Group 5 Alkyltantalum and Ureate Catalyst Systems: Hydroaminoalkylation Reactivity and Applications in Selective Syntheses of Structurally Diverse Amines

by

Rebecca Claire DiPucchio

B.Sc., McMaster University, 2015

A Thesis Submitted In Partial Fulfillment Of The Requirements For The Degree Of

Doctor of Philosophy

in

The Faculty Of Graduate And Postdoctoral Studies

(Chemistry)

The University Of British Columbia

(Vancouver)

August 2020

The following individuals certify that they have read, and recommend to the Faculty of Graduate and Postdoctoral Studies for acceptance, the dissertation entitled:

Group 5 Alkyltantalum and Ureate Catalyst Systems: Hydroaminoalkylation Reactivity and Applications in Selective Syntheses of Structurally Diverse Amines

submitted by Rebecca Claire DiPucchio in partial fulfillment of the requirements for

the degree of Doctor of Philosophy

in Chemistry

Examining Committee:

Laurel Schafer, Chemistry
Supervisor

Parisa Mehrkhodavandi, Chemistry
Supervisory Committee Member

Kristin Orians, Chemistry and Earth and Ocean Sciences
University Examiner

Mark MacLachlan, Chemistry
University Examiner

Additional Supervisory Committee Members:

Jason Hein, Chemistry
Supervisory Committee Member

Abstract

Alkyltantalum precatalysts for intermolecular hydroaminoalkylation reactions between alkene and amine substrates are explored to gain insight into catalyst structure/activity relationships and to develop new methods for the regioselective and diastereoselective synthesis of amines and *N*-heterocycles. This thesis addressed significant challenges with widespread adoption of hydroaminoalkylation towards synthesizing products that display concrete applications in agricultural or pharmaceutical industries.

First, we synthesized alkyltantalum starting materials and combined them with new ureate ligand salts for *in situ* catalyst mixtures that display promising reaction rates. Substrate scope in this section emphasized reactivity using switchable ureate salts for either terminal or internal alkenes while maintaining chemoselectivity with diene substrates. We then probed reaction scope changes that resulted from varying ligand steric and electronic factors. We extended this to study chiral cyclic ureate ligands to attempt enantioselective catalysis, these ligands resulted in poor *ee*'s, but presented unprecedented reactivity with challenging aliphatic amine substrates. Comparative hydroaminoalkylation reactivity with different Ta halides revealed that a brominated Ta started material is slightly more reactive than its chlorinated counterpart, while a fluorinated complex was not active at all.

Catalysis with a new chiral ureate salt accomplished highly chemo- and regioselective C-C bond formation between substituted *N*-methylanilines and either limonene or pinene. We confirmed that hydroaminoalkylation does not racemize allylic stereocentres and can be selective for terminal alkenes. Further, pinene-containing products were consistently generated with high diastereoselectivity. All products were isolated using a simple filtration protocol.

The catalyst system highlighted towards the end of this thesis was the first generally reactive hydroaminoalkylation system. Reactivity was excellent with aromatic or aliphatic amines, terminal or internal alkenes, and most importantly saturated *N*-heterocycles. Exploring substrate scope with these *N*-heterocycles resulted in consistently good yields, with good regio- and diastereoselectivity when unactivated alkene partners are used. However, additional data highlighted the linear dependence of regioisomer product ratios as a function of alkene electronic factors when combining piperidine with styrene partners. This discovery of substrate-controlled product selectivity allowed for only linear product to be obtained in select cases. Final results applied *N*-heterocycle reactivity to a two-step, one-pot catalytic, regiodivergent synthesis of indolizine and quinolizine alkaloids.

Lay Summary

Amines are a class of molecules that have seen a collection of applications in medicinal, agricultural, and fine chemical industries. As the world and its available resources change, we need new strategies to make complex amine products that create less waste and allow us to access previously unattainable products. This work outlines building metal complexes that are reactive enough to combine inexpensive and readily available starting materials into complex products that have potential medicinal activity. We are especially excited about these results because many of the compounds are made in a completely distinct way to traditional strategies, offering opportunities to change how we approach designing amines in the future.

Preface

A version of Chapter 1 will be published later this year (2020) as a review article focused on hydroaminoalkylation across the d block. **DiPucchio, R. C.,** Rosca, S. C. Schafer, L.L. Hydroaminoalkylation as an Emerging Reaction: Catalyst Development Across the d Block and Expanding Applications. *Minireview in Preparation for Chem. Eur. J.* This review was written by me with input via editing and planning from Laurel Schafer.

As noted in the scope of Chapter 2, the work in sections 2.2.1-2.2.4 was completed in collaboration with Dr. Sorin-Claudiu Roşca, where he prepared Ta starting materials and substrates for this paper, while I preformed the vast majority of catalytic reactions and the work on the substrate scope. This collaborative work has been published as both an article and as a worldwide patent. a) **DiPucchio, R. C.***, Rosca, S.C.*, Schafer, L.L. *Catalytic and Atom Economic Csp_3-Csp_3 Bond Formation α-to Nitrogen. Alkyl Tantalum Ureates for Hydroaminoalkylation*. *Angew. Chem. Int. Ed.* **2018**, *130*, 3527. b) Schafer, L. L., **DiPucchio, R.C.,** Rosca, S.C. *Group 5 Metal Complexes for Catalytic Amine Functionalization*. US 62/511,725. Dr. Sorin-Claudiu Roşca wrote an initial draft of the manuscript, with significant edits and input from both Laurel and myself in additional drafts before publication. Both Sorin and myself provided data for the patent and are listed as equal contributors on the patent. Work in Chapter 2 that focused on cyclic ureate ligands is also currently submitted for publication. Daneshmand, P., Roşca, S. C., Dalhoff, R., Kejun, Y., **DiPucchio, R. C.,** Ivanovich, R., A. Polat, D. E., Beauchemin, A. M., Schafer, L. L. *A Cyclic Ureate Ta Catalyst for Preferential Hydroaminoalkylation with Aliphatic Amines. Mechanistic Insights into Substrate Controlled Reactivity*. *J. Am. Chem. Soc.* **2020**. ja-2020-045799. I provided data for the chiral cyclic ureate ligands as both reactivity and enantioselectivity measurements. I provided experimental procedures for these reactions to be included in the supplemental

information. I also synthesized the complex for one crystal structure and edited the manuscript. Last, I have supplied ureate ligands and substrates for the work of Dr. Manfred Manssen and Danfeng Deng to develop Ti-based hydroaminoalkylation catalysts and I will be included on their upcoming paper. Mansen, M., Deng, D., **DiPucchio, R.C.,** Clarkson, J., Schafer, L.L. in situ Generated Highly Active Titanium Ureate Complexes for the Hydroaminoalkylation of Unactivated Terminal and Internal Alkenes. *Manuscript in preparation.* Last, Dr. Daneshmand and Samuel Griffin collected all the data for the crystal structures reported in this chapter. I completed the comparative analyses of all these structures as highlighted in the chapter.

Work in Chapter 3 has been published in its entirety. **DiPucchio, R. C.**; Rosca, S. C.; Athavan, G.; Schafer, L. L. Exploiting Natural Complexity: Synthetic Terpenoid-Alkaloids by Regioselective and Diastereoselective Hydroaminoalkylation Catalysis. *ChemCatChem* **2019**, *11*, 1–7. Dr. Rosca and I co-supervised Gayathri Athavan as an undergraduate researcher during her time working on this project. I planned all reactions to be run, while Gayathri worked to run catalytic reactions and crystallized a product for X-ray analysis. All of the catalysis from Gayathri was repeated by me and all products had to be isolated again. The X-ray data was collected by Sam Griffin. All the reaction products in this paper were synthesized and purified by me. Enantioselectivity data were collected with support from Jordan Daponte and Jason Hein in the Hein lab. Finally, I wrote the paper with support from Laurel Schafer.

A first publication from Chapter 4 is to be submitted. **DiPucchio, R. C.**, Lenzen, K., Daneshmand, P., Erzhova, M., Schafer, L.L. Direct α-Alkylation of *N*-Heterocycles: Substrate Effects for Regiodivergent Product Formation *Revised manuscript submitted with the Journal of the American Chemical Society.* I ran all of the catalysis in this paper and purified all products. I synthesized or supervised the syntheses of all ligands in this work. Dr. Daneshmand synthesized a

first batch of **4.13** and collected the corresponding X-ray data. I helped prepare this crystal data for publication and synthesized subsequent batches of the complex to obtain yields and NMR data. Dr. Karst Lenzen helped with initial reaction screening and purification of large scale hydroaminoalkylation reactions. Maria Erzhova was a huge help with designing and running 2D NMR experiments to characterize products and assign all peak identities. I wrote the resultant paper and prepared the supplemental information. Laurel Schafer has provided direction to help plan and edit the manuscript.

The work towards the end of Chapter 4 focused on the synthesis of fused *N*-heterocycle products was collaborative as noted in the chapter itself. First, a collaborative article with Cameron H.M. Zheng will be published about the synthesis of indolizidine and quinolizine alkaloids where we will be equal contributors. **DiPucchio, R.C.***, Zheng, C.*, Schafer, L.L. Tantalum-Mediated Hydroaminoalkylation for a Two-Step Synthesis of Indolizidine and Quinolizidine Alkaloids. *Manuscript in preparation.* For this paper, I designed the project and mentored Cameron throughout some of his work. I completed the hydroaminoalkylation scope and the associated supplementary information. I also synthesized the first indolizidine and quinolizidine products. Cameron and I planned Ni reactions to screen together, but he performed them and separated the products. He will complete the indolizine and quinolizidine scope while I write an initial draft for the paper and help with supporting information. Next, a collaborative article with Cameron Zheng and Daria Balatsky will be published that focuses on hydroaminoalkylation as a tool to synthesize indole products. I mentored Daria while she worked on this project throughout her 449 undergraduate thesis project. Cameron is going to complete remaining work required for this paper and we will write the manuscript collaboratively. I will work on completing the supporting

information for this paper. As with other projects throughout this thesis, Laurel Schafer will provide input to help design and refine the publications.

Table of Contents

List of Tables

List of Figures

List of Schemes

List of Abbreviations

Å	Angstroms
δ	Chemical shift
°C	Degrees Celcius
σ	Hammett parameter
Ar	Aryl
B:L	Branched:Linear
Bn	Benzyl
BOC	Tert-butoxycarbonyl
BINOL	1,1′-Bi-2-naphthol
bpy	2,2′-Bipyridine
br	Broad
Cat.	Catalyst
COSY	Correlation Spectroscopy
cp	Cyclopentadienyl
%ee	Percent Enantiomeric Excess
d	Doublet
dba	Dibenzylideneacetone
DCM	Dichloromethane
DEPT	Distortionless Enhancement by Polarization Transfer
DG	Directing Group
DIPEA	Diisopropylethylamine

dppf	1,1'-Bis(diphenylphosphino)ferrocene
dppp	1,3-Bis(diphenylphosphino)propane
EDG	Electron-donating group
eq.	Equivalents
EWD	Electron-withdrawing group
g	Grams
GC/MS	Gas Chromatography/Mass Spectrometry
HAT	Hydrogen Atom Transfer
HMBC	Heteronuclear Multiple-Bond Correlation Spectroscopy
HPLC	High Performance Liquid Chromatography
HSQC	Heteronuclear Single Quantum Coherence Spectroscopy
Ind	Indenyl
KIE	Kinetic Isotope Effect
L	Ligand
LED	Light-Emitting Diode
m	Multiplet
Me	Methyl
mg	Milligrams
mL	Milliliters
mmol	Millimoles
NaHMDS	Sodium Hexamethyldisilylazide
NMP	*N*-Methyl-2-pyrrolidone
NMR	Nuclear Magnetic Resonance

NOESY	Nuclear Overhauser Effect Spectroscopy
ORTEP	Oak Ridge Thermal Ellipsoid Plot
Ph	Phenyl
PMP	*Para*-methoxyphenyl
ppm	Parts-per-million
PT	Proton Transfer
q	Quartet
rt	Room Temperature
RuPhos	2-Dicyclohexylphosphino-2′,6′-diisopropoxybiphenyl
s	Singlet
t	Triplet
Ta	Tantalum
t-Bu	*Tert*-butyl
Ti	Titanium
SET	Single Electron Transfer
TBS/TBDMS	Tert-butyldimethylsilyl
TOF	Turnover Frequency
TON	Turnover Number

Acknowledgements

Thank you to everyone who helped me transition from a curious undergraduate scientist to a chemist with many hats to wear for different occasions. Laurel, thank you for having faith in a young organic chemist to tackle and lead a new research direction in the group. I appreciate your exposing me to a new field that I am now not ready to give up. I was so fortunate during moments when I walked into your office with a strange new idea or plan and you were immediately on board.

I'm grateful to NSERC for funding both from the CREATE Sustainable Synthesis program, and for a CGS-D fellowship. Thank you to Dr. Manfred Manssen, Cameron Zheng, Abi Thompson-Killjoy, Maddie Deem, and Jordan Daponte for improving the quality of this thesis along the way. Parisa Mehrkhodavandi provided consistently excellent feedback, and Jason Hein made sure no mistake was missed along the way.

The projects outlined in this thesis would never have been completed without a collection of past and present Schafer members. Thank you Sorin for sharing vital inorganic knowledge, and for helping me discover who I want to be as a mentor throughout my future career. I am immensely grateful for the chance to start the alkyltantalum project with you. I will remember Gordon Carley, Dr. Karst Lenzen, Gayathri Athavan, Dr. Ana Koperniku, Dr. Thibault Bagnol, Samia Zaheer, Dr. Fariba Saadati, Madeline Deem, Cameron Zheng, Jasmin Seibert, and Daria Balatsky as coworkers who helped me develop leadership skills that I hope to continue building. Karst, thank you for arriving at just the right time and helping me to jumpstart the heterocycles project that I am now so proud of. To Cam and Daria, it was an honour to learn alongside both of you. I am so lucky to be a small part of your growth as scientists and I cannot wait to see more of what you both accomplish. Manfred and Pargol filled our lab with valuable new perspectives and helped the little

organometallic chemist in me thrive. Thank you to Abi, Maddie, Cam for being consistent bursts of light in my days (and life). We are not done climbing mountains or investigating ice cream spots yet.

I want to appreciate some of the often unsung heroes in the department. Brian Ditchburn helped me conquer fears and always held a safe space for me to break old glass with a friend. Raz and Ken never questioned my strange design ideas, and somehow could always be found at just the right times. David never found my silly computer questions ridiculous, instead he just instantly solved frustrations that had taken me hours. Adana was so often the key to navigating a new department or solving an unexpected crisis right before an important meeting. Last, chapter 4 of this thesis genuinely would not have been finished without Maria. Thank you for sharing my passion for heterocycles and for running with me through a marathon that we sometimes thought might not end. Jay, not many people look back on TA work as a positive part of their degree. Thank you for making my experience atypical.

I regularly miss all my Inception (now Chinook) colleagues and friends. Thank you for instantly making me feel like a valuable team member, and for reminding me how crucial it is to be a person first and a scientist second. Working with all of you truly was the experience I never knew I needed to grow during my time here.

Thank you Liz.

To my mom, Sara. Thank you for helping me learn persistence and endless determination.

To all the other graduate students who hope that one day science will the most difficult part about completing this degree.

Chapter 1: Introduction

1.1 Importance of Catalytic Amine Functionalization Reactions

Developing efficient catalysts for hydrofunctionalization reactions is a priority among inorganic and organometallic chemists, as these transformations have promising applications in a range of chemical industries.[1] Amine and alkene feedstocks are particularly appealing substrates for such reactions because they are abundant and allow for rapid preparation of structurally complex products in one catalytic step. Currently, most accepted options for generating highly substituted amine products are reductive amination,[2] or complementary C-N bond formations such as Buchwald-Hartwig, Chan-Lam coupling reactions,[3,4] All of these strategies produce waste due to poor atom economy or stochiometric additives. New catalytic amination reactions are particularly desirable, as coupling readily available amines or *N*-heterocycles with different partners can rapidly lead to a library of potential agrochemicals or pharmaceuticals. These options include α C-H arylation or alkylation protocols, with remote C-H alkylation emerging as a newer option for increasingly challenging regioselectivity questions. Strategies for generating substituted amine products with excellent atom economy include hydroamination, hydroaminomethylation, or hydroaminoalkylation.[5] Advantages of these approaches over some stoichiometric methods and other catalytic options can include less waste and regioselective product formation.

Hydroamination adds an N-H bond across a C-C unsaturation to generate a new C-N bond with complete atom economy (Figure 1.1a).[6] This reaction has been prevalent in catalytic amination literature for decades, with catalysts from across the periodic table. Controlled regioselectivity can be obtained by strategic catalyst and substrate selections. Such controlled reactivity results in the efficient synthesis of selectively substituted amines and *N*-heterocycles. Intramolecular hydroamination is much more established than the intermolecular variant, due to

the lower entropic barrier for the intramolecular reaction as intermolecular reactivity is challenging due to the near thermoneutral nature of the transformation. As a result, only limited examples of intermolecular reactions exist and they are restricted to activated alkene substrates such as norbornene, styrene or butadiene substrates. One such example comes from the Nicewicz group, with strategies for anti-Markovnikov photochemical hydroamination reactions using protected aromatic amines with select styrene partners.[7,8] A recent report by the Knowles group illustrated successful intermolecular hydroamination, using an Ir(III) photocatalyst.[9,10] This work reacted amine heterocycles with sterically congested alkene partners to obtain anti-Markovnikov products. Contributions from the Malcolmson group also illustrate intermolecular regioselective hydroamination reactions between aliphatic amines or amine heterocycles and conjugated diene partners.[11,12] Other successful complementary approaches have used activated amine substrates such as hydroxylamine esters[10] or sulfonamides[13] with unactivated alkenes to realize the formal hydroamination of a broad range of unactivated alkenes. Due to the long-standing synthetic challenge associated with hydroamination, this topic has already been extensively reviewed and will not be discussed further here.[14–19]

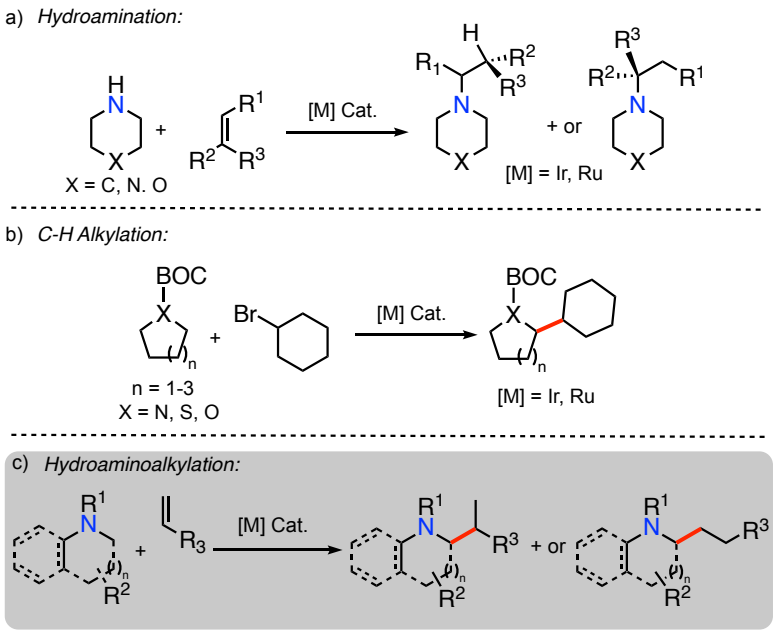

Figure 1.1. Complementary catalytic C-C and C-N bond-forming reactions to generate similar reaction products.

Hydroaminomethylation generates substituted amine products that are often complementary to hydroaminoalkylation, via tandem hydroformylation with CO, reductive amination and then hydrogenation. These reactions sequentially generate C-C and C-N bonds without purification of any reaction intermediates.[20–22] Unlike many typical late transition-metal amination strategies, hydroaminomethylation often does not require amine substrate protection for productive reactivity. As with hydroamination, this reaction strategy has been recently reviewed.[23]

Amine α-C-H arylation reactions helped launch a new series of C-H activation catalysts towards arylated heterocycle products.[24] Such reactions generate Csp^3-Csp^2 bonds, usually by using a late metal catalyst with a heterocycle derivatized with a directing group. Most of the development for this reaction focuses on expanding substrate scope or efforts towards transient directing groups for less waste generation.[25–29] More recent developments emphasized remote C-H activation for selective meta-arylation of amine substrates.[30,31] α-C-H alkylation reactions are

an extension of these arylation strategies to access new Csp^3-Csp^3 bonds by reacting an amine with an alkyl halide partner. These reactions are another alternative to C-N bond-forming hydroamination strategies for making selectively substituted amine products (Figure 1.1b). This transformation typically requires an Ir photocatalyst, and all amine groups must be protected.[32] A transition metal-free alternative exists to generate similar products, using stoichiometric amounts of organolithium reagents with unprotected amine partners.[33,34] Both methods generate linear reaction products exclusively and compounds are often obtained with high diastereoselectivity.

Hydroaminoalkylation is an alternative emerging reaction to add a C-H bond across a C=C unsaturation in an alkene substrate via C-H activation (Figure 1.1c).[5,35–38] Like hydroamination, this hydrofunctionalization reaction is completely atom-economic and can generate either linear or branched regioisomers. Further, hydroaminoalkylation can create stereocenters, and thus reaction development can focus on improved diastereo- and/or enantioselectivity. Early transition-metal, late transition-metal, and photochemical communities all have mechanistically distinct approaches to hydroaminoalkylation and thus reaction development efforts are complementary. For example, most late transition-metal systems are regioselective for the linear product, while their early transition-metal counterparts typically obtain branched products. It should be noted that many late transition-metal chemists refer to hydroaminoalkylation as the C-H alkylation of amines. For consistency, we will exclusively use hydroaminoalkylation for the duration of this work.

This chapter summarizes the development of catalytic transition-metal systems for intra- and intermolecular hydroaminoalkylation reactions, with a focus on catalyst design and ligand selection. Sections are divided by the mechanism of the catalytic reaction to highlight some of the key differences between early transition-metal, late transition-metal, and photocatalytic approaches.

1.2 Early Transition Metal Hydroaminoalkylation

Early transition metal catalyzed hydroaminoalkylation has been known since 1980, when the Maspero group showed that unactivated alkenes such as ethylene, propylene or 1-hexene can react with $HNMe_2$ in the presence of group 4 or 5 metal amido complexes $M(NMe_2)_x$ (Scheme 1.1; M = Zr, x = 4; M = Nb, Ta, x = 5) to give the corresponding α-alkylated product. Other metal amidos such as $Ti(NMe_2)_4$, $V(NMe_2)_5$, $Mo(NMe_2)_5$ or $Sn(NMe_2)_4$ were less reactive and afforded only traces of organic product.[39] Only mono-α-alkylated products were obtained using this method, despite the fact that two potential reactive sites are present. No additional work on this reaction existed for over a decade.

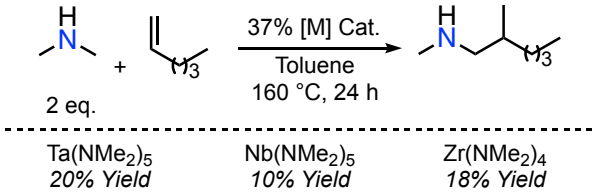

Scheme 1.1. Initial hydroaminoalkylation work by the Maspero group using dimethylamine gas.[39]

Work from the Hartwig group in 2007 sparked a renewed interest in hydroaminoalkylation (Scheme 1.2).[40] Early mechanistic studies that complement this work were performed using deuterium labeling experiments by Nugent and co-workers,[41] who thus proposed an initial C-H activation to generate catalytically active metallaaziridines (Figure 1.2). Insertion of the alkene into the M–C bond results in a 5-membered metallacycle **D**, which later reacts with a molecule of amine substrate to form intermediate **E**. A second C-H activation step generates the hydroaminoalkylation product and regenerates the starting metallaaziridine.

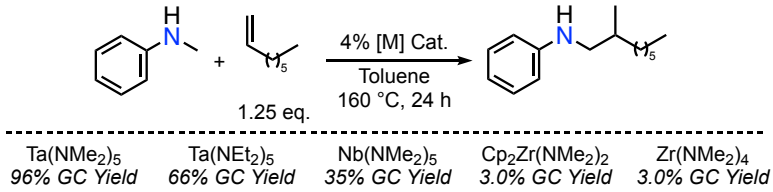

Scheme 1.2. Seminal hydroaminoalkylation efforts from the Hartwig group.[40,42]

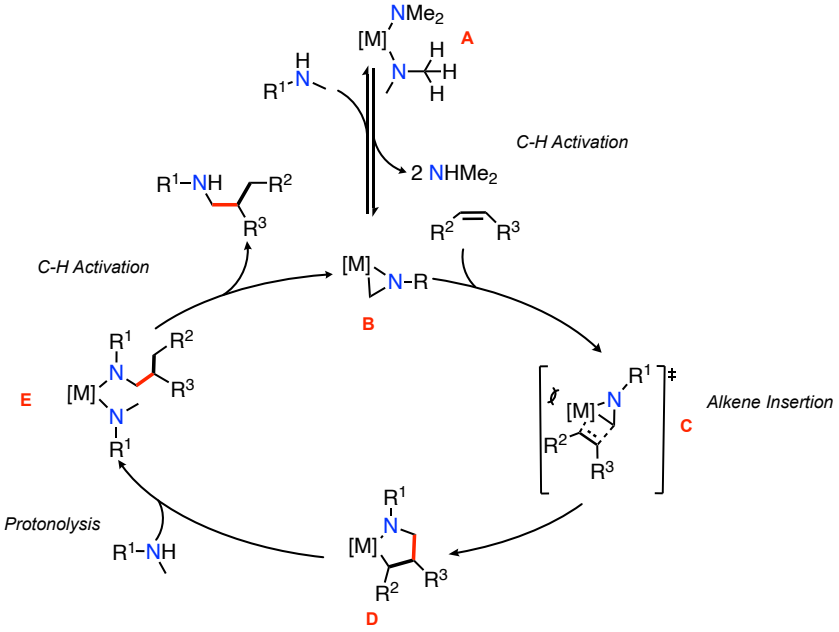

Figure 1.2. The proposed mechanism from Nugent for early transition-metal catalyzed hydroaminoalkylation reactions. This reaction pathway describes reactivity with group 4 or 5 metals.[41] ≠ indicates steric bulk.

Different metals within the early transition-metals have been used for hydroaminoalkylation to deliver metal modified reactivity. Thus, the next subsections are divided by group and contrasting regioselectivities and reactivity with unique substrate classes are highlighted.

1.2.1 Group 3

Scandium catalyzed hydroaminoalkylation was first reported in 2016. Specifically, the Hou group showed that the combination of a Sc alkyl precursor, $Sc(CH_2C_6H_4NMe_2)_3$ and $[Ph_3C][B(C_6F_5)_4]$ generates a cationic Sc complex in situ that can catalyze the reaction of unactivated alkenes with aliphatic tertiary amines (Scheme 1.3a).[43] To date, Sc-based systems are the only early transition-metal reported for the reaction of tertiary amine substrates. Such substrates have not been illustrated in other early-transition metal hydroaminoalkylation publications. Subsequent computational investigations suggest that regioselectivity can be controlled by alkene electronic properties.[44] Alkenes bearing alkyl substituents favor the branched product, whereas substrates containing either $SiMe_3$ or aryl groups exclusively form the linear regioisomer (Figure 1.3). Computational analysis also determined that the turnover limiting step is the C–H bond activation to yield a reactive metallaaziridine. This early work featured the use of a homoleptic complex and did not explore the use of an auxiliary ligand to modify reactivity. However, the Xu group illustrated that tertiary anilines can also undergo C-H activation using cationic Sc (Scheme 1.3b). This scandium complex supported by a tridentate *N,N,P* ligand, in combination with $[PhNHMe_2][B(C_6F_5)_4]$ activator generates a cationic species that promotes the reaction between 1-octene and *N,N*-dimethylaniline (Scheme 1.3b).[45] Xu's ligand was particularly important because it allowed for the first group 3 example of catalyst-controlled selectivity towards only the branched product, despite electronic changes in alkene substrates.

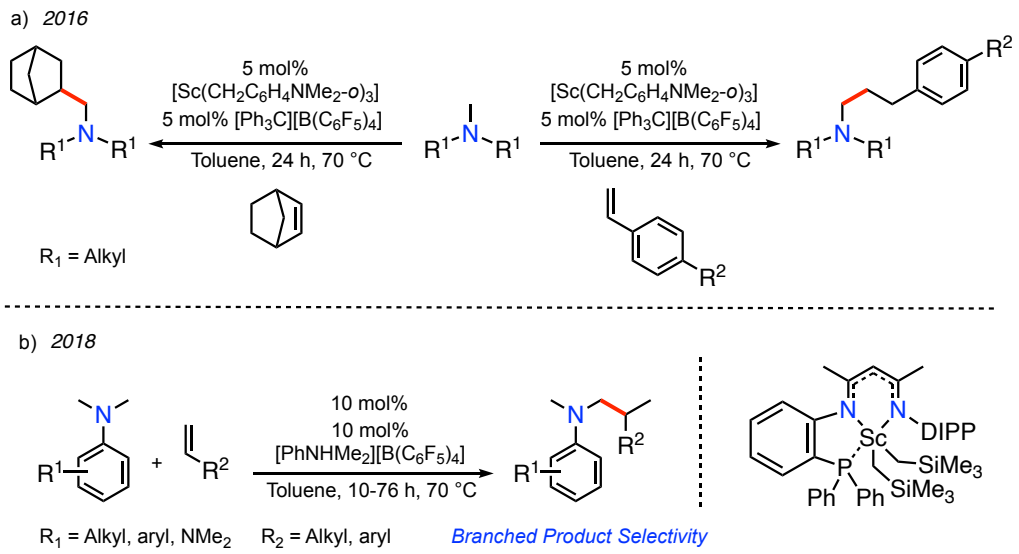

Scheme 1.3. Group 3 systems for intermolecular hydroaminoalkylation from the Hou group (2016) and the Xu group (2018).[43,45]

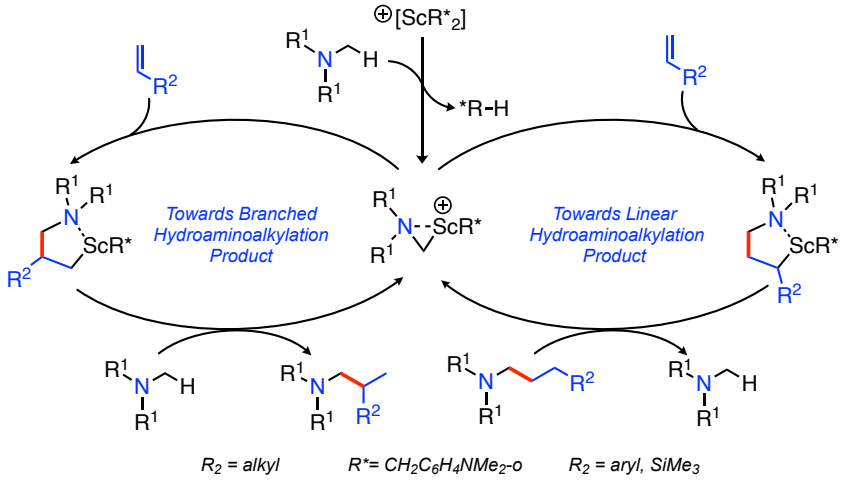

Figure 1.3. Proposed divergent mechanism for Sc-catalyzed hydroaminoalkylation from the Hou group with primary amines. Regioisomer formation is controlled by alkene electronics.[44]

1.2.2 Group 4

The use of $Ti(NMe_2)_4$ in hydroaminoalkylation had been known since the early 80's but the more general application of group 4 metals for this reaction was not revisited until 2009. Since then the Doye and Schafer groups have explored Ti and Zr systems in hydroaminoalkylation.

Using these metals, both intra- and intermolecular reactivity has been established and preliminary trends in the development of auxiliary ligands suitable for modifying reactivity and regioselectivity have been disclosed.

1.2.2.1 Catalysis Using Homoleptic Complexes

The Doye group initially used $Ti(NMe_2)_4$ as an active catalyst for intramolecular hydroaminoalkylation with primary or secondary aminoalkenes to form 5-7 membered rings using high temperatures and long reaction times (160 °C, 72 h; Scheme 1.4).[46] The use of more reactive precursors such as $TiBn_4$ resulted in improved reactivity.[47] These intramolecular reactions displayed some substrate-controlled diastereoselectivity, where R = methyl or alkyl chains. These reactions with alkyl groups resulted in significantly more trans product than when R = phenyl (Scheme 1.4).

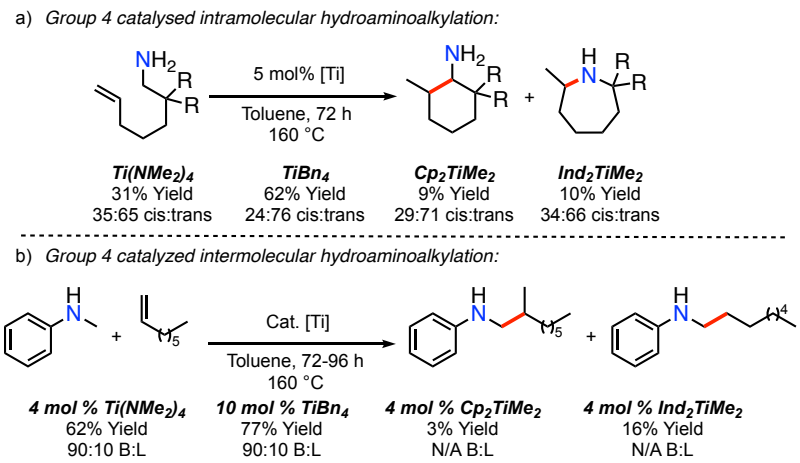

Scheme 1.4. Comparing intra- and intermolecular hydroaminoalkylation reactions by the Doye group with a selection of either commercially available or independently synthesized Ti materials.[46–48]

Intermolecular hydroaminoalkylation with group 4 precursors, such as $Ti(NMe_2)_4$ or $TiBn_4$, were completed for reactions of *N*-methylaniline with 1-octene as a benchmark terminal alkene

substrate showing that $TiBn_4$ had a higher activity than $Ti(NMe_2)_4$ (Scheme 1.4a).[46,47] In contrast to the intramolecular variant, intermolecular hydroaminoalkylation does not compete with the very challenging intermolecular hydroamination, simplifying reaction analyses. Productive reactivity required extended reaction times and high temperatures (96 h, 160 °C), leaving significant potential for catalyst development. Strained internal alkenes such as norbornene can also be used as substrates.

Mechanistic follow-up studies from the Beckhaus and Doye group are consistent with proposals from Nugent and coworkers, further supporting metallaaziridines as the catalytically active species.[49,50] Follow-up experiments from the Beckhaus and Doye groups also isolated an alkene insertion product as proposed.[50,51] Kinetic experiments show that [Ti] must be kept low (< 10 mol %) to avoid the formation of oligomeric Ti species. As in the studies reported by Nugent, a high KIE of 7.3 with a primary aminoalkene for intramolecular hydroaminoalkylation suggests that the rate determining step of the mechanism involves a C–H activation process.[41,49]

The first example of Zr-catalyzed hydroaminoalkylation came from the Basset group, who grafted commercially available Zr materials onto silica surfaces.[52] More recently, the Schafer group became interested in using group 4 systems for reactivity with *N*-silylamines as primary amine surrogates to give the primary amine products upon workup (Scheme 1.5).[53] Notably, this substrate was most compatible with Zr as a catalyst. This was the first example of a catalyst for intermolecular hydroaminoalkylation to afford primary amine products, often as a mixture of regioisomers and diastereomers. Substrate controlled regioselectivity could be leveraged to access the linear products exclusively. For example, the sterically and electronically activated vinyltrimethylsilane gave only linear product while allyltrimethylsilane produces mostly branched product.

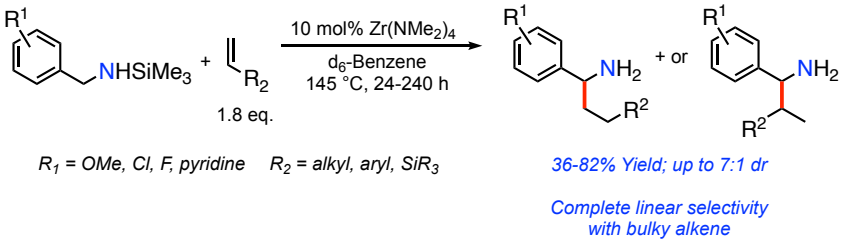

Scheme 1.5. The first example of group 4 catalyzed intermolecular hydroaminoalkylation from the Basset group to generate primary amine products.

1.2.2.2 Metal Complexes Supported By Auxiliary Ligands

Early transition-metals are very electropositive, thus ligands required to stabilize these centers are different than phosphine-based systems that dominate most late transition-metal chemistry. Anionic carbon, oxygen or nitrogen-based donors have been used strategically to modify electronic and steric properties of the resulting catalysts (Scheme 1.4). For example, electron-rich cyclopentadienyl (Cp) ligands are typical for stabilizing early transition-metal centres, but often diminish the corresponding catalytic activity in hydroaminoalkylation due to the fact that this ligand does not afford a sufficiently electrophilic metal center. Thus, Cp_2TiMe_2 provides only trace product for either intra- or intermolecular hydroaminoalkylation (Scheme 1.4).[47,48] Replacing Cp with indenyl (Ind) ligands to make Ind_2TiMe_2 offers slightly improved activity for intramolecular hydroaminoalkylation using *N*–arylaminoalkenes, likely due to the known changes in hapticity (and hence donor capacity and steric encumbrance) of the Ind ligand (Scheme 1.4).[48,54,55] This work was expanded to intermolecular variants, where Ind_2TiMe_2 was shown to catalyze hydroaminoalkylation reactions with activated alkenes such as styrene. The Doye group expanded on excellent reactivity with styrenes to include aromatic butadiene substrates, achieving chemoselectivity for the terminal alkene functionality without any alkene isomerization.[54] These products are obtained as mixtures of linear and branched isomers (Scheme

1.4). Notably, all these complexes with carbon-based auxiliary ligands remain inactive for intermolecular hydroaminoalkylation using *N*-methylaniline and 1-octene as a representative unactivated alkene.

The Doye group reported that some of the challenges with Cp and Ind complexes were due to the dependence of these complexes on the chosen amine substrate.[55] The complex in Scheme 1.6 already contains a tethered amide donor, and provides another method for tuning hydroaminoalkylation reactivity. This complex is an excellent precatalyst for intramolecular hydroaminoalkylation with primary aminoalkene substrates providing excellent regioselectivity and reasonable stereoselectivity for this transformation. However, it is a poor catalyst for intermolecular hydroaminoalkylation reactions with unactivated substrates, requiring extremely long reaction times (96 h) at very high temperatures and loadings (160 C, 10% Ti) for even modest product formation.

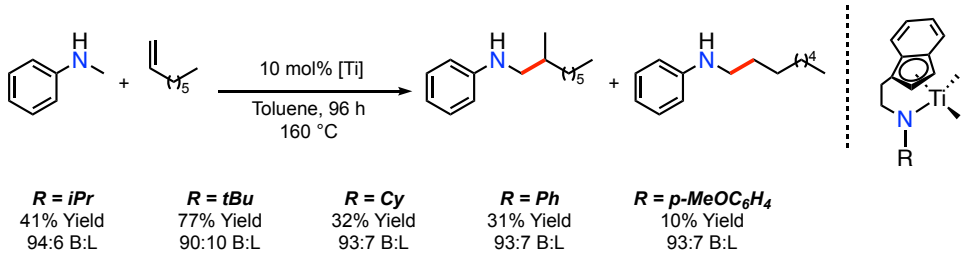

Scheme 1.6. Using a *C,N*-chelating donor for a Ti catalyst by the Doye group towards a benchmark reaction in hydroaminoalkylation.[55]

Another significant focus for group 4 hydroaminoalkylation research is 1,3-*N,N* or *N,O*-chelating ligands, as hemilabile scaffolds to stabilize very electrophilic metal centers. Initial efforts using *N,O*-chelating sulfamide ligands generate dinuclear precatalysts that offer modest reactivity for *N*-methylaniline and styrene (5 mol % Ti, 120 °C, 48 h, 37%, Scheme 1.7).[56] Notably, reactions could be selective for branched reaction products (up to 97:3 branched: linear).

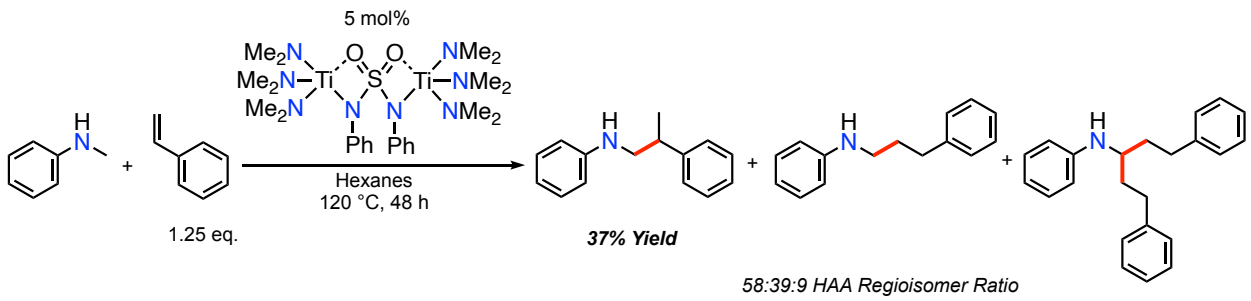

Scheme 1.7. Use of *N,O*-chelating ligands with Ti from the Doye group for dimeric complexes towards intermolecular hydroaminoalkylation reactions.[56]

The Doye group has also explored *N,N*-chelated Ti complexes for hydroaminoalkylation reactions (Figure 1.4). The simplest of these systems, featuring aminopyridinato ligands, was used for the first example of intramolecular hydroaminoalkylation with secondary aromatic aminoalkenes.[57] Complexes in this work were made by reacting commercially available $Ti(NMe_2)_4$ with two equivalents of either 2- (methylamino)pyridine or 2,6-bis(phenylamino)pyridine to generate bis-*N,N*-chelated precatalysts that had been reported by the Eisen group for polymerization catalysis.[58]

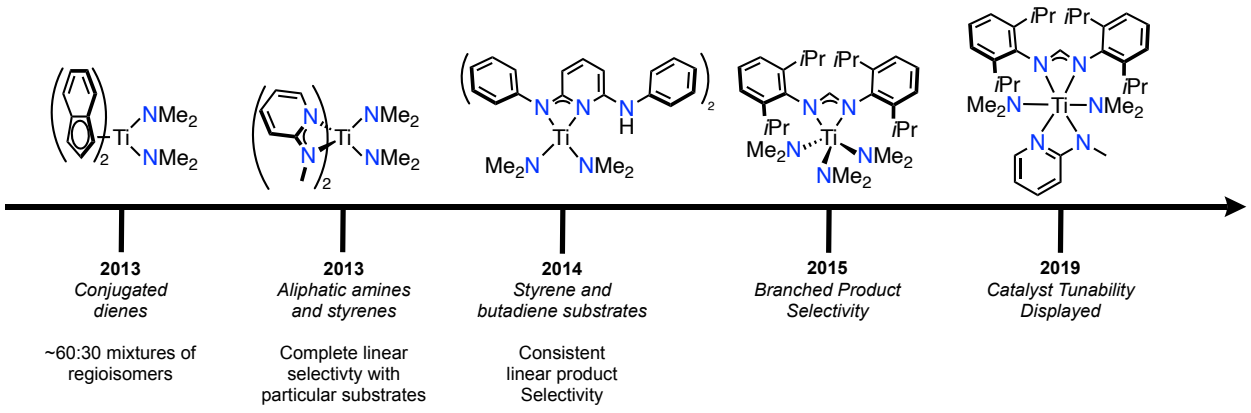

Figure 1.4. A series of *N,N*-chelating Ti hydroaminoalkylation catalysts developed by the Doye group to probe potential changes in regioselectivity.[54,57,59–61]

These complexes showed improved catalyst-controlled linear product selectivity.[59,60] Combining *N*-methylaniline with styrene as an activated alkene (5 mol%, 140 °C, 96 h) yielded only the linear product in 81 % yield (Figure 1.4, 2013, *N,N*-chelating complex).

The 2,6-bis(phenylamino)pyridinate-based Ti catalyst was used to achieve catalyst-controlled regioselectivity for the linear hydroaminoalkylation regioisomer with a variety of substituted N-methylanilines (at least 6:94 branched: linear) including *N*-ethylaniline and *N*-methylbenzylamine (Figure 1.4, 2014).[60] Styrene substrates were still required as activated alkene substrates, though a variety of both electron donating and withdrawing arene substituents were tolerated.

Alternatively, regioselectivity with Ti complexes can be switched to almost entirely branched hydroaminoalkylation products with the use of two equivalents of a mono(formamidinate) ligand as a distinct *N,N*-chelating ligand (Figure 1.4, 2015). Relatively harsh reaction conditions (140-180 °C, 10 mol % Ti, 96 h) allowed for the use of notable substrates including internal alkenes such as cyclopentene and a variety of 1,1-disubstituted alkenes. Challenging quaternary centers can be assembled using this catalyst that selectively yields branched amines.

Unactivated internal alkene substrates are even more challenging starting materials. Reactivity with select examples of these substrates can be accomplished using the same mono(formamidinate) *N,N*-chelated Ti catalyst.[62] High reaction temperatures (180 °C), high catalytic loadings of 10 mol % and long reaction times of 96 h were required for productive reactivity for this demanding reaction. Notably, this group 4 catalyst system can use cyclopentene as a substrate. This catalyst is strongly influenced by substrate steric factors such that α-methylstyrene reacts to give only branched product, while β-methylstyrene reacts to generate the

linear isomer. This catalyst can also be used to advantage for applications in organic synthesis (Figure 1.5, left). For example, this catalyst can be used with gaseous dimethylamine as a hydroaminoalkylation substrate.[63] This report showcases how an easily synthesized catalyst system can be used in combination with simple feedstock chemicals and can be done on multigram scale (48 g). This system also affords control for accessing mono- or dialkylation products simply by increasing alkene equivalents from 1.5 to three respectively. This catalyst can also be used with allene substrates for hydroaminoalkylation.[64] Another gaseous application exists with ethylene, where regioselectivity is no longer a question.[51] Recent work showed that intramolecular aminoallene reactivity can be realized and reactions can be carried out under either kinetic or thermodynamic control to give different major products (Figure 1.5, top).[64]

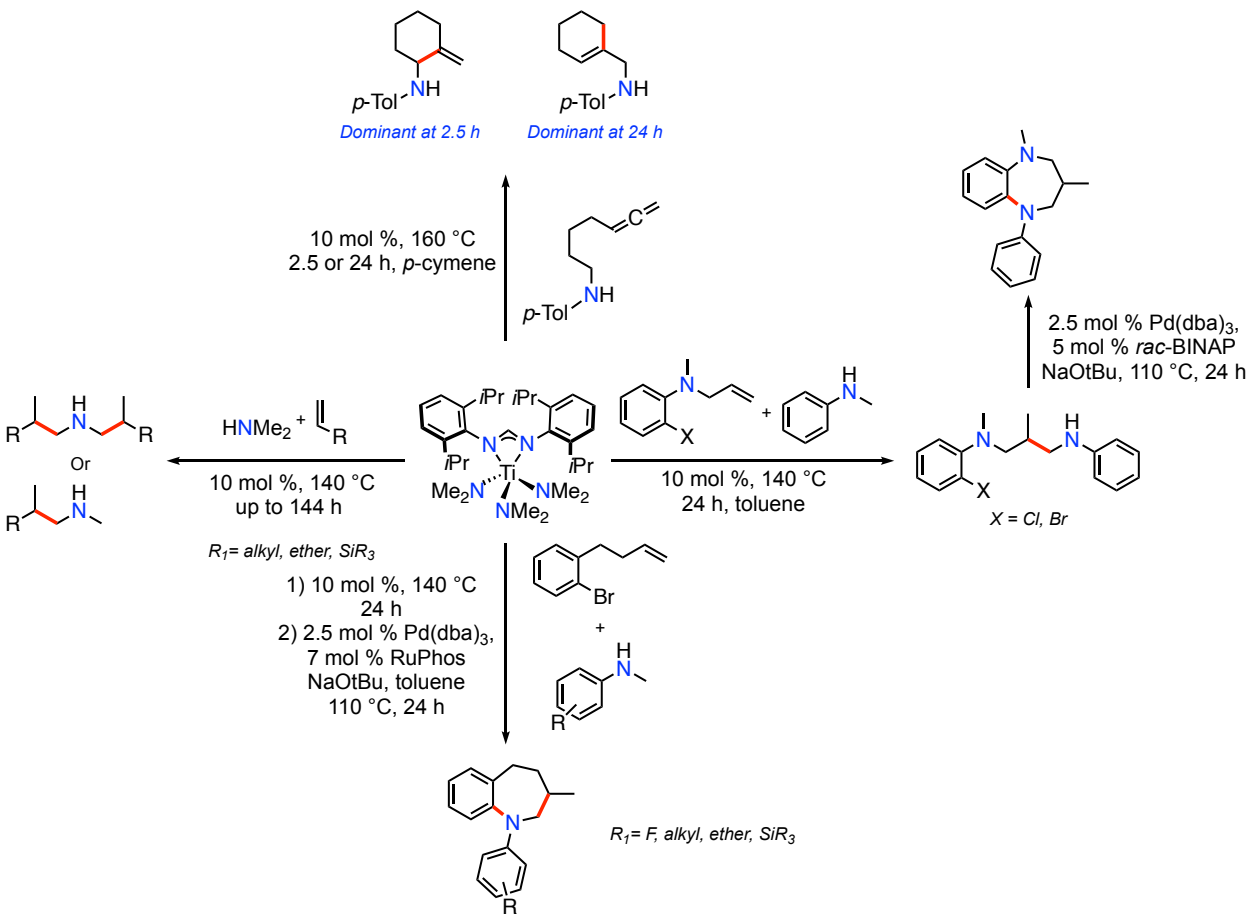

Figure 1.5. Select applications of a mono(formamidinate) Ti catalyst from the Doye group.[59,65,66]

Hydroaminoalkylation with *N,N*-chelating ligands can also be used for post-hydroaminoalkylation functionalization to access more complex heterocycle products.[65,67] For example, ortho-halogenated tertiary *N*-allylanilines with N-methylaniline (10 mol % Ti, 140 °C, 24 h) generate 1,3-diamine products with both secondary and tertiary functionality (Figure 1.5, right). $Pd(dba)_3$ was used in combination with *rac*-BINAP for a subsequent tandem Buchwald-Hartwig amination to prepare 1,5-benzodiazepine products.[66] A similar option uses substituted 4-phenyl-1-butene substrates with N-methylaniline (Figure 1.5, bottom). Buchwald- Hartwig conditions in this case instead combine $Pd(dba)_3$ with RuPhos as an ancillary ligand. The only attempt to modify the hydroaminoalkylation catalyst from Figure 1.5 was published very recently

(Figure 1.4, 2019), where authors added *N*-methylpyridonate as an *N,N*-chelate in place of traditional amido donors. This new complex showed no improvements for reactivity or regioselectivity as compared with the complex highlighted in Figure 1.5.[61]

In contrast, the Schafer group has investigated Ti catalysts with *N,O*-chelating ligands for intramolecular hydroaminoalkylation, where competition with hydroamination is a significant challenge (Scheme 1.8). All previously investigated group 4 or 5 hydroaminoalkylation catalysts gave primarily or entirely hydroamination products.[68] However, sterically and electronically varied pyridonate Ti complexes were explored for controlling chemoselectivity between hydroaminoalkylation and hydroamination, with 3-phenylpyridonate as the ligand with the best selectivity (Scheme 1.8). For optimized reaction conditions, catalyst was added in two separate 10 mol% aliquots over a 48 h reaction time.

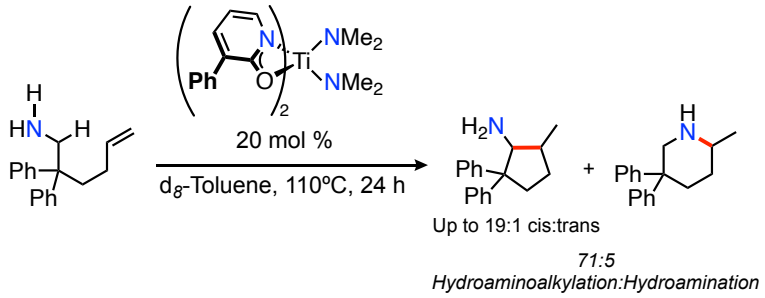

Scheme 1.8. Optimized Ti conditions from the Schafer group for competing hydroamination and hydroaminoalkylation reactions.[68]

A recent study attempts to expand Ti *N,O*-chelating work to phosphoramidate ligand scaffolds. A variety of bis-chelated complexes were generated as in Scheme 1.9. These catalysts were all screened in both hydroamination and hydroaminoalkylation reactions. As displayed, most complexes were inactive for intermolecular hydroaminoalkylation with *para*-methoxy-*N*-

methylaniline as an activated amine with 1-octene. Ongoing work in the Schafer lab will target distinct ligand frameworks for use in group 4 hydroaminoalkylation development.

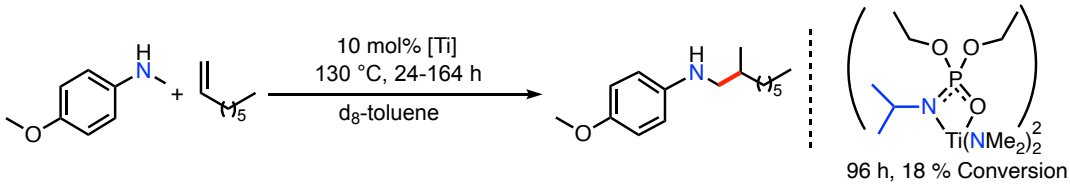

Scheme 1.9. Titanium bis-phosphoramidate complexes as used by the Schafer group with an activated benchmark amine for intermolecular hydroaminoalkylation.[69]

1.2.2.3 *In Situ* Catalytic Systems

In situ formation of catalyst systems, where no organometallic species are isolated, is attractive to synthetic organic chemists interested in utilizing this alternative disconnection strategy. Using $Ti(NMe_2)_4$ with a combination of proteoligands can also allow for rapid access to a family of related catalyst systems. The Doye group showed that in situ mixtures between $Ti(NMe_2)_4$ and 2-(methylamino)pyridine are more reactive than $Ti(NMe_2)_4$ alone and can successfully catalyze the addition of alkylamines to styrenes affording the linear regioisomer as the major product, albeit as a mixture of products (up to 32:68 branched: linear for *N*-methylaniline and styrene, Scheme 1.10).[59]

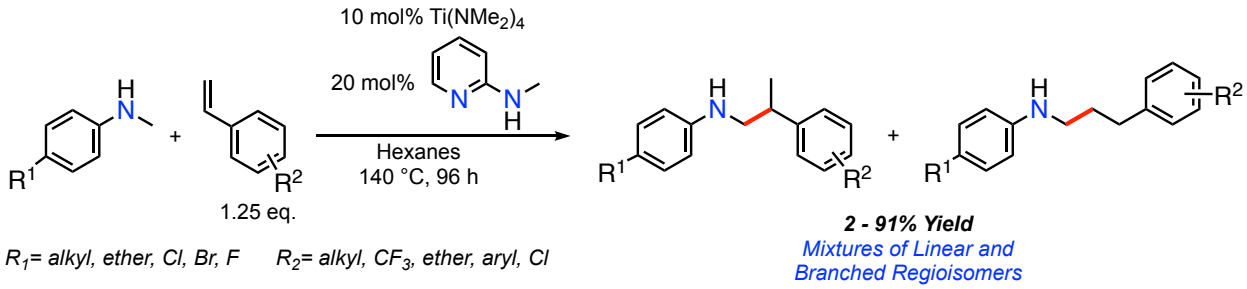

Scheme 1.10. Using an *N,N*-chelating ligand to generate catalysts *in situ* from $Ti(NMe_2)_4$ by the Doye group.[59]

Most recently, the Doye group developed a new *N,N*-chelate that is used in situ with $TiBn_4$ to specifically target neat, rapid reactions (completion in as low as 2 minutes) and exemplify this to make known products in very little time (Scheme 1.11).[70] The ligand in this work requires six steps to synthesize, while the $TiBn_4$ can either be purchased or made using air sensitive techniques. Most products in the amine scope are made with excellent branched product selectivity, while products with varying alkenes resulted in branched/ linear product mixtures. One exciting application of this method was reactivity with silyl-protected methylamine to generate functionalized primary amine products. This reactivity required longer times (12 h) than simpler known products, and was most successful with terminal alkene coupling partners. Earlier discussions have already highlighted the significant challenge that primary amines present as substrates for any hydroaminoalkylation method, so this recent development presents an interesting alternative to reductive amination strategies with ammonia equivalents.

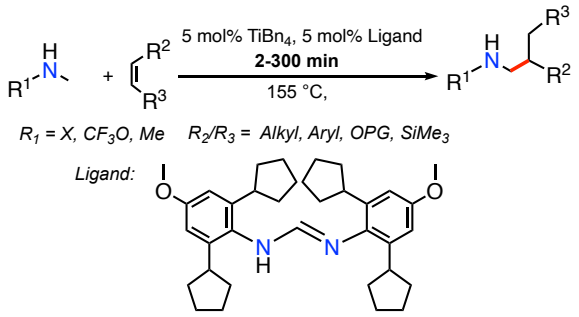

Scheme 1.11. A Ti-based catalyst system for very rapid hydroaminoalkylation reactivity

To date, there is only one example of an isolated Zr ligated complex for hydroaminoalkylation for intramolecular examples (Scheme 1.12).[71] The Schafer group illustrates a distinct system via protonolysis between $Zr(NMe_2)_4$ and two equivalents of 6-tert-butyl-3-phenyl-2-pyridone to generate a bis ligated complex in 98% yield. Reactivity with primary aminoalkenes was successful to generate either 5 or six membered rings in 43-90 % yield, with dr

values ranging significantly from 3:1 to 1:19. Notably, the proposed mechanism for this transformation invoked bimetallic species.

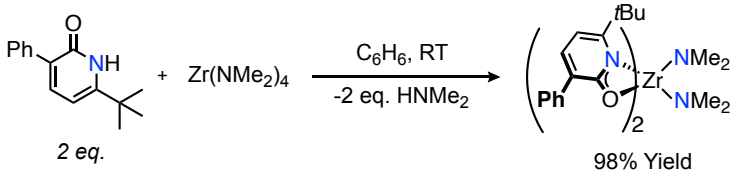

Scheme 1.12. An isolated Zr complex from the Schafer group for hydroaminoalkylation.[71]

1.2.3 Group 5

Ta(V)-based catalysts dominate group 5 hydroaminoalkylation literature. There are rare reports on Nb(V) activity and only one known report of V hydroaminoalkylation.[72–74] The reactivities of group 5 also proceed via a catalytically active metallaaziridine intermediate, although in contrast to group 4, group 5 complexes yield almost exclusively the branched product.

1.2.3.1 Simple Metal Precursors

Following the early disclosure on groups 4 and 5 amido complexes for hydroaminoalkylation by the Maspero group,[39] the investigation of this chemistry remained dormant until 2007. Herzon and Hartwig investigated the catalytic activity of the commercially available $Ta(NMe_2)_5$ and $Ta(NEt_2)_5$.[40,42] This work focused on secondary anilines and terminal alkenes as substrates, with relatively short reaction times of 24 h at 160-165 °C. The reactions in this report were 100% regioselective, exclusively forming the branched isomer. The Doye group showed that $Ta(NMe_2)_5$ can also react with a selection of substituted styrenes to generate branched products (8 mol % Ta, 140 °C, 96 h; Scheme 1.13).[75] $Nb(NMe_2)_5$ was also shown to be catalytically active, though it was outperformed by its tantalum counterpart.

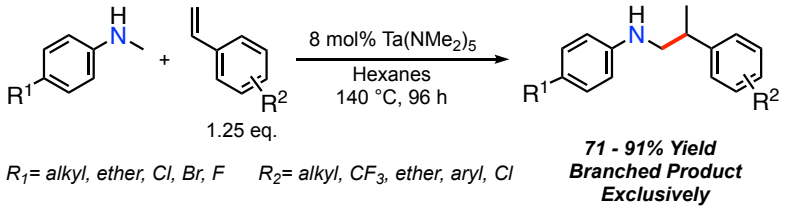

Scheme 1.13. Highlighting the effects of $Ta(NMe_2)_5$ from the Doye group without using additional auxiliary ligands for intermolecular hydroaminoalkylation.[75]

The Basset group showed that heterogeneous hydroaminoalkylation reactions worked when $Ta(NMe_2)_5$ is grafted on to silica to form [≡Si-O-$Ta(NMe_2)_4$].[76,77] Moreover, the Si-supported Ta system can undergo heterogeneous C-H activation hydroaminoalkylation to form a characterized silica-supported tantallaziridine, which can independently catalyze heterogeneous hydroaminoalkylation and allow authors to isolate a resultant azametallacyclopentane (Scheme 1.14).[77]

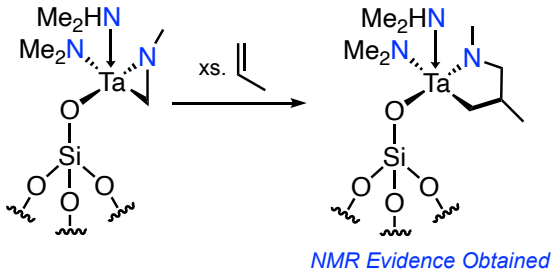

Scheme 1.14. Evidence from the Basset group for surface supported Ta-catalyzed hydroaminoalkylation intermediates.[77]

The incorporation of electron withdrawing ligands such as Cl^- is beneficial for catalysis as $Ta(NMe_3)_2Cl_3$ and $Ta(NEt_3)_2Cl_3$ have higher activities than $Ta(NMe_2)_5$. This higher activity means that the more challenging dialkyl amine substrates can also be used in hydroaminoalkylation.[42] The use of tantalum alkyl species as hydroaminoalkylation catalysts was first introduced by the Schafer group, who reported $TaMe_3Cl_2$ as an efficient catalyst for the benchmark reaction of *N*-

methylaniline and 1-octene (Scheme 1.15).[78] Alkyltantalum starting materials can be advantageous over their Ta amido counterparts because they avoid alkylation of the precatalyst amido ligands (that results in a reaction byproduct), eliminating the need for excess alkene substrate. Despite the fact that the Ta-Me complex can sustain high initial TOFs (up to 6 turnovers in the first hour)[79], its catalytic activity diminishes over longer reaction times due to rapid catalyst decomposition. Further, this Ta starting material is both light and temperature sensitive, making it challenging to work with.

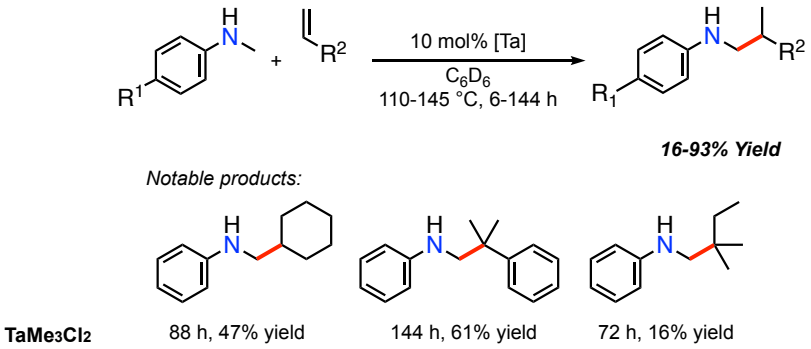

Scheme 1.15. $TaMeCl_2$ as an independent catalyst from the Schafer group for intermolecular hydroaminoalkylation with typically challenging substrates.[78]

1.2.3.2 Metal Complexes Supported By Auxiliary Ligands

The first characterized ligand supported group 5 hydroaminoalkylation precatalysts came from the Schafer group in 2009. *N,O*-chelated Ta amidate complexes were shown to be useful for reactions with secondary anilines and unactivated alkenes (Scheme 1.16).[80] Catalysis using the mono-amidate complex resulted in unprecedented reactivity with a broad range of amine classes and activated internal alkene substrates. It was shown that this amidate complex could alkylate N-heterocycles, such as piperidine or piperazine, to rapidly generate complex products in a highly diastereoselective fashion (dr >20:1).[81] Amidate ligands could also support isolable group 5 tantallaziridine species.[82] Attempts to isolate further catalytic intermediates upon alkene insertion

were unsuccessful. Kinetic experiments performed on tantalum amidate complex in the top of Scheme 1.16 indicate that this variant of hydroaminoalkylation is zero order in amine and first order in catalyst with a nonlinear dependence on alkene concentration.

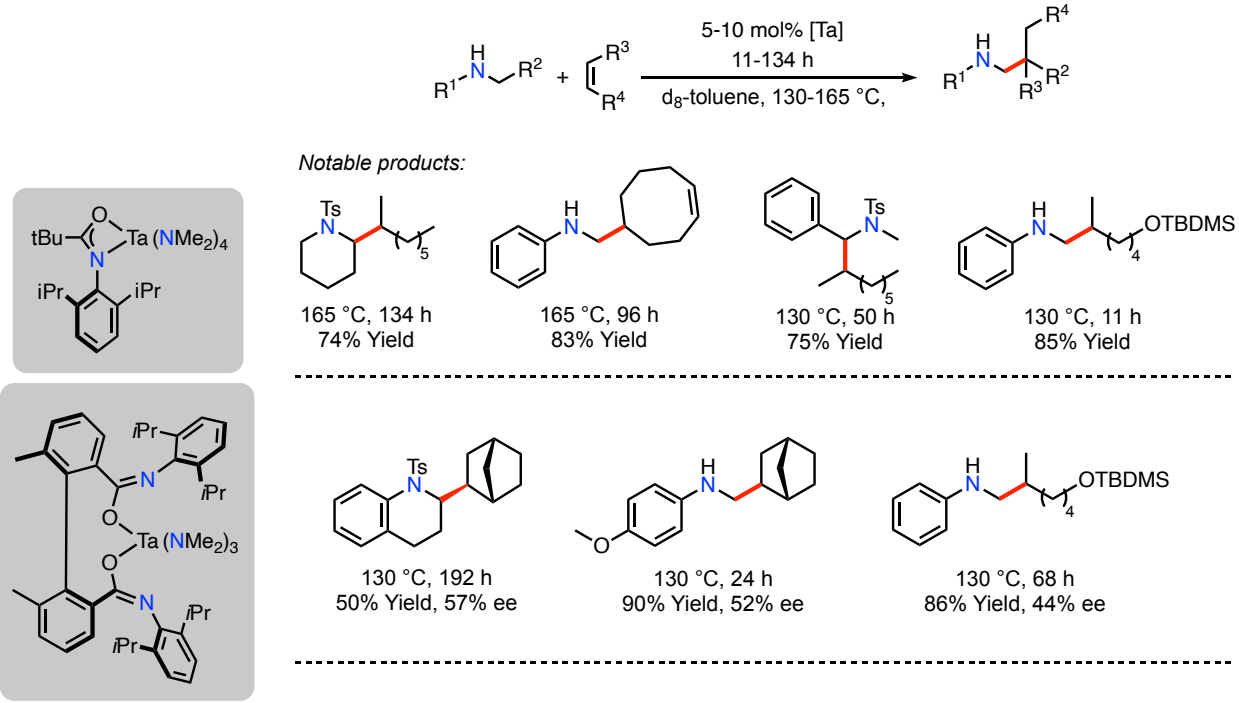

Scheme 1.16. The first isolated group 5 complex from the Schafer group for intermolecular hydroaminoalkylation catalysis.[80]

Another application of early Ta amidate catalysis was the first example of enantioselective hydroaminoalkylation (Scheme 1.16).[80] The tethered bis-amidate scaffold afforded diminished reactivity as compared with its mono-amidate counterpart (5 mol %, 130 °C, 24 h for 84 % conversion with mono-amidate vs. 10 mol %, 130 °C, 68 h, for 86 % yield with bis-amidate). Resultant *ee* values were up to 61 %, leaving lots of room for improvement.

The Zi group also used *N,O*-chelating axially chiral bis-amidate ligands to explore hydroaminoalkylation reactivity with V, Ta, and Nb (Scheme 1.17).[74] In this case *ee*'s up to 93%

were reported. This disclosure also demonstrated that V and Nb catalysts can be used for this reaction, although Ta complexes were preferred. Notably, high *ee* values were very substrate dependent and either a change in amine or a change from a bulky norbornene substrate would result in significantly diminished enantioselectivities.

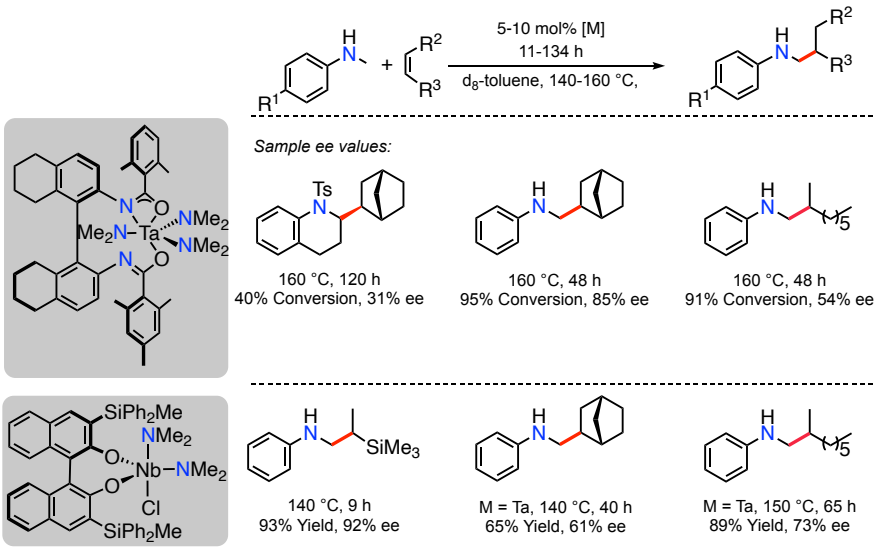

Scheme 1.17. Chelating ligand developments for enantioselective hydroaminoalkylation from the Zi (top) and Hultzsch (bottom) groups.[73,74]

The Hultzsch group used similar ligand scaffolds, with the focus being on Ta and Nb complexes (Scheme 1.17).[73,83] These *O,O*-chelated complexes are derived from axially chiral BINOL. In contrast to the work of Zi, Hultzsch reports Nb catalysts for improved reactivity and enantioselectivity over identical Ta alternatives. As before, high ee values (up to 98%) only exist for either strained or electronically distinct alkene substrates such as vinylsilane or norbornene, while ee's drop to 81% with less sterically demanding substrates.[73] Mechanistic evidence showed reversible metallaaziridine formation, and either alkene insertion or amine protonolysis as the turnover-limiting step in the catalytic cycle.[73] Examples of off-cycle pathways observed include C*sp*^{2}-H activation from the aromatic ring or amine insertion into the aziridine species.

Phosphoramidate ligand systems are an alternative *N,O*-chelating ligand that further enhances electrophilicity at the metal center. In group 4 chemistry described above only minimal reactivity was realized when ligated to Ti and no significant change in reactivity resulted from the use of Ta amido precatalysts.[69] However, these same phosphoramidate ligands could be installed on Ta using the mixed $TaMe_3Cl_2$ starting material to access a mono-*N,O*-chelated catalyst that remains the only early transition-metal complex that can be used at room temperature with unactivated substrates (Scheme 1.18). The reactivity of this complex is much better than that of $TaMe_3Cl_2$ on its own, and the authors attribute this to the electron withdrawing nature of the phosphoramidate backbone as well as the released, unreactive CH_4 byproduct upon catalyst activation.[78] Catalyst instability was a major issue, as the resulting complexes are all light and temperature sensitive. This challenge resulted in high catalyst loadings (10 mol % Ta) and some substrate scope limitations.

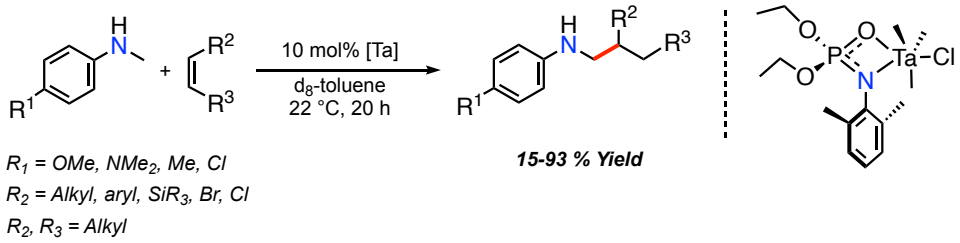

Scheme 1.18. The only example of room-temperature hydroaminoalkylation from the Schafer group with early transition-metals.[84]

A shortcoming in hydroaminoalkylation reactivity generally is the fact that typically only terminal alkene and strained internal alkene substrates could be used. The first catalyst with wide applicability using unactivated internal alkenes came from the Schafer group in 2014 (Scheme 1.19).[85] This work showcased $Ta(NMe_2)_3Cl_2$ with a 3-phenyl-pyridonate ligand salt that could realize excellent reactivity with internal alkenes, including cyclic as well as E and Z alkenes. The

reaction of unsymmetrical internal alkenes offered mixtures of substrate dependent regioisomers with selectivity ratios of 4.4:1.

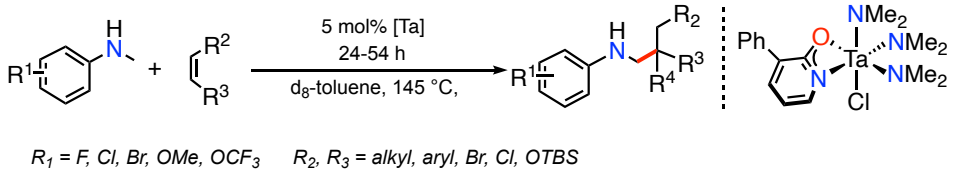

Scheme 1.19. The first early transition-metal catalyst with broad reactivity for internal alkene substrates from the Schafer group.[85]

The effect of electronically and sterically distinct pyridonate variants with substituents at the 3- or 6- positions were explored for their hydroaminoalkylation reactivity trends.[86] Surprisingly, there were no consistent ligand effects that could be attributed to either ligand steric or electronic properties. One of the resultant complexes (Scheme 1.20) was the first examples of catalysts displaying broad reactivity with both internal and terminal alkene substrates, both of which used commercially available pyridone proteoligands. Specifically, work with 3-methylpyridone was very promising.[87] Anion effects were also explored; triflate as an alternative to the chloride ligand diminishes reactivity dramatically. Mechanistic work to understand ligand effects revealed that catalytic activity is dominated by complicated off-cycle equilibria *e.g.* trans-amination and unselective C-H activation events or byproduct formation between alkene substrate with released $HNMe_2$. All these insights suggested the need to avoid [Ta]NMe_2 type precatalysts.

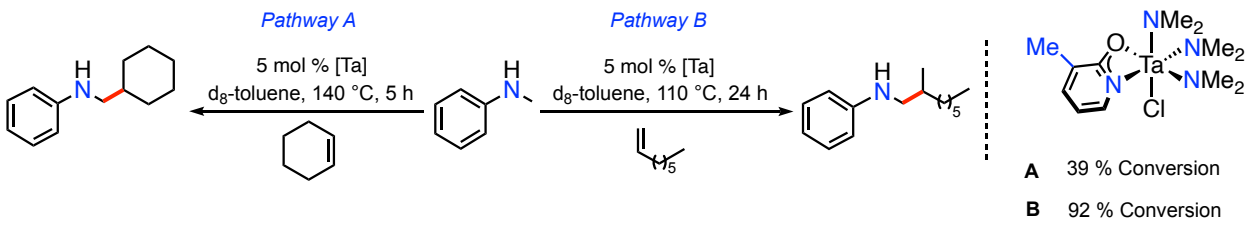

Scheme 1.20. Investigating varying pyridonate steric, electronic, and position effects on hydroaminoalkylation reactivity with two benchmark alkene substrates by the Schafer group.[86]

1.2.3.3 *In Situ* Formed Catalytic Systems

In situ generated group 5 complexes are assembled by either protonolysis or salt metathesis, depending on the metal starting material employed. These methods are more attractive to organic chemists who want a user-friendly strategy to use these air and moisture sensitive catalysts. Depending on the systems employed, these catalyst systems can achieve the same reaction outcomes as their isolated precatalyst counterparts.[86,87] With this goal in mind, the Schafer group developed a Ta catalyst system that can be assembled in situ using syringe techniques and commercially available, soluble starting materials (Scheme 1.21).[87] Combining $Ta(NMe_2)_5$ with an inexpensive 3-methyl-2-pyridone for in situ protonolysis allowed for reactivity with previously challenging functional groups including acetals, ketals or TBS-protected alcohol substrates. Authors also illustrated subsequent ring-closure to access alkylated piperidine products with high diastereoselectivity.

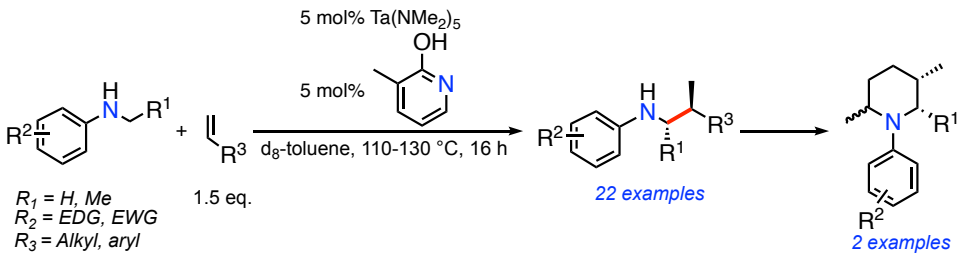

Scheme 1.21. Commercially available Ta and ligand materials for intermolecular hydroaminoalkylation by the Schafer group with *N*-ethylanilines towards select *N*-heterocycles.[87]

Another extension of pyridonate ligand frameworks came from a collaboration between the Schafer and Bräse labs to make paracyclophane-appended pyridonate ligand salts for enantioselective hydroaminoalkylation (Scheme 1.22).[88] These interesting planar chiral ligands had never been explored in hydroaminoalkylation catalysis. From the synthesized proligand, the ligand salt and $Ta(CH_2SiMe_3)_3Cl_2$ resulted in the assembly of chiral complexes suitable for reactivity with both internal and terminal alkene substrates. Some ligand and substrate combinations require long reaction times, high reaction temperatures and/or elevated catalyst loading to access adequate catalytic conversion. Once again, these group 5 catalysts are completely selective for the branched regioisomer, with very high diastereoselectivities (7:1 to >25.1:1) and a maximum of 24 % *ee* when using *N*-methylbenzylaniline.

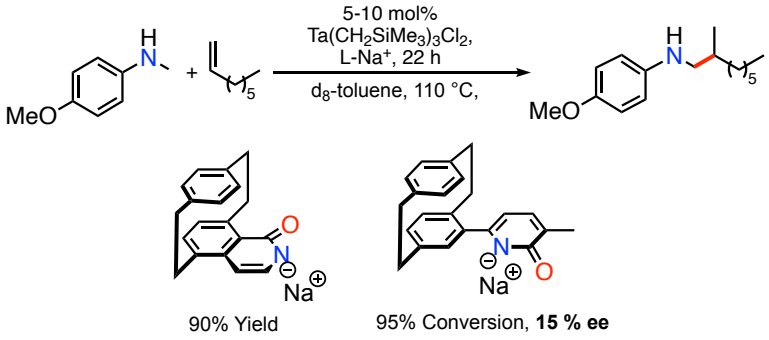

Scheme 1.22. Planar chiral paracyclophanes from the Schafer and Bräse labs for reactivity and enantioselectivity in early transition-metal catalyzed hydroaminoalkylation.[88]

In summary, early transition-metal developments in hydroaminoalkylation focus on careful catalyst and ligand design to drive unique reactivity with a variety of substrate classes. Group 3 systems are still emerging but show promise as the only early transition-metal catalysts for productive tertiary amine reactivity using cationic complexes. In contrast, group 4 efforts span Ti and Zr as well as different types of amines. Notable new directions include initial intermolecular work with primary amine surrogates and *N,N*-chelates for promising Ti reactivity. Finally, group 5 hydroaminoalkylation focuses almost exclusively on Ta, with some initial attempts towards enantioselective catalysis.

1.3 Late Transition Metal Mediated Hydroaminoalkylation

Late transition-metal catalyzed hydroaminoalkylation emerged in the late 1990s.[89] This Csp^3-H alkylation reaction contrasts with better established Csp^2-H arylation or alkylation cross-coupling strategies.[24,27,29,31,90–93] The advances in late metal hydroaminoalkylation are also largely complementary to early transition-metal developments discussed above, as late transition-metal catalysts typically display regioselectivity for the linear product. In addition, most reaction development in this area requires the use of a directing group, and to date limited examples of modified catalysts have been reported. Directing groups play a key mechanistic role by generating a metallacycle through chelation that is required for reactivity and allows for much-improved regioselectivity, as seen in a proposed mechanism from Jun and coworkers (Figure 1.6).[89] Furthermore, precatalysts are prepared in situ from commercially available Ru or Ir starting materials, and substrates employed are quite different from the simple amines emphasized in early transition metal hydroaminoalkylation disclosures.

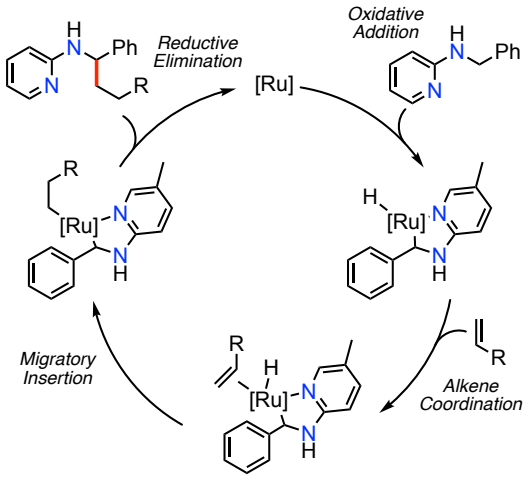

Figure 1.6. Proposed mechanism from the Jun lab for chelation-mediated hydroaminoalkylation.[89]

1.3.1 Modifying Reactivity by Changing the Directing Group

The most widely used directing group is a 2-pyridyl group.[89,94–97] Though crucial for productive Csp^3- Csp^3 bond formation in these disclosures, removing this heterocycle to reveal a free alkylated secondary amine product proves challenging.[97–99] As a result, more recent disclosures emphasize strategies towards easily removed directing groups to increase the usefulness of hydroaminoalkylation (Figure 1.7).[100–105]

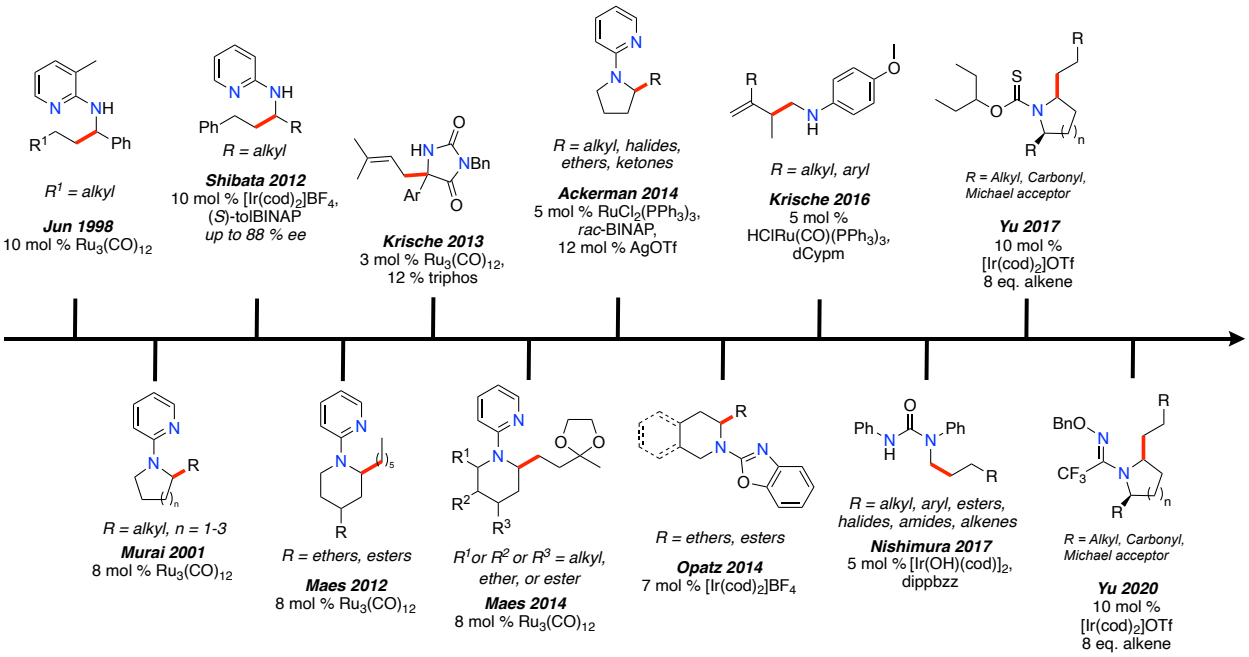

Figure 1.7. Developments in directed late transition-metal catalyzed hydroaminoalkylation realized through substrate or directing group modifications.

1.3.1.1 Ruthenium-Based Methods

An initial example of late transition-metal hydroaminoalkylation from Jun and co-workers focused on alkylating 2-pyridylbenzylamines using $Ru_3(CO)_{12}$ as a precatalyst (Figure 1.7, 1998).[89] Substrate scope in this work utilized a variety of alkyl-substituted alkene substrates. All linear internal alkene substrates in this chemistry isomerize to give the corresponding linear hydroaminoalkylation product. This isomerization is not possible with early transition-metal based hydroaminoalkylation catalysts, explaining the completely different products discussed above. This work represents the beginning of a new family of late transition-metal based hydroaminoalkylation catalysts, while presenting challenges such as high reaction temperatures (130 °C in toluene), relatively high Ru loadings (10 %), and 5 eq. of alkene substrate relative to the amine substrate.

Murai *et al.* used $Ru_3(CO)_{12}$ to realize the first example of heterocycle hydroaminoalkylation (Figure 1.7, 2001).[94] A CO atmosphere proved to be advantageous as this gas reduced catalyst decomposition, allowing for the use of challenging substrates such as pyrrolidines, piperidines, azepanes, and tetrahydroquinolines to be used in pyridine-directed hydroaminoalkylation. However, high reaction temperatures (≥ 140 °C) and a great excess (10 atm) of ethylene substrate resulted in significant bis-alkylation, such that this product was often obtained in greater amounts than the desired mono-alkylation product. Modification of the pyridine directing group with $-CF_3$ as an electron withdrawing group could stop the generation of mixed products.

The Maes group focused on improving yields with challenging six-membered heterocycles by using a hindered alcohol solvent that cannot engage in the potential competing alkene reduction pathway (Figure 1.8).[95] The role of this alcohol is important for suppressing unwanted side reactions. This work also includes esters as hydroaminoalkylation substrates for the first time. Use of a carboxylic acid additive doubles initial reaction rates, and helps suppress alkene reduction that otherwise outcompetes hydroaminoalkylation. Acid also removes the > 1 h induction period and 6 h catalyst decomposition noted in its absence.

The proposed mechanism begins with the carboxylic acid additive coordinating to Ru. Ultimately, a mixed Ru carboxylate hydride is generated as a catalytically active intermediate. The formation of this species is proposed to be promoted by the alcohol solvent. Subsequent alkene addition is rate limiting, thus optimized reaction conditions required a tenfold excess of alkene substrate because kinetic studies indicated a first order rate dependence on alkene concentration. After amine substrate coordination, C-H activation proceeds via concerted metalation-deprotonation and a final reductive elimination step releases the desired alkylated product.

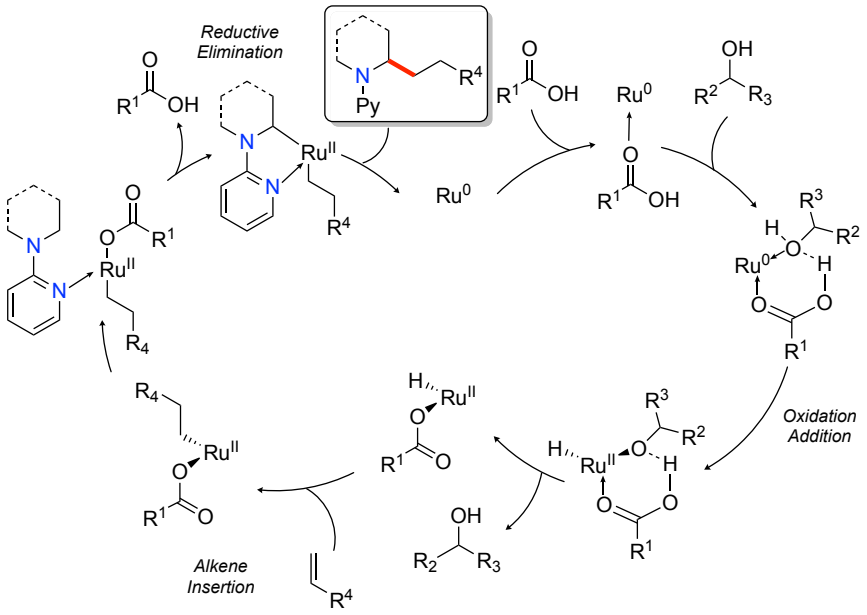

Figure 1.8. Proposed mechanism for hydroaminoalkylation by the Maes group.[95]

A subsequent disclosure in 2014 by Maes *et al.* realized piperidine alkylation with α, β-unsaturated ketones using $Ru_3(CO)_{12}$ by adding 20 equivalents of a chosen alkene substrate.[97] Notably, all alkene substrates protected the ketone as the ketal to avoid reduction as an unwanted side reaction. The selective formation of mono-alkylated products remained a challenge, and products were isolated as a mixture of mono- and bis-alkylated heterocycles.[95,97,106] A temperature of 140 °C in iPrOH was required in this methodology. Further, cis/trans isomer ratios in unsymmetrical piperidine products (≤ 20:62) present a challenge.

With an aim to reduce the amount of bis-alkylated product obtained with saturated heterocyclic substrates, the Ackerman group developed a Ru and Ag co-catalyzed system for pyridine-directed reactivity with pyrrolidines (Scheme 1.23).[102] These authors highlighted the mild reaction conditions (100-120 °C), step economy, and reductive conditions for directing group removal as advantages of their method.

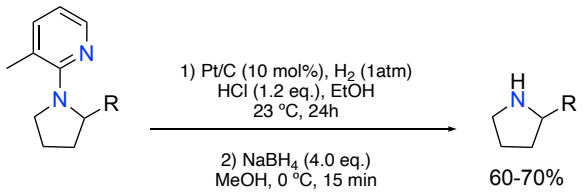

Scheme 1.23. Pyridine directing group removal as developed by Ackerman *et al.*[102]

The Krische group eliminated the pyridine directing group in favour of hydantoins as amine surrogates when isoprene, an activated diene, was chosen as the alkene substrate.[100] Reaction temperatures remained high (140 °C). Conversion of the resulting hydantoin to a benzyl protected amine occurs under strongly reducing conditions (12 eq. $LiAlH_4$, reflux, 60 h).

The same authors illustrated the use of 1,3,5- tris(aryl)-hexahydro-1,3,5-triazines as a way of delivering imine equivalents in combination with $HClRu(CO)(PPh_3)_3$ to generate intermediates that can undergo nucleophilic attack (Figure 1.9).[103,104] Using 4 equivalents of propanol allows for a key protonolysis step to release the desired product in their proposed mechanism.[104] The Krische group was the first to achieve regioselectivity with allenes. Moreover, a recent contribution leveraged a C_2-chiral phosphine, resulting in one example of asymmetric catalysis (88% *ee*.; Scheme 1.24). The triazines of focus in this work must first be made via reductive amination of secondary amines with formaldehyde. Similar to early transition-metal hydroaminoalkylation, all protic functionality in substrates such as additional amines or any alcohols must be protected for productive reactivity.

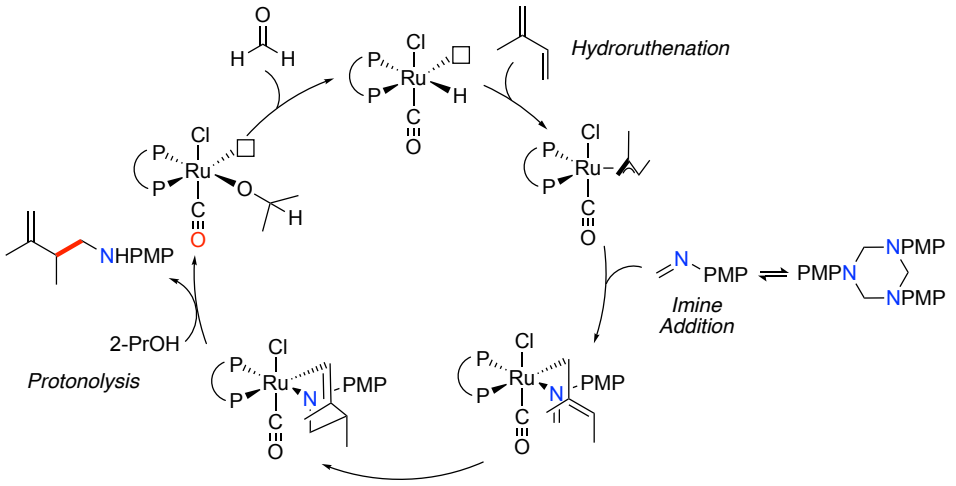

Figure 1.9. Proposed mechanism from the Krische group for using 1,3,5- tris(aryl)-hexahydro-1,3,5-triazines as amine surrogates in hydroaminoalkylation.[104] PMP = paramethoxylphenyl.

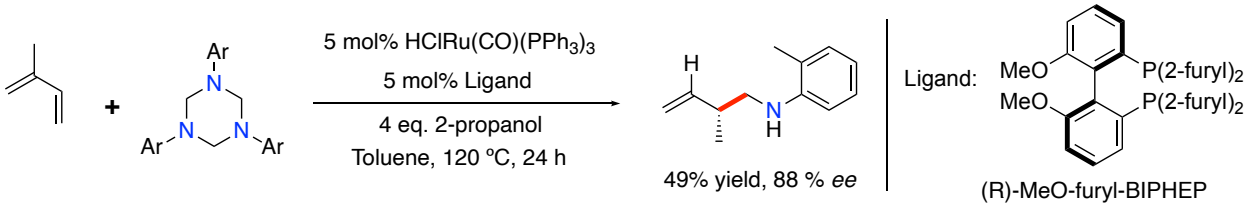

Scheme 1.24. Applying a *C2*-chiral phosphine by the Krische group for enantioselective hydroaminoalkylation using triazines as imine surrogates.

1.3.1.2 Iridium Catalyst Systems

In 2012, Shibata *et al.* presented an example of asymmetric hydroaminoalkylation by combining $[Ir(cod)_2]BF_4$ with (*S*)-tolBINAP *in situ*.[96] In order to obtain enantioenriched products (ee = ≤98%), low reaction temperatures (75 °C) were used with 1-3 day reaction times using 8 eq. of alkene substrate (Scheme 1.25). However, enantioselective transformations with internal alkynes were possible only at 135 °C and using TsOH as an additive.

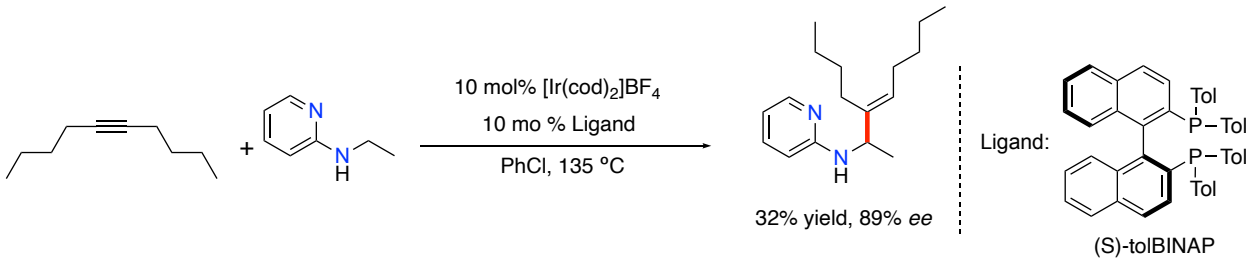

Scheme 1.25. An example of enantioselective hydroaminoalkylation using amines with alkynes from the Shibata group.

Efforts to develop a more easily removable directing group than pyridines involved a benzoxazole as described by the Opatz group in 2014.[101] The amine scope in this method largely focused on tetrahydroquinolines and related saturated heterocycles (Scheme 1.26). Unlike previous reports, use of this directing group results in the completely selective formation of the mono-alkylated product. Authors highlight steric hindrance to explain the regioselective alkylation at the less activated methylene. Two strategies were proposed for removing the benzoxazole with either excess hydride or strong base conditions.

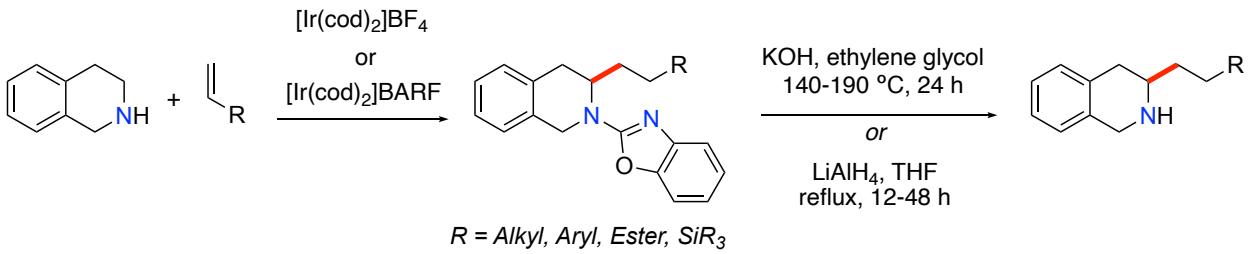

Scheme 1.26. Strategies for removing a benzoxazole directing group by the Opatz group to reveal secondary amine products.[101]

Further, ureas were coupled with a variety of terminal alkenes in the first example of late transition-metal catalyzed hydroaminoalkylation without additional stoichiometric bases or additives (Figure 1.7, 2017).[105] This contribution from the Nishimura group uses a relatively low reaction temperature of 70 °C, and includes substrates with functionality from amides to

phosphites, esters, and halides. Gratifyingly, bis-alkylation is not possible as products generated are tertiary amides, which are then base hydrolyzed to the desired secondary products. Currently, only *N*-methylureas can be used in this method and excess alkene substrate (1.2 eq.) is required.

Last, the Yu group has capitalized further on this idea of urea directing groups and expanded them to thiocarbamate directing groups (Scheme 1.27a) for reactivity with a variety of alkylamines.[107] Notably, this reaction employs 10% Ir and 8 equivalents of the chosen alkene substrate for productive reactivity. However, authors highlight the relatively simple installation of the directing group, though they only isolate the free amine product in one example. The expansion of this work in Scheme 1.27b focused almost entirely on modifying the directing group towards achieving any amount of branched regioisomer that could typically only be generated using early transition-metals.[108] When discussing the design of this directing group, the CF_3 group is reported to restrict free rotation and aid in stereoelectronic control, while the imine helps create a more reactive substrate, and the benzoxy group exists for facile directing group removal. Beyond this, reaction conditions are almost identical to the 2017 work highlighted above. Overall, most substrate combinations resulted in either a separable branched/ linear isomer mixture or only linear product. Complete branched selectivity was only observed when using dimethyl maleate (23%).

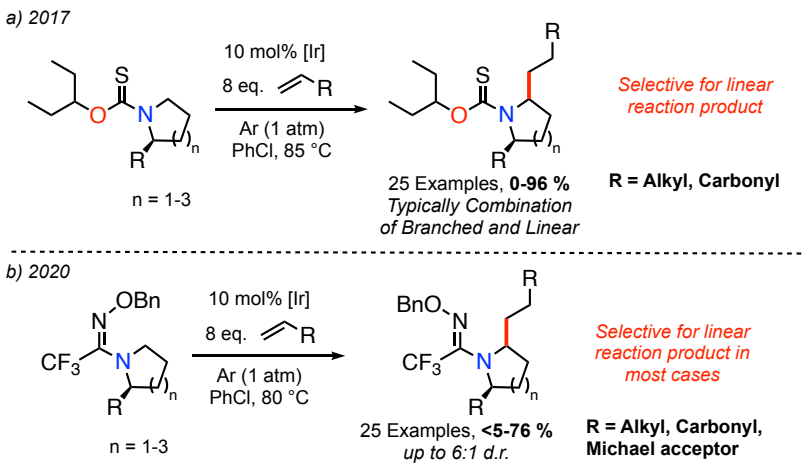

Scheme 1.27. Using thiourea directing groups in the Yu group to modify regioselectivity for hydroaminoalkylation with saturated amine heterocycles. Ar stands for argon gas in this scheme.

1.4 Photoredox Catalysis

1.4.1 Metal-Based Photoredox Catalysis

Photoredox catalysis represents a rapidly progressing field that, when applied towards hydroaminoalkylation, can be used to access unique substrates and reactivity at remarkably low temperatures, sometimes requiring no heat at all (Scheme 1.28).[109–112] As shown below, these examples involve radical-based mechanisms that are distinct from other proposed pathways for hydroaminoalkylation. An initial example from the Nishibayashi group in 2012 employed an Ir(I) photosensitizer for transformations almost exclusively with tertiary amines in combination with activated ethyl crotonates as alkene substrates at room temperature.[109] In contrast to earlier hydroaminoalkylation mediated chemistry, no heterocycles are reported for use with this catalyst system. Instead, most methods in this section use tertiary amine substrates to avoid the use of amine protecting group or amine surrogate substrates.

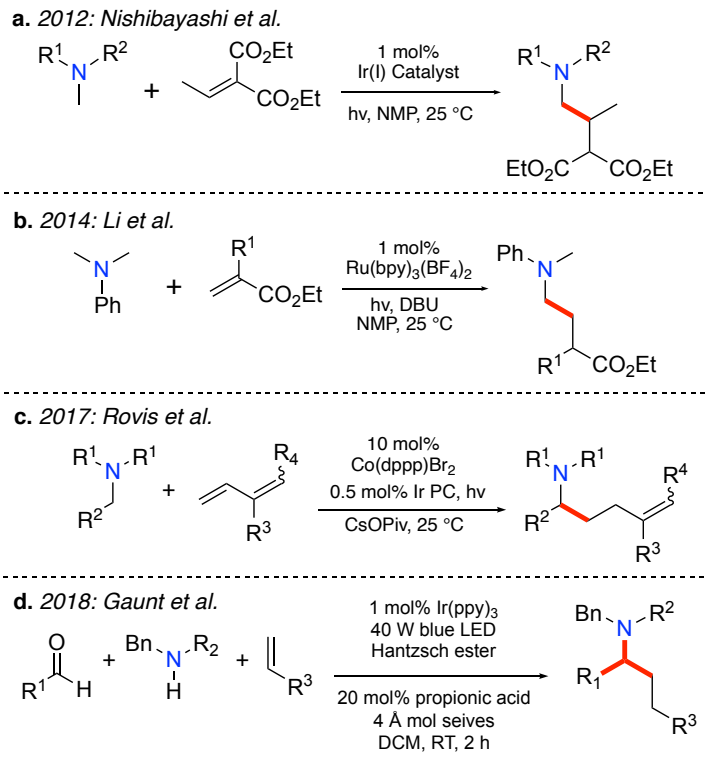

Scheme 1.28. Photoredox catalysis as applied to hydroaminoalkylation. Current methods involve a combination of Ir (a) and (d), Ru (b), and Co co-catalyzed (c) methods.

Xu and Li *et al.* also utilized tertiary amines as substrates with activated Michael acceptors as alkene partners to give products in modest yields (25-73%).[110] This method allows for chemoselectivity with uncommon halide-containing substrates. These are not typically seen in late transition-metal catalysis due to their propensity to undergo oxidative addition. This work also features relatively low Ru loadings (1 mol%) as compared to similar late transition-metal contributions. Furthermore, no bis-alkylation was observed using this method.

A 2017 contribution from the Rovis lab uniquely combined Co and Ir catalysis to feature reactivity using tertiary amines and conjugated dienes.[111] As shown in Figure 1.10, diene isomerization leads to selective reactivity with the terminal alkene functionality. However,

diastereoselectivity in this reaction still remains a challenge, as cis:trans isomer ratios vary from 20:1- 2:1 and these isomers cannot be separated.

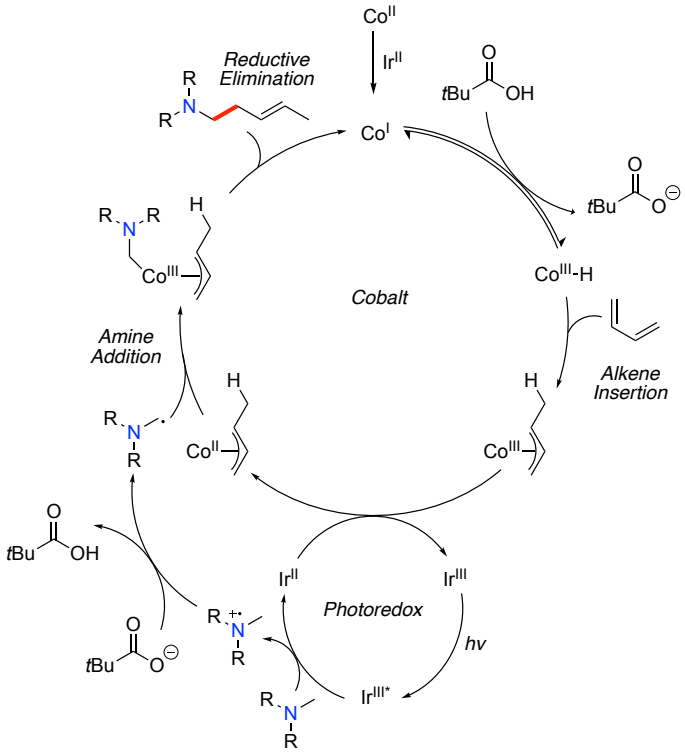

Figure 1.10. Proposed mechanism for Ir and Co co-catalyzed hydroaminoalkylation by the Rovis lab.[111]

In 2019, the Rovis group revisited this reaction to illustrate the first example of photoredox-catalyzed hydroaminoalkylation using protected primary amine substrates (Scheme 1.29).[113] As with many other late transition-metal methods highlighted here, site-selectivity in this work is achieved though using a particular amine protecting group because this group changes the NH pK_a. As with the most reactive diene substrates in 2017, all alkene coupling partners here must be Michael acceptors, where electron acceptors that fit this role could range from phosphonates to sulfonates, amides, or cyano groups. Diastereoselectivity is a challenge with the highest dr being 2.6:1. Their proposed mechanism for this variant of hydroaminoalkylation proceeds via dual

hydrogen atom transfer (HAT) and photoredox catalysis, with quinuclidine as the HAT catalyst (Figure 1.11). The central cycle begins by excited Ir(III) relaxing via a single electron process to in turn generate a quinuclidinium radical cation. This radical cation facilitates HAT with the amine substrate to result in an amine radical anion and a quinuclidinium cation. Reacting with the chosen alkene results in a carbon-centered radical which is in turn trapped before the resulting anion is protonated to reveal the desired product.

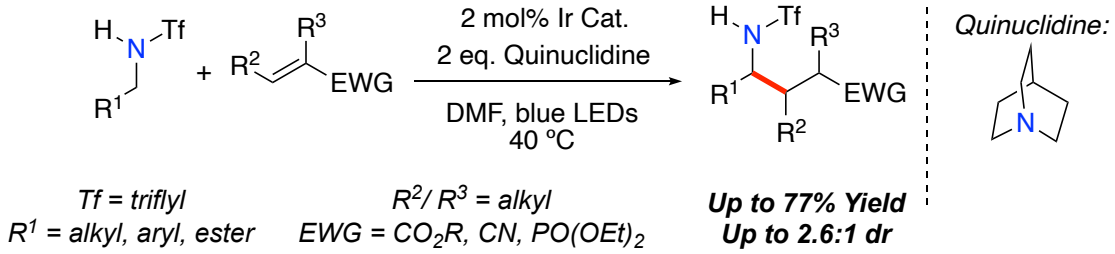

Scheme 1.29. Photocatalytic hydroaminoalkylation from the Rovis group using protected primary amine substrates.

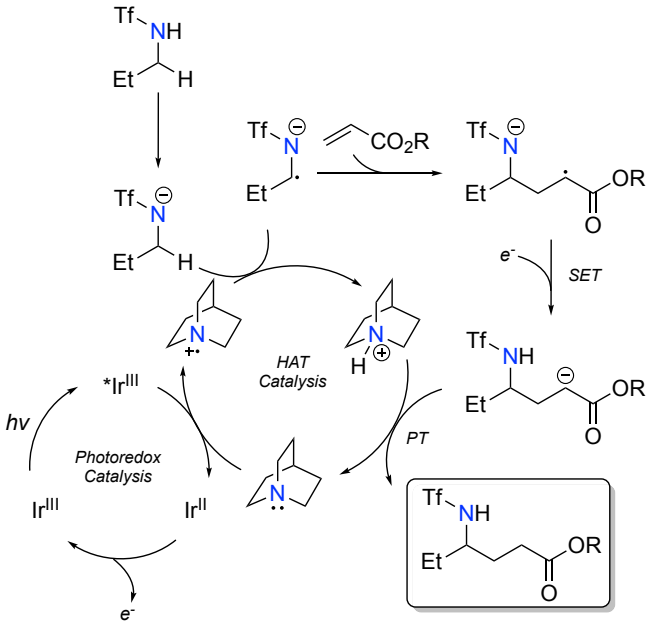

Figure 1.11. Proposed mechanism for hydroaminoalkylation from the Rovis group using protected primary amine substrates.

A late transition-metal hydroaminoalkylation example from the Gaunt group highlights their method as a late-stage amine functionalization strategy.[112] As above, the photocatalytic strategy allows for comparatively mild reaction conditions. Their proposed mechanism begins with imine formation, followed by a single electron transfer event to generate an all-alkyl α-amino radical (Figure 1.12). Alkylation of this radical by a chosen alkene substrate results in an alkyl radical, and a final hydrogen atom transfer step liberates the desired tertiary amine product. Reaction scope is broad, tolerating esters and a variety of heterocyclic substrates. However, no chlorides, bromides, free amines, or alcohols are possible. Further, diastereoselectivity should be a future consideration in this work, with the 5.5:1 being the most impressive dr to date.

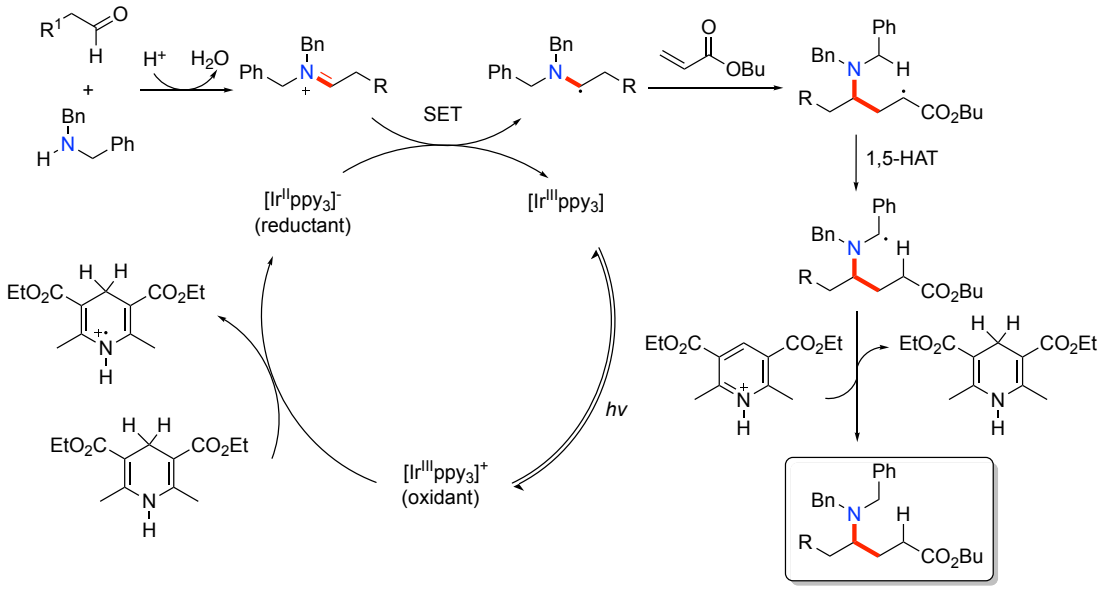

Figure 1.12. Mechanism for the Ir catalyzed multicomponent hydroaminoalkylation by Gaunt group.

1.4.2 Organic Photoredox Catalysis

The Nicewicz group began working with BOC-protected amine heterocycles using an organic acridinium photocatalyst and relatively mild conditions (5 mol %, DCM, 6 h; 20-99 %

yield; Scheme 1.30).[114] This contrasts the rest of the work included in this review thus far as no metal is involved, though products generated are consistent with hydroaminoalkylation reactivity. Functional group tolerance in this work is good; esters, sulfonyls, acetals, and aromatic *N*-heterocycles are all tolerated. One example highlights diastereoselectivity of this method using chiral amine substrates, with a >20:1 dr. Authors invoke a half chair transition state to explain the origin for this observed diastereoselectivity. A more recent disclosure focused on expanding the amine scope to focus on substituted piperazine substrates, as these have multiple potential sites for reactivity when unsymmetrical starting materials are used.[115] Here, authors explored regioselectivity trends using natural population analysis to predict product outcome. This tool was used to predict the major regioisomer as well as the regioselectivity and results were consistent with experimental data for most substrates. Data suggest that regioselectivity in this method is determined by electronic properties of the protected N-heterocycle and its propensity to exist as a radical cation. α-Proton pK_a and steric factors do not play a significant role. Overall, this work presents opportunities for further research as only Michael acceptors are tolerated as alkene substrates and only the linear regioisomer is formed, thus far.

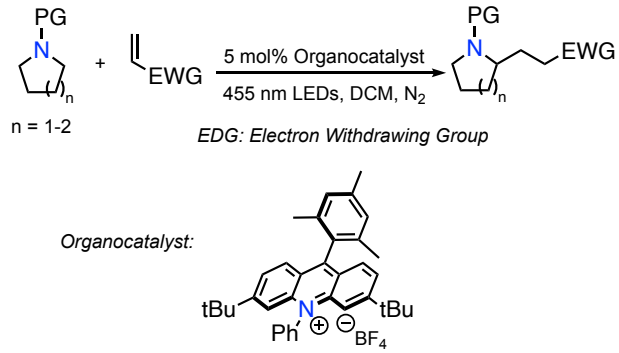

Scheme 1.30. An organocatalyst-based photocatalytic method from the Nicewicz group for hydroaminoalkylation using protected *N*-heterocycles.

1.5 Scope of Thesis

This thesis outlines the beginning of our group's efforts to design alkyltantalum catalysts for atom economic hydroaminoalkylation. Chapter 1 explores previous and continued work in hydroaminoalkylation across the *d* block with distinctly different mechanistic profiles between early transition-metal, late transition-metal, and photocatalytic approaches. This comparison clearly outlines the different attributes of these methods and allows the reader to see the remaining opportunity for catalyst development in this field.

Chapter 2 is focused entirely on catalyst development and exploring types of *N,O* chelate ligand sets in combination with a new alkyltantalum starting material for hydroaminoalkylation. This chapter illustrates effective catalysis using an *in situ* generated system by salt metathesis. This facile reaction set up results in shorter reaction times and simpler product purification using filtration. Ligand development also allowed for preliminary investigations towards enantioselective hydroaminoalkylation. This chapter ends with attempts to modify ligand steric and electronic factors to strategically affect hydroaminoalkylation catalytic activity.

Chapter 3 discusses efforts to leverage the excellent reactivity developed in chapter 2 to realize the synthesis of a more complex class of products; synthetic terpenoid alkaloids. This reaction probes catalyst compatibility with the natural complexity of terpene substrates. By combining commercially available terpenes with simple aromatic amine partners, we explored catalyst-controlled chemoselectivity and substrate-controlled diastereoselectivity in the synthesis of these new amines. We also evaluated another chiral ligand in situ to generate a catalyst for the synthesis of a miniseries of synthetic terpenoid products.

Chapter 4 highlights the use of the broadly active catalyst system discussed in chapter 3 for applications in *N*-heterocycle functionalization. Such heterocycles represent a largely unexplored

area for early transition-metal catalysis, and developing a catalyst that was very reactive with these challenging substrates addressed previously inaccessible research questions around substrate-controlled regio- and diastereoselectivity in hydroaminoalkylation.

The work in this PhD improves hydroaminoalkylation reactivity with previously challenging substrate classes; alkylamines in Chapter 2, terpenes in Chapter 3, and saturated amine heterocycles in Chapter 4. These accomplishments are summarized in Chapter 5, with future directions and preliminary results for new projects outlined at the end of each chapter. Some of these future projects have already begun, with collaboration from other graduate students and postdoctoral fellows in the Schafer group.

Chapter 2: Modifying Tantalum Ureate Complexes for Chemoselective C-C Bond Formation

2.1 Introduction

2.1.1 Hydroaminoalkylation Using Metal Alkyl Starting Materials

Early transition metal complexes have been under development for intermolecular hydroaminoalkylation catalysis since the early 1980s.[39,41] Recent developments use Sc[43,44,116], Ti[47], and Ta[78,84] starting materials for productive catalysis. The background alkyltitanium and alkylscandium research has been discussed extensively in chapter 1. This chapter will focus on group 5 hydroaminoalkylation catalysis. In this case the majority of the work with these metals relies upon the use of metal-amido starting materials. When focusing on group 5 systems, the Schafer group has shown that *N,O*-chelated Ta amido complexes offer a tunable framework for developing enhanced catalysis with improved substrate scope.[36,38,80] However, the reactive amido ligands of the precatalyst result in the generation of complicating equilibria and byproduct formation that reduces TOFs (<4/h) and complicates product isolation.[86,117] Alternatively, we have shown that the organometallic precursor $TaMe_3Cl_2$ can be used either on its own for catalysis[78] or combined with the electron withdrawing, N,O-chelating phosphoramidate ligand[84] to access room temperature reactivity with high initial TOFs. As of 2015, this methyl complex is the only alkyltantalum starting material that has been explored for hydroaminoalkylation.

Unfortunately, Ta methyl complexes exhibit an array of stability issues. For example, each catalyst batch must be stored at -30 ºC and protected from light to avoid both thermal and photochemical decomposition pathways. Also, this complex must be synthesized in small batches that cannot be stored for longer than a few weeks before decomposition is observed. This lack of

robustness results in low TONs (Turnover numbers; <20). Further, the dimethyl zinc used to prepare $TaMe_3Cl_2$ in combination with $TaCl_5$ is also very reactive, mandating starting material syntheses in the dark. Only activated amine substrates with enhanced nucleophilicity could be used with the resultant $TaMe_3Cl_2$ phosphoramidate catalyst.

2.1.2 Urea-Based Ligands for Early Transition Metal Catalysts in Amine Synthesis

Ureate ligands are an alternative N,O-chelating ligand that have been used to generate robust early transition metal hydrofunctionalization catalysts.[118–122] For example, the Schafer group has shown that a zirconium ureate complex, with its very electrophilic metal centre, shows remarkable reactivity in catalytic C-N bond formation by hydroamination.[123] Further, chiral cyclic ureates were synthesized from amino acids to investigate potential enantioselective hydroamination reactions.[121] When this project began, ureate *N,O*-chelating ligands had not been explored for hydroaminoalkylation.

2.1.3 Scope of Chapter

This chapter covers the development of a series of in situ generated alkyltantalum ureate catalysts for hydroaminoalkylation reactions. The work in sections 2.2.1-2.2.4 was completed in collaboration with Dr. Sorin-Claudiu Roşca, where he synthesized the metal starting materials and help me develop those skills for ongoing projects. We synthesized ligands and prepared substrates together. I completed the vast majority of the catalysis, and product purification. Beyond this, electronically and sterically distinct ureate ligands were synthesized for reactivity studies. The resultant catalysts had increased thermal and photochemical stability as compared with previous Ta methyl systems. Two ureate salts in particular were obtained that displayed complementary reactivity with either terminal or internal alkene substrates. Using these ligand salts, we explored reaction scope with a collection of differentially substituted alkene substrates. We accomplished

this while using equimolar amounts of amine and alkene and a protocol for purifying most products without a silica gel column was developed. These results were then expanded, to gain insight into how varied steric and electronic factors of modular ureate ligands result in predictable hydroaminoalkylation reactivity trends. Solid state structures for a selection of N,O-chelated Ta precatalysts were obtained to explore potential patterns in bond metrics and reactivity trends. Finally, chiral cyclic ureate ligand salts were explored as potential candidates for enantioselective hydroaminoalkylation.

2.2 Results and Discussion

2.2.1 Ligand and Metal Starting Material Syntheses

Known Ta organometallic reagents[78,124,125], $TaMe_3Cl_2$, $Ta(CH_2CMe_3)_3Cl_2$, and $Ta(CH_2SiMe_3)_3Cl_2$ as well as Ta amido reagents[40,42] $Ta(NMe_2)_5$ and $[Ta(NMe_2)_3Cl_2]_2$ were screened for hydroaminoalkylation reactivity using a standard benchmark reaction between *N*-methylaniline and 1-octene (Table 2.1). All reactions were run for 1 h at 110 °C, which is a lower temperature than previous state-of-the-art early transition-metal starting materials conditions of >130 °C and up to 96 h for this reaction.[75,80,84] This table gives reaction efficiency measured with turnover frequencies (TOFs), obtained by integrating the *ortho* peaks on the amine product relative to those on the *N*-methylaniline starting material after 1 h of reaction. All reactions presented here generated only the branched regioisomer. $Ta(CH_2SiMe_3)_3Cl_2$ provides promising TOFs (8/h) within the first hour of reaction. In contrast $Ta(CH_2CMe_3)_3Cl_2$ showed no reaction within 1 h, but over 24 h, 21% conversion was observed. The previously explored $TaMe_3Cl_2$ showed good reactivity within the first hour, but this promising reactivity degraded within 5 h, due to known catalyst instability issues at high temperatures.[84] Importantly, $Ta[(NMe_2)_3Cl_2]_2$, showed no

reaction at this lower temperature and time. Thus, $Ta(CH_2SiMe_3)_3Cl_2$ was chosen for further catalytic experiments.

Table 2.1: Screening of tantalum based precursors

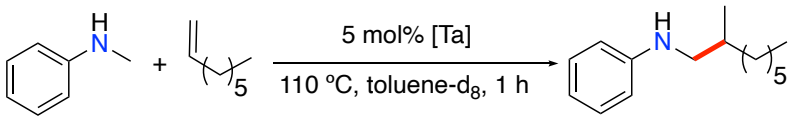

Starting Material	$Ta(CH_2SiMe_3)_3Cl_2$	$Ta(CH_2CMe_3)_3Cl_2$	$TaMe_3Cl_2$	$[Ta(NMe_2)_3Cl_2]_2$
TOF	*8/h*	n. r.[b]	6/h	n.r.[b]

[a.] Reaction conditions: amine (0.5 mmol), 1-octene (0.5 mmol), Ta precursor (0.025 mmol), toluene-d_8 (0.5 g). TOF determined by ^1H NMR spectroscopy. All reactions were run for one hour.
[b.] n. r.: no reaction.

2.2.2 Preliminary Acyclic Ureate Screening and Reaction Optimization

Next, ligand effects on hydroaminoalkylation reactivity were investigated using precatalysts generated in situ (Table 2.2).

Table 2.2: Study of ligand effects on hydroaminoalkylation

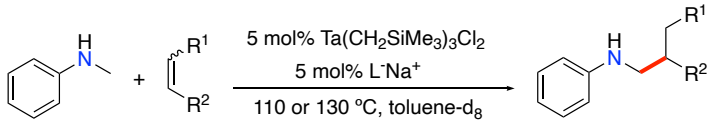

Entry	*Ligand Salt (L^-Na^+)*	*Alkene*	
			
1	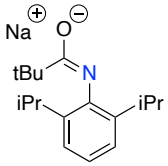 **2.1**	n. r.[b,c]	n. r.[b,d]
2	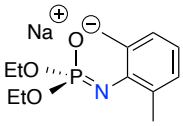 **2.2**	n. r.[b,c]	n. r.[b,d]
3	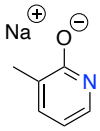 **2.3**	31%[c]	33%[d]
4	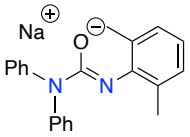 **2.4**	83%[c]	19%[d]
5	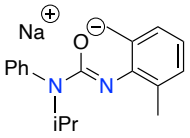 **2.5**	12%[c]	83%[d]
6	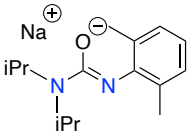 **2.6**	5%[c]	6%[d]

[a.] Reaction conditions: amine (0.5 mmol), 1-octene (0.5 mmol), Ta precursor (0.025 mmol), toluene-d_8 (0.5 g). Percent conversions determined by ^{1}H NMR spectroscopy. All reactions with 1-octene were performed at 110 °C, while those with cyclohexene were performed at 130 °C. [b.] n. r.: no reaction. [c.] Reaction run for 1 hour. [d.] Reaction run for 20 hours.

In order to differentiate between the various ligands and their effect on reactivity, relatively mild reaction conditions were used as above; reactions with 1-octene were carried out at 110 °C for 1 h while cyclohexene was tested at 130 °C for 20 h. Note that the state-of-the-art reaction conditions at the time for an internal alkene substrate used an isolated Ta precatalyst at 145 °C.[85] This in situ catalyst preparation protocol featured ligands previously reported for use with isolated precatalysts; amidate (**2.1**),[80] phosphoramidate (**1.2**),[36] and pyridonate (**2.3**).[85] For the first time, a small selection of ureate (**2.4-2.6**) ligand salts were also explored. All reactions in this chapter were monitored by NMR spectroscopy unless otherwise noted.

Catalytic screening of in situ prepared complexes with amidate **2.1** and phosphoramidate **2.2** resulted in no conversion, regardless of the alkene substrate. In contrast, using the less sterically encumbered pyridonate ligand salt **2.3** proved to be more successful, as 31% and 33% conversions were observed for both terminal and internal alkenes. We next explored ureate salts **2.4**, **2.5**, and **2.6**. Ureate ligands were selected to closely resemble those that were previously explored for successful hydroamination reactions in our group.[126] These ligands were expected to promote the formation of a more electrophilic metal centre that would give improved reactivity. Also, all of these ureate ligands maintained the 2,6-dimethylphenyl substitution on the secondary amine, while the tertiary portion was modified.

The in situ prepared catalyst system with **2.4** was excellent, affording 83% conversion in only 1 h for the reaction between 1-octene and *N*-methylaniline; a TOF of more than 16/h. However, when the more challenging cyclohexene substrate was evaluated, only a modest 19% conversion was observed after 20 h. Remarkably, the substituted ureate ligand with a mixed aryl/alkyl tertiary amine substituent **2.5**, in combination with $Ta(CH_2SiMe_3)_3Cl_2$, resulted in a reversed trend; this system was less effective for the terminal alkene substrate (1 h, 12%) but

realized higher conversion of the internal alkene substrate (20 h, 83%). It is interesting that the steric/electronic effects of the *N*–R substituent can have such a dramatic impact on alkene reactivity, considering that the only change is one *N*-Ph group of **2.4** to an *N*-^{i}Pr moiety in **2.5**. With this empirical observation in hand, we exchanged the remaining Ph group of **2.5** with another iPr group (**2.6**). Unfortunately, this change in ligand design did not improve the catalytic system, as only poor conversions were obtained for both terminal and internal alkenes. We propose that the known hemilability of *N,O*-chelating ligands, coupled with variable coordination modes of ureate ligands, result in a flexible coordination environment about the reactive metal centre. Overall, these results indicate that simple alkyl vs. aryl steric factors do not define the reactivity for these Ta precatalysts, and that something more complicated is at play in these systems. Section 2.2.5 will outline more efforts to understand these reactivity trends.

2.2.3 Amine Scope

With these highly reactive catalyst systems in hand we sought to explore the amine substrate scope of the catalyst prepared with **2.4** for terminal alkene (1-octene) and **2.5** for internal alkene (cyclooctene; Table 2.3) hydroaminoalkylation. Reaction times were adapted to favor full conversion of substrate and facilitate product isolation i.e. 2 h for 1-octene and 6 h for cyclooctene. Upon reaction completion the toluene solvent was removed, and the desired amine products were redissolved in pentane. Filtration of the pentane solution through Celite® and subsequent concentration resulted in isolation of the desired products in >95% purity, and typically column chromatography could be avoided. A variety of methylated aniline derivatives, with different functionality, could be used. For example, the reaction between *N*-methylaniline and 1-octene (**2.7**) resulted in nearly complete conversion and afforded the desired product in 88% yield after simple filtration. Furthermore, using 1 mol% of this catalyst system resulted in complete conversion (TON

= 100), as measured by ^{1}H NMR spectroscopy. With **2.8**, cyclooctene was fully converted within 6 h, offering an excellent isolated yield of product (83%). Consistent with previous work, *para*-substituted *N*-methylaniline derivatives are well tolerated and products can be isolated in good to excellent yields in all cases. Notably, the *para*-methoxyphenyl substituent (**2.9** and **2.10**) can be oxidatively cleaved to access *β*-alkylated primary amine products. Halide substituents on the aromatic ring (**2.11-2.16**) are completely compatible with this d^0 metal that does not engage in oxidative addition/reductive elimination chemistry. Furthermore, aryl halides allow for subsequent elaboration via cross-coupling reactions.[78] These Lewis acidic tantalum catalysts are compatible with the pharmaceutically relevant trifluoromethoxy substituted aniline (**2.17** and **2.18**). Impressively, the presence of a catechol derivative was also well tolerated (**2.19**).

Table 2.3: Substrate scope in amine[a]

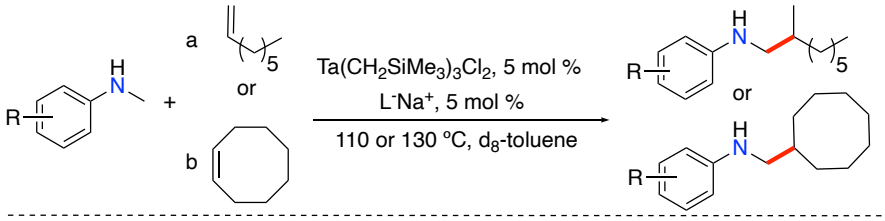

Compound	*Amine*	*Alkene*	*Isolated Yield (%)*
2.7	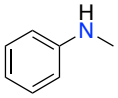	a	88
2.8		b	83
2.9	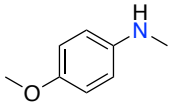	a	77
2.10		b	70
2.11	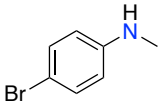	a	86
2.12		b	95
2.13	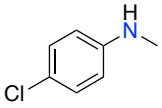	a	90
2.14		b	93
2.15	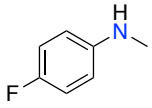	a	85
2.16		b	88
2.17	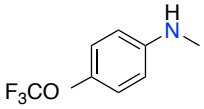	a	92
2.18		b	85
2.19	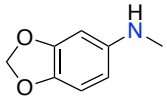	a	85

[a] Reaction conditions: amine (0.5 mmol), alkene (0.5 mmol), $Ta(CH_2SiMe_3)_3Cl_2$ (0.025 mmol), ligand salt (0.025 mmol), d_8-toluene (0.5 g). **2.4** was used for all terminal alkene substrates at 110 °C and **2.5** was used for internal alkene substrates at 130 °C.

In all cases, the various amines were compatible with both ligand salts **2.4** and **2.5** However, efforts to use more challenging dialkyl substituted amines were not successful with either of these in situ prepared catalysts.

2.2.4 Alkene Scope

We next explored the alkene substrate scope with the aforementioned systems assembled using **2.4** for terminal alkenes and **2.5** for internal alkenes (Table 2.5). Alkenes containing silyl protected alcohols easily reacted with *N*-methylaniline within 2 h to give the product in 75% yield (**2.19**). Such aminosilylether products have been shown to be valuable precursors to *β*-alkylated heterocycles.[81,87] Compounds **2.20** and **2.21** show that aryl or alkyl groups can be incorporated into the alkene substrates. Notably, a gem-disubstituted alkene can be used for the facile installation of a *β*-quaternary centre in high yield (**2.22**). The dienes used to prepare **2.23** and **2.24** demonstrate the outstanding chemoselectivity of the in situ catalyst system assembled using **2.4**; only the terminal alkene undergoes hydroaminoalkylation, leaving the internal alkene available for further functionalization.

Table 2.4: Substrate scope in alkene[a]

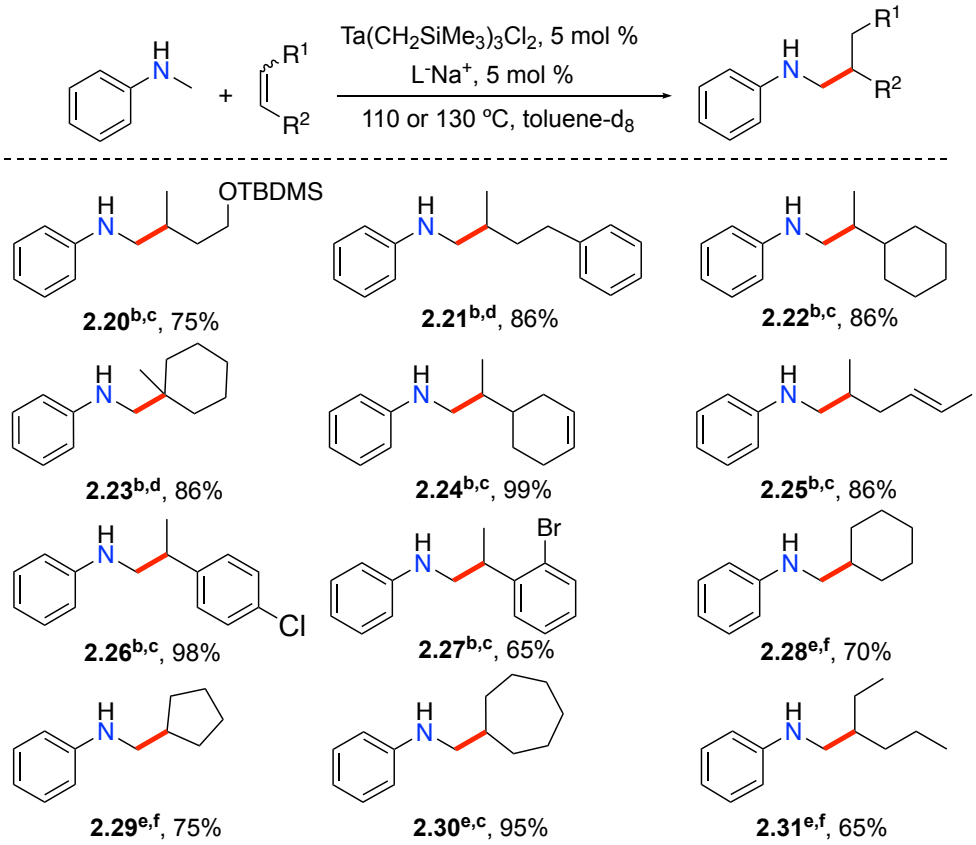

2.20[b,c], 75% **2.21**[b,d], 86% **2.22**[b,c], 86%

2.23[b,d], 86% **2.24**[b,c], 99% **2.25**[b,c], 86%

2.26[b,c], 98% **2.27**[b,c], 65% **2.28**[e,f], 70%

2.29[e,f], 75% **2.30**[e,c], 95% **2.31**[e,f], 65%

[a] Reaction conditions: amine (0.5 mmol), alkene (0.5 mmol), $Ta(CH_2SiMe_3)_3Cl_2$ (0.025 mmol), ligand salt (0.025 mmol), toluene-d_8 (0.5 g). [b] Reaction was run using ligand **2.4** at 110 °C. [c] 2 h reaction time. [d] 3 h reaction time. [e] Reaction was run using ligand **2.5** at 130 °C. [f] 20 h reaction time.

However, when **2.5** is used, the internal alkene does not react preferentially and instead a reduced yield of **2.25** is obtained, as a mixture of two regioisomeric products. Halide substituted styrene derivatives are also compatible with this d^0 metal system (**2.26**), including an example with the halide in the sterically hindered ortho–position (**2.27**). This observation is in contrast to the finding that sterically congested 2-methylstyrene does not react under these conditions. Notably, **2.27** has been shown to undergo a one-pot reaction of hydroaminoalkylation and subsequent Buchwald-Hartwig coupling to give the β-alkylated indoline product.[78]

Having obtained such promising results with terminal alkenes, we next investigated the substrate scope with the more challenging internal alkenes. Table 2.3 and Table 2.4, compounds **2.28** and **2.29**, **2.30**, **2.31** show that cyclic alkenes ranging from 5-8-membered rings are all viable substrates for hydroaminoalkylation. Due to ring-strain, cycloheptene is the most reactive cyclic alkene, requiring only 2 h to reach full conversion. However, linear internal alkenes have reduced reactivity, and cis-3-hexene (**2.31**) takes 20 h to reach 77% conversion to give 65% isolated yield. For comparison, the only other reported catalyst for the hydroaminoalkylation of internal alkenes requires 44 h at 145 °C to obtain 69% yield of **2.10**.[85] The stereochemistry of the internal alkene affects reactivity, as trans-3-hexene results in only 15% conversion when using the ligand **2.5** catalyst system.

2.2.5 Varying Ureate Steric and Electronic Factors

After slightly varying a previously explored ureate ligand to obtain complementary reactivity, we were interested in further manipulating ligand steric and electronic parameters to empirically assess potential improvements in reactivity as a result of these changes. All the ureate proteoligands and ligand salts in this subsection were synthesized using triphosgene, as had been done in previous hydroamination work from our group.[126] Yields range from 38% for **2.32** to 86% isolated for **2.33** among all the proteoligands in this subsection and their respective salts are highlighted in the experimental section for this chapter. Note that ligand salts are not typically purified beyond being dried well before use. Each ligand made was screened for reactivity with three benchmark substrates: *N*-methylaniline as an aromatic amine, *N*-methylcyclohexylamine as an aliphatic amine, and cyclohexene as an internal alkene. *N*-methylaniline and *N*-methylcyclohexylamine have been widely used as substrates that are representative of aromatic and alkyl amine reactivity in hydroaminoalkylation.[38] Further, literature highlights the importance

of sterically bulky ligands for early transition-metals in C-H activation.[127] Thus, we hypothesized that ureate ligand salts with increased steric bulk would result in more productive catalysis across a variety of substrate classes.

Table 2.5 shows the miniseries of sterically distinct ligands we have synthesized and tested (**2.32** - **2.36**). Ligand salts **2.32**, **2.33**, and **2.36** modify steric factors on the secondary amine fragment while **2.34** and **2.35** modify the tertiary amine fragment. The top two rows of Table 2.5 illustrate that increasing size for the secondary amine fragment from methyl to isopropyl leads to an increase in the in situ activity with a terminal alkene (15% in 1 h to 37% in 1 h) and a contrasting decrease in activity using an internal alkene substrate (58% in 20 h to 34% in 30 h). This 30 h reaction had initially been performed for only 20 h, and time was increased with a subsequent reaction to probe if conversion could be improved.

When instead modifying the tertiary amine substituents, we focused on alkyl amines with mixed aryl/ alkyl substituents containing variable bulk that were readily accessible. Changing from isopropyl to benzhydryl, activity with a terminal alkene worsened (40% in 1 h to 20% in 1 h) while results were unchanged with an alkylamine and catalysis using an internal alkene substrate was much improved (32% in 20 h to 70% in 20 h).

Table 2.5. Sterically varied ureate ligands and their reactivity in hydroaminoalkylation benchmark reactions.

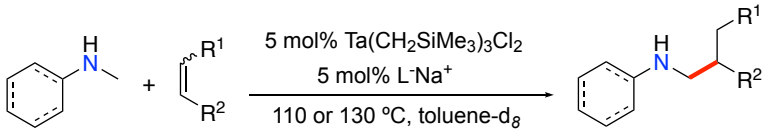

Entry	*Ligand Salt*	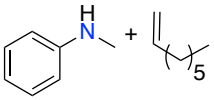	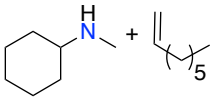	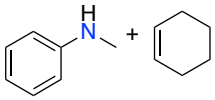
1	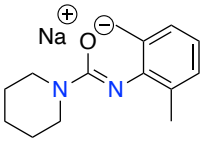 **2.32**	15%[b] (2 h, 55%)	0%[c]	58%[c,d]
2	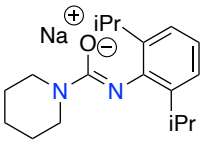 **2.33**	37%[b]	Reaction Not Run	20 h, 34%[c,d]
3	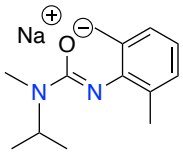 **2.34**	40%[b]	32%[b]	32%[c]
4	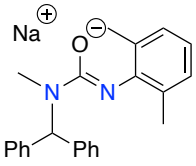 **2.35**	20%[b]	38%[b]	70%[c]
5	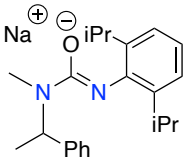 **2.36**	30%[b]	Reaction Not Run	42%[c]

[a.] Reaction conditions: amine (0.5 mmol), 1-octene (0.5 mmol), Ta precursor (0.025 mmol), toluene-d_8 (0.5 g). Conversion determined by ^{1}H NMR spectroscopy. All reactions with 1-octene were performed at 110 °C, while those with cyclohexene were performed at 130 °C. [b.] Reaction run for 1 h. [c.] Reaction run for 20 h. [d.] Reaction run at 145 °C

In contrast, Table 2.6 highlights efforts to electronically modify ureate ligand substituents towards improved reactivity with the same three benchmark reactions highlighted above. We

continued with the same tertiary amine from **2.36** for the electronically varied ureas because the amine starting material was the most inexpensive and available option without compromising reactivity in a significant way. Here, we hypothesized that electron withdrawing substituents would favor the formation of an electron poor ureate donor, resulting in a more electrophilic Ta centre with improved catalysis across different substrate classes. Salts **2.2**, **2.3**, and **2.4** highlight using methyl or halide substituents in the para position of the secondary amine for these preliminary investigations. We chose to electronically modify the secondary amine component of these ureas first for the most facile ligand synthesis. One goal in this chemistry is to make hydroaminoalkylation with early transition-metals more accessible to organic chemists by maintain excellent reactivity with ligands that simple to make.

As shown in Table 2.6, for aryl or alkyl amines with a terminal alkene coupling partner, in situ catalyst mixtures with an electron rich ureate are more productive. These data opposed the trend we proposed when designing these ligands. However, data with cyclohexene as a benchmark internal alkene is completely reversed, where in this case the chlorinated ureate salt was used for the most productive catalyst (20 h, 65%).

In summary, catalytic data from steric and electronic modifications to ureate ligand salts confirms once again that answers to catalytic design for hydroaminoalkylation with alkyltantalum starting materials are more complicated than straightforward structure-activity relationships. Work highlighted in this section was an initial screen aimed less at obtaining reaction parameters for all of these systems and more towards obtaining improved reactivity for potential organic applications that will be discussed further in chapters 3 and 4. The future work section for this chapter highlights more quantitative strategies to assess the role of these ureate ligands in other projects.

Table 2.6. Electronically varying ureate ligands and their reactivity in hydroaminoalkylation benchmark reactions.

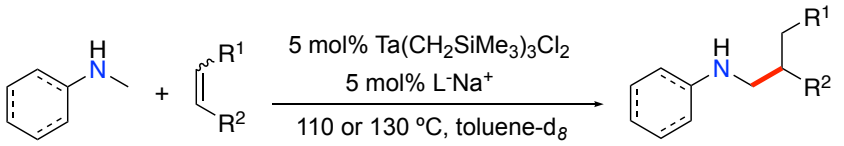

Entry	Ligand Salt	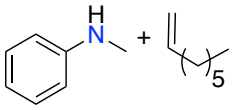	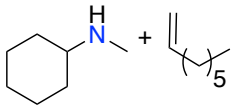	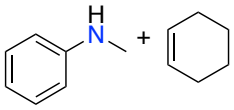
1	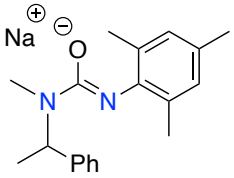 **2.37**	67%[b]	91%[c]	38%[c]
2	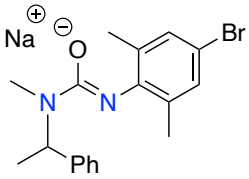 **2.38**	36%[b]	Reaction Not Run	34%[c]
3	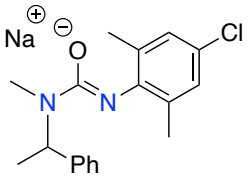 **2.39**	31%[b]	72%[c]	65%[c]

[a.] Reaction conditions: amine (0.5 mmol), 1-octene (0.5 mmol), Ta precursor (0.025 mmol), toluene-d_8 (0.5 g). Conversion determined by ^{1}H NMR spectroscopy. All reactions with 1-octene were performed at 110 °C, while those with cyclohexene were performed at 130 °C. [b.] Reaction run for 2 h. [c.] Reaction run for 20 h.

2.2.6 Isolating Precatalyst Structures

Next, we aimed to isolate the precatalysts associated with the in situ mixtures in the previous sections to observe if any of the reactivity differences manifested as consistent changes in the solid state. The synthesis of the *N,O*-chelated precatalyst series in Figure 2.1 and Table 2.7 was achieved using a salt metathesis reaction, between each ureate salt and one equivalent of

$Ta(CH_2SiMe_3)_3Cl_2$. All products suitable for single crystal X-ray diffraction were crystallized from a concentrated solution of *n*-hexanes at -38 °C. Purifying these ureate precatalysts was initially very challenging, and when an appropriate method was developed, all available ligands were explored for potential crystallization. Initial efforts did not focus on fully characterizing these compounds by NMR spectroscopy as the objective of this work was to develop a practical and useful protocol using in situ generated precatalysts. As a result, this preliminary discussion will focus on information from bond metrics.

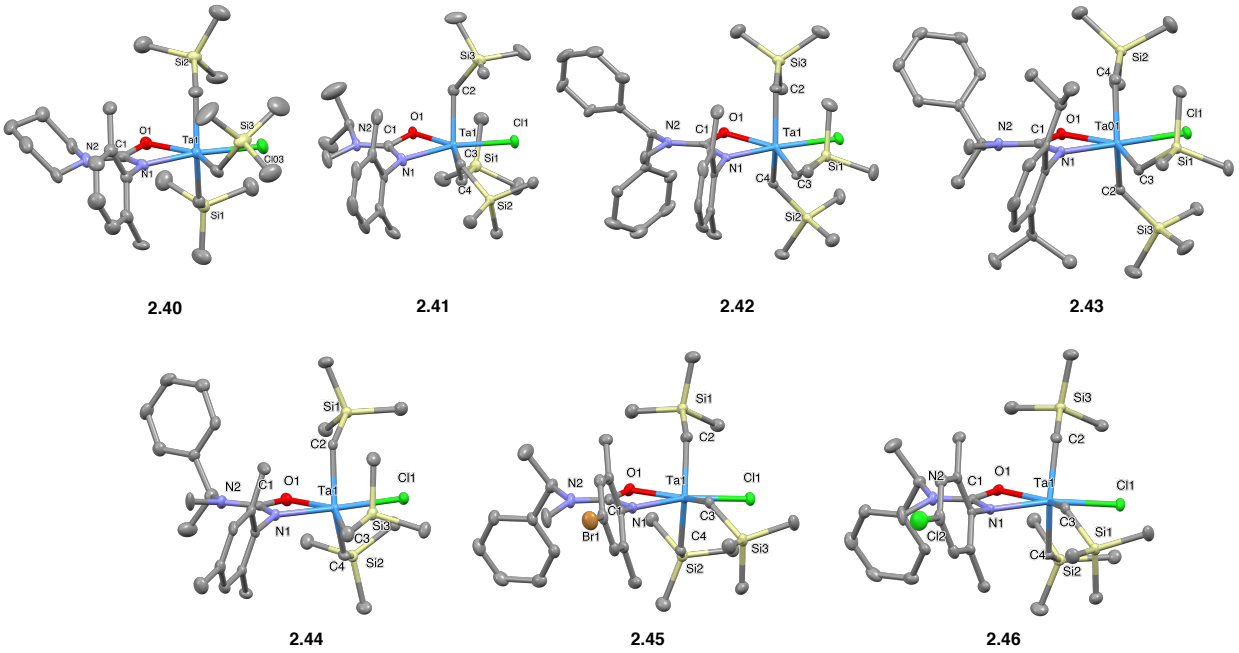

Figure 2.1. Solid-state molecular structures for complexes **2.40**-**2.46**. Ellipsoids in all cases illustrated at 50% probability and H atoms omitted.

Table 2.7. Relevant bonding parameters for **2.40**-**2.46**. Selected bond lengths (Å) and angles (°).

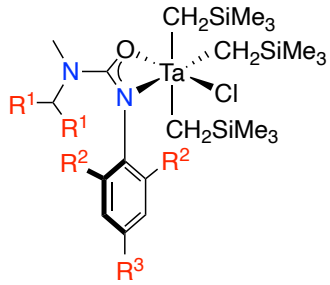

Complex	*R¹/R¹*	*R²*	*R³*	*Ta-O¹*	*C¹-N²*	*C¹-O¹*	*Ta-N¹*	*C¹-N¹*	*O¹-Ta-N¹*	*N¹-Ta-C⁴*
2.40	No R¹, Piperidene as the Amine	Me	H	2.125(5)	1.322(9)	1.305(8)	2.151(5)	1.359(9)	61.0(2)	98.1(3)
2.41	Me, Me	Me	H	2.1542(18)	1.332(3)	1.298(3)	2.137(2)	1.346(3)	59.419	97.74(10)
2.42	Ph, Ph	Me	H	2.166(5)	1.339(9)	1.302(8)	2.151(6)	1.347(8)	60.144	104.3(2)
2.43	Me, Ph	iPr	H	2.158	1.336	1.297	2.151	1.347	60.388	96.964
2.44	Me, Ph	Me	Me	2.144(3)	1.342(5)	1.309(5)	2.162(4)	1.338(5)	60.769	105.58(16)
2.45	Me, Ph	Me	Br	2.146(2)	1.337(4)	1.295(4)	2.167(3)	1.344(4)	60.437	95.52(11)
2.46	Me, Ph	Me	Cl	2.1369(18)	1.339(3)	1.297(3)	2.165(2)	1.339(3)	60.51(8)	95.783

As with previously published pyridonate complexes in the group,[86] these ureate-based precatalysts adopt distorted-octahedral geometries. In these cases, the chloride is consistently in the equatorial plane with one -CH_2SiMe_3 and the *N,O*-chelate. Using complex **2.41** as a representative example, *N,O*-chelates are bound κ^2 to Ta, with conjugation within the ligand as shown with the similar C1-N1 and C1-O1 bond lengths of 1.347(5) Å and 1.296(5) Å, respectively. This conjugation results in sp^2 hybridized atoms in the *N,O*-chelate that allow these ligands to be effective 4-electron sigma donors to Ta.[128]

When considering this octahedral geometry, the Cl-Ta-N1 angle for complex **2.41** is 163.727°, while the C3-Ta-O angle is 140.664°. These angles are smaller than the 180° expected for typical octahedral complexes because of the four-membered metallacycle that a κ^2 *N,O*-chelate mandates, making the bite angle of 59.419 ° much smaller than the 90 ° expected for this portion

of octahedral complexes. O-Ta-N Angles of ~60 ° are typical for other group 5 pyridonate or ureate-containing complexes.[85,86]

However, one important difference here is that the -CH_2SiMe_3 ligands in this work do not adopt the facial arrangement that amido ligated hydroaminoalkylation precatalysts have consistently shown.[80,85,87] This is not surprising since -NR_2 type ligands are considered four-electron π-donor ligands that are cis to each other to minimize trans *pi*-bonding interactions. Alkyl ligands used in this work are only two electron donors and thus do not influence orbital limitations on bonding.[86] Another piece of evidence for this decreased donation with alkyl ligands as compared to their amido counterparts is the increased axial Ta-C bond length of 2.163(4) Å in **2.41** as compared with an axial Ta-N bond length of 1.970(3) Å in a previously published pyridonate precatalyst.[85]

Overall, ureate ligands are held closer to the metal centre than amidate, and pyridonate counterparts.[80,85] Evidence for this includes similar Ta-O bond lengths, but shorter Ta-N bonds with ureate complexes as compared with their older *N,O*-chelate counterparts. For example, the most active Ta amido precatalyst with an amidate *N,O*-chelating ligand for hydroaminoalkylation has a Ta-N1 bond length of 2.447(3) Å, and 2.307(1) Å for a comparable pyridonate vs. an average bound ureate length of 2.155(4) Å.[80,86] We can establish that this shorter length is from the *N,O*-chelate and not the alkyl ligands because a comparable ureate precatalyst with amido ligands still has a short Ta-N1 bond length of 2.145(5) Å.[129] These more tightly bound *N,O*-chelates indicate a more electrophilic metal centre that has been previously invoked for improved hydroaminoalkylation reactivity.[117]

When comparing key bonding metrics between individual structures, we hypothesized that the measurably different reactivity displayed by in situ combinations using ureate salts would

translate to significant variation in bond metrics for their respective *N,O*-chelated precatalysts. However, ligand steric and electronic factors did not have a significant effect in the solid state. One such example was the consistent Ta-O1 bond distances for complexes with electronically distinct ureate ligands; 2.144(3) Å for *para*-methyl, 2.146(2) Å for *para*-bromo, and 2.1369(18) Å for *para*-chloro systems. All of these distances are within 3 standard deviations, indicating no significant length differences. Similarly, previous work that altered similar attributes with pyridonate scaffolds also did not observe large differences.[86]

One other notable point is that complex **2.40** co-crystalized with the bis-*N,O*-chelated complex (**2.47**) in Figure 2.2. These bis-ligated complexes are known to be unreactive in hydroaminoalkylation[86] and its facile formation in this case, even with only one equivalent of ligand salt added, resulted in the lower reactivity observed with the corresponding in situ combination for catalysis; only a fraction of the complexes prepared in situ are participating in catalysis. One prominent bond metric of complex **2.47** is its markedly long Ta-O bond length of 2.171(3) Å, potentially to accommodate the extra bulk of two chelating ligands. This also aligns with the poor reactivity of this compound.

We now have an effective way to prepare and obtain single crystal data for isolated precatalysts that correspond to most of the in situ ureate-containing catalyst systems highlighted in this chapter. Bond metrics suggest a pseudo-octahedral geometry with a tightly bound ureate ligand, but no large differences between complexes that incorporate different ureate ligand salts.

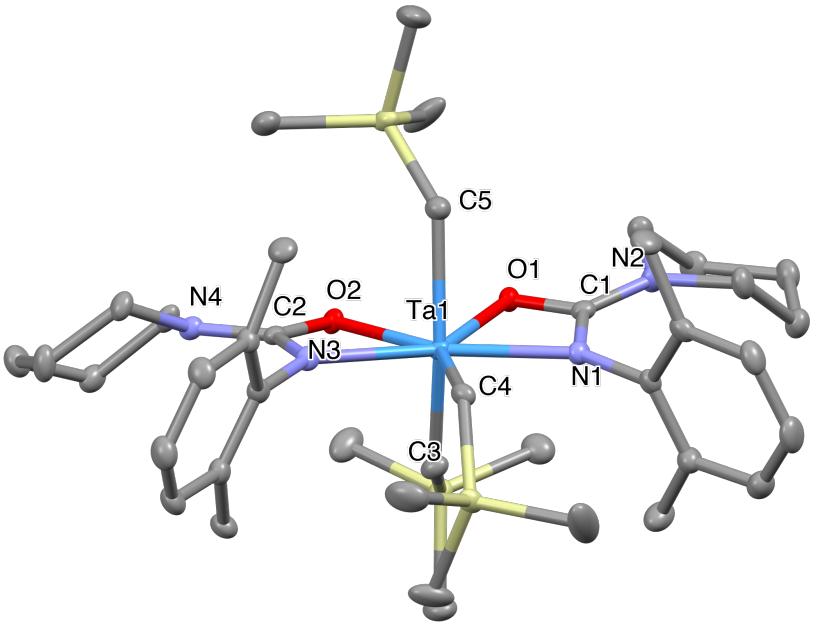

Figure 2.2. Molecular structure of precatalyst **2.47**. Ellipsoids plotted at 50 % probability, H atoms omitted. Selected bond lengths (Å) and angles (°): Ta-O1: 2.171(3), C1-N2: 1.359(5), C1-O1: 1.274(4), Ta-N1: 2.181(3), C1-N1: 1.355(5), O1-Ta-N1: 59.72(11), N1-Ta-C3: 45.195, Ta-O2: 2.185(3), C2-N4: 1.355(5), C2-O2: 1.278(4), Ta-N3: 2.194(3), C2-N3: 1.352(5), O2-Ta-N3: 60.387, N3-Ta-C3: 42.415.

2.2.7 Studies using Cyclic Ureate Ligands

After the results with acyclic ureate ligands above, we decided to explore comparative activity of catalysts with chiral cyclic ureate ligands (**2.48**-H and **2.49** -H, Scheme 2.1). Developing new catalysts for asymmetric hydroaminoalkylation remains a priority, as a generally useful asymmetric catalyst remains an unmet challenge. These ligands were synthesized by Dr. Pippa Payne and were explored in intramolecular enantioselective hydroamination reactions.[51] Hydroamination reaction yields were relatively high (71 - >95%) but enantioselectivities were a modest 5-12% ee. We were also interested in exploring reactivity differences between *N,O*-chelated complexes of $Ta(CH_2SiMe_3)_3Cl_2$ with cyclic vs. acyclic ureate salts, as we proposed that

cyclic 1,3-chelating ligands promote improved accessibility of the metal centre. This idea had been previously observed in the improved reactivity of pyridonate ligands as opposed to amidate counterparts.[86,117]

Another advantage of cyclic ureate ligands, as compared to traditional axially chiral ligand scaffolds, is the ease of their enantiopure syntheses from readily available and inexpensive chiral amino acids (Scheme 2.1).[121] Beginning with amino acids also allows for excellent tunability, especially when considering the diversity of synthetic amino acids available.

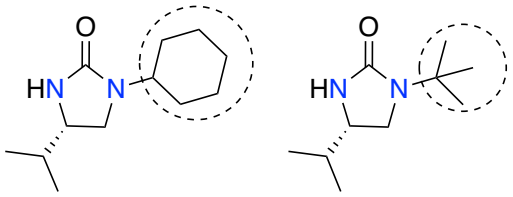

2.48-H **2.49-H**

Scheme 2.1. Differentially substituted urea-based ligands from amino acids.

We began by generating in situ complexes of **2.48** and **2.49** with $[Ta(NMe_2)_3Cl_2]_2$ and $Ta(NMe_2)_5$ to compare hydroaminoalkylation catalytic results using these cyclic ligated systems with previously published acyclic ureate ligated catalysts (Table 2.8). Both ligand salts were screened with *N*-methylaniline as the chosen aromatic amine and 1-octene as a terminal alkene or cyclohexene as an internal alkene. We screened a variety of well-established Ta amido starting materials because it was important to confirm that cyclic ureate ligand salts were also most reactive with alkyltantalum starting materials. Results from experiments with ligand salt **2.48** with $Ta(CH_2SiMe_3)_3Cl_2$ were much more promising than reacting this proligand with $Ta(NMe_2)_5$. This agrees with past reactivity trends from our group and can be attributed to the established improved reactivity of alkyltantalum starting materials as compared with their amido counterparts.[85] With these results, ligand salt **2.49** was combined in equal ratios with $[Ta(NMe_2)_3Cl_2]_2$ to generate

isolated precatalyst **2.50** via salt metathesis, which was then characterized by single crystal X-ray diffraction (Figure 2.3).

Table 2.8: Preliminary investigations with cyclic ureate ligands for hydroaminoalkylation.[a]

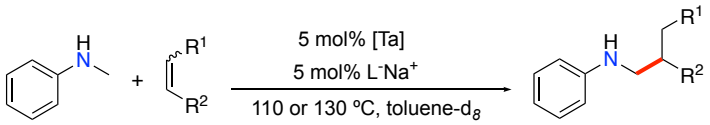

Entry	*[Ta]*	*Ligand Salt*	*Alkene*	
				
1	$Ta(NMe_2)_5$	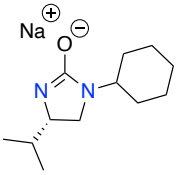 **2.48**	45%[b] **6 % ee**	
2	$[Ta(NMe_2)_3Cl_2]_2$	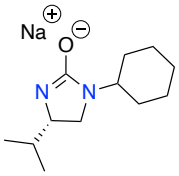 **2.48**	100%[b]	2%
3	$Ta(CH_2SiMe_3)_2Cl_2$	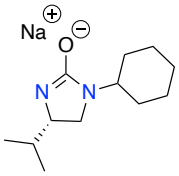 **2.48**	100%[c] **5 % ee**	0%
4	$[Ta(NMe_2)_3Cl_2]_2$	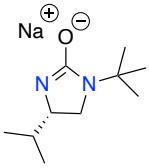 **2.49**	100%[b] **Racemic**	26%
5	$Ta(CH_2SiMe_3)_2Cl_2$	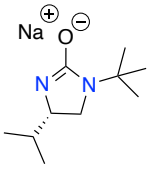 **2.49**	100%[c]	0%

[a.] Reaction conditions: amine (0.5 mmol), alkene (0.5 mmol), [Ta] precursor (0.025 mmol), toluene-d_8 (0.5 g). Percentage values represent conversions as determined by ^{1}H spectroscopy. All reactions with 1-octene were performed at 110 °C, while those with cyclohexene were performed at 130 °C. ee values were determined by chiral HPLC. All reactions with cyclohexene were run for 20 h, while reacition times with 1-octene vary as noted. [b.] Reaction run for 24 h. [c.] Reaction run for 1 h.

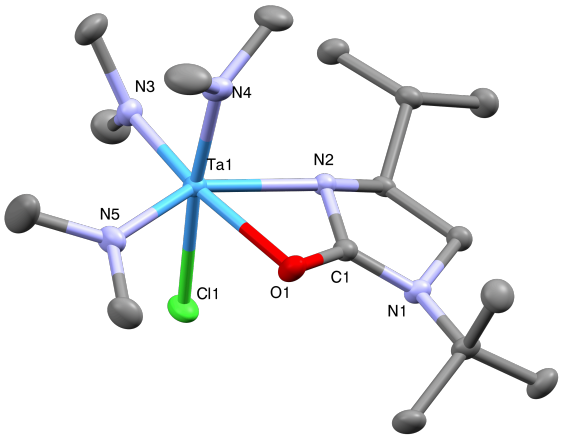

Figure 2.3. Molecular structure of precatalyst **2.50**. Ellipsoids plotted at 50 % probability, H atoms omitted. Selected bond lengths (Å) and angles (°): Ta-O1: 2.243(3), C1-N2: 1.354(5), C1-O1: 1.288(4), Ta-N1: 2.161(3), C1-N1: 1.345(5), O1-Ta-N1: 61.22(10), N3-Ta-Cl1: 173.84(9).

When considering catalysis with Ta alkyl starting materials, these ligands displayed improved reactivity with aromatic amines, where **2.48** and **2.49** showed complete conversion with *N*-methylaniline and 1-octene in 1 h (Table 2.8). This rapid reactivity continued at lower reaction temperatures as well, with completion in 6 h using ligand salt **2.48** at 90 °C. Lowering reaction temperatures to 55 °C stopped all catalytic activity. We were able to monitor this transformation *via* NMR spectroscopy at both 100 °C and 90 °C (Figure 2.4).

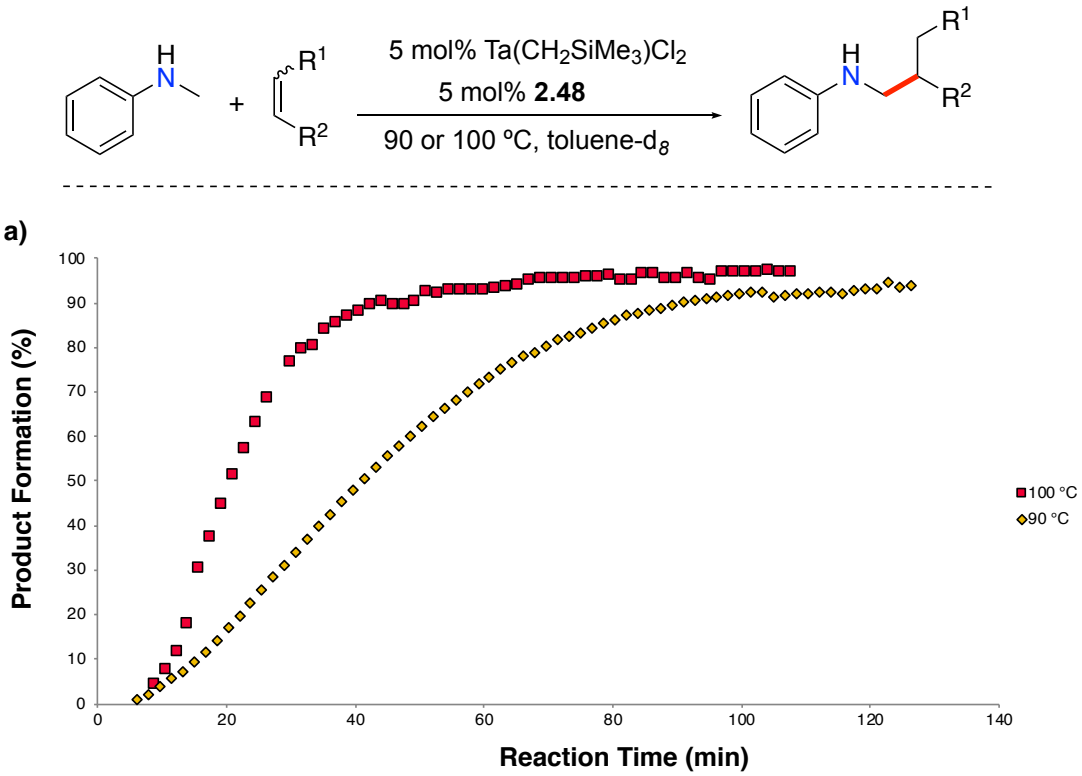

Figure 2.4. ^{1}H NMR spectroscopy-based monitoring of rapid hydroaminoalkylation reactivity at varying temperatures using $Ta(CH_2SiMe_3)_3Cl_2$ with cyclic ureate **2.48**.

In contrast to acyclic ureate ligands, precatalyst complexes using ligands **2.48** and **2.49** both displayed negligible activity with cyclohexene. The best result with these systems was 26 % in 48 h with **2.2.** as an *N,O*-chelating ligand with $[Ta(NMe_2)_3Cl_2]_2$ as starting material (Table 2.8). Amine-based substrate scope investigations for this transformation are mostly limited to substituted *N*-methylanilines. Limited exceptions include the Doye group's success with *N*-ethyl or *N*-benzylaniline, as well one example by our group of direct piperidine alkylation using very harsh conditions (165 °C, 143 h).[59,62,81] Precatalysts using chiral cyclic ureate salts **2.48** and **2.49** displayed excellent reactivity with *N*-methylcyclohexylamine, as exhibited through reaction completion in 30 minutes. This result was surprising, as aliphatic amines are typically more

challenging substrates than their aromatic counterparts. Tolerance for aliphatic amines is dependent on sterics, as catalysis with *N*-methyl-*t*-butylamine displayed no conversion. With this in mind, we were interested in expanding this success with aliphatic amines to *N*-heterocycles such as piperidine or pyrrolidine.

Direct, catalytic functionalization of heterocycles represents a powerful new way to access new alkylated *N*-heterocycles. Preliminary work showed that Ta complexes using cyclic ureate salts are active for piperidine alkylation (Scheme 2.2). Expanding on these observations is a featured achievement of this project and will be discussed in extensive detail in Chapter 4.

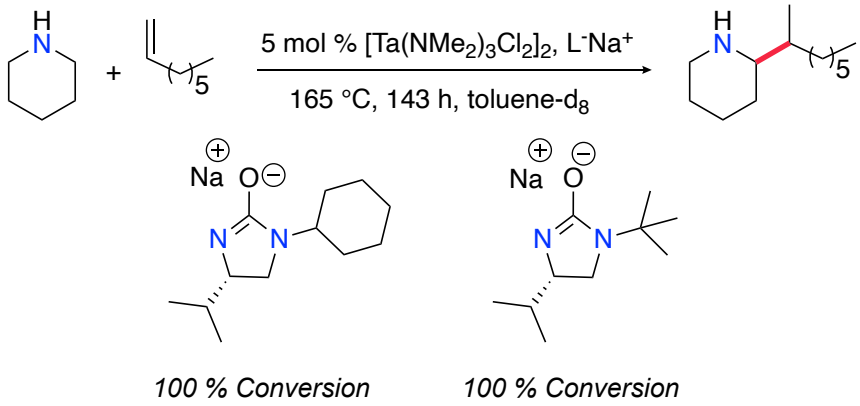

Scheme 2.2. Direct alkylation of piperidine using ureate ligands and Ta starting materials.

Furthermore, the potential for enantioselective catalysis with these ligands was investigated. Reactions with either **2.48** or **2.49** displayed no significant *ee* values at all, even with changes in Ta starting material (Scheme 2.2). We propose that this is because the stereocentre in these ureate ligands is too far from the reactive site at the enantiodetermining step of this reaction. Strategies for improving asymmetric catalysis without compromising reactivity include lower reaction temperatures, increasing bulk at the stereocentre, or relocating the stereocentre entirely to keep it closer to Ta during hydroaminoalkylation.

2.2.8 Effects of Varying Tantalum Halides

Similar to $Ta(CH_2SiMe_3)_3Cl_2$, Dr. Roşca also synthesized $Ta(CH_2SiMe_3)_3Br_2$, and $Ta(CH_2SiMe_3)_3F_2$ for testing that I ran for comparative Ta halides in hydroaminoalkylation.[130] I also made all subsequent batches of $Ta(CH_2SiMe_3)_3Cl_2$ and $Ta(CH_2SiMe_3)_3Br_2$. These Ta halide starting materials allow for the investigation of the role of a halide ion in the mechanism of hydroaminoalkylation. Neither of these materials had been previously investigated for any kind of catalytic transformation to our knowledge. Comparative results for catalysis with different Ta halides are shown in Scheme 2.3, where a preliminary trend exists for improved reactivity with increasing halide size. These initial results are consistent for both aromatic and aliphatic amine substrates when the chiral cyclic ureate ligands discussed above are used.

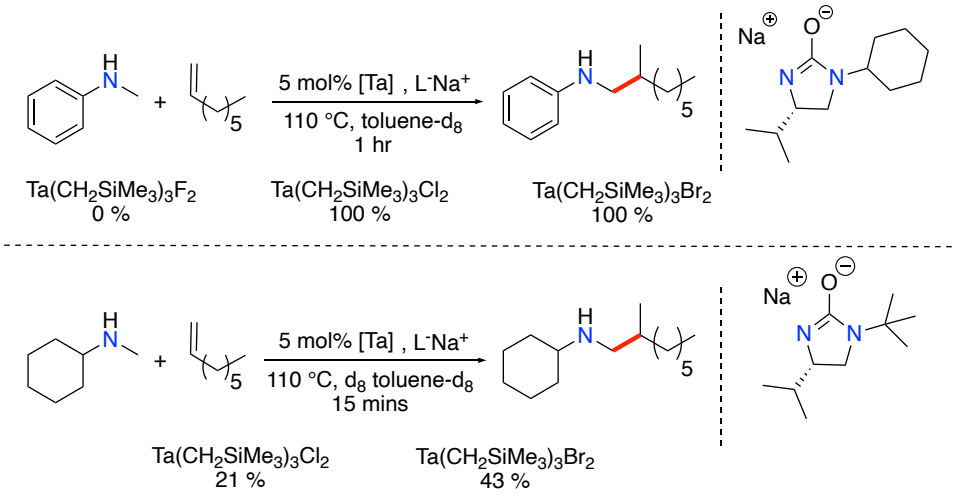

Scheme 2.3. Effect of varying Ta halide starting materials on hydroaminoalkylation reactivity.

After obtaining these data showing excellent reactivity but low *ee* values using chiral cyclic ureate ligands, we decided that the relatively intensive syntheses of these ligands would not be continued. Instead, future work for this section highlights an ongoing project that focuses on simpler cyclic ureate ligands.

2.3 Conclusions

In summary, modified ureate auxiliary ligands in combination with $Ta(CH_2SiMe_3)_3Cl_2$ have been shown to deliver superior TOFs and TONs in the atom- and step-economic hydroaminoalkylation reaction. By leveraging the variable ureate framework excellent activity with either terminal or challenging internal alkenes has been realized. This approach requires no amine protecting groups, directing groups or additives and products can be isolated by simple filtration. Furthermore, this new family of easily prepared catalysts is the only class that uses a stoichiometric combination of commercially available alkene and amine substrates.

Additional work focused on generating steric and electronically varied ureate ligands for catalyst screening to understand and optimize ligand substituent effects. This work clarified that endpoint data with this ureate systems are not sufficient because something more complex is at play than typical structure-activity type relationships.

Working on cyclic ureate ligands derived from enantiopure amino acids allowed us to investigate enantioselective hydroaminoalkylation, without success using these systems. Instead, these cyclic ureate systems allowed for improved reactivity with aliphatic amines over their aromatic counterparts for the first time.

Finally, we assessed activity of different tantalum halide materials, to discover that $Ta(CH_2SiMe_3)_3Br_2$ is slightly more active than $Ta(CH_2SiMe_3)_3Cl_2$, while $Ta(CH_2SiMe_3)_3F_2$ is not active at all for hydroaminoalkylation. As a result, all further experiments in this thesis use $Ta(CH_2SiMe_3)_3Cl_2$, as the small improvement in reactivity with $Ta(CH_2SiMe_3)_3Br_2$ did not justify the increased cost of $TaBr_5$ ($61/ 5 g) compared with $TaCl_5$ ($57/ 10 g).

2.4 Future Work

It is important to note that some aspects of future work for this chapter have already begun or have been completed. First, Dr. Manfred Manßen and Ms. Danfeng Deng are currently using these ureate proteoligands to design productive Ti hydroaminoalkylation catalysts as a potentially less expensive alternative to Ta systems. As well, Dr. Pargol Daneshmand and Dr. Sorin Roşca further explored cylic ureate reactivity in depth using a small series of achiral cyclic ureate ligands that are simpler to synthesize but maintain the reactivity of the cyclic variants discussed in this chapter.[129] Dr. Pargol Daneshmand then investigated the speciation of Ta precatalysts with acyclic ureates to identify what speciation of these complexes when they are prepared in situ.

An initial aspect of future work to still be completed for this portion of the tantalum alkyl catalyst work will focus on better understanding the empirical trends we have observed in ligand structure relative to resultant reactivity. As mentioned above, probing steric and electronic factors in ureate structure has not led to predictable trends that we can harness in future catalyst development. One piece that is missing in our current understanding is reaction monitoring data for a series of ureate ligands when used for the reaction of *N*-methylaniline with 1-octene as benchmark substrates. Dr. Daneshmand's work highlights a sampling strategy to monitor high temperature hydroaminoalkylation reactions on the benchtop without quenching the alkyltantalum catalyst. This is important for hydroaminoalkylation because traditional variable temperature NMR experiments often cannot be run at a high enough temperature for productive reactivity and IR probe setups can allow air/ moisture into a system that may quench the tantalum catalyst. We propose that collecting initial rate and activation parameter data for in situ catalyst mixtures with each of the acyclic ureate ligands may reveal critical insight into catalyst activation and resting states that would impact catalysis. Such insights will be more helpful than just endpoint data.

Further, many of the in situ mixtures discussed here have afforded crystals but the complexes and the mixtures of complexes formed upon catalyst preparation in situ have not been fully characterized. We are interested in obtaining full NMR data for these complexes and comparing their data and reactivity to their corresponding in situ mixtures. These data would help us confirm that the mono-*N,O*-chelated complex is the active catalytic species in hydroaminoalkylation reactions. Unpublished work in the group has highlighted identical reactivity for in situ catalyst mixtures with these ureate ligands as compared with their isolated counterparts. Replicating that experiment with the various ligand combinations in this chapter would confirm the innocence of the 5 mol% NaCl generated with in situ reactions.

2.5 Experimental

2.5.1 Materials and Methods

All reactions were performed under a N_2 atmosphere using Schlenk or glovebox techniques, unless otherwise stated. $TaCl_5$ (Strem), $Ta(NMe_2)_5$ (Strem), (trimethylsilyl)methylmagnesium chloride (Aldrich), 1-chloro-2,2-dimethylpropane (Aldrich), (chloromethyl)trimethylsilane (Aldrich), N,N-diphenylamine (Alfa), N-isopropylaniline (Combi-Blocks), triphosgene (Oakwood) and 2,6-dimethylaniline (Aldrich) were used as received. $NaN(SiMe_3)_2$ (Aldrich) was recrystallized from a hot toluene solution before use. All amines and alkenes were commercially available, dried over CaH_2 and distilled and degassed prior to use in catalytic experiments. $[Ta(NMe_2)_3Cl_2]_2$,[131] $Ta(CH_2CMe_3)_3Cl_2$,[125] and $Ta(CH_2SiMe_3)_3Cl_2$[124] were synthesized according to literature protocols. The proteo-ligands and their corresponding ligand salts **2.** -**2.3**, **2.6**[132] and $TaMe_3Cl_2$,[125,133] can be prepared as previously described. All glassware was dried in a 180 °C oven overnight before use. Toluene, hexanes and Et_2O were dried over activated alumina columns and stored over activated molecular sieves (4 Å). d8-Toluene was dried

over sodium and distilled prior to use. Experiments conducted on an NMR tube scale were performed in J. Young NMR tubes (8" x 5 mm) sealed with screw-type Teflon caps.

^{1}H and $^{13}C\{1H\}$ NMR spectra were recorded on Bruker 300 MHz and 400 MHz Avance spectrometers at ambient temperature. Chemical shifts (δ) are given relative to the corresponding residual protio solvent and are reported in parts per million (ppm). Coupling constants J are given in Hertz (Hz). The following abbreviations are used to indicate signal multiplicity: s = singlet, d = doublet, t = triplet, q = quartet, m = multiplet, and br = broad. Assignment of the signals was carried out using 1D (^{1}H, $^{13}C\{^{1}H\}$) and 2D (COSY, HSQC and HMBC) NMR experiments. Mass spectra (MS) were measured at the Department of Chemistry, Simon Fraser University on a Kratos MS-50 spectrometer using a Bruker maXis Ultra-High Resolution tandem TOF (UHR-Qq-TOF) mass spectrometer using a positive electrospray ionization source. Fragment signals are given in mass per charge number (m/z).

2.5.2 Synthesis and Characterization of Urea Proligands

General procedure for the synthesis of urea based proteoligands: Prepared following a modified literature procedure in which 2,6-dimethylaniline (1 equiv.) was dissolved in dichloromethane and the solution was cooled to 0 °C. Triphosgene (0.35 equiv.) was added in portions as a solid. The solution was stirred for five minutes after which N,N-diisopropylethylamine (DIPEA) (2 equiv.) was added and the cold bath removed. The solution was stirred for 1 h and then the appropriate amine (1 equiv.) and a second portion of DIPEA (1 equiv.) was added. The solution was stirred for an additional hour, and then diluted with 1M HCl. The organic phase was washed three times with 1M HCl dried over $MgSO_4$, filtered, and concentrated by rotary evaporation to give the crude product.

Note: triphosgene was only used in a fumehood and stored in a fridge. Reactions also all had an oil bubbler to safely release any pressure. All equipment that came in contact with triphosgene was quenched with water and left in a fumehood overnight before disposal or further cleaning outside the fumehood.

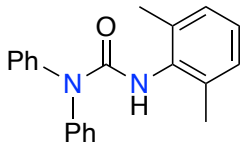

Synthesis of 3-(2,6-dimethylphenyl)-1,1-diphenylurea (2.4-H): Prepared following the general procedure outlined above: 2,6-dimethylaniline (3.64 g, 30 mmol), triphosgene (2.83 g, 9.55 mmol), DIPEA (11.64 g, 90 mmol), diphenylamine (5.08 g, 30 mmol). Recrystallization from a concentrated ethyl acetate solution at -30 °C provided the desired compound as a white solid (2.24 g, 24%): ^{1}H NMR ($CDCl_3$, 300 MHz, 298 K): δ 7.42-7.38 (overlapping m, 8H, o-C_6H_5 and m-C_6H_5), 7.29-7.18 (m, 2H, p-C6H5), 7.05 (s, 3H, 2,6-$Me_2C_6H_3$), 5.86 (br s, 1H, NH), 2.34 (s, 6H, CH_3) ppm. ^{13}C{^{1}H} NMR ($CDCl_3$, 75 MHz, 298 K): δ 153.93 (C=O), 142.72 (i-C_6H_5), 135.67 (o-C_6H_3), 134.55 (i-C_6H_3), 129.53 (m-C_6H_5), 128.11 (m-C_6H_3), 127.28 (o-C_6H_5), 126.84 (p-C_6H_5), 126.39 (p-C_6H_3), 18.62 (CH_3) ppm. HRMS (ESI): m/z calcd for $C_{21}H_{20}N_2O$ [M+H+]: 317.1654. Found: 317.1648.

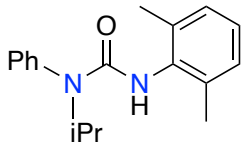

Synthesis of 3-(2,6-dimethylphenyl)-1-isopropyl-1-phenylurea (2.5-H): Prepared following the general procedure outlined above: 2,6-dimethylaniline (5.18 g, 43 mmol), triphosgene (4.43 g, 15 mmol), DIPEA (16.57 g, 129 mmol), *N*-isopropylaniline (5.78 g, 43 mmol). Prepared following the general procedure outlined above. Recrystallization from a concentrated ethyl acetate solution at -30 °C provided the desired compound as a white solid (7.65 g, 63%*)*: ^{1}H NMR ($CDCl_3$, 400 MHz, 298 K): *δ* 7.61-7.28 (overlapping m, 5H, *o,m,p*-C_6H_5), 7.00 (s, 3H, C_6H_3), 5.24 (br s, 1H, N*H*), 4.96 (hept, $J_{H–H}$ = 6.5 Hz, 1H, C*H*(CH_3)$_2$), 2.20 (s, 6H, 2,6-(C*H*$_3$)$_2$C$_6$H$_3$), 1.15 (d, J_{H-H} = 6.2 Hz, 6H, CH(C*H*$_3$)$_2$) ppm. ^{13}C{^{1}H} NMR ($CDCl_3$, 101 MHz, 298 K): *δ* 154.61 (*C*=O), 138.16 (*i*-C_6H_5),

135.70 (*o*-C_6H_3), 135.17 (*i*-C_6H_3), 131.20 (*m*-C_6H_3), 129.83 (*o*-C_6H_5), 128.66 (*p*-C_6H_5), 127.93 (*m*-C_6H_3), 126.37 (*p*-C_6H_3), 46.58 ($CH(CH_3)_2$), 21.66 ($CH(CH_3)_3$), 18.47 (2,6-$(CH_3)_2C_6H_3$) ppm. HRMS (ESI): *m/z* calcd for $C_{18}H_{22}N_2O$ [M+H$^+$]: 283.1810. Found: 283.1805. Anal. Calcd. for $C_{18}H_{22}N_2O$: C, 76.56; H, 7.85; N, 9.92; Found: C, 76.31 ; H, 8.05 ; N, 10.04.

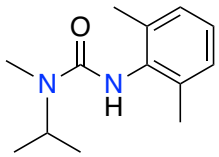

Synthesis of 3-(2,6-dimethylphenyl)-1-isopropyl-1-methylurea (2.34-H): Prepared following the general procedure outlined above: 2,6-dimethylaniline (1.5 g, 20.5 mmol), triphosgene (2.02 g, 7.41 mmol), DIPEA (7.95 g, 61.5 mmol), *N*-isopropylaniline (2.5 g, 20.5 mmol). Recrystallization from a concentrated ethyl acetate solution provided the desired compound as a white solid (3.20 g, 65 %): ^{1}H NMR ($CDCl_3$, 400 MHz, 298 K): δ 7.05 (s, 3H, *o,m,p*-C_6H_5), 5.69 (br s, 1H, N*H*), 4.56-4.49 (m, 1H, C*H*$(CH_3)_2$), 2.86 (s, 3H, CH_3), 2.24 (s, 6H, 2,6-$(CH_3)_2C_6H_3$), 1.17 (d, $J_{H\text{-}H}$ = 1.7 Hz, 6H, $CH(CH_3)_2$) ppm. ^{13}C{^{1}H} NMR ($CDCl_3$, 101 MHz, 298 K): δ 156.00 (*C*=O), 135.70, 135.57, 128.20, 126.40, 45.89, 27.45, 20.21, 18.56 ppm. HRMS (ESI): *m/z* calcd for $C_{13}H_{21}N_2O$ [M+H$^+$]: 221.1654. Found: 221.1656. Anal. Calcd. for $C_{13}H_{21}N_2O$: C, 70.87; H, 9.15; N, 12.72; Found: C, 70.89; H, 9.14; N, 12.63.

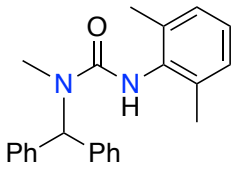

Synthesis of 1-benzhydryl-3-(2,6-dimethylphenyl)-1-methylurea (2.35-H): Prepared following the general procedure outlined above: 2,6-dimethylaniline (307 mg, 2.53 mmol), triphosgene (250.2 mg, 0.843 mmol), DIPEA (981 mg, 7.59 mmol), *N*-methyl-1,1-diphenylmethanamine (500 mg, 2.53 mmol). Recrystallization from a concentrated ethyl acetate solution provided the desired compound as a white solid (750 mg, 86 %): ^{1}H NMR ($CDCl_3$, 400 MHz, 298 K): δ 7.41-7.27 (overlapping m, 10H, *o,m,p*-C_6H_5), 7.04 (s, 3H, *m,p*-C_6H_5), 6.70 (s, 1H, NHC*H*), 5.78 (br s, 1H, N*H*), 2.88 (s, 3H, CH_3), 2.16 (s, 6H, 2,6-$(CH_3)_2C_6H_3$) ppm. ^{13}C{^{1}H} NMR ($CDCl_3$, 101 MHz, 298 K): δ 156.57 (*C*=O), 139.66, 135.47, 135.30, 128.80, 128.77, 128.25, 127.80, 126.49, 63.30, 32.05, 28.48 ppm.

HRMS (ESI): *m/z* calcd for $C_{23}H_{25}N_2O$ [M+H$^+$]: 345.1967 Found: 345.1964. Anal. Calcd. for $C_{23}H_{25}N_2O$: C, 80.20; H, 7.02; N, 8.13; Found: C, 80.50; H, 7.12; N, 8.18.

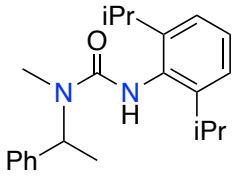

Synthesis of 3-(2,6-diisopropylphenyl)-1-methyl-1-(1-phenylethyl)urea (2.36-H): Prepared following the general procedure outlined above: 2,6-dimethylaniline (1.32 g, 7.40 mmol), triphosgene (724 mg, 2.44 mmol), DIPEA (2.87 g, 22.2 mmol), *N*-methyl-1,1-diphenylmethanamine (1.0 g, 7.40 mmol). Recrystallization from a concentrated ethyl acetate solution provided the desired compound as a white solid (1.81 g, 72.3 %*)*: ^{1}H NMR ($CDCl_3$, 400 MHz, 298 K): *δ* 7.51-7.50 (overlapping m, 4H), 7.45-7.39 (overlapping m, 2H), 7.37-7.35 (m, 1H), 7.28 (m, 1H), 5.78-5.72 (overlapping m, 2H), 3.22-3.12 (m, 2H, C*H*(CH_3)$_2$), 3.00 (s, 3H, CH_3), 1.72 (s, 3H, CH_3), 1.31 (s, 12H, CH(C*H*$_3$)$_2$) ppm. ^{13}C{^{1}H} NMR ($CDCl_3$, 101 MHz, 298 K): *δ* 157.22 (*C*=O), 146.52, 142.12, 132.80, 128.73, 127.63, 127.41, 126.95, 123.36, 52.99, 29.82, 28.79, 23.81 ppm. HRMS (ESI): *m/z* calcd for $C_{22}H_{31}N_2O$ [M+H$^+$]: 339.2437. Found: 339.2444. Anal. Calcd. for $C_{22}H_{31}N_2O$: C, 78.06; H, 8.73; N, 8.28; Found: C, 78.18; H, 8.96; N, 8.31.

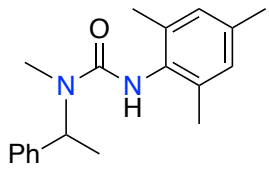

Synthesis of 3-mesityl-1-methyl-1-(1-phenylethyl)urea (2.37-H): Prepared following the general procedure outlined above: 2,4,6-trimethylaniline (2.28 g, 15.8 mmol), triphosgene (1.39 g, 7.40 mmol), DIPEA (12.3 mL, 68.0 mmol), *N*-methyl-1-phenylethan-1-amine (2.5 g, 15.8 mmol). Recrystallization from a concentrated ethyl acetate solution provided the desired compound as a white solid (4.53 g, 91 %): ^{1}H NMR ($CDCl_3$, 400 MHz, 298 K): δ 7.37 (m, 4H, o,m-C_6H_5), 7.30 (m, 1H, p-C_6H_5), 6.86 (S, 2H), 5.72 (br s, 1H, NH), 5.59 (m, 1H, CH(CH_3)$_2$), 2.81 (s, 3H, CH_3), 2.25 (s, 3H, CH_3), 2.15 (s, 6H, CH_3), 1.59 (d, JH-H = 1.6 Hz, 3H, CH_3) ppm. ^{13}C{^{1}H} NMR ($CDCl_3$, 101 MHz, 298 K): δ 156.57 (C=O), 141.92, 136.01, 135.36, 132.89, 128.90, 128.72,

127.36, 126.97, 52,90, 29.68, 20.98, 18.42, 17.13 ppm. HRMS (ESI): m/z calcd for $C_{19}H_{24}N_2O$ [M+H+]: 297.1963. Found: 297.1967.

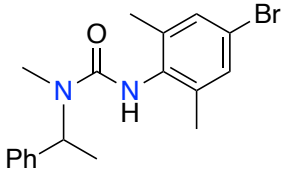

Synthesis of 3-(4-bromo-2,6-dimethylphenyl)-1-methyl-1-(1-phenylethyl)urea (2.38-H): Prepared following the general procedure outlined above: 4-bromo-2,6-dimethylaniline (2.34 g, 11.7 mmol), triphosgene (0.96 g, 3.89 mmol), DIPEA (9.15 mL, 52.5 mmol), *N*-methyl-1-phenylethan-1-amine (1.58 g, 11.7 mmol). Recrystallization from a concentrated ethyl acetate solution provided the desired compound as a white solid (2.36 g, 56 %): ^{1}H NMR ($CDCl_3$, 400 MHz, 298 K): δ 7.37 (m, 4H, o,m-C_6H_5), 7.30 (m, 1H, p-C_6H_5), 6.86 (s, 2H, m-CH), 5.72 (broad s, 1H, NH), 5.99 (m, 1H, CH(CH_3Ph)), 2.81 (s, 3H, CH_3), 2.25 (s, 3H, CH_3), 2.15 (s, 6H, CH_3), 1.59 (d, 3H, CH_3) ppm. ^{13}C{^{1}H} NMR ($CDCl_3$, 101 MHz, 298 K): δ 156.57 (C=O), 141.92, 136.01, 135.36, 132.89, 128.90, 128.72, 127.36, 126.97, 52.90, 29.68, 20.98, 18.42, 17.13 ppm. Anal. Calcd. for $C_{18}H_{21}BrN_2O$: C, 59.84; H, 5.86; N, 7.75; Found: C, 59.91; H, 5.89; N, 7.73.

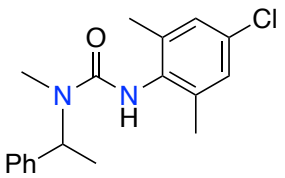

Synthesis of 3-(4-chloro-2,6-dimethylphenyl)-1-methyl-1-(1-phenylethyl)urea (2.39-H): Prepared following the general procedure outlined above: 4-chloro-2,6-dimethylaniline (2.50 g, 15.8 mmol), triphosgene (1.30 g, 5.26 mmol), DIPEA (12.3 mL, 68.0 mmol), *N*-methyl-1-phenylethan-1-amine (2.34 g, 15.8 mmol). Recrystallization from a concentrated ethyl acetate solution provided the desired compound as a white solid (0.94 g, 38 %): ^{1}H NMR ($CDCl_3$, 400 MHz, 298 K): δ 7.36 (m, 4H, o,m-C_6H_5), 7.31 (m, 1H, p-CH_3), 7.03 (s, 2H, CH), 5.84 (br s, 1H, NH), 5.56 (m, 1H, CH(CH_3Ph)), 2.84 (s, 3H, CH_3), 2.14 (s, 6H, 2,6-$(CH_3)_2C_6H_3$), 1.60 (d, 3H, CH_3) ppm. ^{13}C{^{1}H} NMR (CDCl3, 101 MHz, 298 K): δ 156.12 (C=O), 141.69, 137.36, 134.23, 131.59, 128.87,

128.01, 127.58, 126.95, 53.23, 29.92, 18.48, 17.29 ppm. HRMS (ESI): m/z calcd for $C_{16}H_{17}ClN_2O$ [M+H+]: 317.1419. Found: 317.1421.

2.5.3 Synthesis and Characterization of Ureate Ligand Salts

General procedure for the synthesis of ligand salts: $NaN(SiMe_3)_2$ (1 equiv.) was added in portions to a suspension of the corresponding proteoligand (1 equiv.) in Et_2O (~10 mL) and stirred overnight at room temperature. The volatiles were then removed at low pressure and the resulting solid was thoroughly washed with hexanes (3 x 5 mL) and dried to give the sodium salt in quantitative yield as a colorless powder. The resulting ligand salts were used directly without further purification via storage in a glove box. NMR characterization was precluded due to poor solubility in common NMR solvents (e.g. d_6-benzene or d_8-toluene).

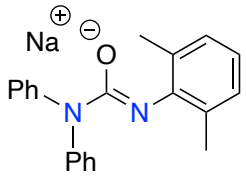

Synthesis of sodium (2,6-dimethylphenyl)(diphenylcarbamoyl)amide (2.4): Prepared following the general procedure outlined above: 3-(2,6-dimethylphenyl)-1,1-diphenylurea (0.68 g, 2.17 mmol), $NaN(SiMe_3)_2$ (0.40 g, 2.17 mmol).

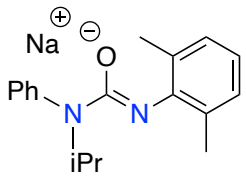

Synthesis of sodium (2,6-dimethylphenyl)(isopropyl(phenyl)carbamoyl)amide (2.5): Prepared following the general procedure outlined above: 3-(2,6-dimethylphenyl)-1-isopropyl-1-phenylurea (0.74 g, 2.64 mmol), $NaN(SiMe_3)_2$ (0.48 g, 2.64 mmol).

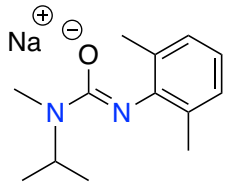

Synthesis of sodium (2,6-dimethylphenyl)(isopropyl(phenyl)carbamoyl)amide (2.34): Prepared following the general procedure outlined above: 3-(2,6-dimethylphenyl)-1-isopropyl-1-phenylurea (1.81 g, 2.64 mmol), $NaN(SiMe_3)_2$ (0.48 g, 2.64 mmol).

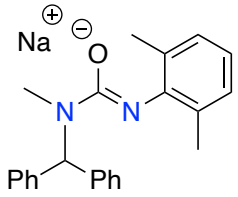

Synthesis of sodium (2,6-dimethylphenyl)(diphenylcarbamoyl)amide (2.35): Prepared following the general procedure outlined above: 3-(2,6-dimethylphenyl)-1,1-diphenylurea (0.68 g, 2.17 mmol), $NaN(SiMe_3)_2$ (0.40 g, 2.17 mmol).

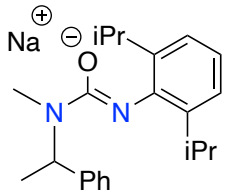

Synthesis of sodium (2,6-diisopropylphenyl)(methyl(1-phenylethyl)carbamoyl)amide (2.36): Prepared following the general procedure outlined above: 3-(2,6-diisopropylphenyl)-1-methyl-1-(1-phenylethyl)urea (0.74 g, 5.35 mmol), $NaN(SiMe_3)_2$ (0.98 g, 5.35 mmol).

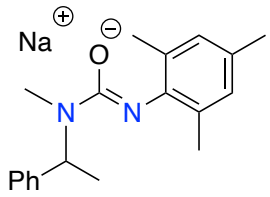

Synthesis of sodium mesityl(methyl(1-phenylethyl)carbamoyl)amide (2.37): Prepared following the general procedure outlined above: 3-mesityl-1-methyl-1-(1-phenylethyl)urea (4.53 g, 14.37 mmol), $NaN(SiMe_3)_2$ (2.64 g, 14.37 mmol).

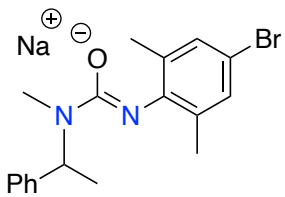

Synthesis of sodium (4-bromo-2,6-dimethylphenyl)(methyl(1-phenylethyl)carbamoyl)amide (2.38): Prepared following the general procedure outlined above: 3-(4-bromo-2,6-dimethylphenyl)-1-methyl-1-(1-phenylethyl)urea (2.36 g, 6.55 mmol), $NaN(SiMe_3)_2$ (1.20 g, 6.55 mmol).

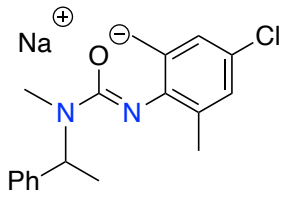

Synthesis of sodium (4-chloro-2,6-dimethylphenyl)(methyl(1-phenylethyl)carbamoyl)amide (2.39): Prepared following the general procedure outlined above: 3-(4-chloro-2,6-dimethylphenyl)-1-methyl-1-(1-phenylethyl)urea (0.94 g, 6.00 mmol), $NaN(SiMe_3)_2$ (1.10 g, 6.00 mmol).

2.5.4 *in situ* Generation of Tantalum Precatalysts

The in situ formation of the tantalum based precatalysts was studied by reacting equimolar amounts of $Ta(CH_2SiMe_3)_3Cl_2$ and the ligand salts **2.4** or **2.5** in a sealed J young tube in toluene-d_8 (vide infra). In the case of the reaction between $Ta(CH_2SiMe_3)_3Cl_2$ and **2.4**, complete signal disappearance for $SiCH_3$ (2.05 ppm) and CH_2SiMe_3 (2.05 ppm) protons of $Ta(CH_2SiMe_3)_3Cl_2$ was observed after 15 minutes. New sets of signals corresponding to the new complex appear at δ 0.29 ppm ($SiCH_3$ peak) and δ 2.23 ppm (CH_2SiMe_3 peak). On the other hand, the NMR tube containing the in situ mixture between $Ta(CH_2SiMe_3)_3Cl_2$ and **2.4** indicated no reaction between the two reactants at room temperature.

2.5.5 General Catalytic Procedure

$Ta(CH_2SiMe_3)_3Cl_2$ (0.025 mmol) was weighed into a vial, followed by addition of the chosen ligand salt (0.025 mmol). Toluene-d_8 (0.3 g) was added and the resultant mixture was left for 15 minutes. A chosen amine substrate was then added (0.5 mmol) with a micropipette, which was then followed by addition the alkene (0.5 mmol). The resultant reaction mixture was transferred into a J. Young NMR tube and the vial was rinsed with an additional 0.2 g of d8-toluene. An initial 1H NMR spectrum was recorded, and the sample was added to a pre-heated oil bath. All conversion values were determined by ^{1}H NMR spectroscopy. After removal of all reaction solvent by rotary evaporation, pentane was added to the reaction mixture and a white precipitate formed instantaneously. The solution was cooled to -80 °C until the solution was no longer turbid, then residual tantalum salts and proteoligands were removed by filtering the pentane solution through Celite®. Unreacted amine or alkene starting materials were removed at 40 °C under low pressure. In all cases, ^{1}H NMR spectroscopy still showed the presence of proteoligands in low amounts (2-4 %), which can be entirely removed by column chromatography. Note, all

compounds except N-(2-propylhexyl)aniline and N-(2-ethylpentyl)aniline, were isolated using the filtration protocol and spectra presented are of these easily isolated products. In the case of N-(2-propylhexyl)aniline, and N-(2-ethylpentyl)aniline there was evidence of decomposition from heating under vacuum and therefore these products were purified by column chromatography. In the case of N-(cyclooctylmethyl)-4-methoxyaniline, the starting amine is a solid so the reaction must be purified by column chromatography to remove any residual reactants.

Please note, in all proton spectra below,◆ indicates residual ligand peaks.

2.5.6 Characterization of Amine Scope Products

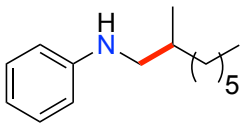

***N*-(2-methyloctyl)aniline (2.7)**: *N*-methylaniline (54 mg, 0.5 mmol), 1-octene (56 mg, 0.5 mmol), $Ta(CH_2SiMe_3)_3Cl_2$ (13 mg, 0.025 mmol), **2.4** (8 mg, 0.025 mmol). Reaction time: 2 h. Yield 88%. The chemical shifts for the title compound match those reported in the literature.

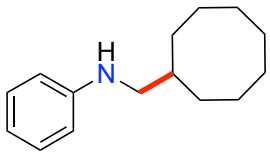

***N*-(cyclooctylmethyl)aniline (2.8)**: *N*-methylaniline (54 mg, 0.5 mmol), cyclooctene (55 mg, 0.5 mmol), $Ta(CH_2SiMe_3)_3Cl_2$ (13 mg, 0.025 mmol), **2.5** (8 mg, 0.025 mmol). Reaction time: 6 h. Yield 83%. The chemical shifts for the title compound match those previously reported in the literature.[85]

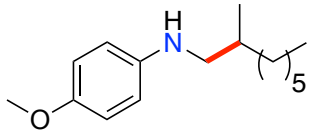

4-methoxy-*N*-(2-methyloctyl)aniline (2.9): 4-methoxy-*N*-methylaniline (96 mg, 0.5 mmol), 1-octene (0.056 g, 0.5 mmol), $Ta(CH_2SiMe_3)_3Cl_2$ (13 mg, 0.025 mmol), **2.4** (8 mg, 0.025 mmol). Reaction time: 2 h. Yield 77%. The chemical shifts for the title compound match those previously reported in the literature.[84]

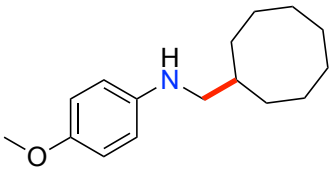

***N*-(cyclooctylmethyl)-4-methoxyaniline (2.10)**: 4-methoxy-*N*-methylaniline (96 mg, 0.5 mmol), cyclooctene (55 mg, 0.5 mmol), $Ta(CH_2SiMe_3)_3Cl_2$ (13 mg, 0.025 mmol), **2.5** (8 mg, 0.025 mmol). Reaction time: 6 h. Yield 70%. ^1H NMR ($CDCl_3$, 300 MHz, 298 K): δ 6.84-6.76 (m, 2H, m-C_6H_4), 6.64-6.55 (m, 2H, o-C_6H_4), 3.76 (br s, 1H, NH), 3.58 (s, 3H, OCH_3), 2.91 (d, JH-H = 6.7 Hz, 2H, NCH_2), 1.90-1.27 (m, 15H, CH and CH_2) ppm. $^{13}C\{^1H\}$ NMR ($CDCl_3$, 75 MHz, 298 K): δ 152.04 (i-C_6H_4), 142.80 (p-C_6H_4), 115.00 (m-C_6H_4), 114.18 (m-C_6H_4), 55.91 (OCH_3), 52.44 (NCH_2), 37.41 (CH), 30.74 (CH_2), 27.16 (CH_2), 26.42 (CH_2), 25.60 (CH_2) ppm. HRMS (ESI): m/z calcd for $C_{16}H_{25}NO$ [M+H+]: 248.2014. Found: 248.2015.

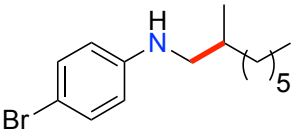

4-bromo-*N*-(2-methyloctyl)aniline (2.11): 4-bromo-*N*-methylaniline (93 mg, 0.5 mmol), 1-octene (56 mg, 0.5 mmol), $Ta(CH_2SiMe_3)_3Cl_2$ (13 mg, 0.025 mmol), **2.4** (8 mg, 0.025 mmol). Reaction time: 2 h. Yield 86%. ^1H NMR ($CDCl_3$, 300 MHz, 298 K): δ 7.23 (d, J_{H-H} = 8.7 Hz, 2H, m-C_6H_4), 6.48 (d, J_{H-H} = 8.9 Hz, 2H, o-C_6H_4), 3.92 (br s, 1H, NH), 3.01 (dd, J_{H-H} = 5.9, 12.2 Hz, 1H, NC(H)H), 2.84 (dd, J_{H-H} = 7.1, 12.1 Hz, 1H, NC(H)H), 1.78-1.65 (m, 1H, CH), 1.51-1.08 (m, 10H, CH_2), 0.96 (d, J_{H-H} = 6.6 Hz, 3H, CHCH3), 0.89 (t, J_{H-H} = 6.9 Hz, 3H, CH_2CH_3) ppm. $^{13}C\{^1H\}$ NMR ($CDCl_3$, 100 MHz, 298 K): δ 147.58 (i-C_6H_4), 132.00 (m-C_6H_4), 114.41 (p-C_6H_4), 108.63 (o-C_6H_4), 50.56, 34.88, 32.94, 31.99, 29.72, 27.05, 22.80, 18.16 (CH_3), 14.25 (CH_3) ppm. HRMS (ESI): m/z calcd for $C_{15}H_{24}BrN$ [M+H+]: 298.1170. Found: 298.1175.

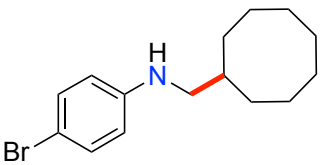

4-bromo-*N*-(cyclooctylmethyl)aniline (2.12): 4-bromo-*N*-methylaniline (93 mg, 0.5 mmol), cyclooctene (55 mg, 0.5 mmol), $Ta(CH_2SiMe_3)_3Cl_2$ (13 mg, 0.025 mmol), **2.5** (8 mg, 0.025 mmol). Reaction time: 6 h. Yield 95%. ^1H NMR ($CDCl_3$, 300 MHz, 298 K): δ 7.27 (m, J_{H-H} = 8.8 Hz, 2H,

m-C6H4), 6.49 (m, JH–H = 8.8 Hz, 2H, o-C6H4), 3.77 (br s, 1H, NH), 2.92 (d, J_{H-H} = 6.8 Hz, 2H, NCH_2), 1.88-1.30 (overlapping m, 15H, CH and CH_2) ppm. $^{13}C\{^1H\}$ NMR (CDCl3, 75 MHz, 298 K): δ 147.64 (i-C_6H_4), 131.99 (m-C_6H_4), 114.24 (o-C_6H_4), 108.39 (p-C_6H_4), 51.21 (NCH_2), 37.34 (CH_2), 30.67 (CH_2), 27.13 (CH_2), 26.42 (CH_2), 25.58 (CH_2) ppm. HRMS (ESI): m/z calcd for $C_{15}H_{22}BrN$ [M+H+]: 296.1014 Found: 296.1008.

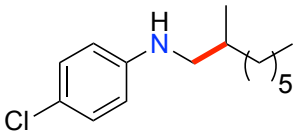

4-chloro-*N*-(2-methyloctyl)aniline (2.13): 4-chloro-*N*-methylaniline (71 mg, 0.5 mmol), 1-octene (56 mg, 0.5 mmol), $Ta(CH_2SiMe_3)_3Cl_2$ (13 mg, 0.025 mmol), **2.4** (8 mg, 0.025 mmol). Reaction time: 2 h. Yield 90%. The chemical shifts for the title compound match those previously reported in the literature.[73]

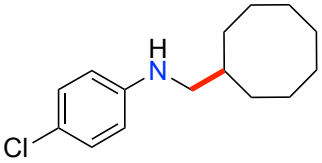

4-chloro-*N*-(cyclooctylmethyl)aniline (2.14): 4-chloro-*N*-methylaniline (71 mg, 0.5 mmol), cyclooctene (55 mg, 0.5 mmol), $Ta(CH_2SiMe_3)_3Cl_2$ (13 mg, 0.025 mmol), **2.5** (8 mg, 0.025 mmol). Reaction time: 6 h. Yield 93%. ^1H NMR ($CDCl_3$, 300 MHz, 298 K): δ 7.13 (m, 2H, m-C_6H_4), 6.53 (m, 2H, o-C_6H_4), 3.73 (s, 1H, NH), 2.92 (d, J_{H-H} = 6.8 Hz, 2H, NCH_2), 1.87-1.28 (overlapping m, 15h H, CH and CH_2) ppm. $^{13}C\{^1H\}$ NMR ($CDCl_3$, 75 MHz, 298 K): δ 147.32 (i-C_6H_4), 129.13 (m-C_6H_4), 121.45 (p-C_6H_4), 113.76 (o-C_6H_4), 51.37 (NCH_2), 37.42 (CH_2), 30.74 (CH_2), 27.19 (CH_2), 26.48 (CH_2), 25.64 (CH_2) ppm. HRMS (ESI): m/z calcd for $C_{15}H_{22}ClN$ [M+H+]: 252.1519. Found: 252.1514.

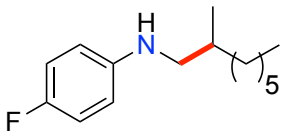

4-fluoro-*N*-(2-methyloctyl)aniline (2.15): 4-fluoro-*N*-methylaniline (63 mg, 0.5 mmol), 1-octene (56 mg, 0.5 mmol), $Ta(CH_2SiMe_3)_3Cl_2$ (13 mg, 0.025 mmol), **2.4** (8 mg, 0.025 mmol). Reaction time: 2 h. Yield 88%. The chemical shifts for the title compound match those previously reported in the literature.[40]

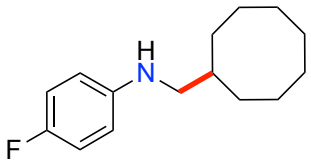

***N*-(cyclooctylmethyl)-4-fluoroaniline (2.16)**: 4-fluoro-*N*-methylaniline (63 mg, 0.5 mmol), cyclooctene (55 mg, 0.5 mmol), $Ta(CH_2SiMe_3)_3Cl_2$ (13 mg, 0.025 mmol), **2.5** (8 mg, 0.025 mmol). Reaction time: 6 h. Yield 88%. ^1H NMR ($CDCl_3$, 300 MHz, 298 K): δ 6.89 (m, 2H, m-C_6H_4), 6.57-6.49 (m, 2H, o-C_6H_4), 3.58 (br s, 1H, NH), 2.90 (d, $J_{H–H}$ = 6.7 Hz, 2H, NCH_2), 1.88-1.22 (overlapping m, 13H, CH and CH_2) ppm. $^{13}C\{^1H\}$ NMR ($CDCl_3$, 100 MHz, 298 K):δ 155.67 (d, $J_{C–F}$ = 234.2 Hz, 2H, *p*-C_6H_4), 145.05 (*i*-C_6H_4), 115.66 (d, $J_{C–F}$ = 22.2 Hz, m-C_6H_4), 113.49 (d, $J_{C–F}$ = 7.3 Hz, o-C_6H_4), 52.00 (NCH_2), 37.41 (CH_2), 30.73 (CH_2), 27.15 (CH_2), 26.44 (CH_2), 25.61 (CH_2) ppm . ^{19}F NMR ($CDCl_3$, 282.4 MHz, 298 K): δ -129.00 (tt, $J_{H–F}$ = 4.5 Hz, 1F, C_6H_4F) ppm. HRMS (ESI): m/z calcd for $C_{15}H_{22}FN$ [M+H+]: 236.1814. Found: 236.1809.

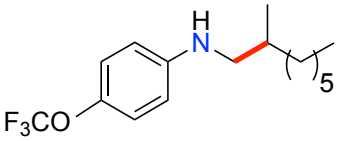

***N*-(2-methyloctyl)-4-(trifluoromethoxy)aniline (2.17)**: *N*-methyl-4-(trifluoromethoxy)aniline (96 mg, 0.5 mmol), 1-octene (56 mg, 0.5 mmol), $Ta(CH_2SiMe_3)_3Cl_2$ (13 mg, 0.025 mmol), **2.4** (8 mg, 0.025 mmol). Reaction time: 3 h. Yield 92%. ^1H NMR ($CDCl_3$, 300 MHz, 298 K): δ 7.03 (d, $J_{H–H}$ = 8.2 Hz, 2H, m-C_6H_4), 6.59-6.50 (m, 2H, *o*-C_6H_4), 3.80 (br s, 1H, NH), 3.03 (dd, $J_{H–H}$ = 5.9, 12.2 Hz, 1H, NC(H)H), 2.87 (dd, $J_{H–H}$ = 7.3, 12.2 Hz, 1H, NC(H)H), 1.79-1.68 (m, 1H, CH), 1.51-1.12 (m, 10H, CH_2), 0.97 (d, $J_{H–H}$ = 6.7 Hz, 3H, $CHCH_3$), 0.90 (t, $J_{H–H}$ = 6.9 Hz, 3H, CH_2CH_3) ppm. $^{13}C\{^1H\}$ NMR ($CDCl_3$, 300 MHz, 298 K): δ 147.51 (*i*-C_6H_5), 122.52 (*m*-C_6H_5), 112.89 (*o*-C_6H_5), 50.68 (NCH_2), 34.90, 33.02, 32.01, 29.74, 27.08, 22.81, 18.18 (CH_3), 14.24 (CH_3) ppm. ^{19}F NMR ($CDCl_3$, 282.4 MHz, 298 K): δ -58.81 (s, 3F, CF_3) ppm. HRMS (ESI): m/z calcd for $C_{16}H_{24}F_3NO$ [M+H+]: 304.1888. Found: 304.1883.

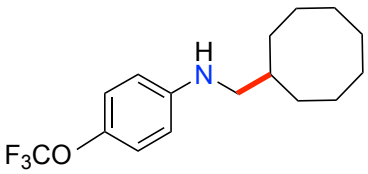

***N*-(cyclooctylmethyl)-4-(trifluoromethoxy)aniline (2.18)**: *N*-methyl-4-(trifluoromethoxy)aniline (96 mg, 0.5 mmol), cyclooctene (55 mg, 0.5 mmol), $Ta(CH_2SiMe_3)_3Cl_2$ (13 mg, 0.025 mmol), **2.5** (8 mg, 0.025 mmol). Reaction time: 6 h. Yield 85%. ^1H NMR ($CDCl_3$, 300 MHz, 298 K): δ 7.03 (d, $J_{H–H}$ = 9.0 Hz, 2H, *m*-C_6H_4), 6.59-6.50 (m, 2H, *o*-C_6H_4), 3.77 (br s, 1H, NH), 2.92 (d, $J_{H–H}$ = 6.5 Hz, 2H, NCH_2), 1.89-1.21 (overlapping m, 15H, CH and CH_2) ppm. $^{13}C\{^1H\}$ NMR ($CDCl_3$, 75 MHz, 298 K): δ 147.54 (*i*-C_6H_4), 122.51 (*m*-C_6H_4), 112.80 (*o*-C_6H_4), 51.43 (NCH_2), 37.48, 30.73, 27.18, 26.45, 25.62 ppm. ^{19}F NMR ($CDCl_3$, 282.4 MHz, 298 K): δ –58.79 (s, 3F, CF_3) ppm. HRMS (ESI): m/z calcd for $C_{16}H_{22}F_3NO$ [M+H+]: 302.1732. Found: 302.1726.

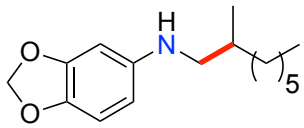

***N*-(2-methyloctyl)benzo[d][1,3]dioxol-5-amine (2.19)**: *N*-methylbenzo[d][1,3]dioxol-5-amine (76 mg, 0.5 mmol), 1-octene (56 mg, 0.5 mmol), $Ta(CH_2SiMe_3)_3Cl_2$ (13 mg, 0.025 mmol), **2.4** (8 mg, 0.025 mmol). Reaction time: 2 h. Yield 85%. ^1H NMR ($CDCl_3$, 300 MHz, 298 K): δ 6.66 (d, $J_{H–H}$ = 8.3 Hz, 2H, *m*-C_6H_3), 6.25 (d, $J_{H–H}$ = 8.3 Hz, 1H, *o*-C_6H_3), 6.04 (dd, $J_{H–H}$ = 2.3, 8.3 Hz, 1H, *o*-C_6H_3), 5.85 (s, 2H, OCH_2), 3.52 (br s, 1H, NH), 2.99 (dd, $J_{H–H}$ = 5.9, 12.0 Hz, 1H, NC(H)H), 2.82 (dd, $J_{H–H}$ = 5.0, 12.2 Hz, 1H, NC(H)H), 1.81-1.62 (m, 1H, CH), 1.50-1.08 (m, 10H, CH_2), 0.96 (d, $J_{H–H}$ = 6.7 Hz, 3H, $CHCH_3$), 0.90 (t, $J_{H–H}$ = 7.1 Hz, 3H, CH_2CH_3) ppm. $^{13}C\{^1H\}$ NMR ($CDCl_3$, 75 MHz, 298 K): δ 148.45 (*i*-C_6H_3), 144.63, 139.39, 108.74 (C_6H_3), 104.34 (C_6H_3), 100.61 (CH_2), 95.90 (C_6H_3), 51.55 (CH_2), 34.95 (CH_2), 33.03 (CH), 32.00 (CH_2), 29.74 (CH_2), 27.07 (CH_2), 22.81 (CH_2), 18.20 (CH_3), 14.24 (CH_3) ppm. HRMS (ESI): m/z calcd for $C_{16}H_{25}NO_2$ [M+H+]: 264.1964. Found: 264.1958.

2.5.7 Characterization of Alkene Scope Products

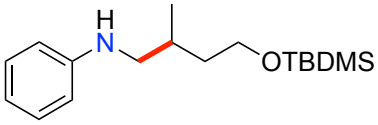

***N*-(4-((tert-butyldimethylsilyl)oxy)-2-methylbutyl)aniline (2.20)**: *N*-methylaniline (54 mg, 0.5 mmol), (but-3-en-1-yloxy)(tert-butyl)dimethylsilane (93 mg, 0.5 mmol), $Ta(CH_2SiMe_3)_3Cl_2$ (13 mg, 0.025 mmol), **2.4** (8 mg, 0.025 mmol). Reaction time: 2 h. Yield 75%. ^1H NMR ($CDCl_3$, 300 MHz, 298 K): δ 7.24-7.16 (m, 2H, *m*-C_6H_4), 6.74-6.67 (m, 1H, *p*-C_6H_5), 6.60-6.66 (m, 2H, *o*-C_6H_4), 3.85 (br s, 1H, NH), 3.81-3.65 (m, 2H, OCH_2), 3.09 (dd, J_{H-H} = 6.3, 12.2 Hz, 1H, NC(H)H), 2.96 (dd, J_{H-H} = 6.9, 12.2 Hz, 1H, NC(H)H), 1.95 (oct, J_{H-H} = 6.7 Hz, 1H, $OCH_2C(H)H$), 1.76-1.61 (m, 1H, $CHCH_3$), 1.53-1.39 (m, 1H, $OCH_2C(H)H$), 1.02 (dd, J_{H-H} = 6.7 Hz, J_{H-H} = 1.0 Hz, 3H, $CHCH_3$), 0.93 (s, 9H, $SiC(CH_3)_3$), 0.09 (s, 6H, $SiCH_3$) ppm. $^{13}C\{^1H\}$ NMR ($CDCl_3$, 75 MHz, 298 K): δ 148.70 (*i*-C_6H_5), 129.32 (*m*-C_6H_5), 116.99 (*p*-C_6H_5), 112.74 (*o*-C_6H_5), 61.21 (NCH_2), 50.43 (OCH_2CH_2), 37.94, 29.99, 26.10 ($SiC(CH_3)_3$), 18.45 ($CHCH_3$), -5.17 ($Si(CH_3)_3$) ppm. HRMS (ESI): m/z calcd for $C_{17}H_{31}NOSi$ [M+H+]: 294.2253. Found: 294.2248.

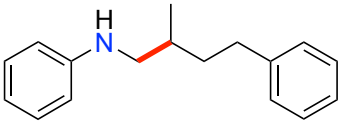

***N*-(2-methyl-4-phenylbutyl)aniline (2.21)**: *N*-methylaniline (54 mg, 0.5 mmol), 4-phenyl-1-butene (66 mg, 0.5 mmol), $Ta(CH_2SiMe_3)_3Cl_2$ (13 mg, 0.025 mmol), **2.4** (8 mg, 0.025 mmol). Reaction time: 3 h. Yield 87%. The chemical shifts for the title compound match those reported in the literature.[73]

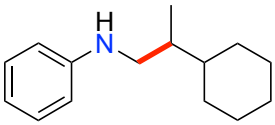

***N*-(2-cyclohexylpropyl)aniline (2.22)**: *N*-methylaniline (54 mg, 0.5 mmol), vinylcyclohexane (55 mg, 0.5 mmol), $Ta(CH_2SiMe_3)_3Cl_2$ (13 mg, 0.025 mmol), **2.4** (8 mg, 0.025 mmol). Reaction time: 2 h. Yield 86%. The chemical shifts for the title compound match those reported.[78]

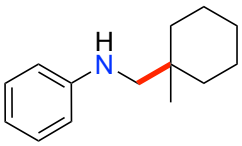

***N*-((1-methylcyclohexyl)methyl)aniline (2.23)**: *N*-methylaniline (54 mg, 0.5 mmol), vinylcyclohexane (48 mg, 0.5 mmol), $Ta(CH_2SiMe_3)_3Cl_2$ (13 mg, 0.025 mmol), **2.4** (8 mg, 0.025 mmol). Reaction time: 3 h. Yield 99%. The chemical shifts for the title compound match those reported in the literature.[62,78]

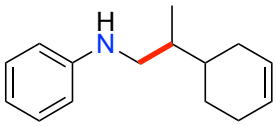

***N*-(2-(cyclohex-3-en-1-yl)propyl)aniline (2.24)**: *N*-methylaniline (54 mg, 0.5 mmol), vinylcyclohexane (55 mg, 0.5 mmol), $Ta(CH_2SiMe_3)_3Cl_2$ (13 mg, 0.025 mmol), **2.4** (8 mg, 0.025 mmol). Reaction time: 2 h. Yield 98%. The chemical shifts for the title compound match those reported in the literature.[59]

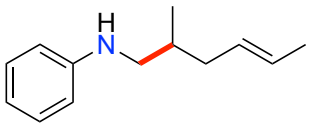

(*E*)-*N*-(2-methylhex-4-en-1-yl)aniline (2.25): *N*-methylaniline (54 mg, 0.5 mmol), (*E*)-hexa-1,4-diene (41 mg, 0.5 mmol), $Ta(CH_2SiMe_3)_3Cl_2$ (13 mg, 0.025 mmol), **2.4** (8 mg, 0.025 mmol). Reaction time: 2 h. Yield 86%. ^1H NMR ($CDCl_3$, 300 MHz, 298 K): δ 7.23-7.17 (m, 2H, m-C_6H_4), 6.74-6.71 (m, 1H, *p*-C_6H_5), 6.69-6.64 (m, 2H, *o*-C_6H_4), 5.50-5.46 (m, 2H, HC=CH), 3.71 (br s, 1H, NH), 3.12-3.06 (m, 1H, NC(H)H), 2.96-2.90 (m, 1H, NC(H)H), 2.19-2.00 (m, 1H, C(H)H), 1.98-1.91 (m, 1H, C(H)H), 1.88-1.77 (m, 1H, CH), 1.72-1.70 (d, J_{H-H} = 1.72 Hz, 3H, CH_3), 1.03-1.00 (m, 3H, CH_3) ppm. $^{13}C\{^1H\}$ NMR (CDCl3, 75 MHz, 298 K): δ 148.69 (*i*-C_6H_5), 129.34 (*m*-C_6H_5), 129.19 (CH_2CH), 126.89 (CH), 117.09 (*p*-C_6H_5), 112.80 (*o*-C_6H_5), 49.96 (NCH_2), 38.08 (CH_2), 33,29 (CH), 18.33 (CH_3), 18.10 (CH_3) ppm. HRMS (ESI): m/z calcd for $C_{13}H_{20}N$ [M+H+]: 190.1596. Found: 190.1597.

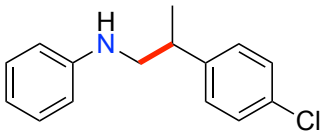

***N*-(2-(4-chlorophenyl)propyl)aniline (2.26)**: *N*-methylaniline (54 mg, 0.5 mmol), 4-chlorostyrene (70 g, 0.5 mmol), $Ta(CH_2SiMe_3)_3Cl_2$ (13 mg, 0.025 mmol), **2.4** (8 mg, 0.025 mmol). Reaction time : 2 h. Yield 98%. The chemical shifts for the title compound match those reported.[78]

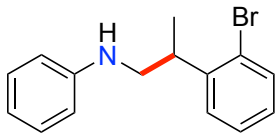

***N*-(2-(2-bromophenyl)propyl)aniline (2.27)**: *N*-methylaniline (54 mg, 0.5 mmol), 2-bromostyrene (92 mg, 0.5 mmol), $Ta(CH_2SiMe_3)_3Cl_2$ (13 mg, 0.025 mmol), **2.4** (8 mg, 0.025 mmol). Reaction time: 2 h. Yield 65%. ^{1}H NMR ($CDCl_3$, 300 MHz, 298 K): δ 7.60 (dd, J_{H-H} = 8.0, 0.8 Hz, 1H, C_6H_4Br), 7.45-7.25 (m, 3H, *m*-C_6H_5), 7.24-7.14 (m, 2H, C_6H_4Br), 7.11 (ddd, J_{H-H} = 8.1, 6.6, 2.4 Hz, 1H, C_6H_4Br), 6.73 (t, J_{H-H} = 7.3 Hz, 1H, *p*-C_6H_5), 6.68-6.62 (m, 2H, *o*-C_6H_5), 3.65 (sext, J_{H-H} = 7.0 Hz, 1H, CH), 3.40 (dd, J_{H-H} = 12.3, 7.3 Hz, 1H, C(H)H), 3.28 (dd, J_{H-H} = 12.3, 7.0 Hz, 1H, C(H)H), 1.37 (d, J_{H-H} = 6.9 Hz, 3H, CH_3) ppm. $^{13}C\{^1H\}$ NMR ($CDCl_3$, 75 MHz, 298 K): δ 148.01 (*i*-C_6H_5), 143.49 (*i*-C_6H_4Br), 133.20 (C_6H_4Br), 129.32 (*m*-C_6H_5), 128.11 (C_6H_4Br), 127.98 (C_6H_4Br), 127.49 (*p*-C_6H_5), 117.58 (C_6H_4Br), 113.08 (*o*-C_6H_5), 50.06 (CH_2), 38.03 (CH), 19.07 (CH_3) ppm. HRMS (ESI): m/z calcd for $C_{15}H_{16}BrN$ [M+H+]: 290.0544. Found: 290.0539.

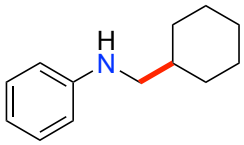

***N*-(cyclohexylmethyl)aniline (2.28)**: *N*-methylaniline (54 mg, 0.5 mmol), cyclohexene (41 mg, 0.5 mmol), $Ta(CH_2SiMe_3)_3Cl_2$ (13 mg, 0.025 mmol), **2.5** (8 mg, 0.025 mmol). Reaction time: 20 h. Yield 70%. The chemical shifts for the title compound match those previously reported in the literature.[62,78,85]

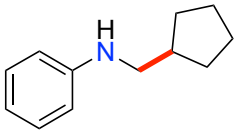

***N*-(cyclopentylmethyl)aniline (2.29)**: *N*-methylaniline (54 mg, 0.5 mmol), cyclopentene (34 mg, 0.5 mmol), $Ta(CH_2SiMe_3)_3Cl_2$ (13 mg, 0.025 mmol), **2.5** (8 mg, 0.025 mmol). Reaction time: 20 h. Yield 74%. The chemical shifts for the title compound match those reported in the literature.[85]

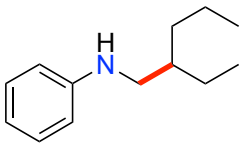

***N*-(2-ethylpentyl)aniline (2.31)**: **Method A**. *N*-methylaniline (54 mg, 0.5 mmol), cis-3-hexene (42 mg, 0.5 mmol), $Ta(CH_2SiMe_3)_3Cl_2$ (13 mg, 0.025 mmol), **2.5** (8 mg, 0.025 mmol). Reaction time: 20 h. Yield 56%. **Method B**. N-methylaniline (54 mg, 0.5 mmol), trans-3-hexene 42 mg, 0.5 mmol), $Ta(CH_2SiMe_3)_3Cl_2$ (13 mg, 0.025 mmol), **2.5** (8 mg, 0.025 mmol). Reaction time: 20 h. Conversion 10% (observed by ^1H NMR spectroscopy). The chemical shifts for the title compound match those reported in the literature.[85]

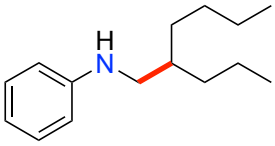

***N*-(2-propylhexyl)aniline**: *N*-methylaniline (54 mg, 0.5 mmol), cis-4-octene (56 mg, 0.5 mmol), $Ta(CH_2SiMe_3)_3Cl_2$ (13 mg, 0.025 mmol), **2.5** (8 mg, 0.025 mmol). Reaction time: 20 h. Yield 45 %. ^1H NMR ($CDCl_3$, 300 MHz, 298 K): δ 7.19 (m, 2H, *m*-C_6H_5), 6.76-6.64 (overlapping m, 3H, *p*-C_6H_5 and *o*-C_6H_5), 3.03 (d, J_{H-H} = 6.2 Hz, 2H, NCH_2), 1.66-1.61 (m, 1H, CH), 1.44-1.24 (overlapping m, 10H, CH_2), 0.99-0.82 (overlapping m, 6H, CH_3) ppm. $^{13}C\{^1H\}$ NMR ($CDCl_3$, 75 MHz, 298 K): δ 148.12 (*i*-C_6H_5), 129.38 (*m*-C_6H_5), 117.76 (*p*-C_6H_5), 113.40 (*o*-C_6H_5), 48.17 (NCH_2), 37.47 (CH), 34.59 (CH_2), 31.95 (CH_2), 29.05 (CH_2), 23.23 (CH_2), 20.01 (CH_2), 14.60 (CH_3), 14.23 (CH_3) ppm. HRMS (ESI): m/z calcd for $C_{15}H_{25}N$ [M+H+]: 220.2065. Found: 220.2060.

2.5.8 Hydroaminoalkylation of cis α-methyl styrene with *N*-methylaniline

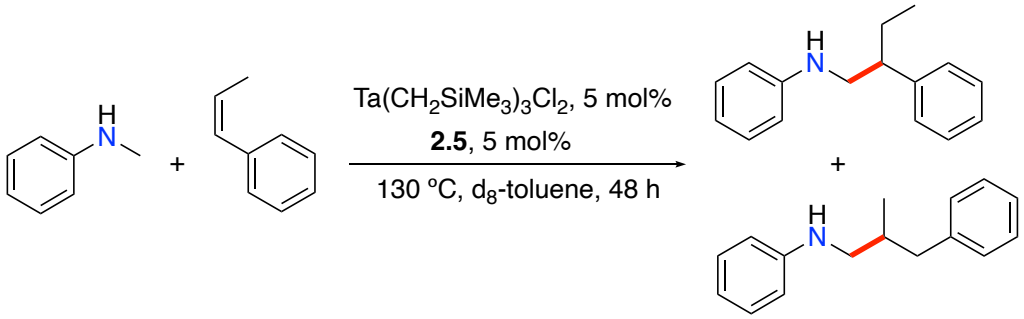

Scheme 2.4. Hydroaminoalkylation reaction between *N*-methylaniline and *cis*-α -methylstyrene.

Reactivity with an unsymmetrical styrene derivative proved challenging as *cis*-α-methylstyrene required unexpectedly long reaction times (48 h) to realize nearly complete conversion. This substrate gave a mixture of regioisomeric products with a modest preference for generating the methylated product. Note that careful reaction monitoring showed that alkene isomerization did not precede Csp^3-Csp^3 bond formation.

2.5.9 Characterization data for isolated Ta precatalysts

General procedure for precatalyst preparations: In a glovebox, to a stirring suspension of $Ta(CH_2SiMe_3)_3Cl_2$ (0.33 mmol) in toluene (~3 mL) in a 20 mL vial, a suspension of sodium (2,6-dimethylphenyl)(methyl(1-phenylethyl)carbamoyl)amide (0.100 g, 0.33 mmol) in toluene (~3 mL) was added dropwise over 5 minutes. The mixture was stirred at ambient temperature for 1 h, filtered through a plug of Celite, and concentrated *in vacuo* overnight. The resulting crude residue was dissolved in minimal hexanes (~2 mL), storage at -35 °C overnight produced a yellow precipitate. A sample from these crystals was used for single crystal X-ray structure analysis. NMR spectra and elemental analyses for compounds highlighted in this section need to be determined in future work due to a lab shutdown.

Chapter 3: Terpenes as Substrates in Hydroaminoalkylation Reactions

3.1 Introduction

3.1.1 Medicinal Relevance of Terpenes and Terpenoid Alkaloids

Terpenes represent a structurally diverse set of natural products with a rich history of use in both natural medicines and fragrances.[134–137] Beyond their medicinal applications, terpenes are attractive substrates for catalytic functionalization, due to the high-value products obtained upon regio- and stereoselective transformations. For example, catalytic oxidations of terpene substrates are well established and used in flavor industries.[138–140] However, the direct catalytic amination of terpenes to access aminated terpenes (synthetic terpenoid-alkaloids) is unexplored.

Terpenoid-alkaloids (or pseudoalkaloids) often display enhanced bioactivities as compared to terpenes alone.[138] Specifically, monoterpene alkaloids are employed as treatments for a variety of prevalent diseases including cancer, malaria, and hypertension.[141] Typically pseudoalkaloid syntheses target natural products and are biomimetic or have linear stoichiometric pathways that involve multiple protection/deprotection protocols. Meanwhile, the modification of compounds with natural product-like or natural product-containing cores has emerged as a useful approach for diversity-oriented synthesis with proven success in accessing exciting bioactivity.[142–144]

3.1.2 Terpenes as Substrates in Catalytic Amination Reactions

The direct catalytic amination of terpenes has been rarely reported. One noteworthy example is the industrial synthesis of (-)-menthol via the Takasago process, which proceeds via hydroamination of myrcene.[145] However, a general catalytic route for the catalytic amination of the unactivated alkenes in terpenes remains a synthetic challenge.[9,11–13,146–151] Meanwhile hydroaminoalkylation is a complementary amination strategy for the hydrofunctionalization of alkenes. In this case, the reaction forms a Csp^3-Csp^3 bond adjacent to the N of the amine substrate.

This reaction proceeds via C-H activation and can be mediated by either early or late transition metal-based catalysts. Previously published early transition-metal hydroaminoalkylation catalyst systems discussed in Chapters 1 and 2 can mediate this reaction with secondary amines and simple unactivated alkenes, although these reactions typically result in racemic products with saturated hydrocarbon frameworks that do not readily undergo further synthetic manipulation (Figure 3.1a).[5,35–38,76,152] Furthermore, diastereoselectivity in hydroaminoalkylation has not been extensively reported. Late transition metal variants of this reaction show improved functional group tolerance, but require directing/protecting groups to promote C-H activation (Figure 3.1b),[103–105,153] and photocatalytic hydroaminoalkylation requires multiple catalytic systems and specialized reaction setups.[32,111] Further, the alternative strategy towards these products of tandem hydroformylation-reductive amination has reported the linear regioisomer.[154]

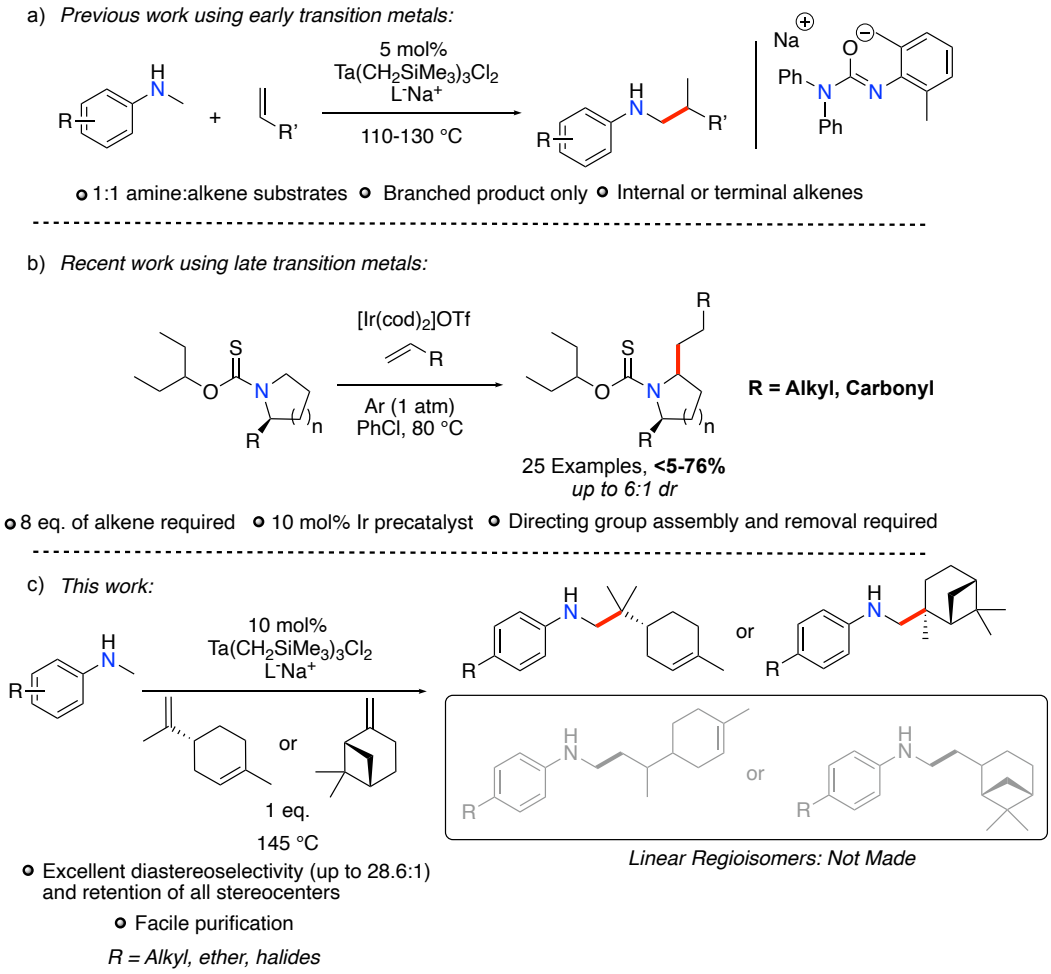

Figure 3.1. a) A recent example of group 5 catalyzed hydroaminoalkylation, b) a summary of reaction scopes for late transition-metal catalyzed hydroaminoalkylation strategies, and c) the goal of this work.[28,79]

3.1.3 Scope of Chapter

Here we show that hydroaminoalkylation using early transition-metals generates the branched regioisomer with excellent diastereoselectivity without epimerizing the stereocenter for terpene substrates (Figure 3.1c). These results demonstrate that hydroaminoalkylation can be used for the direct catalytic amination of terpenes to generate new classes of synthetic terpenoid-alkaloids. Thus, this atom-economic, regioselective and diastereoselective catalytic

functionalization reaction offers a new strategy that can be applied toward diversity-oriented synthesis.

3.2 Results and Discussion

3.2.1 Reaction Optimization

An initial screen of reported Ta-amido and -alkyl precursors confirmed that the known $Ta(CH_2SiMe_3)_3Cl_2$, as previously established in octene hydroaminoalkylation in Chapter 2,[79] showed the most promise for use with the terpene (R)-(+)-limonene as well (See Table 3.1a). This terpene was selected as a readily available, enantiopure, and diene-containing substrate that could be used to exemplify the excellent regioselectivity of our method. Furthermore, hydroaminoalkylation of commercially available (R)-(+)-limonene and (S)-(-)-limonene with $Ta(CH_2SiMe_3)_3Cl_2$ resulted in no appreciable changes in enantiopurity, as determined by chiral HPLC (See Figure. C.1 and Figure. C.2, Appendix C). This shows that Ta catalyzed hydroaminoalkylation does not racemize allylic stereocenters, as is known to occur in other late transition-metal based catalytic transformations of terpenes.[138–140] Furthermore, ^{1}H NMR spectra of reaction mixtures did not indicate any alkene isomerization, which can also occur under alternative catalytic conditions.

Table 3.1a. Screening of tantalum- based precursors for 1-octene and limonene reactivity.

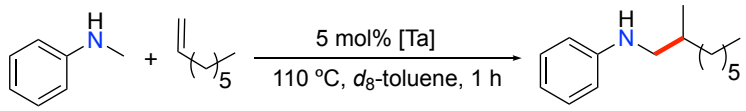

$Ta(NMe_2)_5$	$[Ta(NMe_2)_3Cl_2]_2$	$Ta(CH_2SiMe_3)_3Cl_2$
n.r.[b]	n.r.[b]	39% Conversion

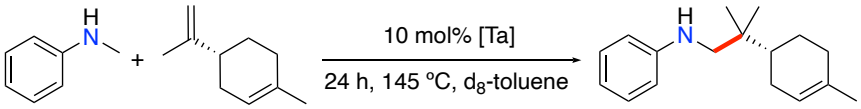

$Ta(NMe_2)_5$	$[Ta(NMe_2)_3Cl_2]_2$	$Ta(CH_2SiMe_3)_3Cl_2$
Traces	39% Conversion	38% Conversion

[a]Reaction conditions: *N*-methylaniline (0.5 mmol), (*R*)-(+)-limonene (0.5 mmol), Ta precursor (0.05 mmol), d_8-toluene (0.5 g). Conversion determined by ^{1}H NMR spectroscopy using 1,3,5-trimethoxybenzene (0.15 mmol) as an internal standard. [b] n.r.: no reaction.

Table 3.1b: Screening N,O-chelating ligands in hydroaminoalkylation[a]

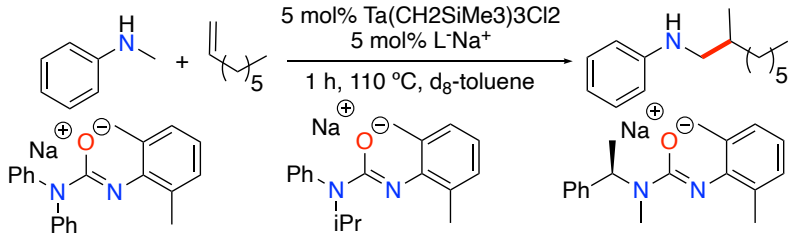

3.1: 83% Conversion	**3.2**: 12% Conversion	**3.3**: 98% Conversion

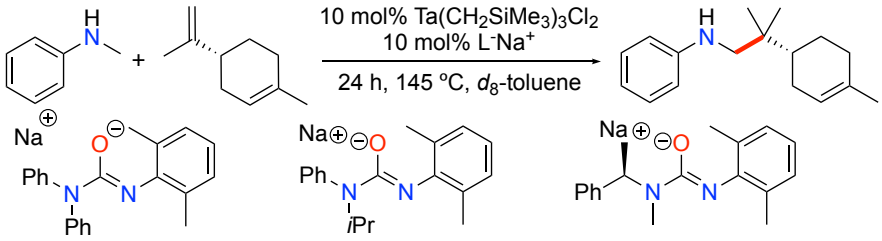

3.1: 38% Conversion[b]	**3.2**: 57% Conversion[b]	**3.3**: 40% Conversion[b,c]

[a]Reaction conditions: amine (0.5 mmol), (*R*)-(+)-limonene (0.5 mmol), $Ta(CH_2SiMe_3)_3Cl_2$ (0.025 mmol), ligand salt (0.025 mmol), d_8-toluene (0.5 g). Conversion determined by ^{1}H NMR spectroscopy. [b] 0.05 mmol $Ta(CH_2SiMe_3)_3Cl_2$ and ligand salt used. [c] The same conversion value was observed when using either enantiopure or racemic batches of **3.3**.

Next, in Table 3.1b, we explored the use of various *N,O*-chelating ureate ligand salts (**3.1**, **3.2**, **3.3**) in combination with our preferred Ta-alkyl starting material to generate catalyst systems in situ. As in previous work in Chapter 2 using $Ta(CH_2SiMe_3)_3Cl_2$ precursors, a 1:1 in situ combination of ligand salt with this Ta-alkyl precursor results in the formation of a catalytic system upon ligand substitution as characterized by ^{1}H-NMR spectroscopy. For example, the combination of $Ta(CH_2SiMe_3)_3Cl_2$ with **3.3** shows a disappearance of $SiCH_3$ (0.24 ppm) and CH_2SiMe_3 (2.04 ppm) protons of the $Ta(CH_2SiMe_3)_3Cl_2$ starting material and new peaks that form at 0.34 ppm, and 2.18 ppm, respectively, upon ligand coordination (Figure. A.50 Appendix A).

Initial efforts focused on using previously reported ligand salts **3.1** and **3.2**[79] and a new ligand **3.3** which features a chiral alkyl substituent. Investigations of 1-octene and (R)-(+)-limonene with *N*-methylaniline showed that **3.3** had comparable reactivity to the best previously reported catalyst with **3.1**, but does not perform as well as **3.2** for the transformation using (R)-(+)-limonene. However, **3.3** offers several practical advantages in that it is easily prepared on multi-gram scale and it is the only soluble ligand salt, making it best for the reliable in situ preparation of the catalyst. Furthermore, **3.3** allows for a comparison of reactivity and selectivity between enantiopure and racemic ligand batches. Unfortunately, investigations using enantiopure **3.3** towards enantioselective catalysis with 1-octene were unsuccessful (ee < 5%), indicating that the location of the stereocenter in this position on the ligand, which is distant to the metal center, does not adequately influence enantioselectivity. This is a similar issue to the one encountered with chiral cyclic ureate ligand strategies in Chapter 2.

The racemic variant of **3.3** was tested and the same conversion over 1 h was observed. In reactions with (R)-(+)-limonene, the Ta *N,O*-chelated catalyst systems offer selectivity for the branched product, as evidenced by two diastereotopic singlets at 0.97 and 0.93 ppm, integrating

for 3H each, in reference to the multiplet, integrating to 1H, of the enantiotopic proton. Stereochemical reaction outcomes were identical using both enantiopure and racemic **3.3** (Figure. C.3, Figure. C.4, Appendix C). Due to the practical advantages and the lack of influence of the remote stereocenter, the racemic variant was used for the remainder of this chapter and this thesis.

3.2.2 Substrate Scope

Next, we explored the hydroaminoalkylation substrate scope using our *in situ* formed catalyst system with both (*R*)-(+)-limonene, (1*S*)-(-)-β-pinene as representative terpenes (Table 3.2; limonene at the top and pinene at the bottom). Regioselectivity for (R)-(+)-limonene hydroaminoalkylation can be determined by NMR spectroscopy, as described above. Here, regardless of the aniline derivative, only the branched product and unreacted starting materials were observed. This clean reactivity lends itself to rapid isolation and purification of the targeted amine products. By using a simple filtration with a silica plug, the desired product is always first to elute, with some contaminating unreacted alkene substrate. Unreacted terpene can be easily removed under vacuum to give pure products as yellow oils, as evidenced by ^{1}H and $^{13}C\{^{1}H\}$ NMR spectroscopy, and further characterized by GC-MS or HPLC (see Experimental section). Note these isolated yields are reported for consistent reaction conditions and have not been optimized for each substrate combination.

Table 3.2. Hydroaminoalkylation scope using (R)-(+)-limonene and pinene (1S)-(-)-β-pinene.

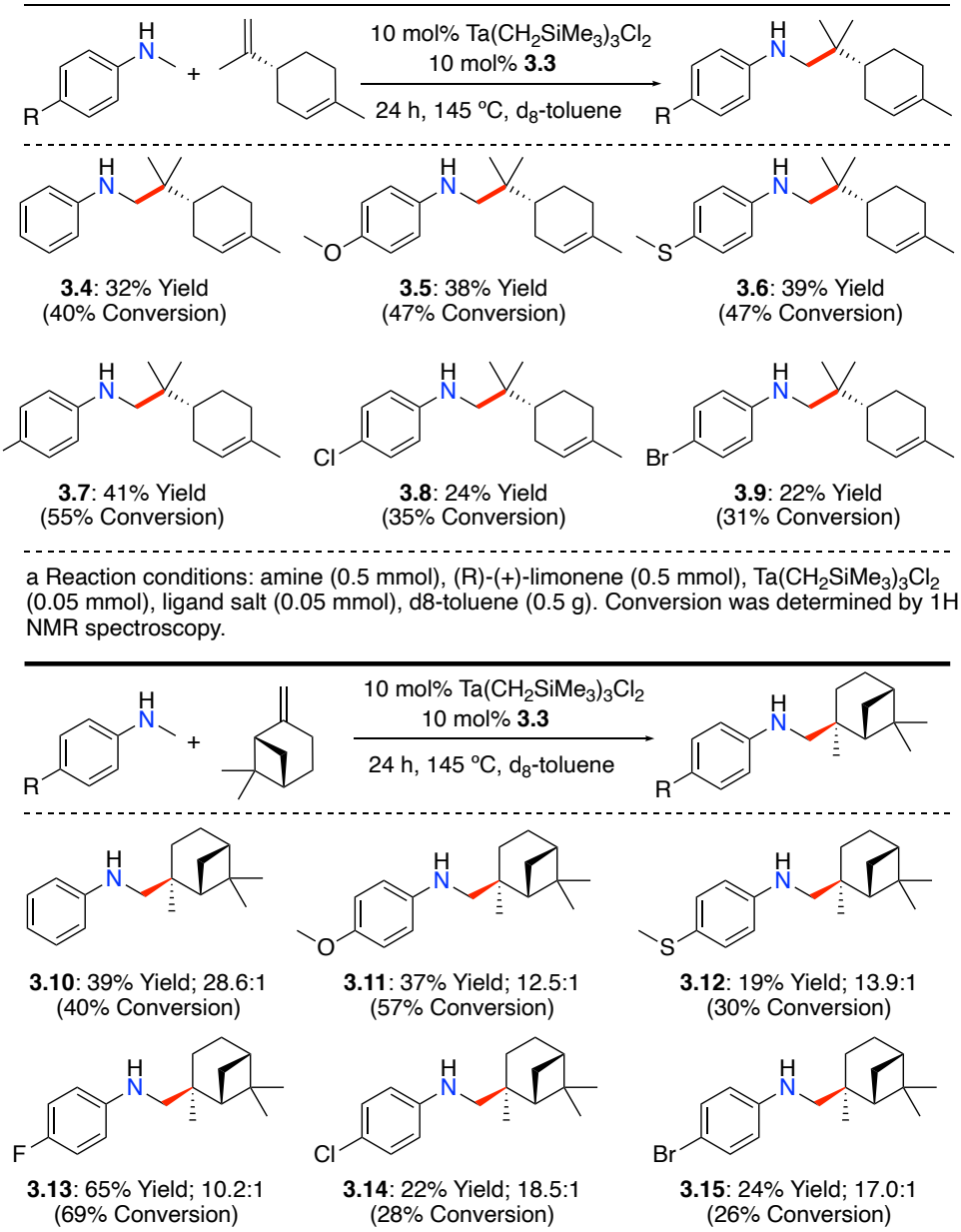

a Reaction conditions: amine (0.5 mmol), (R)-(+)-limonene (0.5 mmol), $Ta(CH_2SiMe_3)_3Cl_2$ (0.05 mmol), ligand salt (0.05 mmol), d8-toluene (0.5 g). Conversion was determined by 1H NMR spectroscopy.

a Reaction conditions: amine (0.5 mmol), (1S)-(-)-pinene (0.5 mmol), $Ta(CH_2SiMe_3)_3Cl_2$ (0.05 mmol), ligand salt (0.05 mmol), d8-toluene (0.5 g). Conversion was determined by ^1H NMR spectroscopy. Diastereoselectivity values are displayed as ratios, with the major diastereomer drawn and the ratio determined by GC-MS analysis.

As a demonstration that improved yields can be obtained for **3.4**, two sequential additions of 10 mol% catalyst solution (the second aliquot being added after 24 h) can be added to the

substrate solution to increase the conversion from 48% to 71% (Scheme 3.1). Notably, prolonged reaction times (up to 48 h) without the sequential addition of catalyst do not improve reaction yields. Likewise, one reaction with 20 mol% catalyst loading added in one batch only offers 51% conversion. These results are consistent with slow catalyst decomposition that appears to occur when using these naturally sourced substrates due to suspected trace impurities in terpene substrates.

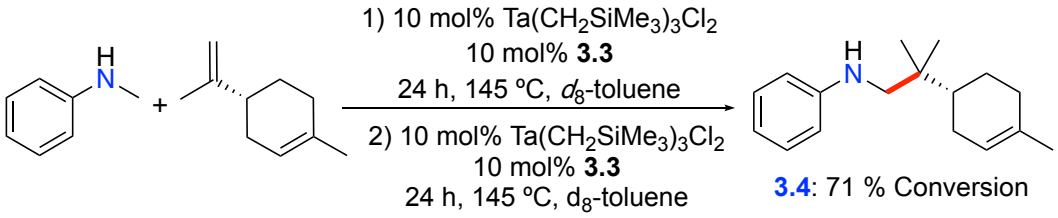

Scheme 3.1. Optimized hydroaminoalkylation conditions using (R)-(+)-limonene as an alkene substrate.

When choosing amine substrates, we focused on commercially available aniline derivatives that included functionality that may be medicinally relevant (Table 3.1; products **3.5**-**3.9**). Furthermore, the inclusion of chloride (**3.8**) or bromide (**3.9**) substituents allows for subsequent modification. Also, ethers and thioethers can be demethylated,[155,156] to yield alcohols or thiols, which are suitable for additional reactions. Substrate electronic properties have a notable effect on reaction productivity, in which electron rich, pi-donating substituents typically result in higher reaction conversions. This is proposed to be due to the increased amine nucleophilicity resulting in improved coordination to promote associative protonolysis of Ta-C bonds in the turnover limiting step of the catalytic cycle (*vide infra*, Figure 3.3).[157]

Catalysis using (1S)-(-)-β-pinene presents steric and stereochemical challenges. First, the exocyclic double bond is incorporated into a sterically demanding strained bicycle that is prone to

isomerization.[158–161] Furthermore, diastereomeric products could be generated in the hydroaminoalkylation reaction, which sets a new stereocenter, in addition to the two defined stereocenters of the starting material (products **3.10**-**3.15**). This substrate is the only previously reported example of terpene hydroaminoalkylation, although reactivity required 54 h at 145 °C to realize 57% yield with a 16:1 d.r. [85] As noted above, hydroformylation and reductive amination strategies are often used to generate complex amine products. Both this strategy and typical late metal reactions would yield the complementary linear regioisomer. When using the catalyst system with **3.3**, the regioselectivity in the hydroaminoalkylation reaction remained excellent for the branched product, as characterized by the appearance of the diagnostic singlet of the enantiotopic methyl group (such as 1.32 ppm for product **3.10**).

3.2.3 Stereochemical Assignments and Mechanistic Implications

The stereochemical assignment of diastereomer **3.10** was made by comparing with previous literature[85], and further confirmed by X-ray crystallography of **3.13** (Figure 3.2). The *exo*-product is obtained preferentially and despite the steric congestion proximal to the newly formed C-C bond, the reaction proceeded smoothly. Excellent diastereoselectivity was observed for each product in Table 3.2b, as established by GC-MS and confirmed by ^{1}H-NMR spectroscopy. Next, we confirmed the retained enantiopurity of the product for product **7** using chiral HPLC (see Appendix C). Reactions using enantiopure or racemic batches of **3.3** resulted in the identical enantiopure product.

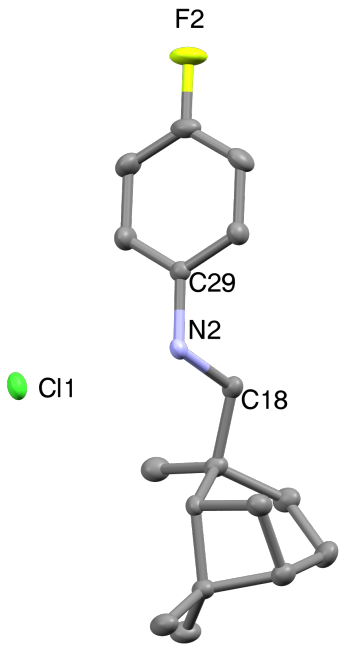

Figure 3.2. ORTEP representation of the X-ray crystallographic structure compound **3.13**. Ellipsoids plotted at 50% probability; nontertiary hydrogens omitted for clarity.

The proposed mechanism for group 5 catalyzed hydroaminoalkylation using Ta alkyl precursors is presented in Figure 3.3. This mechanism was discussed in more detail in chapters 1 and 2. In this chapter, the most important section is the alkene insertion (**C** to **E**) as it defines the regiochemistry and stereochemistry of the final product. Recent computational chemistry investigations of the mechanism of hydroaminoalkylation[44,157] showed that regioselectivity is affected by electronic effects consistent with the build-up of partial positive charge on the more substituted carbon during the alkene insertion step.[44] We believe that the catalyst system discussed throughout this chapter results in poor enantioselectivity because the stereocentre is too far from the reactive metal centre to have a significant influence on how alkene insertion proceeds. This idea was also discussed in Chapter 2.

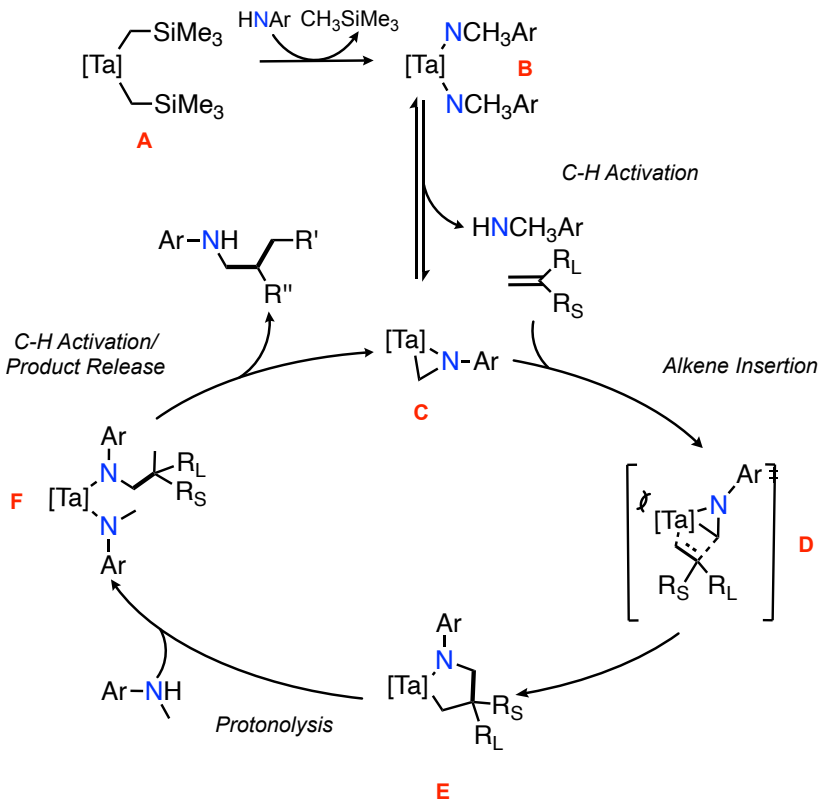

Figure 3.3. Proposed mechanism for hydroaminoalkylation using Ta alkyl precursors.

Overall, the synthetic terpenoid alkaloids generated in this chapter are vastly different than any previously terpenoid alkaloids discussed in total synthesis articles.[141] This is partly because hydroaminoalkylation represents a completely distinct disconnection strategy than most organic chemists would include when designing a retrosynthesis. As a result, I think the true power of hydroaminoalkylation is in diversity-oriented synthesis towards products that are based on privileged natural scaffolds. Through this early stage reaction, we are able to functionalize feedstocks as illustrated in this chapter and generate new products for biological testing. Chapter 4 expands on this idea in much more detail.

3.3 Conclusions

In summary, we have presented a hydroaminoalkylation catalyst system that can mediate reactivity with naturally occurring terpenes to access a new class of readily modified synthetic terpenoid-alkaloid products. The combination of $Ta(CH_2SiMe_3)_3Cl_2$ with a soluble, chiral ureate salt as a ligand allows for regioselective and diastereoselective catalysis in good yields. Although **3.3** is not a suitable candidate for asymmetric catalysis, we conclude that future work should focus on incorporating chiral elements into the ligand in closer proximity to the metal center. This catalyst system does yield only one product and no isomerization of the terpene framework is observed. This facilitates isolation of the desired aminated terpenes as pure oils. Thus, these readily accessed and modified products offer opportunities in diversity-oriented synthesis that could be used to access interesting biological activity.

3.4 Future Work

As noted throughout this chapter, the only terpene substrates used were limonene and pinene. The original goal of work with terpenes was to apply our hydroaminoalkylation methodology to more complex natural substrates, while highlighting potential chemoselectivity with diene substrates. We anticipate that many other commercially available terpenes that are produced by Canadian conifers can be competent substrates in regio- and diastereoselective hydroaminoalkylation. Figure 3.3 highlights examples of possible monoterpenes, sesquiterpenes and diterpene substrates. Further, using different amines, such as saturated amine heterocycles, in this chemistry can allow us to access more complex terpenoid alkaloid products. Chapter 4 will discuss efforts towards this research direction in more detail.

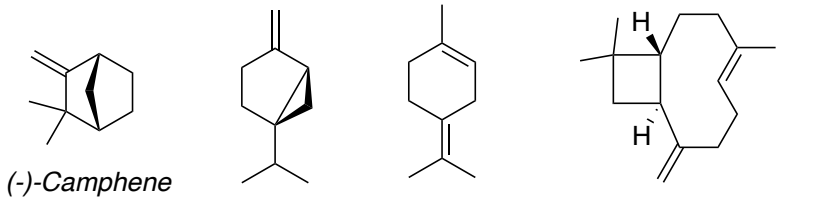

Figure 3.4. Examples of commercially available terpenes that we are interested in using for hydroaminoalkylation.

3.5 Experimental

3.5.1 Materials and Methods

All reactions were performed under a N_2 atmosphere using Schlenk or glovebox techniques, unless otherwise stated. $TaCl_5$ (Strem), $Ta(NMe_2)_5$ (Strem), (trimethylsilyl)methylmagnesium chloride (Aldrich), 1-chloro-2,2-dimethylpropane (Aldrich), (chloromethyl)trimethylsilane (Aldrich), *N*-methyl-1-phenylethanamine (Oakwood), triphosgene (Oakwood) and 2,6-dimethylaniline (Aldrich) were used as received. With the exception of *N*-methyl-4-(methylthio)aniline, all amines and alkenes were commercially available, dried over CaH_2 and distilled and degassed prior to use in catalytic experiments. 4-*N*-Methyl-4-(methylthio)aniline was synthesized according to literature protocols.[162] $[Ta(NMe_2)_3Cl_2]_2$,[131] and $Ta(CH_2SiMe_3)_3Cl_2$[124] were synthesized according to literature protocols. The ligand salts **3.1** and **3.2** were synthesized as previously reported.[79] All glassware was dried in a 180 °C oven overnight before use. Toluene, hexanes and Et_2O were dried over activated alumina columns and stored over activated molecular sieves (4 Å). d_8-Toluene was degassed using freeze-pump-thaw cycles and dried on molecular sieves before use. Experiments conducted on an NMR tube scale were performed in J. Young NMR tubes (8" x 5 mm) sealed with screw-type Teflon caps.

^{1}H and $^{13}C\{^{1}H\}$ NMR spectra were recorded on Bruker 300 MHz and 400 MHz Avance spectrometers at ambient temperature. Chemical shifts (δ) are given relative to the corresponding residual protio solvent and are reported in parts per million (ppm). Coupling constants J are given in Hertz (Hz). The following abbreviations are used to indicate signal multiplicity: s = singlet, d = doublet, t = triplet, q = quartet, m = multiplet, and br = broad. Assignment of the signals was carried out using 1D (^{1}H, $^{13}C\{^{1}H\}$) and 2D (COSY, HSQC and HMBC) NMR experiments. High resolution mass-spectra (HRMS) were measured by the mass spectrometry services at University of British Columbia, UBC on a Kratos MS-50 spectrometer using a Bruker maXis Ultra-High Resolution tandem TOF (UHR-Qq-TOF) mass spectrometer using a positive electrospray ionization source. Fragment signals are given in mass per charge number (m/z). HPLC analyses were run on an Agilent Series 1100 (detector: UV/VIS, operating at the stated wavelength given in nm) using the specified column (Chiralcel OJ-RH, length: 15 cm, inner diameter: 4.6 mm, particle size: 5 μm), flow rate of the solvent (0.5 mL/min), and sample injection volume (1 μL; sample concentration approximately 1 mg/mL) unless otherwise stated. Solvent system for all HPLC runs was 55% MeCN and 45% H_2O, each with 0.5% TFA by volume. The total runtime was 15 min, with a maximum pressure of 85 bar. Retention times t_R are stated in minutes (min). GC/MS analyses were conducted on an Agilent 7890B GC with an Agilent 5977 inert CI mass detector, utilizing methane as the ionization gas. Single-crystal X-ray structure determination was performed on an APEX II diffractometer at the Department of Chemistry, University of British Columbia, by Samuel Griffin.

3.5.2 Synthesis of a Urea Proligand and Ligand Salt

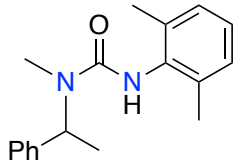

Synthesis of 3-(2,6-dimethylphenyl)-1-methyl-1-(1-phenylethyl)urea: Prepared following a modified literature procedure[163] in which 2,6-dimethylaniline (2.25 g, 18.5 mmol) was dissolved in dichloromethane and the solution was cooled to 0 °C. Triphosgene (1.81 g, 6.10 mmol) was added in portions as a solid. The solution was stirred for five minutes after which *N,N*-diisopropylethylamine (4.78 g, 37 mmol) was added and the cold bath removed. The solution was stirred for 1 h and *N*-methyl-1-phenylethan-1-amine (2.5 g, 18.5 mmol) and a second portion of *N,N*-diisopropylethylamine (2.39 g, 18.5 mmol) were added. The solution was stirred for an additional hour, and then diluted with 1M HCl. The organic phase was washed three times with 1M HCl, dried over $MgSO_4$, filtered, and concentrated by rotary evaporation to give the crude product. Recrystallization from a concentrated ethyl acetate solution provided the desired compound as a white solid (3.48 g, 66.9%*)*: ^{1}H NMR ($CDCl_3$, 300 MHz, 298 K): δ 7.41-7.26 (overlapping m, 5H, *o*-C_6H_5 *m*-C_6H_5, and *p*-C_6H_5), 7.04 (s, 3H, C_6H_3), 5.86 (br s, 1H, N*H*), 5.59 (q, $^3J_{H\text{-}H}$ = 6.9 Hz, 1H, C*H*CH_3), 2.79 (s, 3H, CH_3), 2.19 (s, 6H, 2,6-(CH_3)$_2C_6H_3$), 1.57 (d, $^3J_{H\text{-}H}$ = 7.1 Hz,C(Ph)CH_3) ppm. ^{13}C{^{1}H} NMR ($CDCl_3$, 75 MHz, 298 K): δ 156.35 (*C*=O), 141.83, 135.62, 135.57, 128.67, 128.10, 127.32, 126.92, 126.38, 77.16, 52.82, 29.55, 18.46, 17.05 ppm. HRMS (ESI): *m/z* calcd for $C_{18}H_{23}N_2O$ [M+H$^+$]: 283.1810. Found: 283.1809. Anal. Calcd. for $C_{18}H_{22}N_2O$: C, 76.56; H, 7.85; N, 9.92; Found: C, 76.77 ; H, 7.81 ; N, 9.93 (avg. of two runs).

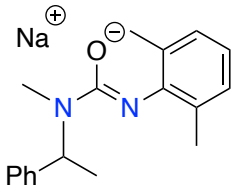

Synthesis of sodium (2,6-dimethylphenyl)(methyl(1-phenylethyl)carbamoyl)amide: $NaN(SiMe_3)_2$ (1.88 g, 10.26 mmol) was added in portions to a suspension of 3-(2,6-dimethylphenyl)-1-methyl-1-(1-phenylethyl)urea (2.9 g, 10.28 mmol) in toluene (~5 mL) and stirred overnight at room

temperature. The volatiles were then removed at low pressure and the resulting solid was thoroughly washed with hexanes (3 x 5 mL) and dried to give the sodium salt as a colorless powder. Yield (2.69 g, 86%). NMR data hints towards the existence of pair of isomers in solution that can be observed at a NMR time scale. Due to this, the chemical shifts in the ^{13}C NMR spectrum are given as an average, instead of having each chemical shift assigned to each isomer. ^{1}H NMR (toluene-d_8, 300 MHz, 298 K): δ 7.14-6.88 (overlapping m, 7H, *o*-C_6H_5 *m*-C_6H_5, and C_6H_3), 6.79 (t, $J_{H\text{-}H}$ = 7.4 Hz, 1H, *p*-C_6H_5), 5.30-5.11 (m, 1H, C*H*CH_3), 2.25 (s, 3H, NCH_3), 2.16 (s, 6H, 2,6-(CH_3)$_2C_6H_3$), 1.21 (d, $^{3}J_{H\text{-}H}$ = 7.00 Hz,C(Ph)CH_3) ppm. $^{13}C\{^{1}H\}$ NMR (toluene-d_8, 100 MHz, 298 K): δ 161.78 (C=O), 150.57 (*i*-C_6H_3), 144.50(*i*-C_6H_5), 129.62 (*m*-C_6H_3), 126.87 (*m*-C_6H_5), 126.14 (*o*-C_6H_5), 119.71 (*p*-C_6H_3), 54.68 (*C*H), 30.92 (N*C*H_3), 19.57 (C(Ph)CH_3) 18.13 (C(Ph)CH_3) ppm.

3.5.3 In situ Generation of the Precatalyst

The *in situ* formation of the tantalum-based precatalysts was studied by reacting equimolar amounts of $Ta(CH_2SiMe_3)_3Cl_2$ and the ligand salt **3.3** in a sealed J young tube in d_8-toluene (*vide infra*). Partial signal disappearance for SiCH_3 (0.24 ppm) and CH_2SiMe$_3$ (2.04 ppm) protons of $Ta(CH_2SiMe_3)_3Cl_2$ was observed after 1 h. New sets of signals corresponding to the new complex appear at δ 0.34 ppm (SiCH_3 peak) and δ 2.18 ppm (CH_2SiMe$_3$ peak).

3.5.4 General Catalytic Procedure

Unless otherwise stated, $Ta(CH_2SiMe_3)_3Cl_2$ (0.05) was weighed into a vial, followed by addition of the ligand salt (0.05 mmol). Toluene-d_8 (200 mg) was added and the resultant mixture was left for 15 minutes. Aniline (0.5 mmol), followed by limonene or β-pinene were then added (0.5 mmol) with a micropipette. The vials were rinsed with 300 mg of toluene-d_8 and transferred into a J. Young NMR tube. An initial ^{1}H NMR spectrum was recorded, and the sample was added to a pre-heated oil bath at 145 °C for 24 h. All conversion values were determined by ^{1}H NMR

spectroscopy. After quenching the reaction and removal of all reaction solvent, the resulting amine was purified *via* a silica-filtration (hexanes:EtOAc = 9:1) and dried *in vacuo* overnight to afford the desired product.

3.5.5 Characterization of Amine Products and Enantioselectivity Data

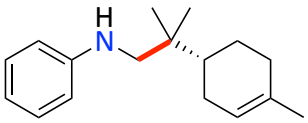

Synthesis of (*R*)-*N*-(2-methyl-2-(4-methylcyclohex-3-en-1-yl)propyl)aniline: Synthesized using the above description: limonene (71 mg, 0.5 mmol), *N*-methylaniline (54 mg, 0.5 mmol), **3.3** (15 mg, 0.5 mmol), $Ta(CH_2SiMe_3)_3Cl_2$ (25 mg, 0.5 mmol). Yield (39 mg, 32%). HPLC (OJ-RH, MeCN/H_2O = 55/45, 0.5 mL/min): t_R 12.7; indicating the presence of one enantiomer. ^{1}H NMR (400 MHz, $CDCl_3$, 298 K): δ 7.23-7.14 (m, 2H, Ar*H*), 6.74-6.58 (overlapping m, 2H, Ar*H*), 5.40 (s, 1H, C*H*=C(CH_3)), 2.98 (s, 2H, NCH_2), 2.11-1.76 (overlapping m, 5H, C*H* and CH_2), 1.67 (s, 3H, CH_3), 1.57-1.45 (m, 1H, C(*H*)H), 1.37-1.20 (m, 1H, C*H*), 0.97 (s, 3H, CH_3), 0.97 (s, 3H, CH_3) ppm. ^{13}C{^{1}H} NMR (100 MHz, $CDCl_3$, 298 K): δ 149.13, 134.11, 129.33, 121.12, 117.06, 112.78, 52.94, 40.36, 36.06, 31.54, 26.49, 24.09, 23.44, 23.31, 22.96 ppm. HRMS (ESI): m/z calcd for [M+H$^+$]: 244.2065, found: 244.2070.

Noted method differences for the data obtained in in Figure C.3 are as follows:

HPLC analyses were run on an Agilent Series 1100 (detector: UV/VIS, operating at the stated wavelength given in nm) using the specified column (Chiralcel OJ-RH, length: 15 cm, inner diameter: 4.6 mm, particle size: 5 µm), flow rate of the solvent (0.5 mL/min), and sample injection volume (1 µL; sample concentration approximately 1 mg/mL). Solvent for system was 55% MeCN and 45% H_2O, with 1% TFA by volume. The total runtime was 20 min, with a maximum pressure of 90 bar. The gradient stated above was used for the first 15 min of runtime, followed by 100%

MeCN for the final 5 min. Further, Optima solvents were purchased and used as received for analyses.

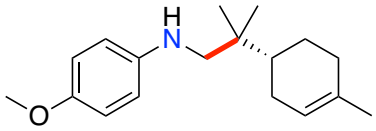

Synthesis of (*R*)-4-methoxy-*N*-(2-methyl-2-(4-methylcyclohex-3-en-1-yl)propyl)aniline: Synthesized using the above description: limonene (68 mg, 0.5 mmol), 4-methoxy-*N*-methylaniline (68 mg, 0.5 mmol), **3.3** (15 mg, 0.05 mmol), $Ta(CH_2SiMe_3)_3Cl_2$ (25 mg, 0.05 mmol). Yield (52 mg, 38%). ^{1}H NMR (400 MHz, $CDCl_3$, 298 K): δ 6.81-6.74 (m, 2H, Ar*H*), 6.63-6.56 (m, 2H, Ar*H*), 5.38 (s, 1H, C*H*=C(CH_3)), 3.75 (s, 3H, OCH_3), 2.91 (s, 2H, NCH_2), 2.08-1.72 (overlapping m, 5H, C*H* and CH_2), 1.64 (s, 3H, CH_3), 1.56-1.41 (m, 1H, C(*H*)H), 1.34-1.19 (m, 1H, C*H*), 0.99 (s, 3H, CH_3), 0.94 (s, 3H, CH_3) ppm. ^{13}C{^{1}H} NMR (100 MHz, $CDCl_3$, 298 K): δ 149.21, 129.31, 117.01, 112.76, 77.16, 55.63, 50.08, 40.99, 39.49, 38.53, 28.60, 28.34, 27.89, 26.54, 25.74, 24.41 ppm. HRMS (ESI): m/z calcd for [M+H$^+$]: 274.2171, found: 274.2174.

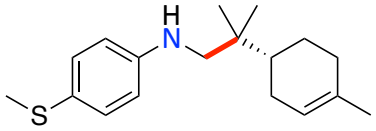

Synthesis of (R)-N-(2-methyl-2-(4-methylcyclohex-3-en-1-yl)propyl)-4-(methylthio)aniline: Synthesized using the above description: limonene (68 mg, 0.5 mmol), *N*-methyl-4-(methylthio)aniline (77 mg, 0.5 mmol), **3.3** (15 mg, 0.05 mmol), $Ta(CH_2SiMe_3)_3Cl_2$ (26 mg, 0.05 mmol). Yield (56 mg, 39%). ^{1}H NMR (400 MHz, $CDCl_3$, 298 K): δ 7.25-7.18 (m, 2H, Ar*H*), 6.61-6.51 (m, 2H, Ar*H*), 5.38 (s, 1H, C*H*=C(CH_3)), 3.67 (br s , 1H, N*H*), 2.95 (s, 2H, NCH_2), 2.41 (s, 3H, OCH_3), 2.05-1.75 (overlapping m, 5H, C*H* and CH_2), 1.65 (s, 3H, CH_3), 1.53-1.42 (m, 1H, C*H*), 1.33-1.20 (m, 1H, CH(*H*)), 0.97 (s, 3H, CH_3), 0.93 (s, 3H, CH_3) ppm. ^{13}C{^{1}H} NMR (100 MHz, $CDCl_3$, 298 K): δ 148.06, 134.12, 131.92, 123.65, 121.03, 113.31, 52.89, 40.29, 36.08, 31.49, 26.46, 24.06, 23.43, 23.28, 22.90, 19.56 ppm. HRMS (ESI): m/z calcd for [M+H$^+$]: 290.1942, found: 290.1939.

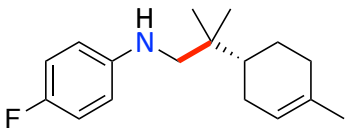

Synthesis of (*R*)-4-fluoro-*N*-(2-methyl-2-(4-methylcyclohex-3-en-1-yl)propyl)aniline: Synthesized using the above description: limonene (71 mg, 0.5 mmol), 4-fluoro-*N*-methylaniline (62 mg, 0.5 mmol), **3.3** (15 mg, 0.5 mmol), $Ta(CH_2SiMe_3)_3Cl_2$ (25 mg, 0.5 mmol). Yield (53 mg, 41%). ^{1}H NMR (400 MHz, $CDCl_3$, 298 K): δ 6.93-6.83 (m, 2H, Ar*H*), 6.59-6.49 (m, 2H, Ar*H*), 5.40 (s, 1H, C*H*=C(CH_3)), 3.49 (br s, 1H, N*H*), 2.92 (s, 2H, NCH_2), 2.08-1.77 (overlapping m, 5H, C*H* and CH_2), 1.66 (s, 3H, CH_3), 1.54-1.44 (m, 1H, C(*H*)H), 1.34-1.20 (m, 1H, C*H*), 0.98 (s, 3H, CH_3), 0.94 (s, 3H, CH_3) ppm. ^{13}C{^{1}H} NMR (100 MHz, $CDCl_3$, 298 K): δ 155.69 (d, J = 234.3 Hz), 145.57, 134.16, 121.10, 115.70 (d, J = 22.2 Hz), 113.51 (d, J = 7.3 Hz), 53.75, 40.33, 36.05, 31.52, 26.47, 24.07, 23.45, 23.32, 22.92 ppm. ^{19}F NMR (282 MHz, $CDCl_3$, 298 K): δ -128.99 ppm. HRMS (ESI): m/z calcd for [M+H$^+$]: 262.1971, found: 262.1969.

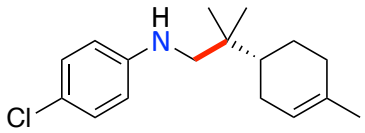

Synthesis of (*R*)-4-chloro-*N*-(2-methyl-2-(4-methylcyclohex-3-en-1-yl)propyl)aniline: Synthesized using the above description: limonene (68 mg, 0.5 mmol), 4-chloro-*N*-methylaniline (68 mg, 0.5 mmol), **3.3** (15 mg, 0.05 mmol), $Ta(CH_2SiMe_3)_3Cl_2$ (25 mg, 0.05 mmol). Yield (34 mg, 24%). ^{1}H NMR (400 MHz, $CDCl_3$, 298 K): δ 7.13-7.06 (m, 2H, Ar*H*), 6.58-6.48 (m, 2H, Ar*H*), 5.37 (s, 1H, C*H*=C(CH_3)), 2.92 (s, 2H, NCH_2), 2.08-1.73 (overlapping m, 5H, C*H* and CH_2), 1.64 (s, 3H, CH_3), 1.53-1.39 (m, 1H, C(*H*)H), 1.36-1.17 (m, 1H, C*H*), 0.97 (s, 3H, CH_3), 0.93 (s, 3H, CH_3) ppm. ^{13}C{^{1}H} NMR (100 MHz, $CDCl_3$, 298 K): δ 147.55, 134.20, 129.13, 121.01, 113.95, 53.23, 40.35, 36.14, 31.51, 26.48, 24.08, 23.45, 23.30, 22.92 ppm. HRMS (ESI): m/z calcd for [M+H$^+$]: 278.1675, found: 278.1671.

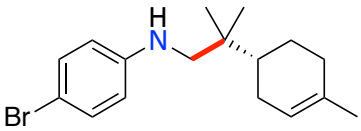

Synthesis of (*R*)-4-bromo-*N*-(2-methyl-2-(4-methylcyclohex-3-en-1-yl)propyl)aniline: Synthesized using the above description: limonene (71 mg, 0.5 mmol), 4-bromo-*N*-methylaniline (93 mg, 0.5 mmol), **3.3** (15 mg, 0.5 mmol), $Ta(CH_2SiMe_3)_3Cl_2$ (25 mg, 0.5 mmol). Yield (40 mg, 22%). ^{1}H NMR (400 MHz, $CDCl_3$, 298 K): δ 7.26-7.20 (m, 2H, Ar*H*), 6.51-6.45 (m, 2H, Ar*H*), 5.38 (s, 1H, C*H*=C(CH_3)), 3.64 (br s, 1H, N*H*), 2.92 (s, 2H, NCH_2), 2.08-1.72 (overlapping m, 5H, C*H* and CH_2), 1.65 (s, 3H, CH_3), 1.53-1.39 (m, 1H, C(*H*)H), 1.35-1.18 (m, 1H, C*H*), 0.98 (s, 3H, CH_3), 0.94 (s, 3H, CH_3) ppm. ^{13}C{^{1}H} NMR (100 MHz, $CDCl_3$, 298 K): δ 152.21, 134.14, 121.14, 115.09, 114.35, 114.33, 56.05, 40.39, 36.04, 31.55, 26.50, 24.09, 23.45, 23.34, 22.99 ppm. HRMS (ESI): m/z calcd for [M+H$^+$]: 322.1170, found: 322.1171.

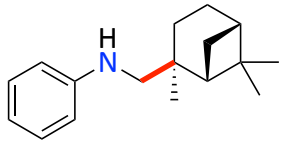

Synthesis of *N*-(((1*R*,2*S*,5*S*)-2,6,6-trimethylbicyclo[3.1.1]heptan-2-yl)methyl)aniline: Synthesized using the above description: pinene (68 mg, 0.5 mmol), *N*-methyl-aniline (54 mg, 0.5 mmol), **3.3** (15 mg, 0.05 mmol), $Ta(CH_2SiMe_3)_3Cl_2$ (26 mg, 0.05 mmol). Diastereoselectivity (GC): d.r > 20:1. HPLC (OJ-RH, MeCN/H_2O = 55/45, 0.5 mL/min): t_R 12.7; indicating the presence of one enantiomer. Yield (48 mg, 39%). ^{1}H NMR (400 MHz, $CDCl_3$, 298 K): δ 7.24-7.15 (m, 2H, Ar*H*), 6.74-6.60 (m, 5H, Ar*H*), 3.61 (br s, 1H, N*H*), 3.10 (d, $J_{H\text{-}H}$ = 11.7 Hz, NC(*H*)H), 2.91 (d, $J_{H\text{-}H}$ = 11.7 Hz, NC(H)*H*), 2.28-2.13 (m, 1H, C*H*), 2.05-1.77 (overlapping m, 4H, CH_2), 1.66-1.54 (overlapping m, 2H, CH_2), 1.32-1.26 (overlapping m, CH_3 and C*H*), 1.19 (s, 3H, CH_3), 1.12 (s, 3H, CH_3) ppm. The chemical shift match those reported previously in the literature.[85] HRMS (ESI): m/z calcd for [M+H$^+$]: 244.2065, found: 244.2061.

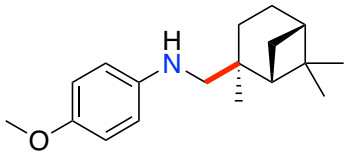

Synthesis of 4-methoxy-N-(((1R,2S,5S)-2,6,6-trimethylbicyclo[3.1.1]heptan-2-yl)methyl)aniline: Synthesized using the above description: β-pinene (68 mg, 0.5 mmol), 4-methoxy-*N*-methylaniline (68 mg, 0.5 mmol), **3.3** (15 mg, 0.05 mmol), $Ta(CH_2SiMe_3)_3Cl_2$ (25 mg, 0.05 mmol). Diastereoselectivity (GC): d.r > 10:1. Yield (50 mg, 37%). ^{1}H NMR (400 MHz, $CDCl_3$, 298 K): δ 6.81-6.75 (m, 2H, Ar*H*), 6.63-6.56 (m, 2H, Ar*H*), 3.75 (s, 3H, OCH_3), 3.03 (d, $J_{H\text{-}H}$ = 11.5 Hz, NC(*H*)H), 2.83 (d, $J_{H\text{-}H}$ = 11.5 Hz, NC(H)*H*), 2.23-2.12 (m, 1H, C*H*), 2.00-1.78 (overlapping m, 4H, CH_2), 1.67-1.51 (overlapping m, 2H, CH_2), 1.32-1.22 (overlapping m, CH_3 and C*H*), 1.16 (s, 3H, CH_3), 1.09 (s, 3H, CH_3) ppm. ^{13}C{^{1}H} NMR (100 MHz, $CDCl_3$, 298 K): δ 151.91, 143.63, 115.03, 114.02, 56.86, 56.00, 50.06, 40.97, 39.48, 38.47, 28.59, 28.31, 27.97, 26.54, 25.75, 24.41 ppm. HRMS (ESI): m/z calcd for [M+H$^+$]: 274.2171, found: 274.2172

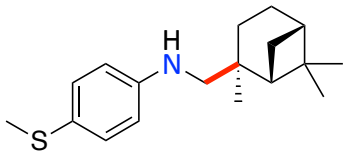

Synthesis of 4-(methylthio)-*N*-(((1*R*,2*S*,5*S*)-2,6,6-trimethylbicyclo[3.1.1]heptan-2-yl)methyl)aniline: Synthesized using the above description: β-pinene (68 mg, 0.5 mmol), *N*-methyl-4-(methylthio)aniline (77 mg, 0.5 mmol), **3.3** (15 mg, 0.05 mmol), $Ta(CH_2SiMe_3)_3Cl_2$ (25 mg, 0.05 mmol). Diastereoselectivity (GC): d.r > 10:1. Yield (28 mg, 19%). ^{1}H NMR (400 MHz, $CDCl_3$, 298 K): δ 7.25-7.18 (m, 2H, Ar*H*), 6.59-6.51 (m, 2H, Ar*H*), 3.63 (br s, 1H, N*H*), 3.05 (d, $J_{H\text{-}H}$ = 11.9 Hz, NC(*H*)H), 2.86 (d, $J_{H\text{-}H}$ = 11.9 Hz, NC(H)*H*), 2.40 (s, 3H, SCH_3), 2.22-2.13 (m, 1H, C*H*), 1.99-1.76 (overlapping m, 4H, CH_2), 1.65-1.48cc (overlapping m, 2H, CH_2), 1.28-1.21 (overlapping m, CH_3 and C*H*), 1.14 (s, 3H, CH_3), 1.08 (s, 3H, CH_3) ppm. ^{13}C{^{1}H} NMR (100 MHz, $CDCl_3$, 298 K): δ 148.22, 131.96, 123.54, 113.26, 55.54, 50.01, 40.95, 39.48, 38.55, 28.57, 28.33, 27.83, 26.50, 25.70, 24.40, 19.61 ppm. HRMS (ESI): m/z calcd for [M-Cl$^-$]: 290.1942, found: 290.1944.

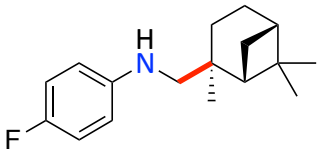

Synthesis of 4-fluoro-*N*-(((1R,2S,5S)-2,6,6-trimethylbicyclo[3.1.1]heptan-2-yl)methyl)aniline: Synthesized using the above description: β-pinene (68 mg, 0.05 mmol), 4-fluoro-*N*-methylaniline (62 mg, 0.5 mmol), **3.3** (15 mg, 0.05 mmol), $Ta(CH_2SiMe_3)_3Cl_2$ (25 mg, 0.05 mmol). Yield (84 mg, 65%). Diastereoselectivity (GC): d.r > 10:1. ^{1}H NMR (400 MHz, $CDCl_3$, 298 K): δ 6.95-6.86 (m, 2H, Ar*H*), 6.61-6.53 (m, 2H, Ar*H*), 3.45 (br s, 1H, N*H*), 3.06 (d, $J_{H\text{-}H}$ = 11.6 Hz, NC(*H*)H), 2.85 (d, $J_{H\text{-}H}$ = 11.6 Hz, NC(H)*H*), 2.26-2.17 (m, 1H, C*H*), 2.03-1.81 (overlapping m, 4H, CH_2), 1.69-1.53 (overlapping m, 2H, CH_2), 1.31 (s, 3H, CH_3), 1.28 (d, $J_{H\text{-}H}$ = 9.9 Hz, 1H, C*H*) 1.19 (s, 3H, CH_3), 1.13 (s, 3H, CH_3) ppm. ^{13}C{^{1}H} NMR (100 MHz, $CDCl_3$, 298 K): δ 155.67 (d, J = 234.2 Hz), 145.73 (d, J = 1.9 Hz), 115.70 (d, J = 22.2 Hz), 113.53 (d, J = 7.3 Hz), 56.41, 50.02, 40.95, 39.46, 38.48, 28.56, 28.30, 27.89, 26.48, 25.70, 24.38 ppm. ^{19}F NMR (282 MHz, $CDCl_3$, 298 K): δ -128.92 ppm. HRMS (ESI): m/z calcd for [M+H$^+$]: 262.1971, found: 262.1978.

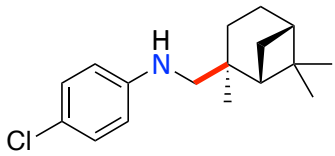

Synthesis of 4-chloro-*N*-(((1R,2S,5S)-2,6,6-trimethylbicyclo[3.1.1]heptan-2-yl)methyl)aniline: Synthesized using the above description: β-pinene (68 mg, 0.5 mmol), 4-chloro-*N*-methylaniline (70 mg, 0.5 mmol), L^-Na^+ (15 mg, 0.05 mmol), $Ta(CH_2SiMe_3)_3Cl_2$ (25 mg, 0.05 mmol). Diastereoselectivity (GC): d.r > 20:1. Yield (31 mg, 22%). ^{1}H NMR (400 MHz, $CDCl_3$, 298 K): δ 7.12-7.05 (m, 2H, Ar*H*), 6.55-6.48 (m, 2H, Ar*H*), 3.59 (br s, 1H, N*H*), 3.83 (d, $J_{H\text{-}H}$ = 11.8 Hz, NC(*H*)H), 2.85 (d, $J_{H\text{-}H}$ = 11.8 Hz, NC(H)*H*), 2.22-2.13 (m, 1H, C*H*), 1.99-1.76 (overlapping m, 4H, CH_2), 1.65-1.47 (overlapping m, 2H, CH_2), 1.26 (s, 3H, CH_3), 1.23 (d, $J_{H\text{-}H}$ = 10.3 Hz, 1H, C*H*) 1.14 (s, 3H, CH_3), 1.08 (s, 3H, CH_3) ppm. ^{13}C{^{1}H} NMR (100 MHz, $CDCl_3$,

298 K): δ 147.80, 129.10, 121.40, 113.76, 55.72, 50.01, 40.96, 39.50, 38.59, 28.58, 28.35, 27.85, 26.51, 25.70, 24.41 ppm. HRMS (ESI): m/z calcd for [M+H$^+$]: 278.1675, found: 278.1672.

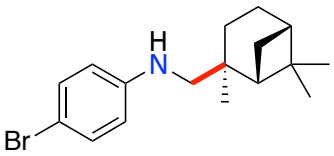

Synthesis of 4-bromo-*N*-(((1R,2S,5S)-2,6,6-trimethylbicyclo[3.1.1]heptan-2-yl)methyl)aniline: Synthesized using the above description: β-pinene (68 mg, 0.5 mmol), 4-bromo-*N*-methylaniline (94 mg, 0.5 mmol), L$^-$Na$^+$ (15 mg, 0.1 mmol), $Ta(CH_2SiMe_3)_3Cl_2$ (25 mg, 0.1 mmol). Diastereoselectivity (GC): d.r > 20:1. Yield (38 mg, 24%). ^{1}H NMR (400 MHz, $CDCl_3$, 298 K): δ 7.25-7.19 (m, 2H, Ar*H*), 6.50-6.44 (m, 2H, Ar*H*), 3.60 (br s, 1H, N*H*), 3.02 (d, $J_{H\text{-}H}$ = 11.7 Hz, NC(*H*)H), 2.82 (d, $J_{H\text{-}H}$ = 11.7 Hz, NC(H)*H*), 2.23-2.11 (m, 1H, C*H*), 2.00-1.75 (overlapping m, 4H, CH_2), 1.67-1.46 (overlapping m, 2H, CH_2), 1.26 (s, 3H, CH_3), 1.23 (d, $J_{H\text{-}H}$ = 10.2 Hz, 1H, C*H*) 1.13 (s, 3H, CH_3), 1.07 (s, 3H, CH_3) ppm. ^{13}C{^{1}H} NMR (100 MHz, $CDCl_3$, 298 K): δ 148.22, 131.96, 114.28, 108.35, 55.60, 50.03, 40.98, 39.50, 38.61, 29.85, 28.58, 28.35, 27.84, 26.51, 25.70, 24.41 ppm.. HRMS (ESI): m/z calcd for [M+H$^+$]: 322.1170, found: 322.1169.

Chapter 4: Hydroaminoalkylation Reactivity with *N*-Heterocycles

4.1 Introduction

4.1.1 C-H Alkylation of *N*-Heterocycles

N-heterocycles are privileged scaffolds in drug development, representing 59% of recently approved small-molecule treatments.[1] Saturated systems such as piperidine, azepane, and tetrahydroquinoline are particularly prevalent yet remain some of the most challenging heterocycles to selectively functionalize. The ability to selectively C-H activate amine heterocycles allows for the rapid generation of complex amine products from simple starting materials in one catalytic step. According to a recent review of catalytic C-H functionalization of heterocycles, less than 8% of reports disclose the ability to C-H functionalize saturated *N*-heterocycles and most demand the use of protected amine substrates.[164] Current literature to react saturated amine heterocycles systems is dominated by Csp^3-Csp^2 arylation[24,27,28], and Csp^3-Csp cyanation/alkynylation.[165,166] Photocatalytic cross-coupling can realize the α-C-H alkylation of protected saturated amines with activated electrophiles, such as such as aldehydes or alkyl halides.[32,112,167,168] The stoichiometric α-alkylation of unprotected *N*-heterocycles can be achieved by the addition of simple linear organometallic nucleophiles to transiently generated imines.[33,34] These methods require customized syntheses of activated alkylating agents that result in the generation of stoichiometric amounts of waste. An atom-economic alternative is to use simple alkenes as reagents for the catalytic alkylation of *N*-heterocycles by hydroaminoalkylation.

4.1.2 Hydroaminoalkylation of *N*-Heterocycles

Various catalytic approaches exist to address the challenge of directly alkylating saturated *N*-heterocycles by hydroaminoalkylation (Figure 4.1). Recently developed photocatalytic strategies (Figure 4.1a) employ protected *N*-heterocycles in combination with Michael acceptors

to generate the linear alkylation product.[109–111,114,169] Established late transition metal hydroaminoalkylation strategies for heterocycle alkylation[94,170] benefit from good functional group tolerance and dominant regioselectivity for the linear reaction product with modest diastereoselectivity (Figure 4.1b). However, late transition metal hydroaminoalkylation requires the use of protected *N*-heterocycles.[89,94,96–98,102,106,107,100,103,104]

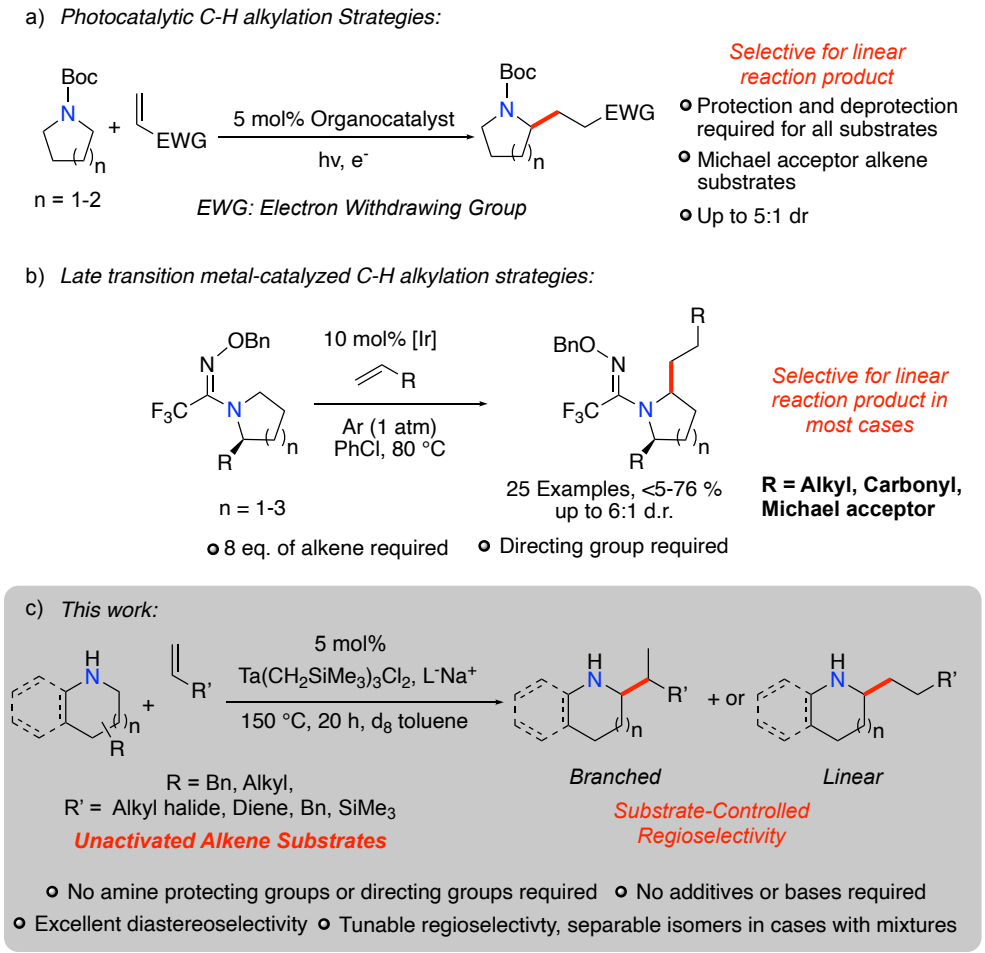

Figure 4.1. a) Photocatalytic C-H alkylation strategies for protected amine functionalization, b) A recent late transition-metal catalyzed method for reactions using amine surrogates, c) This work: a Ta-based catalyst system for reactions with unprotected amines and unactivated alkene substrates.

Early transition-metal hydroaminoalkylation is a powerful reaction for the preparation of the branched α-alkylation product with a variety of secondary aryl and alkyl amines *without* the need for protecting/directing groups or cocatalysts/additives.[5,35,36,38] Even though early transition metals are more abundant, less toxic and less expensive than their late transition metal counterparts, early transition metal catalyzed hydroaminoalkylation of *N*-heterocycles remains largely unexplored. To date, the only example using piperidine employs very reaction high temperatures (165 °C), long reaction times (143 h), and high catalyst loadings (10 mol %) to give the desired products.[81,88]

4.2 Scope of Chapter

This chapter focuses on developing a productive early transition-metal catalyst for reactivity with saturated *N*-heterocycles. Parts of this work are collaborative with students I have mentored throughout my PhD, and these will be outlined as they arise. Developing a truly broadly reactive hydroaminoalkylation catalyst allowed us to preliminarily probe isolated vs. *in situ* catalytic activity and investigate new substrate combinations. Most importantly, rapid *N*-heterocycle reactivity at relatively low catalytic loadings resulted in exploring questions around regioselectivity and diastereoselectivity that previously could not be explored due to unreactive catalysts. In later sections, we illustrate how hydroaminoalkylation can be used as a key step in novel disconnections towards different types of complex amine heterocycles.

Work in chapters 2 and 3 showed that highly active tantalum ureate hydroaminoalkylation catalysts can be prepared *in situ* for the efficient alkylation of both aryl and alkyl *N*-Me amines.[79,171] These chapters and ensuing publications showcased the tunable nature of ureate ligand salts to achieve improved catalytic activity and enhanced substrate scope, although reactivity with *N*-heterocycles was not achieved. Here we report tantalum ureate catalysts that can

be used for the rapid α-C-H alkylation of saturated *N*-heterocycles with alkene coupling partners (Figure 4.1c). A simple protocol for catalyst assembly *in situ* is featured, rigorous precatalyst characterization and catalytic evaluation is also presented. We show that this new catalyst system can be used at 5 mol% loading to give isolable unprotected α-alkylated 6 & 7 membered ring *N*-heterocycles. Investigations into alkene substrate scope revealed steric and electronic effects on regioisomeric control, with branched products being favored for unactivated alkenes while activated styrene derivatives could be used for the substrate-controlled formation of the linear regioisomer.

4.3 Results and Discussion

4.3.1 Screening Metal Starting Materials and *N,O*-Chelating Ligands

Initial reaction development efforts began by investigating the reaction between piperidine and 1-octene as benchmarks for *N*-heterocycle reactivity (see Experimental Section). Both substrates are inexpensive, commercially available, and represent challenging unactivated feedstocks. The first experiments tested the reactivity of $Ta(CH_2SiMe_3)_3Cl_2$, that has been shown to offer access to best-in-class catalysts using activated *N*-methylanilines as substrate.[79,171] Here, the benchmark reaction with piperidine over 24 h at 165 °C gave only 6 % conversion, as determined by ^{1}H NMR spectroscopy. ^{1}H NMR conversions were determined by integrating the peak at 2.96 ppm corresponding to one H of the CH_2 α to nitrogen in the hydroaminoalkylation product as compared with a disappearing piperidine peak at 2.63 ppm (see Supporting Information).

However, when $Ta(CH_2SiMe_3)_3Cl_2$ was combined with various *N,O*-chelating ureate salts, seven very active catalyst combinations resulted (Figure 4.2; ligands **4.1, 4.2, 4.5, 4.7, 4.9-4.11**). These reactions achieved full conversion after only 6 h of reaction time at 150 °C. Only branched

product was obtained in all cases as indicated by the diagnostic doublet at 0.84 ppm in the ^{1}H NMR spectrum. A cyclic ureate ligand salt (**4.4**) that has shown excellent reactivity with linear dialkyl amines was less effective when used with piperidine, even at longer reactions times of 12 h. When comparing these ureate ligand reactivities, small structural changes resulted in unpredictable changes in reactivity (eg. **4.5** vs **4.6**). Ligands **4.9**-**4.11** explore electronic effects upon catalysis, but no advantages could be realized with these varied *N*-aryl substituents.

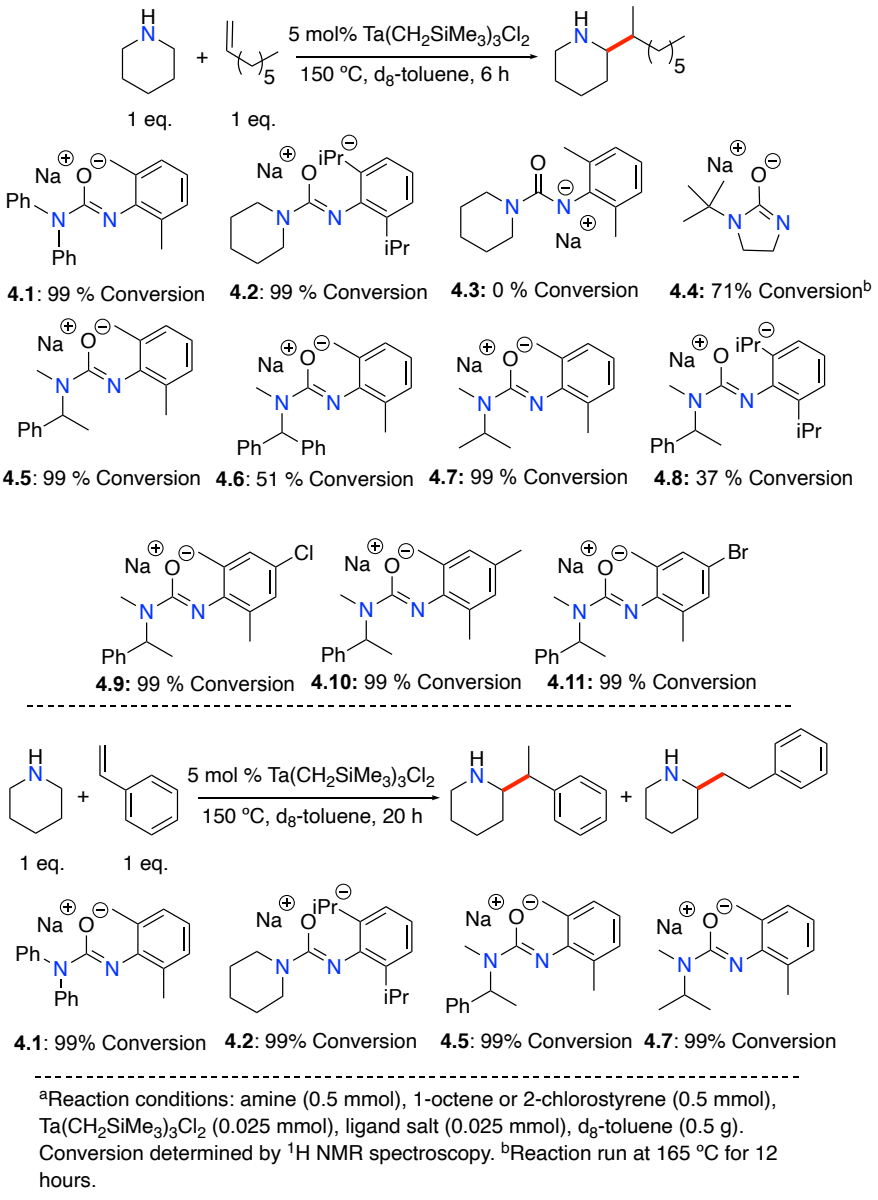

[a]Reaction conditions: amine (0.5 mmol), 1-octene or 2-chlorostyrene (0.5 mmol), $Ta(CH_2SiMe_3)_3Cl_2$ (0.025 mmol), ligand salt (0.025 mmol), d_8-toluene (0.5 g). Conversion determined by ^1H NMR spectroscopy. [b]Reaction run at 165 °C for 12 hours.

Figure 4.2. Screening ureate ligand salts for piperidine reactivity with 1-octene (top) and styrene (bottom).

Of the seven ureate options showing excellent reactivity, we chose to explore reactivity with styrene as an activated alkene substrate that is typically more reactive than octene, but has remained more challenged when combined with piperidine. The bottom scheme in Figure 4.2 highlights that a representative group of the catalyst mixtures displaying impressive reactivity with

1-octene could replicate these results using styrene, though longer reaction times of 20 h were required in these cases. This catalyst mixture is the only hydroaminoalkylation catalyst for the reaction of styrenes with piperidine. Further, these examples show that a group 5 hydroaminoalkylation catalyst can access substrate-dependent linear regioselectivity with styrene substrates as all entries in this bottom scheme generated significant amounts of the linear regioisomer. These are the first group 5 catalysts to consistently generate linear reaction products with any substrate combination in hydroaminoalkylation. Proposals around this regioselectivity shift and strategies to manipulate it are presented in a later section.

Overall, we chose to continue with a known ligand salt (Figure 4.2, ligand **4.5**)[171], as this proteoligand can be synthesized in large batches (up to 10 g in a single batch) with a high recrystallized yield of 86%. Further, the corresponding sodium salt for this ligand is soluble in toluene, improving the ease of reaction setup. This ligand is chiral, though previous work has shown that the remote incorporation of a stereocenter is not useful for enantioselective hydroaminoalkylation.[171] All work reported here was done using the racemic ureate ligand (+/-**4.5**, now written as **4.5** throughout this thesis).

4.3.2 A Broadly Reactive Catalyst

The *in situ* catalyst system above using ligand **4.5** is the only catalyst mixture that displays reactivity with all benchmark substrates for hydroaminoalkylation. This is the first truly general hydroaminoalkylation catalyst. As discussed in Chapter 2, alkyltantalum systems were identified as the most reactive since they could be used for reacting aromatic amine substrates with either terminal or internal alkene partners.[79] However, different combinations were required for either a terminal or internal alkene. These catalyst systems were also not reactive with aliphatic amines or *N*-heterocycles. As highlighted in an upcoming publication,[129] cyclic ureas display excellent

reactivity with aliphatic amines but cannot be used with internal alkenes or saturated *N*-heterocycles effectively. These limitations left significant opportunity for the development of a catalyst where users did not have to select different systems for each substrate combination.

Figure 4.3 shows reactions that were performed with a 1:1 amine: alkene ratio as with many of the other reactions outlined in this thesis. All four benchmark reactions were successful and results in reactivity comparable to previous best-in-class catalysts.[79,80,85,129] This catalyst is also simpler to use, as other options require isolated precatalysts, excess alkene, and sometimes laborious ligand syntheses. Recall, results in Chapter 3 highlighted the ease of synthesis, excellent solubility profile, and scalability of ligand **4.5**. Preliminary ^{1}H NMR reaction monitoring data for this catalyst system using *N*-methylaniline and 1-octene (Figure 4.4) illustrates rapid product formation.

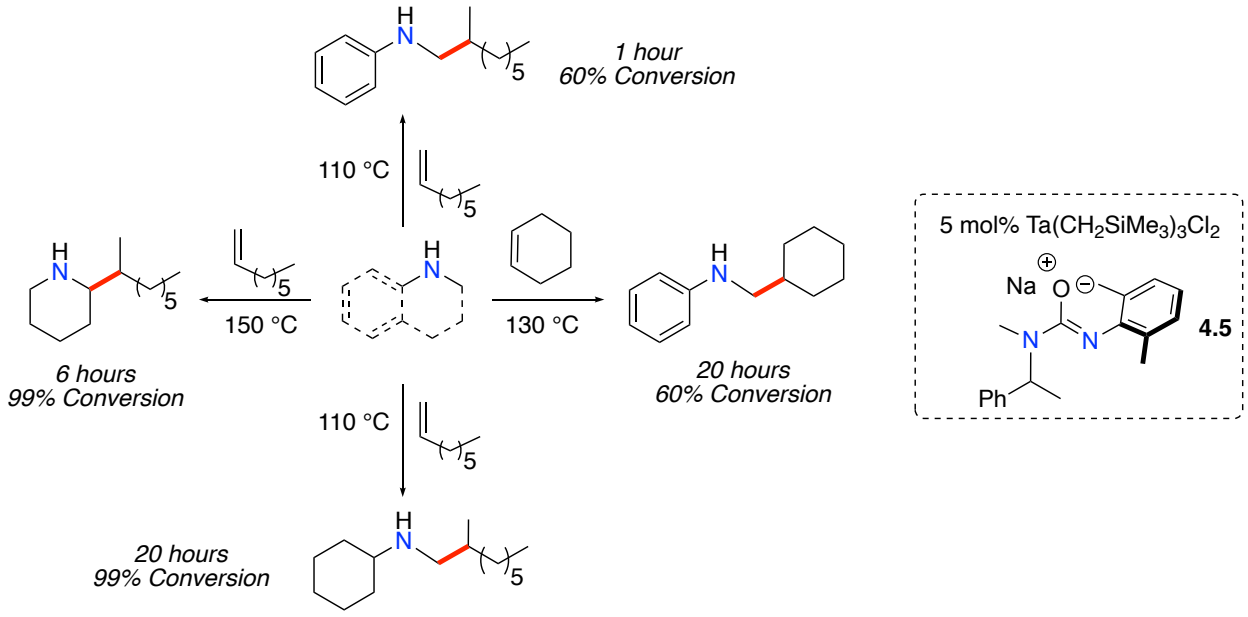

Figure 4.3. Optimized conditions for four different benchmark hydroaminoalkylation reactions with the first broadly applicable *in situ* catalyst system.

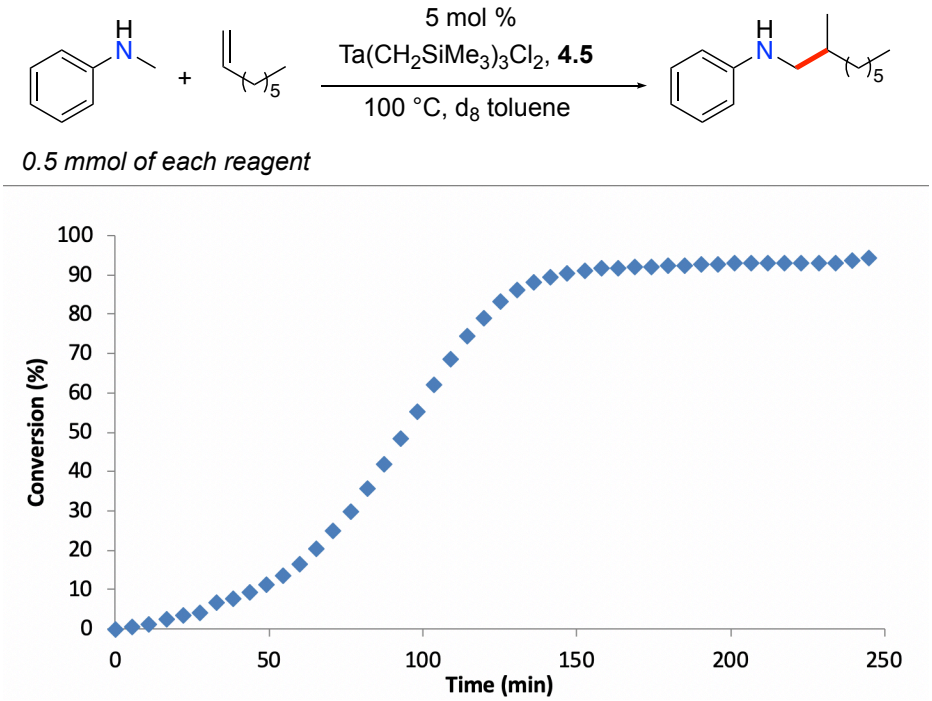

Figure 4.4. Preliminary reaction monitoring for hydroaminoalkylation using *N*-methylaniline and 1-octene with a broadly active *in situ* Ta ureate catalyst prepared using **4.5**. This reaction was monitored by NMR spectroscopy, data was not fitted at this time.

Beyond the impressive *N*-heterocycle reactivity displayed by this catalyst, it is also the only option to date for reactions of aliphatic amines with internal alkene partners (Scheme 4.1). Reactions using either aliphatic amines or internal alkenes are challenging in their own right, often requiring higher loadings or reaction temperatures in the few cases where they can be used at all.[38,172]

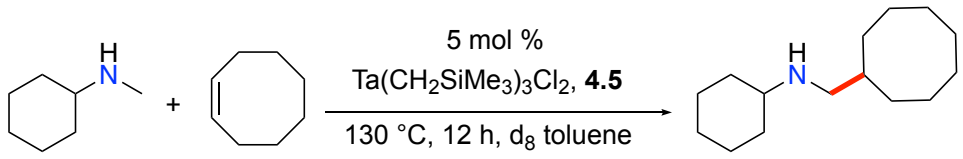

0.5 mmol of each reagent

4.12. *71% Conversion (Product Observed by GC-MS and ^{1}H NMR)*

Scheme 4.1. Using an *in situ* alkyltantalum ureate catalyst for previously unexplored reactivity between *N*-methylcyclohexylamine and cyclooctene as a representative internal alkene partner.

4.3.3 Isolated Precatalyst Characterization

Isolation of Ta ureate complexes has previously proven challenging.[79,171] Here, the isolation, purification and crystallographic characterization of the *N,O*-chelated complex resulting from the 1:1 reaction of ligand salt to $Ta(CH_2SiMe_3)_3Cl_2$ could be achieved (Figure 2b, **4.13**). The precatalyst **4.13** is confirmed to be monoligated, though these ureate ligands are bound much closer to Ta than comparable amidate or pyridonate ligand scaffolds (Ta-N lengths of 2.447(3) Å, and 2.307(1) Å for prominent amidate and pyridonate systems, respectively), [86,117] This is consistent with a more electrophilic metal centre. A more electron poor Ta results in more ionic bonding, behavior that has been previously invoked for improved polarization of metal-ligand bonds, which can help facilitate hydroaminoalkylation reactivity.[173]

The catalytic activity of the isolated precatalyst **4.13** was compared with *in situ* reactivity to ensure that the isolated material reactivity was consistent with the catalyst system assembled in situ. Both experiments provided complete conversion to the branched product using optimized reaction conditions (20 h, 150 °C, 5 mol%). Almost identical peaks between the ^{1}H NMR spectrum of isolated **4.13** and a previously published[171] spectrum of the corresponding *in situ* catalyst mixture further confirms **4.13** as the active catalytic species. All further reactions in this work were done using an in situ precatalyst generation for synthetic ease.

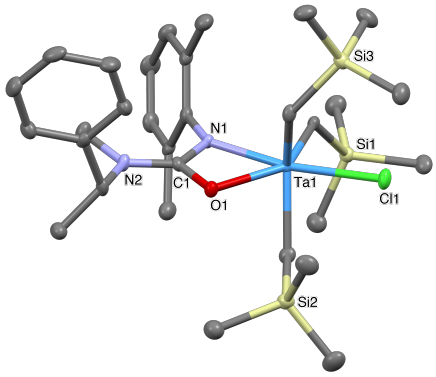

Figure 4.5. X-ray crystallographic data for the isolated precatalyst **4.13** that resulted in optimized reactivity with N-heterocycle substrates. Ellipsoids plotted at 50 % probability, H atoms omitted. Selected bond lengths (Å) and angles (°): Ta-O1: 2.164(2), C1-N2: 1.338(4), C1-O1: 1.305(4), Ta-N1: 2.155(3), C1-N1: 1.341(4), O1-Ta-N1: 60.29(9), N1-Ta-C4: 99.672.

4.3.4 Amine Scope with 1-Octene

With an easy-to-use catalyst system in hand, further exploration of the *N*-heterocycle substrate scope was undertaken. As shown in Figure 4.6 *in situ* assembled catalyst **4.13** (with ligand **4.5**) tolerates fused ring systems, varied ring sizes, and substituted *N*-heterocycles to give exclusively branched product formation with a simple unactivated alkene. 1-Octene was used in particular as this would allow us to directly compare reactivity using piperidine with that of other simpler amines highlighted in Chapters 2 and 3. High yields are observed with most heterocycles (entries **4.14**-**4.21**) and even a piperazine derivative can undergo hydroaminoalkylation in moderate yield (**4.22**). Tetrahydroquinoline or tetrahydroisoquinoline are the only other heterocycles that can be used with a variety of catalysts, although equally forcing conditions are required.[78,85] Furthermore, typically these products had to be isolated as the *N*-tosylate protected

products due to challenges in purifying and characterizing the free N-H functionalized heterocyclic products.

Here, the illustrated diastereoselective generation of the branched product (**4.14**, 11:1 dr as determined by GC-MS), can be rationalized by the mechanism (Figure 4.6b). Relative stereochemistry was determined by combining information from previous work[81] with 1D/2D NOESY experiments (see Experimental Section). This fused metallacycle undergoes alkene insertion via transition state **D** to five-membered metallacycle **E**. Another molecule of piperidine then initiates protonolysis, before C-H activation to release the desired product and regenerate the metallaaziridine **C**. As shown in Figure 4.6b, a catalytically active intermediate fused metallaaziridine-piperidine system undergoes facially selective alkene insertion such that the alkyl substituent is positioned on the opposite face of the metallaaziridine ring **C** (see in Figure 4.6b).[82,86,117,157]

a)

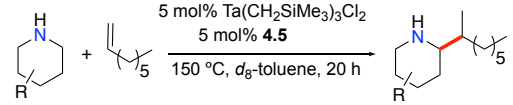

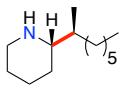

4.14: 99% Yield; 11:1 dr

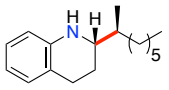

4.15: 65% Yield; >20:1 dr

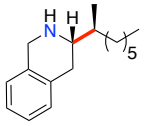

4.16: 99% Yield; >20:1 dr
4:1 rr

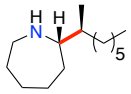

4.17: 91% Yield; >20:1

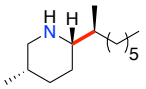

4.18: 99% Yield; 8:1:1 dr

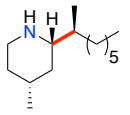

4.19: 84% Yield; 9:1:1 dr

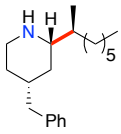

4.20: 84% Yield; 12:1 dr

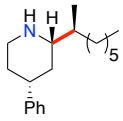

4.21: 99% Yield; >20:1 dr

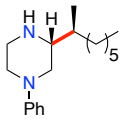

4.22: 48% Yield; >20:1 dr

[a] Reaction conditions: amine (1 mmol), alkene (1 mmol), $Ta(CH_2SiMe_3)_3Cl_2$ (0.05 mmol), ligand salt (0.05 mmol), d_8-toluene (0.6 g). Conversion was determined by ^1H NMR spectroscopy. NMR yields were determined using 1,3,5-trimethoxybenzene as an internal standard. Diastereoselectivity values are displayed as ratios, with the major diastereomer drawn and the ratio determined by GC-MS analysis.

b)

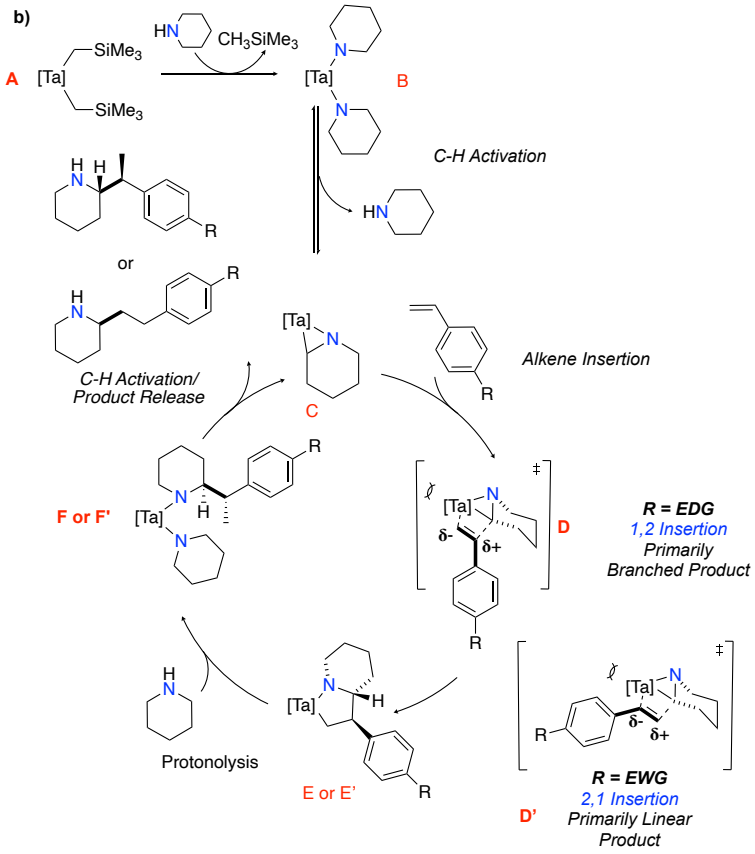

Figure 4.6. a) Amine heterocycle scope for C-H alkylation. All amines were reacted and purified as free amine substrates. b) The proposed mechanism for hydroaminoalkylation with alkyltantalum precursors and saturated *N*-heterocycles.

This preferred relative stereochemistry of the α,β-stereocenters in hydroaminoalkylation products is consistent across all heterocycles, including a 7-membered ring (Figure 4.6a, **4.17**). The desired free amine products for the major diastereomer can be isolated from its minor isomer counterpart by column chromatography, although isolated yields are reduced due to product that does not elute from the column. The tetrahydroisoquinoline substrate (**4.16**) shows good regioselectivity, as determined by NMR spectroscopy, as the isolated methylene group α to nitrogen at 3.97 ppm remained a singlet in the major product of the crude reaction mixture. While the benzylic C-H bond of this N-heterocycle has a lower bond dissociation energy, it is sterically inhibited from reactivity. Pyrrolidine was not reactive with this catalyst, potentially due to aggregation/oligomerization.[153] This observation contrasts reactivity observed with late transition-metal catalysts that typically prefer 5-membered rings over piperidine-based systems.[108,112]

Notably, **4.18**-**4.21**, in Figure 4.6a highlight the ability of this method to set the relative stereochemistry of up to three positions in a single, diastereoselective catalytic step. The relative configurations were confirmed using 1D- and 2D-NOESY NMR spectroscopy (See Experimental Section). We propose that this orientation of the substituent at the 3- or 4- position is due to steric interactions of this stereocenter with the octyl group during the alkene insertion step (Figure 4.6b, **D**). Substituted piperidine substrates were highly reactive, while 2-methylpiperidine showed no reactivity, even after 20 h. The substituted piperazine in **4.22** highlights the potential for additional heteroatoms in this methodology, albeit with a lower yield (48%). Unfortunately, 4-

methylpiperazine, unprotected piperazine, and morpholine show only starting materials remaining after heating and are all unsuitable substrates.

4.3.5 Alkene Scope

With the reactivity of *N*-heterocycles in hand, next the alkene scope of reactivity with piperidine was explored (Table 4.1). As expected, aliphatic alkenes (Table 4.1, **4.23**-**4.25**) generate only branched product with terminal alkenes and no reactivity with unactivated internal alkene substrates can be achieved, even with prolonged reaction conditions. This trend can be used to advantage to obtain complete selectivity for the terminal alkene of a representative diene substrate, albeit with lower diastereoselectivity (Table 4.1, **4.23**). A protected alcohol (Table 4.1, **4.24**) resulted in a product with excellent diastereoselectivity. Likewise, **4.25** illustrates reactivity with allyltrimethylsilane with excellent diastereoselectivity.

Next, an evaluation of reactivity with styrene derivatives was undertaken. The use of a variety of halide-containing styrene substrates in entries **4.32**-**4.37** and **4.40**-**4.46** expands the functional group tolerance of this method. These products all allow for access to post-hydroaminoalkylation cross-coupling strategies. Such halides are typically not possible for use in related late transition metal or photoredox-based hydroaminoalkylation catalysts. As shown previously,[81,87] vinyltrimethylsilane (Table 4.1, **4.47**) can be used to highlight the effect of alkene electronic effects on product regiochemistry, whereby only the linear product is observed with vinyltrimethylsilane. This result is consistent with a dominating α-silyl stabilized anion effect that inverts charge distribution in this vinyltrimethylsilane.[84]

Table 4.1. Alkene scope for hydroaminoalkylation with piperidine.

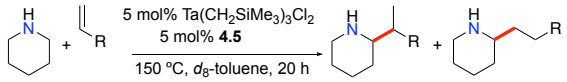

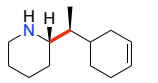

4.23: 99% Yield; 2.7:1

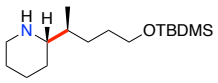

4.24: 94% Yield; 9:1

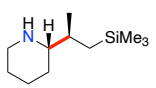

4.25: 99% Yield; 10:1

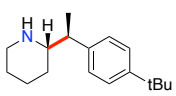

4.26: 65% Yield; 20:1 (99% Conversion)

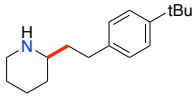

2.5: 1 Branched: Linear

4.27: 34% Yield (99% Conversion)

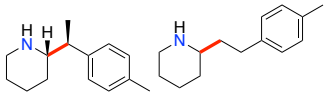

2.5: 1 Branched: Linear

4.28: 67% Yield; 14:1 (99 % Conversion)

4.29: 29% Yield (99% Conversion)

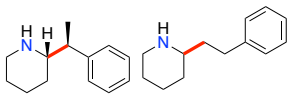

1:7: 1 Branched: Linear

4.30: 60% Yield; 5:1 (99% Conversion)

4.31: 40% Yield (99% Conversion)

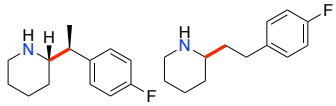

1.5: 1 Branched: Linear

4.32: 60% Yield; 19:1 (99% Conversion)

4.33: 39% Yield (99% Conversion)

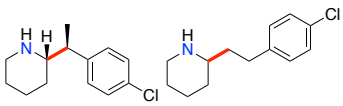

1.3: 1 Branched: Linear

4.34: 54% Yield; 20:1 (99% Conversion)

4.35: 46% Yield (99% Conversion)

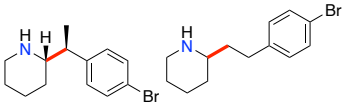

1.4: 1 Branched: Linear

4.36: 58% Yield; >20:1 (99% Conversion)

4.37: 42% Yield (99% Conversion)

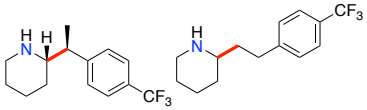

0.63: 1 Branched: Linear

4.38: 37% Yield; 20:1 (99% Conversion)

4.39: 55% Yield (99% Conversion)

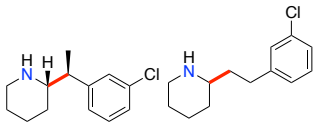

1: 1 Branched: Linear

4.40: 45% Yield; 20:1 (99% Conversion)

4.41: 53% Yield (99% Conversion)

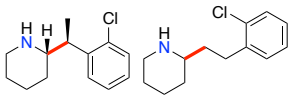

1.15: 1 Branched: Linear

4.42: 51% Yield; 5:1 (99% Conversion)

4.43: 49% Yield (99% Conversion)

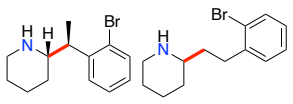

1.15: 1 Branched: Linear

4.44: 99% Conversion 5:1 dr

4.45: 99% Conversion

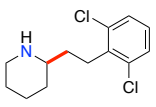

4.46: 45% Yield

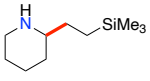

4.47: 68% Yield; 5.5:1

[a] Reaction conditions: amine (1 mmol), alkene (1 mmol), $Ta(CH_2SiMe_3)_3Cl_2$ (0.05 mmol), ligand salt (0.05 mmol), d_8-toluene (0.6 g). Conversion was determined by ^1H NMR spectroscopy. Yields are determined by NMR with 1,3,5-trimethoxybenzene as an internal standard. Diastereoselectivity values are displayed as ratios, with the major diastereomer drawn and the ratio determined by GC-MS analysis.

As noted in Table 4.1, all styrene substrates used resulted in significant amounts of both branched and linear regioisomers. By modifying the electronic features of these styrenes with different aryl substituents, substrate-controlled regioselectivity is realized while maintaining excellent reactivity. All reactions afforded product mixtures that were analyzed by quantitative NMR spectroscopy and GC-MS to determine product ratios. Notably, regioisomers and diastereomers could be separated, and often diastereoenrichment was observed upon purification on silica to obtain the major stereoisomer as a pure product (see Experimental Section).

Products **4.26**-**4.39** highlight hydroaminoalkylation reaction products from reacting piperidine with a series of electronically varied, para-substituted styrene substrates. The changes in regioselectivity can be correlated with previously observed alkene electronic effects using scandium[44] and titanium[60] catalyzed hydroaminoalkylation, whereby electron withdrawing substituents allow access to increasing amounts of linear products. A comparison of all the Cl containing styrene derivatives (**4.34** & **4.35**, **4.40** – **4.43**), in which only small differences in regioselectivity are observed, confirms that inductive electronic effects dominate over steric effects for altering regioselectivities. Meanwhile, diastereoselectivity values for the branched products were typically excellent. For example, reactivity with a representative *meta*-chlorostyrene maintained 20:1 diastereoselectivity (**4.40**). Only the sterically congested *ortho*-substituted styrene substrates eroded this diastereoselectivity to ~5:1 (Table 4.1, **4.42** and **4.44**).

With clear electronic trends observed in the regioselectivity of reactions with different styrene derivatives, a Hammett study was undertaken. Figure 4.7 depicts the quantitative dependence of branched: linear regioisomer ratios on the electronic effect of each styrene, as depicted using Hammett parameters for para-substituted materials.[174,175] Overall, reactions using styrenes with electron donating substituents resulted in more branched product (up to 2.5:1 B:L

with *para*-*tert*-butylstyrene), while styrenes with electron withdrawing groups could be used to generate more linear regioisomer (up to 1:1.6 B:L with *para*-trifluoromethylstyrene) at reaction completion. The two accessible alkene insertion transition states (Figure 4.6b) are proposed to be influenced by electronic effects such that electron withdrawing groups favor the polarization of substituted styrenes that support a buildup of negative charge in the transition state at the substituted carbon of the alkene. However, this effect with a tantalum catalyst is much more profound with piperidine, as the same optimized catalyst affords mostly branched product (~9:1 B:L) when *N*-methylaniline is reacted with styrene. The rationale for multiple regioisomers with piperidine substrates can be attributed to the bulky fused-ring tantallaziridine **C** that makes the typical branched product less sterically favorable.

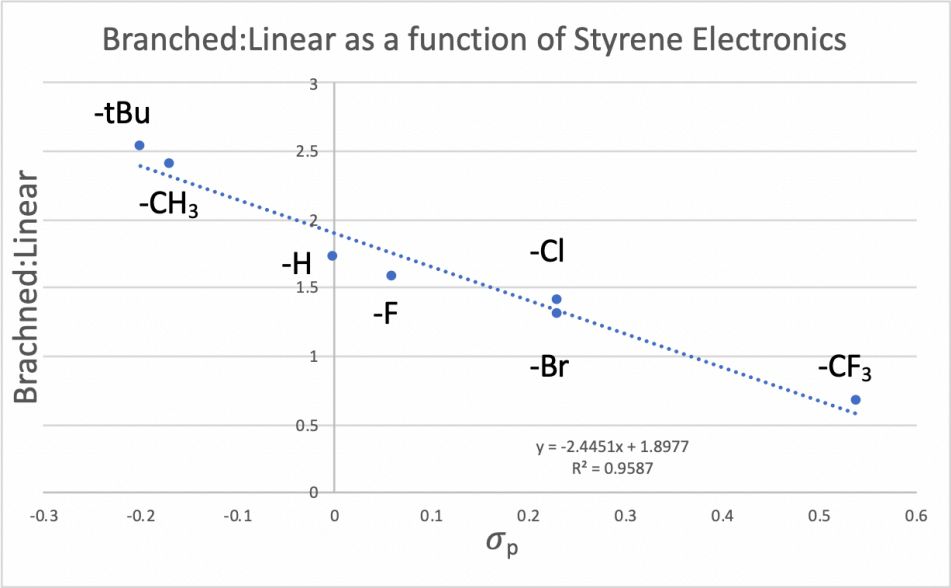

Figure 4.7. Branched: linear regioisomer ratios as plotted against Hammett parameters for hydroaminoalkylation reactions with a series of substituted styrene substrates.

4.3.6 Towards Hydroaminoalkylation Reactivity on the Benchtop

With a very promising catalyst system and excellent reactivity with challenging *N*-heterocycles in hand, the next sections of this chapter focus on making hydroaminoalkylation accessible to more organic chemists. First, we have patented this methodology with an eventual goal of making $Ta(CH_2SiMe_3)_3Cl_2$ commercially available as a stock solution in toluene so users could dispense this into reactions, as is done with alkylithium reagents. Dr. Rosca (who had helped developed the Ta alkyl catalysts in Chapter 2) has unpublished results where he has studied the stability of this Ta starting material in toluene solution and notes that it maintains its catalytic activity over months. It is important to recall in this section that $Ta(CH_2SiMe_3)_3Cl_2$ is not pyrophoric, so potential errors by users would not result in dangerous situations. As well, we highlighted ligand **4.5** in Chapter 3 as being soluble in toluene in both its protic and sodium salt forms. This allows for storage as a stock solution as well.

Thus, these stock solutions allowed for the test of hydroaminoalkylation reactions between piperidine and 1-octene with minimal glove box use (see Experimental Section). This experimental setup relied on syringe techniques with stock solutions of all reagents instead of weighing out solids in a glove box. Further, Schlenk techniques were not required.

Using such a modified catalyst preparation it was noted that after 20 h at 150 °C the results were identical (99% conversion) to those from reactions using *in situ* catalyst preparation in the glove box. We were also able to further challenge the system by using a batch of piperidine that was not distilled. Instead, the commercially available amine was dissolved in toluene and dried over activated sieves in a Teflon-sealed round bottomed flask for 30 minutes prior to use. These results illustrate the possibility for other groups to apply our *N*-heterocycle reactivity with easy to use alkyltantalum catalysts for the synthesis of complex amine materials.

4.3.7 Applications in Fused Heterocycle Syntheses

4.3.7.1 Indolizidine and Quinolizidine Alkaloids

After this initial work focusing on reactivity with *N*-heterocycles and the resulting product selectivity questions this raised, we shifted efforts towards making hydroaminoalkylation products that could undergo a second catalytic step and generate fused heterocycles. The first example of this aimed to synthesize indolizidine and quinolizidine products because these are complex scaffolds that could be rapidly accessed to exemplify the utility of hydroaminoalkylation.

Indolizidine and quinolizidine fused heterocyclic natural products are considered privileged structures in medicinal chemistry, yet published syntheses focus almost entirely on the natural variants without opportunity for significant diversification.[176–183] Further, there are few known strategies to access the non-natural variants targeted here.[184–186] Previous reports include stoichiometric transformations, generating significant waste and rarely incorporating catalysts. These methods also require the synthesis of specific substrates for each product combination, thereby limiting the potential of using these strategies for investigating structure-activity relationships of the resultant indolizidine or quinolizidine products (Figure 4.8a-c).[184–186]

Chapter 3 presented the importance of diversity-oriented synthesis, and here we are interested in expanding that approach to access entirely synthetic indolizidine and quinolizidine alkaloids in two catalytic steps. Furthermore, the strategy employed here features different disconnections than previously designed synthetic routes for accessing these products (Figure 4.8d).

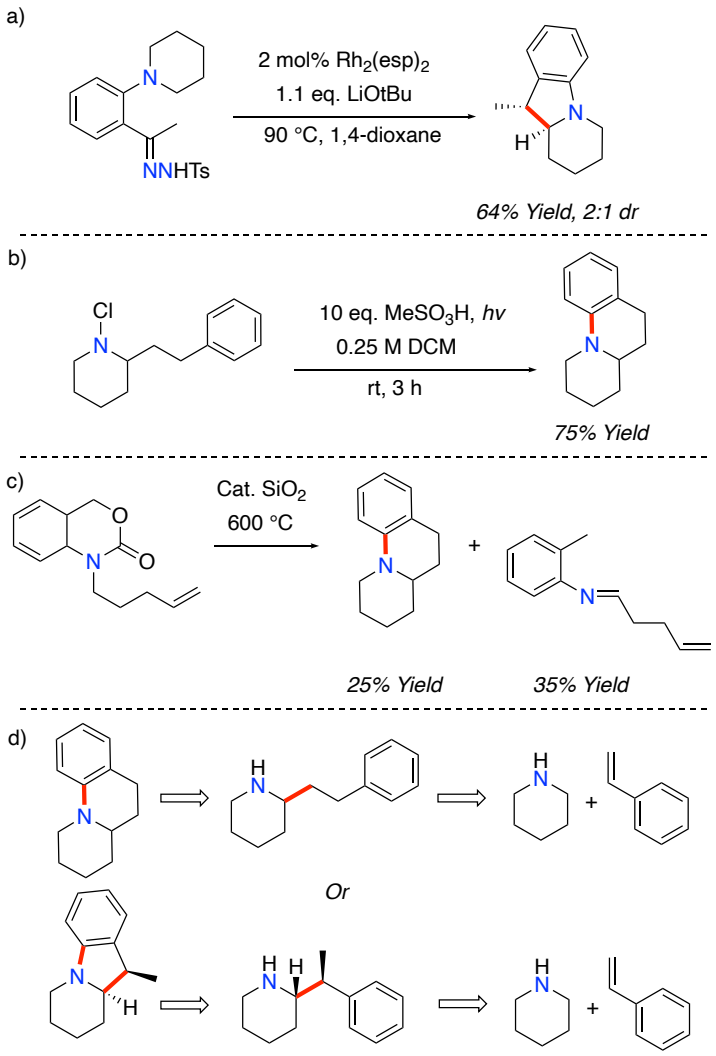

Figure 4.8. a) The only known previous strategy for making our desired benchmark indolizidine alkaloid. b) A radical-mediated strategy for synthesizing our desired benchmark quinolizidine product. c) A vacuum pyrolysis strategy for our quinolizidine product. d) The proposed disconnections for our fused alkaloid synthesis.

We became interested in these specific products because we could design them through a synthesis that uses halide-containing substrates that are often a challenge for late transition-metal counterparts. Our goal was to design a sequential hydroaminoalkylation then C-N bond formation

strategy to generate both indolizidine and quinolizidine alkaloid products in two catalytic steps (Scheme 4.2). It was important that this strategy featured substrates that were easily accessible and relatively inexpensive while using inexpensive and metals that are more abundant that late transition metals. In the scheme outlined below, the indolizine product is generated from the branched hydroaminoalkylation product and the quinolizidine originates the linear hydroaminoalkylation regioisomer.

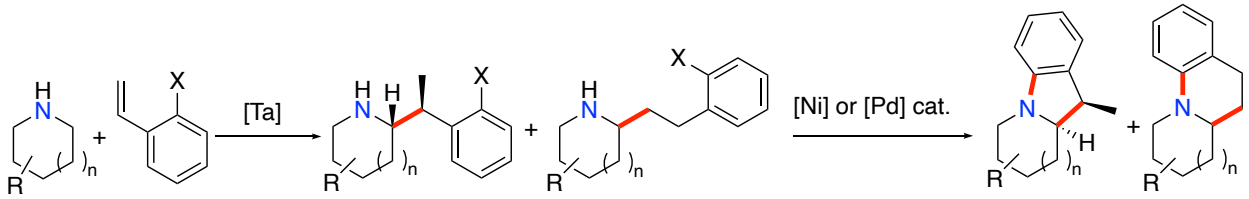

R = Alkyl, Aryl, OMe, NMe_2, n = 1,2, X = H, Cl, Br

Scheme 4.2. A sequential hydroaminoalkylation/ C-N bond formation strategy for the synthesis of indolizidine and quinolizidine alkaloids.

The results in this section of Chapter 4 have been completed in collaboration with both Dr. Karst Lenzen and Mr. Cameron Zheng, during their time as Schafer group members. I supervised Dr. Lenzen in screening potential C-H activation strategies for amination reactions that would have expanded that potential substrate scope for this method and reduced overall waste. I have mentored Cameron as he spends a portion of his graduate degree on developing Buchwald-Hartwig reaction conditions using Ni as the preferred catalyst. Complete data from Mr. Zheng will be presented in his own thesis at a later date.

When designing this method, hydroaminoalkylation conditions that had already been developed for the reaction of piperidine with a series of substituted styrene partners (5 mol% cat., 150 °C, 20 h) were explored. No further development of those conditions was developed in this section. Initial work with Dr. Lenzen aimed to employ a C-H activation catalyst to form the C-N

bond of the desired indolizidine and quinolizidine products. The success of a C-H activation strategy would allow us to use almost any styrene coupling partner, without restrictions on *ortho* substituents that might be required for the Buchwald-Hartwig reaction.

To test different C-H activation reactions, a model hydroaminoalkylation reaction was scaled up with piperidine and p-chlorostyrene as test substrates; over 1 g (5 mmol each) of alkene and amine starting materials were used (Scheme 4.3). This styrene was selected because it displays excellent reactivity in hydroaminoalkylation, and the *para* substituent allows for cleaner crude ^{1}H NMR spectra to assess potential C-H activation activity. Despite the larger reaction scale, there were no changes made to setup or purification as compared with smaller scale (0.1 mmol) reactions reported in earlier sections. This reaction was set up using a 20 mL scintillation vial instead of a typical 8 mL vial and a metal heating block as before. Purifying these reaction products allowed for enough isolated branched and linear regioisomeric material for screening of Pd-based C-H activation conditions. The reactions highlighted in Table 4.2 were inspired by literature examples available at the time.[3,187–193] We restricted these attempts to reactions involving homogeneous catalyst options.

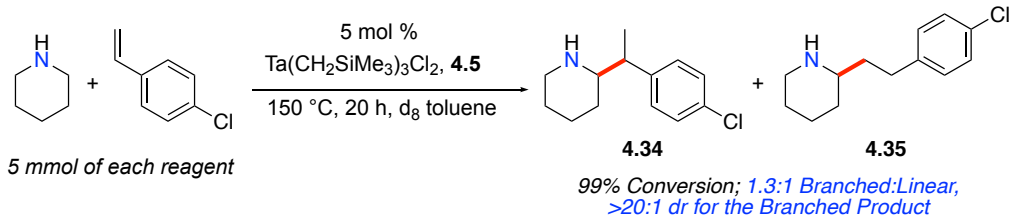

Scheme 4.3. An example of scaling up a hydroaminoalkylation reaction between piperidine and *p*-chlorostyrene.

Table 4.2. Attempts to use C-H activation for C-N bond formation in fused heterocycles.

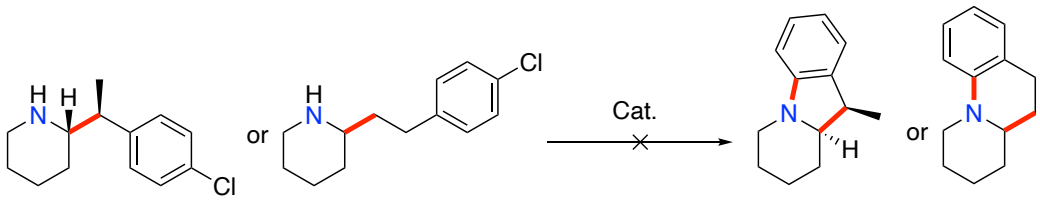

Entry	B or L?	Cat. Loading	Metal	Additive	Temp (C)	Solvent	Time (h)	Yield
1	B	20 mol%	$Pd(OAc)_2$	1 eq. $Cu(OAc)_2$	120	DMSO	16	-
2	L	20 mol%	$Pd(OAc)_2$	1 eq. $Cu(OAc)_2$	120	DMSO	16	-
3	B	20 mol%	$Pd(OAc)_2$	1 eq. Ag_2CO_3 [d]	120	DMSO	16	-
4	L	20 mol%	$Pd(OAc)_2$	1 eq. Ag_2CO_3 [d]	120	DMSO	16	-
5	B	20 mol%	$Pd(OAc)_2$	1 eq. $Cu(OAc)_2$ [d]	120	DMSO	16	-
6	L	20 mol%	$Pd(OAc)_2$	1 eq. $Cu(OAc)_2$ [d]	120	DMSO	16	-
7	B	20 mol%	$Pd(OAc)_2$	1 eq. Ag_2CO_3 [b,d]	120	DMSO	16	-
8	L	20 mol%	$Pd(OAc)_2$	1 eq. Ag_2CO_3 [b,d]	120	DMSO	16	-
9	B	20 mol%	$Pd(OAc)_2$	1.1 eq. $PhI(OAc)_2$	120	Toluene	16	-
10	L	20 mol%	$Pd(OAc)_2$	1.1 eq. $PhI(OAc)_2$	120	Toluene	16	-
11	B	20 mol%	$Pd(OAc)_2$	1.1 eq. $PhI(OAc)_2$	120	Toluene	16	-
12	L	20 mol%	$Pd(OAc)_2$	1.1 eq. $PhI(OAc)_2$	120	Toluene	16	-
13	B	-	-	1.1 eq. $PhI(OAc)_2$	120	Toluene	1	-
14	B	20 mol%	$Pd(OAc)_2$	1 eq.Ag_2CO_3 [b,d]	120	DMSO	16	-
15	B	20 mol%	$Pd(OAc)_2$	1 eq.Ag_2CO_3 [b,d]	120	Toluene	16	-
16	B	20 mol%	$Pd(OAc)_2$	-	120	DMSO	16	-
17	B	20 mol%	$Pd(OAc)_2$	1 eq.Ag_2CO_3 [b]	120	Toluene	16	-
18	B	20 mol%	$Pd(OAc)_2$	0.3 eq. DPEPhos [c]	120	Toluene	16	-

[a.] All reactions were screened for conversion by GC-MS analysis. Note that B means only the branched hydroaminoalkylation regioisomer was used, while L means only the linear regioisomer was used. Only starting material remained in all cases. [b.] 2 eq. K2CO3 added. [c.] 1.5 eq. Cs2CO3 added. [d.] 1 eq. PivOH added.

Reactions in Table 4.2 were analyzed by both ^{1}H NMR spectroscopy and GC-MS. As noted in this table, all reactions resulted in only unreacted starting material. We quickly realized that a general C-H activation protocol would not be possible at this time without extensive late transition-

metal reaction development and instead focused future efforts on Buchwald-Hartwig reaction strategies. With this in mind, initial proof of concept Buchwald-Hartwig amination reactions were attempted with 5 mol% $Pd(PPh_3)_4$ as catalyst (Scheme 4.4). Purified material from the hydroaminoalkylation reaction between piperidine and o-bromostyrene was used as brominated arenes are compatible reaction partners for Pd-mediated coupling reactions. A related hydroaminoalkylation, Buchwald-Hartwig cross-coupling sequence had been previously used in the group to generate methylated indoline.[78]

Using this approach yields of 43% for **4.48** and 70% for **4.49** show the promise of these single reaction runs on small scale (10 mg of each hydroaminoalkylation product). This proof-of-concept work encouraged us to further explore the amine hydroaminoalkylation scope and refine an effective Ni catalyzed Buchwald-Hartwig reaction.

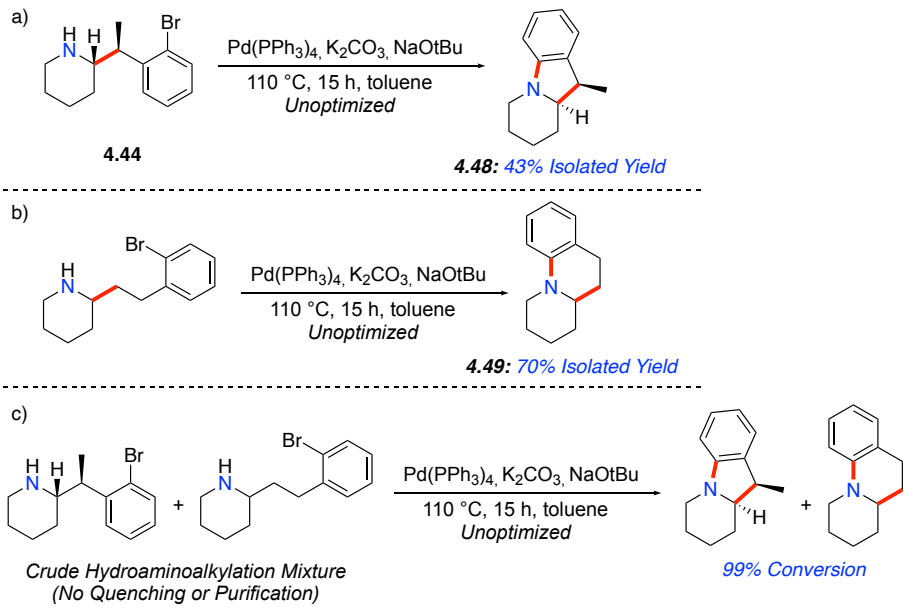

Scheme 4.4. Preliminary Buchwald-Hartwig reaction screening using a Pd catalyst system.

When exploring the amine scope for hydroaminoalkylation with *o*-chlorostyrene, we initially used many of the same amine substrates as in section 4.2.4. As noted in Table 4.3 the

different amines used did not significantly alter regioselectivity as compared with simple piperidine and *o*-chlorostyrene (1.15:1 branched: linear, Table 4.1). For example, 3-methylpiperidine and 4-methylpiperidine resulted in branched: linear ratios of 1:1 and 1:1.1 respectively. Larger regioselectivity changes could be observed when azepane was used as an amine substrate (1:4 branched: linear), and we believe that this is due to the increased metallaaziridine steric bulk, due to the bigger N-heterocyclic ring, that makes alkene insertion reaction favor the linear product. Unlike products in sections 4.2.4 and 4.2.5, data in this section still requires quantitative ^{1}H NMR spectra with 1,3,5-trimethoxybenzene as an internal standard. As a result, these preliminary data are presented as reaction conversions and discussion here will focus on diastereoselectivity and product assignments.

Diastereoselectivity values were consistently good across all products in Table 4.3 (5:1 for **4.42** – 13:1 for **4.52**). Unlike in most products in sections 4.2.4 or 4.2.5, we were sometimes able to separate and characterize both the major and minor diastereomer for these products and that data is reflected in the experimental section for this chapter. Also, the major diastereomer for branched products has been illustrated as determined by 1D and 2D NOESY experiments for the product from 4-methylpiperidine (**4.54**). Note that the stereochemical assignment in this section matches that from products in section 4.2.4. This was expected since the steric factors discussed in that section that govern diastereoselectivity during alkene addition have not changed with *o*-chlorostyrene being used instead of 1-octene. Diastereomer orientations have not been illustrated for the linear isomers of products with 3- or 4- substituted piperidine substrates (**4.55**, **4.57**, **4.59**) because NOESY NMR spectroscopy has not yet been completed for these products.

Table 4.3. Preliminary scope of amine heterocycles for reactivity with *o*-chlorostyrene.

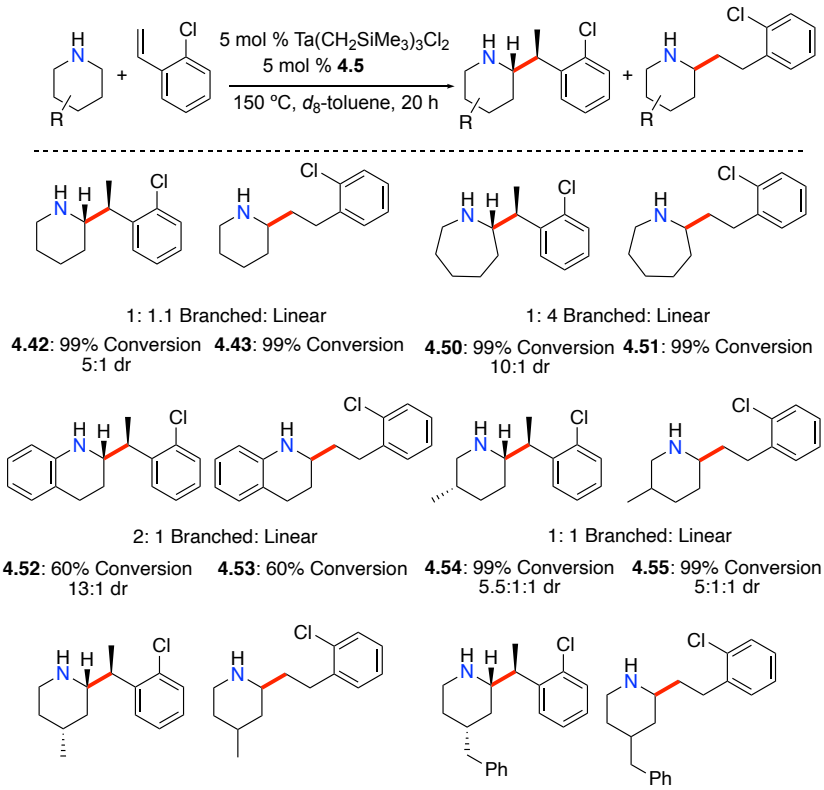

[a] Reaction conditions: amine (0.5 mmol), (1S)-(-)-pinene (0.5 mmol), $Ta(CH_2SiMe_3)_3Cl_2$ (0.05 mmol), ligand salt (0.05 mmol), d_8-toluene (0.5 g). Conversion was determined by ^1H NMR spectroscopy. Diastereoselectivity values are displayed as ratios, with the major diastereomer drawn and the ratio determined by GC-MS analysis.

Interesting preliminary data came from exploring the role of a second heteroatom in the saturated *N*-heterocycles for hydroaminoalkylation. When discussing amine reactivity with 1-octene earlier in this chapter, we added that morpholine, thiomorpholine, and 4-methylpiperazine were all unreactive. We were interested in trying other heteroatom-containing substrates where the N or O was further away from the reactive metal centre. These amines are exciting because resultant products would offer excellent synthetic handles for further product diversification. As noted in Scheme 4.5, 4-methoxypiperidine and 4-*N,N*-dimethylpiperidine were both competent hydroaminoalkylation substrates when combined with either o-chlorostyrene or 1-octene.

Regioselectivity was not altered significantly when using these amines, as compared with piperidine. However, diastereoselectivity was completely eroded in all cases with oxygen-containing products and partially in nitrogen-containing products. We propose that this disrupted reactivity with additional heteroatoms is due to a chelating or hydrogen-bonding effect from the heteroatom that alters how alkene addition can proceed. In future work experiments to understand these data are proposed.

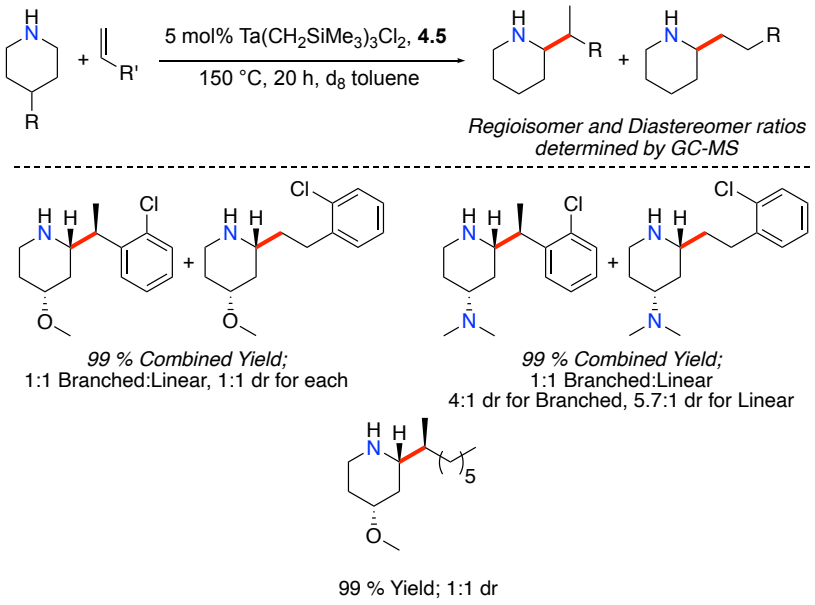

Scheme 4.5. Preliminary hydroaminoalkylation reactivity using 4-methoxypiperidine and 4-*N,N*-dimethylpiperidine.

As mentioned earlier in this section, Ni catalyzed Buchwald-Hartwig reactions as well as the scope of indolizidine and quinolizidine products are part of Mr. Zheng's degree program, under my initial guidance, so this section summarizes some of the most relevant findings thus far. First, $Ni(COD)_2$ was identified as the most productive catalyst starting material and optimized reaction conditions combine 5 mol% of Ni with 10% dppf for *in situ* catalyst generation

(Scheme 4.6).[194] Notably, all screening data in this section were done using crude hydroaminoalkylation mixtures. No quenching or purification of any kind was required before proceeding directly to the next reaction step.

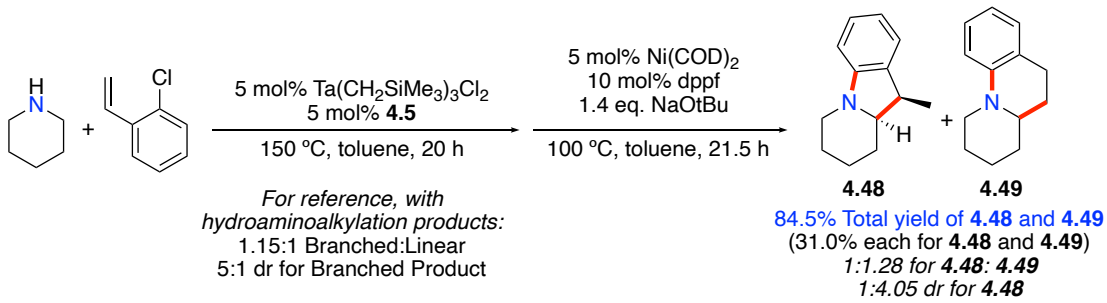

Scheme 4.6. Optimized Ni-mediated Buchwald-Hartwig amination conditions for use with crude hydroaminoalkylation mixtures.

When examining Buchwald-Hartwig product mixtures, GC-MS data from crude mixtures illustrates a clean reaction that does not generate side products, and regioselectivity and diastereoselectivity from the previous hydroaminoalkylation step is maintained. Crude ^{1}H NMR spectroscopy data from the crude reaction mixture can also be used to confirm the ~4:1 dr ratio for the branched product, with a doublet indicative of the methyl group for each diastereomer of the branched product. Last, isolated yields over two steps illustrated in the scheme above identify the relative ease of purification for these tertiary amine products as compared with their secondary amine counterparts in sections 4.2.4 and 4.2.5.

4.3.7.2 Synthesis of *N*-Arylated Indole Products

The strategy of sequential hydroaminoalkylation followed by Buchwald-Hartwig amination reactions lends itself well to applications in the synthesis of *N*-arylated indoles (Scheme 4.7). In this case, substituted *N*-methylanilines can be screened with *o*-chlorostyrene and either isolated as a single branched hydroaminoalkylation regioisomer or directly reacted with Ni(COD)$_2$

as above. The C-N bond formation results in one indoline product that can also be isolated and reacted with *o*-chloranil to generate the corresponding indole. This project was supervised by me and completed by Ms. Daria Balatsky during her 449 Honour's thesis project in our group.

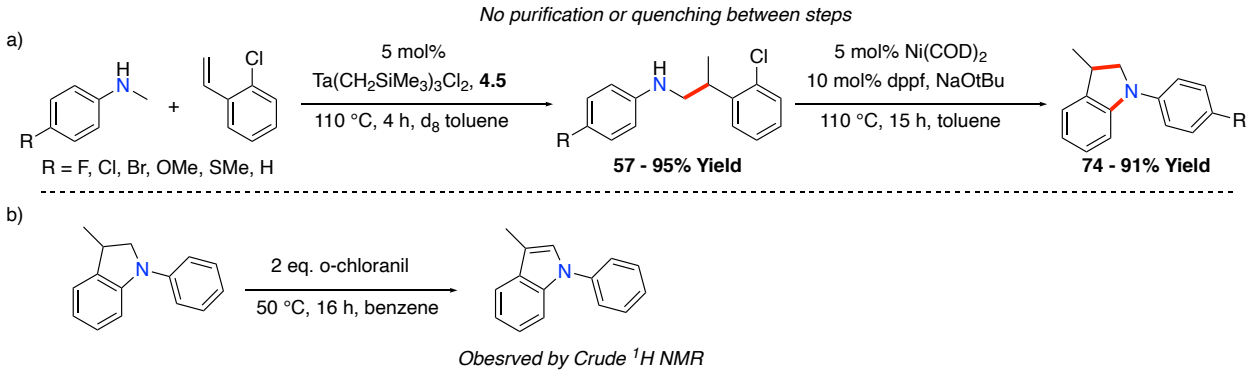

Scheme 4.7. Using hydroaminoalkylation of *N*-arylated substrates as a key step in synthesizing indoles.

4.4 Conclusion

In summary, we have developed the first productive early transition metal catalyst for reactivity with challenging *N*-heterocycle substrates. Exploring reactivity with this catalyst system unveiled the first broadly applicable hydroaminoalkylation catalyst. This catalyst displays excellent reactivity with all major substrate classes for this reaction. One notable example was almost complete conversion when combining an aliphatic amine with an internal alkene coupling partner, a combination that has not yet been accessed in hydroaminoalkylation.

For the first time using group 5 catalysts, variable styrene substrates reacted with piperidine allowed us to access regiodivergent product formation. Such catalysis occurs with a 5 mol% catalyst loading to obtain full conversion in as little as 6 h, depending on the chosen substrate. Isolated and *in situ* versions of our most active catalyst showed identical reactivity, allowing for the use of an easily assembled *in situ* catalyst system for hydroaminoalkylation.

Variously substituted piperidines allowed for the investigation of diastereoselectivity in this reaction, where most compounds were generated as a major diastereomer that can be predicted based on mechanistic insights for the key alkene insertion step. Changes in regioselectivity allowed us to better understand the role of alkene electronic effects, as interpreted by a Hammet study, on product distribution and reaction mechanism. Last, all of this reactivity was explored using syringe techniques to obtain excellent reactivity with challenging *N*-heterocycles. These data will help make the organic-oriented applications in this chapter more accessible to organic or medicinal chemists going forward.

Current work in our group is focused on using hydroaminoalkylation as a key step in the synthesis of complex fused heterocycle products. Specifically, work in this chapter focused on preliminary efforts for generating indolizidine and quinolizidine alkaloid products in two catalytic steps. We accomplished this using Ta and Ni as inexpensive metals and extended the approach to the synthesis of a series of indoline products.

4.5 Future Work

As with Chapter 2, future work in this chapter has already begun. Cameron is currently finishing the indolizine and quinolizine scope for an upcoming publication featuring fused heterocycles. It is also interesting to use currently available drugs as *N*-heterocycle substrates in hydroaminoalkylation. For example, desloratadine is an over-the-counter allergy medication that can be used as a substrate in combination with 1-octene (Scheme 4.8). As well, lorcaserin would be exciting to use because it is chiral, so we may be able to generate an enantiopure product as discussed in Chapter 3 with amination of chiral terpenes (Figure 4.9).

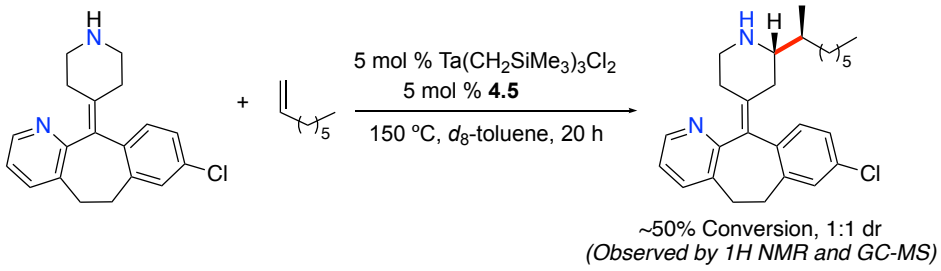

Scheme 4.8. Preliminary reactivity with desloratadine in hydroaminoalkylation.

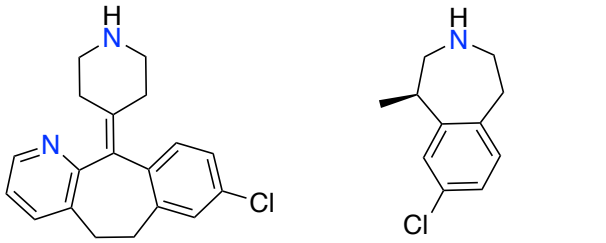

Deslortadine
Allergy Medication

Lorcaserin
Weight Loss Medication

Figure 4.9. Desloratadine and lorcaserin as N-heterocycle substrates in hydroaminoalkylation.

Mr. Zheng will also add finishing details to Ms. Balatzky's work make indoles using hydroaminoalkylation as the key step. Another publication will be submitted later this year to outline applications for that prevalent scaffold. Additional future directions will focus on both potential mechanistic questions and organic applications associated with this exciting *N*-heterocycle reactivity.

One notable question surrounding the current *N*-heterocycle work is the change in reactivity and selectivity when heteroatom-containing amine substrates are used. These data were highlighted in section 4.2.5 for reactivity between 4-methoxy or 4-*N*,*N*-dimethyl substituted piperidines with either 1-octene or o-chlorostyrene. As well, experiments suggest that oxygen has a more prominent effect on this reactivity as 4-methoxypiperidine has a 1:1 dr for either branched or linear product when combined with *o*-chlorostyrene, while 4-*N*,*N*-dimethylpiperidine still maintains a relatively some diastereoselectivity with a small dr of 4:1:1 for the branched or 5.7:1:1

for the linear products. We propose that heteroatoms need to be a certain distance away from the reactive metal centre to allow for productive reactivity, as 4-methoxypiperidine is a productive substrate but morpholine is not. Of course, these proposals need to be better supported by mechanistic and hopefully computational investigations.

Applications of this work focus on hydroaminoalkylation substrates that have been successfully used, and employing these products in subsequent catalytic or stoichiometric steps to access other types of fused heterocycles. The first example is the reactivity we observed between piperidine and a protected alcohol coupling partner (Scheme 4.9). We propose that these alcohol-containing products could be deprotected and cyclized in one step to generate a distinct series of indolizidine and quinolizidine alkaloids. This C-N bond forming reaction has been used previously in our group with simpler *N*-methylaniline-based products to generate a substituted piperidine.[87] Unlike the products that are discussed in the results section of this chapter, these indolizidine and quinolizidine alkaloid products would not have a fused aryl ring and thus would more closely resemble their natural counterparts.

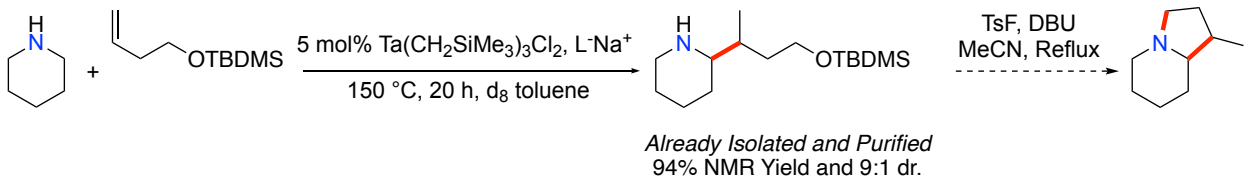

Scheme 4.9. Strategies for hydroaminoalkylation reactions with *N*-heterocycles and protected alcohols towards fused heterocycle products.

A particularly exciting result focuses on developing a sequential hydroaminoalkylation-hydroamination protocol using entirely early transition-metal catalysts. The strategy for this project would capitalize on the reactivity in this chapter between piperidine and diene partners (Scheme 4.10). These products have already been generated. Further, a catalyst already exists in

our group for intramolecular hydroamination between aliphatic amines and internal alkene substrates.[118] I synthesized a batch of this catalyst and added it to the crude hydroaminoalkylation mixture, for about ~50% conversion as qualitatively observed by GC-MS. The associated crude NMR spectrum was too difficult to analyze as a combination of hydroaminoalkylation and hydroamination material. This result is exciting because it is the first example of sequential hydroaminoalkylation-hydroamination. I envision that conditions for the hydroamination step could be optimized for complete conversion with increased catalyst loading, reaction times, or higher reaction temperatures. Further, Figure 4.10 below highlights potential hydroaminoalkylation products that could then be used as substrates in this method. One of the most exciting is the conjugated phenylbutadiene, a substrate that has been used in group 4 catalyst development[54] but no Ta-based systems have explored conjugated alkenes to date. Another product in Figure 4.10 allows for exploring conjugated enynes as substrates. We have already observed that terminal alkynes are not competent substrates because they are too acidic, but internal alkyne substrates have not been thoroughly explored with early transition-metal catalysts.

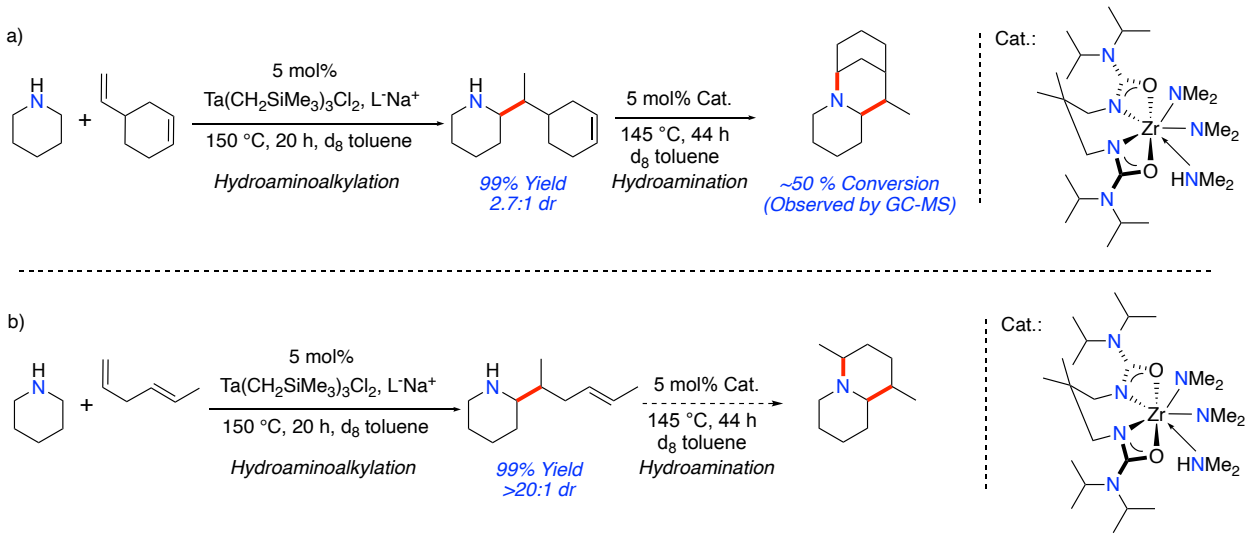

Scheme 4.10. Preliminary data towards a sequential hydroaminoalkylation-hydroamination methodology.

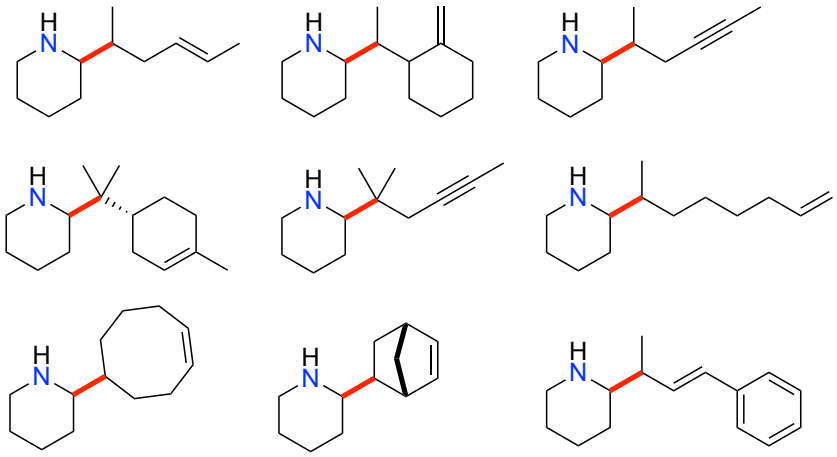

Figure 4.10. Potential hydroaminoalkylation products for use in a subsequent hydroamination step.

Finally, I explored preliminary reactions using norbornadiene as a substrate for hydroaminoalkylation with piperidine as a coupling partner (Scheme 4.11). This substrate was interesting first because it is a diene that raised regioselectivity questions, but also because it is regularly used by our group's polymer chemists as an alkene for hydroaminoalkylation and subsequent ring-opening metathesis polymerization (ROMP) to make amine-containing polymers.[195,196] In an alternate pathway in Scheme 4.11, this strained alkene was very reactive, and quickly (2 h 150 °C) alkylated both possible sites on either side of the piperidine structure. Note that this structure was not rigorously characterized, but is proposed based on preliminary GC-MS and crude NMR data for the corresponding reaction. Optimizing the conditions by either lowering reaction temperatures or times to stop the reaction at one alkylation would allow for another strategy towards fused quinolizidine products (Scheme 4.11). Reactivity with *N*-heterocycles and strained diene partners like norbornadiene or cyclooctadiene is also an exciting

area for potential expansion of the *N*-containing polymer projects because the current published work focuses entirely on properties of polymers from aromatic amine substrates. This is partly because our group has not had access to a catalyst with useful reactivity for challenging saturated *N*-heterocycles.

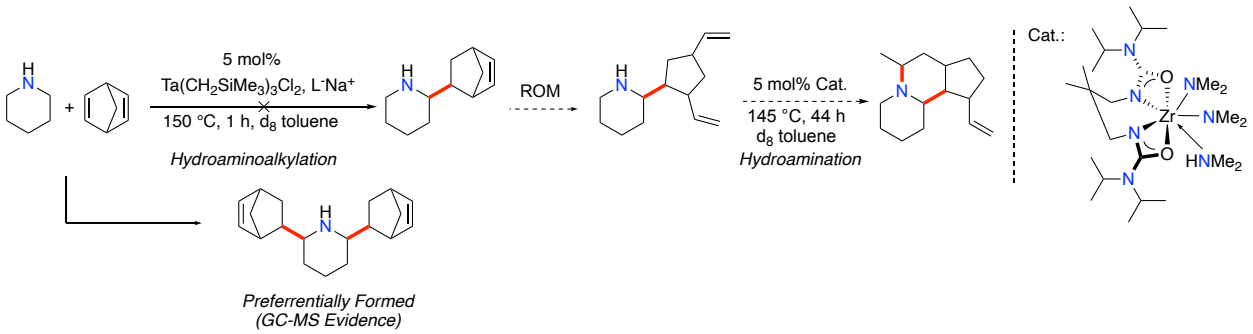

Scheme 4.11. Reactivity data using norbornadiene as a substrate with piperidine. This scheme highlights a strategy towards saturated fused heterocycle products.

4.6 Experimental

4.6.1 Materials and Instrumentation

All reactions were performed under a N_2 atmosphere using Schlenk or glovebox techniques, unless otherwise stated. $TaCl_5$ (Strem), $Ta(NMe_2)_5$ (Strem), (chloromethyl)trimethylsilane (Aldrich), *N,N*-diphenylamine (Alfa), *N*-isopropylaniline (Combi-Blocks), triphosgene (Oakwood), 2,6-dimethylaniline (Aldrich), and 2,6-diisopropylaniline (Alfa), *N*-methyl-1-phenylethan-1-amine (CombiBlocks), *N*-methyl-1,1-diphenylmethanamine (CombiBlocks), *N*-methylpropan-2-amine (CombiBlocks), 2,4,6-trimethylaniline (Aldrich), 4-bromo-2,6-dimethylaniline (Aldrich), and 4-chloro-2,6-dimethylaniline (Aldrich)were used as received. All amines and alkenes were commercially available, dried over CaH_2 and distilled and degassed prior to use in catalytic experiments. $[Ta(NMe_2)_3Cl_2]_2$,[131] $Ta(CH_2CMe_3)_3Cl_2$,[125] $Ta(CH_2SiMe_3)_3Cl_2$,[124] all proteo-ligands and their corresponding ligand salts[84,86,129,197,198] and

$TaMe_3Cl_2$[133] were prepared as previously described. Specifically, preparation for ligands **4.6**, **4.7**, **4.8**, **4.9**, **4.10**, and **4.11** is outlined in the experimental section of Chapter 2. All glassware was dried in a 180 °C oven overnight before use. Toluene, and hexanes were dried over activated alumina columns and stored over activated molecular sieves (4 Å). d_8-Toluene was dried over sieves, sparged, and freeze/pump/thawed prior to use. Experiments conducted on an NMR tube scale were performed in J. Young NMR tubes (8" x 5 mm) sealed with screw-type Teflon caps.

^1H and $^{13}C\{^1H\}$ NMR spectra were recorded on Bruker 300 MHz and 400 MHz Avance spectrometers at ambient temperature. Chemical shifts (δ) are given relative to the corresponding residual protio solvent and are reported in parts per million (ppm). Coupling constants *J* are given in Hertz (Hz). The following abbreviations are used to indicate signal multiplicity: s = singlet, d = doublet, t = triplet, q = quartet, m = multiplet, and br = broad. Assignment of the signals was carried out using 1D (^1H, $^{13}C\{^1H\}$) and 2D (COSY, HSQC and HMBC) NMR experiments. High resolution mass-spectra (HRMS) were measured by the mass spectrometry services at University of British Columbia, UBC on a Kratos MS-50 spectrometer using a Bruker maXis Ultra-High Resolution tandem TOF (UHR-Qq-TOF) mass spectrometer using a positive electrospray ionization source. Fragment signals are given in mass per charge number (*m/z*). GC/MS analyses were conducted on an Agilent 7890B GC with an Agilent 5977 inert CI mass detector, utilizing methane as the ionization gas. Single-crystal X-ray structure determination was performed on a APEX II diffractometer at the Department of Chemistry, University of British Columbia, by Dr. Pargol Daneshmand.

4.6.2 Obtaining and Characterizing an Isolated Catalyst

Mono(*N*-(2,6-dimethylphenyl)-*N*-methyl-*N*-(1-phenylethyl)carbamoylamidate)-tris(methylenetrimethylsilane)chlorotantalum: In a glovebox, to a stirring suspension of

$Ta(CH_2SiMe_3)_3Cl_2$ (0.169 g, 0.33 mmol) in toluene (~3 mL) in a 20 mL vial, a suspension of sodium (2,6-dimethylphenyl)(methyl(1-phenylethyl)carbamoyl)amide (0.100 g, 0.33 mmol) in toluene (~3 mL) was added dropwise over 5 minutes. The mixture was stirred at ambient temperature for one h, filtered through a plug of Celite, and concentrated *in vacuo* overnight. The resulting crude residue was dissolved in minimal hexanes (~2 mL), storage at -35 °C overnight produced a yellow precipitate. The supernatant was decanted and the white crystals (0.0813 g, 31%) were obtained and dried *in vacuo* overnight. A sample from these crystals was used for single crystal X-ray structure analysis: ^{1}H NMR ($CDCl_3$, 400 MHz, 298 K): δ 7.18 (m, 3H), 7.05 (m, 2H), 6.84 (m, 3H), 6.05 (m, 1H), 2.22 (s, 3H), 2.17 (s, 3H), 2.13 (m, 4H), 1.72 (s, 3H), 1.45 (m, 6H), 1.22 (m, 3H), 0.38 (s, 27H) ppm. ^{13}C{^{1}H} NMR ($CDCl_3$, 101 MHz, 298 K): δ 164.71, 142.01, 139.17, 135.23, 135.05, 126.82, 93.17, 86.58, 52.71, 35.02, 32.06, 28.16, 23.12, 15.74, 2.96 ppm.

4.6.3 General Procedures for Qualitative and Quantitative Catalysis

General procedure for qualitative catalytic experiments:

Unless otherwise stated, $Ta(CH_2SiMe_3)_3Cl_2$ (0.005 mmol, 26.0 mg) was weighed into a vial, followed by addition of the ligand salt (0.005 mmol, 15.2 mg). Toluene-d_8 (300 mg) was added and the resultant mixture was left for 15 minutes. Aniline (1 mmol), followed by alkene (1 mmol) were then added by mass with a micropipette. The reaction vials were rinsed with 300 mg of toluene-d_8 and transferred into a J. Young NMR tube. An initial ^{1}H NMR spectrum was recorded, and the sample was added to a pre-heated oil bath at 150 °C for 20 h. All conversion values were determined by ^{1}H NMR spectroscopy by integrating the product peak at 2.96 ppm (1H) relative to one of the alkene peaks. After quenching the reaction, rinsing the NMR tube with dichloromethane, and removal of all reaction solvent, the resulting amine was purified *via* a silica-filtration and fractions were dried *in vacuo* overnight to afford the desired product.

General Procedure for Quantitative Catalytic Experiments:

Unless otherwise stated, $Ta(CH_2SiMe_3)_3Cl_2$ (0.005 mmol, 26.0 mg) was weighed into a vial, followed by addition of the ligand salt (0.005 mmol, 15.2 mg). A solution of 0.033 mmol (0.33 eq) trimethoxybenzene in toluene-d_8 (300 mg total of solution) was added and the resultant mixture was left for 15 minutes. Aniline (1 mmol), followed by alkene (1 mmol) were then added by mass with a micropipette. The reaction vials were rinsed with 300 mg of toluene-d_8 and transferred into a J. Young NMR tube. An initial ^{1}H NMR spectrum was recorded, and the sample was added to a pre-heated oil bath at 150 °C for 20 h. All NMR yield values were determined by ^{1}H NMR spectroscopy but integrating the product peak at 2.96 ppm (1H) relative to the internal standard peak for the three methyl groups at 3.40 ppm (integrated to 3H instead of 9H due to 0.33 equivalents relative to amine being used). **Note that for all quantitative NMR reactions, D1 values were determined to be and set as 200 s.** After quenching the reaction, rinsing the NMR tube with dichloromethane, and removal of all reaction solvent, the resulting amine was purified *via* a silica-filtration and fractions were dried *in vacuo* overnight to afford the desired product.

4.6.4 Synthesis and Characterization of Hydroaminoalkylation Reaction Products

4.6.4.1 Amine Scope Products with 1-Octene

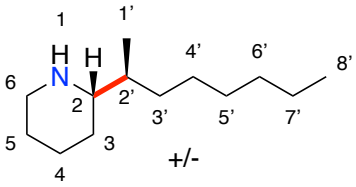

Synthesis of 2-(octan-2-yl)piperidine (4.14): Prepared following the general procedure outlined above: 26.0 mg Ta, 15.2 mg Ligand, piperidine (85.15 mg, 1.0 mmol), 1-octene (122.12 mg, 1.0 mmol). The reaction was subsequently concentrated, and the yield was determined to be 99 % by NMR (1,3,5-trimethoxybenzene as a standard). Purification via column chromatography (7:2.5:0.5 hexanes : ethyl acetate : triethyl amine) .chemical shifts for the title compound match those reported in the literature.[88]

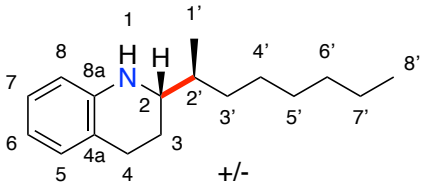

Synthesis of 2-(octan-2-yl)-1,2,3,4-tetrahydroquinoline (4.15): Prepared following the general procedure outlined above: 26.0 mg Ta, 15.2 mg Ligand, 1,2,3,4-tetrahydroquinoline (133.19 mg, 1.0 mmol), 1-octene (122.12 mg, 1.0 mmol). The reaction was subsequently concentrated, and the yield was determined to be 65 % by NMR (1,3,5-trimethoxybenzene as a standard). Purification via column chromatography (7:2.5:0.5 hexanes : ethyl acetate : triethyl amine). The chemical shifts for the title compound match those reported in the literature.[85]

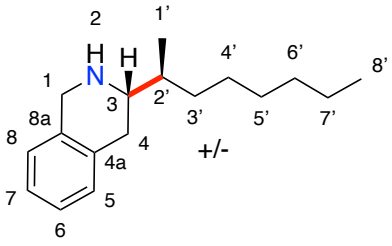

Synthesis of 3-(octan-2-yl)-1,2,3,4-tetrahydroisoquinoline (4.16): Prepared following the general procedure outlined above: 26.0 mg Ta, 15.2 mg Ligand, 1,2,3,4-tetrahydroisoquinoline (133.19 mg, 1.0 mmol), 1-octene (112.22 mg, 1.0 mmol). The reaction was subsequently concentrated, and the yield was determined to be 99 % by NMR (1,3,5-trimethoxybenzene as a standard). Purification via column chromatography (7:2.5:0.5 hexanes : ethyl acetate : triethyl amine): ^{1}H NMR ($CDCl_3$, 400 MHz, 298 K): 7.03 (m, 2H, **6** and **7**), 6.99 (m, 1H, **5**), 6.92 (m, 1H, **8**), 3.97 (s, 2H, **1**), 2.68, (m, 1H, **3**), 2.58 (m, 2H, **4**), 1.78 (broad s, 1H, NH), 1.50 (m, 1H, **2'**), 1.45 (m, 1H, ½ of **3'**), 1.29 (m, 2H, **4'/5'/6'/7'**), 1.24 (m, 2H, **4'/5'/6'/7'**), 1.21 (m, 2H, **4'/5'/6'/7'**), 1.20 (m, 2H, **4'/5'/6'/7'**), 1.18 (m, 1H, ½ of **3'**), 1.16 (m, 1H, ½ of **3**), 0.91 (d, J = 0.91, 3H, **1'**), 0.81 (t, 3H, **8'**), 0.61 (d, J = 0.61, 3H, **1' of minor diastereomer**) ppm. ^{13}C{^{1}H} NMR ($CDCl_3$, 101 MHz, 298 K): δ 133.83 (minor), 136.49 (minor), 135.91, 135.40, 129.46, 129.16 (minor), 126.07, 126.00, 125.95 (minor), 125.69, 125.65 (minor), 125.56 (minor), 59.55 (minor), 58.28, 49.22, 43.04 (minor), 37.88, 37.71 (minor), 34.53 (minor), 32.94, 32.38,

32.00, 30.61 (minor), 29.73, 27.97 (minor), 27.43, 22.77, 15.58, 14.20, 13.46 ppm. HRMS (ESI): *m/z* calcd for $C_{17}H_{27}N$ [M+H$^+$]: 246.2221 Found: 246.2220.

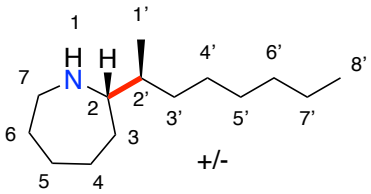

Synthesis of 2-(octan-2-yl)azepane (4.17): Prepared following the general procedure outlined above: 26.0 mg Ta, 15.2 mg Ligand, azepane (99.17 mg, 1.0 mmol), 1-octene (112.22 mg, 1.0 mmol). The reaction was subsequently concentrated, and the yield was determined to be 91 % by NMR (1,3,5-trimethoxybenzene as a standard). Purification via column chromatography (7:2.5:0.5 hexanes : ethyl acetate : triethyl amine): ^{1}H NMR ($CDCl_3$, 400 MHz, 298 K): δ 3.00 (m, 1H, ½ of **7**), 2.64 (m, 1H, ½ of **7**), 2.47 (m, 1H, **2**), 1.69 (m, 1H, ½ of **3/4**), 1.63 (m, 1H, ½ of **3/4**), 1.60 (m, 2H, **6/5**), 1.57 (m, 1H, ½ of **3/4**), 1.46 (m, 2H, **6/5**), 1.42 (m, 1H, **2'**), 1.38 (m, 1H, ½ of **3'/4'**), 1.35 (m, 1H, ½ of **3/4**), 1.27 (m, 1H, ½ of **3/4**), 1.26 (m, 2H, **5'/6'/7'**), 1.24 (m, 2H, **5'/6'/7'**), 1.20 (m, 2H, **5'/6'/7'**), 1.14 (m, 1H, ½ of **3'/4'**), 1.09 (m, 1H, ½ of **3'/4'**), 0.85 (overlapping t, 3H, **8'**), 0.81 (overlapping d, 3H, **1'**) ppm. ^{13}C{^{1}H} NMR ($CDCl_3$, 101 MHz, 298 K): δ 63.17, 55.33, 48.70, 39.59, 33.82, 33,59, 32.01, 31.33, 29.77, 27.74, 26.97, 22.76, 15.36, 14.16 ppm. HRMS (ESI): *m/z* calcd for $C_{14}H_{29}N$ [M+H$^+$]: 212.2378 Found: 212.2372.

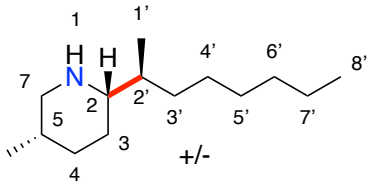

Synthesis of 4-methyl-2-(octan-2-yl)piperidine (4.18): Prepared following the general procedure outlined above: 26.0 mg Ta, 15.2 Ligand, 3-methylpiperidine (99.17 mg, 1.0 mmol), 1-octene (112.22 mg, 1.0 mmol). The reaction was subsequently concentrated, and the yield was determined to be 86 % by NMR (1,3,5-trimethoxybenzene as a standard). Purification via column chromatography (7:2.5:0.5 hexanes : ethyl acetate : triethyl amine): ^{1}H NMR ($CDCl_3$, 400 MHz, 298 K): δ 3.03 (m, 1H, ½ of **7**), 2.33 (minor diastereomer) and 2.26 (m, 1H, **2**), 2.21 (m, 1H, ½ of **7**), 1.89 (broad s, 1H, NH), 1.78 (m, 1H, ½ of **4**), 1.59 (m, 1H, ½ of **3**), 1.46 (m, 1H, **5**), 1.41 (m,

1H, ½ of **3'/4'**), 1.37 (m, 1H, **2'**), 1.32 (m, 1H, ½ of **4'/3'**), 1.28 (m, 2H, **5'/6'/7'**), 1.26 (m, 2H, **5'/6'/7'**), 1.25 (m, 2H, **5'/6'/7'**), 1.23 (m, 1H, ½ of **3**), 1.20, (m, 1H, ½ of **3'/4'**), 1.08 (m, 1H, ½ of **3'/4'**), 0.98 (m, 1H, ½ of **4**), 0.87 (overlapping d, 3H, **1'**), 0.86 (overlapping t, 3H, **8'**), 0.81 (d, J = 0.81, 3H, **6**) ppm. $^{13}C\{^{1}H\}$ NMR ($CDCl_3$, 101 MHz, 298 K): δ 61.41 (major) and 61.41 (minor), 54.43 (major), 54.30 (minor), 37.23 (major), 33.17 (major), 32.33 (major), 31.31 (major), 31.04 (major), 29.46 (minor), 28.76 (major), 28.73 (minor), 27.38 (minor), 26.58 (major), 26.51 (minor), 23.59 (major), 21.80 (major), 18.64 (major), 16.32 (minor), 14.75 (minor), 14.68 (major), 13.22 (major). HRMS (ESI): *m/z* calcd for $C_{14}H_{29}N$ $[M+H^+]$: 212.2378 Found: 212.2381.

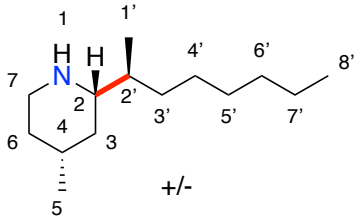

Synthesis of 4-methyl-2-(octan-2-yl)piperidine (4.19): Prepared following the general procedure outlined above: 26.0 Ta, 15.2 Ligand, 4-methylpiperidine (99.17 mg, 1.0 mmol), 1-octene (250.2 mg, 1.0 mmol). The reaction was subsequently concentrated, and the yield was determined to be 84 % by NMR (1,3,5-trimethoxybenzene as a standard). Purification via column chromatography (7:2.5:0.5 hexanes : ethyl acetate : triethyl amine): ^{1}H NMR ($CDCl_3$, 400 MHz, 298 K): δ 3.09 (m, 1H, ½ of **7**), 2.59 (m, 1H, ½ of **7**), 2.33 (m, 1H, **2**), 1.99 (broad s, 1H, NH), 1.59 (m, 1H, ½ of **6**), 1.55 (m, 1H, ½ of **3**), 1.44 (m, 1H, **4**), 1.42 (m, 1H, ½ of **3'**), 1.36 (m, 1H, **2'**), 1.30 (m, 1H, ½ of **4'**), 1.28 (m, 2H, **5'/6'/7'**), 1.26 (m, 2H, **5'/6'/7'**), 1.25 (m, 2H, **5'/6'/7'**), 1.17 (m, 1H, ½ of **4'**), 1.08 (m, 1H, ½ of **3'**), 1.01 (m, 1H, ½ of **6**), 0.90 (d, J = 0.90, 3H, **5**), 0.88 (overlapping d, 3H, **1'**), 0.87 (overlapping t, 3H, **8'**), 0.80 (m, 1H, ½ of **3**) ppm. $^{13}C\{^{1}H\}$ NMR ($CDCl_3$, 101 MHz, 298 K): δ 61.52, 55.44, 47.29, 38.52, 38.38, 35.37, 33.26, 32.05, 31.85, 29.77, 27.62, 22.81, 15.62, 14.22 ppm. HRMS (ESI): *m/z* calcd for $C_{14}H_{29}N$ $[M^+]$: 212.2299 Found: 212.2310.

Note: The 1D/2D NMR spectroscopy data for this compound is a representative example of how we were able to assign all proton and carbon signals conclusively in products with 1-octene as a coupling partner as well as assign relative stereochemistry for all compounds.

For NOESY experiments: The 1D NOESY experiment illustrated irradiated the peak at 2.59 ppm (1/2 of **7**) selectively. This data suggests that this proton interacts spatially with the other peak on the same methylene (3.09 (m, 1H, ½ of **7**)), as well as the CH at 2.33 ppm (m, 1H, **2**). This tells us that the proton at 2.59 ppm represents the half of **7** that faces of out of the page. Other important interactions in the 1D NOESY include with the proton at 1.59 ppm (m, 1H, ½ of **6**) and with the CH at 1.44 ppm (m, 1H, **4**). This interaction with 4 is key, because it shows that the methyl group **5** is facing into the page as illustrated in the major diastereomer above. 2D NOESY data shown below was used to further corroborate this analysis and rule out the other possible orientation.

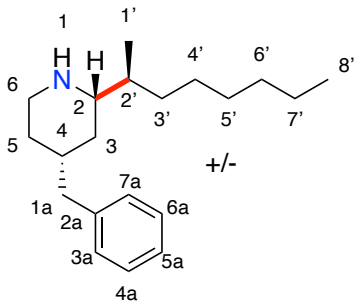

Synthesis of 4-benzyl-2-(octan-2-yl)piperidine (4.20): Prepared following the general procedure outlined above: 26.0 mg Ta, 15.2 mg Ligand, 4-benzylpiperazine (175.3 mg, 1.0 mmol), 1-octene (112.22 mg, 1.0 mmol). The reaction was subsequently concentrated, and the yield was determined to be 84 % by NMR (1,3,5-trimethoxybenzene as a standard). Purification via column chromatography (7:2.5:0.5 hexanes : ethyl acetate : triethyl amine): ^{1}H NMR ($CDCl_3$, 400 MHz, 298 K): δ 7.31 (m, 2H, **4a** and **6a**), 7.23 (m, 1H, **5a**), 7.18 (m, 2H, **3a** and **7a**), 3.58 (broad s, 1H, NH), 3.30 (m, 1H, ½ of **6**), 2.68 (m, 1H, ½ of **6**), 2.60 (m, 1H, **4**), 2.55 (m, 1H, **2**), 1.75 (m, 1H, ½ of **3**), 1.71 (m, 1H, ½ of **5**/**3'**), 1.67 (m, 1H, ½ of **5**/**3'**), 1.61 (m, 1H, ½ **5**/**3'**), 1.51 (m, 1H, **2'**), 1.37 (m, 1H, ½ **5**/**3'**) 1.33 (m, 2H, **1a**), 1.30 (m, 2H, **4'**/**5'**/**6'**/**7'**), 1.29 (m, 2H, **4'**/**5'**/**6'**/**7'**), 1.26 (m, 2H, **4'**/**5'**/**6'**/**7'**), 1.23 (m, 2H, **4'**/**5'**/**6'**/**7'**), 1.17 (m, 1H, ½ of **3**), 0.98 (d, J = 0.98, 3H, **1'**), 0.91 (t, 3H, **8'**) ppm. ^{13}C{^{1}H}

NMR ($CDCl_3$, 101 MHz, 298 K): δ ppm. HRMS (ESI): *m/z* calcd for $C_{20}H_{33}N$ [$M+H^+$]: 288.2691 Found: 288.2692.

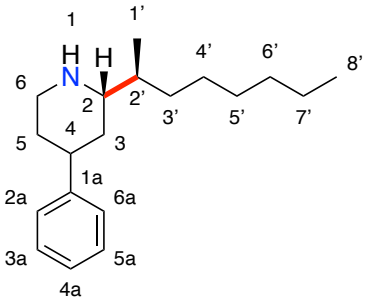

Synthesis of 2-(octan-2-yl)-4-phenylpiperidine (4.21): Prepared following the general procedure outlined above: 26.0 mg Ta, 15.2 mg Ligand, 4-phenylpiperidine (307 mg, 1.0 mmol), 1-octene (250.2 mg, 1.0 mmol). The reaction was subsequently concentrated, and the yield was determined to be 99 % by NMR (1,3,5-trimethoxybenzene as a standard). Purification via column chromatography (7:2.5:0.5 hexanes : ethyl acetate : triethyl amine): ^{1}H NMR ($CDCl_3$, 400 MHz, 298 K): δ 7.31 (m, 2H, **3a** and **5a**), 7.24 (m 2H, **2a** and **6a**), 7.20 (m, 1H, **4a**), 3.26 (m 1H, ½ of **6**), 2.79 (m, 1H, ½ of **6**), 2.61 (m, 1H, **4**), 2.53 (m, 1H, **2**), 1.90 (broad s, 1H, NH), 1.83 (m, 1H, ½ of **3**), 1.80 (m, 1H, ½ of **5**), 1.64 (m, 1H, ½ of **5**), 1.49 (m, 1H, ½ of **4'**), 1.44 (m 1H, **2'**), 1.39 (m, 1H, ½ of **3**), 1.32 (m, 1H, ½ of **3'**), 1.28 (m, 2H, **5'/6'/7'**), 1.26 (m, 2H, **5'/6'/7'**), 1.24 (m, 2H, **5'/6'/7'**), 1.21 (m, 1H, ½ of **3'**), 1.14 (m, 1H, ½ of **4'**), 0.92 (d, J = 0.93, 3H, **1'**), 0.88 (overlapping t, 3H, **8'**) ppm. ^{13}C{^{1}H} NMR ($CDCl_3$, 101 MHz, 298 K): δ 146.99, 128.56, 127.00, 126.23, 61.89, 47.51, 43.56, 38.46, 37.68, 34.12, 33.23, 32.03, 29.76, 27.62, 22.80, 15.67, 14.23 ppm. HRMS (ESI): *m/z* calcd for $C_{19}H_{31}N$ [M^+]: 273.2456 Found: 273.2464.

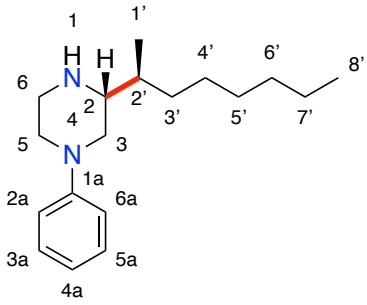

Synthesis of 3-(octan-2-yl)-1-phenylpiperazine (4.22): Prepared following the general procedure outlined above: 26.0 mg Ta, 15.2 Ligand, 4-phenylpiperazine (162.24 mg, 1.0 mmol), 1-octene (112.22 mg, 1.0 mmol). The reaction was subsequently concentrated, and the yield was determined to be 48 % by NMR (1,3,5-trimethoxybenzene as a standard). Purification via column chromatography (7:2.5:0.5

hexanes : ethyl acetate : triethyl amine). The chemical shifts for the title compound match those reported in the literature.[88]

4.6.4.2 Alkene Scope Products

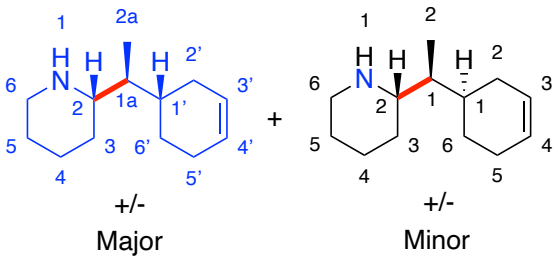

Synthesis of 2-(1-(cyclohex-3-en-1-yl)ethyl)piperidine (4.23): Prepared following the general procedure outlined above: 26.0 mg Ta, 15.2 mg Ligand, piperidine (85.15 mg, 1.0 mmol), vinylcyclohexene (108.18 mg, 1.0 mmol). The reaction was subsequently concentrated, and the yield was determined to be 99 % by NMR (1,3,5-trimethoxybenzene as a standard). Purification via column chromatography (7:2.5:0.5 hexanes : ethyl acetate : triethyl amine): ^{1}H NMR ($CDCl_3$, 400 MHz, 298 K): δ 5.63 (m, 2H, **3'** and **4'** and **3'** and **4'**), 3.09 (m, 1H, ½ of **6** and **6**), 2.57 (m, 1H, ½ of **6** and **6**), 2.47 (m, 1H, **2** and **2**), 2.03 (m, 2H, **5'**), 1.96 (m, 1H, ½ of **5'**), 1.89 (m, 1H, ½ of **2'** and **2'**), 1.81 (m, 1H, ½ of **5'**), 1.75 (m, 1H, ½ of **4** and **4**), 1.69 (m, 1H, ½ of **2'** and **2'**), 1.63 (m, 1H, ½ of **1'** and **1'**), 1.60 (m, 1H, ½ of **6'** and **6'**), 1.57 (m, 1H, ½ of **3** and **3**), 1.54 (m, 1H, ½ of **5** and **5**), 1.39 (m, 1H, ½ of **4** and **4**), 1.34 (m, 1H, ½ of **6'** and **6'**), 1.28 (m, 1H, ½ of **5** and **5**), 1.23 (m, 1H, **1a** and **1a**), 1.17 (m, 1H, ½ of **3** and **3**), 0.86 (d, J = 0.95, 3H, **2a**), 0.84 (d, 3H, **2a**), ppm. ^{13}C{^{1}H} NMR ($CDCl_3$, 101 MHz, 298 K): δ 127.15 (major and minor), 127.05 (major and minor), 126. 91 (major and minor), 58.98 (major and minor), 47.70 (major), 47.67 (minor), 43.17 (major), 42.71 (minor), 35.26 (minor), 35.11 (minor), 31.19 (minor), 31.12 (major), 30.73 (major and minor), 27.81 (major), 27.69 (minor), 26.80 (minor), 26.76 (major), 26.11 (major), 25.96 (minor), 25.46 (minor), 25.39 (major), 11.61 (minor), 11.19 (major) ppm. HRMS (ESI): *m/z* calcd for **major**: $C_{13}H_{23}N$ [M^+]: 193.1830 Found: 193.1834 and **minor**: $C_{13}H_{23}N$ [$M+H^+$]: 193.1830 Found:193.1832.

Note: With these diastereomers, we obtained enough sample for each pure diastereomer to get a clean GC-MS sample for each. However, NMR peaks are reported for the mixture.

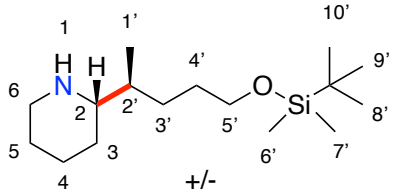

Synthesis of 2-(5-((tert-butyldimethylsilyl)oxy)pentan-2-yl)piperidine (4.24): Prepared following the general procedure outlined above: 26.0 mg Ta, 15.2 mg Ligand, piperidine (85.15 mg, 1.0 mmol), tert-butyldimethyl(pent-4-en-1-yloxy)silane (200.4 mg, 1.0 mmol). The reaction was subsequently concentrated, and the yield was determined to be 93 % by NMR (1,3,5-trimethoxybenzene as a standard). Purification via column chromatography (7:2.5:0.5 hexanes : ethyl acetate : triethyl amine): ^{1}H NMR ($CDCl_3$, 400 MHz, 298 K): δ 3.57 (m, 2H, **5'**), 3.09 (m, 1H, ½ of **6**), 2.59 (m, 1H, ½ of **6**), 2.33 (m, 1H, **2**), 2.17 (broad s, 1H, NH), 1.78 (m, 1H, ½ of **4**), 1.60 (m, 1H, ½ of **3'**), 1.57 (m, 1H, ½ of **4'**), 1.55 (m, 1H, ½ of **5**), 1.47 (m, 1H, ½ of **4'**), 1.42 (m, 1H, ½ of **3**), 1.38 (m, 1H, **2'**), 1.34 (m 1H, ½ of **5**), 1.29 (m, 1H, ½ of **4**), 1.17 (m, 1H, ½ of **3'**), 1.12 (m, 1H, ½ of **3**), 0.89 (overlapping d, 3H, **1'**), 0.87 (s, 9H, **8'** and **9'** and **10'**), 0.03 (s, 6H, **6'** and **7'**) ppm. ^{13}C{^{1}H} NMR ($CDCl_3$, 101 MHz, 298 K): δ 63.65, 61.64, 47.68, 38.21, 30.83, 29.77, 29.24, 26.70, 26.10, 25.27, 18.47, 15.62, -5.13 ppm. HRMS (ESI): *m/z* calcd for $C_{16}H_{35}NOSi$ [M+H$^+$]: 285.2488 Found: 285.2492.

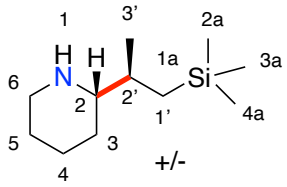

Synthesis of 2-(1-(trimethylsilyl)propan-2-yl)piperidine (4.25): Prepared following the general procedure outlined above: 26.0 mg Ta, 15.2 mg Ligand, piperidine (85.15 mg, 1.0 mmol), allyltrimethylsilane (114.26 mg, 1.0 mmol). The reaction was subsequently concentrated, and the yield was determined to be 99 % by NMR (1,3,5-trimethoxybenzene as a standard). Purification via column chromatography (7:2.5:0.5 hexanes : ethyl acetate : triethyl amine): ^{1}H NMR ($CDCl_3$, 400 MHz, 298 K): δ 3.12 (m 1H, ½ of **6**), 2.60 (m, 1H, ½ of **6**), 2.25 (m, 1H, **2**), 1.95 (broad s, 1H, NH), 1.81

(m, 1H, ½ of **4**), 1.60 (m, 1H, ½ of **3**), 1.57 (m, 1H, ½ of **2**), 1.54 (m, 1H, **2'**), 1.40 (m, 1H, ½ of **5**), 1.29 (m, 1H, ½ of **4**), 1.15 (m, 1H, ½ of **3**), 0.90 (d, J = 0.90, 3H, **3'**), 0.71 (m, 1H, ½ of **1'**), 0.36 (m, 1H, ½ of **1'**), 0.00, (s, 9H, **2a** and **3a** and **4a**) ppm. $^{13}C\{^{1}H\}$ NMR ($CDCl_3$, 101 MHz, 298 K): δ 64.74, 48.32, 35.46, 29.65, 27.25, 25.84, 21.22, 19.10, 0.00 ppm. HRMS (ESI): *m/z* calcd for $C_{11}H_{26}N_1Si_1$ $[M+H^+]$: 200.1835 Found: 200.1835.

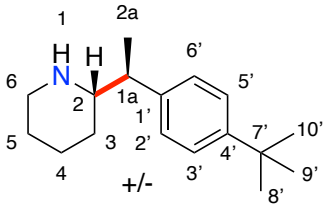

Synthesis of 2-(1-(4-(tert-butyl)phenyl)ethyl)piperidine (4.26): Prepared following the general procedure outlined above: 26.0 mg Ta, 15.2 mg Ligand, piperidine (85.15 mg, 1.0 mmol), para-t-butylstyrene (160.13 mg, 1.0 mmol). The reaction was subsequently concentrated, and the yield was determined to be 65 % by NMR (1,3, 5-trimethoxybenzene as a standard). Purification via column chromatography (7:2.5:0.5 hexanes : ethyl acetate : triethyl amine): ^{1}H NMR ($CDCl_3$, 400 MHz, 298 K): δ 7.34 (m, 2H, **3'** and **5'**), 7.14 (m, 2H, **2'** and **6'**), 3.12 (m, 1H, ½ of **6**), 2.69 (m, 1H, **1a**), 2.63 (m, 1H, ½ of **6**), 2.57 (m, 1H, **2**), 1.93 (broad s, 1H, NH), 1.75 (m, 1H, ½ of **4**), 1.57 (m, 1H, ½ of **5**), 1.49 (m, 1H, ½ of **3**), 1.40 (m, 1H, ½ of **5**), 1.34 (s, 9H, **8'** and **9'** and **10'**), 1.32 (d, J = 1.32, 3H, **2a**), 1.27 (m, 1H, ½ of **4**), 1.10 (m, 1H, ½ of **3**) ppm. $^{13}C\{^{1}H\}$ NMR ($CDCl_3$, 101 MHz, 298 K): δ 148.86, 141.88, 127.44, 125.11, 47.47, 45.03, 34.37, 31.44, 30.79, 26.46, 25.02, 17.00 ppm. HRMS (ESI): *m/z* calcd for $C_{17}H_{27}N$ $[M+H^+]$: 245.2143 Found: 245.2147.

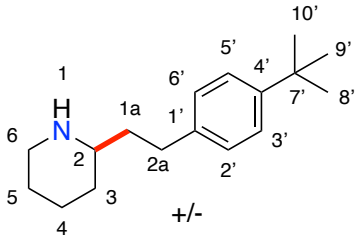

Synthesis of 2-(4-(tert-butyl)phenethyl)piperidine (4.27): Prepared following the general procedure outlined above: 26.0 mg Ta, 15.2 mg Ligand, piperidine (85.15 mg, 1.0 mmol), para-t-butylstyrene (160.13 mg, 1.0 mmol). The reaction was subsequently concentrated, and the yield was determined to be 34 % by NMR (1,3,5-trimethoxybenzene as a standard). Purification via column chromatography (7:2.5:0.5 hexanes : ethyl acetate : triethyl amine): ^{1}H NMR ($CDCl_3$, 400 MHz, 298 K): δ 7.33 (m, 2H, **3'** and **5'**), 7.15 (m, 2H, **2'** and **6'**), 3.12 (m, 1H, ½ of **6**), 2.70 (m, 1H, ½ of **6**), 2.64 (m, 2H, **2a**), 2.56 (m, 1H, **2**), 2.26 (broad s, 1H, NH), 1.82 (m, 1H, ½ of **4**), 1.77 (m, 1H, ½ of **3**), 1.70 (m, 2H, **1a**), 1.63 (m, 1H, ½ of **5**), 1.48 (m, 1H, ½ of **5**), 1.41 (m, 1H, ½ of **4**), 1.34 (s, 9H, **8'** and **9'** and **10'**), 1.18 (m, 1H, ½ of **3**) ppm. ^{13}C{^{1}H} NMR ($CDCl_3$, 101 MHz, 298 K): δ 148.55, 139.22, 127.97, 125.26, 56.56, 47.05, 39.01, 34.36, 32.75, 31.72, 31.42, 26.46, 24.76 ppm. HRMS (ESI): *m/z* calcd for $C_{17}H_{27}N$ [M+H$^+$]: 245.2143 Found: 245.2148.

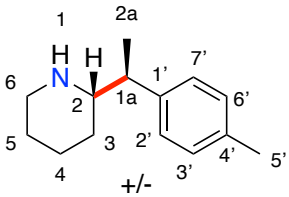

Synthesis of 2-(1-(p-tolyl)ethyl)piperidine (4.28): Prepared following the general procedure outlined above: 26.0 Ta, 15.2 Ligand, piperidine (85.15 mg, 1.0 mmol), 4-methylstyrene (118.18 mg, 1.0 mmol). The reaction was subsequently concentrated, and the yield was determined to be 67 % by NMR (1,3,5-trimethoxybenzene as a standard). Purification via column chromatography (7:2.5:0.5 hexanes : ethyl acetate : triethyl amine): ^{1}H NMR ($CDCl_3$, 400 MHz, 298 K): δ 7.10 (m, 2H, **3'** and **6'**), 7.08 (m, 2H, **2'** and **7'**), 3.12 (m, 1H, ½ of **6**), 2.65 (m, 1H, **1a**), 2.62 (m, 1H, ½ of **6**), 2.54 (m, 1H, **2**), 2.32 (s, 3H, **5'**), 1.95 (broad s, 1H, NH), 1.72 (m, 1H, ½ of **4**), 1.56 (m, 1H, ½ of **5**), 1.45 (m, 1H, ½ of **3**), 1.36 (m, 1H, ½ of **5**), 1.29 (d, J = 1.28, 3H, **2a**), 1.24 (m, 1H, ½ of **4**), 1.06 (m, 1H, ½ of **3**) ppm. ^{13}C{^{1}H} NMR ($CDCl_3$, 101 MHz, 298 K): δ 142.07, 135. 79, 129.11, 127.84, 62.64, 47.54,

45.26, 30.83, 26.46, 25.04, 21.13, 17.43 ppm. HRMS (ESI): *m/z* calcd for $C_{14}H_{22}N$ [M+H$^+$]: 204.1752 Found: 204.1748.

Note: The 1D/2D NMR spectroscopy data for this compound is a representative example of how we were able to assign all proton and carbon signals conclusively in products with styrenes as coupling partners.

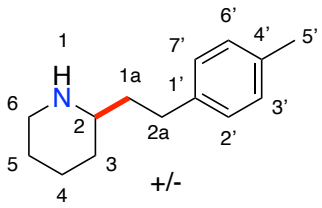

Synthesis of 2-(4-methylphenethyl)piperidine (4.29): Prepared following the general procedure outlined above: 26.0 Ta, 15.2 Ligand, piperidine (85.15 mg, 1.0 mmol), para-methylstyrene (118.18 mg, 1.0 mmol). The reaction was subsequently concentrated, and the yield was determined to be 29 % by NMR (1,3,5-trimethoxybenzene as a standard). Purification via column chromatography (7:2.5:0.5 hexanes : ethyl acetate : triethyl amine): ^{1}H NMR ($CDCl_3$, 400 MHz, 298 K): δ 7.08 (m, 4H, **2'** and **3'** and **6'** and **7'**), 3.09 (m, 1H, ½ of **6**), 2.65 (m, 1H, ½ of **6**), 2.59 (m, 2H, **2a**), 2.52 (m, 1H, **2**), 2.31 (s, 3H, **5'**), 1.96 (broad s, 1H, NH), 1.81 (m, 1H, ½ of **4**), 1.73 (m, 1H, ½ of **3**), 1.68 (m, 2H, **1a**), 1.58 (m, 1H, ½ of **5**), 1.45 (m, 1H, ½ of **5**), 1.35 (m, 1H, ½ of **4**), 1.14 (m, 1H, ½ of **3**) ppm. ^{13}C{^{1}H} NMR ($CDCl_3$, 101 MHz, 298 K): δ 139.29, 135.33, 129.19, 128.34, 56.60, 47.17, 39.22, 32.82, 31.92, 26.53, 24.84, 21.12 ppm. HRMS (ESI): *m/z* calcd for $C_{14}H_{22}N$ [M+H$^+$]: 204.1752 Found: 204.1755.

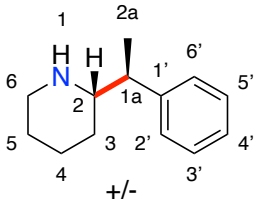

Synthesis of 2-(1-phenylethyl)piperidine (4.30): Prepared following the general procedure outlined above: 26.0 mg Ta, 15.2 mg Ligand, piperidine (85.15 mg, 1.0 mmol), styrene (104.15 mg, 1.0 mmol). The reaction was subsequently concentrated, and the yield was determined to be 60 % by NMR (1,3,5-trimethoxybenzene as a standard). Purification via column chromatography (7:2.5:0.5 hexanes : ethyl acetate : triethyl amine): ^{1}H NMR ($CDCl_3$, 400 MHz, 298 K): δ 7.22 (m, 2H, **3'** and **5'**), 7.16 (m, 2H, **2'** and **6'**), 7.12 (m, 1H, **4'**), 3.07 (m, 1H, ½ of **6**), 2.63 (m, 1H, **1a**), 2.52 (m, 1H, ½ of **6**), 2.52 (m, 1H, **2**), 1.92 (broad s, 1H, NH), 1.68 (m, 1H, ½ of **4**), 1.52 (m, 1H, ½ of **5**), 1.39 (m, 1H, ½ of **3**), 1.30 (m, 1H, ½ of **5**), 1.25 (d, J = 1.26, 3H, **2a**), 1.19 (m, 1H, ½ of **4**), 1.00 (m, 1H, ½ of **3**) ppm. ^{13}C NMR ($CDCl_3$, 101 MHz, 298 K): δ 145.12, 128.43, 127.98, 126.34, 62.61, 47.53, 45.72, 30.85, 26.43, 25.01, 17.42 ppm. HRMS (ESI): *m/z* calcd for $C_{13}H_{20}N$ [M+H$^+$]: 190.1596 Found: 190.1594.

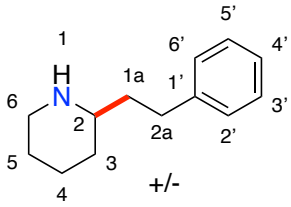

Synthesis of 2-phenethylpiperidine (4.31): Prepared following the general procedure outlined above: 26.0 Ta, 15.2 Ligand, piperidine (85.15 mg, 1.0 mmol), styrene (104.15 mg, 1.0 mmol). The reaction was subsequently concentrated, and the yield was determined to be 40 % by NMR (1,3,5-trimethoxybenzene as a standard). Purification via column chromatography (7:2.5:0.5 hexanes : ethyl acetate : triethyl amine): ^{1}H NMR ($CDCl_3$, 400 MHz, 298 K): δ 7.23 (m, 2H, **3'** and **5'**), 7.16 (m, 2H, **2'** and **6'**), 7.14 (m, 1H, **4'**), 3.07 (m, 1H, ½ of **6**), 2.66 (m, 2H, **2a**), 2.59 (m, 1H, ½ of **6**), 2.50 (m, 1H, **2**), 2.19 (broad s, 1H, NH), 1.76 (m, 1H, ½ of **4**), 1.70 (m, 2H, **1a**), 1.64 (m, ½ of **3**), 1.55 (m, 1H, ½ of **5**), 1.41 (m, 1H, ½ of **5**), 1.31 (m, 1H, ½ of **4**), 1.14 (m, 1H, ½ of **3**) ppm. ^{13}C{^{1}H} NMR ($CDCl_3$, 101 MHz, 298 K): δ 142.37, 128.51, 128.47, 125.90, 56.61, 47.14, 39.04,

32.77, 32.38, 26.48, 24.81 ppm. HRMS (ESI): *m/z* calcd for $C_{13}H_{20}N$ [M+H$^+$]: 190.1596 Found: 190.1592.

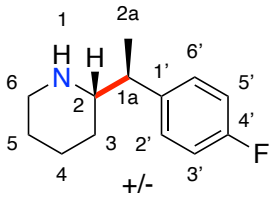

Synthesis of 2-(1-(4-fluorophenyl)ethyl)piperidine (4.32): Prepared following the general procedure outlined above: 26.0 mg Ta, 15.2 mg Ligand, piperidine (85.15 mg, 1.0 mmol), para-fluorostyrene (122.05 mg, 1.0 mmol). The reaction was subsequently concentrated, and the yield was determined to be 60 % by NMR (1,3,5-trimethoxybenzene as a standard). Purification via column chromatography (7:2.5:0.5 hexanes : ethyl acetate : triethyl amine): ^{1}H NMR ($CDCl_3$, 400 MHz, 298 K): δ 7.12 (m, 2H, **3'** and **5'**), 6.96 (m, 2H, **2'** and **6'**), 3.09 (m, 1H, ½ of **6**), 2.64 (m, 1H, **1a**), 2.58 (m, 1H, ½ of **6**), 2.50 (m, 1H, **2**), 1.74 (broad s, 1H, NH), 1.70 (m, 1H, ½ of **4**), 1.55 (m, 1H, ½ of **5**), 1.37 (m, 1H, ½ of **4**), 1.32 (m, 1H, ½ of **5**), 1.25 (d, J = 1.26, 3H, **2a**), 1.21 (m, 1H, ½ of **4**), 1.02 (m, 1H, ½ of **3**) ppm. ^{13}C{^{1}H} NMR ($CDCl_3$, 101 MHz, 298 K): δ 162.70-160-27 (d, J = 242.97), 140.79, 129.24-129.17 (d, J = 7.546), 115.20-114.99 (J = 20.8689), 62.60, 47.54, 45.06, 30.83, 26.54, 25.03, 17.51 ppm. HRMS (ESI): *m/z* calcd for $C_{13}H_{18}FN$ [M+H$^+$]: 207.1423 Found: 207.1427.

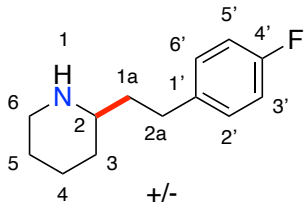

Synthesis of 2-(4-fluorophenethyl)piperidine (4.33): Prepared following the general procedure outlined above: 26.0 mg Ta, 15.2 mg Ligand, piperidine (85.15 mg, 1.0 mmol), para-fluorostyrene (122.05 mg, 1.0 mmol). The reaction was subsequently concentrated, and the yield was determined to be 39 % by NMR (1,3,5-trimethoxybenzene as a standard). Purification via column chromatography (7:2.5:0.5 hexanes : ethyl acetate : triethyl amine): ^{1}H NMR ($CDCl_3$, 400 MHz, 298 K): δ 7.13 (m, 2H, **3'** and **5'**), 6.95 (m, 2H, **2'** and **6'**), 3.07 (m, 1H, ½ of **6**), 2.66 (m, 2H, **1a**), 2.58 (m, 1H, ½ of **6**), 2.49 (m, 1H, **2**), 2.08 (broad s, 1H, NH), 1.79 (m, 1H, ½ of **4**), 1,71 (m, 2H, **2a**), 1.64 (m, 1H, ½ of **3**), 1.58 (m, 1H, ½ of **5**), 1.42 (m, 1H, ½ of **5**), 1.34 (m, 1H, ½ of **4**), 1.12 (m, 1H, ½ of **3**) ppm. ^{13}C{^{1}H} NMR ($CDCl_3$, 101 MHz, 298 K): δ 161.56-160.14 (d, J = 243.074), 138.03-138.00 (d, J = 3.382), 129.77-129.69 (q, J = 7.762), 115.32-115.11 (q, J = 21.148), 56.46, 47.19, 39.31, 32.92, 31.58, 26.62, 24.87 ppm. HRMS (ESI): *m/z* calcd for $C_{13}H_{18}FN$ [M+H$^+$]: 207.1423 Found: 207.1427.

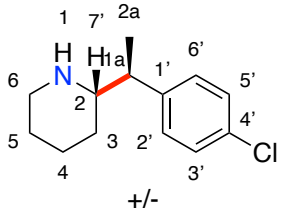

Synthesis of 2-(1-(4-chlorophenyl)ethyl)piperidine (4.34): Prepared following the general procedure outlined above: 26.0 Ta, 15.2 Ligand, piperidine (85.15 mg, 1.0 mmol), 4-chlorostyrene (138.59 mg, 1.0 mmol). The reaction was subsequently concentrated, and the yield was determined to be 54 % by NMR (1,3,5-trimethoxybenzene as a standard). Purification via column chromatography (7:2.5:0.5 hexanes : ethyl acetate : triethyl amine): ^{1}H NMR ($CDCl_3$, 400 MHz, 298 K): δ 7.25 (m, 2H, **3'** and **5'**), 7.11 (m, 2H, **2'** and **6'**), 3.11 (m, 1H, ½ of **6**), 2.65 (m, 1H, **1a**), 2.59 (m, 1H, ½ of **6**), 2.52 (m, 1H, **2**), 1.85 (broad s, 1H, NH), 1.71 (m, 1H, ½ of **4**), 1.57 (m, 1H, ½ of **5**), 1.41 (m, 1H, ½ of **3**), 1.33 (m, 1H, ½ of **5**), 1.26 (d, J = 1.31, 3H, **2a**), 1.22 (m, 1H, ½ of **4**), 1.03 (m, 1H, ½ of **3**) ppm. ^{13}C{^{1}H} NMR ($CDCl_3$, 101 MHz, 298 K): δ 143.42, 131.88, 129.17, 128.43, 62.38, 47.38,

45.06, 30.63, 26.25, 24.81, 17.35 ppm. HRMS (ESI): *m/z* calcd for $C_{13}H_{19}NCl$ [M+H$^+$]: 224.1206 Found: 224.1201.

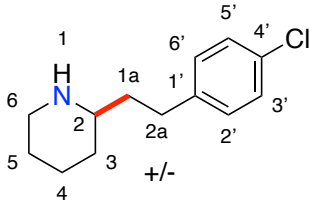

Synthesis of 2-(4-chlorophenethyl)piperidine (4.35): Prepared following the general procedure outlined above: 26.0 Ta, 15.2 Ligand, piperidine (85.15 mg, 1.0 mmol), 4-chlorostyrene (138.59 mg, 1.0 mmol). The reaction was subsequently concentrated, and the yield was determined to be 46 % by NMR (1,3,5-trimethoxybenzene as a standard). Purification via column chromatography (7:2.5:0.5 hexanes : ethyl acetate : triethyl amine): ^{1}H NMR ($CDCl_3$, 400 MHz, 298 K): δ 7.22 (m, 2H, **3'** and **5'**), 7.10 (m, 2H, **2'** and **6'**), 3.14 (m, 1H, ½ of **6**), 2.66 (m, 2H, **2a**), 2.64 (m, 1H, ½ of **6**), 2.53 (m, 1H, **2**), 2.45, (broad s, 1H, NH), 1.82 (m, 1H, ½ of **4**), 1.74 (m, 2H, **1a**), 1.69 (m, 1H, ½ of **3**), 1.61 (m, 1H, ½ of **5**), 1.48 (m, 1H, ½ of **5**), 1.34 (m, 1H, ½ of **4**), 1,22 (m, 1H, ½ of **3**) ppm. ^{13}C{^{1}H} NMR ($CDCl_3$, 101 MHz, 298 K): δ 140.87, 131.55, 129.77, 128.55, 56.42, 47.22, 39.11, 32.95, 31.71, 26.66, 24.86 ppm. HRMS (ESI): *m/z* calcd for $C_{13}H_{19}NCl$ [M+H$^+$]: 224.1206 Found: 224.1207.

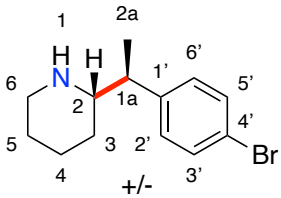

Synthesis of 2-(1-(4-bromophenyl)ethyl)piperidine (4.36): Prepared following the general procedure outlined above: 26.0 mg Ta, 15.2 mg Ligand, piperidine (85.15 mg, 1.0 mmol), para-bromostyrene (181.9 mg, 1.0 mmol). The reaction was subsequently concentrated, and the yield was determined to be 58 % by NMR (1,3,5-trimethoxybenzene as a standard). Purification via column chromatography (7:2.5:0.5 hexanes : ethyl acetate : triethyl amine): ^{1}H NMR ($CDCl_3$, 400 MHz, 298 K): δ 7.40 (m, 2H, **3'** and **5'**), 7.07 (m, 2H, **2'** and **6'**), 3.11 (m, 1H, ½ of **6**), 2.65 (m, 1H, **1a**), 2.59 (m, 1H, ½ of **6**), 2.52 (m, 1H, **2**), 1.81 (broad s, 1H, NH), 1.71 (m, 1H, ½ of **4**), 1.54 (m, 1H, ½ of **5**), 1.39 (m, 1H, ½ of **3**), 1.34 (m, 1H, ½ of **5**), 1.26 (d, J = 1.27, 3H, **2a**), 1.22 (m, 1H, ½ of **4**), 1.02 (m, 1H, ½ of **3**) ppm. ^{13}C{^{1}H} NMR ($CDCl_3$, 101 MHz, 298 K): δ 144.17, 131.47, 129.71, 120.00, 62.41, 47.53, 45.32, 30.84, 26.51, 25.00, 17.32 ppm. HRMS (ESI): *m/z* calcd for $C_{13}H_{18}BrN$ [M+H$^+$]: 267.0623 Found: 267.0626.

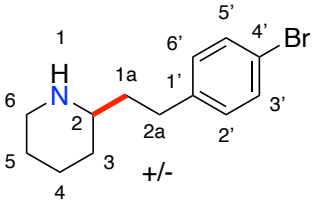

Synthesis of 2-(4-bromophenethyl)piperidine (4.37): Prepared following the general procedure outlined above: 26.0 mg Ta, 15.2 mg Ligand, piperidine (85.15 mg, 1.0 mmol), para-bromostyrene (181.9 mg, 1.0 mmol). The reaction was subsequently concentrated, and the yield was determined to be 42 % by NMR (1,3,5-trimethoxybenzene as a standard). Purification via column chromatography (7:2.5:0.5 hexanes : ethyl acetate : triethyl amine): ^{1}H NMR ($CDCl_3$, 400 MHz, 298 K): δ 7.39 (m, 2H, **3'** and **5'**), 7.04 (m, 2H, **2'** and **6'**), 3.11 (m, 1H, ½ of **6**) 2.82 (broad s 1H, NH), 2.65 (m, 1H, ½ of **6**), 2.60 (m, 2H, **2a**), 2.52 (m, 1H, **2**), 1.79 (m, 1H, ½ of **4**), 1.73 (m, 1H, ½ of **3**), 1.67 (m, 2H, **1a**), 1.61 (m, 1H, ½ of **5**), 1.45 (m, 1H, ½ of **5**), 1.36 (m, 1H, ½ of **4**), 1.18 (m, 1H, ½ of **3**) ppm. ^{13}C{^{1}H} NMR ($CDCl_3$, 101 MHz, 298 K): δ 141.22, 131.56, 130.23, 119.65, 56.34, 46.88,

38.58, 32.46, 31.70, 26.30, 24.64 ppm. HRMS (ESI): *m/z* calcd for $C_{13}H_{18}BrN$ [M+H$^+$]: 267.0623 Found: 267.0625.

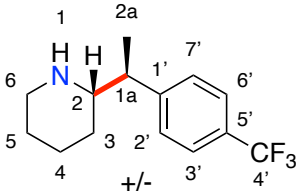

Synthesis of 2-(1-(4-(trifluoromethyl)phenyl)ethyl)piperidine (4.38): Prepared following the general procedure outlined above: 26.0 mg Ta, 15.2 mg Ligand, piperidine (85.15 mg, 1.0 mmol), para-trifluoromethylstyrene (172.05 mg, 1.0 mmol). The reaction was subsequently concentrated, and the yield was determined to be 37 % by NMR (1,3,5-trimethoxybenzene as a standard). Purification via column chromatography (7:2.5:0.5 hexanes : ethyl acetate : triethyl amine): ^{1}H NMR ($CDCl_3$, 400 MHz, 298 K): δ 7.53 (m, 2H, **3'** and **6'**), 7.28 (m, 2H, **2'** and **7'**), 3.12 (m, 1H, ½ of **6**), 2.74 (m, 1H, **1a**), 2.61 (overlapping dt, 1H, ½ of **6**), 2.57 (m, 1H, **2**), 2.02 (broad s, 1H, NH), 1.70 (m, 1H, ½ of **4**), 1.56 (m, 1H, ½ of **5**), 1.38 (m, 1H, ½ of **3**), 1.34 (m, 1H, ½ of **5**), 1.31 (d, J = 1.31, 3H, **2a**), 1.22 (m, 1H, ½ of **4**), 1.02 (m, 1H, ½ of **3**) ppm. ^{13}C{^{1}H} NMR ($CDCl_3$, 101 MHz, 298 K): δ 149.24 , 128.76 (q, J = 32), 128.54, 128.29 (q, J = 271.26), 125.36, 63.33, 47.45, 45.73, 30.78, 26.32, 25.88, 17.42 ppm. HRMS (ESI): *m/z* calcd for $C_{14}H_{18}F_3N$ [M+H$^+$]: 257.2391 Found: 257.1395.

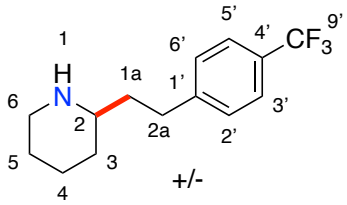

Synthesis of 2-(4-(trifluoromethyl)phenethyl)piperidine (4.39): Prepared following the general procedure outlined above: 26.0 mg Ta, 15.2 mg Ligand, piperidine (85.15 mg, 1.0 mmol), para-trifluoromethylstyrene (172.05 mg, 1.0 mmol). The reaction was subsequently concentrated, and the yield was determined to be 55 % by NMR (1,3,5-trimethoxybenzene as a standard). Purification via column chromatography (7:2.5:0.5 hexanes : ethyl acetate : triethyl amine): ^{1}H NMR ($CDCl_3$, 400 MHz, 298 K): δ 7.53 (m, 2H, **2'** and **3'**), 7.29 (m, 2H, **3'** and **5'**), 3.09 (m, 1H, ½ of **6**), 2.72 (m, 2H, **2a**), 2.62 (m, 1H, ½ of **6**), 2.50 (m, 1H, **2**), 2.00 (broad s, 1H, NH), 1.80 (m, 1H, ½ of **4**), 1.72 (m, 1H, ½ of **3**), 1.68 (m, 2H, **1a**), 1.60 (m, 1H, ½ of **5**), 1.41 (m, 1H, ½ of **5**), 1.35 (m, 1H, ½ of **4**), 1.14 (m, 1H, ½ of **3**) ppm. ^{13}C{^{1}H} NMR ($CDCl_3$, 101 MHz, 298 K): δ 146.63, 128.75 (q, J = 32.42), 125.84 (q, J = 4.063), 125.44 (q, J = 272.85), 56.43, 47.20, 38.93, 32.95, 32.24, 25.66, 24.85 ppm. HRMS (ESI): *m/z* calcd for $C_{14}H_{18}F_3N$ [M+H$^+$]: 257.2391 Found: 257.1394.

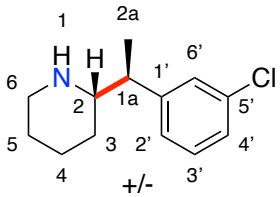

Synthesis of 2-(1-(3-chlorophenyl)ethyl)piperidine (4.40): Prepared following the general procedure outlined above: 26.0 mg Ta, 15.2 mg Ligand, piperidine (85.15 mg, 1.0 mmol), meta-chlorostyrene (138.59 mg, 1.0 mmol). The reaction was subsequently concentrated, and the yield was determined to be 45 % by NMR (1,3,5-trimethoxybenzene as a standard). Purification via column chromatography (7:2.5:0.5 hexanes : ethyl acetate : triethyl amine): ^{1}H NMR ($CDCl_3$, 400 MHz, 298 K): δ 7.23 (m, 1H, **3'**), 7.18 (m, 1H, **4'**), 7.16 (m, 1H, **6'**), 7.05, (m, 1H, **2'**), 3.09 (m, 1H, ½ of **6**), 2.63 (m, 1H, **1a**), 2.59 (m, 1H, ½ of **6**), 2.53 (m, 1H, **2**), 2.00 (broad s, 1H, NH), 1.72 (m, 1H, ½ of **4**), 1.54 (m, 1H, ½ of **5**), 1.41 (m, 1H, ½ of **3**), 1.34 (m, 1H, ½ of **5**), 1.27 (d, J = 1.28, 3H, **2a**), 1.23 (m, 1H, ½ of **4**), 1.02 (m, 1H, ½ of **3**) ppm. ^{13}C{^{1}H} NMR ($CDCl_3$, 101 MHz, 298 K): δ 147.20,

134.12, 129.55, 127.90, 126.41, 126.13, 62.24, 47.37, 45.54, 30.76, 26.30, 24.83, 17.27 ppm. HRMS (ESI): *m/z* calcd for $C_{13}H_{18}ClN$ [M+H$^+$]: 223.1128 Found: 223.1135.

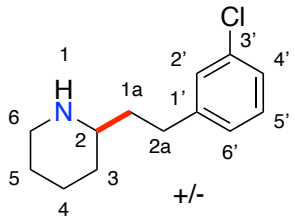

Synthesis of 2-(3-chlorophenethyl)piperidine (4.41): Prepared following the general procedure outlined above: 26.0 mg Ta, 15.2 mg Ligand, piperidine (85.15 mg, 1.0 mmol), meta-chlorostyrene (138.59 mg, 1.0 mmol). The reaction was subsequently concentrated, and the yield was determined to be 53 % by NMR (1,3,5-trimethoxybenzene as a standard). Purification via column chromatography (7:2.5:0.5 hexanes : ethyl acetate : triethyl amine): ^{1}H NMR ($CDCl_3$, 400 MHz, 298 K): δ 7.19 (m, 1H, **4'**), 7.17 (m, 1H, **2'/6'**), 7.16 (m, 1H, **2'/6'**), 7.05 (m, 1H, **5'**), 3.12 (m, 1H, ½ of **6**), 2.65 (m, 2H, **2a**), 2.63 (m, 1H, ½ of **6**), 2.54 (m, 1H, **2**), 1.81 (m, 1H, ½ of **4**), 1.73 (m, 1H, ½ of **3**), 1.71 (m, 2H, **1a**), 1.60 (m, 1H, ½ of **5**), 1.47 (m, 1H, ½ of **5**), 1.35, (m, 1H, ½ of **4**), 1.20 (m, 1H, ½ of **3**) ppm. ^{13}C{^{1}H} NMR ($CDCl_3$, 101 MHz, 298 K): δ 144.13, 134.13, 129.65, 128.48, 126.54, 126.04, 56.31, 46.73, 38.25, 32.21, 31.82, 25.95, 24.44 ppm. HRMS (ESI): *m/z* calcd for $C_{13}H_{18}ClN$ [M+H$^+$]: 223.1128 Found: 223.1137.

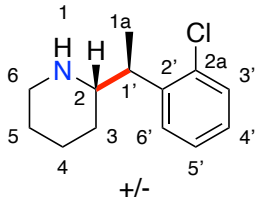

Synthesis of 2-(1-(2-chlorophenyl)ethyl)piperidine (4.42): Prepared following the general procedure outlined above: 26.0 mg Ta, 15.2 mg Ligand, piperidine (85.15 mg, 1.0 mmol), 2-chlorostyrene (138.59 mg, 1.0 mmol). The reaction was subsequently concentrated, and the yield was determined to be 51 % by NMR (1,3,5-trimethoxybenzene as a standard). Purification via column chromatography (7:2.5:0.5 hexanes : ethyl acetate : triethyl amine): ^{1}H NMR ($CDCl_3$, 400 MHz, 298 K): δ 7.57 (m, 1H, **3'**), 7.47 (m, 1H, **5'/6'**), 7.43 (m, 1H, **5'/6'**), 7.33 (m, 1H, **4'**), 3.52 (m, 1H, **1'**), 3.33 (m, 1H, ½ of **6**), 2.86 (m, 1H, **2**), 2.80 (m, 1H, ½ of **6**), 2.00 (broad s, 1H, NH), 1.92 (m, 1H, ½ of **4**), 1.75 (m, 1H, ½ of **5**), 1.64 (m, 1H, ½ of **5**), 1.57 (m, 1H, ½ of **3**), 1.48 (d, J = 1.49, 3H, **1a**), 1.45 (m, 1H. ½ of

4), 1.38 (m, 1H, ½ of **3**) ppm. $^{13}C\{^{1}H\}$ NMR ($CDCl_3$, 101 MHz, 298 K): δ ppm. HRMS (ESI): *m/z* calcd for $C_{13}H_{19}NCl$ $[M+H^+]$: 224.1206 Found: 224.1208.

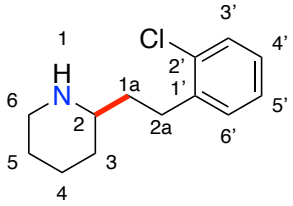

Synthesis of 2-(1-(2-chlorophenyl)ethyl)piperidine (4.43): Prepared following the general procedure outlined above: 26.0 mg Ta, 15.2 mg Ligand, piperidine (85.15 mg, 1.0 mmol), 2-chlorostyrene (138.59 mg, 1.0 mmol). The reaction was subsequently concentrated, and the yield was determined to be 49 % by NMR (1,3,5-trimethoxybenzene as a standard). Purification via column chromatography (7:2.5:0.5 hexanes : ethyl acetate : triethyl amine): ^{1}H NMR ($CDCl_3$, 400 MHz, 298 K): δ 7.33 (m, 1H, **3'**), 7.21 (m, 1H, **6'**), 7.14 (m, 2H, **4'** and **5'**), 3.12 (m, 1H, ½ of **6**), 2.77 (m, 2H, **2a**), 2.65 (m, 1H, ½ of **6**), 2.55 (m, 1H, **2**), 2.11 (broad s, 1H, NH), 1.82 (m, 1H, ½ of **4**), 1.76 (m, 1H, ½ of **3**), 1.69 (m, 2H, **1a**), 1.62 (m, 1H, ½ of **5**), 1.47 (m, 1H, ½ of **5**), 1.38 (m, 1H, ½ of **4**), 1.18 (m, 1H, ½ of **3**) ppm. $^{13}C\{^{1}H\}$ NMR ($CDCl_3$, 101 MHz, 298 K): δ 140.01, 134.01, 130.39, 129.61, 127.41, 126.95, 56.74, 47.19, 37.39, 32.77, 30.15, 26.51, 24.83 ppm. HRMS (ESI): *m/z* calcd for $C_{13}H_{19}NCl$ $[M+H^+]$: 224.1206 Found: 224.1208.

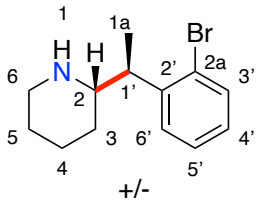

Synthesis of 2-(1-(2-bromophenyl)ethyl)piperidine (4.44): Prepared following the general procedure outlined above: 26.0 mg Ta, 15.2 mg Ligand, piperidine (85.15 mg, 1.0 mmol), 2-bromostyrene (181.9 mg, 1.0 mmol). The reaction was subsequently concentrated. Yield of the reaction mixture could not be determined via solubility issues after styrene polymerization. Total reaction conversion was 99 %. Purification via column chromatography (7:2.5:0.5 hexanes : ethyl acetate : triethyl amine): ^{1}H NMR ($CDCl_3$, 400 MHz, 298 K): δ 7.56 (m, 1H, **3'**), 7.27 (m, 1H, **5'**), 7.23 (m, 1H, **6'**), 7.05 (m, 1H, **4'**), 3.29 (m, 1H, **1a**), 3.11 (m, 1H, ½ of **6**), 2.67 (m, 1H, **2**), 2.60 (m, 1H, ½ of **6**), 1.95 (broad s, 1H, NH), 1.74 (m, 1H, ½ of **4**), 1.55 (m, 1H, ½ of **5**), 1.44 (m, 1H, ½ of **3**), 1.38 (m, 1H, ½ of

5), 1.28 (d, J = 1.27, 3H, **2a**), 1.25 (m, 1H, ½ of **3**), 1.22 (m, 1H, ½ of **4**) ppm. $^{13}C\{^{1}H\}$ NMR ($CDCl_3$, 101 MHz, 298 K): δ 144.51, 133.15, 128.36, 127.65, 127.61, 125.29, 61.70, 47.50, 43.46, 30.70, 26.38, 25.02, 16.84 ppm. HRMS (ESI): *m/z* calcd for $C_{13}H_{19}NBr$ $[M+H^+]$: 268.0701 Found: 268.0704.

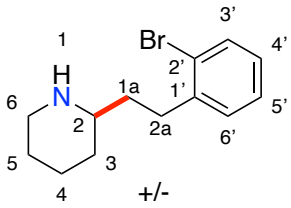

Synthesis of 2-(2-bromophenethyl)piperidine (4.45): Prepared following the general procedure outlined above: 26.0 mg Ta, 15.2 mg Ligand, piperidine (85.15 mg, 1.0 mmol), 2-bromostyrene (181.9 mg, 1.0 mmol). The reaction was subsequently concentrated. Yield of the reaction mixture could not be determined via solubility issues after styrene polymerization. Total reaction conversion was 99 %. Purification via column chromatography (7:2.5:0.5 hexanes : ethyl acetate : triethyl amine): ^{1}H NMR ($CDCl_3$, 400 MHz, 298 K): δ 7.49 (m, 1H, **3'**), 7.19 (m, 2H, **5'** and **6'**), 7.02 (m, 1H, **4'**), 3.08 (m, 1H, ½ of **6**), 2.77 (m, 2H, **2a**), 2.64 (m, 1H, ½ of **6**), 2.54 (m, 1H, **2**), 2.28 (broad s, 1H, NH), 1.80 (m, 1H, ½ of **4**), 1.71 (m, 1H, ½ of 3), 1.66 (m, 1H, **1a**), 1.57 (m, 1H, ½ of **5**), 1.44 (m, 1H, ½ of **5**), 1.35 (m, 1H, ½ of **4**), 1.16 (m, 1H, ½ of **3**) ppm. $^{13}C\{^{1}H\}$ NMR ($CDCl_3$, 101 MHz, 298 K): δ 141.71, 132.86, 130.31, 127.60, 127.56, 124.48, 56.66, 47.17, 37.57, 32.79, 32.70, 26.53, 24.82 ppm. HRMS (ESI): *m/z* calcd for $C_{13}H_{19}NBr$ $[M+H^+]$: 268.0701 Found: 268.0704.

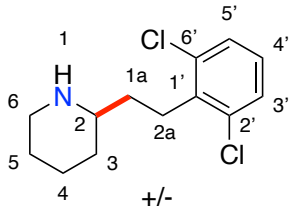

Synthesis of 2-(2,6-dichlorophenethyl)piperidine (4.46): Prepared following the general procedure outlined above: 26.0 mg Ta, 15.2 mg Ligand, piperidine (85.15 mg, 1.0 mmol), 2,6-dichlorostyrene (173.04 mg, 1.0 mmol). The reaction was subsequently concentrated, and the yield was determined to be 45 % by NMR (1,3,5-trimethoxybenzene as a standard). Purification via column chromatography (7:2.5:0.5 hexanes : ethyl acetate : triethyl amine): ^{1}H NMR ($CDCl_3$, 400 MHz, 298 K): δ 7.28 (m, 2H, **3'** and **5'**), 7.07 (m, 1H, **4'**), 3.19 (m, 1H, ½ of **6**), 2.98 (m, 2H, **2a**), 2.73 (m, 1H, ½ of **6**), 2.66 (m, 1H, **2**), 2.22 (broad s, 1H, NH), 1.85 (m, 1H, ½ of **4**), 1.83 (m, 1H, ½ of **3**), 1.73 (m, 2H, **1a**), 1.66 (m, 1H, ½ of **5**), 1.56 (m, 1H, ½ of **5**), 1.43 (m, 1H, ½ of **4**), 1.34 (m, 1H, ½ of **3**) ppm. ^{13}C{^{1}H} NMR ($CDCl_3$, 101 MHz, 298 K): δ 138.08, 135.38, 128.31, 127.73, 57.00, 46.78, 34.78, 31.95, 28.00, 25.82, 24.46 ppm. HRMS (ESI): *m/z* calcd for $C_{13}H_{18}NCl_2$ [M+H$^+$]: 258.0815 Found: 258.0816.

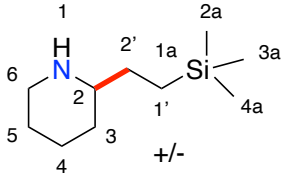

Synthesis of 2-(2-(trimethylsilyl)ethyl)piperidine: Prepared following the general procedure outlined above: 26.0 mg Ta, 15.2 mg Ligand, piperidine (85.15 mg, 1.0 mmol), vinyltrimethylsilane (100.24 mg, 1.0 mmol). The reaction was subsequently concentrated, and the yield was determined to be 68 % by NMR (1,3,5-trimethoxybenzene as a standard). Purification via column chromatography (7:2.5:0.5 hexanes : ethyl acetate : triethyl amine): ^{1}H NMR ($CDCl_3$, 400 MHz, 298 K): δ 3.09 (m, 1H, ½ of **6**), 2.61 (m, 1H, ½ of **6**), 2.33 (m, 1H, **2**), 1.83 (broad s, 1H, NH), 1.79 (m, 1H, ½ of **4**), 1.69 (m, 1H, ½ of **5**), 1.57 (m, 1H, ½ of **5**), 1.41 (m, 2H, **2'**), 1.32 (m, 2H, **1'**), 1.04 (m, 1H, ½ of **3**), 0.52 (m, 1H, ½ of **4**), 0.43 (m, 1H, ½ of **3**), 0.03 (s, 9H, **2a** and **3a** and **4a**) ppm. ^{13}C{^{1}H} NMR ($CDCl_3$, 101 MHz, 298 K): δ 47.40, 32.74, 31.61, 26.78, 25.07, 12.65, -1.67 ppm. HRMS (ESI): *m/z* calcd for $C_{13}H_{18}NCl_2$ [M+H$^+$]: 258.0815 Found: 258.0816.

4.6.4.3 Hydroaminoalkylation Reactions with Minimal Glove Box Use

In these experiments, we used 8 mL septum capped vials that had been store in the oven for both reagent stock solutions and reaction mixtures. Stock solutions for each reagent were prepared in the glove box and immediately brought out for use. Concentrations of stock solutions of $Ta(CH_2SiMe_3)_3Cl_2$ and **4.5** were prepared in toluene at a 0.025 mmol/0.5 mL concentration, such that 0.5 mL of each was used for each reaction. Likewise, stock solutions of piperidine and 1-octene were prepared at a 0.5 mmol/ 0.5 mL (1 mmol/mL) concentration such that 0.5 mL of each of these was used in each test reaction. Empty reaction vials were sparged with N_2 gas for 5 minutes via a nitrogen manifold. All plastic syringes used were backfilled with N_2 gas and emptied three times in a reaction vial before being used. $Ta(CH_2SiMe_3)_3Cl_2$ and ligand salt (0.025 mmol each) were added to the vials via syringe. Reaction vials were then left for 15 minutes to allow for *in situ* salt metathesis to proceed as with a typical glove box reaction setup. Piperidine (0.5 mmol) and 1-octene (0.5 mmol) were then added and reactions were added to a metal heating block that was preheated to 150 °C for 20 h. Figure 4.11 provides additional detail for what this process looked like. Note that there are two reactions vials because the reaction was setup in duplicate.

Stock Solutions for
All Reagents

Sparge Vials
(5 minutes)

Visible NaCl
Formation

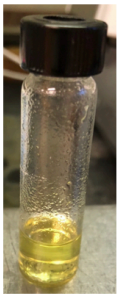

Before
Heating

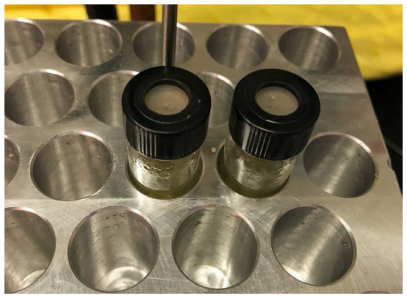

Heating Block

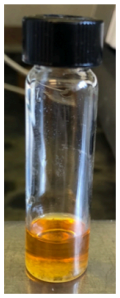

After
Heating

Figure 4.11. Images to depict hydroaminoalkylation reaction setup without using a glove box.

4.6.4.4 Amine Scope Products with o-Chlorostyrene

The products in this section were partially isolated, though all reactions were run. Crude mixtures were analyzed by GC-MS and ^{1}H NMR spectroscopy.

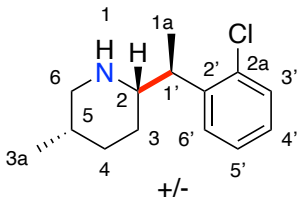

Synthesis of 2-(1-(2-chlorophenyl)ethyl)-5-methylpiperidine (4.54): Prepared following the general procedure outlined above: 26.0 mg Ta, 15.2 mg Ligand, 3-methylpiperidine (99.17 mg, 1.0 mmol), 2-chlorostyrene (138.59 mg, 1.0 mmol). The reaction was subsequently concentrated, and the conversion was determined to be 99 % by ^{1}H NMR. Purification via column chromatography (7:2.5:0.5 hexanes : ethyl acetate : triethyl amine): ^{1}H NMR ($CDCl_3$, 400 MHz, 298 K): δ 7.36 (m, 1H, **3'**), 7.24 (m, 1H, **6'**), 7.22 (m, 1H, **5'**), 7.12 (m, 1H, **4'**), 3.31 (m, 1H, **1'**), 3.08 (m, 1H, ½ of **6**), 2.60 (m, 1H, **2**), 2.21 (m, 1H, ½ of **6**), 1.71 (m, 1H, ½ of **4**), 1.51 (m, 1H, **5**), 1.43 (m, 1H, ½ of **3**), 1.31 (d, 3H, J = 1.31 Hz, **1a**), 1.23 (m, 1H, ½ of **3**), 0.92 (m, 1H, ½ of **4**), 0.81 (d, 3H, J = 1.31 Hz, **3a**) ppm. ^{13}C{^{1}H} NMR ($CDCl_3$, 101 MHz, 298 K): δ 142.86, 134.19, 129.80, 128.35, 127.30, 126.97, 61.35, 55.07, 40.80, 33.83, 31.87, 30.72, 19.57, 16.91 ppm. HRMS (ESI): *m/z* calcd for $C_{14}H_{20}NCl$ [M-H$^+$]: 236.1206 Found: 236.1214.

With this compound, we were also able to characterize its minor diastereomer. Below are spectra that indicate data for this isomer as much as possible as mixed with the major isomer highlighted just above. Note that in this portion, we are only reporting/ integrating peaks we can identify as for specifically the minor isomer. We have not illustrated stereochemistry for this isomer, as we were not able to run NOESY experiments with such a small amount of the diastereomer.

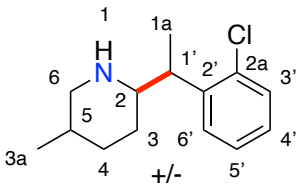

Minor Diastereomer

Synthesis of 2-(1-(2-chlorophenyl)ethyl)-5-methylpiperidine (4.54): Prepared following the general procedure outlined above: 26.0 mg Ta, 15.2 mg Ligand, 3-methylpiperidine (99.17 mg, 1.0 mmol), 2-chlorostyrene (138.59 mg, 1.0 mmol). The reaction was subsequently concentrated, and the conversion was determined to be 99 % by ^{1}H NMR. Purification via column chromatography (7:2.5:0.5 hexanes : ethyl acetate : triethyl amine): ^{1}H NMR ($CDCl_3$, 400 MHz, 298 K): δ 3.22 (m, 1H, **1'**), 2.91 (m, 1H, ½ of **6**), 2.66 (m, 1H, **2**), 2.19 (m, 1H, ½ of **6**), 1.86 (m, 1H, ½ of **3**), 1.79 (m, 1H, ½ of **4**), 1.68 (m, 1H, ½ of **4**), 1.52 (m, 1H, **5**), 1.16 (m, 1H, ½ of **3**), 0.98 (m, 1H, ½ of **4**) ppm. ^{13}C{^{1}H} NMR ($CDCl_3$, 101 MHz, 298 K): δ 142.75, 134.62, 129.95, 128.03, 127.39, 127.16, 61.15, 60.53, 41.57, 33.21, 31.80, 29.90, 19.23, 17.65 ppm.

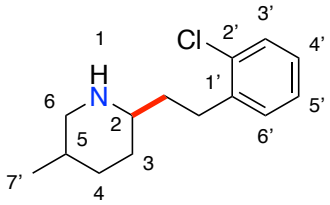

Synthesis of 2-(2-chlorophenethyl)-5-methylpiperidine (4.55): Prepared following the general procedure outlined above: 26.0 mg Ta, 15.2 mg Ligand, 3-methylpiperidine (99.17 mg, 1.0 mmol), 2-chlorostyrene (138.59 mg, 1.0 mmol). The reaction was subsequently concentrated, and the conversion was determined to be 99 % by ^{1}H NMR. Purification via column chromatography (7:2.5:0.5 hexanes : ethyl acetate : triethyl amine). HRMS (ESI): *m/z* calcd for $C_{14}H_{20}NCl$ [M-H^{+}]: 236.1206 Found: 236.1207.

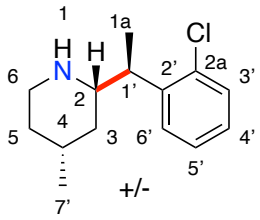

Synthesis of 2-(1-(2-chlorophenyl)ethyl)-4-methylpiperidine (4.56): Prepared following the general procedure outlined above: 26.0 mg Ta, 15.2 mg Ligand, 4-methylpiperidine (99.17 mg, 1.0 mmol), 2-chlorostyrene (138.59 mg, 1.0 mmol). The reaction was subsequently concentrated, and the conversion was determined to be 99 % by ^{1}H NMR. Purification via column chromatography (7:2.5:0.5 hexanes : ethyl acetate : triethyl amine): ^{1}H NMR ($CDCl_3$, 400 MHz, 298 K): δ 7.35 (m, 1H, **3'**), 7.26 (m, 1H, **5'**/**6'**), 7.20 (m, 1H, **5'**/**6'**), 7.14 (m, 1H, **4'**), 3.31 (m, 1H, **1'**), 3.15 (m, 1H, ½ of **6**), 2.70 (m, 1H, **2'**), 2.60 (m, 1H, ½ of **6**), 2.05 (broad s, 1H, NH), 1.59 (m, 1H, ½ of **5**), 1.42 (m, 1H, ½ of **5**), 1.36 (m, 1H, **4**), 1.29 (d, 3H, J = 1.30 Hz, **1a**), 1.06 (m, 1H. ½ of **3**), 0.93 (m, 1H, ½ of **3**), 0.85 (d, 3H, J = 0.84 Hz, **7'**) ppm. ^{13}C{^{1}H} NMR ($CDCl_3$, 101 MHz, 298 K): δ 142.73, 134.22, 129.84, 128.37, 127.33, 126.99, 61.31, 47.17, 40.90, 39.31, 34.85, 31.63, 22.62, 16.79 ppm. HRMS (ESI): *m/z* calcd for $C_{14}H_{20}NCl$ [M+H$^+$]: 238.1363 Found: 238.1361.

Note: The 1D/2D NMR spectroscopy data for this compound is a representative example of how we were able to assign all proton and carbon signals conclusively in products with 2-chlorostyrene as a coupling partner as well as assign relative stereochemistry for all compounds.

For NOESY experiments: The 1D NOESY experiment illustrated irradiated the peak at 2.70 ppm and was analyzed as with a similar amine product with 1-octene above. Results identified the same major diastereomer as above through the same interactions identified.

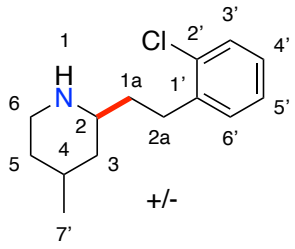

Synthesis of 2-(2-chlorophenethyl)-4-methylpiperidine (4.57): Prepared following the general procedure outlined above: 26.0 mg Ta, 15.2 mg Ligand, 4-methylpiperidine (99.17 mg, 1.0 mmol), 2-chlorostyrene (138.59 mg, 1.0 mmol). The reaction was subsequently concentrated, and the conversion was determined to be 99 % by ^{1}H NMR. Purification via column chromatography (7:2.5:0.5 hexanes : ethyl acetate : triethyl amine): ^{1}H NMR ($CDCl_3$, 400 MHz, 298 K): δ 7.32 (m, 1H, **3'**), 7.22 (m, 1H, **6'**), 7.17 (m, 1H, **5'**), 7.33 (m, 1H, **4'**), 3.12 (m, 1H, ½ of **6**), 2.79 (m, 2H, **2a**), 2.65 (m, 1H, ½ of **6**), 2.56 (m, 1H, **2**), 2.17 (broad s, 1H, NH), 1.76 (m, 1H, ½ of **3**), 1.71 (m, 2H, **2a**), 1.62 (m, 1H, ½ of **5**), 1.47 (m, 1H, **4**), 1.11 (m, 1H, ½ of **5**), 0.93 (d, 3H, J = 0.95, **7'**), 0.84 (m, 1H, ½ of **3**) ppm. ^{13}C{^{1}H} NMR ($CDCl_3$, 101 MHz, 298 K): δ 139.95, 134.01, 130.41, 129.62, 127.44, 126.97, 56.56, 46.84, 41.36, 37.24, 34.93, 31.42, 30.17, 22.66 ppm. HRMS (ESI): *m/z* calcd for $C_{14}H_{20}NCl$ [M+H$^+$]: 238.1363 Found: 238.1359.

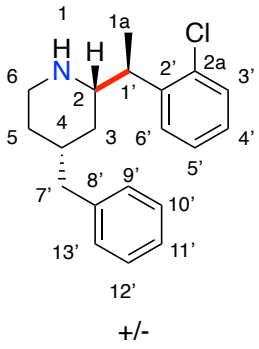

Synthesis of 4-benzyl-2-(1-(2-chlorophenyl)ethyl)piperidine (4.58): Prepared following the general procedure outlined above: 26.0 mg Ta, 15.2 mg Ligand, 4-methylpiperidine (99.17 mg, 1.0 mmol), 2-chlorostyrene (138.59 mg, 1.0 mmol). The reaction was subsequently concentrated, and the conversion was determined to be 99 % by ^{1}H NMR. Purification via column chromatography (7:2.5:0.5 hexanes : ethyl acetate : triethyl amine): ^{1}H NMR ($CDCl_3$, 400 MHz, 298 K): δ 7.36 (m, 1H, **3'**), 7.25 (m, 2H, **10'**/**12'**), 7.22 (m, 2H, **5'**/**6'**), 7.16 (m, 1H, **11'**), 7.12 (m, 1H, **4'**), 7.09 (m, 2H, **9'**/ **13'**), 3.34 (m, 1H, **1'**), 3.12 (m, 1H, ½ of **6**), 2.69 (m, 1H, **2**), 2.57 (m, 1H, ½ of **7'**), 2.51 (m, 1H, ½ of **6**), 2.37 (m, 1H, ½ of **7'**), 2.01 (broad s, 1H, NH), 1.58 (m, 1H, **4**), 1.54 (m, 1H, ½ of **5**), 1.51 (m, 1H, ½ of **3**), 1.31 (d, 3H, J = 1.30 Hz, **1a**), 1.10 (m, 1H, ½ of **3**), 1.02 (m, 1H, ½ of **5**) ppm. ^{13}C NMR ($CDCl_3$, 101 MHz, 298 K): δ 142.51, 140.58, 134.21,

129.84, 129.27, 128.37, 128.24, 127.40, 126.98, 125.89, 61.09, 47.01, 43.88, 40.74, 38.67, 37.59, 32.55, 16.36 ppm. HRMS (ESI): *m/z* calcd for $C_{20}H_{25}NCl$ [M+H$^+$]: 314.1675 Found: 314.1676.

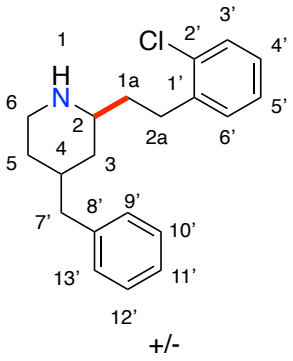

Synthesis of 4-benzyl-2-(2-chlorophenethyl)piperidine (4.59): Prepared following the general procedure outlined above: 26.0 mg Ta, 15.2 mg Ligand, 4-methylpiperidine (99.17 mg, 1.0 mmol), 2-chlorostyrene (138.59 mg, 1.0 mmol). The reaction was subsequently concentrated, and the conversion was determined to be 99 % by ^{1}H NMR. Purification via column chromatography (7:2.5:0.5 hexanes : ethyl acetate : triethyl amine): ^{1}H NMR ($CDCl_3$, 400 MHz, 298 K): δ 7.31 (m, 1H, **3'**), 7.29 (m, 1H, **10'**), 7.26 (m, 2H, **12'**), 7.23 (m, 1H, **6'**), 7.21 (m, 1H, **5'**), 7.14 (m, 1H, **11'**), 7.12 (m, 2H, **5'**/**4'**), 7.10 (m, 1H, **13'**), 3.33 (m, 1H, ½ of **6**), 2.81 (m, 2H, **1a**), 2.73 (m, 1H, **2**), 2.67 (m, 1H, ½ of **6**), 2.57 (m, 2H, **2a**), 2.09 (m, 1H, ½ of **7'**), 1.93 (m, 1H, ½ of **7'**), 1.86 (m, 1H, ½ of **3**), 1.72 (m, 1H, ½ of **5**), 1.65 (m, 1H, **4**), 1.50 (m, 1H, ½ of **5**), 1.32 (m, 1H, ½ of **3**) ppm. ^{13}C{^{1}H} NMR ($CDCl_3$, 101 MHz, 298 K): δ 139.20, 137.91, 133.92, 130.67, 129.71, 129.17, 128.66, 127.97, 127.18, 126.54, 56.92, 44.89, 42.63, 36.99, 35.13, 33.47, 29.19, 28.56 ppm. HRMS (ESI): *m/z* calcd for $C_{20}H_{25}NCl$ [M+H$^+$]: 314.1675 Found: 314.1670.

4.6.4.5 Preliminary Data for Using Hydroaminoalkylation to Synthesize Fused Heterocycles

General procedure for Pd catalyzed Buchwald-Hartwig amination reactions:

A 2-dram screw thread vial was charged with chosen Pd starting material (0.025 mmol, 5 mol %), Ligand (0.05 mmol, 10 mol %), as well as base and/or additive of choice (2 eq.) to the chosen hydroaminoalkylation product. Toluene (1.4 mL) was then added and the vial was heated to 100 °C with stirring for 21.5 h.

Chapter 5: Conclusions

5.1 Summary

This thesis outlined the development of alkyltantalum catalysts with ureate ligands for hydroaminoalkylation reactions. Chapters 2-4 explore the use of alkyltantalum catalyst systems with ureate ligand salts for reaction development and applications in organic synthesis. First, the literature review in Chapter 1 is the first direct comparison as a review of early and late transition-metal based hydroaminoalkylation strategies. Both families of catalysts have seen impressive developments in a reaction motif that remains far from its full potential. The advantages of early transition-metal chemistry include rapid reactivity with secondary arylamine substrates, excellent regioselectivity with group 5 metals, as well as unparalleled reactivity with terminal and internal alkene substrates. Notably, these secondary amine substrates require no derivatization prior to the reaction. Linear and branched regioselectivities can be accessed, and the development of highly regioselective catalysts remains an outstanding challenge. Limited substrate scope, remaining opportunities in stereoselectivity, as well as air and moisture sensitivity were significant challenges towards widespread adoption of early transition-metal mediated hydroaminoalkylation.

In contrast, late transition-metal or photoredox catalyzed hydroaminoalkylation strategies are typically entirely selective for the linear regioisomer and have presented impressive results with saturated, directing group-incorporated *N*-heterocycle substrates for the last two decades. Recent disclosures[108,113] have also applied photoredox principles for use with other tertiary amines. Late transition-metal and photoredox catalyst systems are less air and moisture sensitive, though reactions are still not run in an ambient environment. Unfortunately, these strategies rely on often-high loadings of expensive metals (Ru and Ir) and lack step economy, as directing groups or amine

surrogates are consistently required. As a result, reactions with free primary or secondary amines are not yet known.

Chapter 2 focuses exclusively on catalyst development, where we began by comparing the reactivity of different Ta-based starting materials without the use of exogenous chelating ligands. This investigation identified $Ta(CH_2SiMe_3)_3Cl_2$ as the most reactive and easy to use option, so most investigations in this thesis focused on catalyst systems with this precursor. Next, by exploring a small series of 1,3-*N,O*-chelating ligand salts for *in situ* reactivity, several combinations using ureate salts **2.4** and **2.5** (Scheme 5.1) were identified as being the most reactive with unprecedented TOFs for this reaction. Interestingly, using **2.4** resulted in excellent reactivity with terminal alkene substrates but diminished reactivity with internal alkene substrates while using **2.5** completely reversed that trend to favour internal alkene substrates. We thus used careful ligand choice to generate a scope of hydroaminoalkylation products that combined aryl amines with either terminal or internal alkene partners. All products were generated as only the branched regioisomer. Notably, using alkyltantalum materials eliminated the need for excess alkene, allowing for 1:1 amine: alkene. This also meant that most products could be purified with a simple filtration protocol and did not require column chromatography. Understanding these unexpected differences in reactivity remains a challenge, but one that future work for Chapter 2 outlines strategies to address.

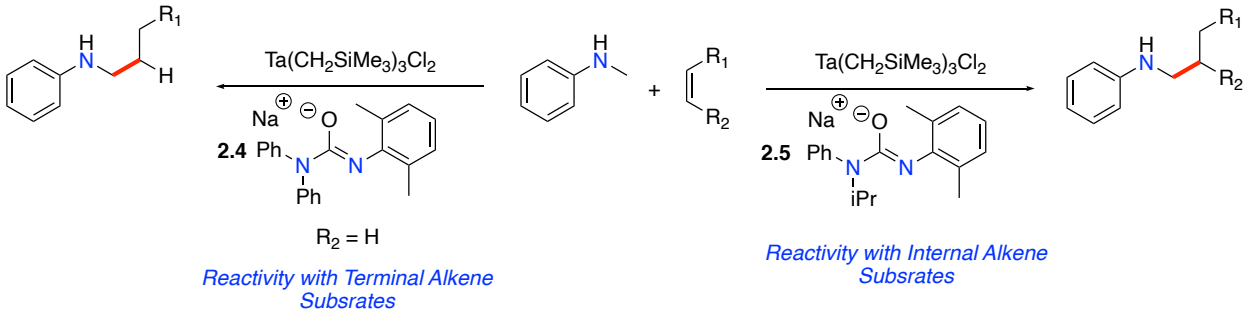

Scheme 5.1. Alkyltantalum catalyst systems as developed in Chapter 2 for tunable reactivity with terminal or internal alkene substrates.

Additional work in Chapter 2 attempted to understand why relatively small changes in ureate ligand structure resulted in significant changes to hydroaminoalkylation reactivity. Unfortunately, simple structure-activity relationships with steric and electronically varied ureate salts did not address these questions. Further, the analysis of solid state molecular structures for most precatalysts discussed in this chapter only showed that reactivity changes do not correspond to measurable differences in bond metrics available from X-ray data. X-ray parameters were similar for all structures despite the associated changes in ureates used. The future work section of Chapter 2 suggests additional experiments to quantitatively measure differences in reactivity that can be achieved using different ureate salts as ligands. The final sections of this chapter present preliminary data from chiral cyclic ureate ligand salts that had been previously used for hydroamination reactions. Using these ligands results in excellent hydroaminoalkylation reactivity with aromatic amine substrates and even higher TOFs with typically challenging aliphatic amine substrates. The %*ee* values with these ligands were not promising, but the aliphatic amine reactivity inspired further work using achiral cyclic ureate salts.

Results in Chapter 3 directly expanded on Chapter 2 by applying the now developed alkyltantalum catalysts to react substituted *N*-methylaniline substrates with either limonene or

pinene coupling partners (Scheme 5.2). Optimizing reactivity for these challenging substrates required new ureate ligand salts. The most reactive salt **3.3** was chiral and allowed us to investigate potential enantioselective hydroaminoalkylation once again. These investigations were not successful so all other reactions in this thesis used a racemic version of **3.3**. Beyond the impressive reactivity noted in Chapter 3, **3.3** can be synthesized in large batches of up to 10 g at a time with a high recrystallized yield. HPLC studies from reactions with this catalyst system indicate that the allylic stereocentre on limonene is not racemized during hydroaminoalkylation. Reactivity with limonene was also selective for only the terminal alkene functionality. When using pinene as a coupling partner, branched products had all three stereocentres set with excellent diastereoselectivity. Crystalizing the HCl salt for one of these pinene-based products allowed us to identify the absolute stereochemical orientation for compounds in the mini-series generated. Lastly, the products in this chapter are all synthetic terpenoid alkaloids that were submitted for medicinal testing at the Centre for Drug Research and Discovery at UBC.

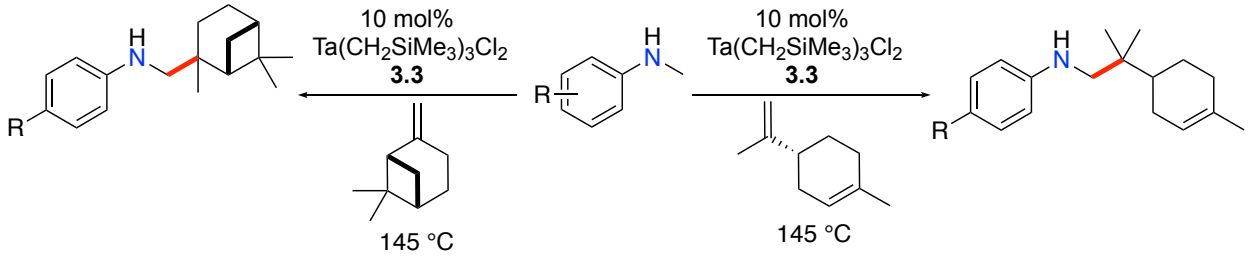

Scheme 5.2. Using hydroaminoalkylation for synthesizing terpenoid alkaloid products in Chapter 3.

Chapter 4 is completely dedicated to hydroaminoalkylation reactivity with saturated *N*-heterocyclic substrates. Chapters 1 and 2 both briefly discussed the challenges presented by these substrates; piperidine would typically require a week-long reaction time at very high temperatures with high loadings to generate any product. Further, all previous examples isolate protected amine compounds only. We began by using the ligand salt from in Chapter 3 (**3.3** in Chapter 3 and **4.5** in Chapter 4) to obtain the first generally applicable hydroaminoalkylation catalyst. This system can be used for reactivity with aromatic amine, aliphatic amine, internal alkene, and saturated *N*-heterocyclic substrates. We were particularly excited about reducing reaction times to 6 h with piperidine as a representative *N*-heterocycle. Full conversion was realized with only 5 % catalyst loading and exclusively the branched regioisomer was formed diastereoselectively. The reaction of different heterocycle substrates with 1-octene generated products in excellent diastereoselectivity, and using substituted piperidine materials allowed us to set three stereocentres in one catalytic step. 1D and 2D NOESY experiments helped us to identify relative configurations in reaction products.

Interestingly, the reaction of various styrene substrates with piperidine accessed a significant amount of the linear regioisomer for the first time and we used this observation to quantify the relationship between hydroaminoalkylation regiochemistry and alkene electronic properties (Scheme 5.3). These data showed that using electron-rich styrene partners results in more branched product, while electron-poor substrates can be used towards more linear product. These results indicate that the polarizability of each styrene influences how it adds to the tantallaziridine during the reaction mechanism. Notably, these regioisomers are separable and all products were isolated and characterized as free secondary amines.

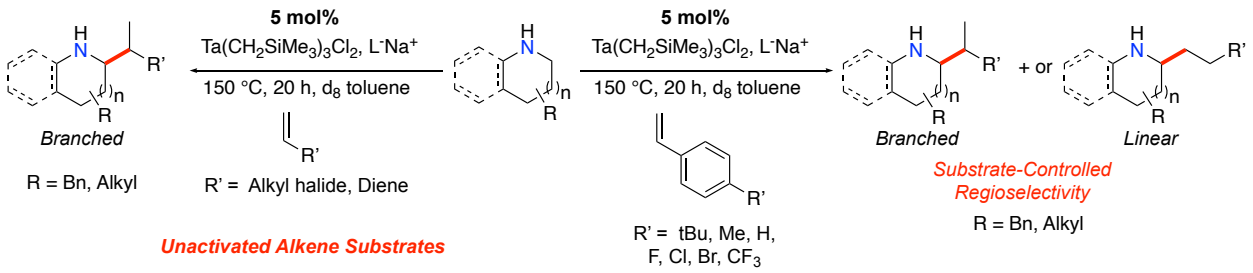

Scheme 5.3. A group 5 hydroaminoalkylation strategy for regiodivergent product formation as dependent on alkene electronic properties.

Follow-up work in Chapter 4 uses the *N*-heterocycle hydroaminoalkylation method we developed as a key step in synthesizing fused indolizidine and quinolizidine alkaloid products. These privileged scaffolds are laborious to access, and typical syntheses are not geared towards the identical synthetic products, which may have new biological activity profiles. Our optimized approach involves hydroaminoalkylation of piperidine with a halogenated alkene coupling partner followed immediately by a Ni-catalyzed Buchwald Hartwig amination step (Scheme 5.4). As above, we first generated a small scope of products that now varied amine partners with *o*-chlorostyrene. Regiochemical and stereochemical trends for these compounds did not vary significantly as compared with reactivity between unsubstituted piperidine and *o*-chlorostyrene. Overall, this two-step strategy is one-pot sequential, as the Buchwald-Hartwig catalyst system is added directly to the hydroaminoalkylation reaction mixture without any quenching or purification required. Products are then separated and isolated for yields over two steps.

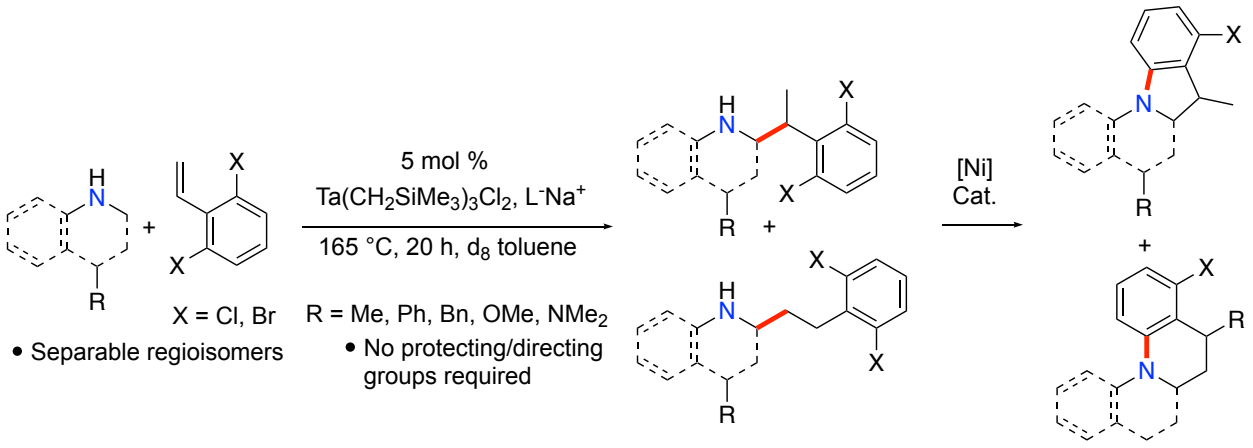

Scheme 5.4. Hydroaminoalkylation as a key step in synthesizing indolizidine and quinolizidine alkaloids.

5.2 Concluding Remarks

This thesis presents a building story about optimizing and applying alkyltantalum catalysts for hydroaminoalkylation reactions. Work flows from catalyst development in Chapter 2, to simpler applications in Chapter 3 culminate in strategies to build more complex *N*-heterocycles in Chapter 4. This work has inspired new research directions within our group, advances in mechanistic insights and organic synthesis will continue to emerge in years to come.

Overall, catalysis with alkyltantalum ureate complexes addresses most of the challenges with early transition-metal hydroaminoalkylation catalysis. We have lowered catalytic loadings, decreased reaction temperatures, significantly dropped reaction times, and created the first generally applicable catalyst. All of this resulted in unprecedented organic applications for early transition-metal systems in the entirely catalytic synthesis of fused *N*-heterocycle products. These alkyltantalum systems are the most promising options we currently have for unique disconnections to generate amine products through hydroaminoalkylation.

References

(1) Vitaku, E.; Smith, D. T.; Njardarson, J. T. Analysis of the Structural Diversity, Substitution Patterns, and Frequency of Nitrogen Heterocycles among U.S. FDA Approved Pharmaceuticals. *J. Med. Chem.* **2014**, *57*, 10257–10274.

(2) Baxter, E. W.; Reitz, A. B. Reductive Aminations of Carbonyl Compounds with Borohydride and Borane Reducing Agents. *Organic Reactions*. 2004, 1–714.

(3) Louillat, M. L.; Patureau, F. W. Oxidative C-H Amination Reactions. *Chem. Soc. Rev.* **2014**, *43*, 901–910.

(4) Cernak, T.; Dykstra, K. D.; Tyagarajan, S.; Vachal, P.; Krska, S. W. The Medicinal Chemist's Toolbox for Late Stage Functionalization of Drug-like Molecules. *Chem. Soc. Rev.* **2016**, *45*, 546–576.

(5) Dong, Z.; Ren, Z.; Thompson, S. J.; Xu, Y.; Dong, G. Transition-Metal-Catalyzed C-H Alkylation Using Alkenes. *Chem. Rev.* **2017**, *117*, 9333–9403.

(6) Lepori, C.; Hannedouche, J. First-Row Late Transition Metals for Catalytic (Formal) Hydroamination of Unactivated Alkenes. *Synthesis.*. **2017**, *49*, 1158–1167.

(7) Nguyen, T. M.; Nicewicz, D. A. Anti-Markovnikov Hydroamination of Alkenes Catalyzed by an Organic Photoredox System. *J. Am. Chem. Soc.* **2013**, *135*, 9588–9591.

(8) Nguyen, T. M.; Manohar, N.; Nicewicz, D. A. Anti -Markovnikov Hydroamination of Alkenes Catalyzed by a Two- Component Organic Photoredox System : Direct Access to Phenethylamine Derivatives. *Angew. Chem. Int. Ed.* **2014**, *53*, 6198–6201.

(9) Musacchio, A. J.; Lainhart, B. C.; Zhang, X.; Naguib, S. G.; Sherwood, T. C.; Knowles, R. R. Catalytic Intermolecular Hydroaminations of Unactivated Olefins with Secondary Alkyl Amines. *Science.* **2017**, *355*, 727–730.

(10) Zhu, Q.; Graff, D. E.; Knowles, R. R. Intermolecular Anti-Markovnikov Hydroamination of Unactivated Alkenes with Sulfonamides Enabled by Proton-Coupled Electron Transfer. *J. Am. Chem. Soc.* **2018**, *140*, 741–747.

(11) Adamson, N. J.; Hull, E.; Malcolmson, S. J. Enantioselective Intermolecular Addition of Aliphatic Amines to Acyclic Dienes with a Pd-PHOX Catalyst. *J. Am. Chem. Soc.* **2017**, *139*, 7180–7183.

(12) Adamson, N. J.; Jeddi, H.; Malcolmson, S. J. Preparation of Chiral Allenes through Pd-Catalyzed Intermolecular Hydroamination of Conjugated Enynes: Enantioselective Synthesis Enabled by Catalyst Design. *J. Am. Chem. Soc.* **2019**, *141*, 8574–8583.

(13) Yang, Y.; Shi, S. L.; Niu, D.; Liu, P.; Buchwald, S. L. Catalytic Asymmetric Hydroamination of Unactivated Internal Olefins to Aliphatic Amines. *Science.* **2015**, *349*, 62–66.

(14) Bytschkov, I.; Doye, S. Group-IV Metal Complexes as Hydroamination Catalysts. *European J. Org. Chem.* **2003**, *6*, 935–946.

(15) Hong, S.; Marks, T. J. Organolanthanide-Catalyzed Hydroamination. *Acc. Chem. Res.* **2004**, *37*, 673–686.

(16) Severin, R.; Doye, S. The Catalytic Hydroamination of Alkynes. *Chem. Soc. Rev.* **2007**, *36*, 1407–1420.

(17) Mueller, T. E.; Hultzsch, K. C.; Yus, M.; Foubelo, F.; Tada, M. Hydroamination: Direct Addition of Amines to Alkenes and Alkynes. *Chem. Rev.* **2008**, *108*, 3795–3892.

(18) Gooßen, L. J.; Huang, L.; Arndt, M.; Gooßen, K.; Heydt, H. Late Transition Metal-Catalyzed Hydroamination and Hydroamidation. *Chem. Rev.* **2015**, *115*, 2596–2697.
(19) Reznichenko, A. L.; Oy, B. P.; Box, P. O.; Hultzsch, K. C. Hydroamination of Alkenes. *Organic Reactions*; **2016**; *88*, 1–553.
(20) Zimmermann, B.; Herwig, J.; Beller, M. The First Efficient Hydroaminomethylation with Ammonia : With Dual Metal Catalysts and Two-Phase Catalysis to Primary Amines *Angew. Chem. Int. Ed.* **1999**, *38*, 2372–2375.
(21) Ahmed, M.; Seayad, A. M.; Jackstell, R.; Beller, M. Amines Made Easily: A Highly Selective Hydroaminomethylation of Olefins. *J. Am. Chem. Soc.* **2003**, *125*, 10311–10318.
(22) Crozet, D.; Urrutigoïty, M.; Kalck, P. Recent Advances in Amine Synthesis by Catalytic Hydroaminomethylation of Alkenes. *ChemCatChem* **2011**, *3*, 1102–1118.
(23) Kalck, P.; Urrutigoïty, M. Tandem Hydroaminomethylation Reaction to Synthesize Amines from Alkenes. *Chem. Rev.* **2018**, *118*, 3833–3861.
(24) Baudoin, O. Transition Metal-Catalyzed Arylation of Unactivated C(Sp3)–H Bonds. *Chem. Soc. Rev.* **2011**, *40*, 4902–4911.
(25) Mcnally, A.; Prier, C. K.; Macmillan, D. W. C. Discovery of an a-Amino C-H Arylation Reaction Using the Strategy of Accelerated Serendipity. *Science.* **2011**, *334*, 1114–1118.
(26) Chen, W.; Wilde, R. G.; Seidel, D. Redox-Neutral a-Arylation of Amines. *Org. Lett.* **2014**, *16*, 730–732.
(27) He, C.; Gaunt, M. J. Ligand-Enabled Catalytic C-H Arylation of Aliphatic Amines by a Four-Membered-Ring Cyclopalladation Pathway. *Angew. Chem. - Int. Ed.* **2015**, *54*, 15840–15844.
(28) Jain, P.; Verma, P.; Xia, G.; Yu, J.-Q. Enantioselective Amine α-Functionalization via Palladium-Catalysed C–H Arylation of Thioamides. *Nat. Chem.* **2016**, *9*, 1–5.
(29) Hoyt, C. B.; Lee, L. C.; He, J.; Yu, J. Q.; Jones, C. W. Selective C(sp^3)–H Monoarylation Catalyzed by a Covalently Cross-Linked Reverse Micelle-Supported Palladium Catalyst. *Adv. Synth. Catal.* **2017**, *359*, 3611–3617.
(30) Tang, R.; Li, G.; Yu, J. Conformation-Induced Remote Meta-C-H Activation of Amines. *Nature* **2014**, *507*, 215–220.
(31) Wang, P.; Verma, P.; Xia, G.; Shi, J.; Qiao, J. X.; Tao, S.; Cheng, P. T. W.; Poss, M. A.; Farmer, M. E.; Yeung, K. S.; Yu, J. Q. Ligand-Accelerated Non-Directed C-H Functionalization of Arenes. *Nature* **2017**, *551*, 489–493.
(32) Le, C.; Liang, Y.; Evans, R. W.; Li, X.; MacMillan, D. W. C. Selective Sp3 C-H Alkylation via Polarity-Match-Based Cross-Coupling. *Nature* **2017**, *547*, 79–83.
(33) Chen, W.; Ma, L.; Paul, A.; Seidel, D. Direct α-C-H Bond Functionalization of Unprotected Cyclic Amines. *Nat. Chem.* **2018**, *10*, 165–169.
(34) Paul, A.; Seidel, D. α-Functionalization of Cyclic Secondary Amines: Lewis Acid Promoted Addition of Organometallics to Transient Imines. *J. Am. Chem. Soc.* **2019**, *141*, 8778–8782.
(35) Roesky, P. W. Catalytic Hydroaminoalkylation. *Angew. Chem. - Int. Ed.* **2009**, *48*, 4892–4894.
(36) Chong, E.; Garcia, P.; Schafer, L. Hydroaminoalkylation: Early-Transition-Metal-Catalyzed α-Alkylation of Amines. *Synthesis.* **2014**, *46*, 2884–2896.
(37) Ryken, S. A.; Schafer, L. L. N,O-Chelating Four-Membered Metallacyclic Titanium(IV) Complexes for Atom-Economic Catalytic Reactions. *Acc. Chem. Res.* **2015**, *48*, 2576–

2586.
(38) Edwards, P. M.; Schafer, L. L. Early Transition Metal-Catalyzed C-H Alkylation: Hydroaminoalkylation for Csp3-Csp3 Bond Formation in the Synthesis of Selectively Substituted Amines. *Chem. Commun.* **2018**, *54*, 12543–12560.
(39) Clerici, M. G.; Maspero, F. Catalytic C-Alkylation of Secondary Amines with Alkenes. *Synthesis.* **1980**, *91*, 305–306.
(40) Herzon, S. B.; Hartwig, J. F. Direct, Catalytic Hydroaminoalkylation of Unactivated Olefins with N-Alkyl Arylamines. *J. Am. Chem. Soc.* **2007**, *129*, 6690–6691.
(41) Nugent, W. A.; Ovenall, D. W.; Holmes, S. J. Catalytic C-H Activation in Early Transition-Metal Dialkylamides and Alkoxides. *Organometallics* **1983**, *2*, 161–162.
(42) Herzon, S.; Hartwig, J. Ta(V)-Catalyzed Hydroaminoalkylation of Olefins with Dialkylamines. *J. Am. Chem. Soc.* **2009**, *2009*, 193–193.
(43) Nako, A. E.; Oyamada, J.; Nishiura, M.; Hou, Z. Scandium-Catalysed Intermolecular Hydroaminoalkylation of Olefins with Aliphatic Tertiary Amines. *Chem. Sci.* **2016**, *7*, 6429–6434.
(44) Liu, F.; Luo, G.; Hou, Z.; Luo, Y. Mechanistic Insights into Scandium-Catalyzed Hydroaminoalkylation of Olefins with Amines: Origin of Regioselectivity and Charge-Based Prediction Model. *Organometallics* **2017**, *36*, 1557–1565.
(45) Gao, H.; Su, J.; Xu, P.; Xu, X. Scandium-Catalyzed C(sp^3)-H Alkylation of: N, N-Dimethyl Anilines with Alkenes. *Org. Chem. Front.* **2018**, *5*, 59–63.
(46) Kubiak, R.; Prochnow, I.; Doye, S. Titanium-Catalyzed Hydroaminoalkylation of Alkenes by C-H Bond Activation at sp^3 Centers in the α-Position to a Nitrogen Atom. *Angew. Chemie - Int. Ed.* **2009**, *48*, 1153–1156.
(47) Prochnow, I.; Kubiak, R.; Frey, O. N.; Beckhaus, R.; Doye, S. Tetrabenzyltitanium: An Improved Catalyst for the Activation of Sp3 C-H Bonds Adjacent to Nitrogen Atoms. *ChemCatChem* **2009**, *1*, 162–172.
(48) Kubiak, R.; Prochnow, I.; Doye, S. [Ind_2TiMe_2]: A Catalyst for the Hydroaminomethylation of Alkenes and Styrenes. *Angew. Chem. Int. Ed.* **2010**, *49*, 2626–2629.
(49) Prochnow, I.; Zark, P.; Müller, T.; Doye, S. The Mechanism of the Titanium-Catalyzed Hydroaminoalkylation of Alkenes. *Angew. Chem. - Int. Ed.* **2011**, *50*, 6401–6405.
(50) Manßen, M.; Lauterbach, N.; Dörfler, J.; Schmidtmann, M.; Saak, W.; Doye, S.; Beckhaus, R. Efficient Access to Titanaaziridines by C-H Activation of N-Methylanilines at Ambient Temperature. *Angew. Chem. - Int. Ed.* **2015**, *54*, 4383–4387.
(51) Rosien, M.; Töben, I.; Schmidtmann, M.; Beckhaus, R.; Doye, S. Titanium-Catalyzed Hydroaminoalkylation of Ethylene. *Chem. - A Eur. J.* **2020**, *26*, 2138–2142.
(52) Hamzaoui, B.; El Eter, M.; Abou-Hamad, E.; Chen, Y.; Pelletier, J. D. A.; Basset, J. M. Well-Defined Single-Site Monohydride Silica-Supported Zirconium from Azazirconacyclopropane. *Chem. Eur. J.* **2015**, *21*, 4294–4299.
(53) Koperniku, A.; Foth, P. J.; Sammis, G. M.; Schafer, L. L. Zirconium Hydroaminoalkylation. An Alternative Disconnection for the Catalytic Synthesis of α-Arylated Primary Amines. *J. Am. Chem. Soc.* **2019**, *141*, 18944–18948.
(54) Preub, T.; Saak, W.; Doye, S. Titanium-Catalyzed Intermolecular Hydroaminoalkylation of Conjugated Dienes. *Chem. Eur. J.* **2013**, *19*, 3833–3837.
(55) Rohjans, S. H.; Ross, J. H.; Lühning, L. H.; Sklorz, L.; Schmidtmann, M.; Doye, S.

Titanium Catalysts with Linked Indenyl-Amido Ligands for Hydroamination and Hydroaminoalkylation Reactions. *Organometallics* **2018**, *37*, 4350–4357.
(56) Jaspers, D.; Saak, W.; Doye, S. Dinuclear Titanium Complexes with Sulfamide Ligands as Precatalysts for Hydroaminoalkylation and Hydroamination Reactions. *Synlett* **2012**, *23*, 2098–2102.
(57) Dorfler, J.; Bytyqi, B.; Huller, S.; Mann, N. M.; Brahms, C.; Schmidtmann, M.; Doye, S. An Aminopyridinato Titanium Catalyst for the Intramolecular Hydroaminoalkylation of Secondary Aminoalkenes. *Adv. Synth. Catal.* **2015**, *357*, 2265–2276.
(58) Elkin, T.; Kulkarni, N. V.; Tumanskii, B.; Botoshansky, M.; Shimon, L. J. W.; Eisen, M. S. Synthesis and Structure of Group 4 Symmetric Amidinate Complexes and Their Reactivity in the Polymerization of α-Olefins. *Organometallics* **2013**, *32*, 6337–6352.
(59) Dörfler, J.; Doye, S. Aminopyridinato Titanium Catalysts for the Hydroaminoalkylation of Alkenes and Styrenes. *Angew. Chem. - Int. Ed.* **2013**, *52*, 1806–1809.
(60) Dörfler, J.; Preuß, T.; Schischko, A.; Schmidtmann, M.; Doye, S. A 2,6-Bis(Phenylamino)Pyridinato Titanium Catalyst for the Highly Regioselective Hydroaminoalkylation of Styrenes and 1,3-Butadienes. *Angew. Chem. - Int. Ed.* **2014**, *53*, 7918–7922.
(61) Bielefeld, J.; Kurochkina, E.; Schmidtmann, M.; Doye, S. New Titanium Complexes and Their Use in Hydroamination and Hydroaminoalkylation Reactions. *Eur. J. Inorg. Chem.* **2019**.
(62) Dörfler, J.; Preuß, T.; Brahms, C.; Scheuer, D.; Doye, S. Intermolecular Hydroaminoalkylation of Alkenes and Dienes Using a Titanium Mono(Formamidinate) Catalyst. *Dalton. Trans.* **2015**, *44*, 12149–12168.
(63) Bielefeld, J.; Doye, S. Dimethylamine as a Substrate in Hydroaminoalkylation Reactions. *Angew. Chem. - Int. Ed.* **2017**, *56*, 15155–15158.
(64) Bielefeld, J.; Mannhaupt, S.; Schmidtmann, M.; Doye, S. Hydroaminoalkylation of Allenes. *Synlett* **2019**, *30*, 967–971.
(65) Lühning, L. H.; Rosien, M.; Doye, S. Thieme Chemistry Journals Awardees - Where Are They Now? Titanium-Catalyzed Hydroaminoalkylation of Vinylsilanes and a One-Pot Procedure for the Synthesis of 1,4-Benzoazasilines. *Synlett* **2017**, *28*, 2489–2494.
(66) Kaper, T.; Doye, S. Hydroaminoalkylation/Buchwald-Hartwig Amination Sequences for the Synthesis of Benzo-Annulated Seven-Membered Nitrogen Heterocycles. *Tetrahedron* **2019**, 73, 4343-4350.
(67) Lühning, L. H.; Strehl, J.; Schmidtmann, M.; Doye, S. Hydroaminoalkylation of Allylsilanes and a One-Pot Procedure for the Synthesis of 1,5-Benzoazasilepines. *Chem. Eur. J.* **2017**, *23*, 4197–4202.
(68) Chong, E.; Schafer, L. L. 2-Pyridonate Titanium Complexes for Chemoselectivity. Accessing Intramolecular Hydroaminoalkylation over Hydroamination. *Org. Lett.* **2013**, *15*, 6002–6005.
(69) Perry, M. R.; Gilmour, D. J.; Schafer, L. L. Mono, Bis, and Tris(Phosphoramidate) Titanium Complexes: Synthesis, Structure, and Reactivity Investigations. *Dalton. Trans.* **2019**, 9782–9790.
(70) Bielefeld, J.; Doye, S. Fast Titanium-Catalyzed Hydroaminomethylation of Alkenes and the Formal Conversion of Methylamine. *Angew. Chem. - Int. Ed.* **2020**.
(71) Bexrud, J. A.; Eisenberger, P.; Leitch, D. C.; Payne, P. R.; Schafer, L. L. Selective C-H

Activation α to Primary Amines. Bridging Metallaaziridines for Catalytic, Intramolecular α-Alkylation. *J. Am. Chem. Soc.* **2009**, *131*, 2116–2118.
(72) Zi, G.; Zhang, F.; Song, H. Highly Enantioselective Hydroaminoalkylation of Secondary Amines Catalyzed by Group 5 Metal Amides with Chiral Biarylamidate Ligands. *Chem. Commun.* **2010**, *46*, 6296–6298.
(73) Reznichenko, A. L.; Hultzsch, K. C. The Mechanism of Hydroaminoalkylation Catalyzed by Group 5 Metal Binaphtholate Complexes. *J. Am. Chem. Soc.* **2012**, *134*, 3300–3311.
(74) Zhang, F.; Song, H.; Zi, G. Synthesis and Catalytic Activity of Group 5 Metal Amides with Chiral Biaryldiamine-Based Ligands. *Dalt. Trans.* **2011**, *40*, 1547–1566.
(75) Dörfler, J.; Doye, S. A Commercially Available Tantalum Catalyst for the Highly Regioselective Intermolecular Hydroaminoalkylation of Styrenes. *European J. Org. Chem.* **2014**, *2014*, 2790–2797.
(76) Pelletier, J. D. A.; Basset, J. M. Catalysis by Design: Well-Defined Single-Site Heterogeneous Catalysts. *Acc. Chem. Res.* **2016**, *49*, 664–677.
(77) Hamzaoui, B.; Pelletier, J. D. A.; El Eter, M.; Chen, Y.; Abou-Hamad, E.; Basset, J. M. Isolation and Characterization of Well-Defined Silica-Supported Azametallacyclopentane: A Key Intermediate in Catalytic Hydroaminoalkylation Reactions. *Adv. Synth. Catal.* **2015**, *357*, 3148–3154.
(78) Zhang, Z.; Hamel, J. D.; Schafer, L. L. TaMe3Cl2-Catalyzed Intermolecular Hydroaminoalkylation: A Simple Complex for Enhanced Reactivity and Expanded Substrate Scope. *Chem. Eur. J.* **2013**, *19*, 8751–8754.
(79) DiPucchio, R. C.; Roşca, S. C.; Schafer, L. L. Catalytic and Atom-Economic Csp^3−Csp^3 Bond Formation: Alkyl Tantalum Ureates for Hydroaminoalkylation. *Angew. Chem. - Int. Ed.* **2018**, *57*, 3469–3472.
(80) Eisenberger, P.; Ayinla, R. O.; Lauzon, J. M. P.; Schafer, L. L. Tantalum-Amidate Complexes for the Hydroaminoalkylation of Secondary Amines: Enhanced Substrate Scope and Enantioselective Chiral Amine Synthesis. *Angew. Chem. Int. Ed.* **2009**, *48*, 8361–8365.
(81) Payne, P. R.; Garcia, P.; Eisenberger, P.; Yim, J. C. H.; Schafer, L. L. Tantalum Catalyzed Hydroaminoalkylation for the Synthesis of α- and β-Substituted N-Heterocycles. *Org. Lett.* **2013**, *15*, 2182–2185.
(82) Lauzon, J. M. P.; Schafer, L. L. Tantallaaziridines: From Synthesis to Catalytic Applications. *Dalton. Trans.* **2012**, *41*, 11539.
(83) Klauber, E. G.; Reznichenko, A. L.; Emge, T. J.; Aud, S.; Hultzsch, K. C.; Schmidt, B.; Golm, D.-. Group 5 Metal Binaphtholate Complexes for Catalytic Asymmetric Hydroaminoalkylation and Hydroamination / Cyclization. **2011**, No. d, 921–924.
(84) Garcia, P.; Lau, Y. Y.; Perry, M. R.; Schafer, L. L. Phosphoramidate Tantalum Complexes for Room-Temperature C-H Functionalization: Hydroaminoalkylation Catalysis. *Angew. Chem. Int. Ed.*. **2013**, *52*, 9144–9148.
(85) Chong, E.; Brandt, J. W.; Schafer, L. L. 2-Pyridonate Tantalum Complexes for the Intermolecular Hydroaminoalkylation of Sterically Demanding Alkenes. *J. Am. Chem. Soc.* **2014**, *136*, 10898–10901.
(86) Brandt, J. W.; Chong, E.; Schafer, L. L. Ligand Effects and Kinetic Investigations of Sterically Accessible 2-Pyridonate Tantalum Complexes for Hydroaminoalkylation. *ACS Catal.* **2017**, *7*, 6323–6330.

(87) Edwards, P. M.; Schafer, L. L. In Situ Generation of a Regio- and Diastereoselective Hydroaminoalkylation Catalyst Using Commercially Available Starting Materials. *Org. Lett.* **2017**, *19*, 5720–5723.
(88) Braun, C.; Nieger, M.; Bräse, S.; Schafer, L. L. Planar-Chiral [2.2]Paracyclophane-Based Pyridonates as Ligands for Tantalum-Catalyzed Hydroaminoalkylation. *ChemCatChem* **2019**, 1–6.
(89) Jun, C.-H. Chelation-Assisted Alkylation of Benzylamine Derivatives by Ru(0) Catalyst. *Chem. Commun.* **1998**, *13*, 1405–1406.
(90) Arockiam, P. B.; Bruneau, C.; Dixneuf, P. H. Ruthenium(II)-Catalyzed C-H Bond Activation and Functionalization. *Chem. Rev.* **2012**, *112*, 5879–5918.
(91) Zuo, Z.; Cong, H.; Li, W.; Choi, J.; Fu, G. C.; MacMillan, D. W. C. Enantioselective Decarboxylative Arylation of α-Amino Acids via the Merger of Photoredox and Nickel Catalysis. *J. Am. Chem. Soc.* **2016**, *138*, 1832–1835.
(92) Cruz, F. A.; Zhu, Y.; Tercenio, Q. D.; Shen, Z.; Dong, V. M. Alkyne Hydroheteroarylation: Enantioselective Coupling of Indoles and Alkynes via Rh-Hydride Catalysis. *J. Am. Chem. Soc.* **2017**, *139*, 10641–10644.
(93) Cuthbertson, J. D.; MacMillan, D. W. C. The Direct Arylation of Allylic Sp^3 C-H Bonds via Organic and Photoredox Catalysis. *Nature* **2015**, *519*, 74–77.
(94) Chatani, N.; Asaumi, T.; Yorimitsu, S.; Ikeda, T.; Kakiuchi, F.; Murai, S. Ru3(CO)12-Catalyzed Coupling Reaction of sp^3 C-H Bonds Adjacent to a Nitrogen Atom in Alkylamines with Alkenes. *J. Am. Chem. Soc.* **2001**, *123*, 10935–10941.
(95) Bergman, S. D.; Storr, T. E.; Prokopcová, H.; Aelvoet, K.; Diels, G.; Meerpoel, L.; Maes, B. U. W. The Role of the Alcohol and Carboxylic Acid in Directed Ruthenium-Catalyzed C(sp^3)-H α-Alkylation of Cyclic Amines. *Chem. Eur. J.* **2012**, *18*, 10393–10398.
(96) Pan, S.; Matsuo, Y.; Endo, K.; Shibata, T. Cationic Iridium-Catalyzed Enantioselective Activation of Secondary sp^3 C-H Bond Adjacent to Nitrogen Atom. *Tetrahedron* **2012**, *68*, 9009–9015.
(97) Kulago, A. A.; Van Steijvoort, B. F.; Mitchell, E. A.; Meerpoel, L.; Maes, B. U. W. Directed Ruthenium-Catalyzed C(sp^3)-H α-Alkylation of Cyclic Amines Using Dioxolane-Protected Alkenones. *Adv. Synth. Catal.* **2014**, *356*, 1610–1618.
(98) Smout, V.; Peschiulli, A.; Verbeeck, S.; Mitchell, E. A.; Herrebout, W.; Bultinck, P.; Vande Velde, C. M. L.; Berthelot, D.; Meerpoel, L.; Maes, B. U. W. Removal of the Pyridine Directing Group from α-Substituted N-(Pyridin-2-Yl)Piperidines Obtained via Directed Ru-Catalyzed sp^3 C-H Functionalization. *J. Org. Chem.* **2013**, *78*, 9803–9814.
(99) Prokopcová, H.; Bergman, S. D.; Aelvoet, K.; Smout, V.; Herrebout, W.; Van Der Veken, B.; Meerpoel, L.; Maes, B. U. W. C-2 Arylation of Piperidines through Directed Transition-Metal-Catalyzed sp^3 C-H Activation. *Chem. Eur. J.* **2010**, *16*, 13063–13067.
(100) Schmitt, D. C.; Lee, J.; Dechert-Schmitt, A.-M. R.; Yamaguchi, E.; Krische, M. J. Ruthenium Catalyzed Hydroaminoalkylation of Isoprene via Transfer Hydrogenation: Byproduct-Free Prenylation of Hydantoins. *Chem. Commun.* **2013**, *49*, 6096–6098.
(101) Lahm, G.; Opatz, T. Unique Regioselectivity in the C(sp^3)-H α-Alkylation of Amines: The Benzoxazole Moiety as a Removable Directing Group. *Org. Lett.* **2014**, *16*, 4201–4203.
(102) Schinkel, M.; Wang, L.; Bielefeld, K.; Ackermann, L. Ruthenium(II)-Catalyzed C(sp^3)–H α-Alkylation of Pyrrolidines. *Org. Lett.* **2014**, *16*, 1876–1879.
(103) Oda, S.; Sam, B.; Krische, M. J. Hydroaminomethylation beyond Carbonylation: Allene-

Imine Reductive Coupling by Ruthenium-Catalyzed Transfer Hydrogenation. *Angew. Chemie - Int. Ed.* **2015**, *54*, 8525–8528.
(104) Oda, S.; Franke, J.; Krische, M. J. Diene Hydroaminomethylation via Ruthenium-Catalyzed C–C Bond Forming Transfer Hydrogenation: Beyond Carbonylation. *Chem. Sci.* **2016**, *7*, 136–141.
(105) Yamauchi, D.; Nishimura, T.; Yorimitsu, H. Hydroxoiridium-Catalyzed Hydroalkylation of Terminal Alkenes with Ureas by C(sp^3)−H Bond Activation. *Angew. Chem. Int. Ed.*. **2017**, *56*, 7200–7204.
(106) Mitchell, E. A.; Peschiulli, A.; Lefevre, N.; Meerpoel, L.; Maes, B. U. W. Direct α-Functionalization of Saturated Cyclic Amines. *Chem. Eur. J.* **2012**, *18*, 10092–10142.
(107) Tran, A. T.; Yu, J.-Q. Practical Alkoxythiocarbonyl Auxiliaries for Iridium(I)-Catalyzed C-H Alkylation of Azacycles. *Angew. Chem. Int. Ed.* **2017**, *56*, 10530–10534.
(108) Verma, P.; Richter, J. M.; Chekshin, N.; Qiao, J. X.; Yu, J.-Q. Iridium(I)-Catalyzed #-C(Sp)–H Alkylation of Saturated Azacycles. *J. Am. Chem. Soc.* **2020**, No. I, 1–9.
(109) Miyake, Y.; Nakajima, K.; Nishibayashi, Y. Visible-Light-Mediated Utilization of α-Aminoalkyl Radicals: Addition to Electron-Deficient Alkenes Using Photoredox Catalysts. *J. Am. Chem. Soc.* **2012**, *134*, 3338–3341.
(110) Dai, X.; Cheng, D.; Guan, B.; Mao, W.; Xu, X.; Li, X. The Coupling of Tertiary Amines with Acrylate Derivatives via Visible-Light Photoredox Catalysis. *J. Org. Chem.* **2014**, *79*, 7212–7219.
(111) Thullen, S. M.; Rovis, T. A Mild Hydroaminoalkylation of Conjugated Dienes Using a Unified Cobalt and Photoredox Catalytic System. *J. Am. Chem. Soc.* **2017**, *139*, 15504–15508.
(112) Trowbridge, A.; Reich, D.; Gaunt, M. J. Multicomponent Synthesis of Tertiary Alkylamines by Photocatalytic Olefin-Hydroaminoalkylation. *Nature* **2018**, *561*, 522–527.
(113) Ashley, M. A.; Yamauchi, C.; Chu, J. C. K.; Otsuka, S.; Yorimitsu, H.; Rovis, T. Photoredox-Catalyzed Site-Selective α-C(sp^3)−H Alkylation of Primary Amine Derivatives. *Angew. Chem. Int. Ed.* **2019**, *58*, 4002–4006.
(114) McManus, J. B.; Onuska, N. P. R.; Nicewicz, D. A. Generation and Alkylation of α-Carbamyl Radicals via Organic Photoredox Catalysis. *J. Am. Chem. Soc.* **2018**, *140*, 9056–9060.
(115) McManus, J. B.; Onuska, N. P. R.; Jeffreys, M. S.; Goodwin, N. C.; Nicewicz, D. A. Site-Selective C-H Alkylation of Piperazine Substrates via Organic Photoredox Catalysis. *Org. Lett.* **2020**, *22*, 679–683.
(116) Su, J.; Zhou, Y.; Xu, X. Hydroaminoalkylation of Sterically Hindered Alkenes with N, N-Dimethyl Anilines Using a Scandium Catalyst. *Org. Biomol. Chem.* **2019**, *17*, 2013–2019.
(117) Lauzon, J. M.; Eisenberger, P.; Roşca, S. C.; Schafer, L. L. Amidate Complexes of Tantalum and Niobium for the Hydroaminoalkylation of Unactivated Alkenes. *ACS Catal.* **2017**, *7*, 5921–5931.
(118) Leitch, D. C.; Payne, P. R.; Dunbar, C. R.; Schafer, L. L. Broadening the Scope of Group 4 Hydroamination Catalysis Using a Tethered Ureate Ligand. *J. Am. Chem. Soc.* **2009**, *131*, 18246–18247.
(119) Leitch, D. C.; Turner, C. S.; Schafer, L. L. Isolation of Catalytic Intermediates in Hydroamination Reactions: Insertion of Internal Alkynes into a Zirconium-Amido Bond. *Angew. Chemie - Int. Ed.* **2010**, *49*, 6382–6386.

(120) Leitch, D. C.; Platel, R. H.; Schafer, L. L. Mechanistic Elucidation of Intramolecular Aminoalkene Hydroamination Catalyzed by a Tethered Bis(Ureate) Complex: Evidence for Proton-Assisted C-N Bond Formation at Zirconium. *J. Am. Chem. Soc.* **2011**, *133*, 15453–15463.
(121) Payne, P. R.; Bexrud, J. a.; Leitch, D. C.; Schafer, L. L. Asymmetric Hydroamination Catalyzed by in Situ Generated Chiral Amidate and Ureate Complexes of Zirconium — Probing the Role of the Tether in Ligand Design. *Can. J. Chem.* **2011**, *89*, 1222–1229.
(122) Lauzon, J. M. P.; Schafer, L. L. Tethered Bis(Amidate) and Bis(Ureate) Supported Zirconium Precatalysts for the Intramolecular Hydroamination of Aminoalkenes. *Zeitschrift fur Anorg. und Allg. Chemie* **2015**, *641*, 128–135.
(123) Platel, R. H.; Schafer, L. L. Zirconium Catalyzed Alkyne Dimerization for Selective Z-Enyne Synthesis. *Chem. Commun.* **2012**, *48*, 10609–10611.
(124) Moorhouse, B. S.; Wilkinson, G. Bis[(Trimethylsilyl)Methyl]- and Bis(Neopentyl)-Zinc and Tris[(Trimethylsilyl)Methyl]Aluminum-Diethyl Ether; Their Use as Alkylating Agents in Forming Niobium and Tantalum Alkyls. *Dalt. Trans* **1974**, 2187–2190.
(125) Chcme, M. C.; Schrock, R. R.; Fellmann, J. D. Multiple Metal-Carbon Bonds. Preparation, Characterization, and Mechanism of Formation of the Tantalum and Niobium Neopentylidene Complexes, $M(CH_2CMe_3)_3(CHCMe_3)$. *J. Am. Chem. Soc.* **1978**, *3*, 3359.
(126) Leitch, D. C.; Schafer, L. L. Zirconium Alkyl Complexes Supported by Ureate Ligands: Synthesis, Characterization, and Precursors to Metal-Element Multiple Bonds. *Organometallics* **2010**, *29*, 5162–5172.
(127) Ninković, D. B.; Moncho, S.; Petrović, P. V.; Zarić, S. D.; Hall, M. B.; Brothers, E. N. Methane Activations by Titanium Neopentylidene Complexes: Electronic Resilience and Steric Control. *Inorg. Chem.* **2017**, *56*, 9264–9272.
(128) Smith, M. B.; March, J. *March's Advanced Organic Chemistry*; Wiley-VCH: New York, 2006.
(129) Daneshmand, P.; Roşca, S. C.; Dalhoff, R.; Kejun, Y.; DiPucchio, R. C.; Ivanovich, R. A.; Polat, D. E.; Beauchemin, A. M.; Schafer, L. L. A Cyclic Ureate Ta Catalyst for Preferential Hydroaminoalkylation with Aliphatic Amines. Mechanistic Insights into Substrate Controlled Reactivity. *J. Am. Chem. Soc.* **2020**. Submitted.
(130) Guzyr, O. I.; Schormann, M.; Schimkowiak, J.; Roesky, H. W.; Lehmann, C.; Walawalkar, M. G.; Murugavel, R.; Schmidt, H.-G.; Noltemeyer, M. Conversion of Alkyltantalum Chlorides to Fluorides Using Trimethyltin Fluoride as a Fluorinating Agent. Crystal Structures of $(p\text{-}MeC_6H_4CH_2)_3TaF_2$, $(Me_3SnF.TaF_5)n$, $(Me_3Si)_3CHTaCl_4$, $\{(Me_3Si)_2CHTaCl_4.[Me_3Si)_2CH]_2Ta_2Cl_6(U_2\text{-}O)\}$, and $(Me_3Si)_2CHTaF_4$. *Organometallics* **1999**, *18*, 832–836.
(131) Chisholm, M. H.; Huffman, J. C.; Tan, L. S. Chloro(Dimethylamido) Compounds of Tantalum(V): Preparations, Properties, and Structures of $[Ta(NMe_2)_3Cl_2]_2$, $TaCl_3(NMe_2)_2(HNMe_2)$, $Ta(NMe_2)_3Cl_2(HNMe_2)$, and $[TaCl_2(NMe_2)_2(HNMe_2)]_2O$. *Inorg. Chem.* **1981**, *20*, 1859–1866.
(132) Leitch, D. C.; Beard, J. D.; Thomson, R. K.; Wright, V. A.; Patrick, B. O.; Schafer, L. L. N,O-Chelates of Group 4 Metals: Contrasting the Use of Amidates and Ureates in the Synthesis of Metal Dichlorides. *Eur. J. Inorg. Chem.* **2009**, *2009*, 2691–2701.
(133) Sattler, A.; Ruccolo, S.; Parkin, G. Structural Characterization of $TaMe_3Cl_2$ and $Ta(PMe_3)_2Me_3Cl_2$,A Pair of Five and Seven-Coordinate D0 Tantalum Methyl

Compounds. *Dalt. Trans.* **2011**, *40*, 7777–77782.
(134) van Vuuren, S. F.; Viljoen, A. M. Antimicrobial Activity of Limonene Enantiomers and 1,8-Cineole Alone and in Combination. *Flavour Fragr. J.* **2007**, *22*, 540–544.
(135) da Silva, A. Cristin. R.; Lopes, P. Monteir.; de Azevedo, M. Mari. B.; Costa, D. Cristin. M.; Alviano, C. S. ale.; Alviano, D. Sale. Biological Activities of α-Pinene and β-Pinene Enantiomers. *Molecules* **2012**, *17*, 6305–6316.
(136) Rufino, A. T.; Ribeiro, M.; Judas, F.; Salgueiro, L.; Lopes, M. C.; Cavaleiro, C.; Mendes, A. F. Anti-Inflammatory and Chondroprotective Activity of (+)-α-Pinene: Structural and Enantiomeric Selectivity. *J. Nat. Prod.* **2014**, *77*, 264–269.
(137) Koziol, A.; Stryjewska, A.; Librowski, T.; Salat, K.; Gawel, M.; Moniczewski, A.; Lochynski, S. An Overview of the Pharmacological Properties and Potential Applications of Natural Monoterpenes. *Mini-Reviews Med. Chem.* **2015**, *14*, 1156–1168.
(138) Monteiro, J. L. F.; Veloso, C. O. Catalytic Conversion of Terpenes into Fine Chemicals. *Top. Catal.* **2004**, *27*, 169–180.
(139) Bicas, J. L.; Dionísio, A. P.; Pastore, G. M. Bio-Oxidation of Terpenes: An Approach for the Flavor Industry. *Chem. Rev.* **2009**, *109*, 4518–4531.
(140) Schwab, W.; Fuchs, C.; Huang, F. C. Transformation of Terpenes into Fine Chemicals. *Eur. J. Lipid Sci. Technol.* **2013**, *115*, 3–8.
(141) Cherney, E. C.; Baran, P. S. Terpenoid-Alkaloids: Their Biosynthetic Twist of Fate and Total Synthesis. *Isr. J. Chem.* **2011**, *51*, 391–405.
(142) Zhou, C.; Dubrovsky, A. V.; Larock, R. C. Diversity-Oriented Synthesis of 3-Iodochromones and Heteroatom Analogues via ICl-Induced Cyclization. *J. Org. Chem.* **2006**, *71*, 1626–1632.
(143) Ko, S. K.; Jang, H. J.; Kim, E.; Park, S. B. Concise and Diversity-Oriented Synthesis of Novel Scaffolds Embedded with Privileged Benzopyran Motif. *Chem. Commun.* **2006**, No. 28, 2962–2964.
(144) Spandl, R. J.; Bender, A.; Spring, D. R. Diversity-Oriented Synthesis; A Spectrum of Approaches and Results. *Org. Biomol. Chem.* **2008**, *6*, 1149–1158.
(145) Behr, A.; Johnen, L.; Rentmeister, N. Novel Palladium-Catalysed Hydroamination of Myrcene and Catalyst Separation by Thermomorphic Solvent Systems. *Adv. Synth. Catal.* **2010**, *352*, 2062–2072.
(146) Ryu, J. S.; Li, G. Y.; Marks, T. J. Organolathanide-Catalyzed Regioselective Intermolecular Hydroamination of Alkenes, Alkynes, Vinylarenes, Di- and Trivinylarenes, and Methylenecyclopropanes. Scope and Mechanistic Comparison to Intramolecular Cyclohydroaminations. *J. Am. Chem. Soc.* **2003**, *125*, 12584–12605.
(147) Brunet, J. J.; Chu, N. C.; Diallo, O. Intermolecular Highly Regioselective Hydroamination of Alkenes with Ligandless Platinum(II) Catalysts in Ionic Solvents: Activation Role of n-Bu4PBr. *Organometallics* **2005**, *24*, 3104–3110.
(148) Zhang, Z.; Lee, S. Du; Widenhoefer, R. A. Intermolecular Hydroamination of Ethylene and 1-Alkenes with Cyclic Ureas Catalyzed by Achiral and Chiral Gold(I) Complexes. *J. Am. Chem. Soc.* **2009**, *131*, 5372–5373.
(149) Reznichenko, A. L.; Nguyen, H. N.; Hultzsch, K. C. Asymmetric Intermolecular Hydroamination of Unactivated Alkenes with Simple Amines. *Angew. Chem. Int. Ed.* **2010**, *49*, 8984–8987.
(150) Sevov, C. S.; Zhou, J.; Hartwig, J. F. Iridium-Catalyzed Intermolecular Hydroamination

of Unactivated Aliphatic Alkenes with Amides and Sulfonamides. *J. Am. Chem. Soc.* **2012**, *134*, 11960–11963.
(151) Sevov, C. S.; Zhou, J.; Hartwig, J. F. Iridium-Catalyzed, Intermolecular Hydroamination of Unactivated Alkenes with Indoles. *J. Am. Chem. Soc.* **2014**, *136*, 3200–3207.
(152) Eisenberger, P.; Schafer, L. L. Catalytic Synthesis of Amines and N-Containing Heterocycles: Amidate Complexes for Selective C–N and C–C Bond-Forming Reactions. *Pure Appl. Chem.* **2010**, *82*, 1503–1515.
(153) Chen, T. Y.; Tsutsumi, R.; Montgomery, T. P.; Volchkov, I.; Krische, M. J. Ruthenium-Catalyzed C-C Coupling of Amino Alcohols with Dienes via Transfer Hydrogenation: Redox-Triggered Imine Addition and Related Hydroaminoalkylations. *J. Am. Chem. Soc.* **2015**, *137*, 1798–1801.
(154) Seayad, A.; Ahmed, M.; Klein, H.; Jackstell, R.; Gross, T.; Beller, M. Internal Olefins to Linear Amines. *Science.* **2002**, *297*, 1676–1679.
(155) Kobayashi, S.; Ishitani, H.; Ueno, M. Catalytic Asymmetric Synthesis of Both Syn- and Anti-β-Amino Alcohols. *J. Am. Chem. Soc.* **1998**, *120*, 431–432.
(156) Garst, M. E.; Dolby, L. J.; Esfandiari, S.; Fedoruk, N. A.; Chamberlain, N. C.; Avey, A. A. Reductions with Lithium in Low Molecular Weight Amines and Ethylenediamine. *J. Org. Chem.* **2000**, *65*, 7098–7104.
(157) Gilmour, D. J.; Lauzon, J. M. P.; Clot, E.; Schafer, L. L. Ta-Catalyzed Hydroaminoalkylation of Alkenes: Insights into Ligand-Modified Reactivity Using DFT. *Organometallics* **2018**, *37*, 4387–4394.
(158) Allahverdiev, A. I.; Göndüz, G.; Murzin, D. Y. Kinetics of α-Pinene Isomerization. *Ind. Eng. Chem. Res.* **1998**, *37*, 2373–2377.
(159) Rocha, W. R.; Milagre, H. M. S.; De Almeida, W. B. On the Isomerization of β-Pinene: A Theoretical Study. *J. Mol. Struct.* **2001**, *544*, 213–220.
(160) Chimal-Valencia, O.; Robau-Sánchez, A.; Collins-Martínez, V.; Aguilar-Elguézabal, A. Ion Exchange Resins as Catalyst for the Isomerization of α-Pinene to Camphene. *Bioresour. Technol.* **2004**, *93*, 119–123.
(161) Stelter, L.; Teusch, T.; Bielefeld, J.; Doye, S.; Klüner, T. Theoretical Studies on the Hydroaminoalkylation of Alkenes with Primary and Secondary Amines. *Chem. Eur. J.* **2018**, *24*, 12485–12489.
(162) Sengoden, M.; Bhowmick, A.; Punniyamurthy, T. Stereospecific Copper-Catalyzed Domino Ring Opening and Sp3 C-H Functionalization of Activated Aziridines with N-Alkylanilines. *Org. Lett.* **2017**, *19*, 158–161.
(163) Majer, P.; Randad, S. R. A Safe and Efficient Method for Preparation of N,N'-Unsymmetrically Disubstituted Ureas Utilizing Triphosgene. *J. Org. Chem.* **1994**, *59*, 1937–1938.
(164) Kaur, M.; Van Humbeck, J. F. Recent Trends in Catalytic sp^3 C-H Functionalization of Heterocycles. *Org. Biomol. Chem.* **2020**.
(165) Das, D.; Sun, A. X.; Seidel, D. Redox-Neutral Copper(II) Carboxylate Catalyzed α-Alkynylation of Amines. *Angew. Chem. Int. Ed.* **2013**, *52*, 3765–3769.
(166) Lennox, A. J. J.; Goes, S. L.; Webster, M. P.; Koolman, H. F.; Djuric, S. W.; Stahl, S. S. Electrochemical Aminoxyl-Mediated α-Cyanation of Secondary Piperidines for Pharmaceutical Building Block Diversification. *J. Am. Chem. Soc.* **2018**, *140*, 11227–11231.

(167) Shaw, M. H.; Shurtleff, V. W.; Terrett, J. A.; Cuthbertson, J. D.; MacMillan, D. W. C. Native Functionality in Triple Catalytic Cross-Coupling: sp^3 C-H Bonds as Latent Nucleophiles. *Science.* **2016**, *352*, 1304–1308.
(168) Zhou, W. J.; Cao, G. M.; Shen, G.; Zhu, X. Y.; Gui, Y. Y.; Ye, J. H.; Sun, L.; Liao, L. L.; Li, J.; Yu, D. G. Visible-Light-Driven Palladium-Catalyzed Radical Alkylation of C−H Bonds with Unactivated Alkyl Bromides. *Angew. Chem. Int. Ed.* **2017**, *56*, 15683–15687.
(169) Mcmanus, J. B.; Onuska, N. P. R.; Je, M. S.; Goodwin, N. C.; Nicewicz, D. A. Site-Selective C − H Alkylation of Piperazine Substrates via Organic Photoredox Catalysis. *Org. Lett.* **2019**.
(170) Fukuyama, T.; Chatani, N.; Tatsumi, J.; Kakiuchi, F.; Murai, S. Ru3(CO)12-Catalyzed Site-Selective Carbonylation Reactions at a C-H Bond in Aza-Heterocycles. *J. Am. Chem. Soc.* **1998**, *120*, 11522–11523.
(171) DiPucchio, R. C.; Rosca, S. C.; Athavan, G.; Schafer, L. L. Exploiting Natural Complexity: Synthetic Terpenoid-Alkaloids by Regioselective and Diastereoselective Hydroaminoalkylation Catalysis. *ChemCatChem* **2019**, 1–7.
(172) Hannedouche, J.; Schulz, E. Hydroamination and Hydroaminoalkylation of Alkenes by Group 3–5 Elements: Recent Developments and Comparison with Late Transition Metals. *Organometallics* **2018**, *37*, 4313–4326.
(173) Nazemi, A.; Cundari, T. R. Importance of Nitrogen-Hydrogen Bond p Ka in the Catalytic Coupling of Alkenes and Amines by Amidate Tantalum Complexes: A Computational Study. *J. Phys. Chem. A* **2019**, *123*, 8595–8606.
(174) Hansch, C.; Leo, A.; Taft, R. W. A Survey of Hammett Substituent Constants and Resonance and Field Parameters. *Chem. Rev.* **1991**, *91*, 165–195.
(175) Coote, M. L.; Davis, T. P. Propagation Kinetics of Para-Substituted Styrenes: A Test of the Applicability of the Hammett Relationship to Free-Radical Polymerization. *Macromolecules* **1999**, *32*, 4290–4298.
(176) P Michael, J. Indolizidine and Quinolizidine Alkaloids. *Nat. Prod. Rep.* **1998**, *15*, 571.
(177) P Michael, J. Indolizidine and Quinolizidine Alkaloids. *Nat. Prod. Rep.* **2001**, *17*, 520–542.
(178) Michael, J. P. Simple Indolizidine and Quinolizidine Alkaloids. *Alkaloids Chem. Biol.* **2003**, *20*, 458–475.
(179) P Michael, J. Indolizidine and Quinolizidine Alkaloids. *Nat. Prod. Rep.* **2004**, *21*, 625–649.
(180) P Michael, J. Indolizidine and Quinolizidine Alkaloids. *Nat. Prod. Rep.* **2005**, *21*, 603–626.
(181) Michael, J. P. Simple Indolizidine and Quinolizidine Alkaloids. *Nat. Prod. Rep.* **2007**, *24*, 191–222.
(182) Michael, J. P. Simple Indolizidine and Quinolizidine Alkaloids. *Nat. Prod. Rep.* **2008**, *25*, 139–165.
(183) Michael, J. P. Simple Indolizidine and Quinolizidine Alkaloids. In *The Alkaloids*; Elsevier Ltd, 2016; pp 1–498.
(184) Hodgetts, I.; Noyce, S. J.; Storr, R. C. Catalysis in Flash Vacuum Pyrolysis. *Tetrahedron Lett.* **1984**, *25*, 5435–5438.
(185) Su, N.; Deng, T.; Wink, D. J.; Driver, T. G. Achieving Site Selectivity in Metal-Catalyzed Electron-Rich Carbene Transfer Reactions from N-Tosylhydrazones. *Org. Lett.* **2017**, *19*,

3990–3993.
(186) Cosgrove, S. C.; Plane, J. M. C.; Marsden, S. P. Radical-Mediated Direct C-H Amination of Arenes with Secondary Amines. *Chem. Sci.* **2018**, *9*, 6647–6652.
(187) Jordan-Hore, J. A.; Johansson, C. C. C.; Gulias, M.; Beck, E. M.; Gaunt, M. J. Oxidative Pd(II)-Catalyzed C-H Bond Amination to Carbazole at Ambient Temperature. *J. Am. Chem. Soc.* **2008**, *130*, 16184–16186.
(188) Wang, H.; Wang, Y.; Peng, C.; Zhang, J.; Zhu, Q. A Direct Intramolecular C-H Amination Reaction Cocatalyzed by Copper(II) and Iron(III) as Part of an Efficient Route for the Synthesis of Pyrido[1,2-a]Benzimidazoles from N-Aryl-2-Aminopyridines. *J. Am. Chem. Soc.* **2010**, *132*, 13217–13219.
(189) Lu, J.; Jin, Y.; Liu, H.; Jiang, Y.; Fu, H. Copper-Catalyzed Aerobic Oxidative Intramolecular Alkene C-H Amination Leading to N-Heterocycles. *Org. Lett.* **2011**, *13*, 3694–3697.
(190) Shi, Z.; Zhang, C.; Tang, C.; Jiao, N. Recent Advances in Transition-Metal Catalyzed Reactions Using Molecular Oxygen as the Oxidant. *Chem. Soc. Rev.* **2012**, *41*, 3381–3430.
(191) Shrestha, R.; Mukherjee, P.; Tan, Y.; Litman, Z. C.; Hartwig, J. F. Sterically Controlled, Palladium-Catalyzed Intermolecular Amination of Arenes. *J. Am. Chem. Soc.* **2013**, *135*, 8480–8483.
(192) Shang, M.; Zeng, S. H.; Sun, S. Z.; Dai, H. X.; Yu, J. Q. Ru(II)-Catalyzed Ortho-C-H Amination of Arenes and Heteroarenes at Room Temperature. *Org. Lett.* **2013**, *15*, 5286–5289.
(193) Park, Y.; Kim, Y.; Chang, S. Transition Metal-Catalyzed C-H Amination: Scope, Mechanism, and Applications. *Chem. Rev.* **2017**, *117*, 9247–9301.
(194) Wolfe, J. P.; Buchwald, S. L. Nickel-Catalyzed Amination of Aryl Chlorides. *J. Am. Chem. Soc.* **1997**, *119*, 6054–6058.
(195) Perry, M. R.; Ebrahimi, T.; Morgan, E.; Edwards, P. M.; Hatzikiriakos, S. G.; Schafer, L. L. Catalytic Synthesis of Secondary Amine-Containing Polymers: Variable Hydrogen Bonding for Tunable Rheological Properties. *Macromolecules* **2016**, *49*, 4423–4430.
(196) Kuanr, N.; Tomkovic, T.; Gilmour, D. J.; Perry, M. R.; Hsiang, S. J.; Van Ruymbeke, E.; Hatzikiriakos, S. G.; Schafer, L. L. Dynamic Cross-Linking of Catalytically Synthesized Poly(Aminonorbornenes). *Macromolecules* **2020**, *53*, 2649–2661.
(197) M. Budzelaar, P. H.; van Oort, A. B.; Orpen, A. G. β-Diiminato Complexes of VIII and TiIII – Formation and Structure of Stable Paramagnetic Dialkylmetal Compounds. *Eur. J. Inorg. Chem.* **1998**, *1998*, 1485–1494.
(198) Leitch, D. C.; Beard, J. D.; Thomson, R. K.; Wright, V. A.; Patrick, B. O.; Schafer, L. L. N,O-Chelates of Group 4 Metals: Contrasting the Use of Amidates and Ureates in the Synthesis of Metal Dichlorides. *Eur. J. Inorg. Chem.* **2009**, 2691–2701.

Appendices

Appendix A

This appendix is for NMR spectra.

A.1 Chapter 2 Ureate Ligand Spectra

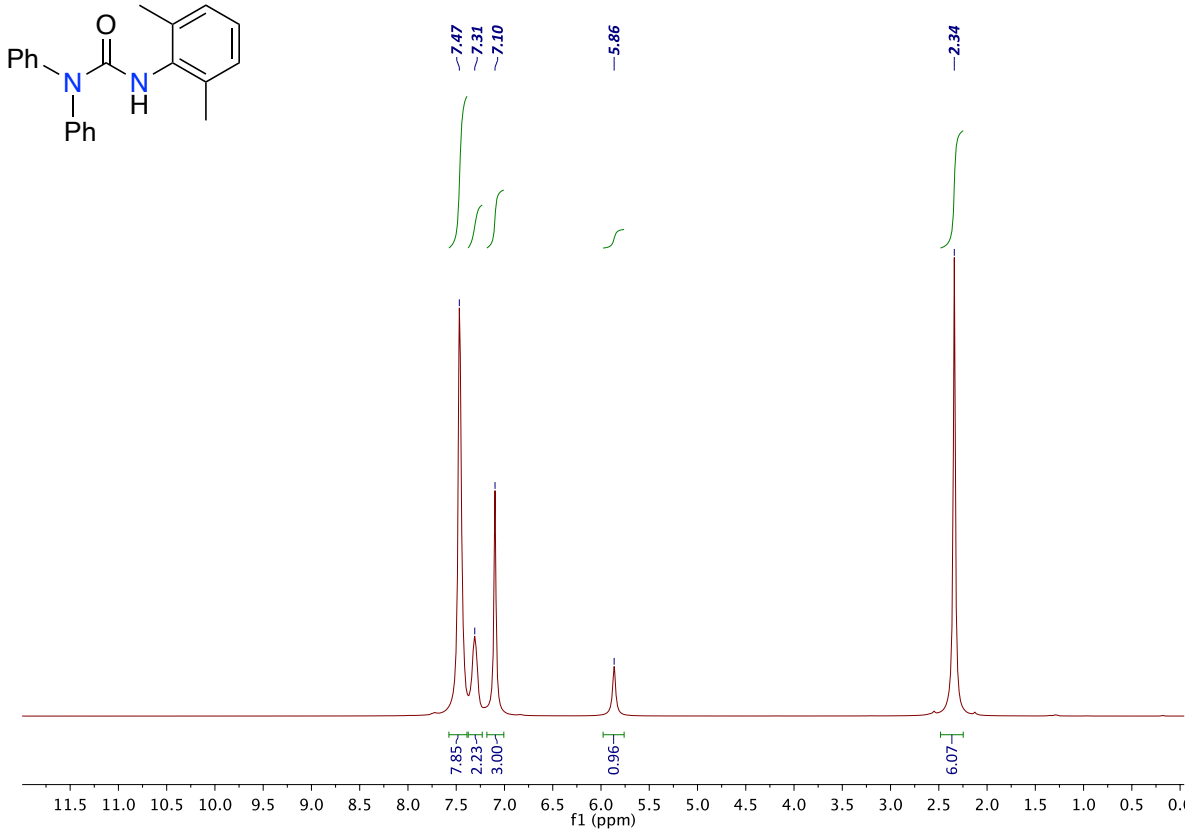

Figure. A.1 . ^{1}H NMR spectrum (300 MHz, $CDCl_3$, 298 K) of 3-(2,6-dimethylphenyl)-1,1-diphenylurea.

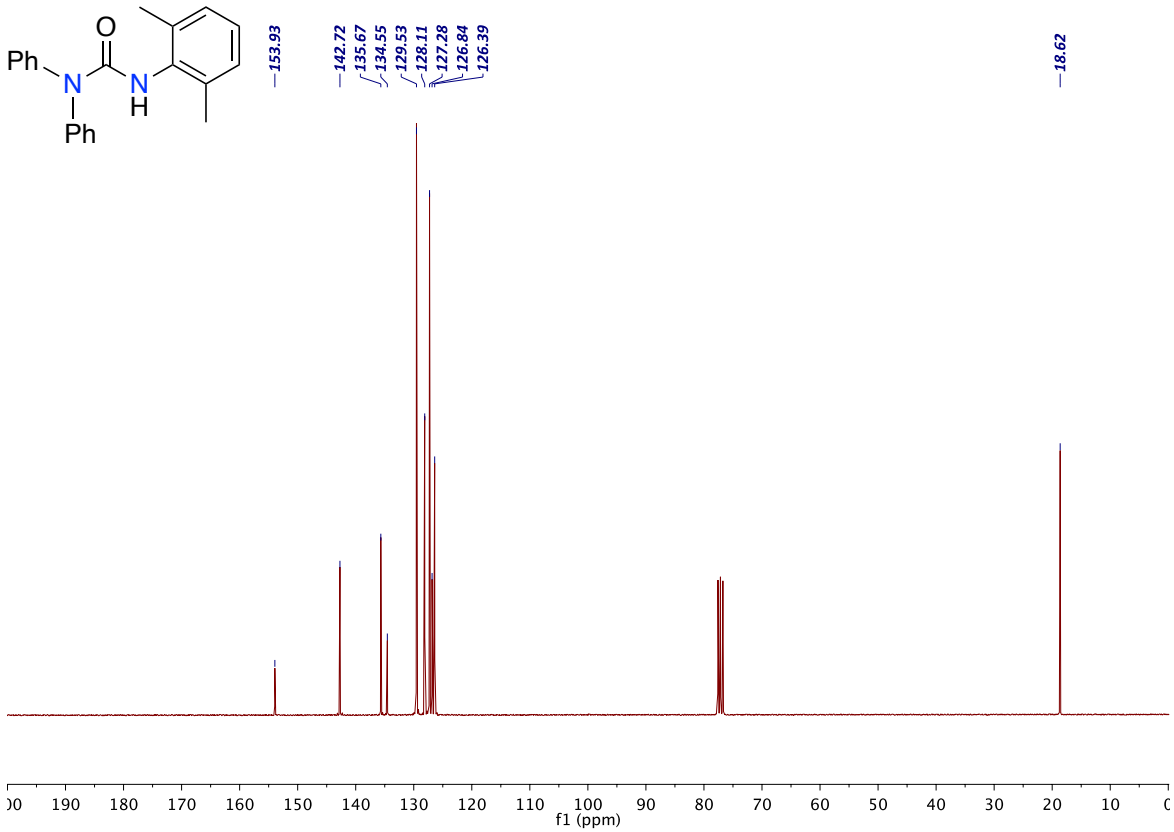

Figure. A.2. $^{13}C\{^{1}H\}$ NMR spectrum (75 MHz, $CDCl_3$, 298 K) of 3-(2,6-dimethylphenyl)-1,1-diphenylurea.

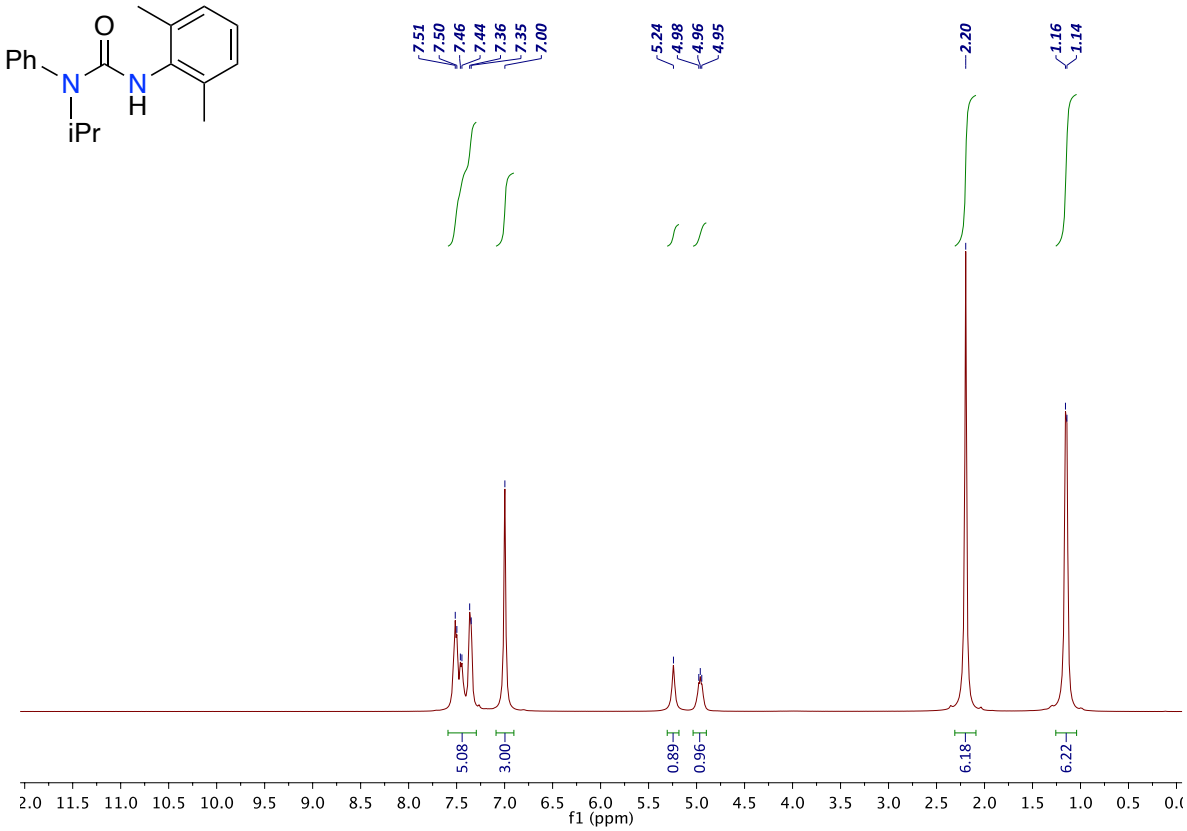

Figure. A.3. ^{1}H NMR spectrum (300 MHz, $CDCl_3$, 298 K) of 3-(2,6-dimethylphenyl)-1-isopropyl-1-phenylurea.

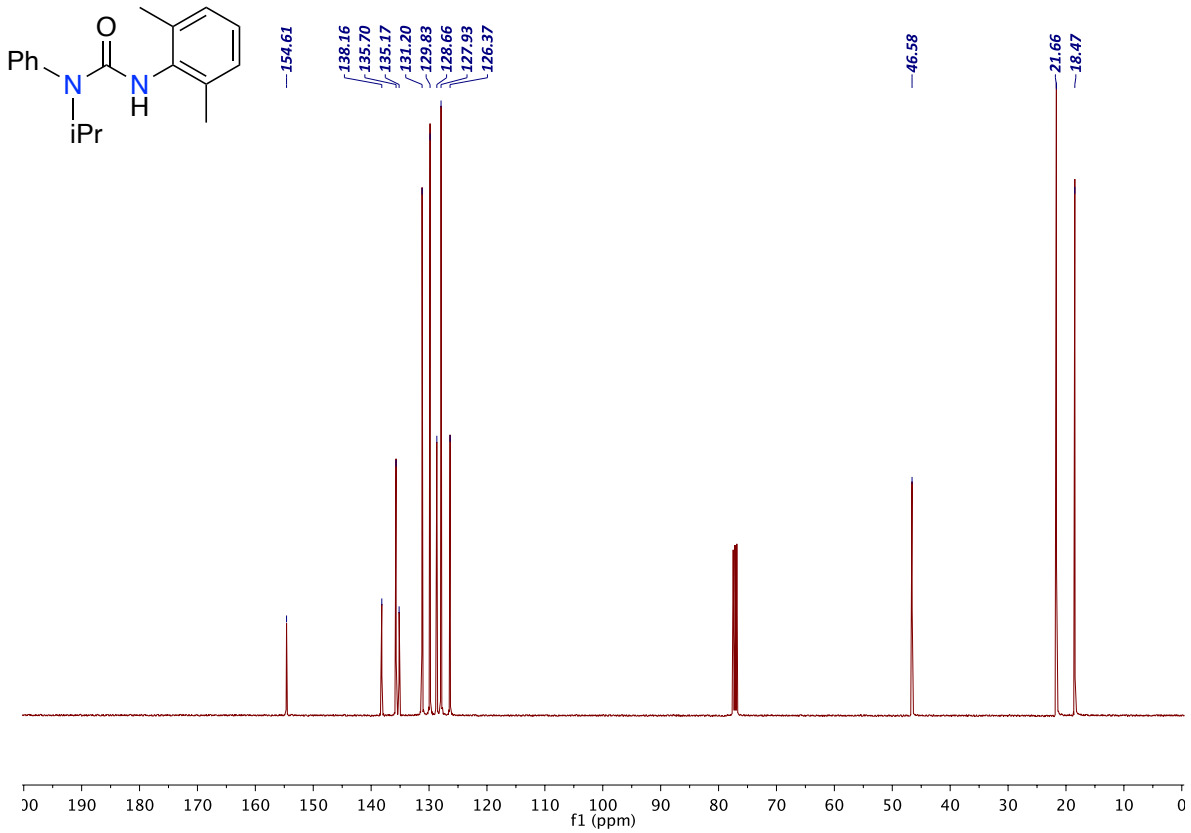

Figure. A.4. $^{13}C\{^{1}H\}$ NMR spectrum (75 MHz, $CDCl_3$, 298 K) of 3-(2,6-dimethylphenyl)-1-isopropyl-1-phenylurea.

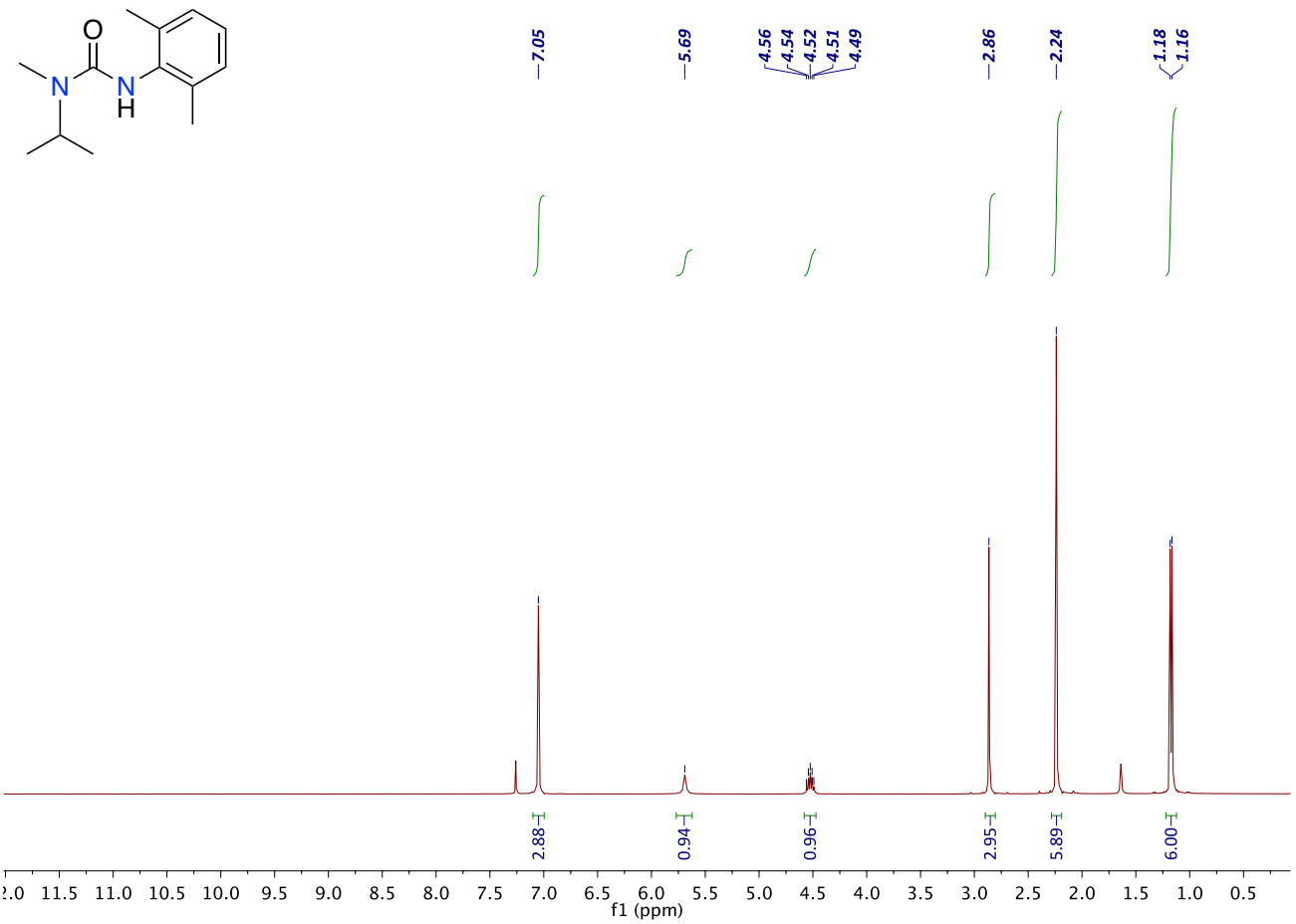

Figure. A.5. ^{1}H NMR spectrum (400 MHz, $CDCl_3$, 298 K) of 3-(2,6-dimethylphenyl)-1-isopropyl-1-phenylurea.

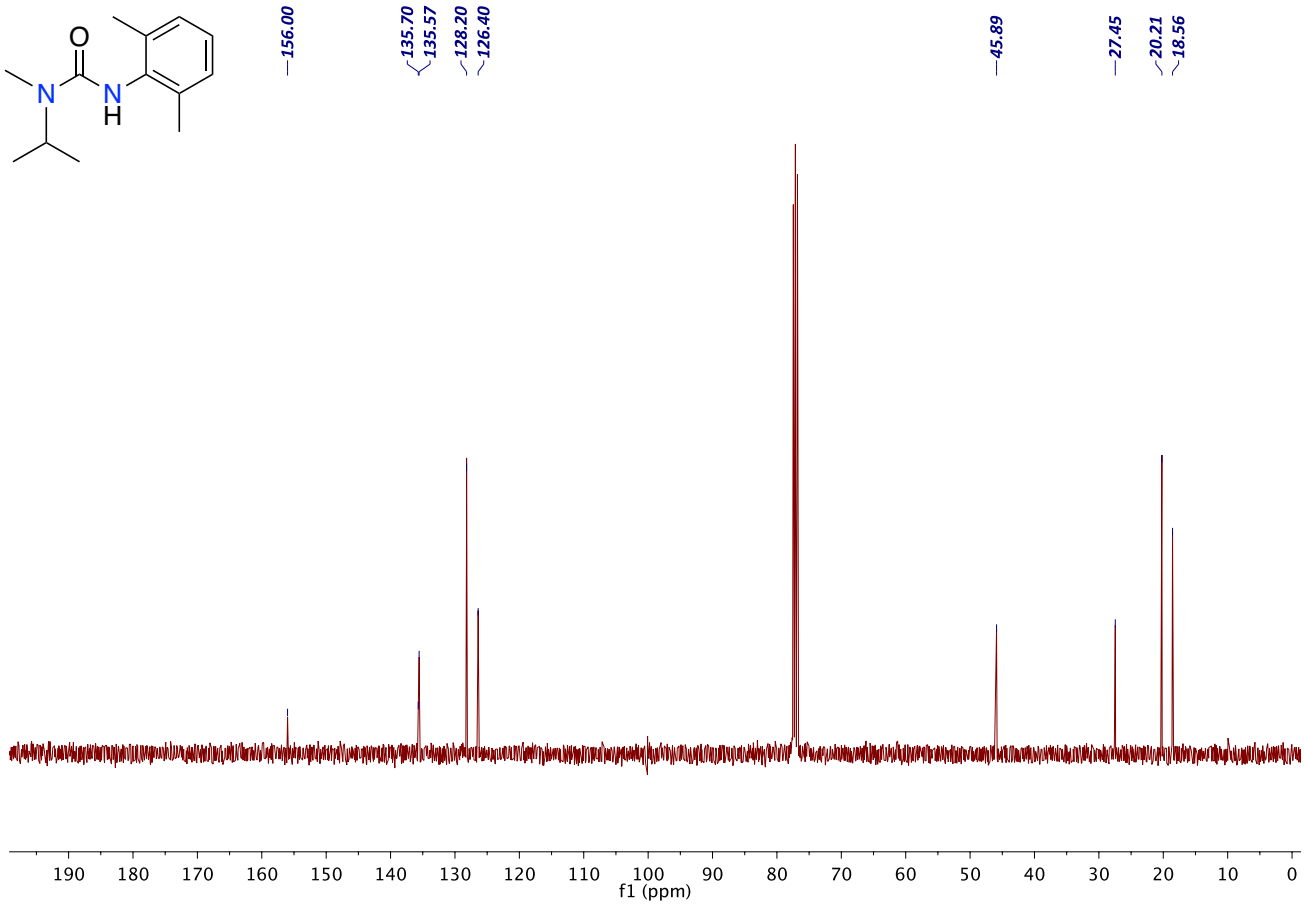

Figure. A.6. $^{13}C\{^{1}H\}$ NMR spectrum (101 MHz, $CDCl_3$, 298 K) of 3-(2,6-dimethylphenyl)-1-isopropyl-1-phenylurea.

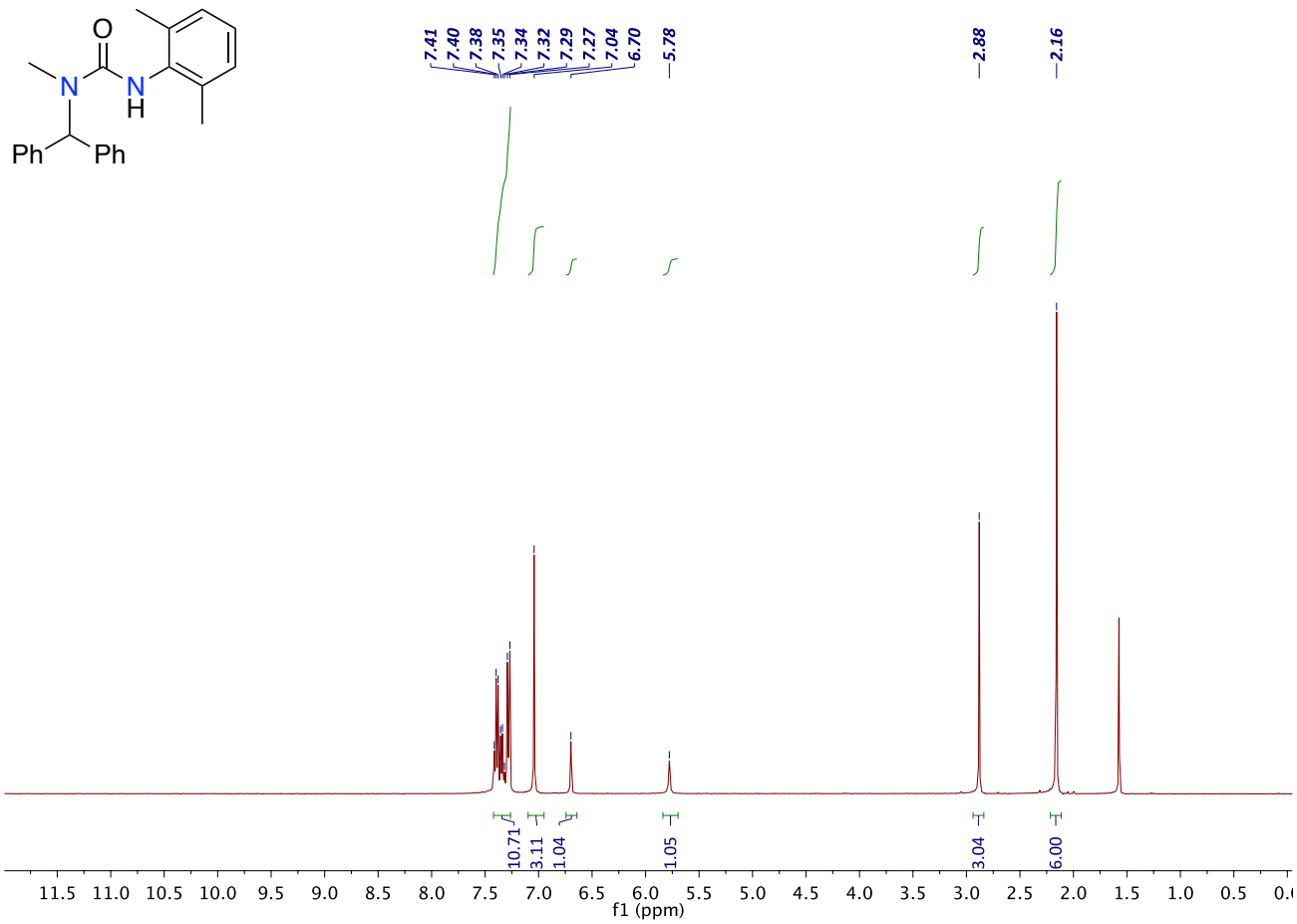

Figure. A.7. ^{1}H NMR spectrum (400 MHz, $CDCl_3$, 298 K) of 1-benzhydryl-3-(2,6-dimethylphenyl)-1-methylurea.

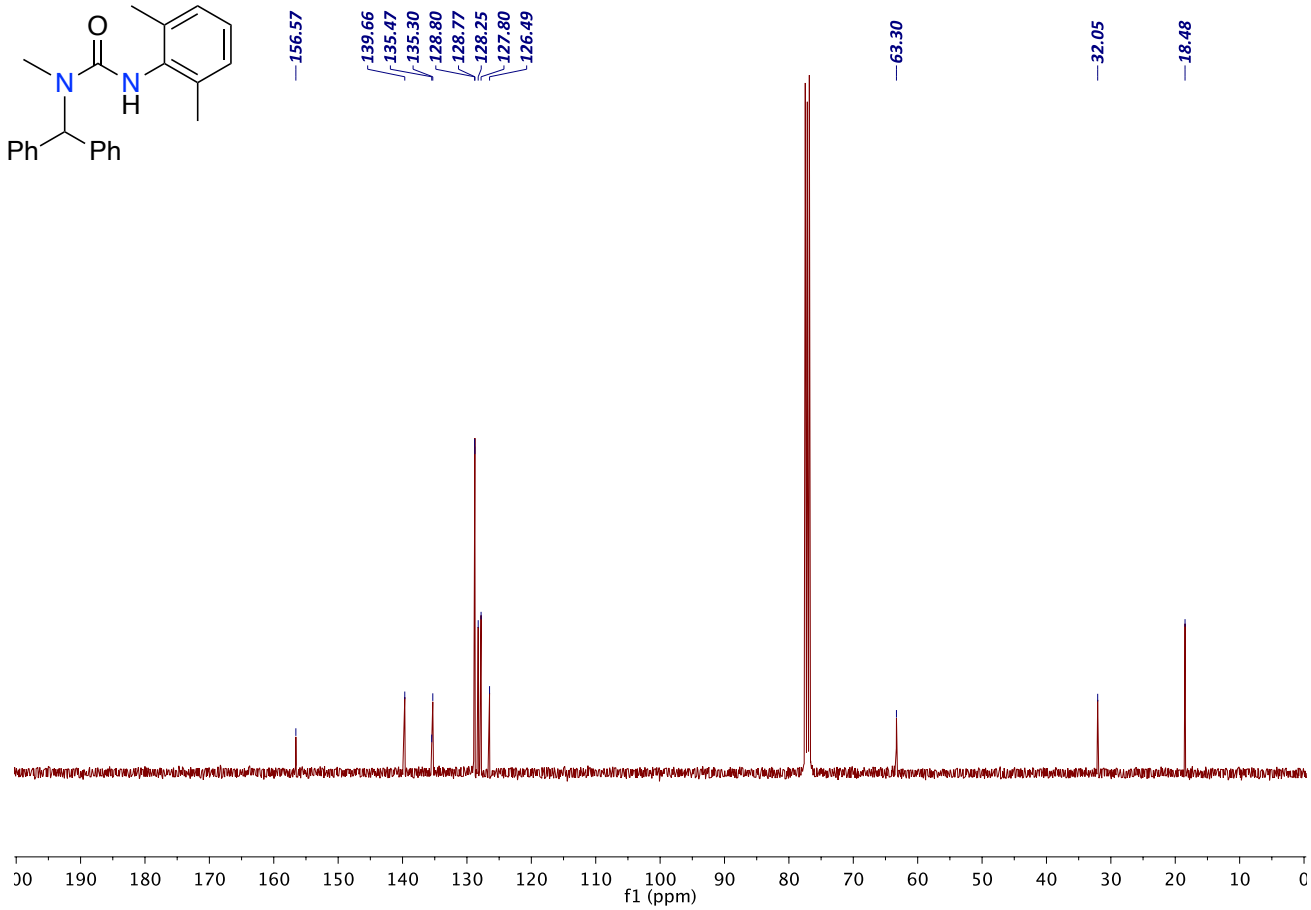

Figure. A.8. $^{13}C\{^{1}H\}$ NMR spectrum (101 MHz, $CDCl_3$, 298 K) of 1-benzhydryl-3-(2,6-dimethylphenyl)-1-methylurea.

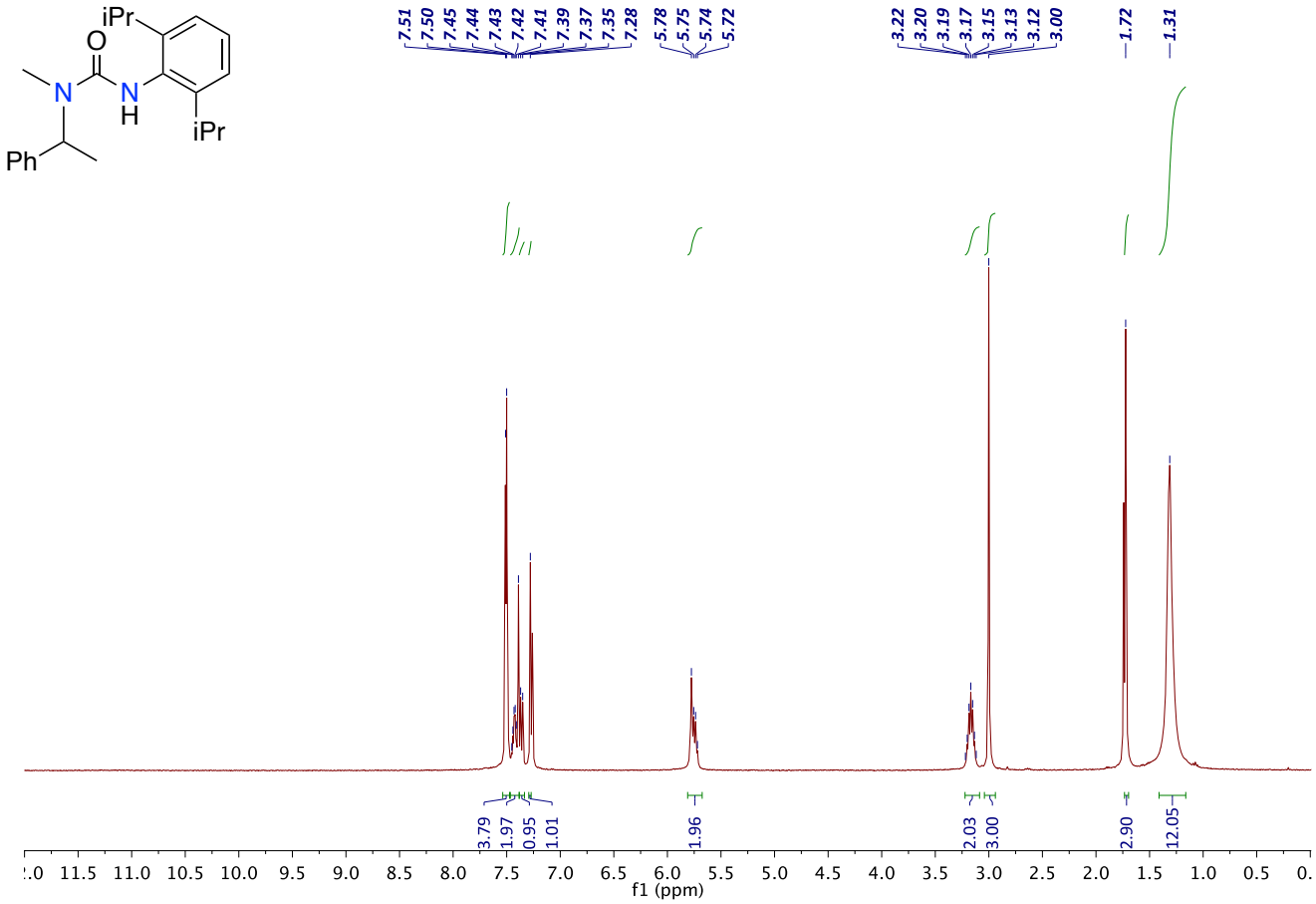

Figure. A.9. ^{1}H NMR spectrum (400 MHz, $CDCl_3$, 298 K) of 3-(2,6-diisopropylphenyl)-1-methyl-1-(1-phenylethyl)urea.

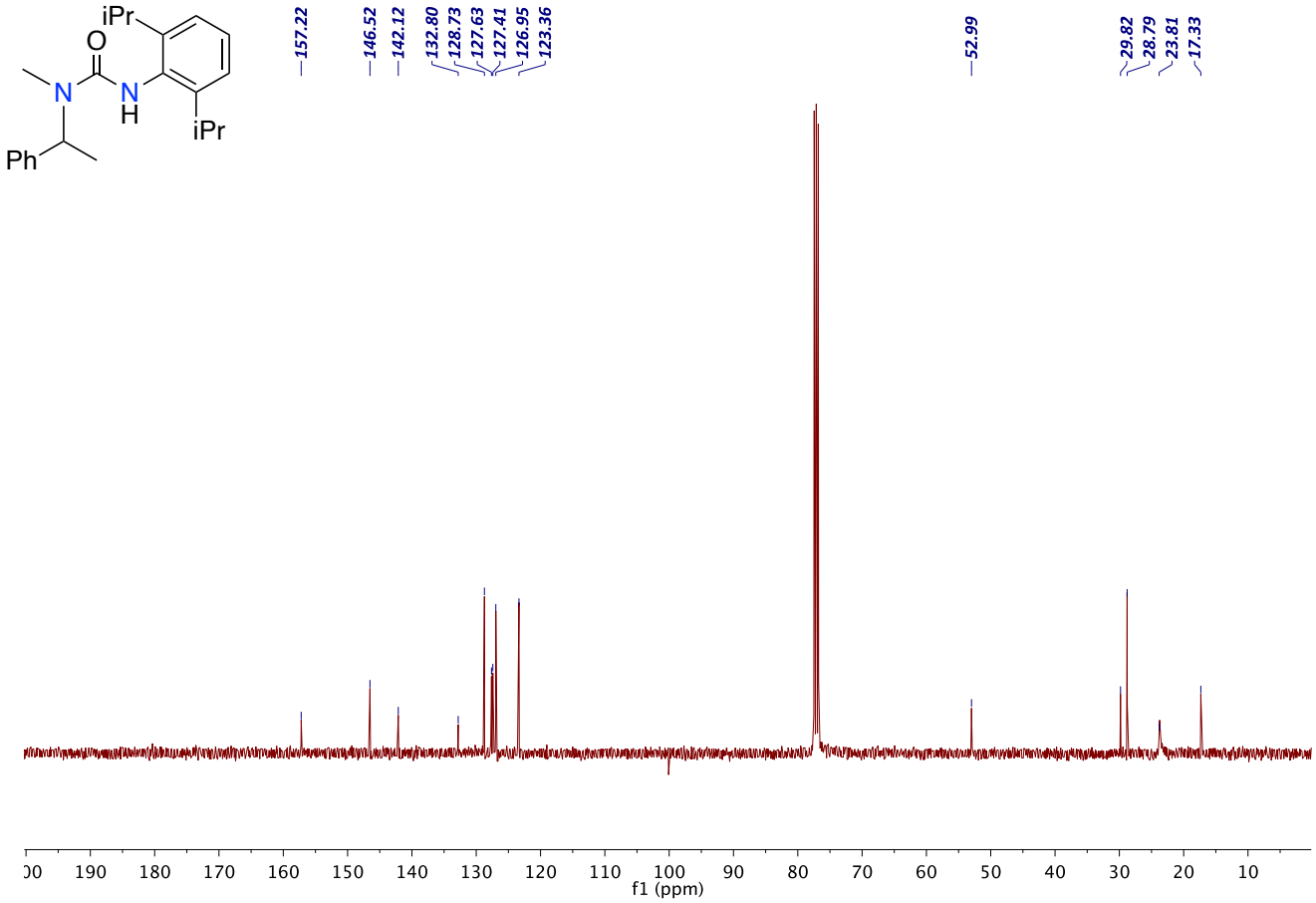

Figure. A.10. $^{13}C\{^{1}H\}$ NMR spectrum (101 MHz, $CDCl_3$, 298 K) of 3-(2,6-diisopropylphenyl)-1-methyl-1-(1-phenylethyl)urea.

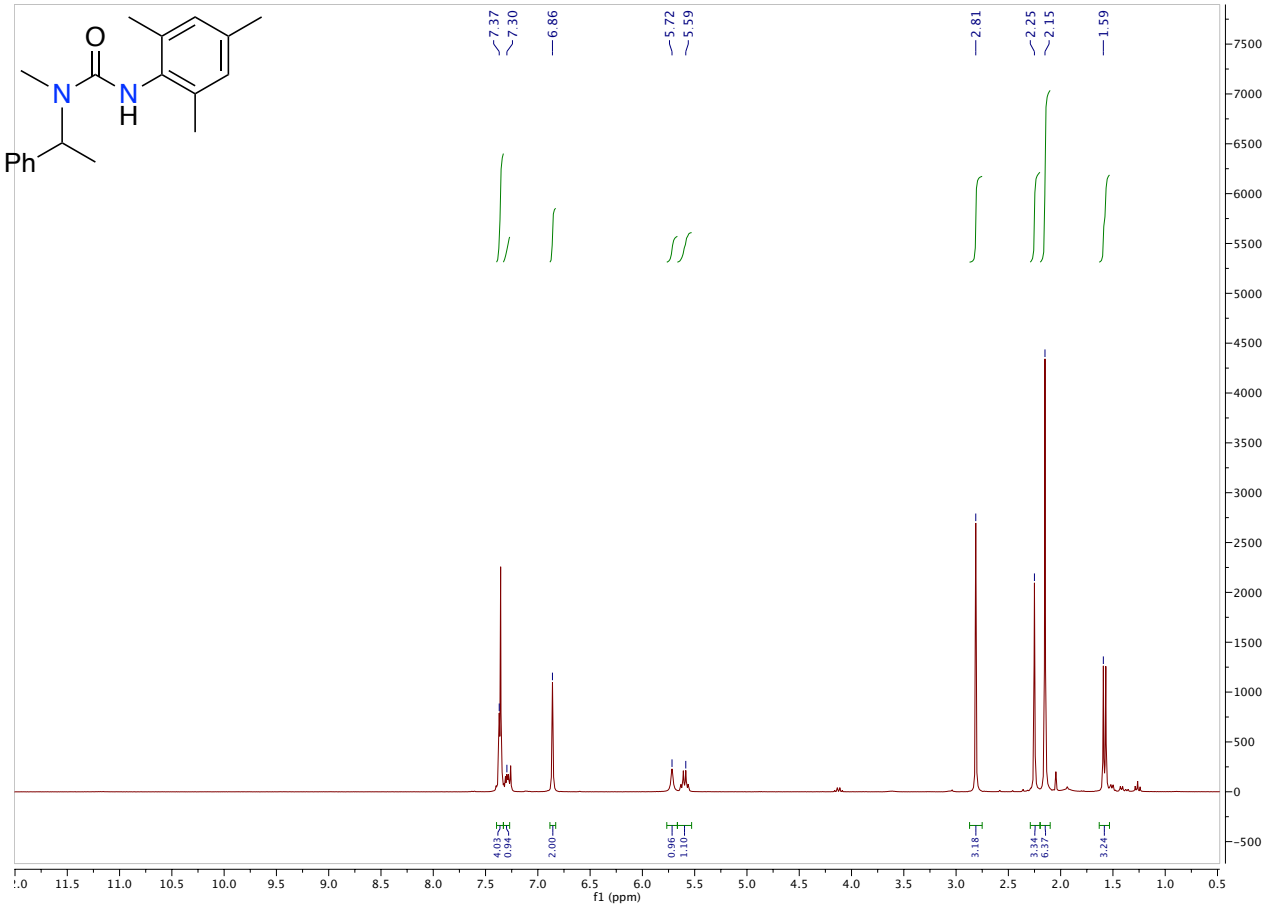

Figure. A.11. ^{1}H NMR spectrum (400 MHz, CDCl3, 298 K) of 3-mesityl-1-methyl-1-(1-phenylethyl)urea.

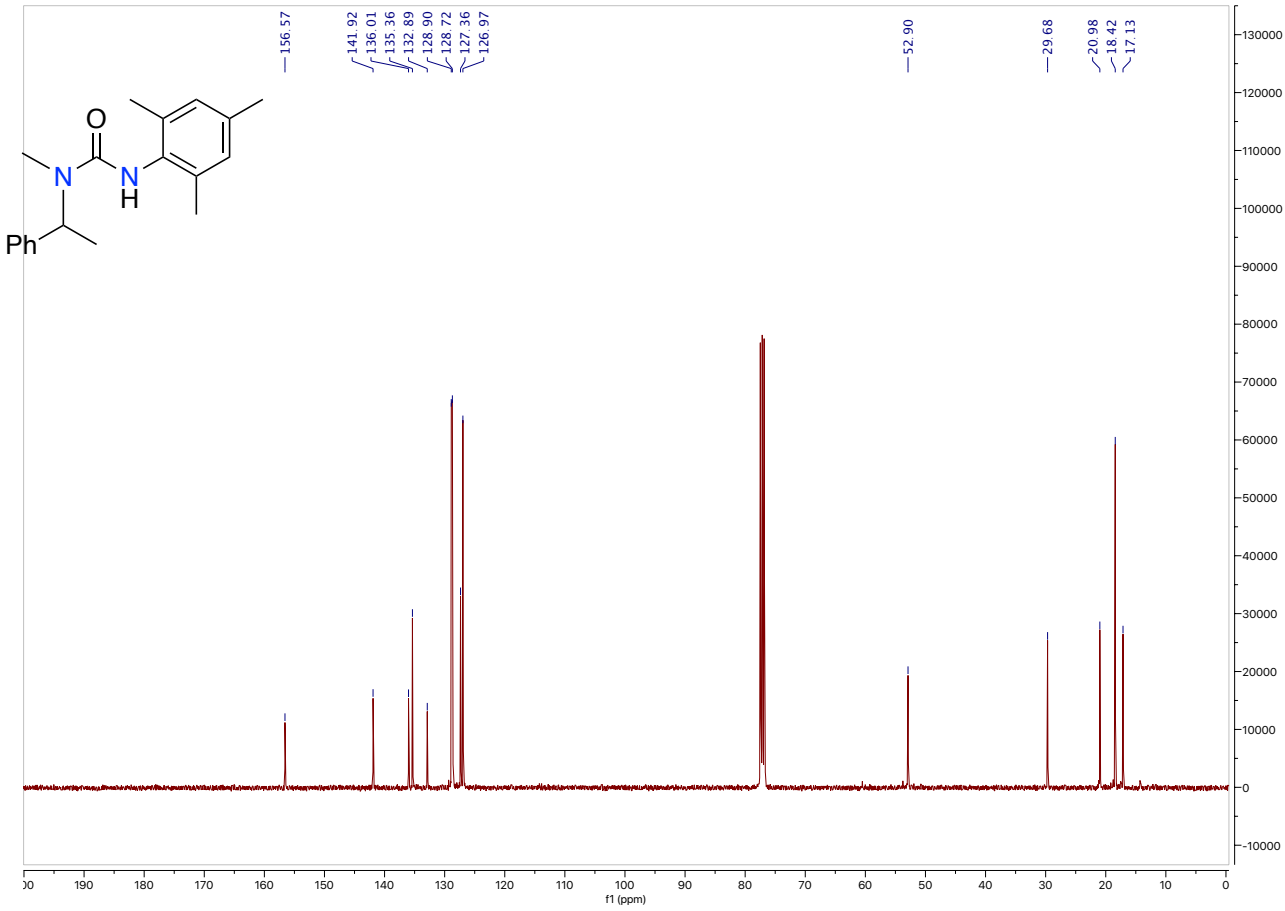

Figure. A.12. $^{13}C\{^{1}H\}$ NMR spectrum (101 MHz, $CDCl_3$, 298 K) of 3-mesityl-1-methyl-1-(1-phenylethyl)urea.

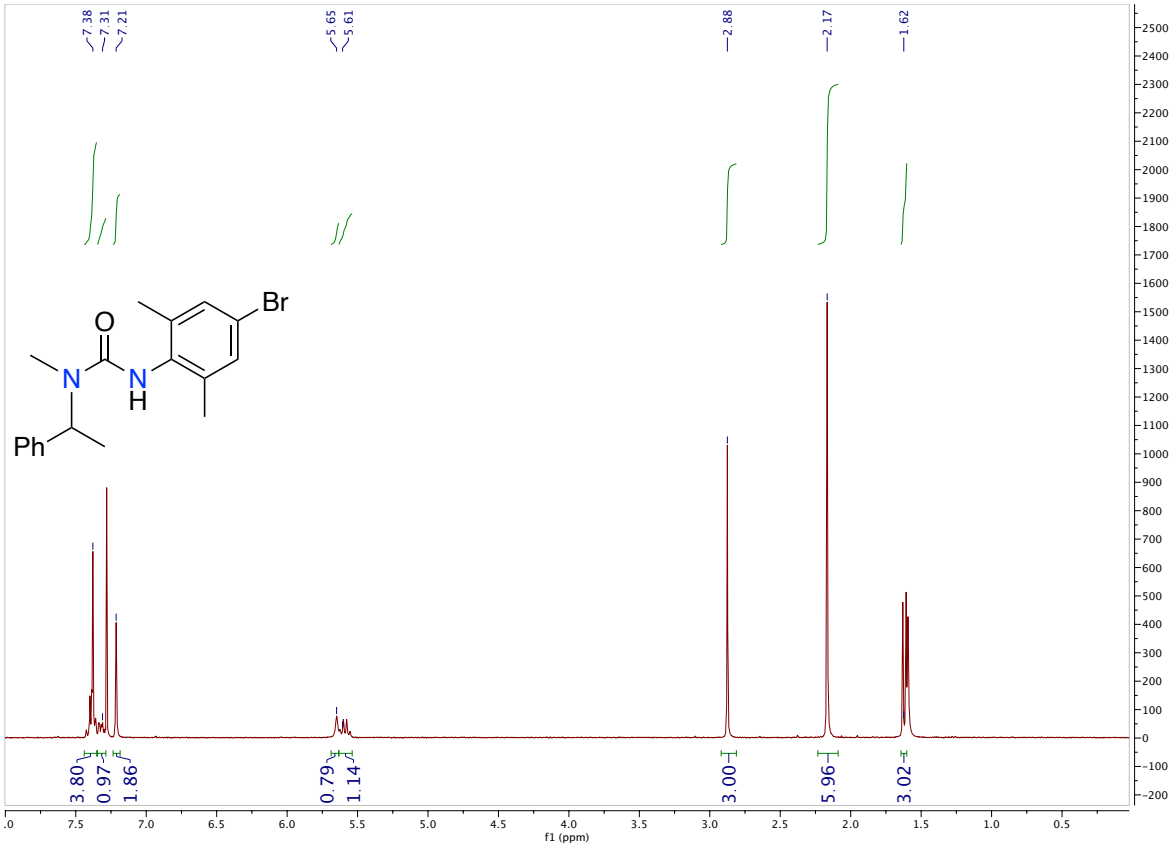

Figure. A.13. ^{1}H NMR spectrum (400 MHz, CDCl3, 298 K) of 3-(4-bromo-2,6-dimethylphenyl)-1-methyl-1-(1-phenylethyl)urea.

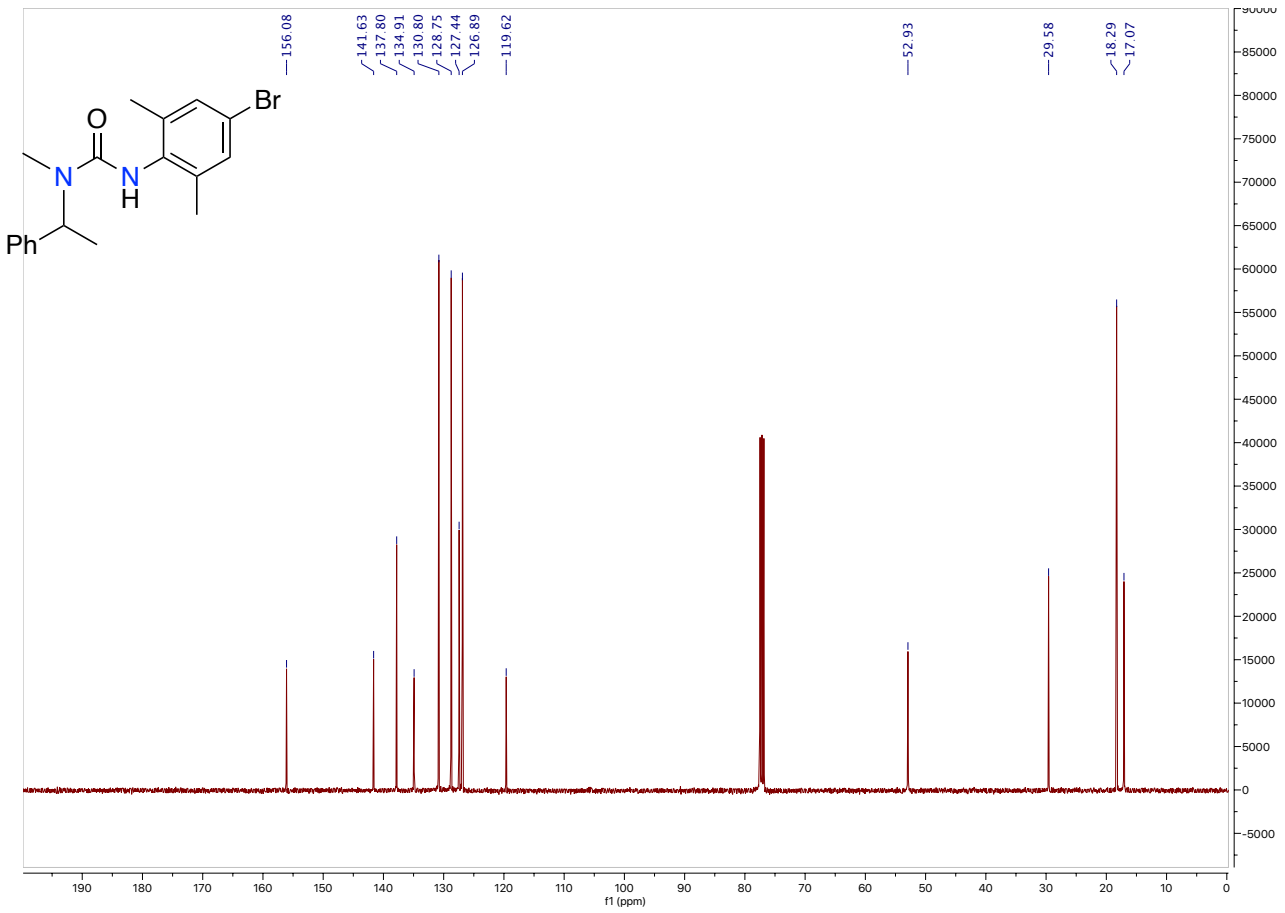

Figure. A.14. $^{13}C\{^{1}H\}$ NMR spectrum (101 MHz, $CDCl_3$, 298 K) of 3-(4-bromo-2,6-dimethylphenyl)-1-methyl-1-(1-phenylethyl)urea.

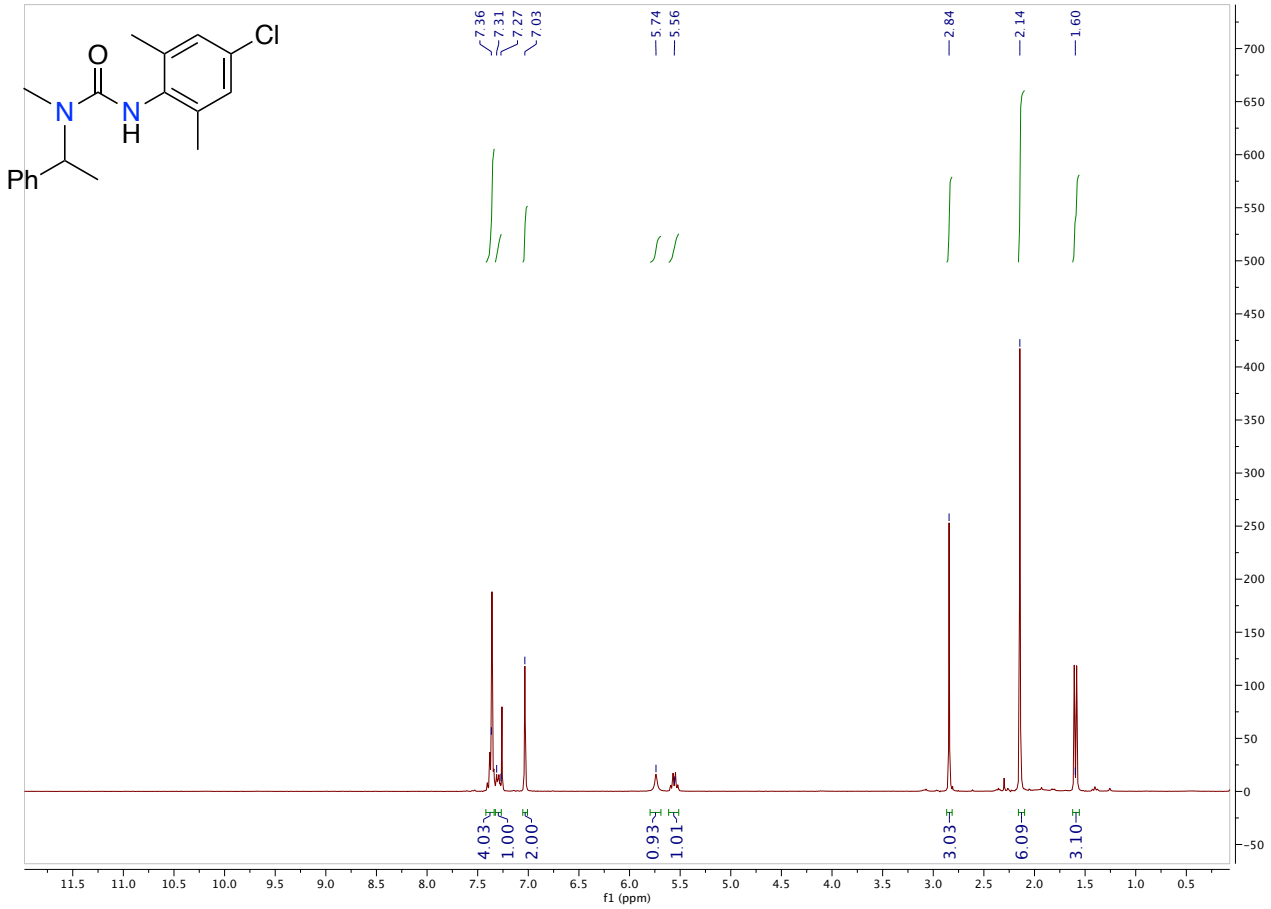

Figure. A.15. ^{1}H NMR spectrum (400 MHz, CDCl3, 298 K) of 3-(4-chloro-2,6-dimethylphenyl)-1-methyl-1-(1-phenylethyl)urea.

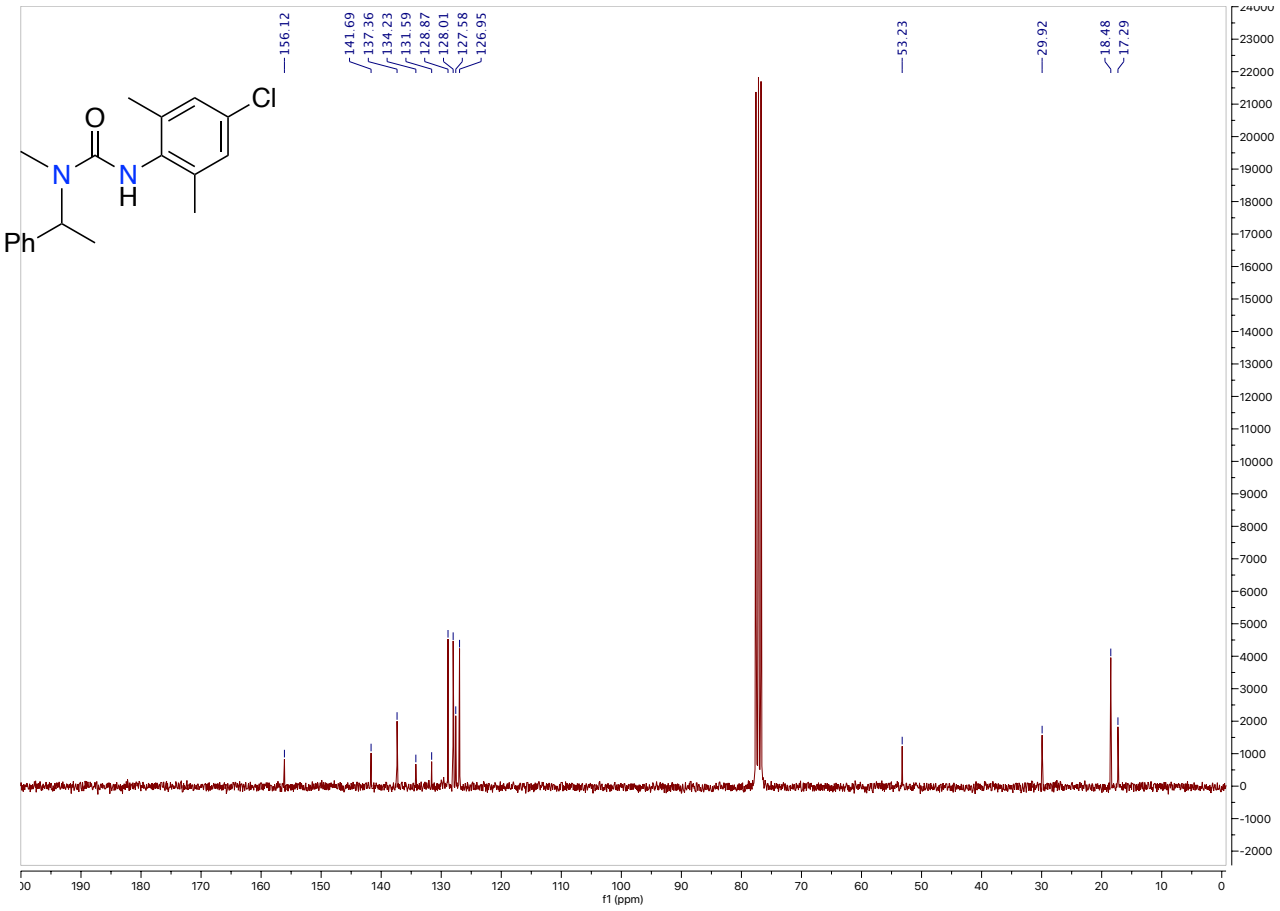

Figure. A.16. $^{13}C\{^{1}H\}$ NMR spectrum (101 MHz, $CDCl_3$, 298 K) of 3-(4-chloro-2,6-dimethylphenyl)-1-methyl-1-(1-phenylethyl)urea.

A.2 Chapter 2 *in situ* Catalysis Spectra

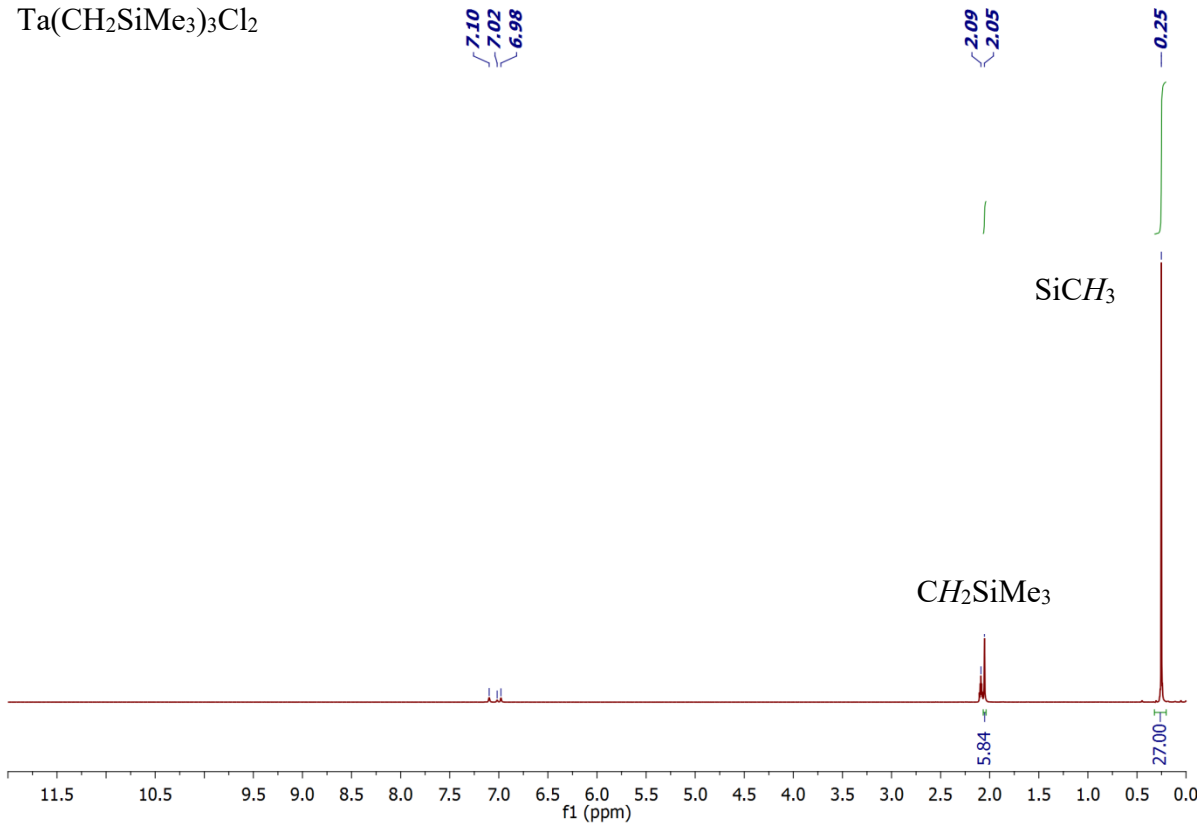

Figure. A.17. ^{1}H NMR spectrum (300 MHz, d8-toluene, 298 K) of $Ta(CH_2SiMe_3)_3Cl_2$.

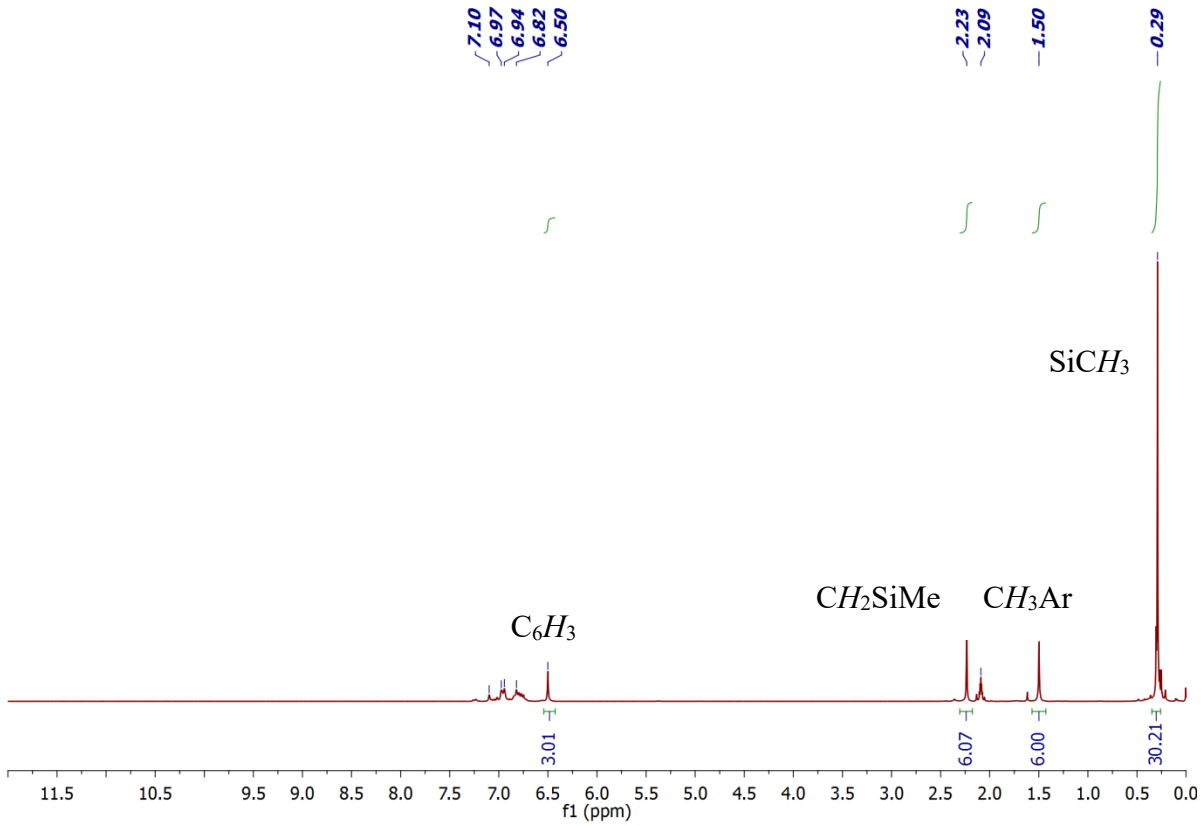

Figure. A.18. ^{1}H NMR spectrum (300 MHz, d8-toluene, 298 K) of the in situ mixture between $Ta(CH_2SiMe_3)_3Cl_2$ and **2.5** showing the formation of the corresponding precatalyst.

A.3 Chapter 2 Amine Scope Products

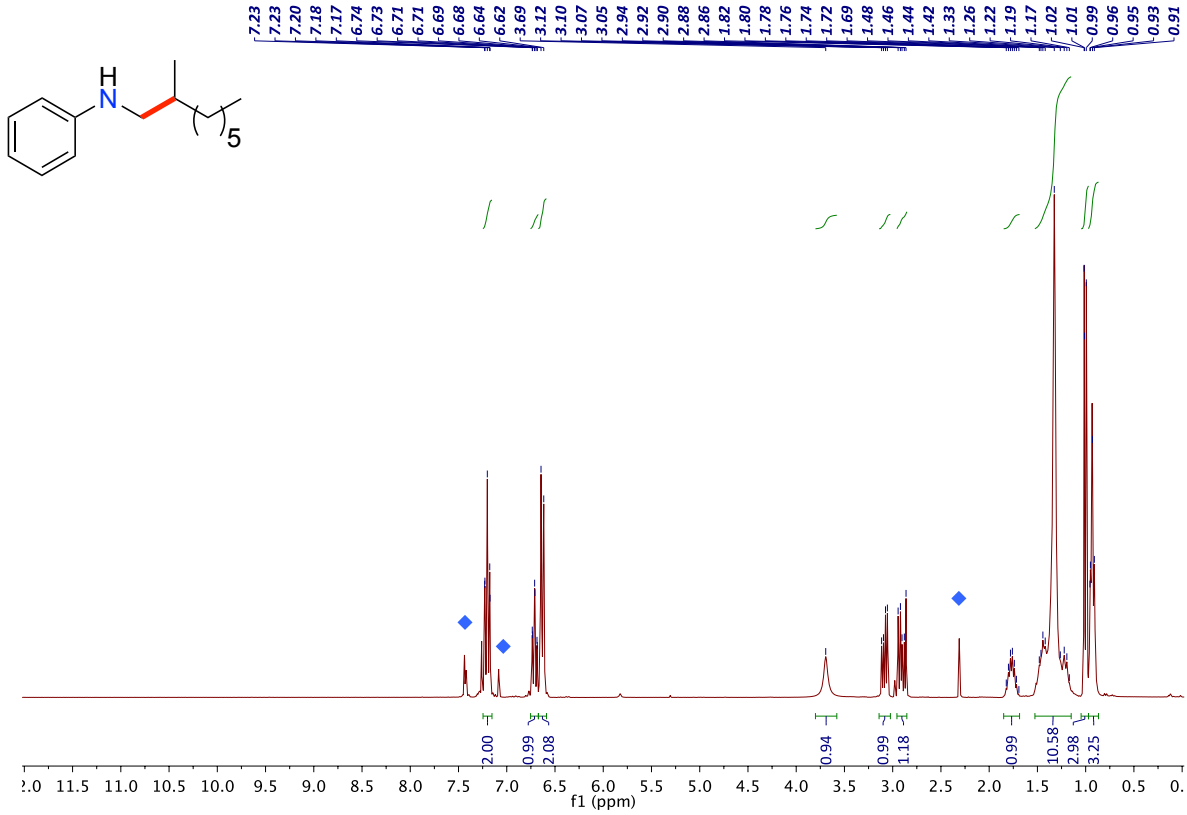

Figure. A.19. ^{1}H NMR spectrum (300 MHz, $CDCl_3$, 298 K) of *N*-(2-methyloctyl)aniline as purified using the general filtration procedure above.

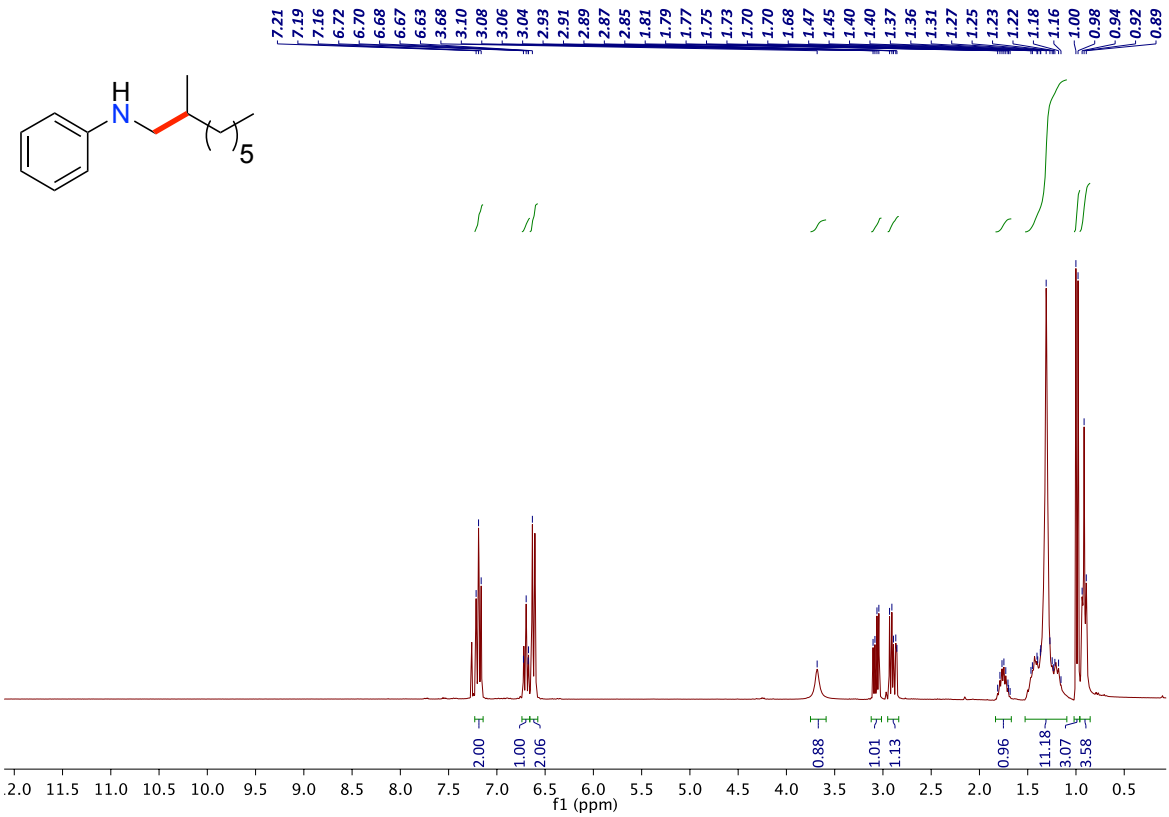

Figure. A.20. ^{1}H NMR spectrum (300 MHz, $CDCl_3$, 298 K) of *N*-(2-methyloctyl)aniline after column chromatography.

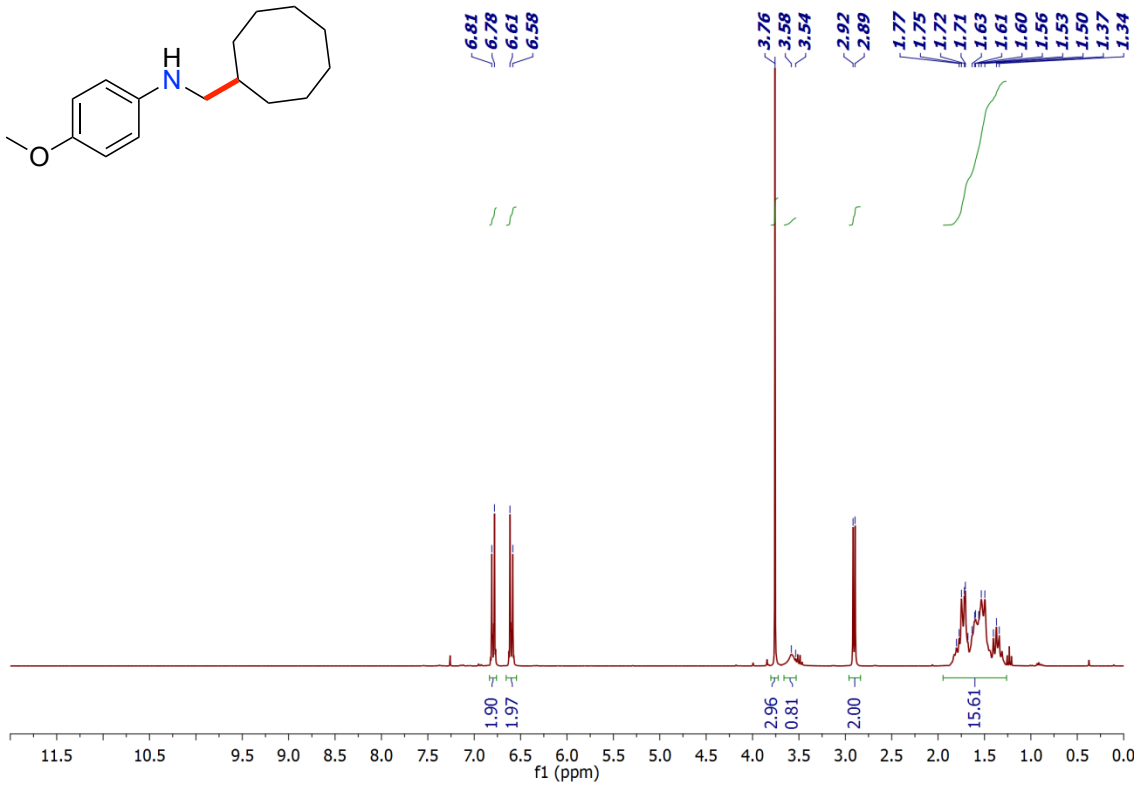

Figure. A.21. ^{1}H NMR spectrum (300 MHz, $CDCl_3$, 298 K) of *N*-(cyclooctylmethyl)-4-methoxyaniline.

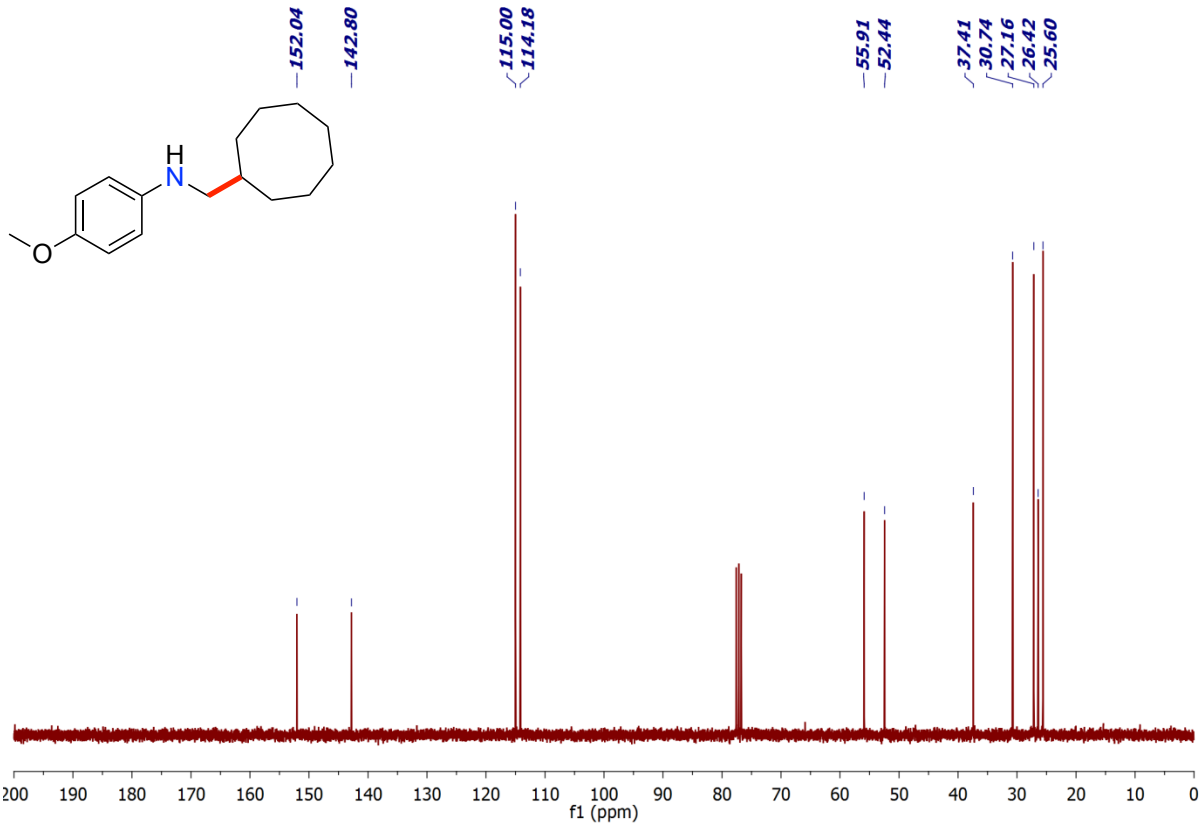

Figure. A.22. $^{13}C\{^{1}H\}$ NMR spectrum (75 MHz, $CDCl_3$, 298 K) of *N*-(cyclooctylmethyl)-4-methoxyaniline.

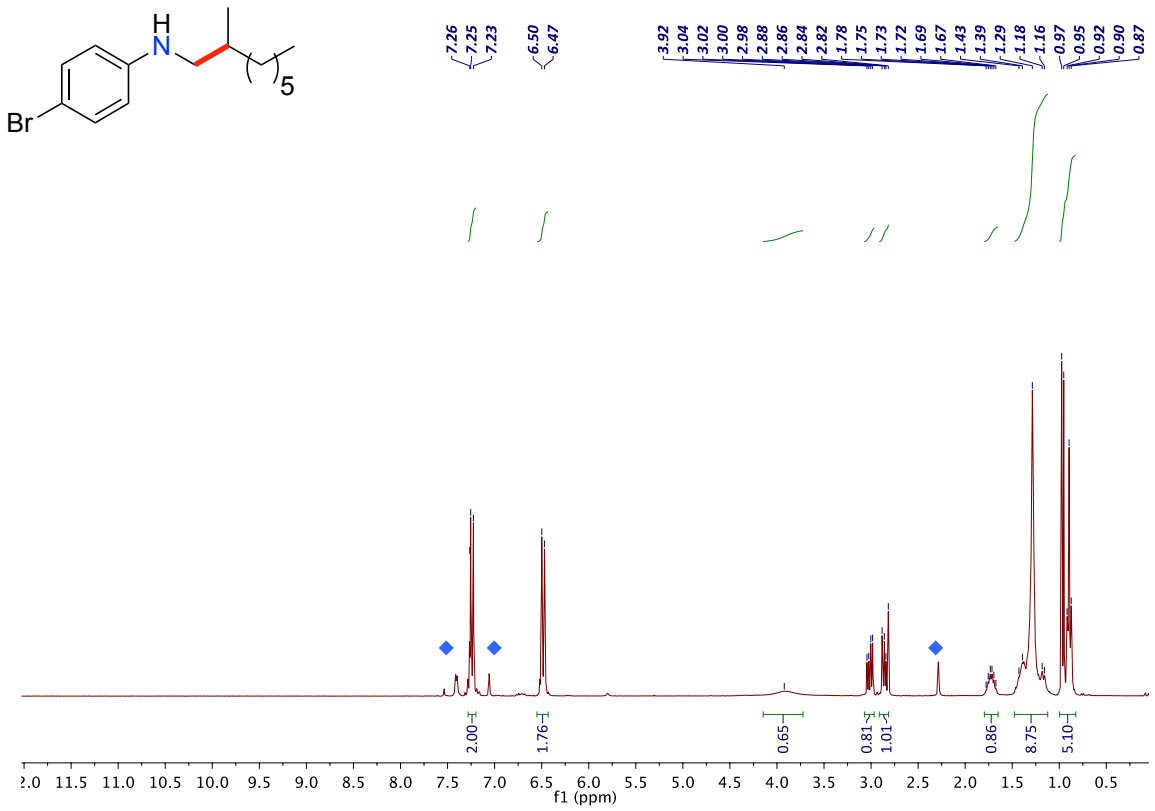

Figure. A.23. ^{1}H NMR spectrum (300 MHz, $CDCl_3$, 298 K) of 4-bromo-*N*-(2-methyloctyl)aniline.

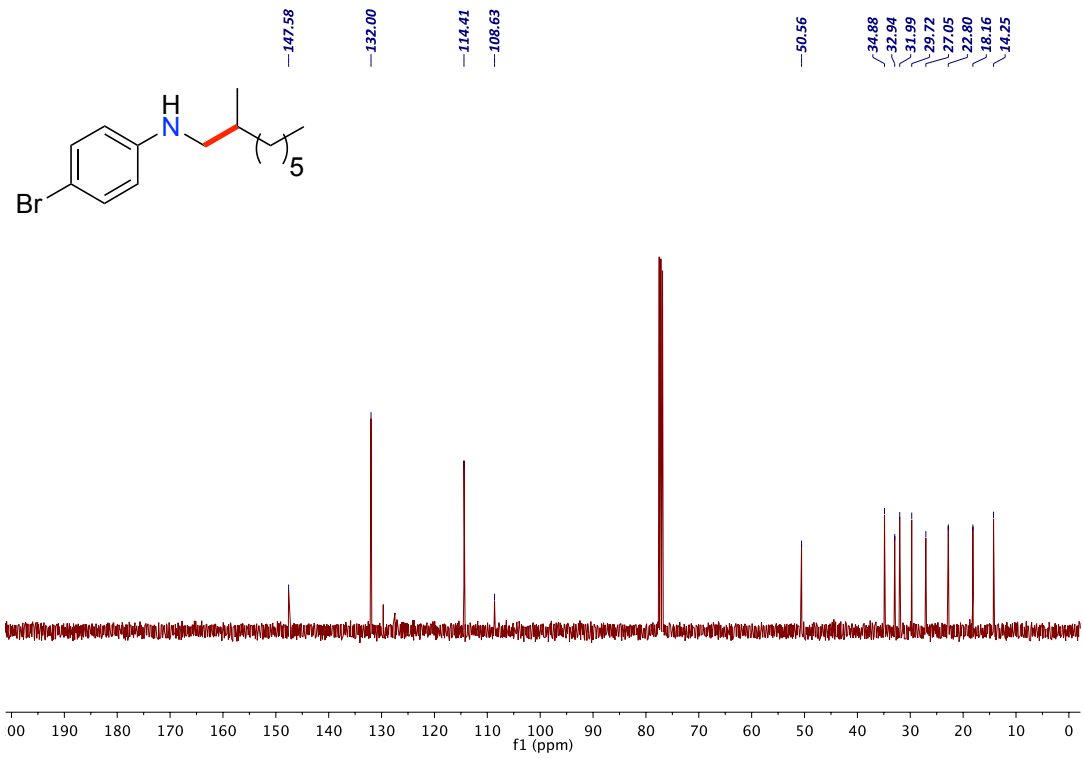

Figure. A.24. $^{13}C\{^{1}H\}$ NMR spectrum (75 MHz, $CDCl_3$, 298 K) of 4-bromo-*N*-(2-methyloctyl)aniline.

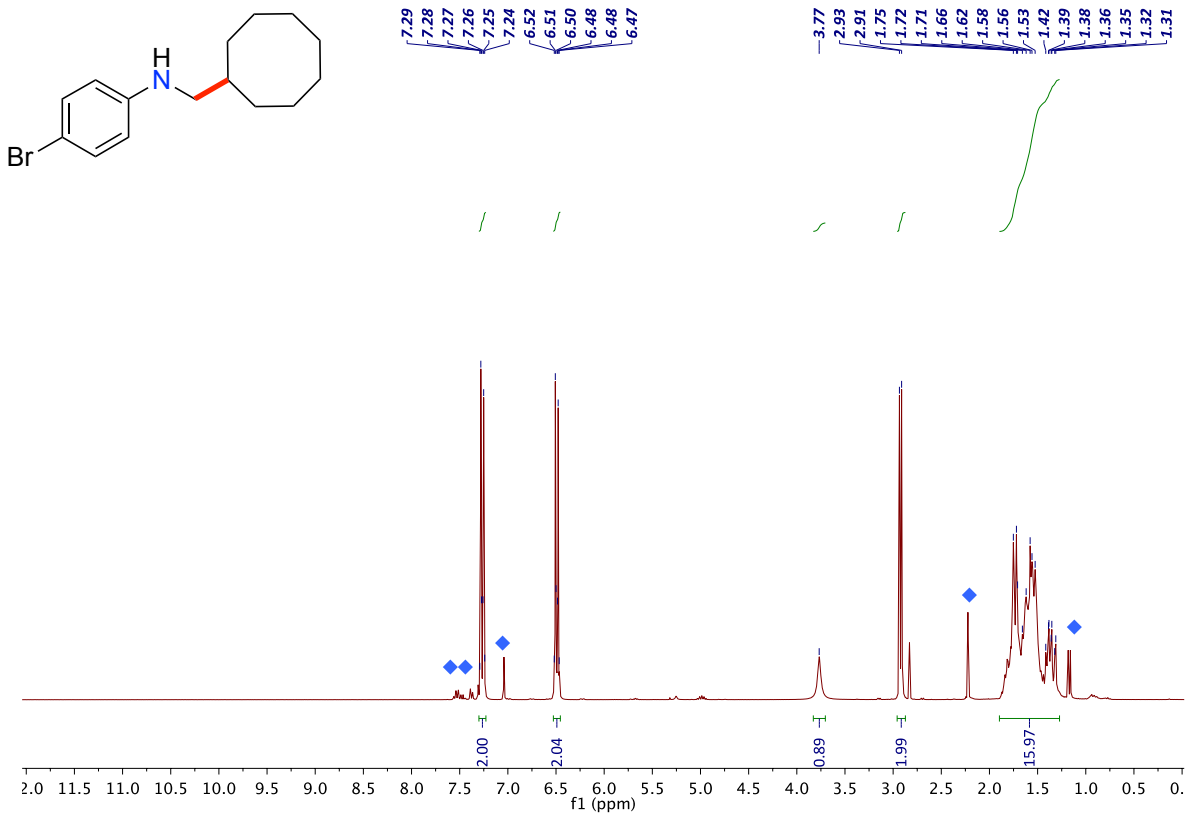

Figure. A.25. ^{1}H NMR spectrum (300 MHz, $CDCl_3$, 298 K) of 4-bromo-*N*-(cyclooctylmethyl)aniline.

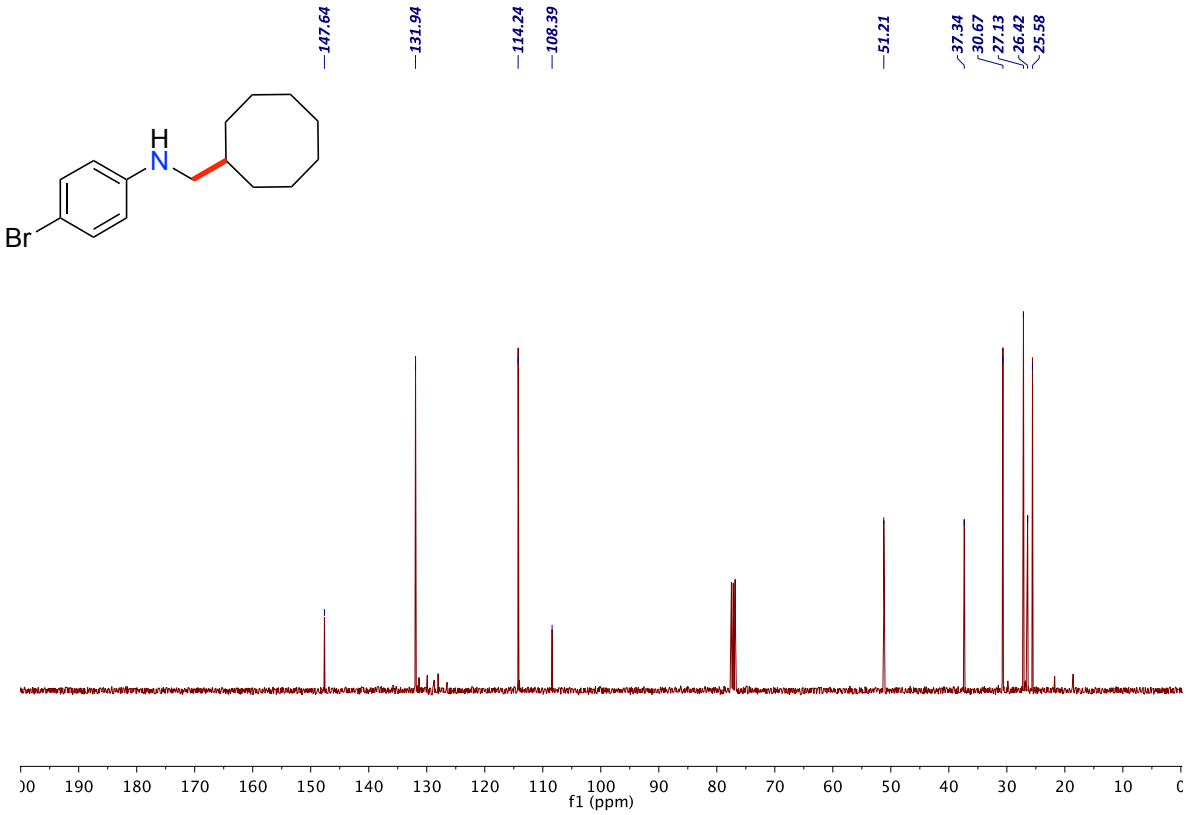

Figure. A.26. $^{13}C\{^{1}H\}$ NMR spectrum (100 MHz, $CDCl_3$, 298 K) of 4-bromo-*N*-(cyclooctylmethyl)aniline.

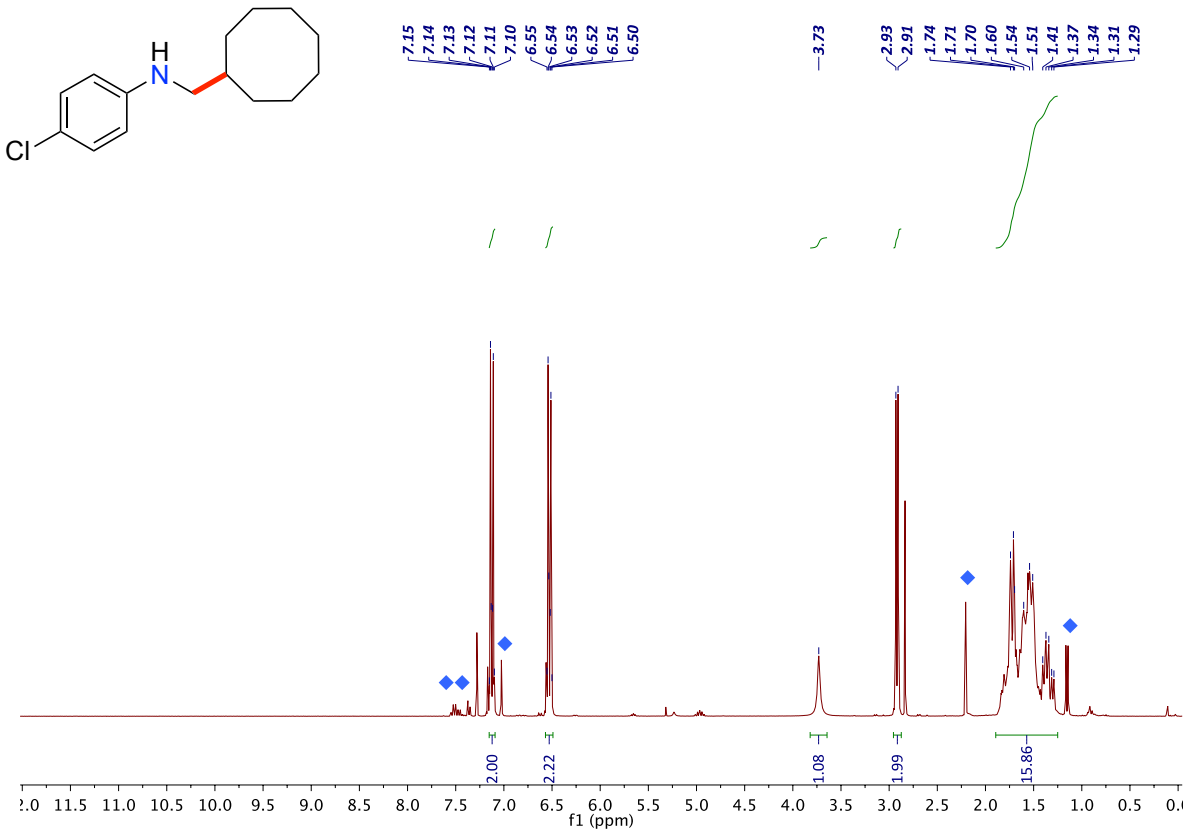

Figure. A.27. ^{1}H NMR spectrum (300 MHz, $CDCl_3$, 298 K) of 4-chloro-*N*-(cyclooctylmethyl)aniline.

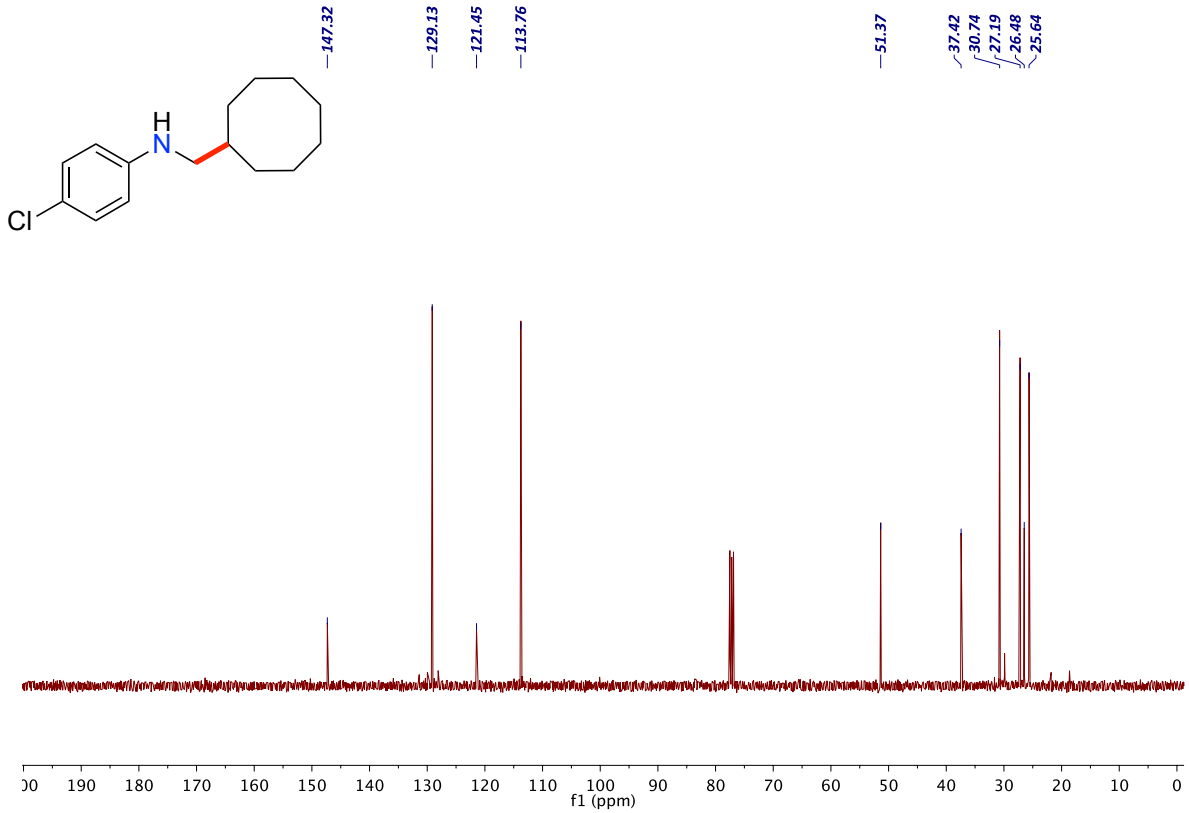

Figure. A.28. $^{13}C\{^{1}H\}$ NMR spectrum (75 MHz, $CDCl_3$, 298 K) of 4-chloro-*N*-(cyclooctylmethyl)aniline.

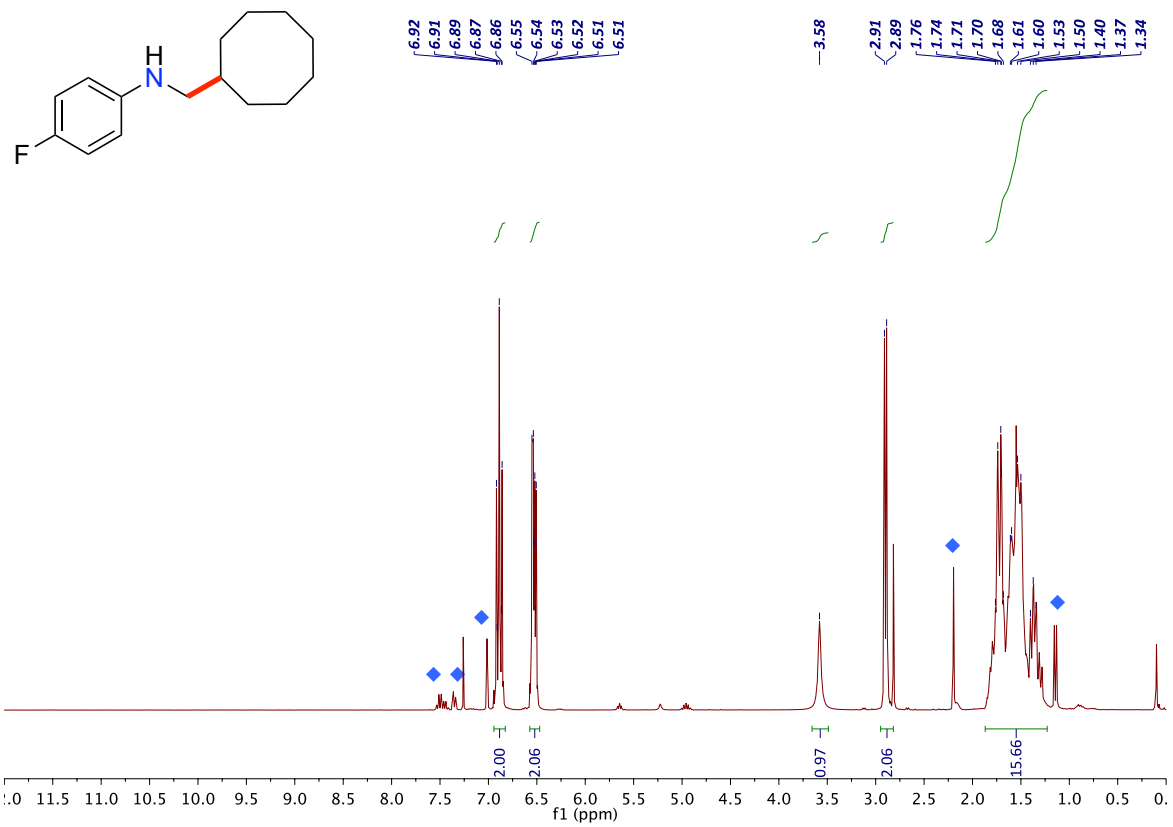

Figure. A.29. ^{1}H NMR spectrum (300 MHz, $CDCl_3$, 298 K) of *N*-(cyclooctylmethyl)-4-fluoroaniline.

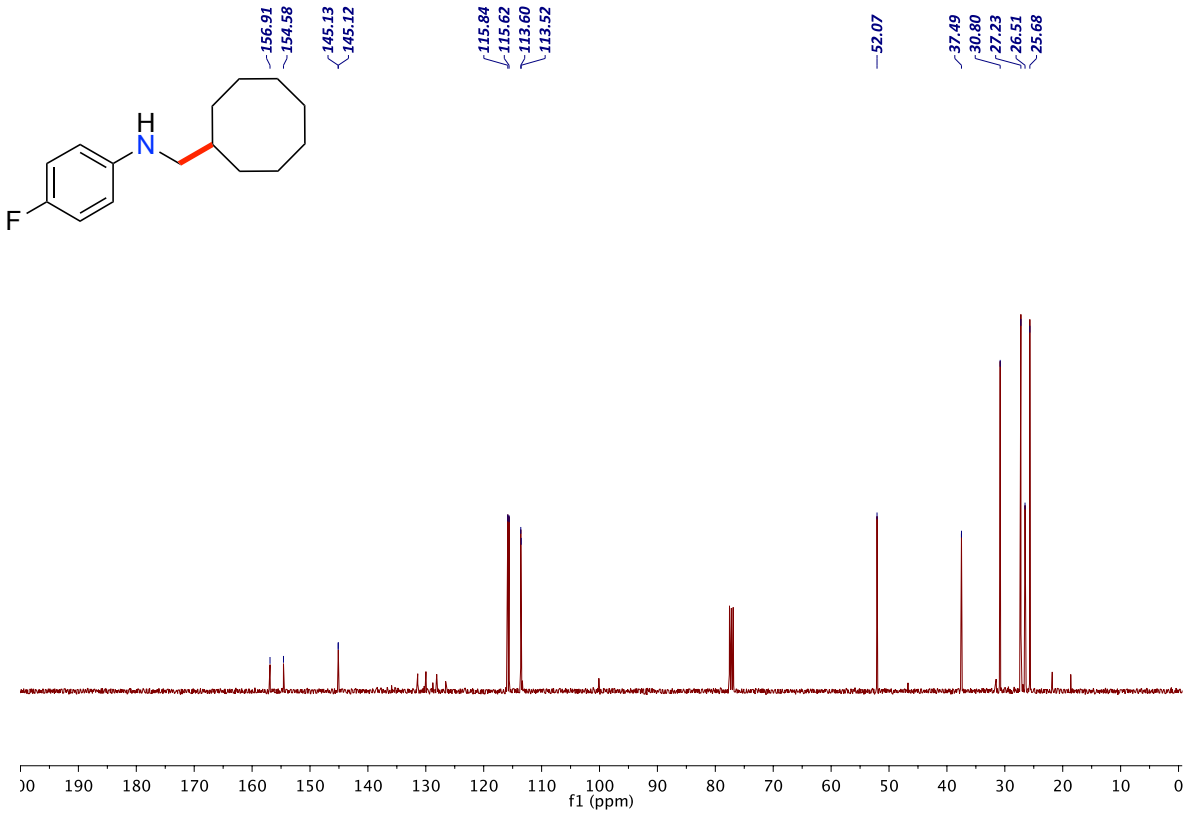

Figure. A.30. $^{13}C\{^{1}H\}$ NMR spectrum (75 MHz, CDCl3, 298 K) of *N*-(cyclooctylmethyl)-4-fluoroaniline.

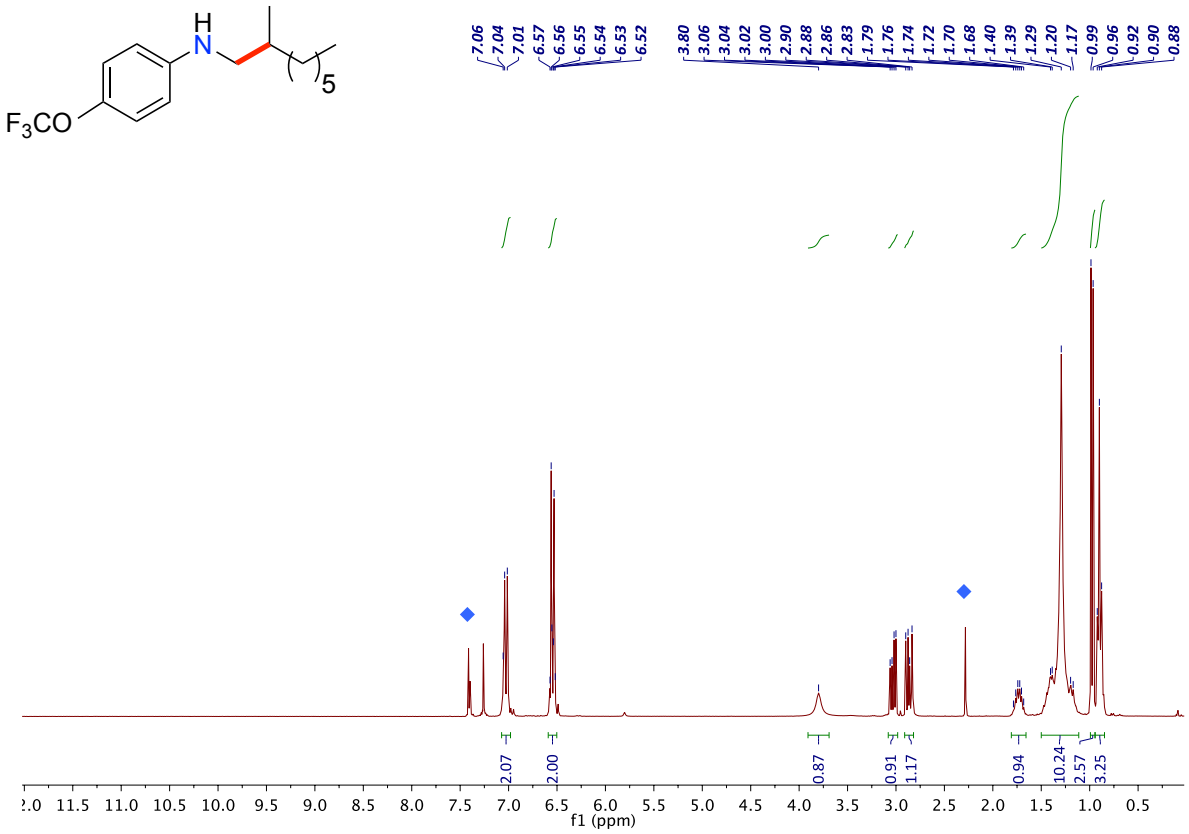

Figure. A.31. ^{1}H NMR spectrum (300 MHz, $CDCl_3$, 298 K) of *N*-(2-methyloctyl)-4-(trifluoromethoxy)aniline.

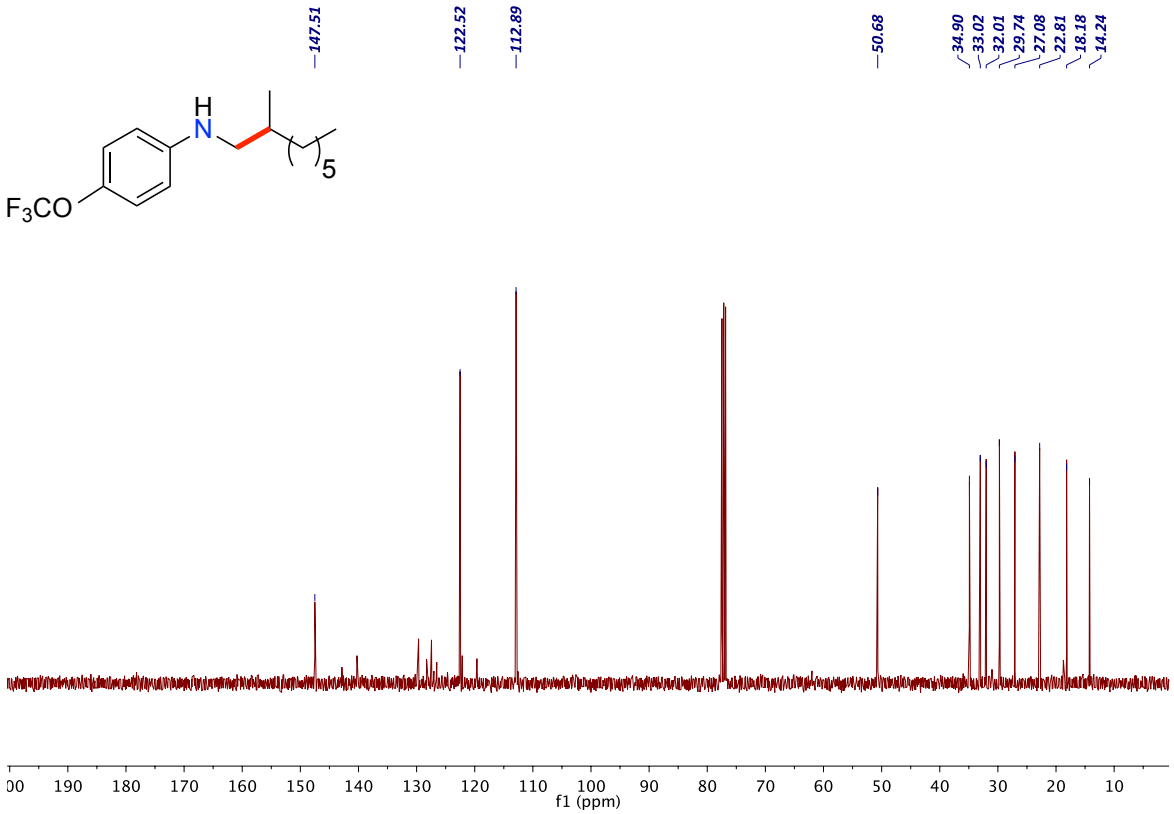

Figure. A.32. $^{13}C\{^{1}H\}$ NMR spectrum (75 MHz, $CDCl_3$, 298 K) of *N*-(2-methyloctyl)-4-(trifluoromethoxy)aniline.

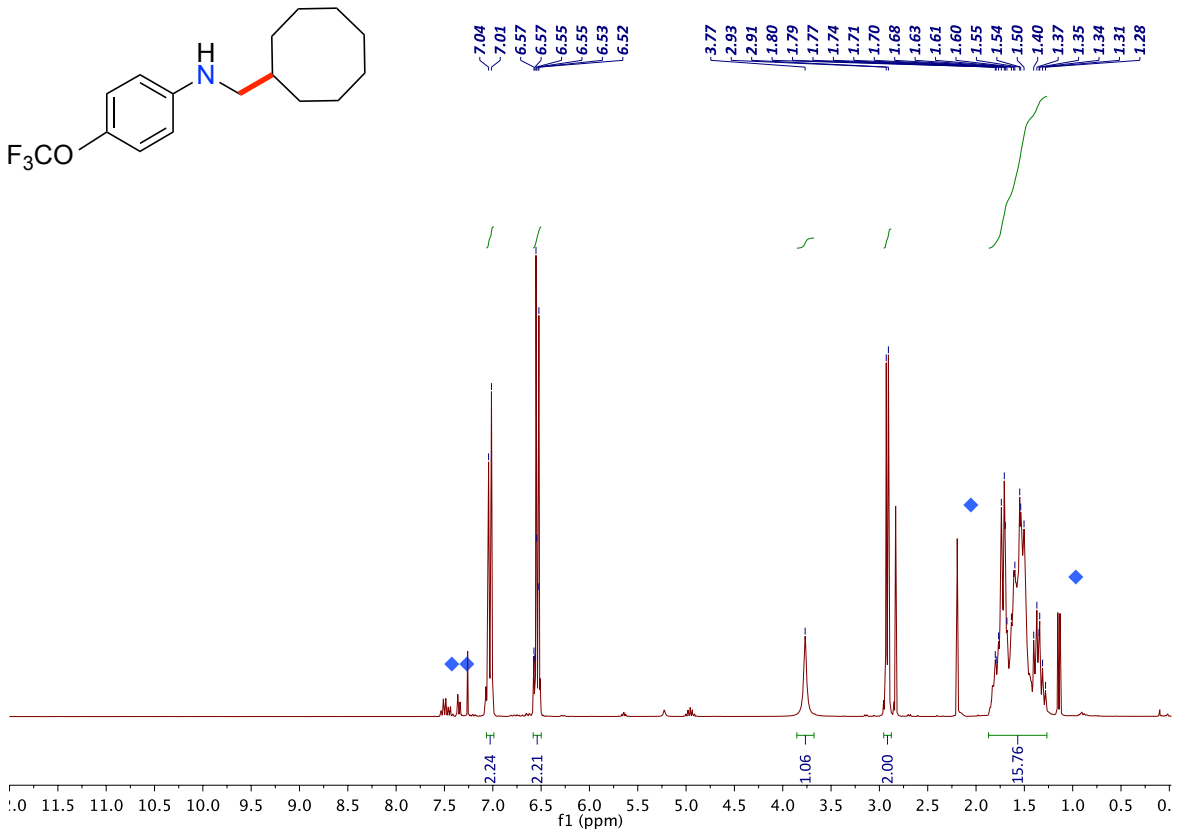

Figure. A.33. ^{1}H NMR spectrum (300 MHz, $CDCl_3$, 298 K) of *N*-(cyclooctylmethyl)-4-(trifluoromethoxy)aniline.

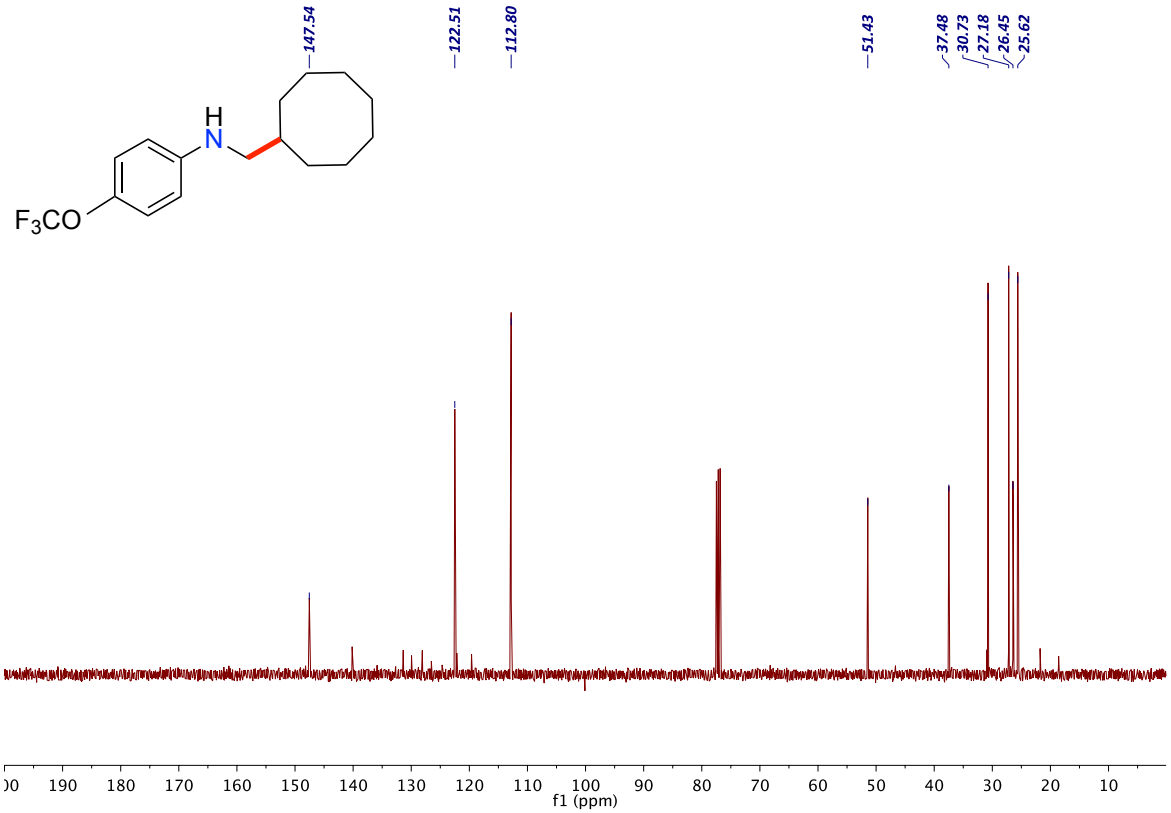

Figure. A.34. $^{13}C\{^{1}H\}$ NMR spectrum (75 MHz, $CDCl_3$, 298 K) of *N*-(cyclooctylmethyl)-4-(trifluoromethoxy)aniline.

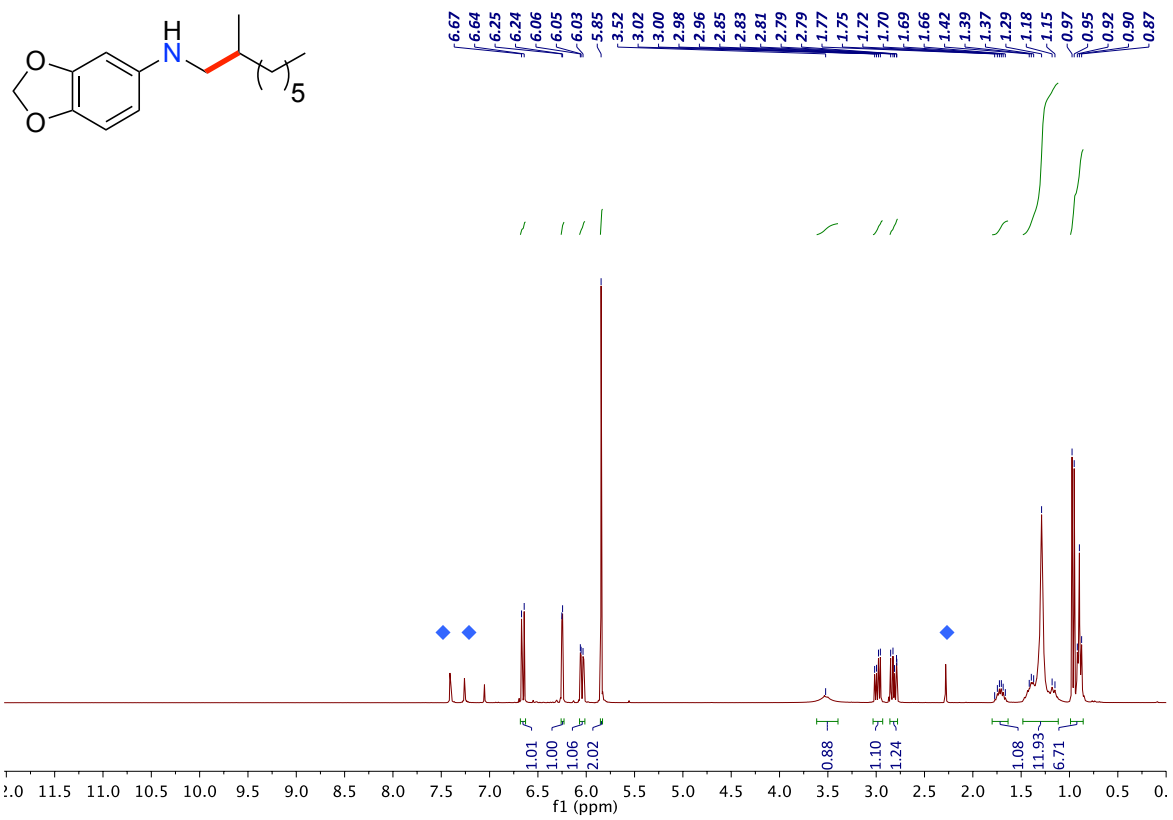

Figure. A.35. ^{1}H NMR spectrum (300 MHz, $CDCl_3$, 298 K) of *N*-(2-methyloctyl)benzo[d][1,3]dioxol-5-amine.

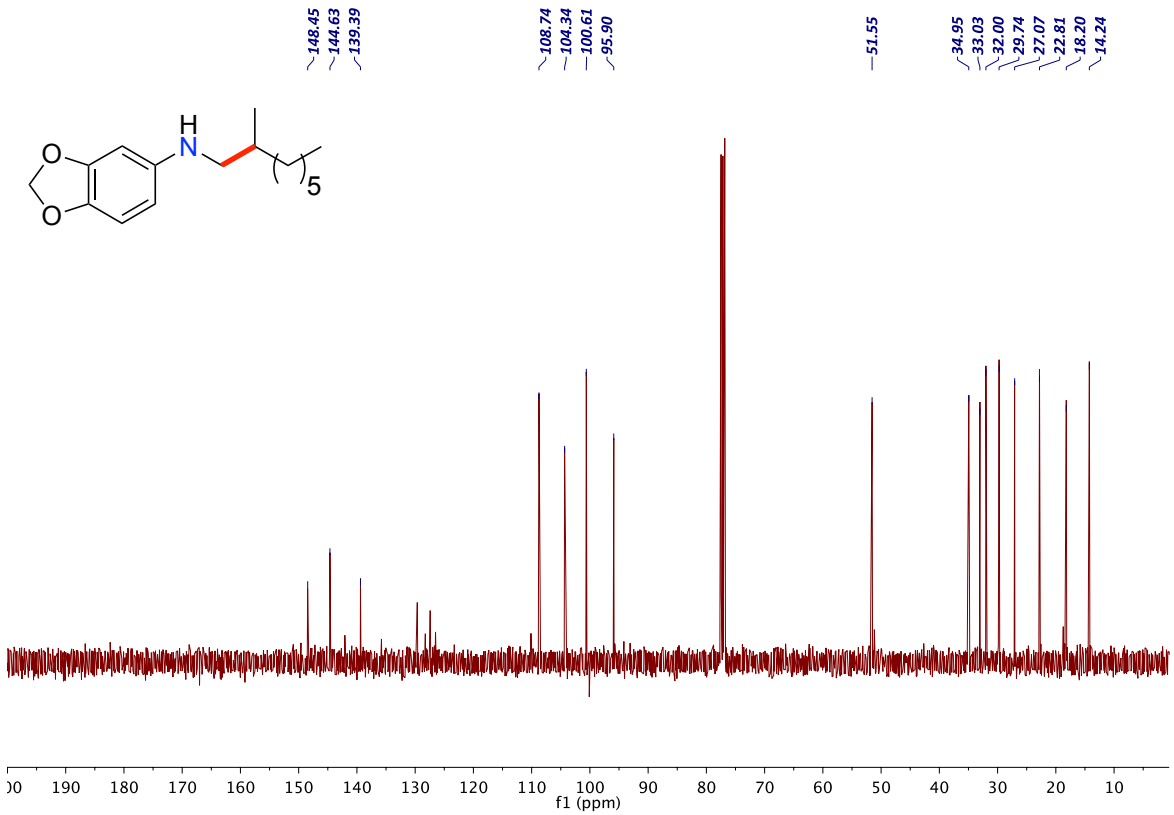

Figure. A.36. $^{13}C\{^{1}H\}$ NMR spectrum (75 MHz, $CDCl_3$, 298 K) of *N*-(2-methyloctyl)benzo[d][1,3]dioxol-5-amine.

A.4 Chapter 2 Alkene Scope Products

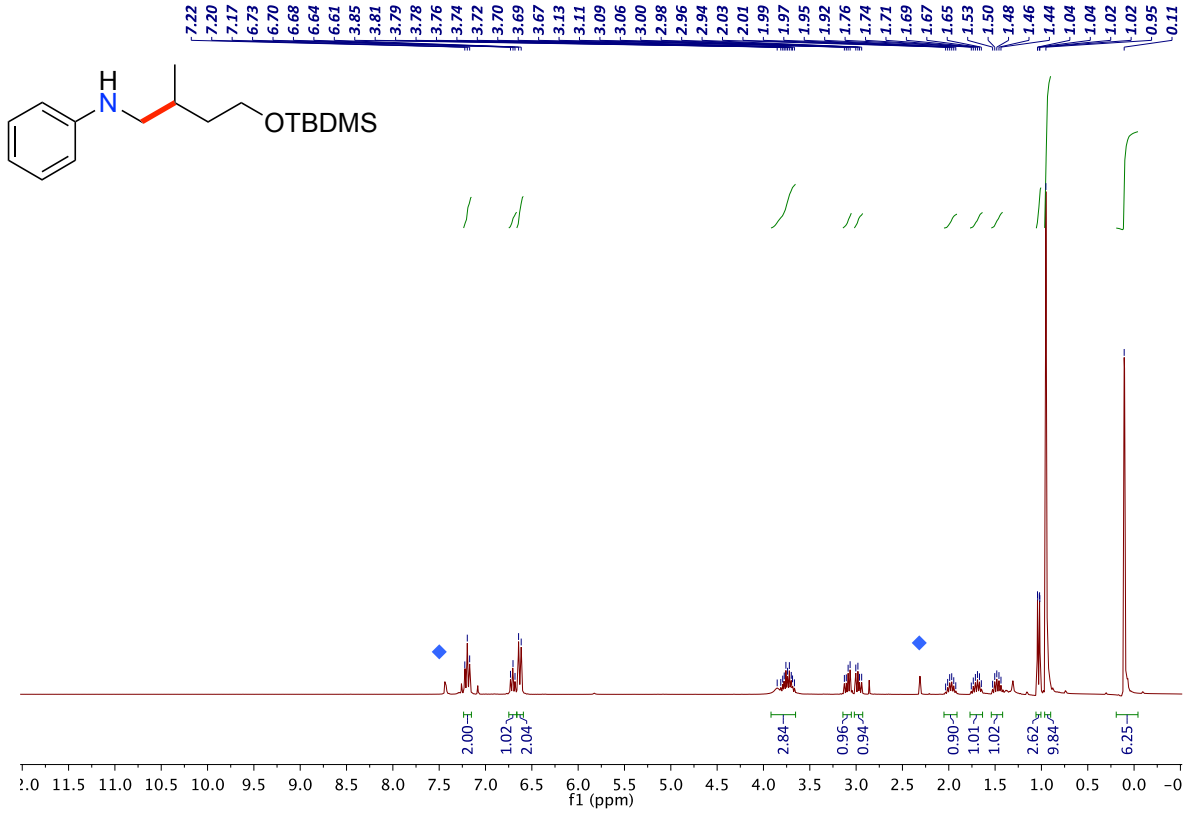

Figure. A.37. ^{1}H NMR spectrum (300 MHz, $CDCl_3$, 298 K) of 4-((tert-butyldimethylsilyl)oxy)-2-methylbutyl)aniline.

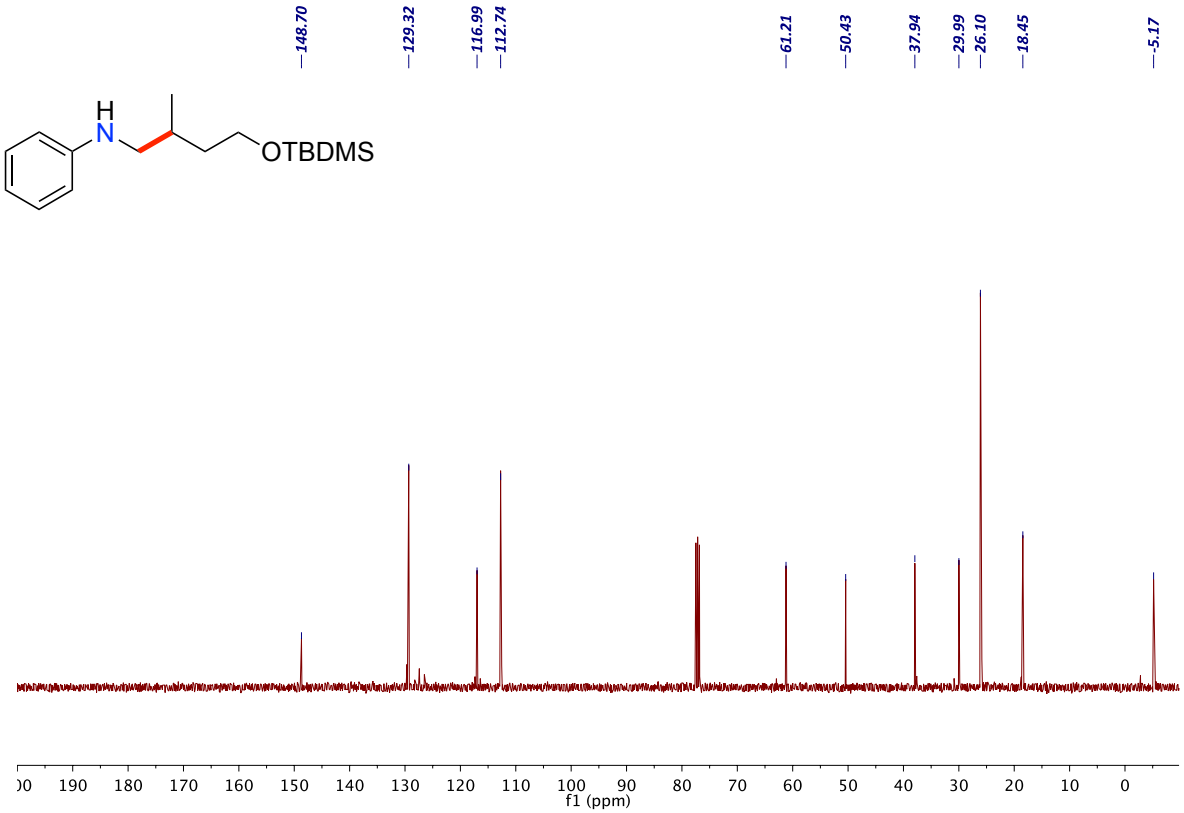

Figure. A.38. $^{13}C\{^{1}H\}$ NMR spectrum (100 MHz, $CDCl_3$, 298 K) of 4-((tert-butyldimethylsilyl)oxy)-2-methylbutyl)aniline.

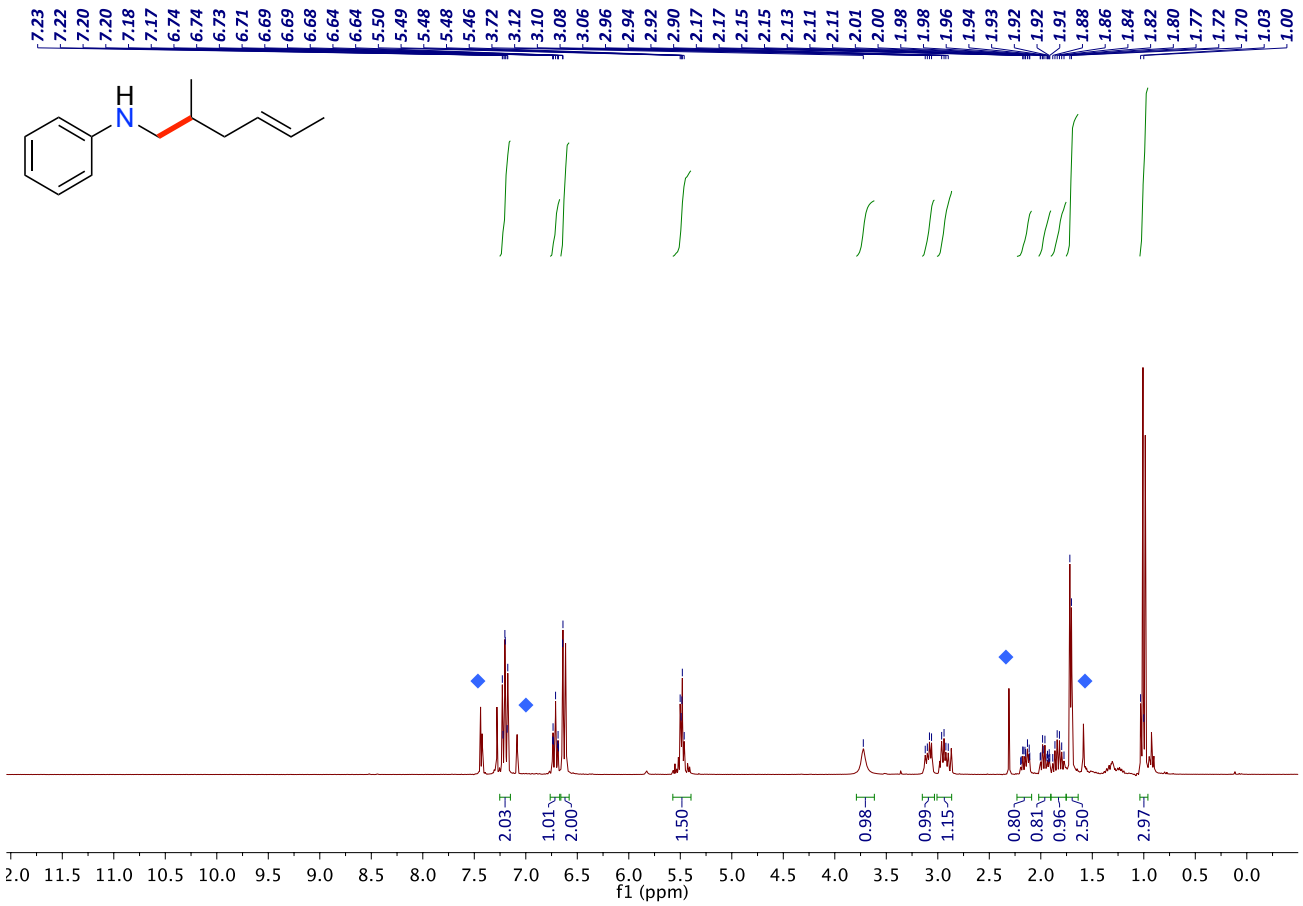

Figure. A.39. ^{1}H NMR spectrum (300 MHz, $CDCl_3$, 298 K) of (*E*)-*N*-(2-methylhex-4-en-1-yl)aniline .

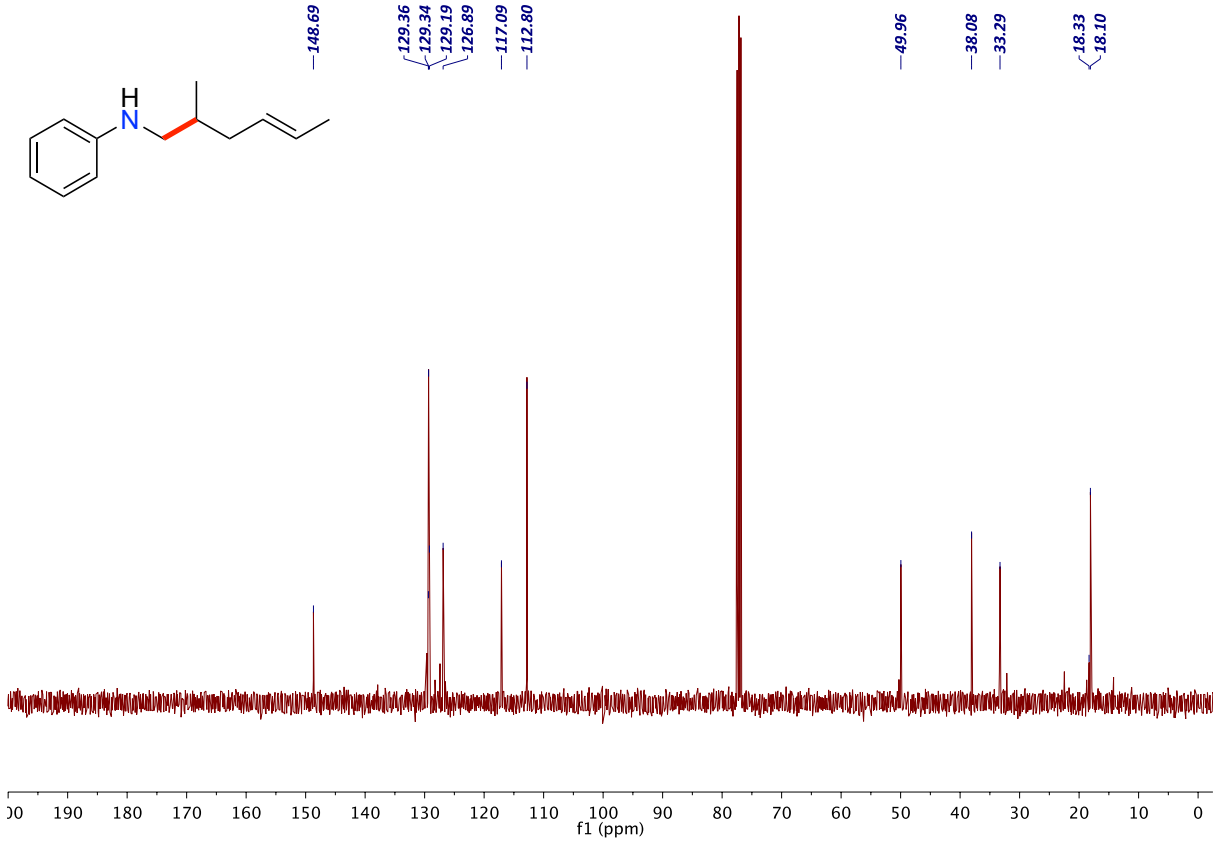

Figure. A.40. $^{13}C\{^{1}H\}$ NMR spectrum (300 MHz, $CDCl_3$, 298 K) of (*E*)-*N*-(2-methylhex-4-en-1-yl)aniline

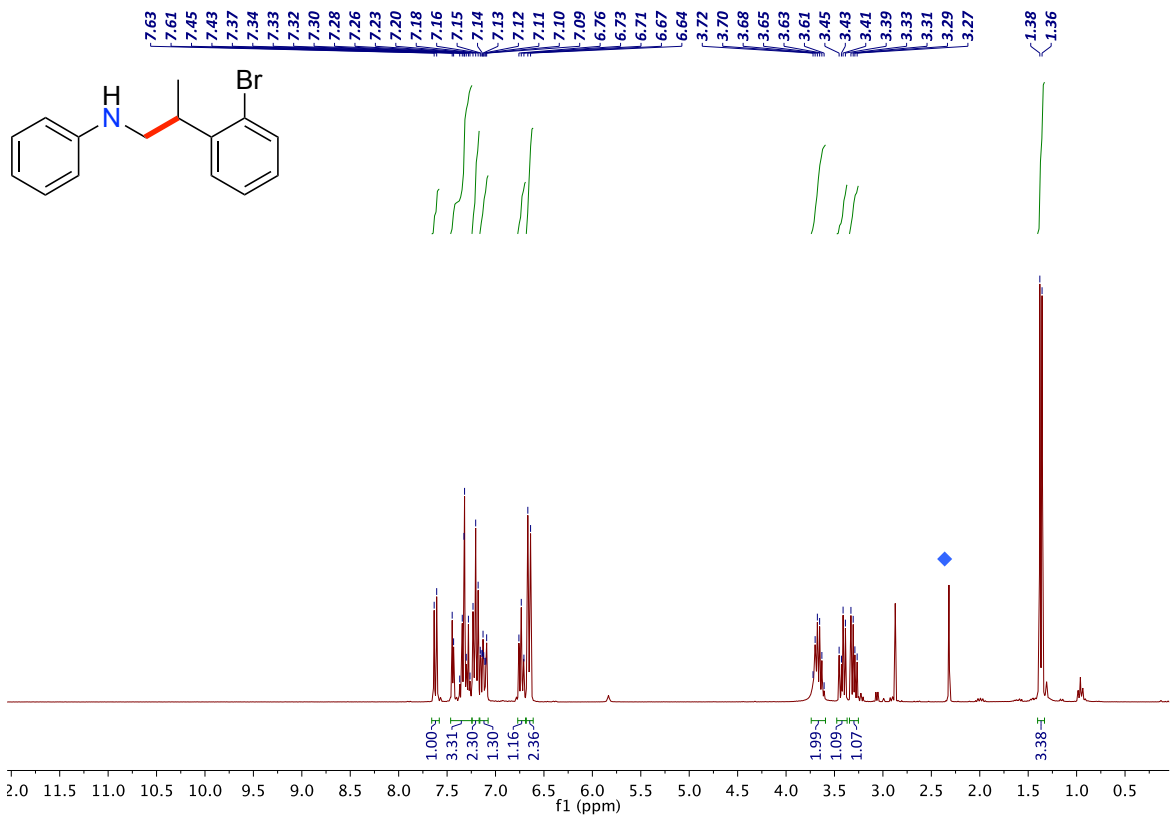

Figure. A.41. ^{1}H NMR spectrum (300 MHz, $CDCl_3$, 298 K) of *N*-(2-(2-bromophenyl)propyl)aniline.

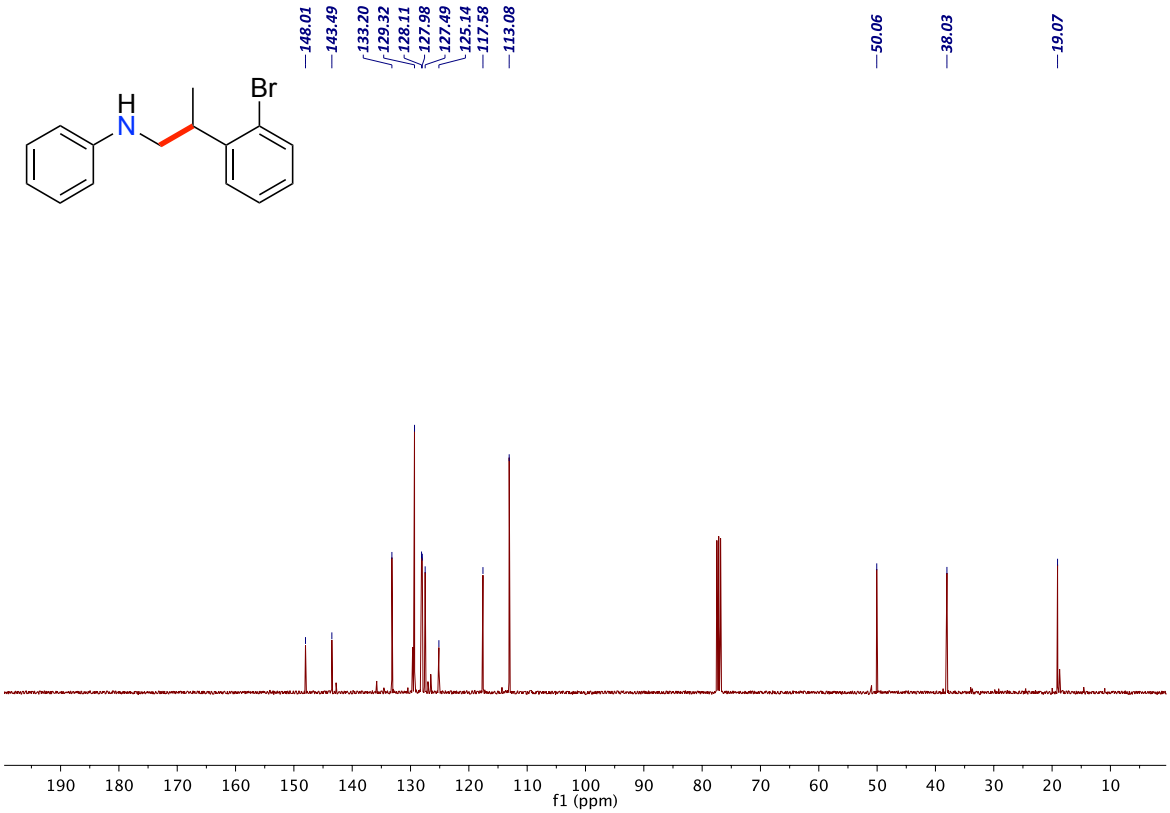

Figure. A.42. $^{13}C\{^{1}H\}$ NMR spectrum (100 MHz, $CDCl_3$, 298 K) of *N*-(2-(2-bromophenyl)propyl)aniline.

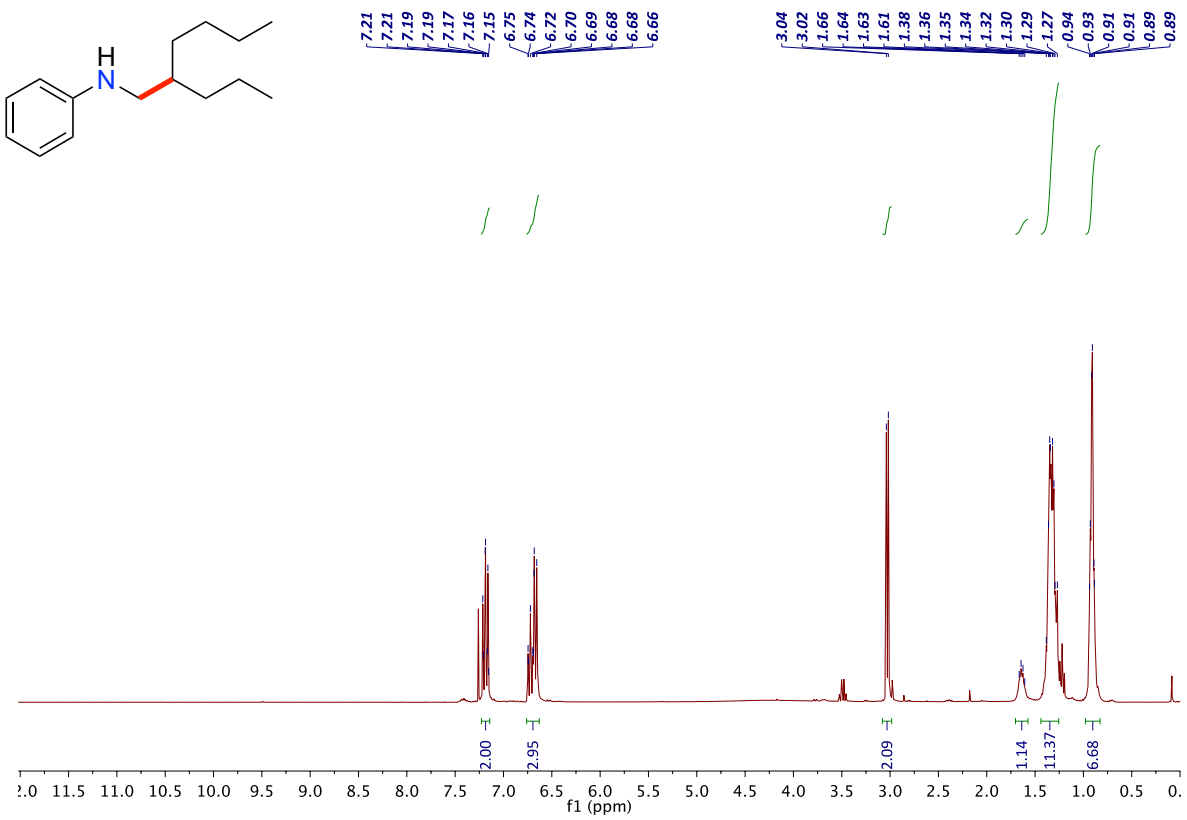

Figure. A.43. ^{1}H NMR spectrum (300 MHz, $CDCl_3$, 298 K) of N-(2-propylhexyl)aniline.

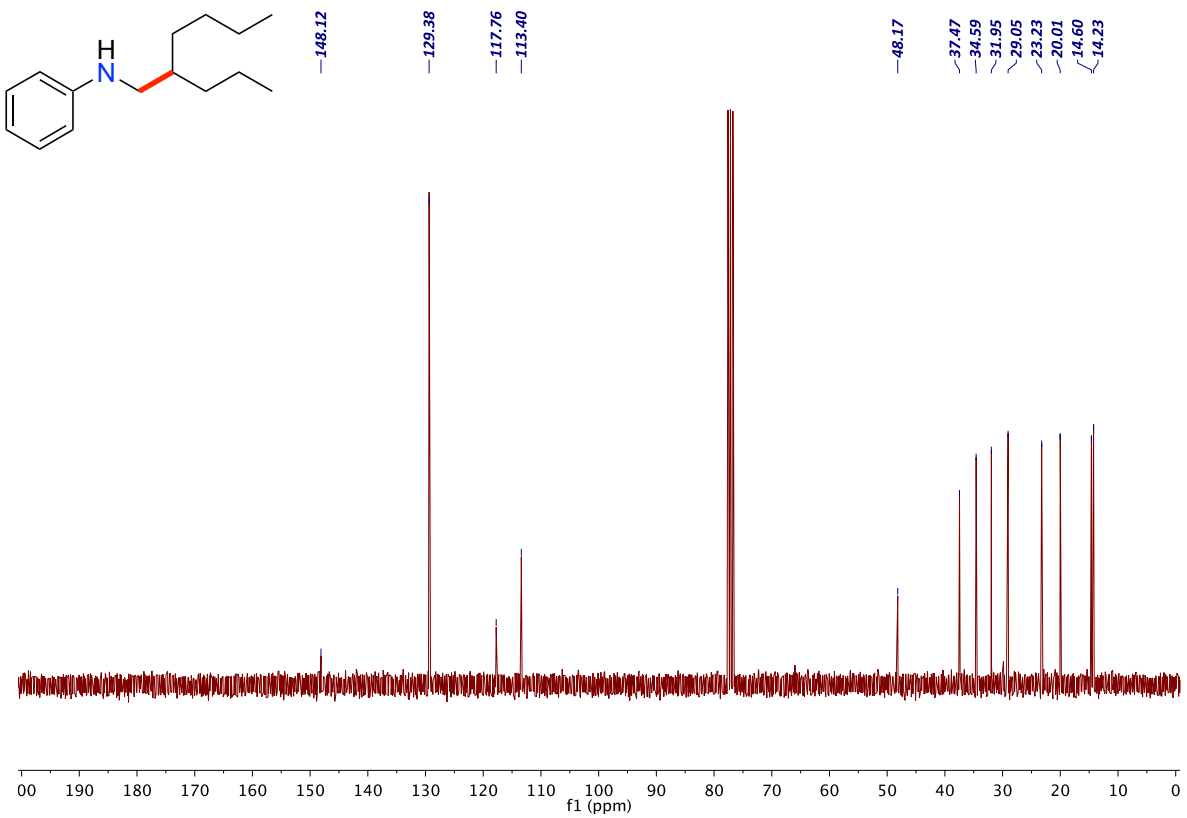

Figure. A.44. $^{13}C\{^{1}H\}$ NMR spectrum (100 MHz, $CDCl_3$, 298 K) of *N*-(2-propylhexyl)aniline.

A.5 Chapter 3 Ureate Ligand Spectra

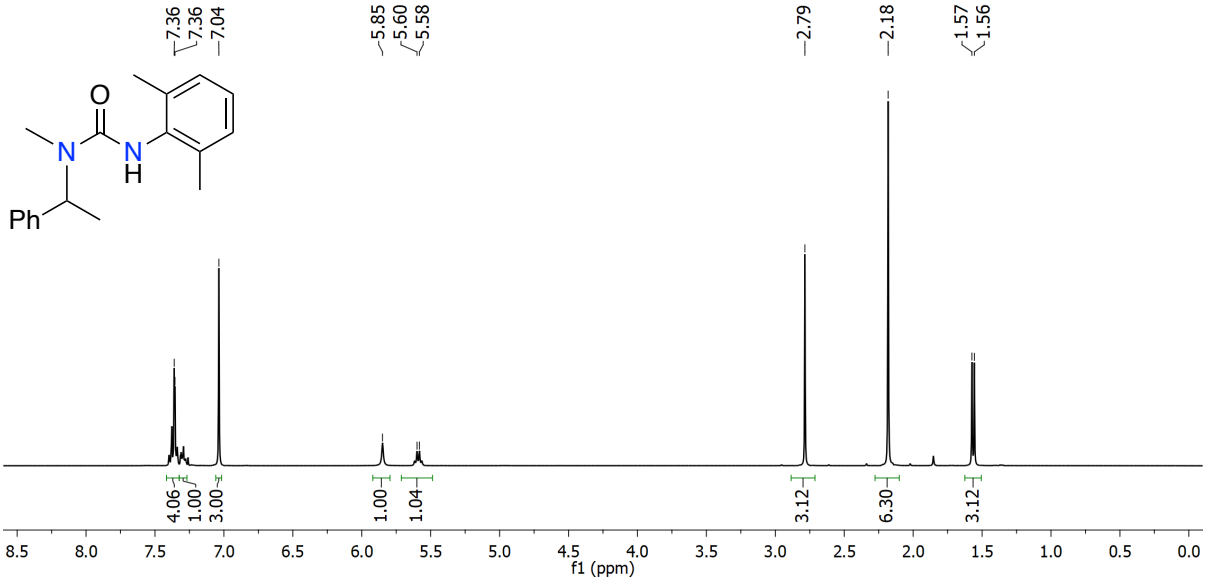

Figure. A.45. ^{1}H NMR spectrum (300 MHz, $CDCl_3$, 298 K) of 3-(2,6-dimethylphenyl)-1-methyl-1-(1-phenylethyl)urea.

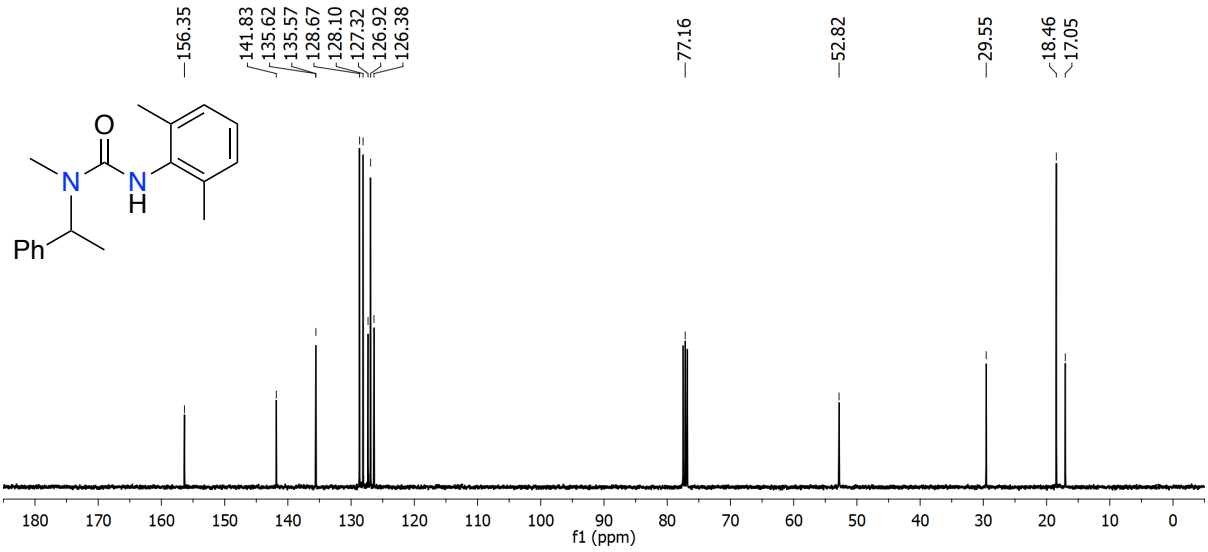

Figure. A.46. $^{13}C\{^{1}H\}$ NMR spectrum (75 MHz, $CDCl_3$, 298 K) of 3-(2,6-dimethylphenyl)-1-methyl-1-(1-phenylethyl)urea.

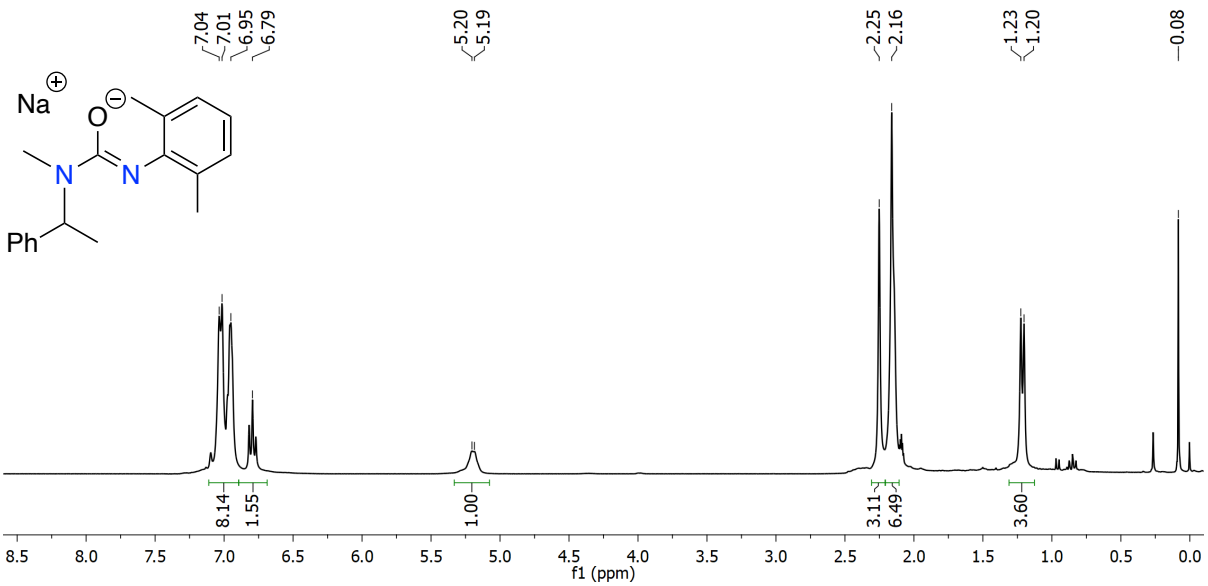

Figure. A.47. ^{1}H NMR spectrum (300 MHz, toluene-d_8, 298 K) of sodium (2,6-dimethylphenyl)(methyl(1-phenylethyl)carbamoyl)amide.

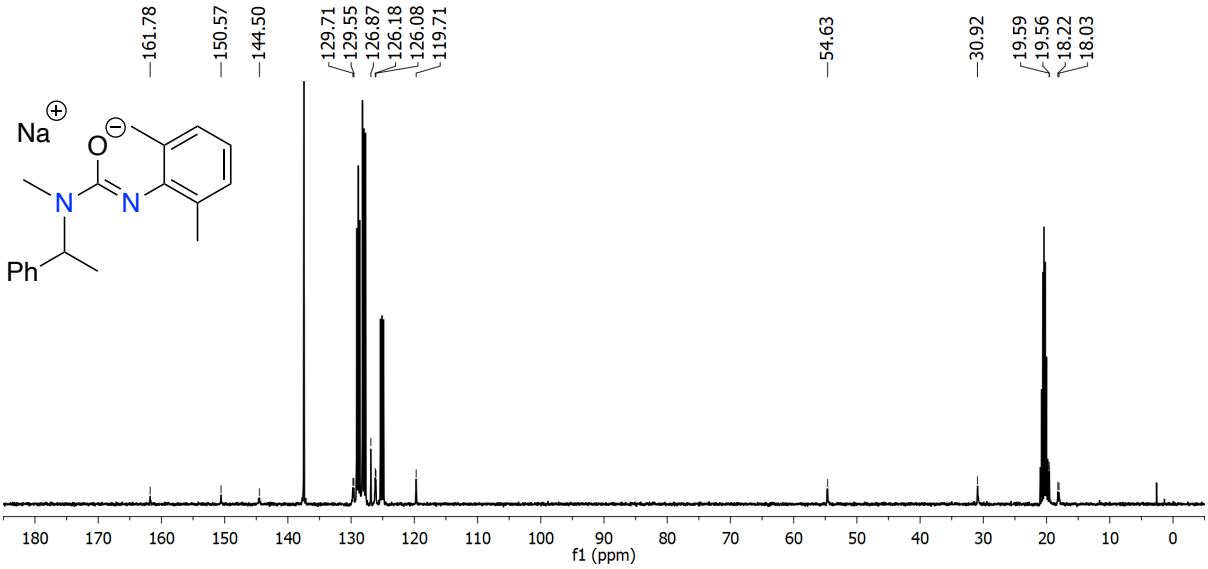

Figure. A.48. ^{13}C{^{1}H} NMR spectrum (100 MHz, toluene-d_8, 298 K) of sodium (2,6-dimethylphenyl)(methyl(1-phenylethyl)carbamoyl)amide.

A.6 Chapter 3 *In Situ* Generated Precatalyst Spectra

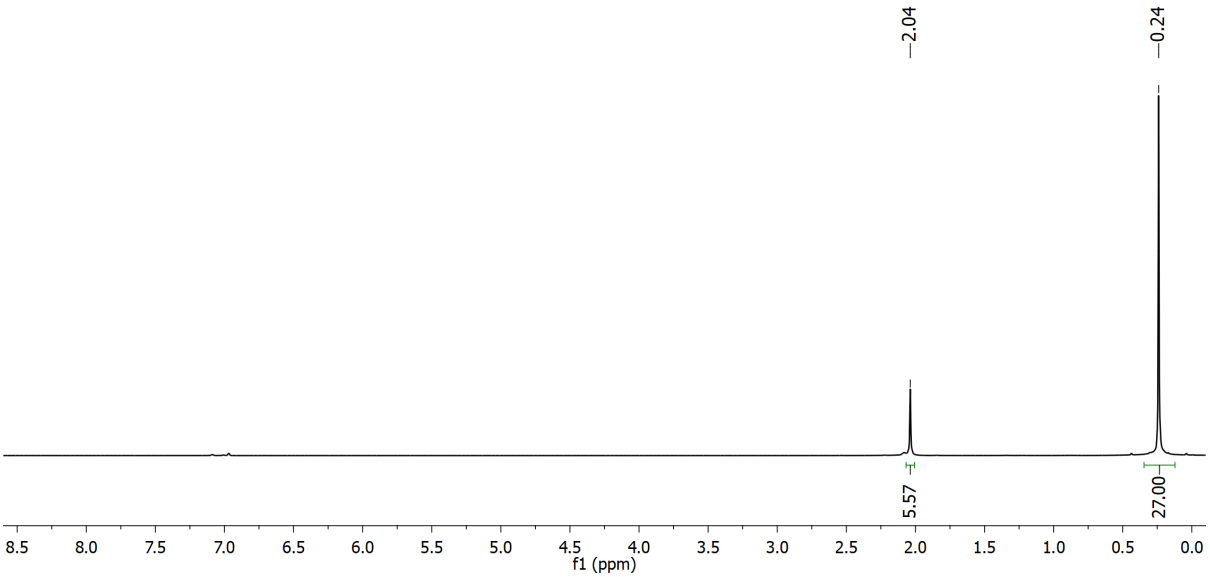

Figure. A.49. ^{1}H NMR spectrum (300 MHz, toluene-d_8, 298 K) of $Ta(CH_2SiMe_3)_3Cl_2$.

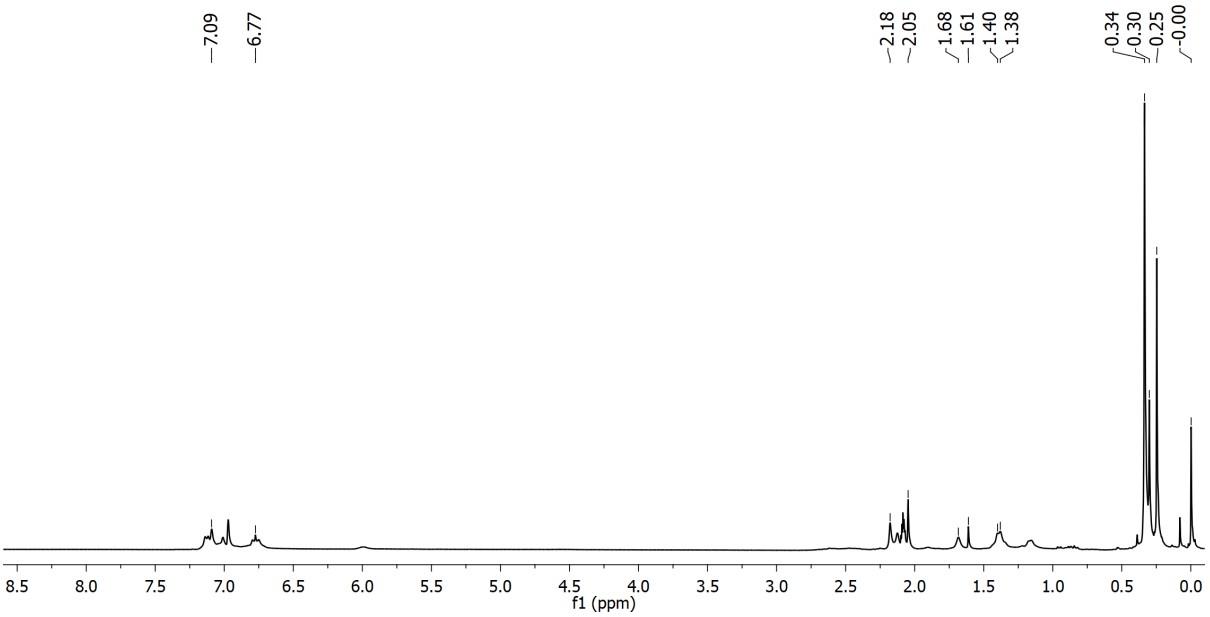

Figure. A.50. ^{1}H NMR spectrum (300 MHz, toluene-d_8, 298 K) of a mixture between $Ta(CH_2SiMe_3)_3Cl_2$ and L3Na recorded one hour after mixing the two reagents.

A.7 Chapter 3 Limonene Scope Spectra

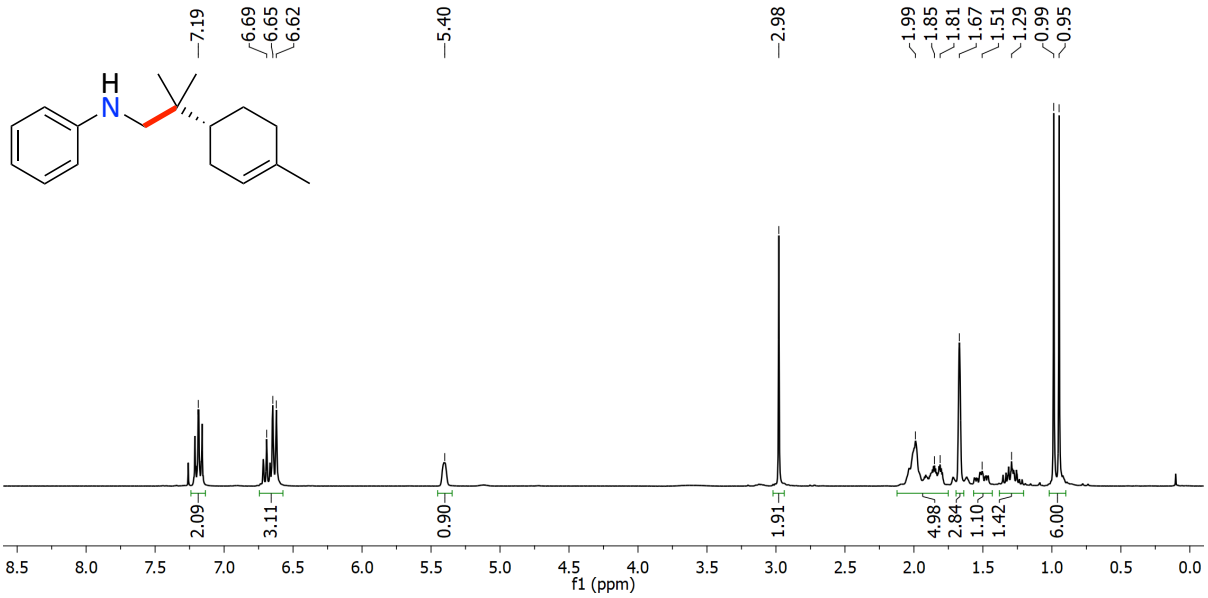

Figure. A.51. ^{1}H NMR spectrum (400 MHz, $CDCl_3$, 298 K) of *N*-(2-methyl-2-(4-methylcyclohex-3-en-1-yl)propyl)aniline.

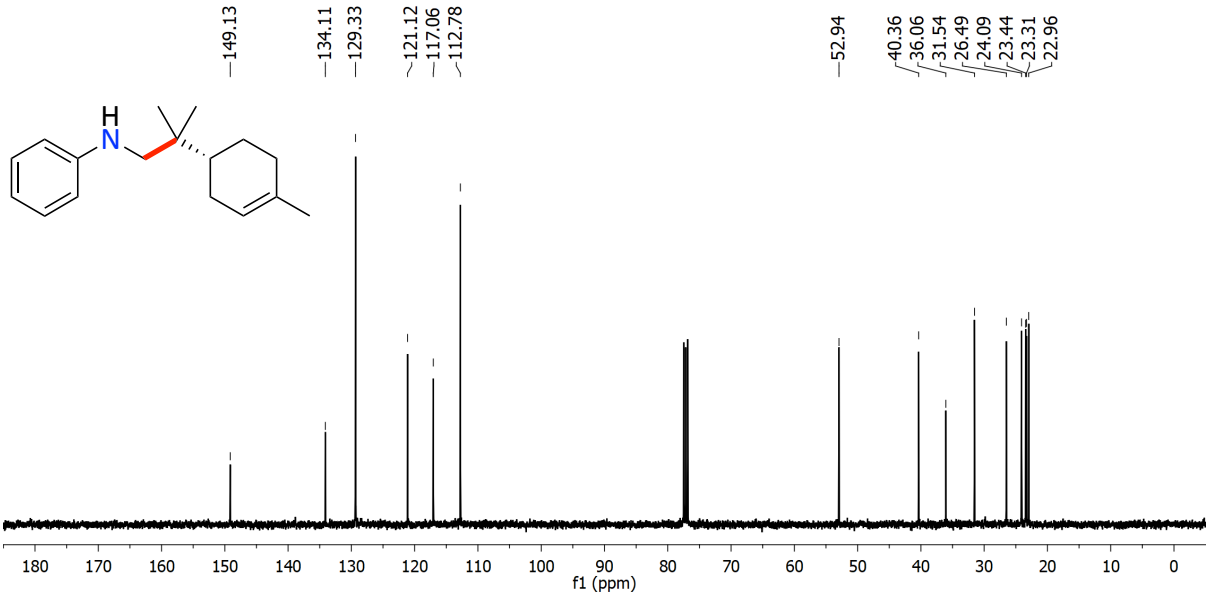

Figure. A.52. ^{13}C{^{1}H} NMR spectrum (100 MHz, $CDCl_3$, 298 K) of *N*-(2-methyl-2-(4-methylcyclohex-3-en-1-yl)propyl)aniline.

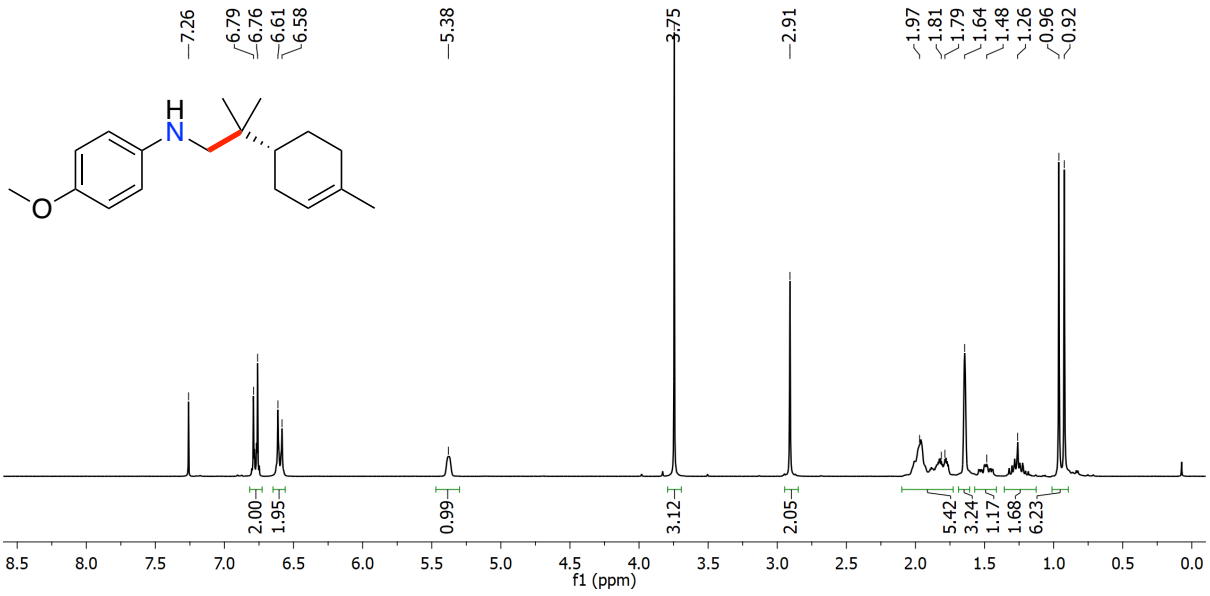

Figure. A.53. ^{1}H NMR spectrum (400 MHz, $CDCl_3$, 298 K) of 4-methoxy-*N*-(2-ethyl-2-(4-methylcyclohex-3-en-1-yl)propyl)aniline.

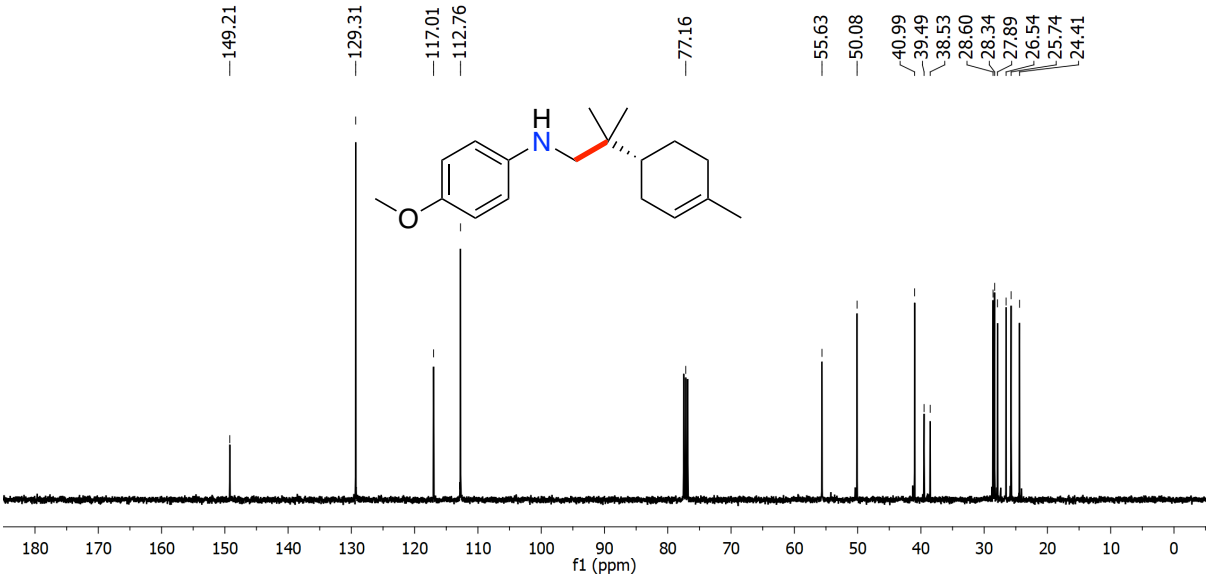

Figure. A.54. ^{13}C{^{1}H} NMR spectrum (100 MHz, methanol-d_4, 298 K) of 4-methoxy-*N*-(2-methyl-2-(4-methylcyclohex-3-en-1-yl)propyl)aniline.

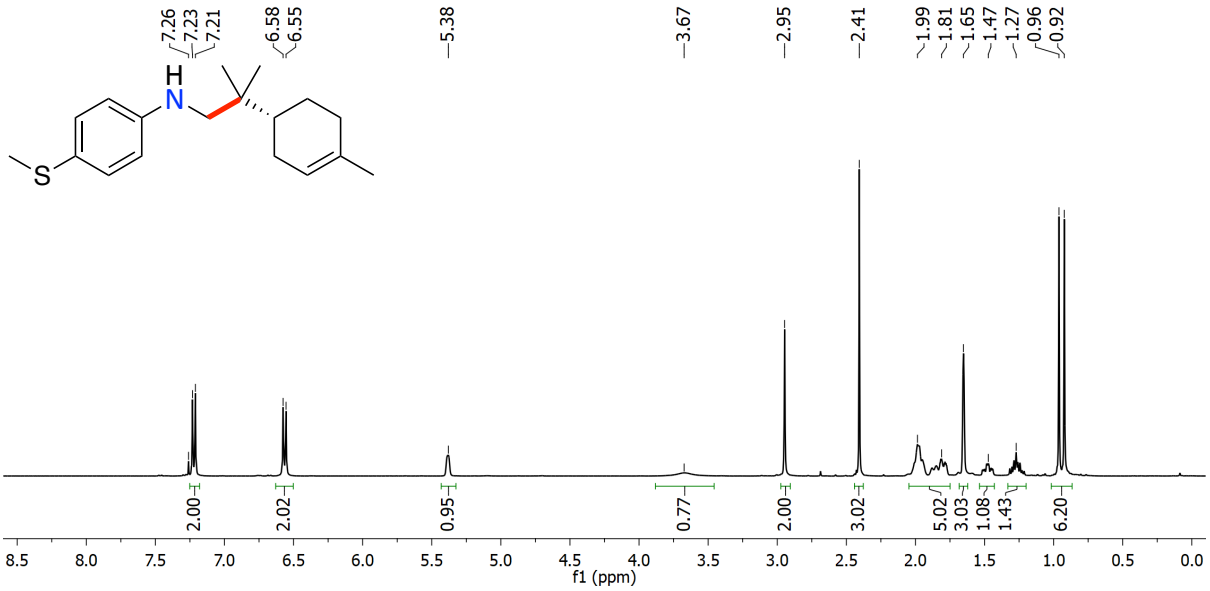

Figure. A.55. ^{1}H NMR spectrum (400 MHz, $CDCl_3$, 298 K) of *N*-(2-methyl-2-(4-methylcyclohex-3-en-1-yl)propyl)-4-(methylthio)aniline.

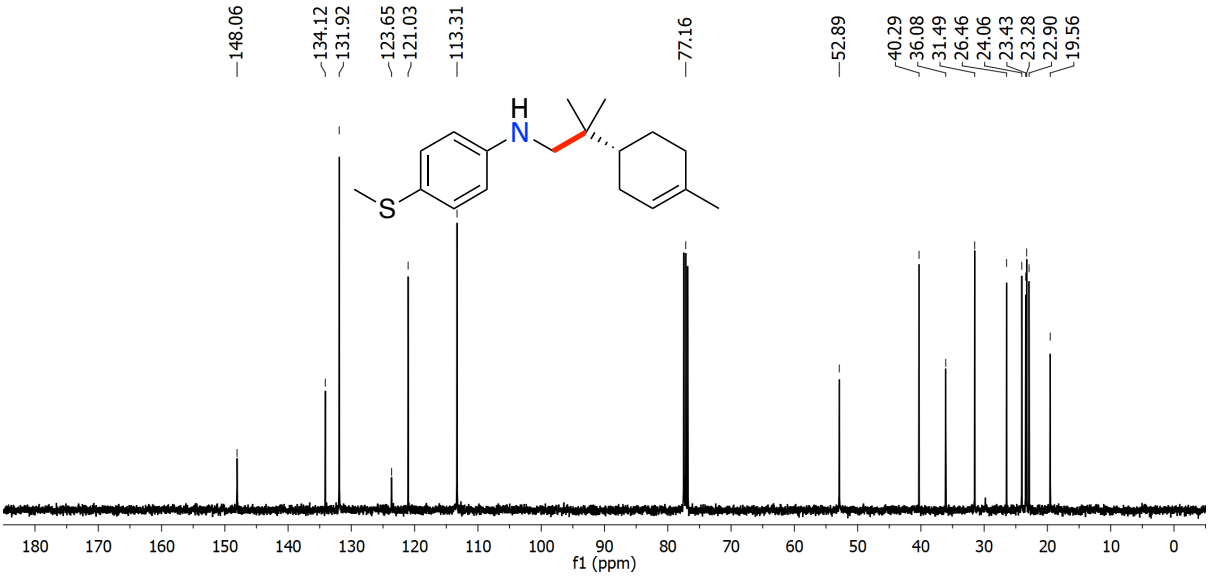

Figure. A.56. ^{13}C{^{1}H} NMR spectrum (100 MHz, $CDCl_3$, 298 K) of *N*-(2-methyl-2-(4-methylcyclohex-3-en-1-yl)propyl)-4-(methylthio)aniline.

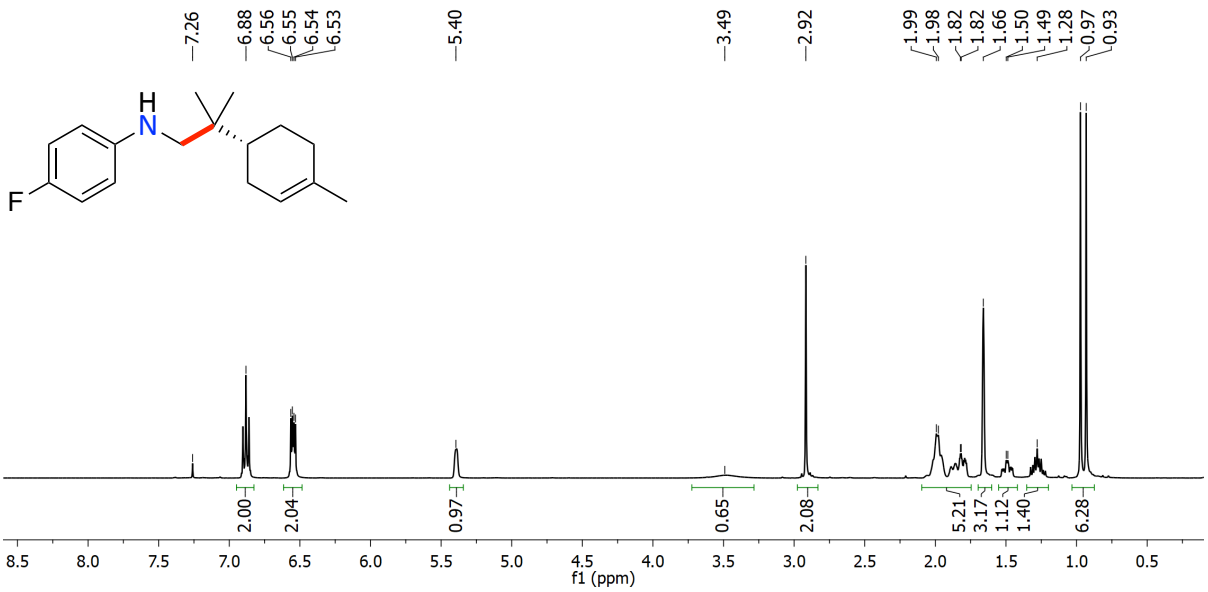

Figure. A.57. ^{1}H NMR spectrum (400 MHz, $CDCl_3$, 298 K) of 4-fluoro-*N*-(2-ethyl-2-(4-methylcyclohex-3-en-1-yl)propyl)aniline.

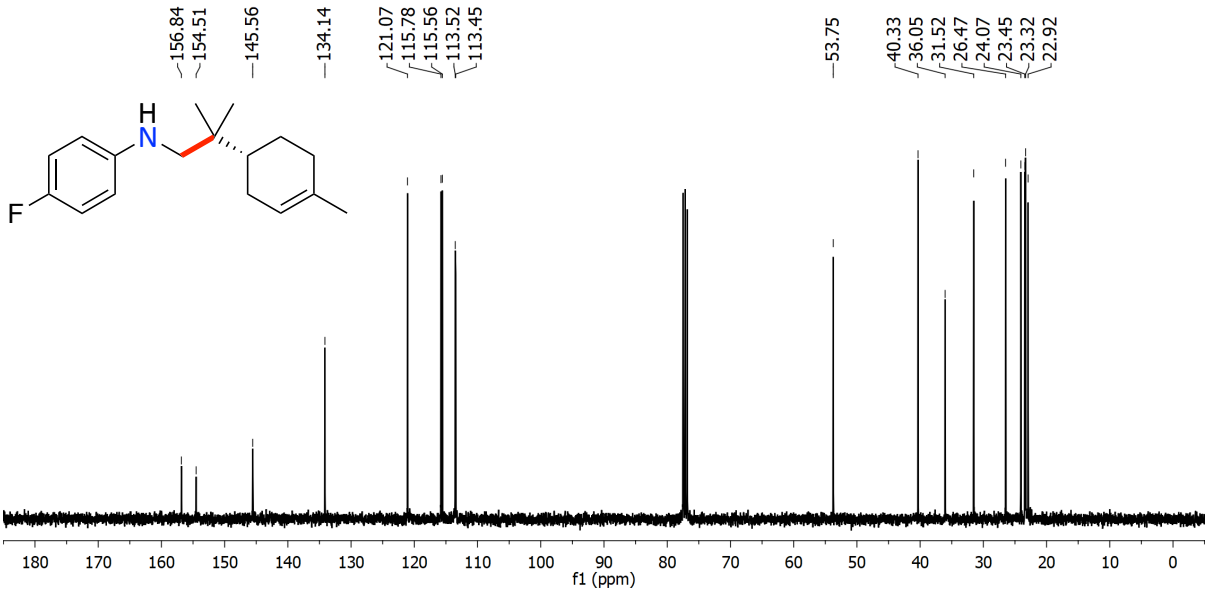

Figure. A.58. ^{13}C{^{1}H} NMR spectrum (100 MHz, $CDCl_3$, 298 K) of 4-fluoro-*N*-(2-methyl-2-(4-methylcyclohex-3-en-1-yl)propyl)aniline.

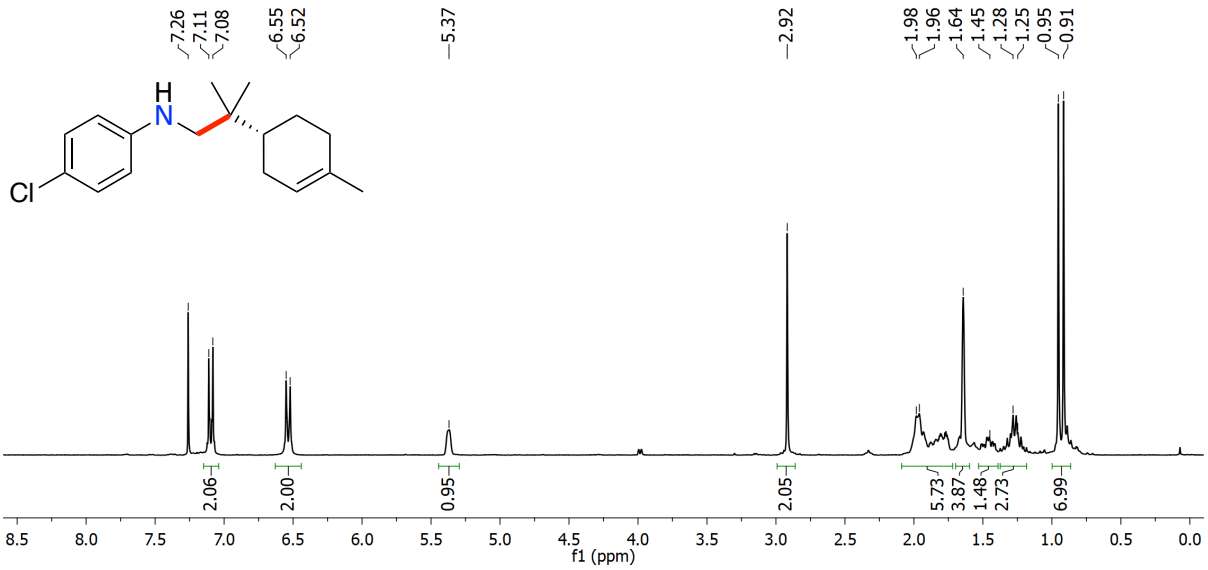

Figure. A.59. ^{1}H NMR spectrum (300 MHz, $CDCl_3$, 298 K) of 4-chloro-*N*-(2-methyl-2-(4-methylcyclohex-3-en-1-yl)propyl)aniline.

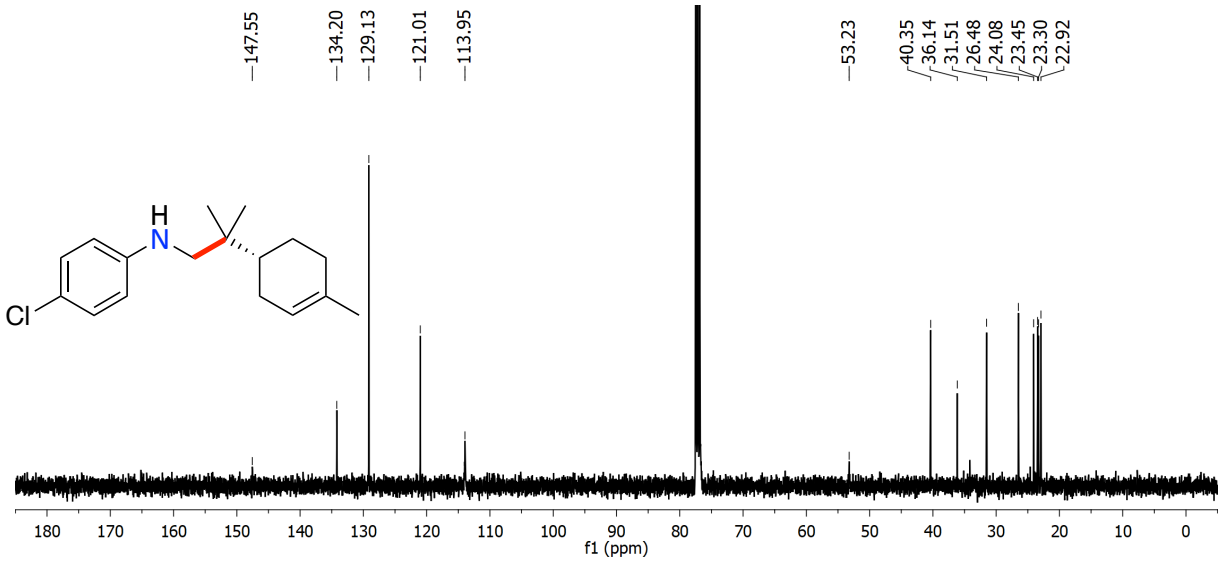

Figure. A.60. ^{13}C{^{1}H} NMR spectrum (100 MHz, $CDCl_3$, 298 K) of 4-chloro-*N*-(2-methyl-2-(4-methylcyclohex-3-en-1-yl)propyl)aniline.

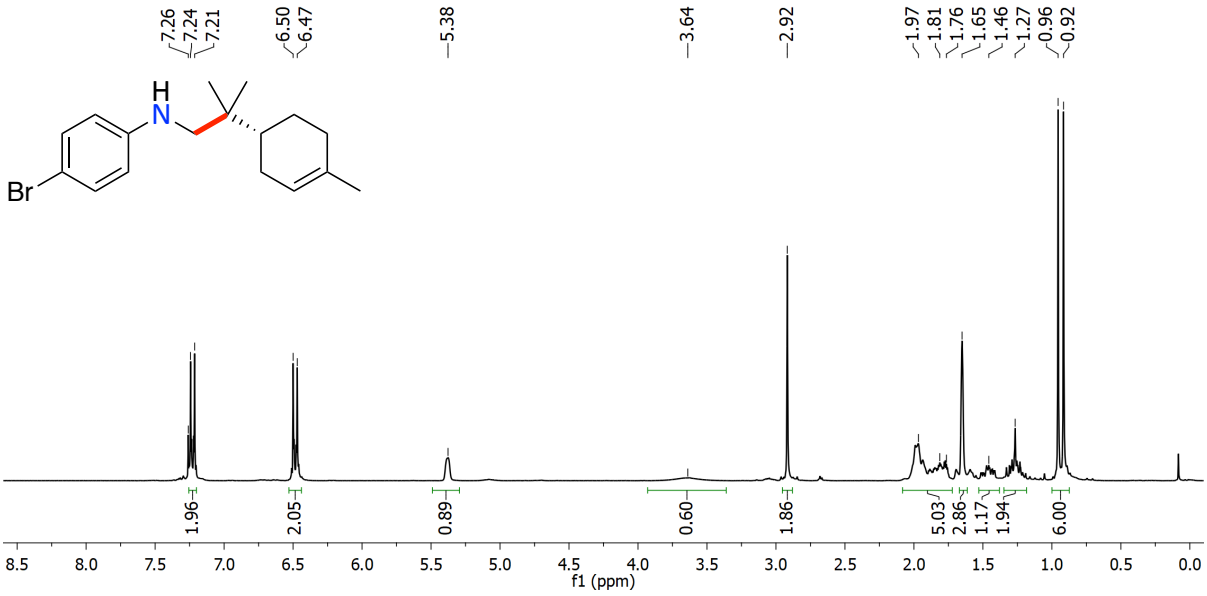

Figure. A.61. ^{1}H NMR spectrum (400 MHz, $CDCl_3$, 298 K) of 4-bromo-*N*-(2-methyl-2-(4-methylcyclohex-3-en-1-yl)propyl)aniline.

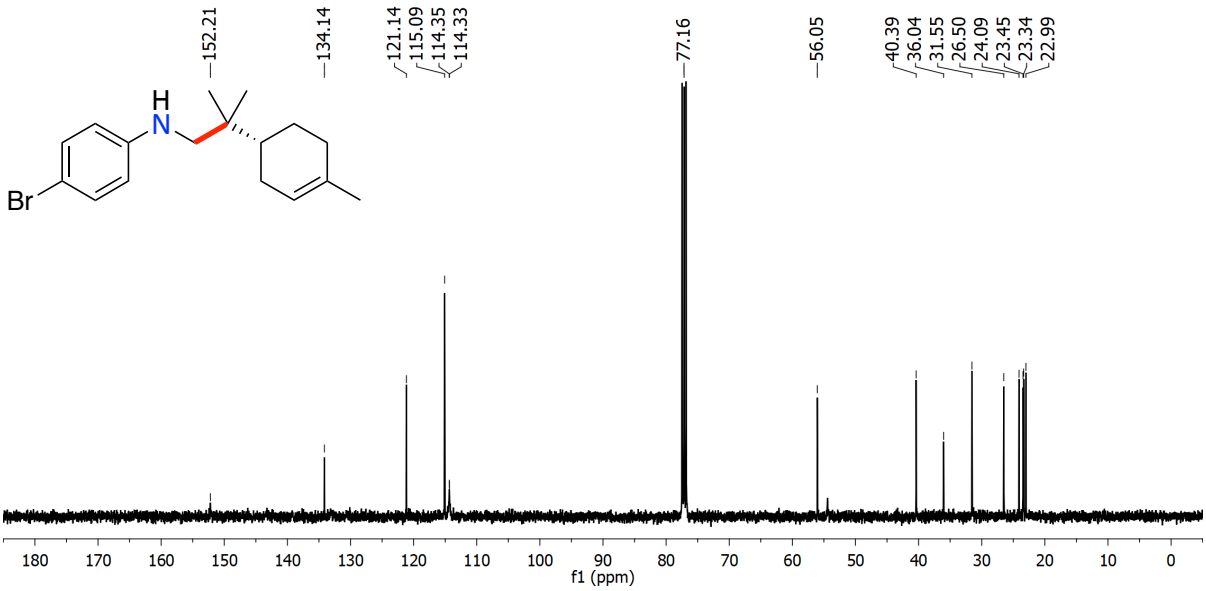

Figure. A.62. ^{13}C{^{1}H} NMR spectrum (100 MHz, $CDCl_3$, 298 K) of 4-bromo-*N*-(2-methyl-2-(4-methylcyclohex-3-en-1-yl)propyl)aniline.

A.8 Chapter 3 Pinene Scope Spectra

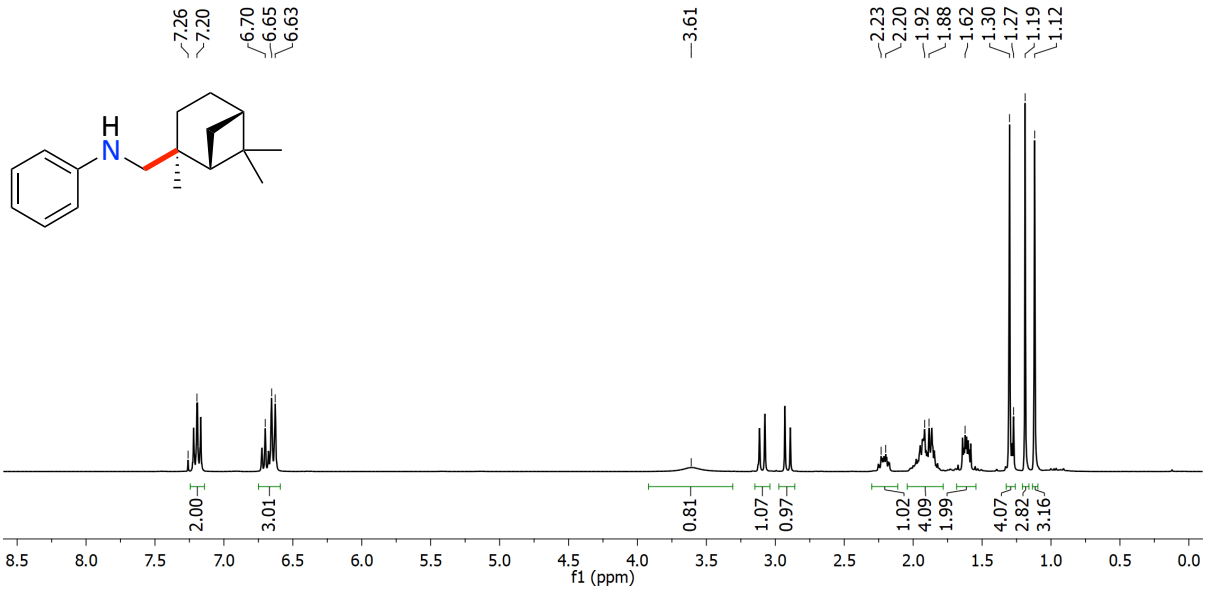

Figure. A.63. ^{1}H NMR spectrum (400 MHz, $CDCl_3$, 298 K) of *N*-((2,6,6-trimethylbicyclo[3.1.1]heptan-2-yl)methyl)aniline.

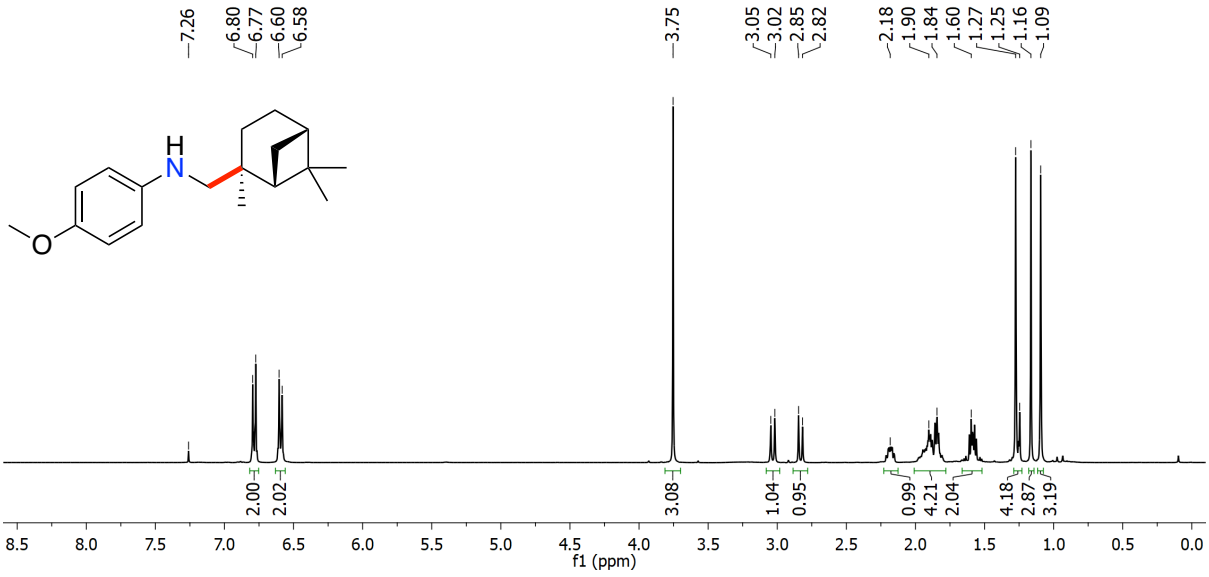

Figure. A.64. ^{1}H NMR spectrum (400 MHz, $CDCl_3$, 298 K) of 4-methoxy-*N*-((2,6,6-trimethylbicyclo[3.1.1]heptan-2-yl)methyl)aniline.

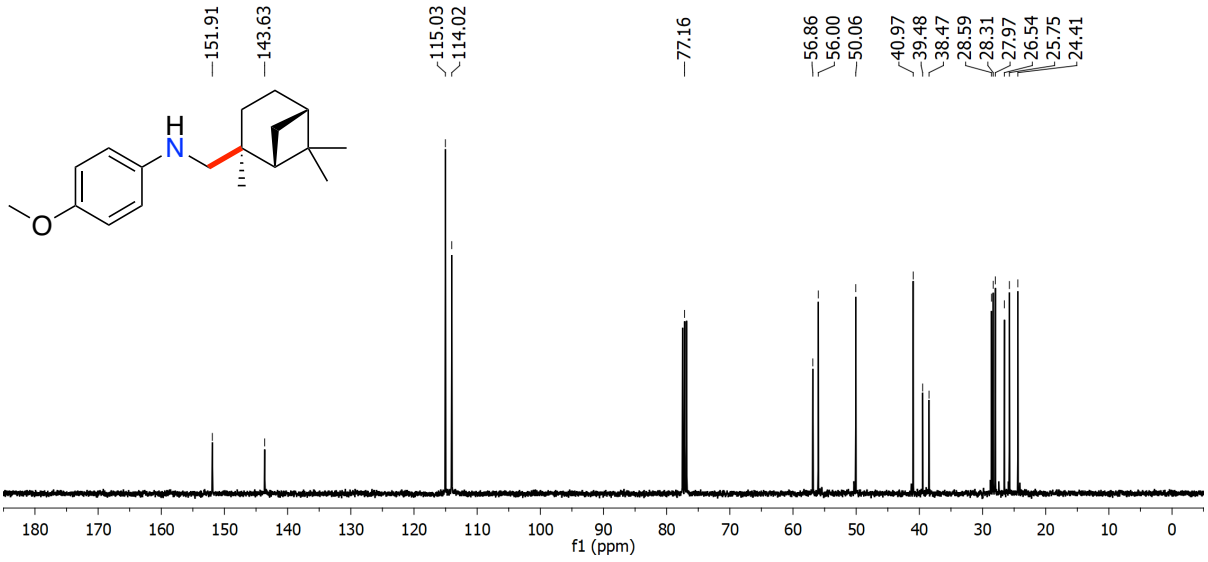

Figure. A.65. $^{13}C\{^{1}H\}$ NMR spectrum (100 MHz, $CDCl_3$, 298 K) of 4-methoxy-*N*-((2,6,6-trimethylbicyclo[3.1.1]heptan-2-yl)methyl)aniline.

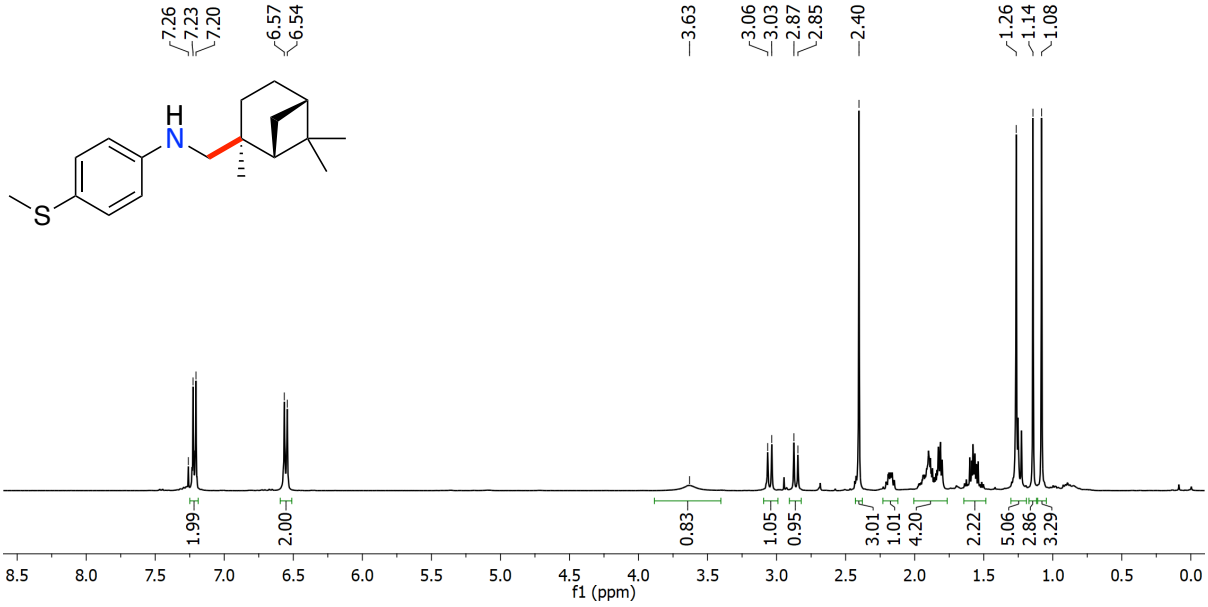

Figure. A.66. ^{1}H NMR spectrum (400 MHz, $CDCl_3$, 298 K) of 4-(methylthio)-*N*-((2,6,6-trimethylbicyclo[3.1.1]heptan-2-yl)methyl)aniline.

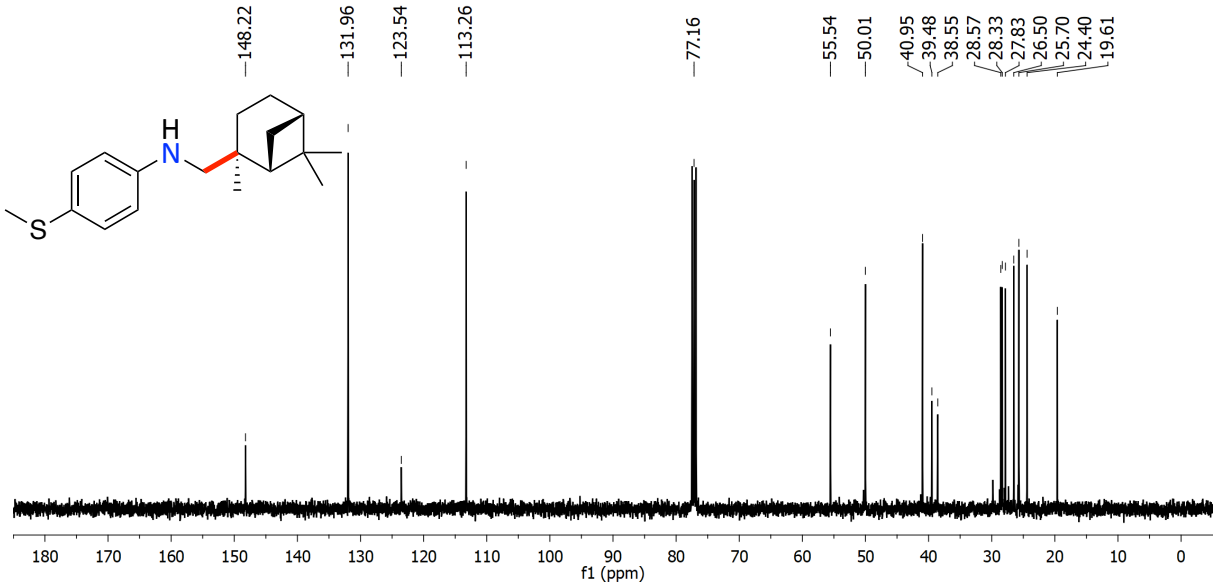

Figure. A.67. $^{13}C\{^{1}H\}$ NMR spectrum (100 MHz, $CDCl_3$, 298 K) of 4-(methylthio)-*N*-((2,6,6-trimethylbicyclo[3.1.1]heptan-2-yl)methyl)aniline.

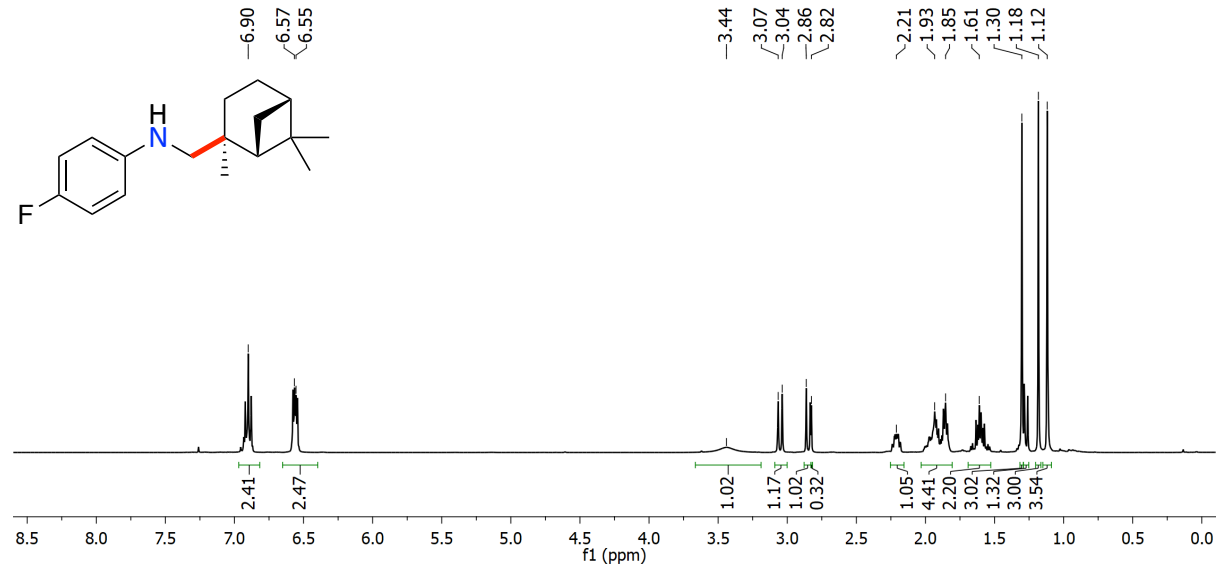

Figure. A.68. ^{1}H NMR spectrum (400 MHz, $CDCl_3$, 298 K) of 4-fluoro-*N*-(((1R,2S,5S)-2,6,6-trimethylbicyclo[3.1.1]heptan-2-yl)methyl)aniline.

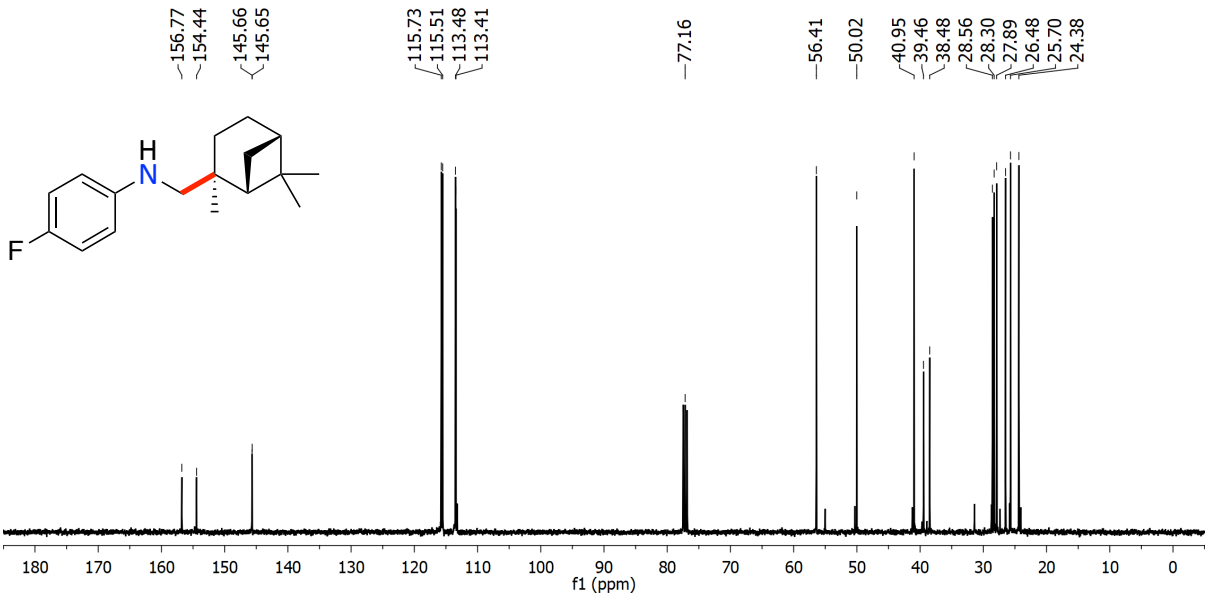

Figure. A.69. $^{13}C\{^{1}H\}$ NMR spectrum (100 MHz, $CDCl_3$, 298 K) of 4-fluoro-*N*-(((1R,2S,5S)-2,6,6-trimethylbicyclo[3.1.1]heptan-2-yl)methyl)aniline.

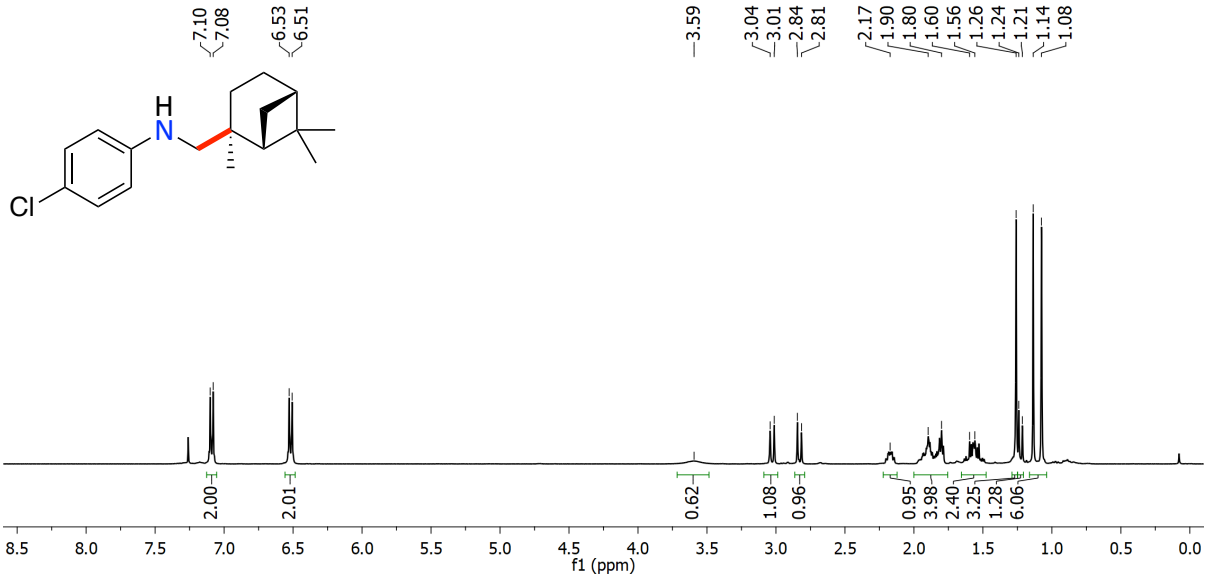

Figure. A.70. ^{1}H NMR spectrum (400 MHz, $CDCl_3$, 298 K) of 4-chloro-*N*-((2,6,6-trimethylbicyclo[3.1.1]heptan-2-yl)methyl)aniline.

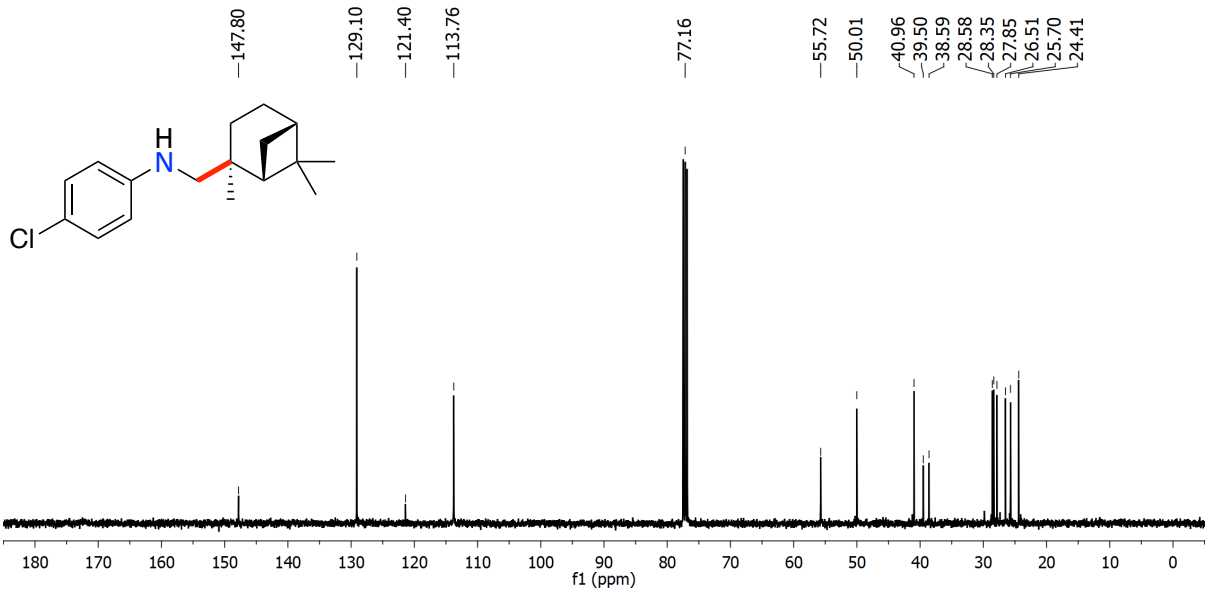

Figure. A.71. $^{13}C\{^{1}H\}$ NMR spectrum (100 MHz, $CDCl_3$, 298 K) of 4-chloro-*N*-((2,6,6-trimethylbicyclo[3.1.1]heptan-2-yl)methyl)aniline.

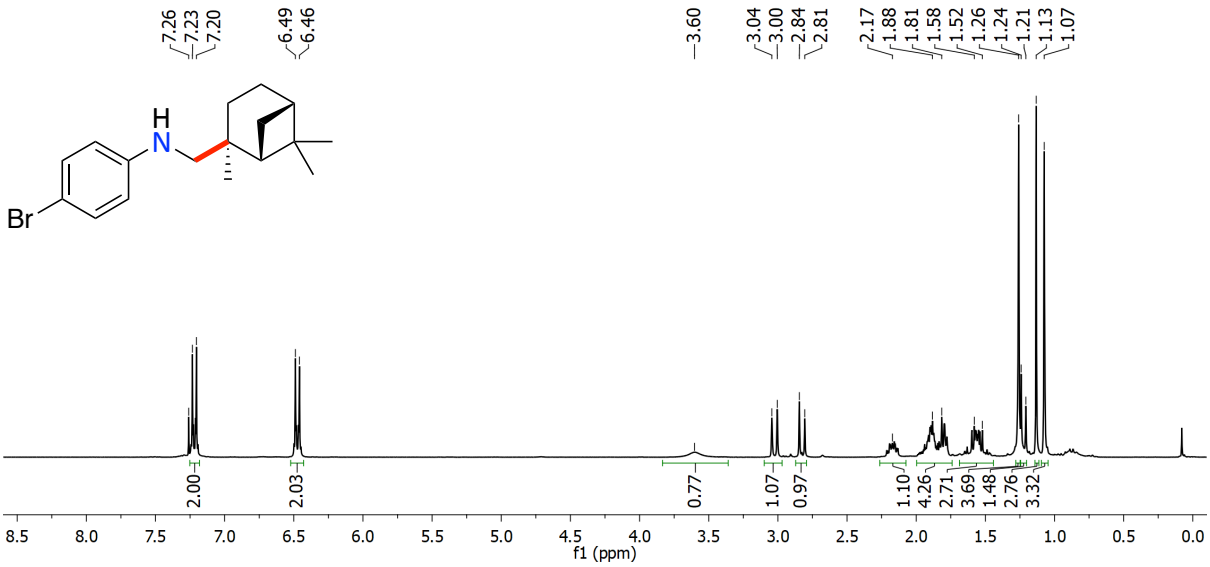

Figure. A.72. ^{1}H NMR spectrum (400 MHz, $CDCl_3$, 298 K) of 4-bromo-*N*-((2,6,6-trimethylbicyclo[3.1.1]heptan-2-yl)methyl)aniline.

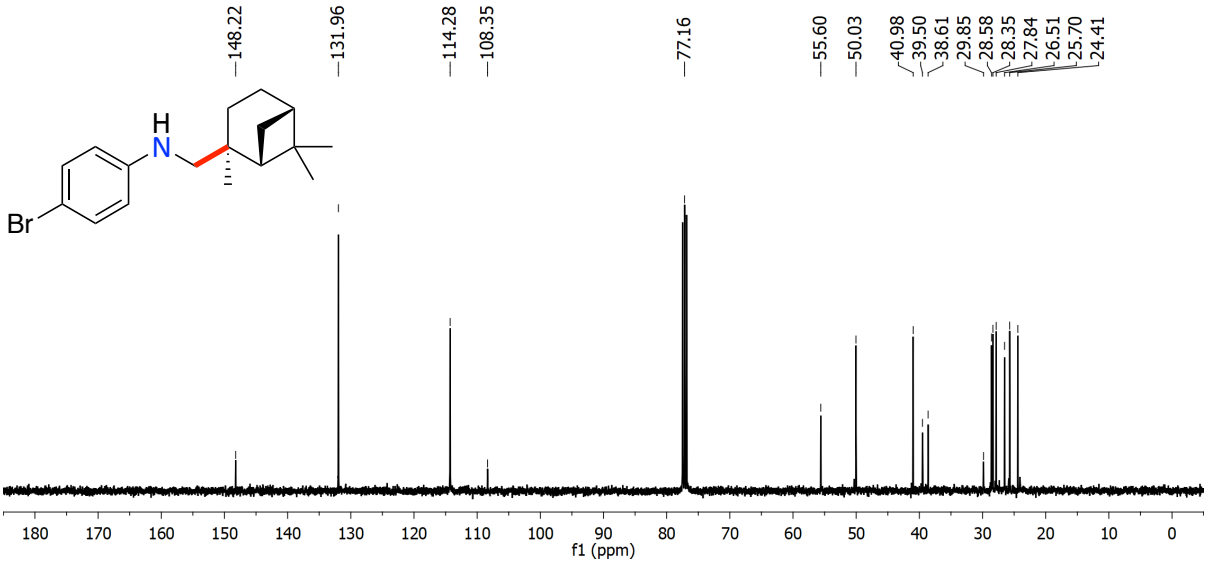

Figure. A.73. $^{13}C\{^{1}H\}$ NMR spectrum (100 MHz, $CDCl_3$, 298 K) of 4-bromo-*N*-((2,6,6-trimethylbicyclo[3.1.1]heptan-2-yl)methyl)aniline.

A.9 Chapter 4 Precatalyst Spectra

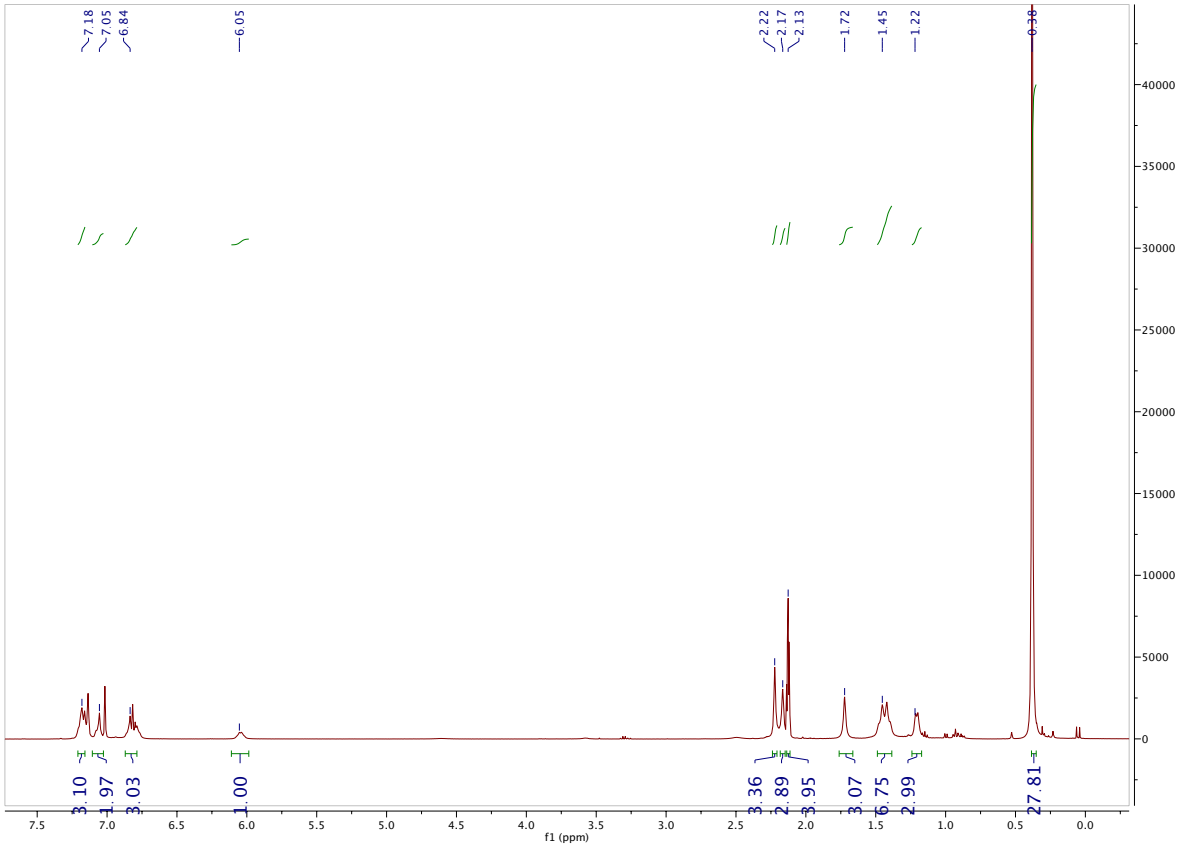

Figure. A.74. ^{1}H NMR spectrum (400 MHz, $CDCl_3$, 298 K) for mono(*N*-(2,6-dimethylphenyl)-*N*-methyl-*N*-(1-phenylethyl)carbamoylamidate)-tris(methylenetrimethylsilane)chlorotantalum

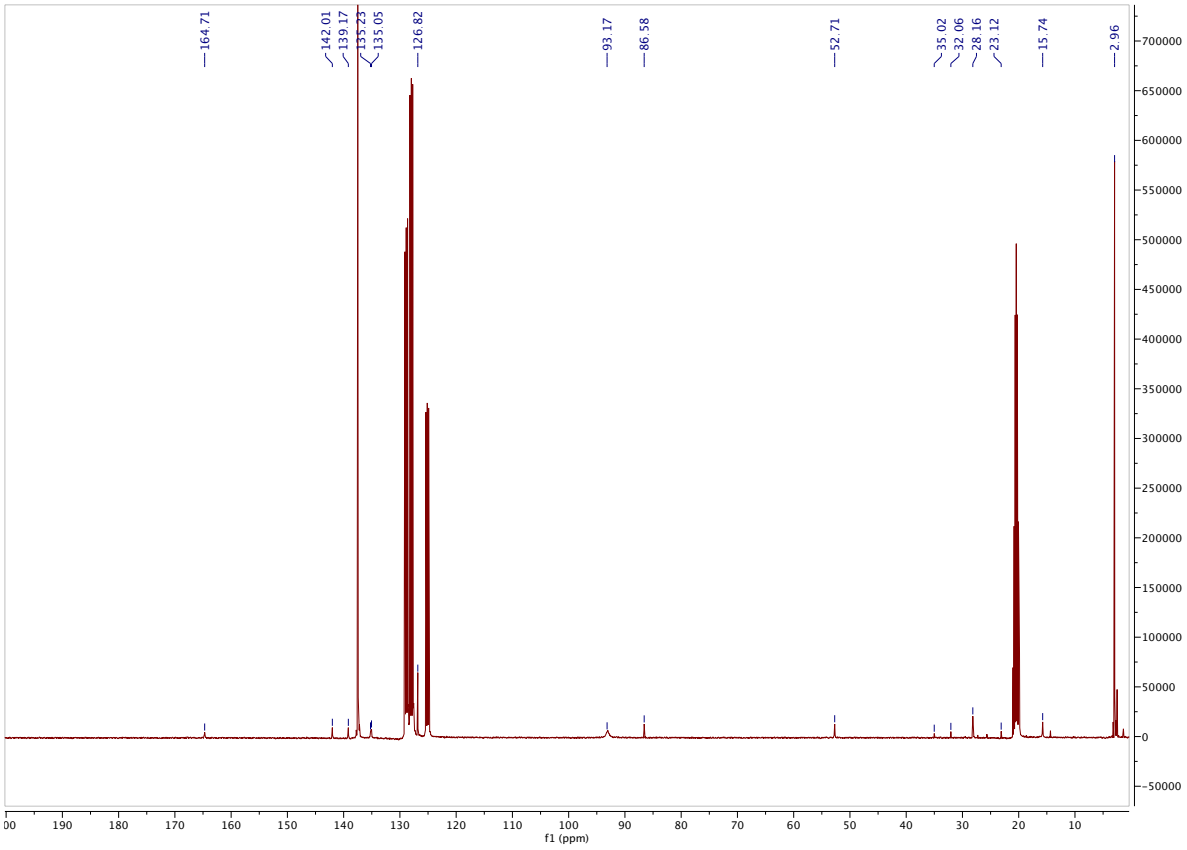

Figure. A.75. $^{13}C\{^{1}H\}$ NMR spectrum (101 MHz, $CDCl_3$, 298 K) for mono(*N*-(2,6-dimethylphenyl)-*N*-methyl-*N*-(1-phenylethyl)carbamoylamidate)-tris(methylenetrimethylsilane)chlorotantalum

A.10 Chapter 4 Spectra from Catalytic Screening

.

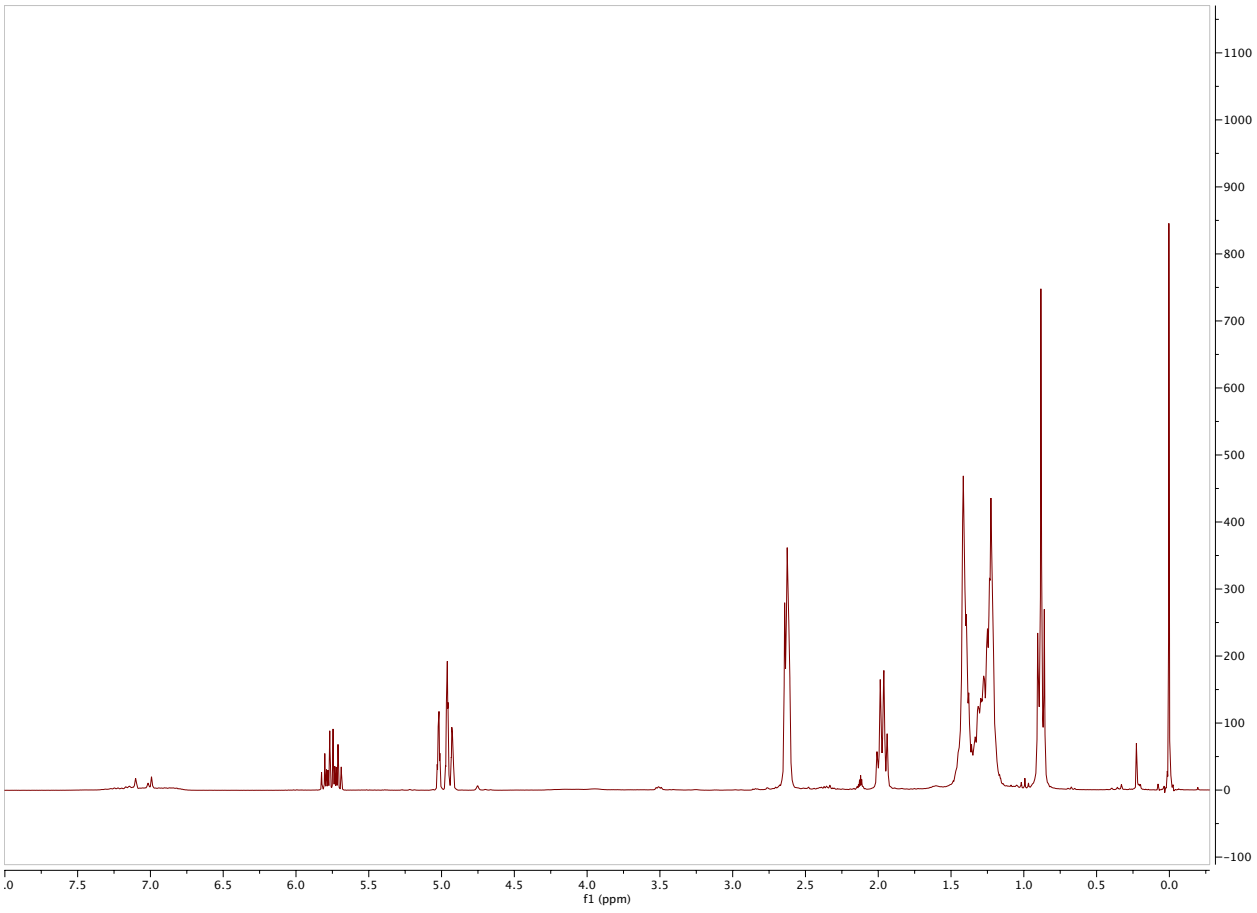

Figure. A.76. ^{1}H NMR spectrum (400 MHz, $CDCl_3$, 298 K) for the crude reaction mixture between piperidine and 1-octene before heating.

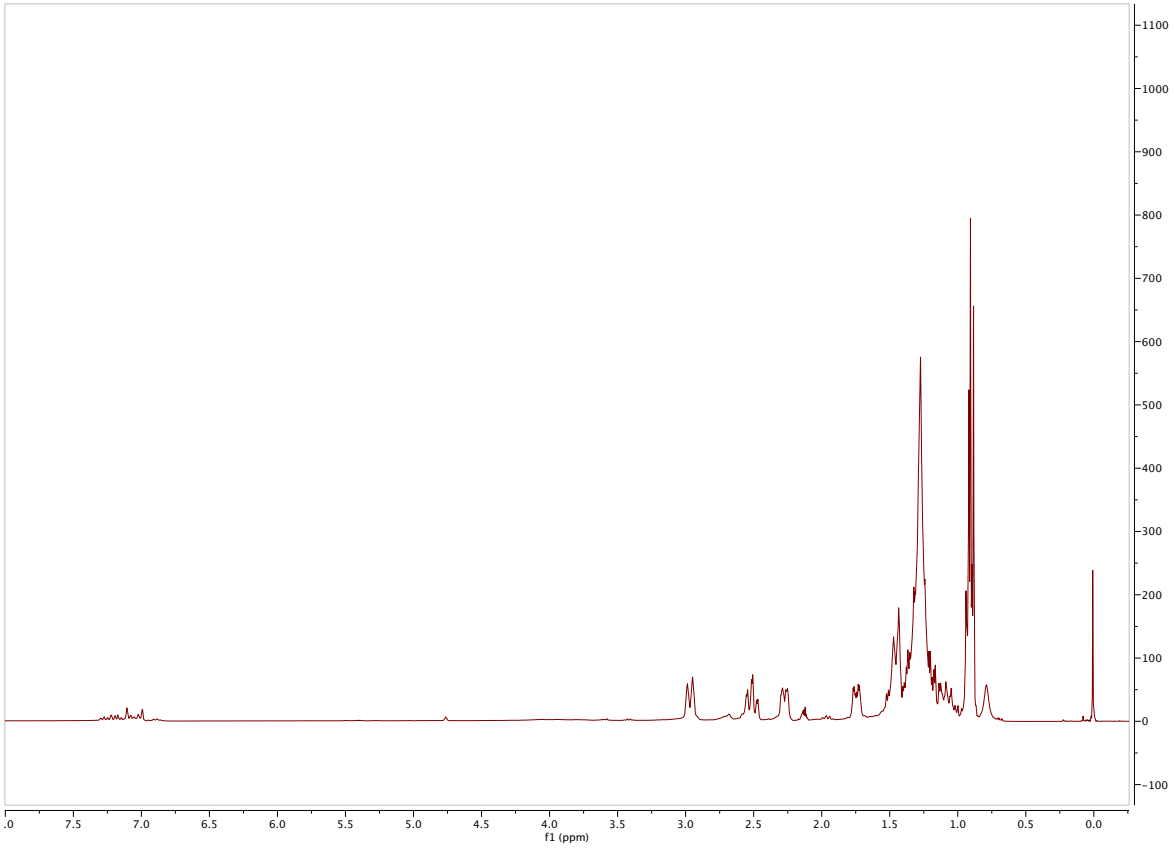

Figure. A.77. ^{1}H NMR spectrum (400 MHz, $CDCl_3$, 298 K) for the crude reaction mixture between piperidine and 1-octene after heating.

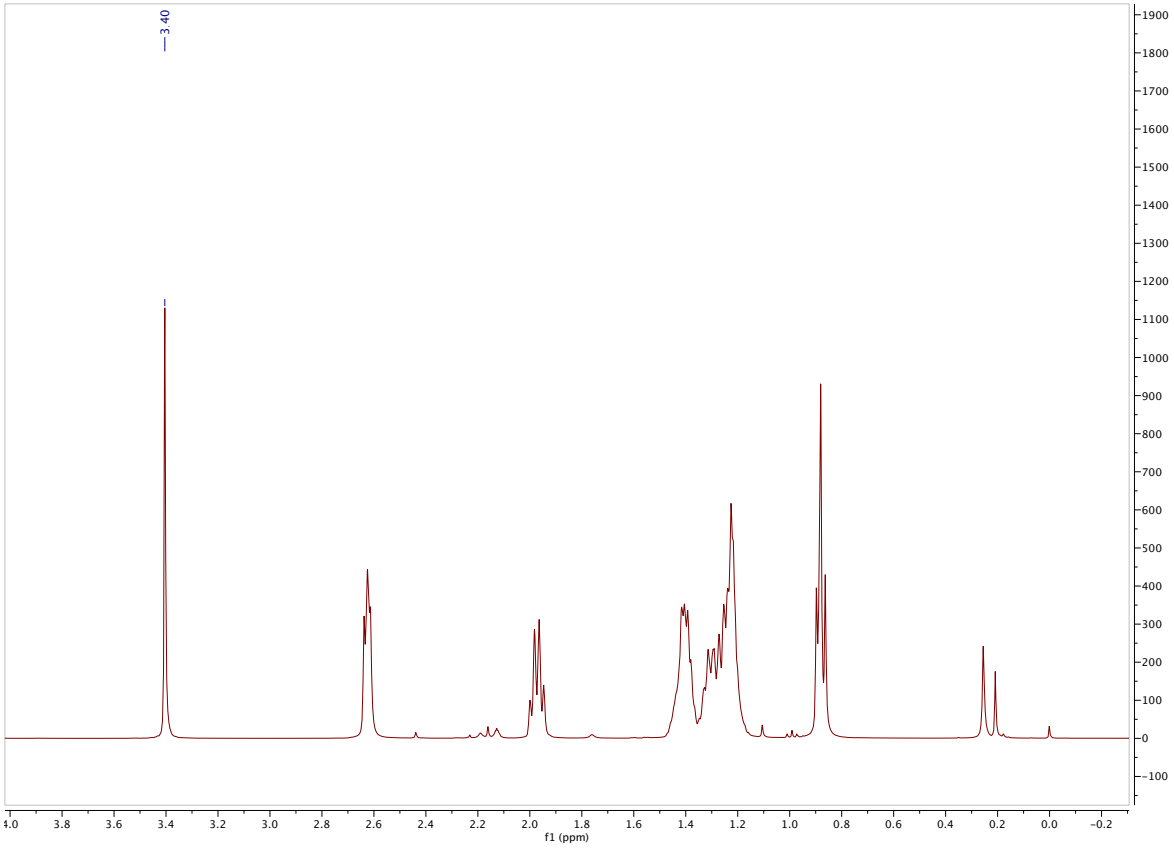

Figure. A.78. ^{1}H NMR spectrum (400 MHz, $CDCl_3$, 298 K) for the crude reaction mixture between piperidine and 1-octene with 1,3,5-trimethoxybenzene as an internal standard (0.33 eq.) before heating. This image is specifically zoomed in on the product region of the NMR spectrum.

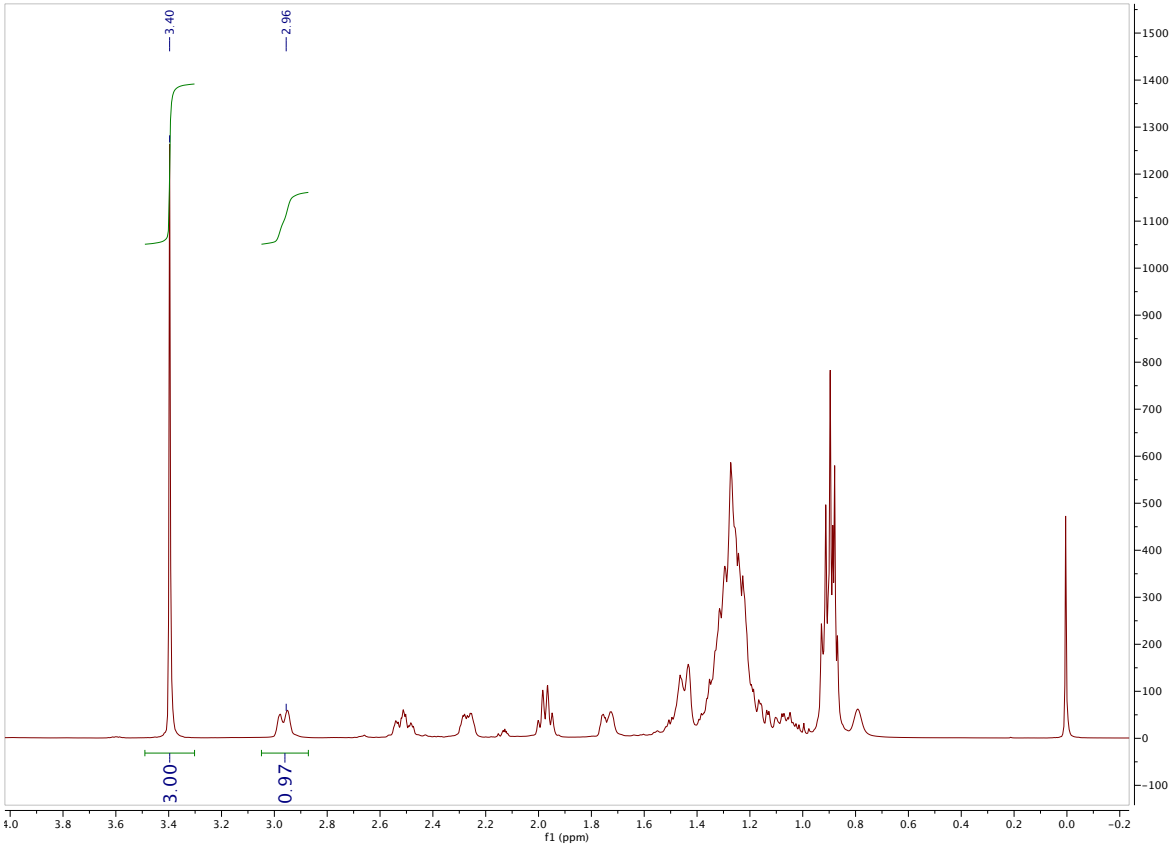

Figure. A.79. ^{1}H NMR spectrum (400 MHz, $CDCl_3$, 298 K) for the crude reaction mixture between piperidine and 1-octene with 1,3,5-trimethoxybenzene as an internal standard (0.33 eq.) after heating. This image is specifically zoomed in on the product region of the NMR spectrum.

A.11 Chapter 4 Amine Scope with 1-Octene

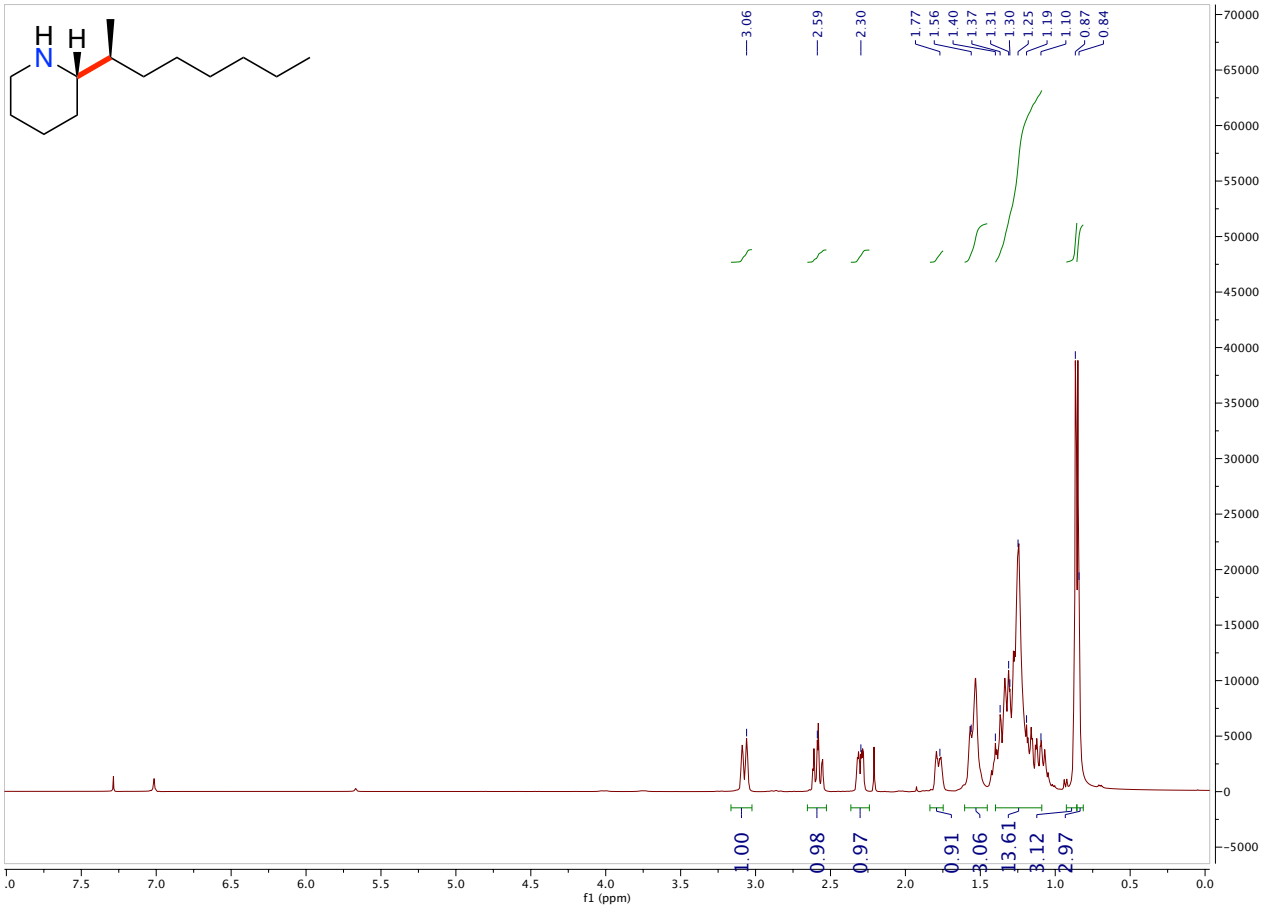

Figure. A.80. ^{1}H NMR spectrum (400 MHz, $CDCl_3$, 298 K) of 2-(octan-2-yl)piperidine.

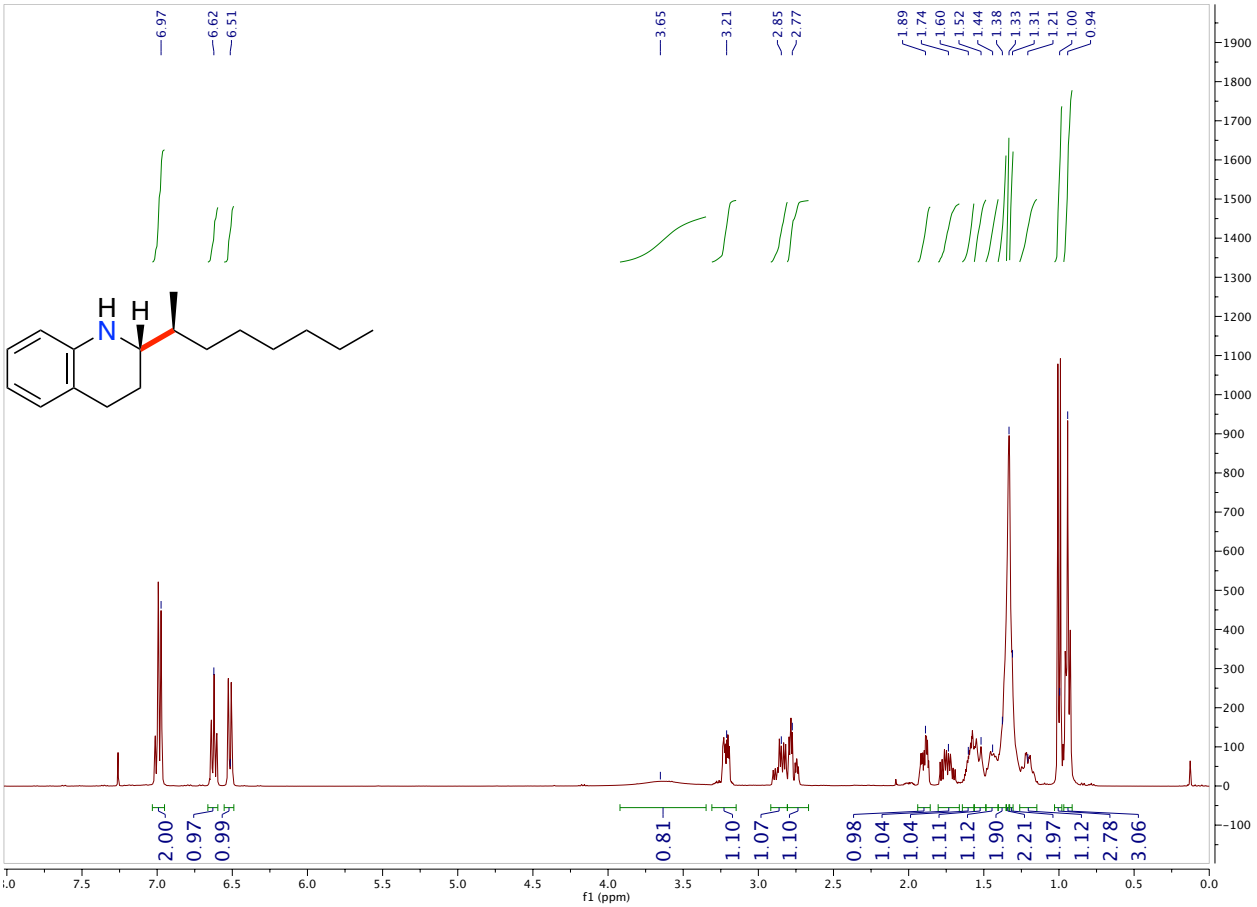

Figure. A.81. ^{1}H NMR spectrum (400 MHz, $CDCl_3$, 298 K) of 2-(octan-2-yl)-1,2,3,4-tetrahydroquinoline.

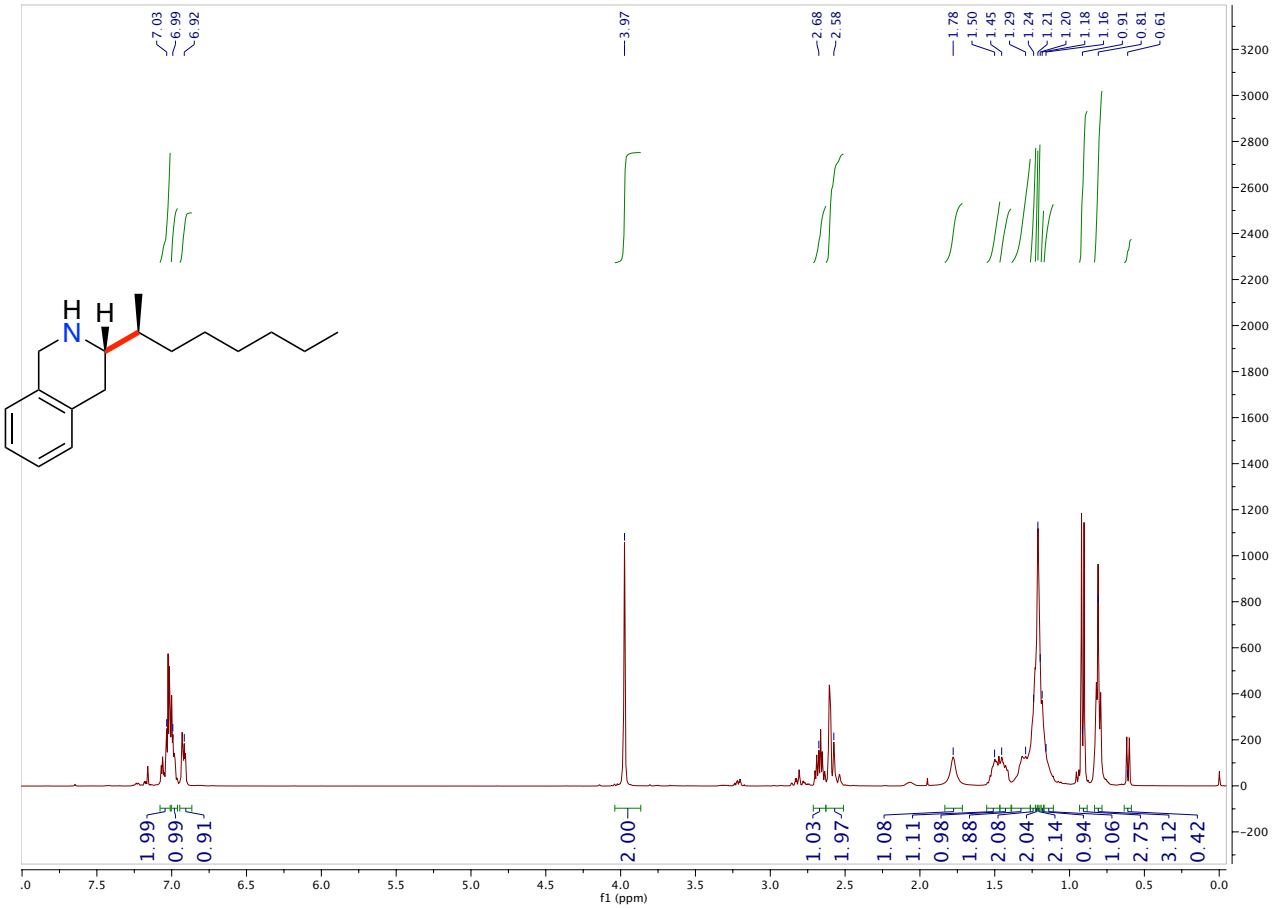

Figure. A.82. ^{1}H NMR spectrum (400 MHz, $CDCl_3$, 298 K) of 3-(octan-2-yl)-1,2,3,4-tetrahydroisoquinoline.

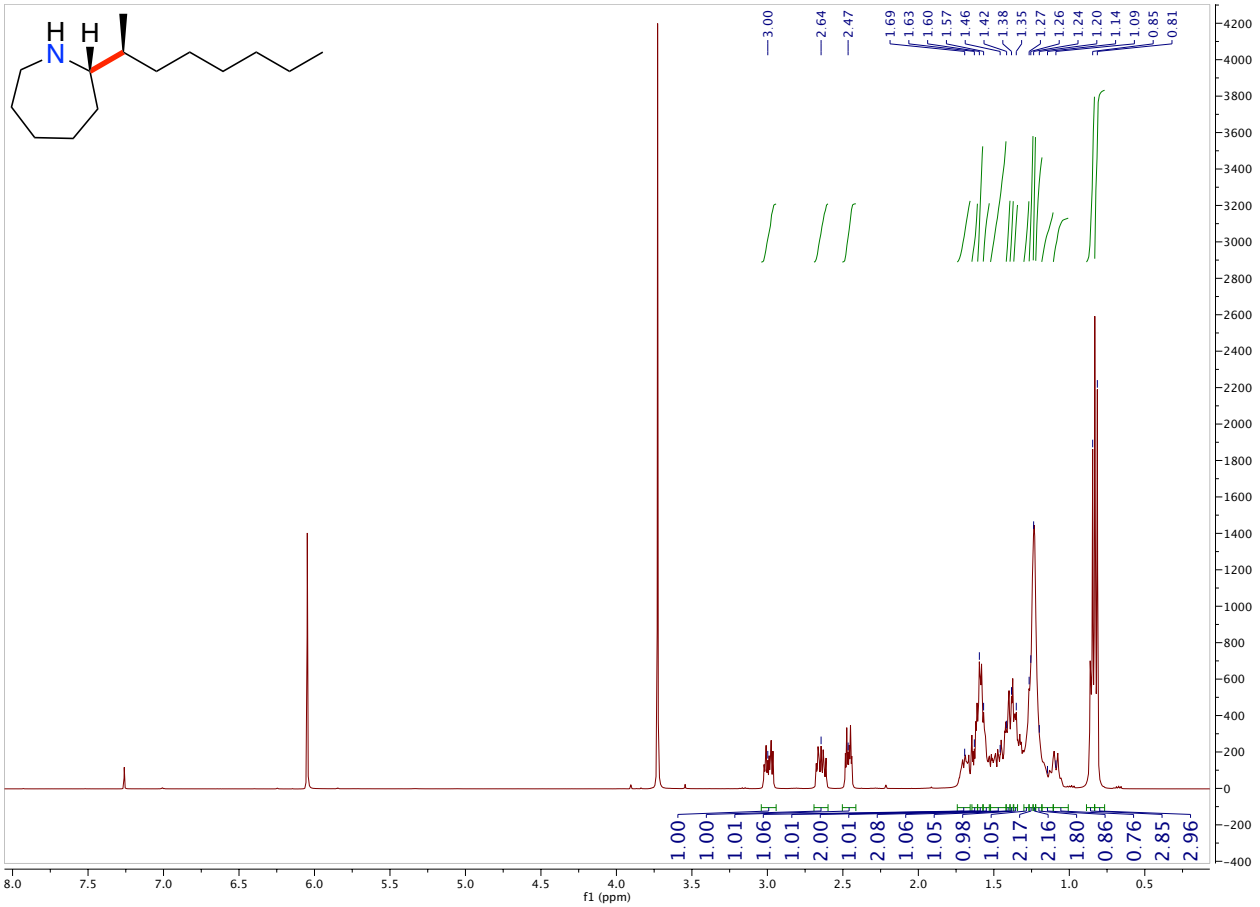

Figure. A.83. ^{1}H NMR spectrum (400 MHz, $CDCl_3$, 298 K) of 2-(octan-2-yl)azepane. Note that peaks at 3.6 and 6.1 ppm represent residual 1,3,5-trimethoxybenzene internal standard.

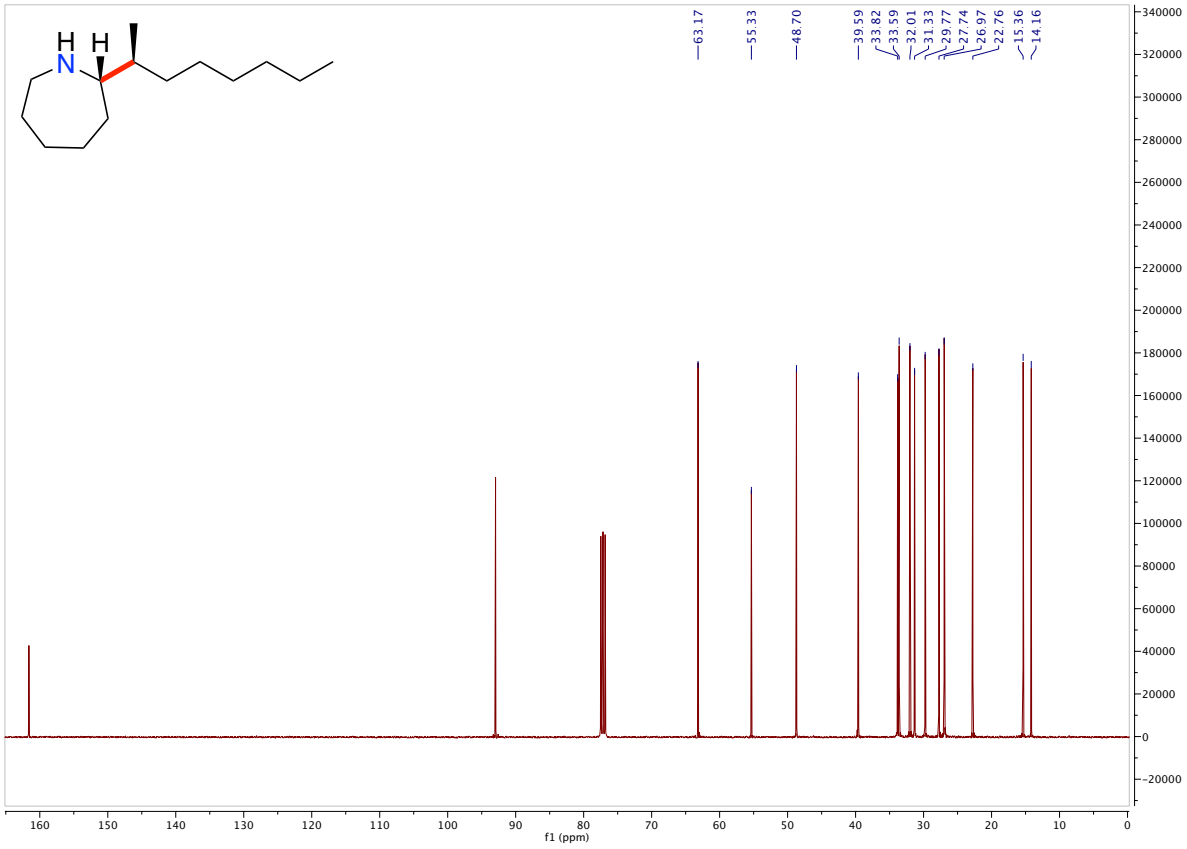

Figure. A.84. $^{13}C\{^{1}H\}$ NMR spectrum (101 MHz, $CDCl_3$, 298 K) of 2-(octan-2-yl)azepane.

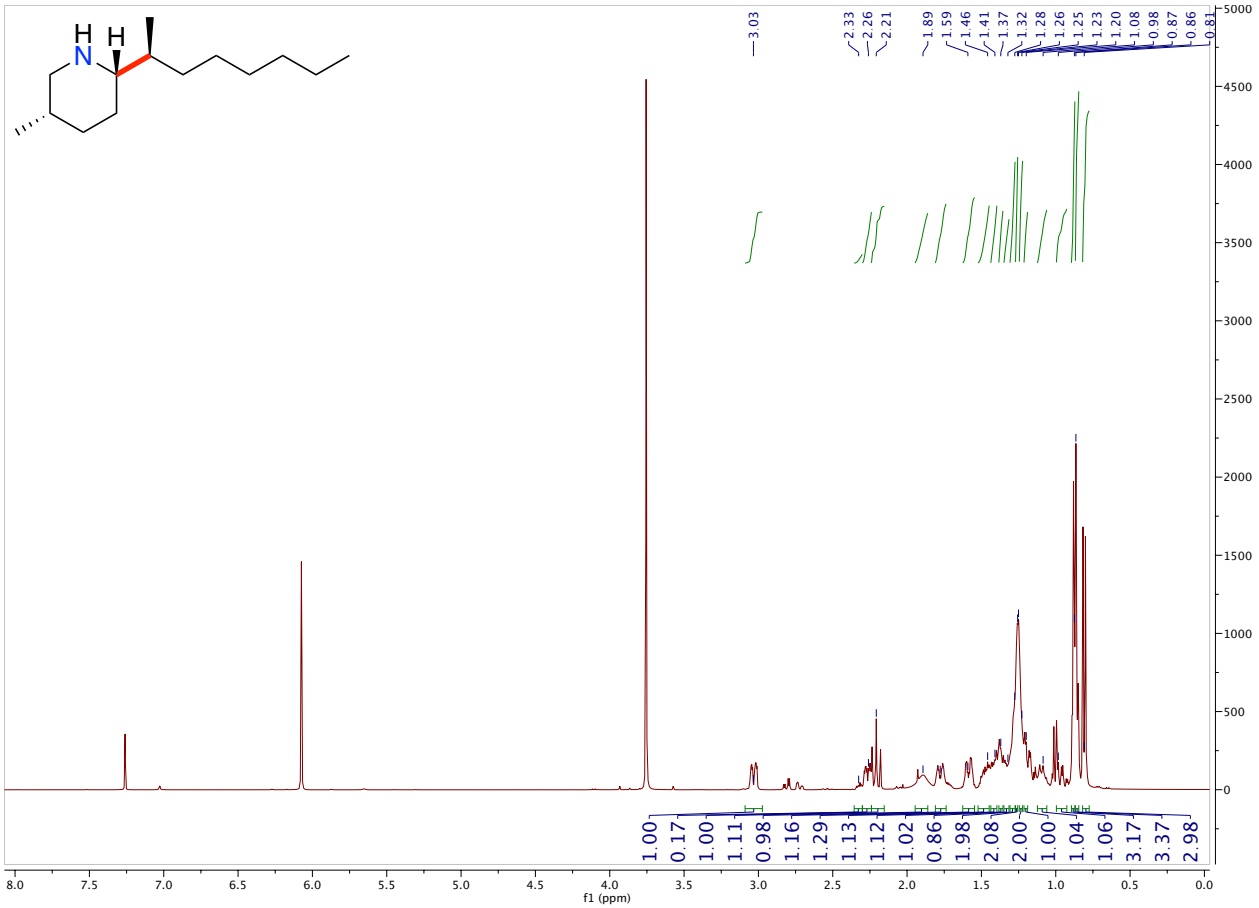

Figure. A.85. ^{1}H NMR spectrum (400 MHz, $CDCl_3$, 298 K) of both diastereomers of 4-methyl-2-(octan-2-yl)piperidine (1:10). Note that peaks at 3.7 and 6.1 ppm represent residual 1,3,5-trimethoxybenzene internal standard.

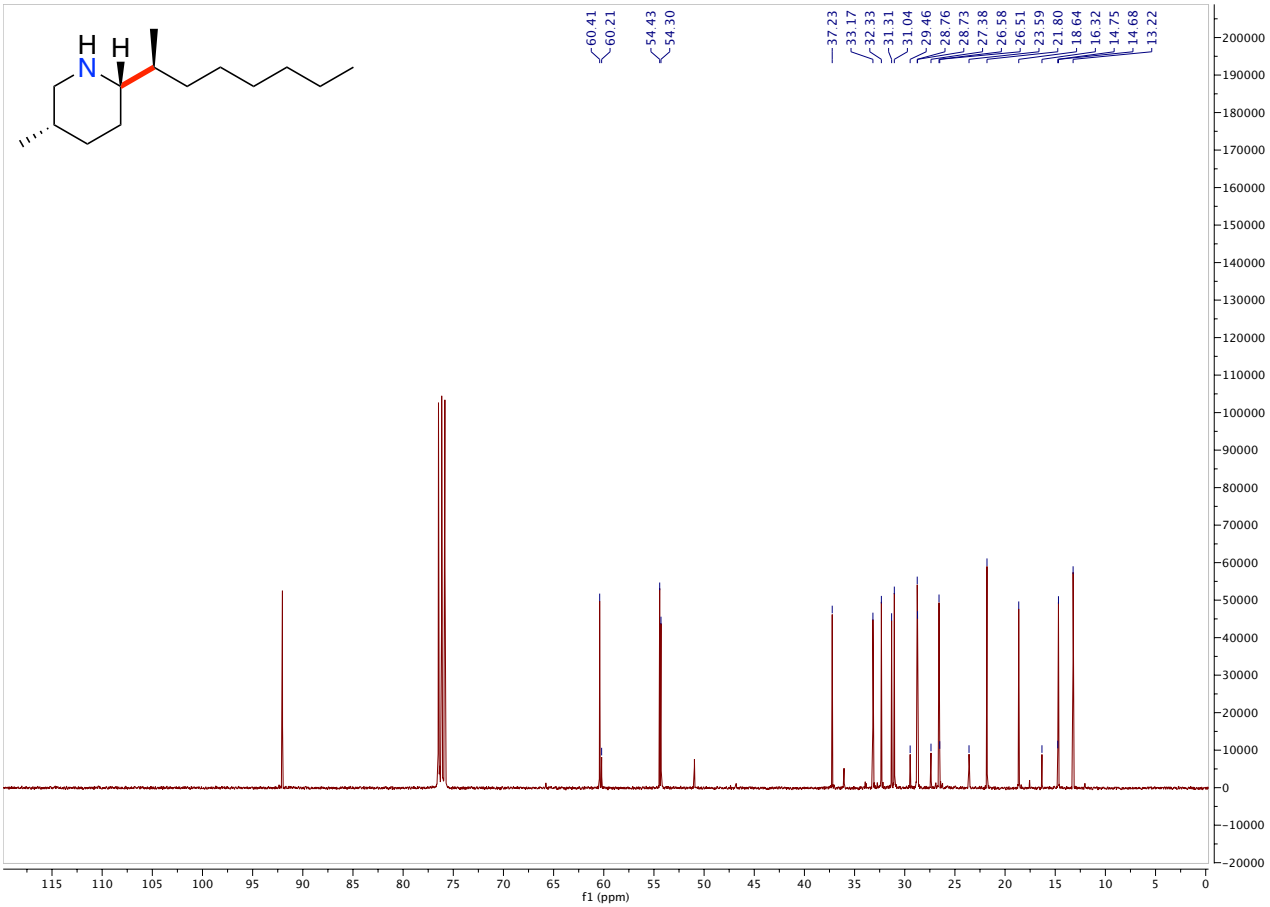

Figure. A.86. $^{13}C\{^{1}H\}$ NMR spectrum (101 MHz, $CDCl_3$, 298 K) of 4-methyl-2-(octan-2-yl)piperidine.

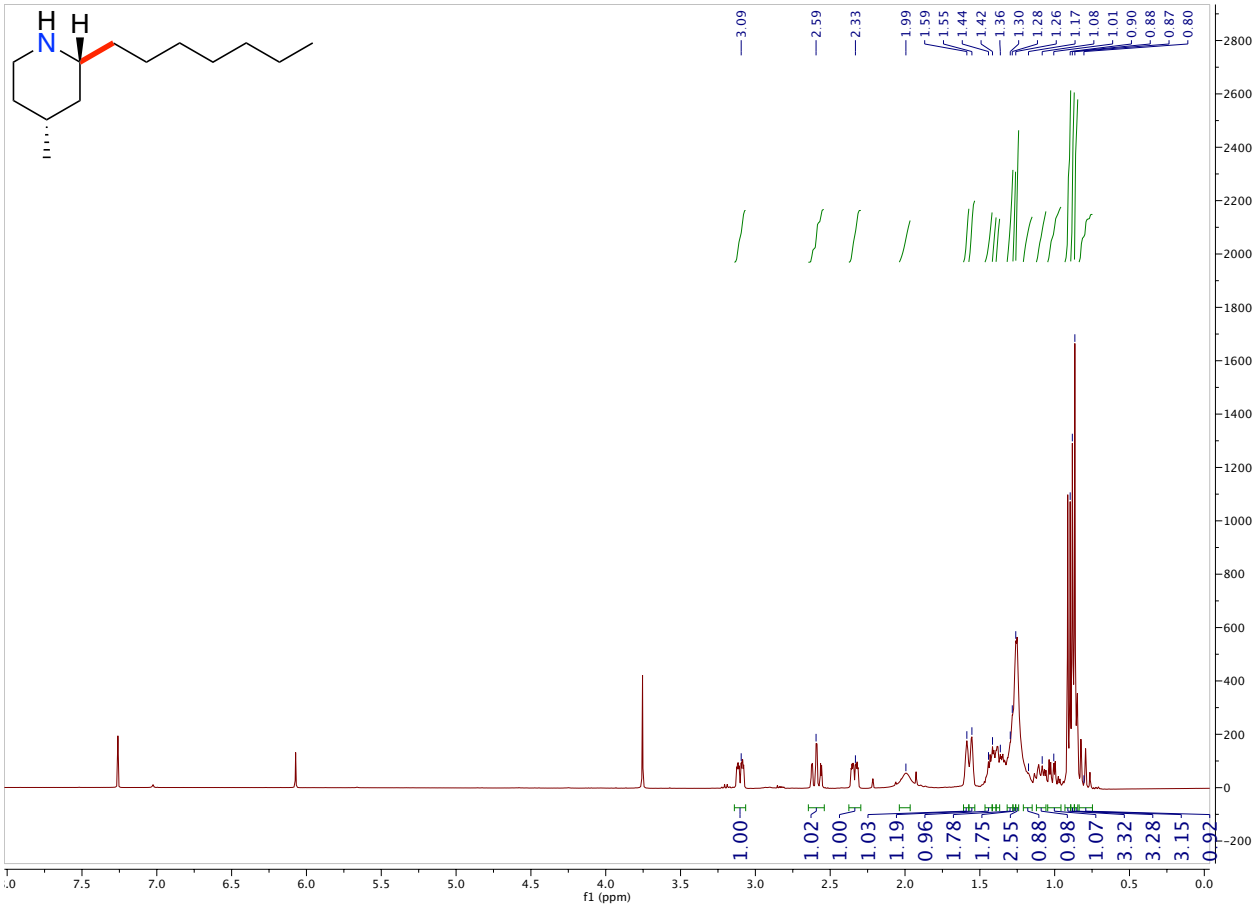

Figure. A.87. ^{1}H NMR spectrum (400 MHz, $CDCl_3$, 298 K) of 4-methyl-2-(octan-2-yl)piperidine.

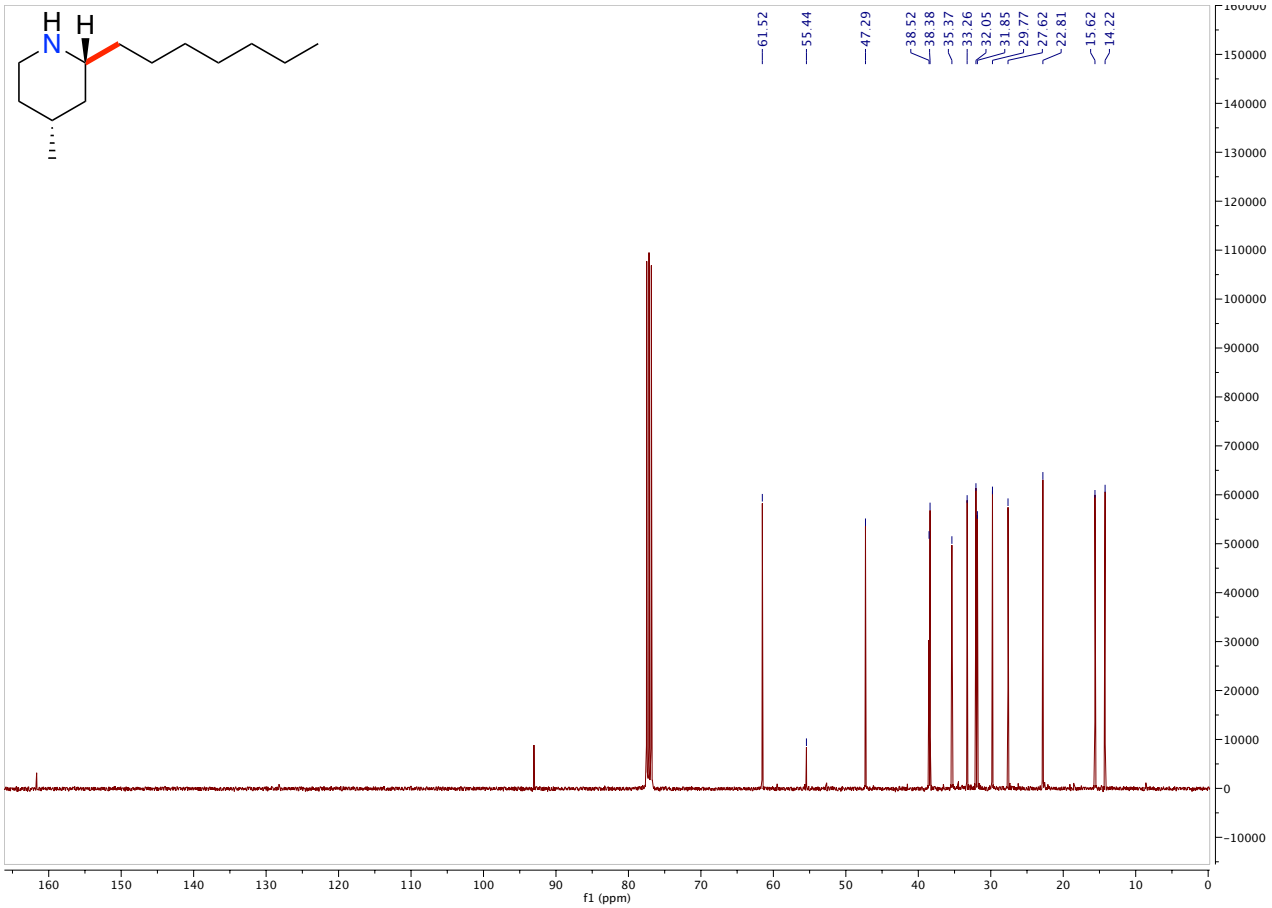

Figure. A.88. $^{13}C\{^{1}H\}$ NMR spectrum (101 MHz, $CDCl_3$, 298 K) of 4-methyl-2-(octan-2-yl)piperidine.

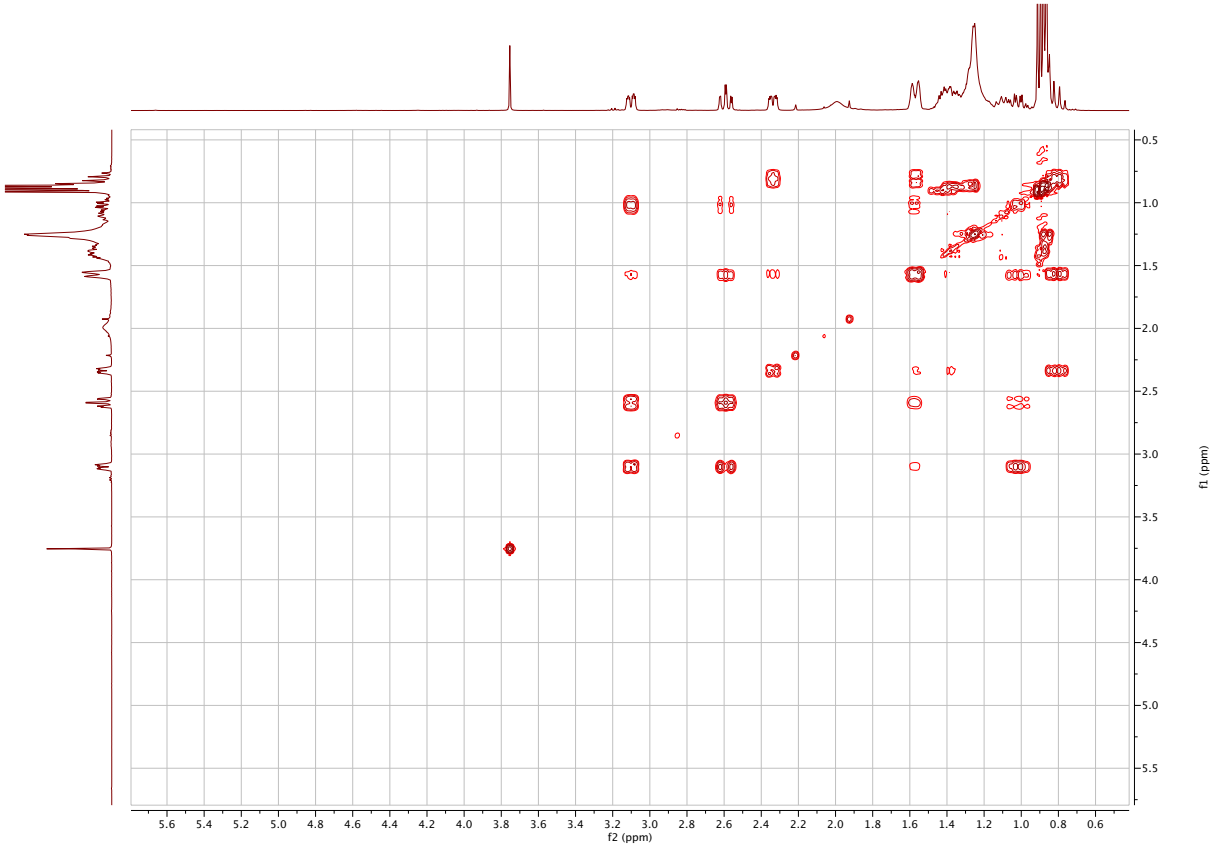

Figure. A.89. COSY spectrum (400 MHz, $CDCl_3$, 298 K) of 4-methyl-2-(octan-2-yl)piperidine.

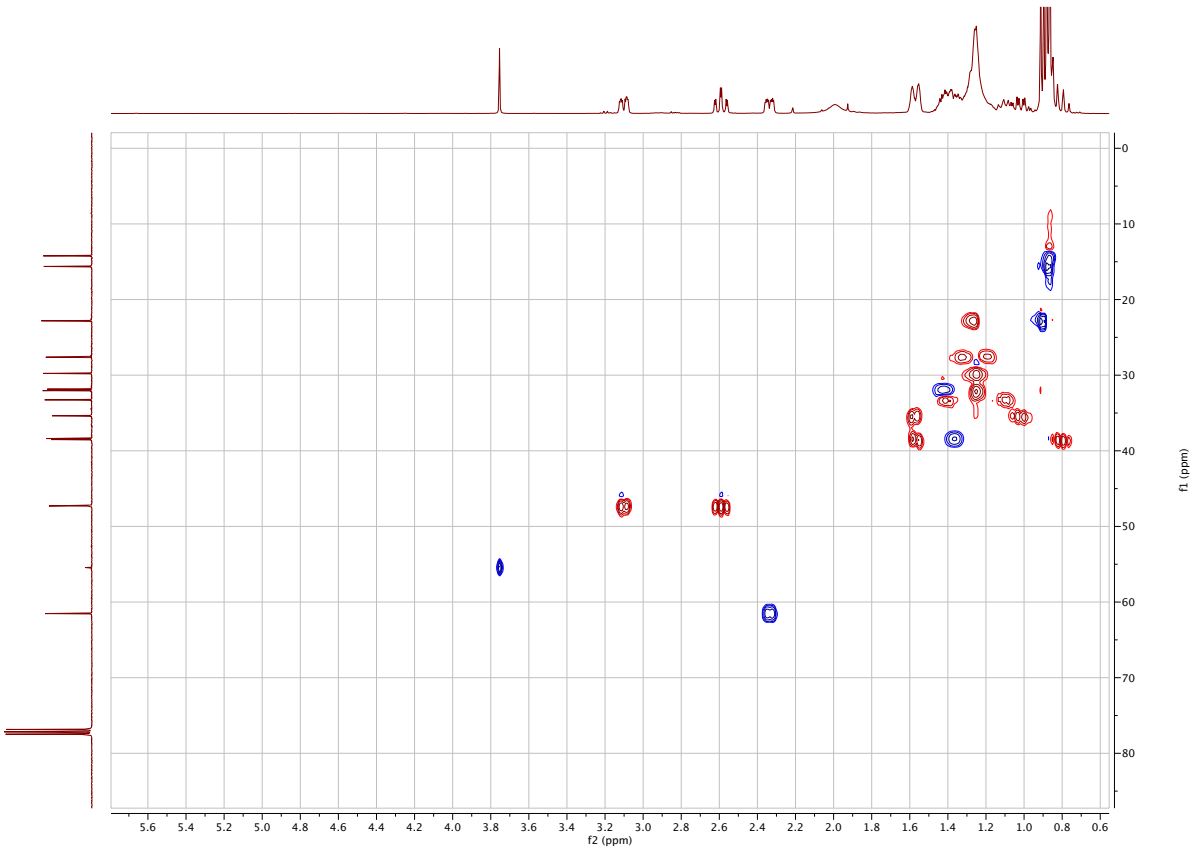

Figure. A.90. HSQC spectrum (101 MHz, $CDCl_3$, 298 K) of 4-methyl-2-(octan-2-yl)piperidine.

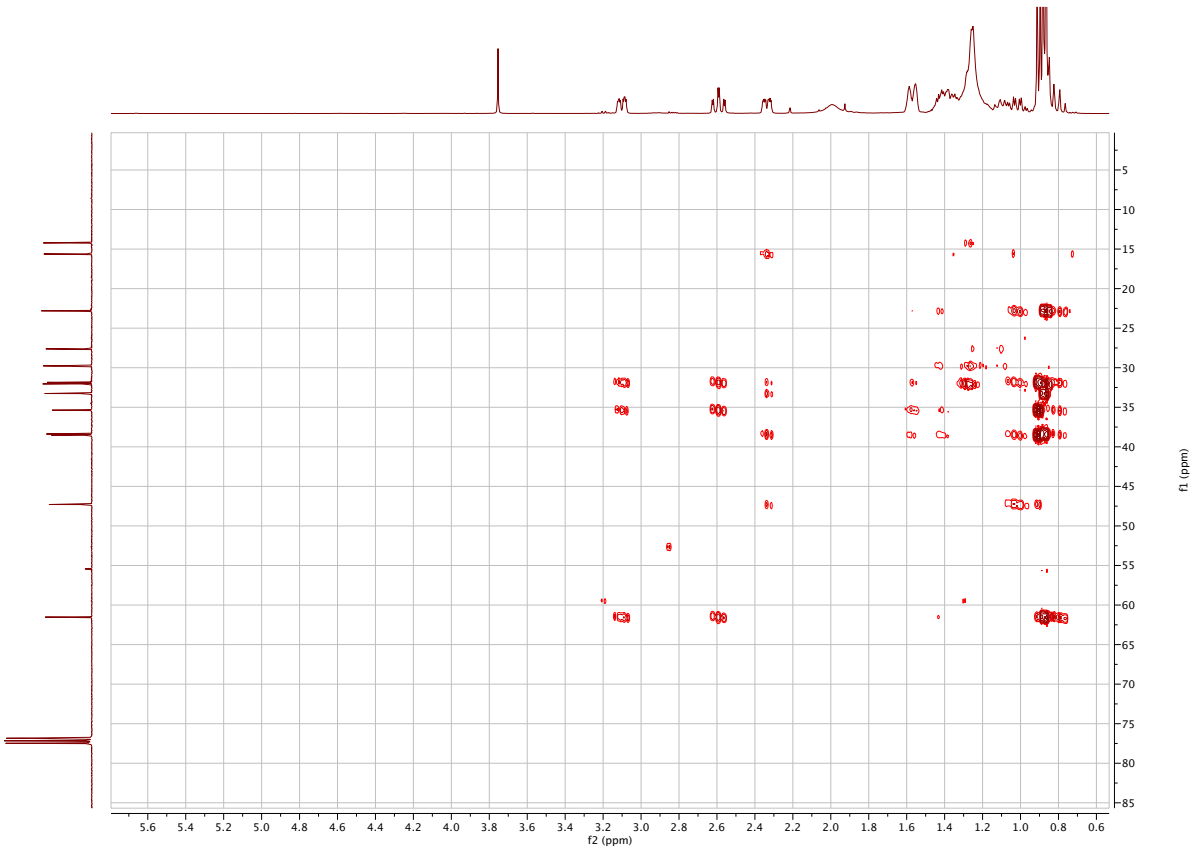

Figure. A.91. HMBC spectrum (101 MHz, $CDCl_3$, 298 K) of 4-methyl-2-(octan-2-yl)piperidine.

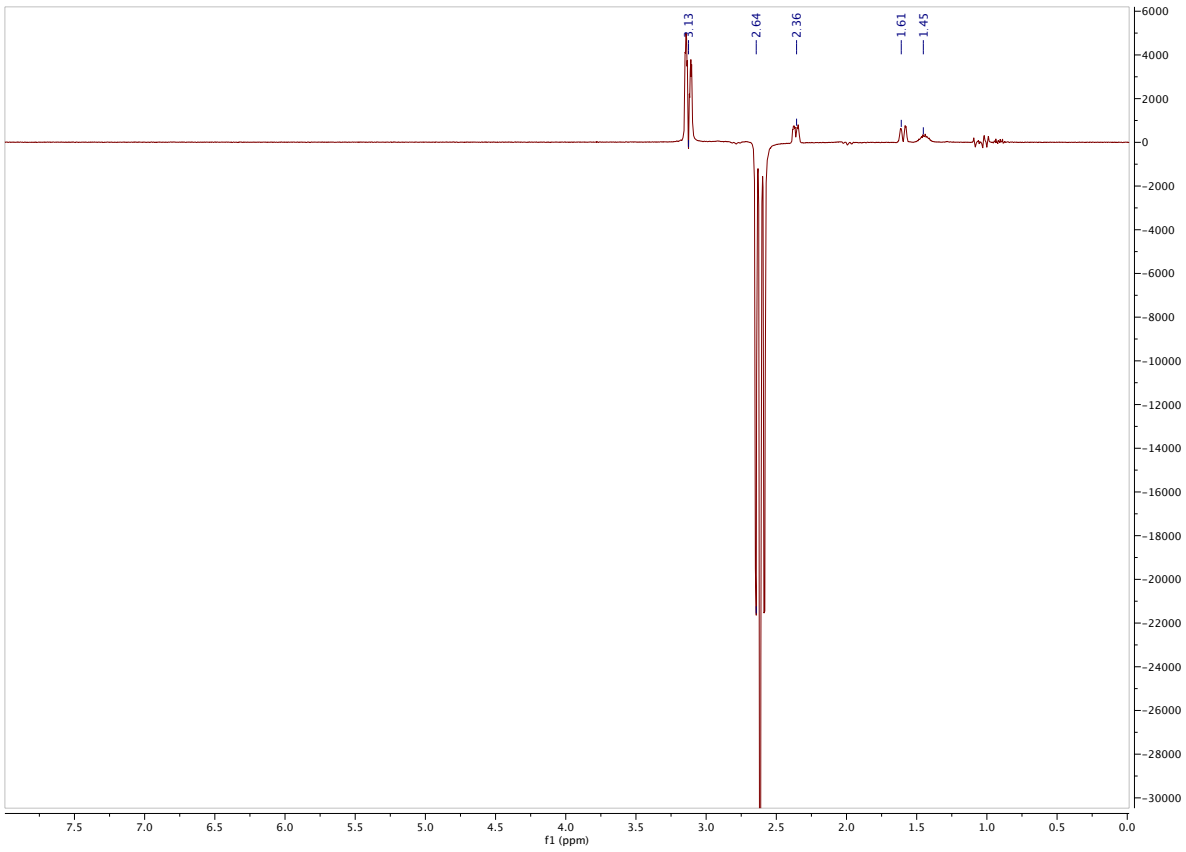

Figure. A.92. 1D NOESY spectrum (400 MHz, $CDCl_3$, 298 K) of 4-methyl-2-(octan-2-yl)piperidine.

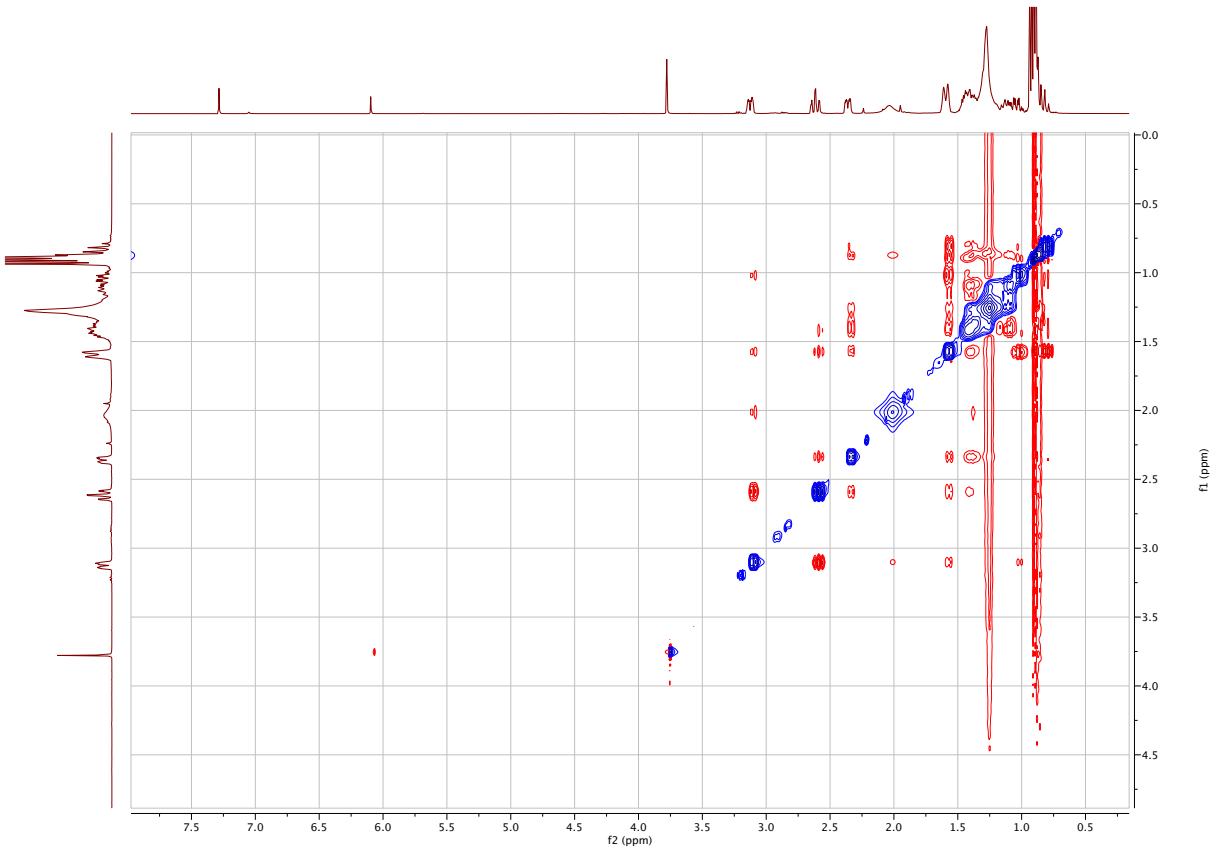

Figure. A.93. 2D NOESY spectrum (400 MHz, $CDCl_3$, 298 K) of 4-methyl-2-(octan-2-yl)piperidine.

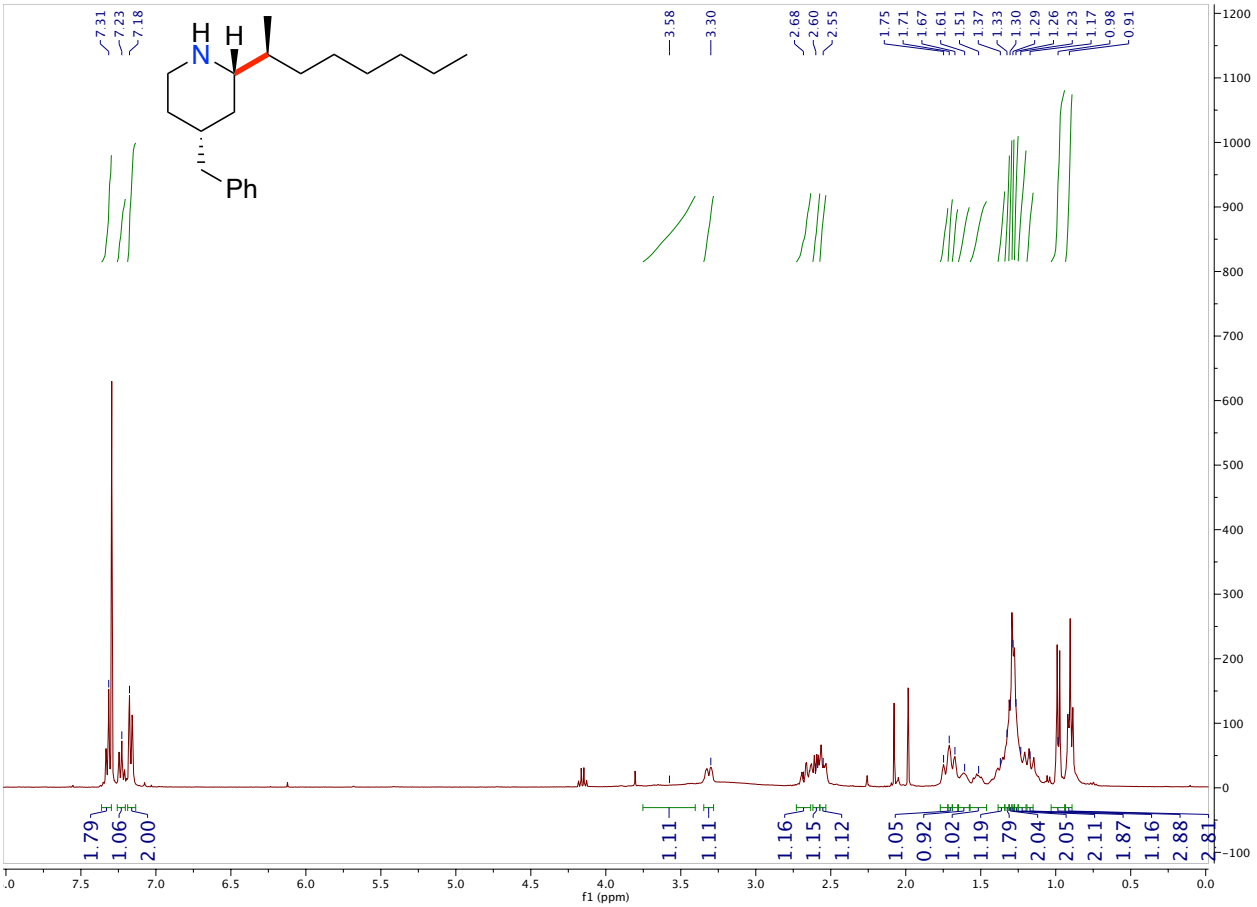

Figure. A.94. ^{1}H NMR spectrum (400 MHz, $CDCl_3$, 298 K) of 4-benzyl-2-(octan-2-yl)piperidine.

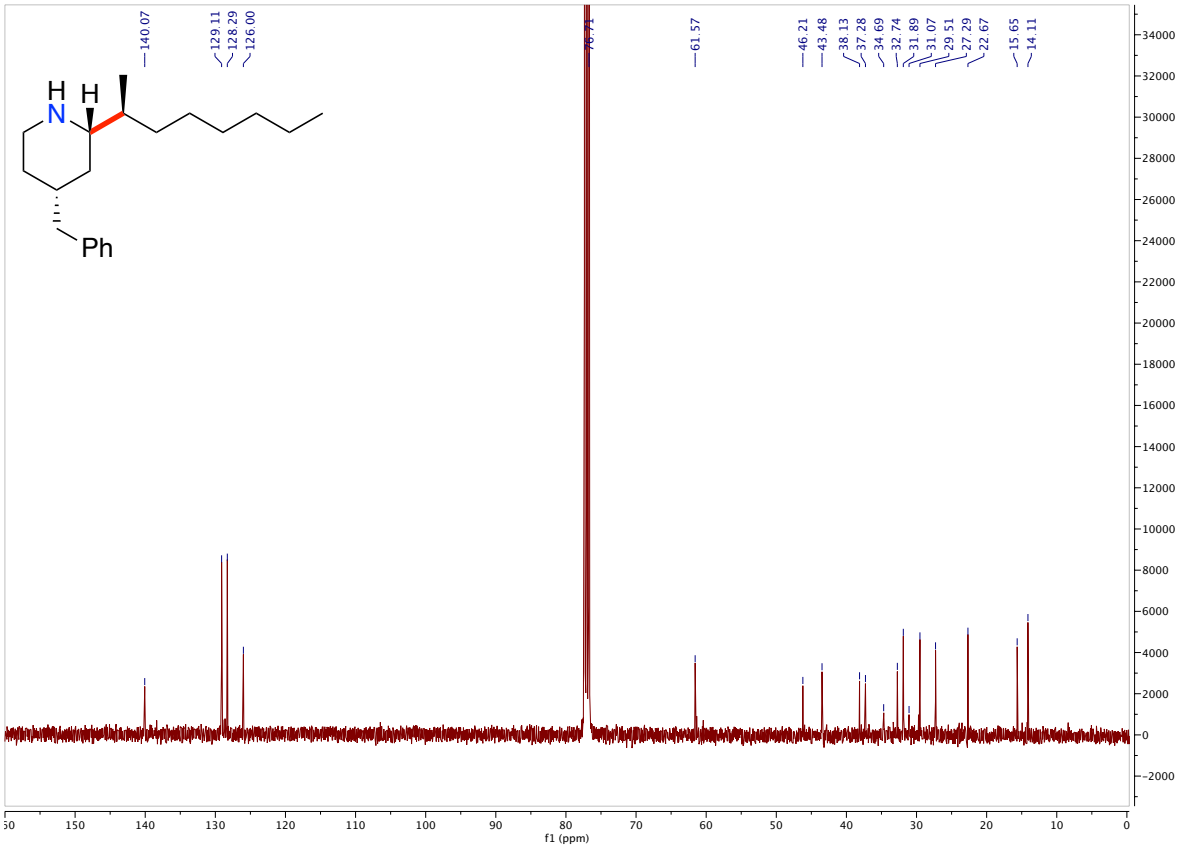

Figure. A.95. $^{13}C\{^{1}H\}$ NMR spectrum (101 MHz, $CDCl_3$, 298 K) of 4-benzyl-2-(octan-2-yl)piperidine.

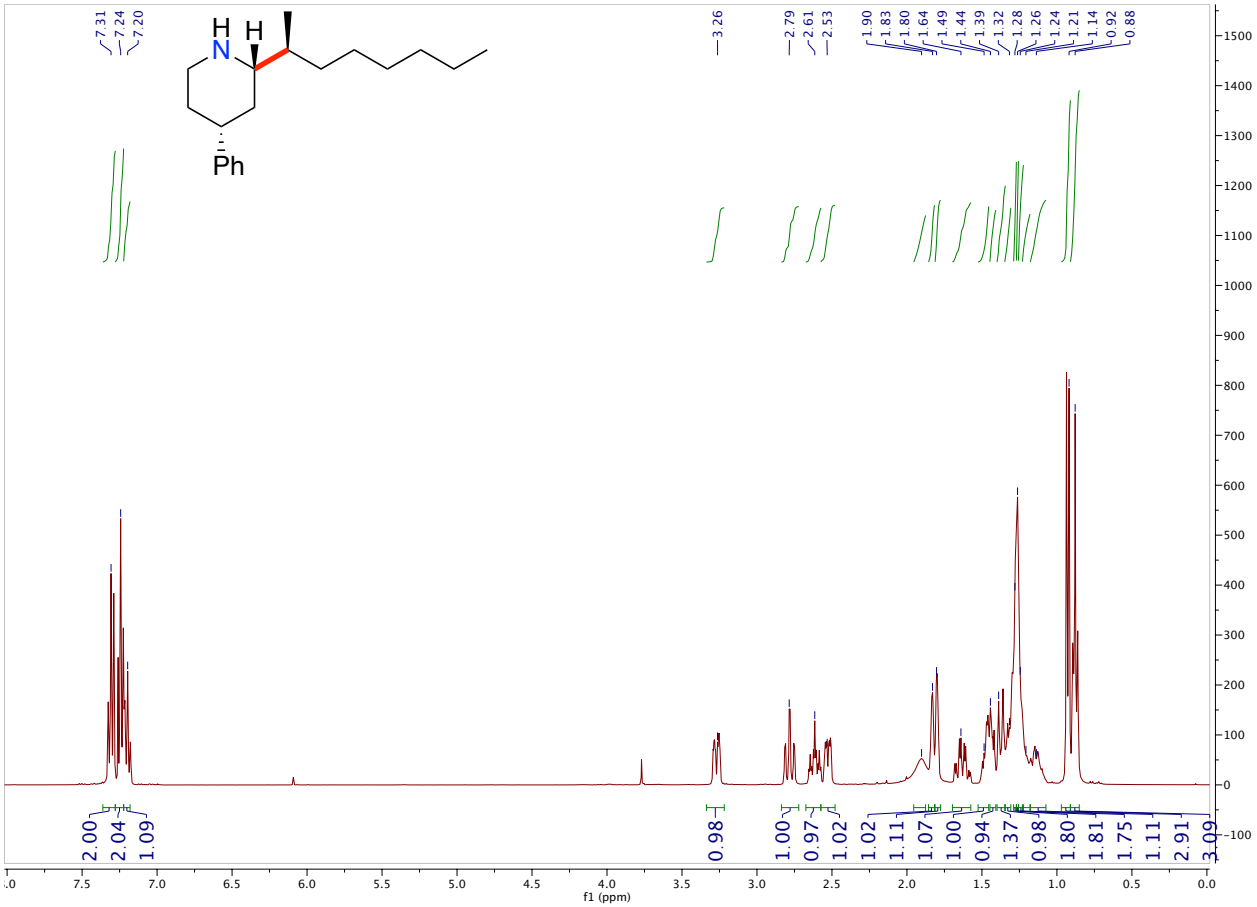

Figure. A.96. ^{1}H NMR spectrum (400 MHz, $CDCl_3$, 298 K) of 2-(octan-2-yl)-4-phenylpiperidine.

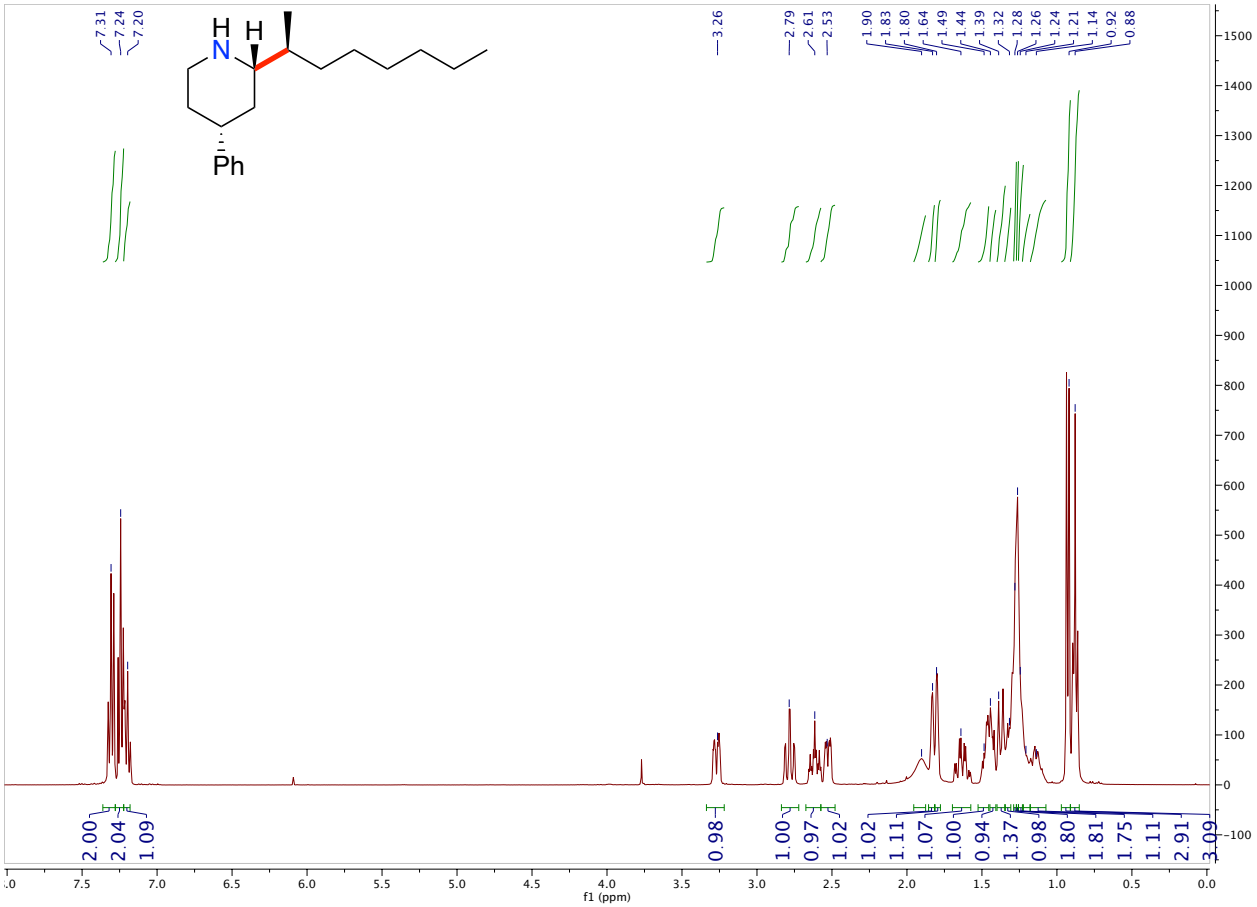

Figure. A.97. ^{1}H NMR spectrum (400 MHz, $CDCl_3$, 298 K) of 2-(octan-2-yl)-4-phenylpiperidine.

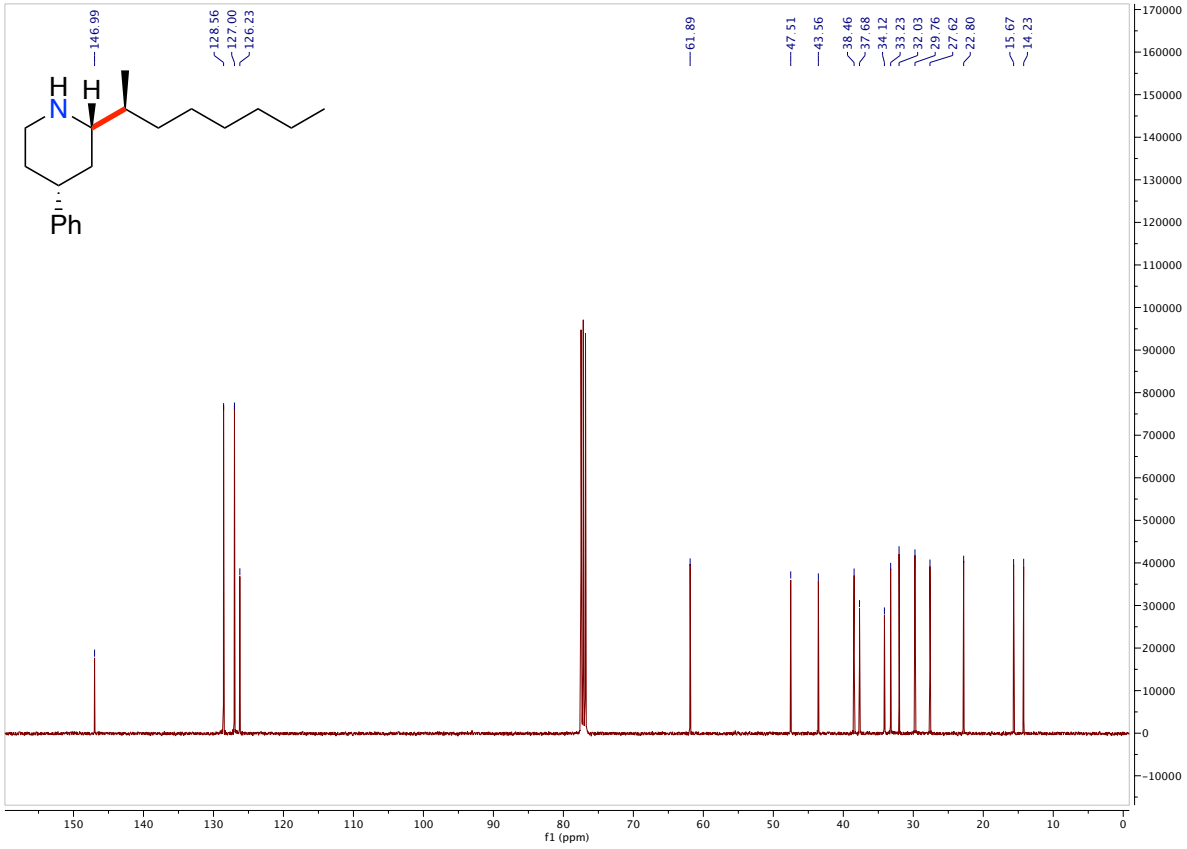

Figure. A.98. $^{13}C\{^{1}H\}$ NMR spectrum (101 MHz, $CDCl_3$, 298 K) of 2-(octan-2-yl)-4-phenylpiperidine.

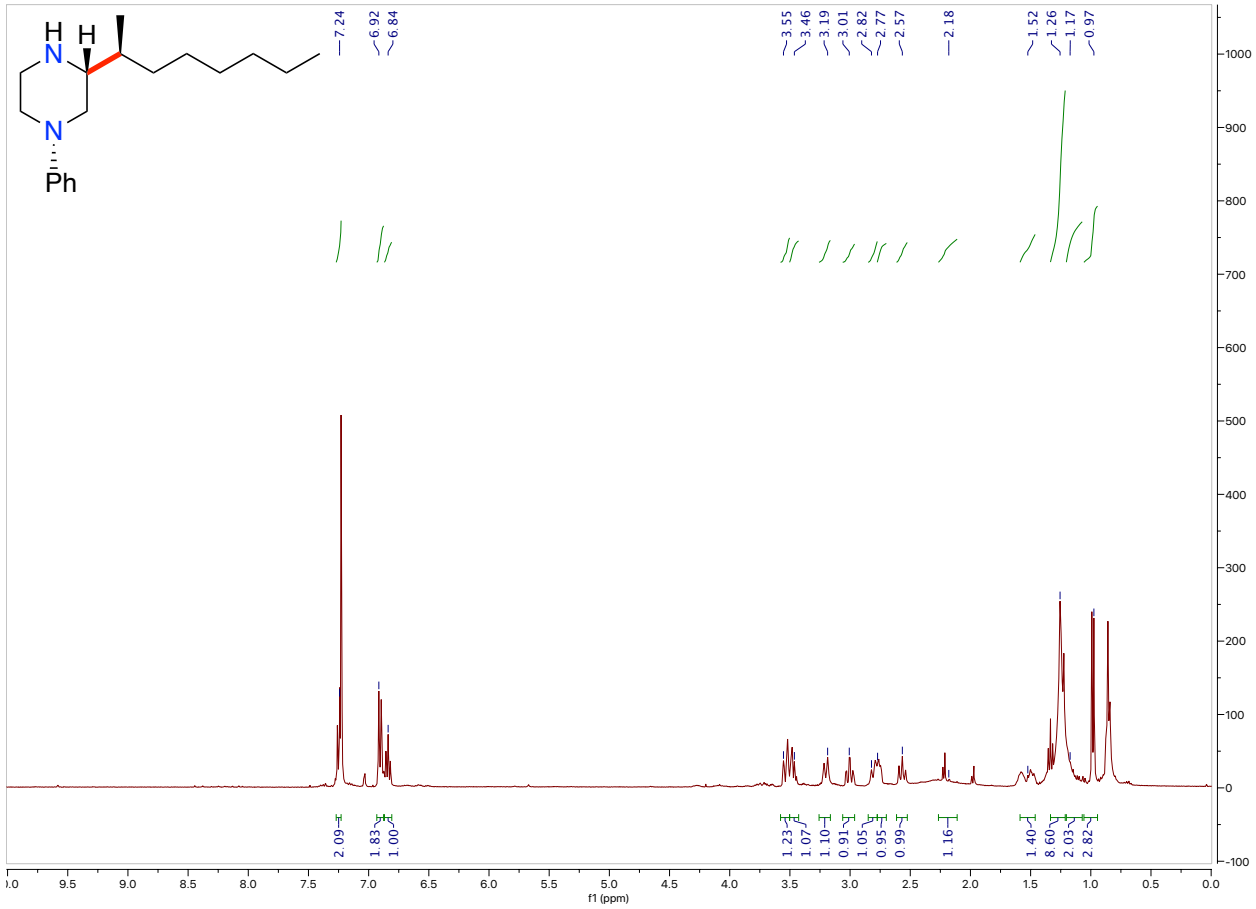

Figure. A.99. ^{1}H NMR spectrum (400 MHz, $CDCl_3$, 298 K) of 3-(octan-2-yl)-1-phenylpiperazine.

A.12 Chapter 4 Alkene Scope

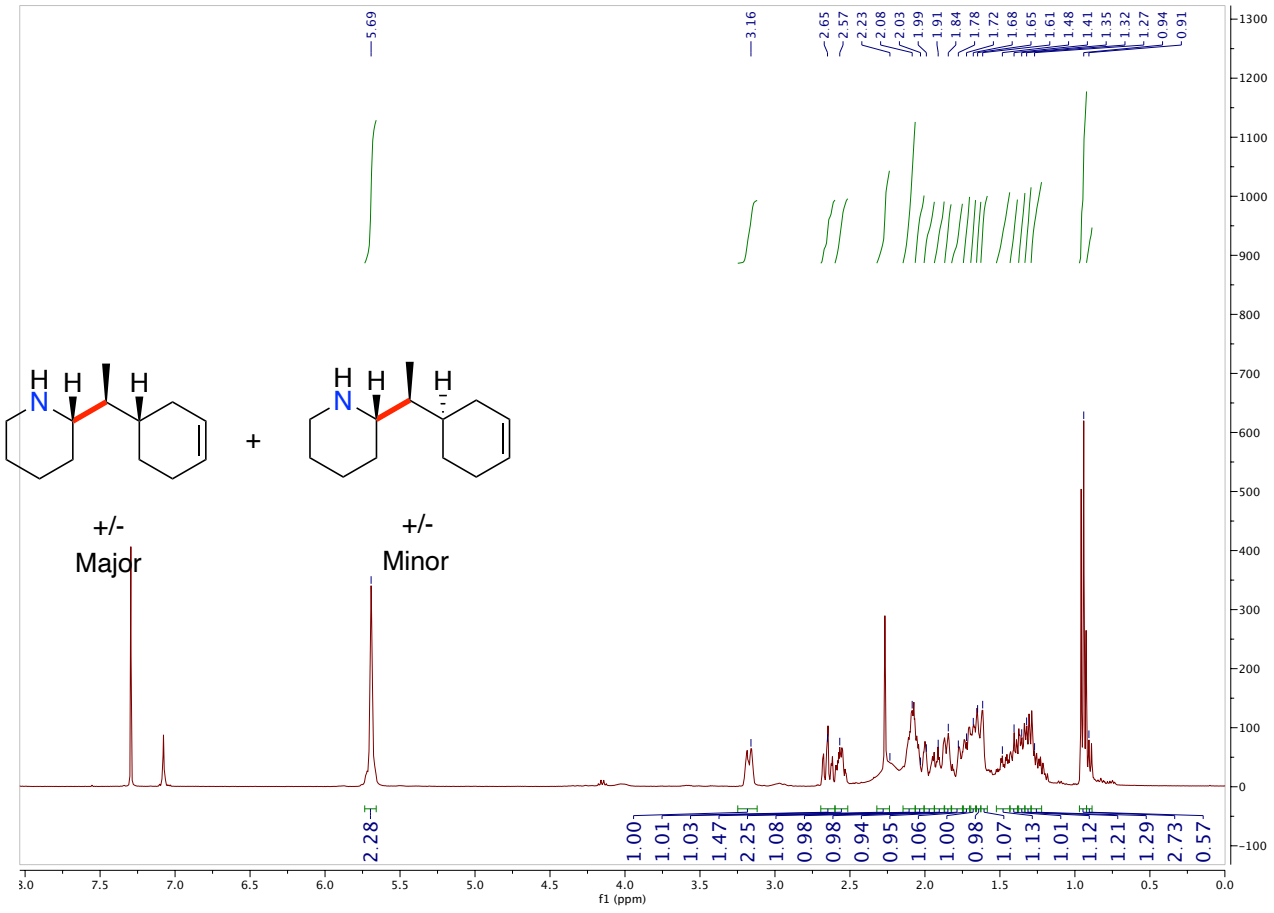

Figure. A.100. ^{1}H NMR spectrum (400 MHz, $CDCl_3$, 298 K) of 2-(1-(cyclohex-3-en-1-yl)ethyl)piperidine.

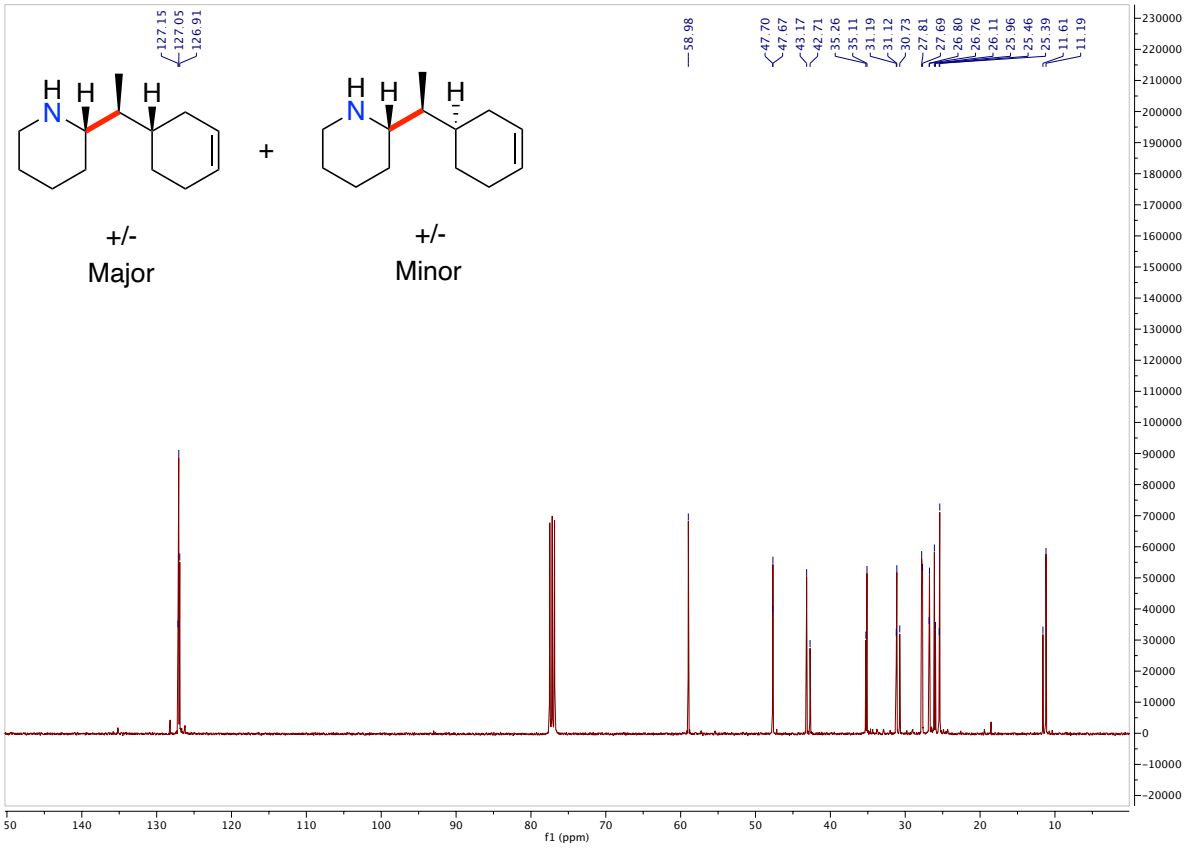

Figure. A.101. $^{13}C\{^{1}H\}$ NMR spectrum (101 MHz, $CDCl_3$, 298 K) of both diastereomers of 2-(1-(cyclohex-3-en-1-yl)ethyl)piperidine.

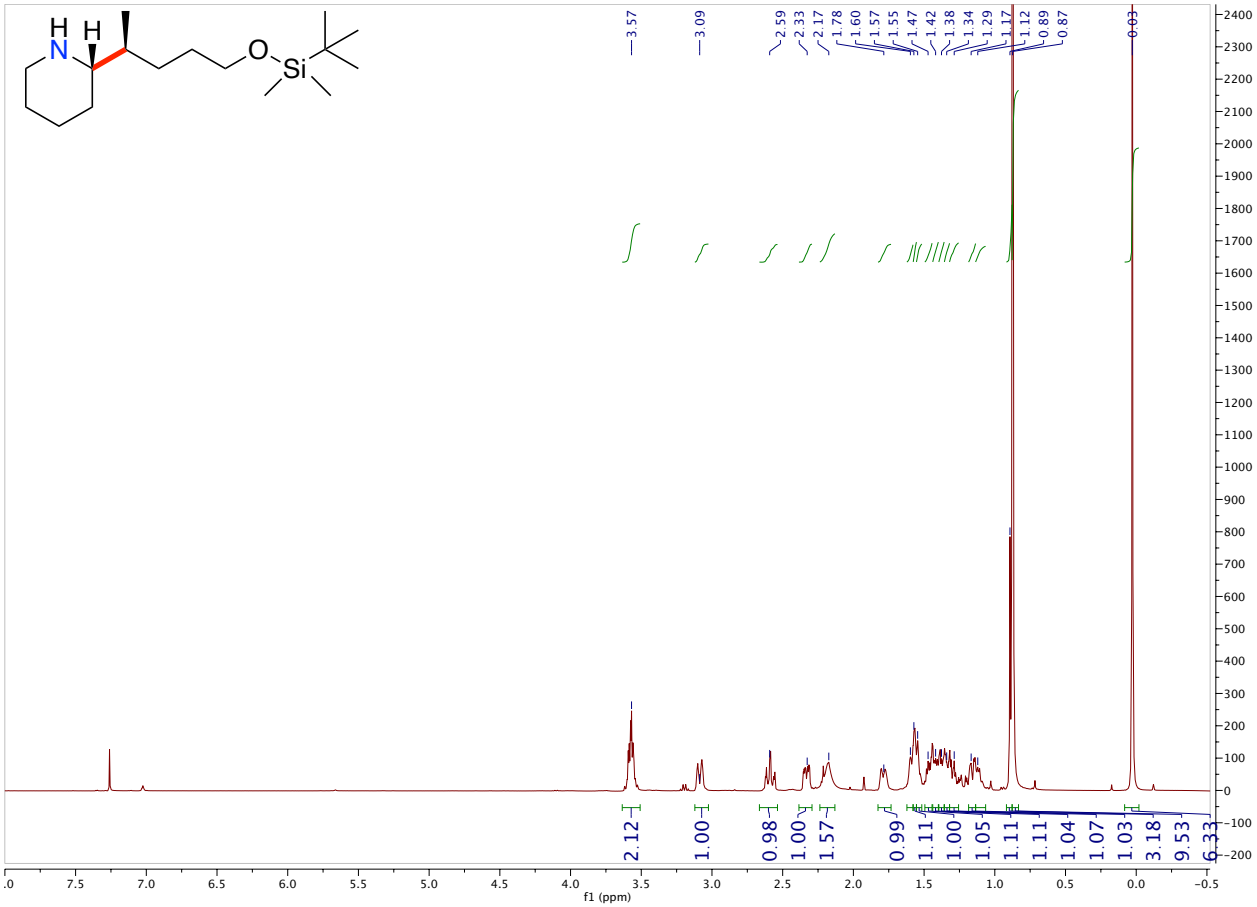

Figure. A.102. ^{1}H NMR spectrum (400 MHz, $CDCl_3$, 298 K) of 2-(5-((tert-butyldimethylsilyl)oxy)pentan-2-yl)piperidine.

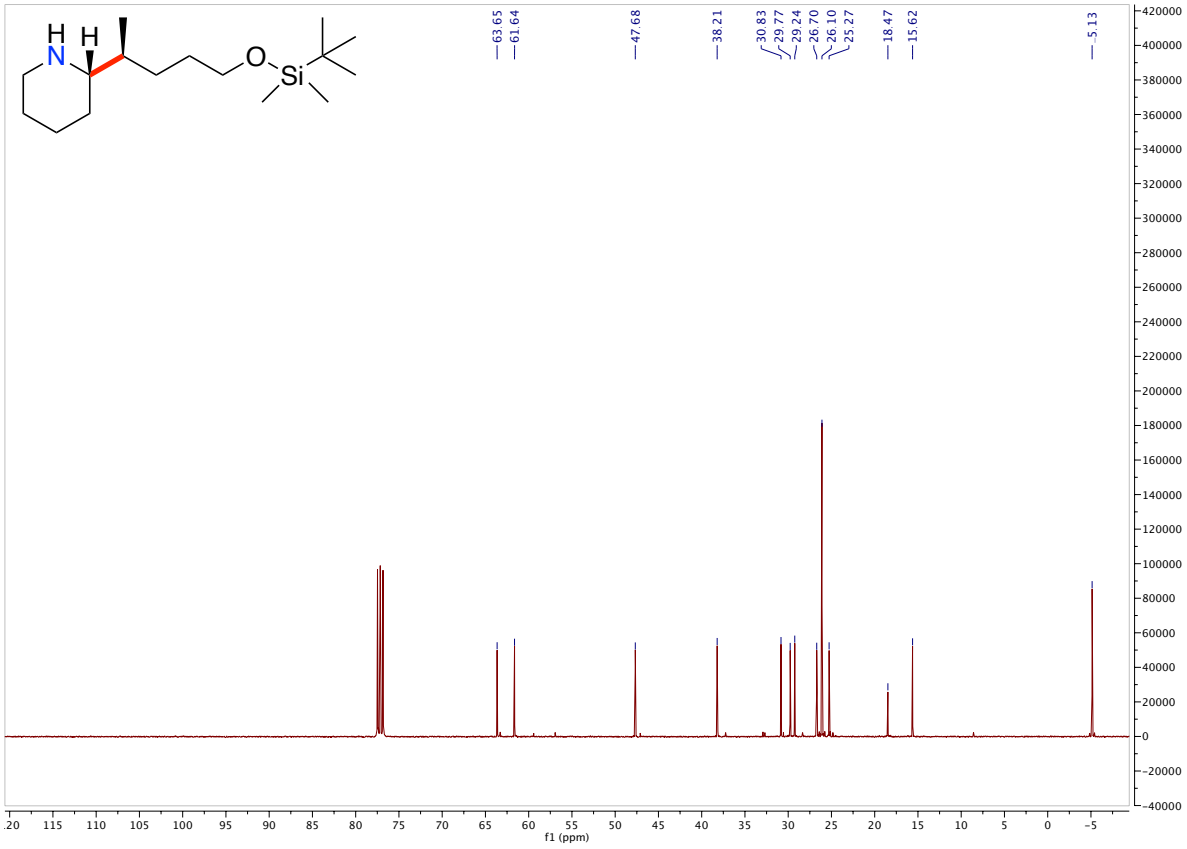

Figure. A.103. $^{13}C\{^{1}H\}$ NMR spectrum (101 MHz, $CDCl_3$, 298 K) of 2-(5-((tert-butyldimethylsilyl)oxy)pentan-2-yl)piperidine.

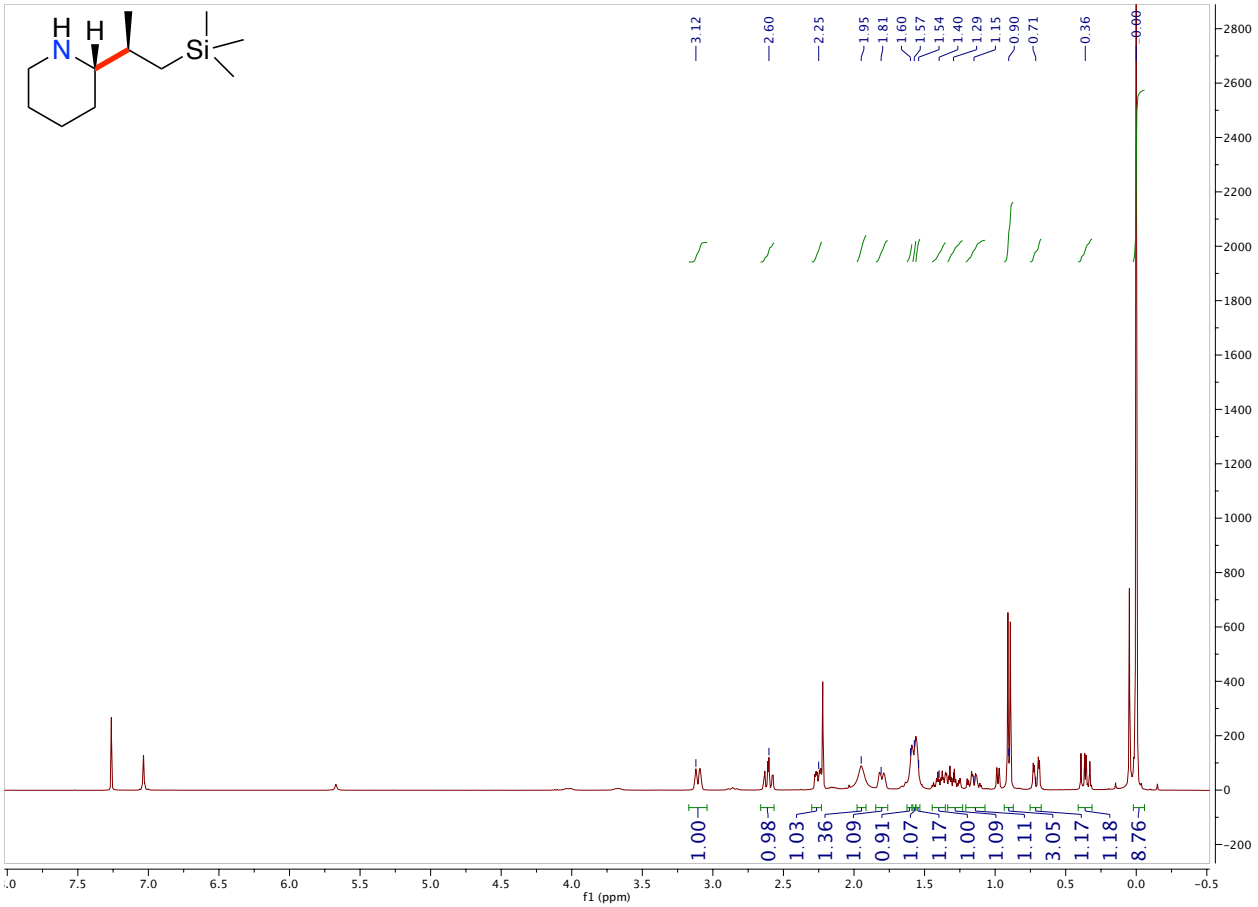

Figure. A.104. ^{1}H NMR spectrum (400 MHz, $CDCl_3$, 298 K) of 2-(1-(trimethylsilyl)propan-2-yl)piperidine.

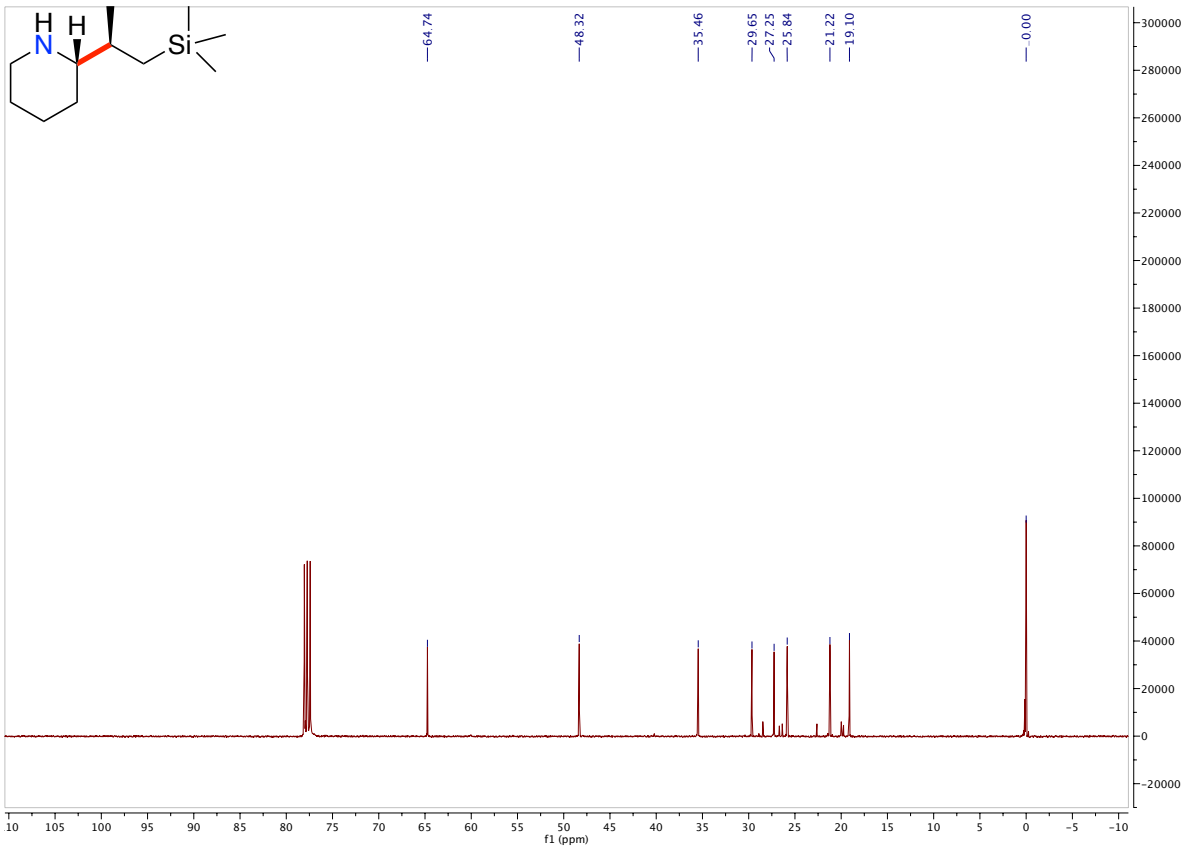

Figure. A.105. $^{13}C\{^{1}H\}$ NMR spectrum (101 MHz, $CDCl_3$, 298 K) of 2-(1-(trimethylsilyl)propan-2-yl)piperidine.

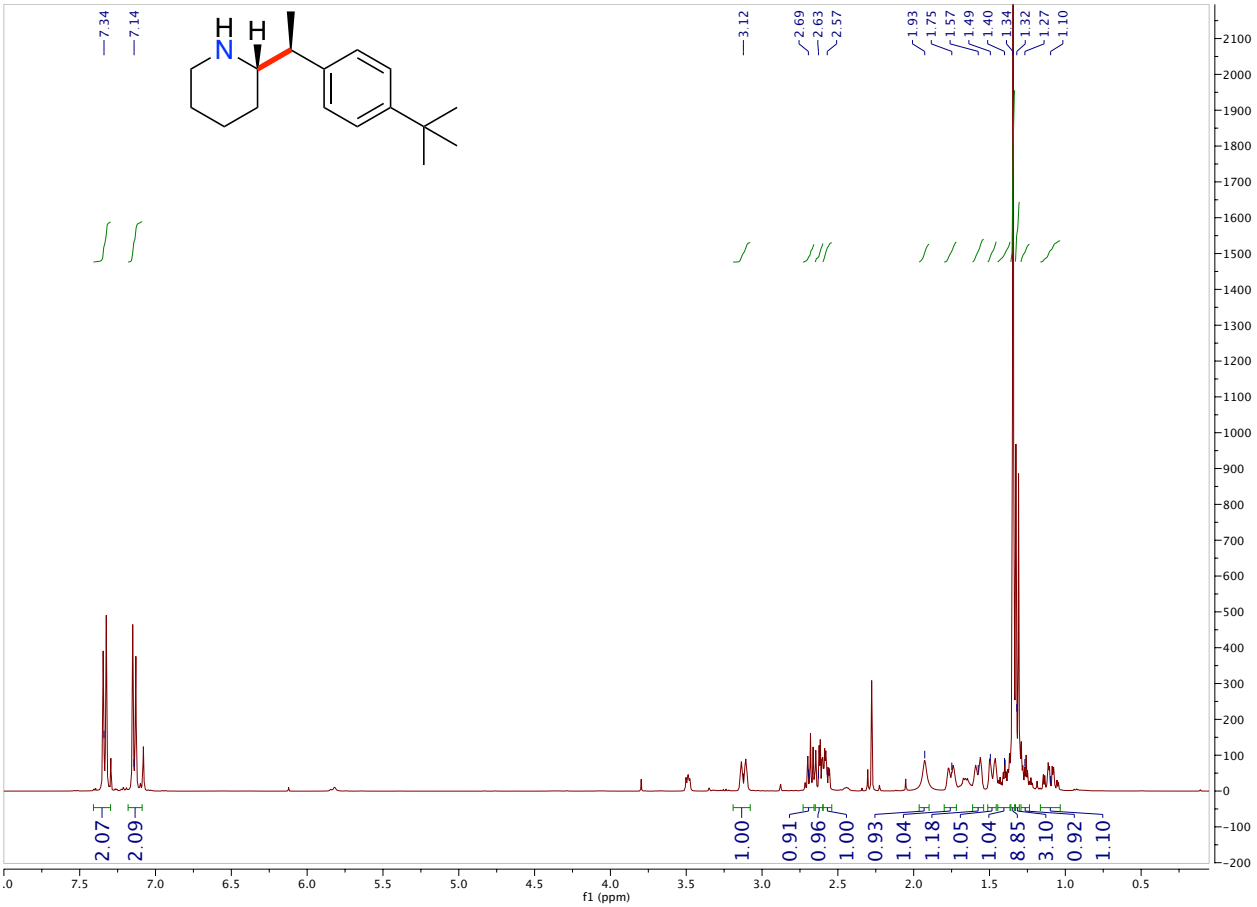

Figure. A.106. ^{1}H NMR spectrum (400 MHz, $CDCl_3$, 298 K) of 2-(1-(4-(tert-butyl)phenyl)ethyl)piperidine.

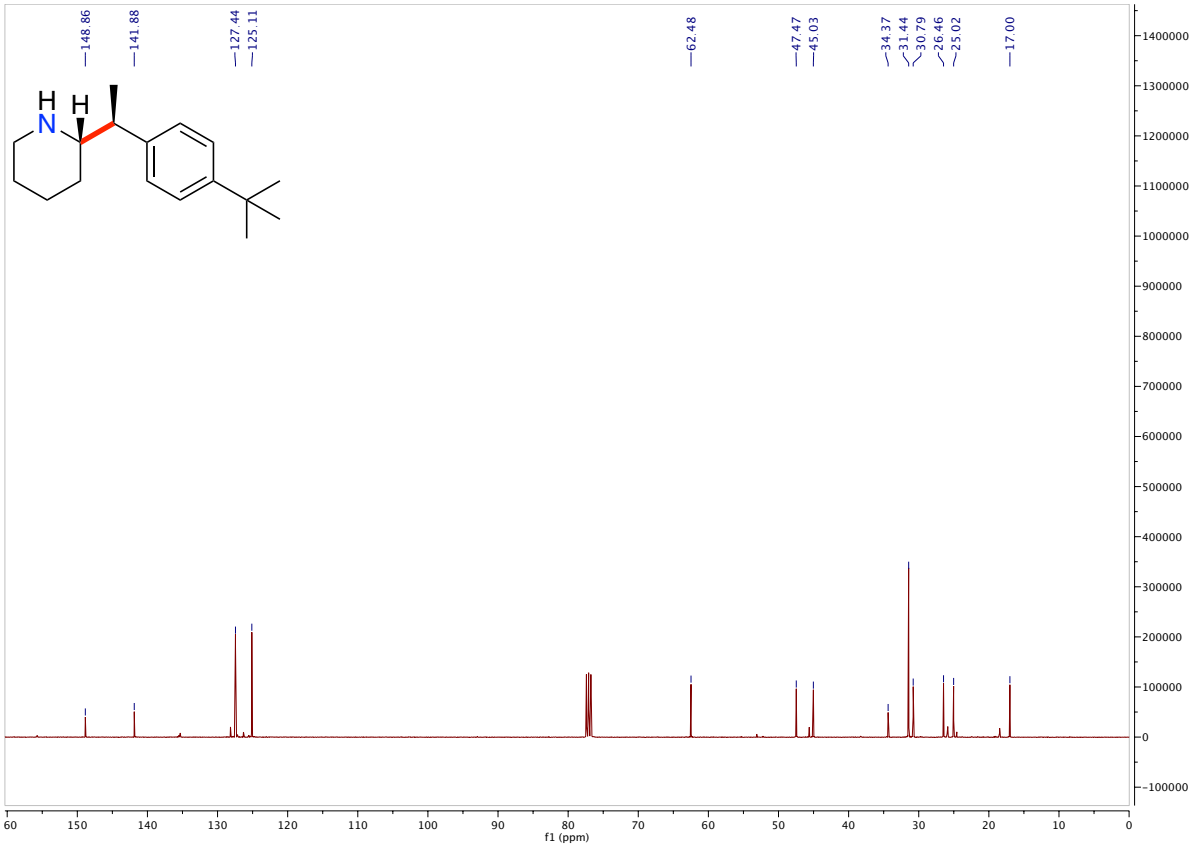

Figure. A.107. $^{13}C\{^{1}H\}$ NMR spectrum (101 MHz, $CDCl_3$, 298 K) 2-(1-(4-(tert-butyl)phenyl)ethyl)piperidine.

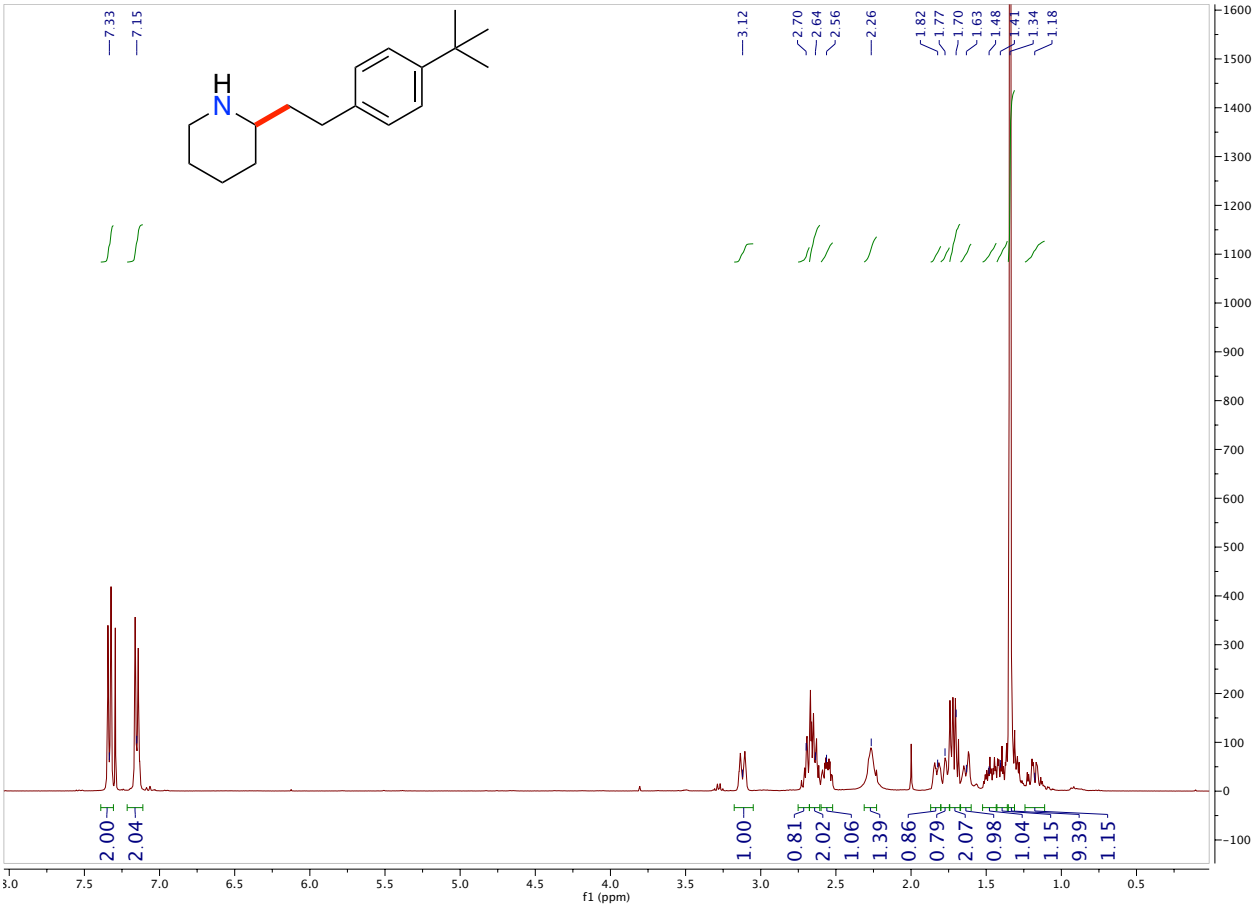

Figure. A.108. ^{1}H NMR spectrum (400 MHz, $CDCl_3$, 298 K) of 2-(4-(tert-butyl)phenethyl)piperidine.

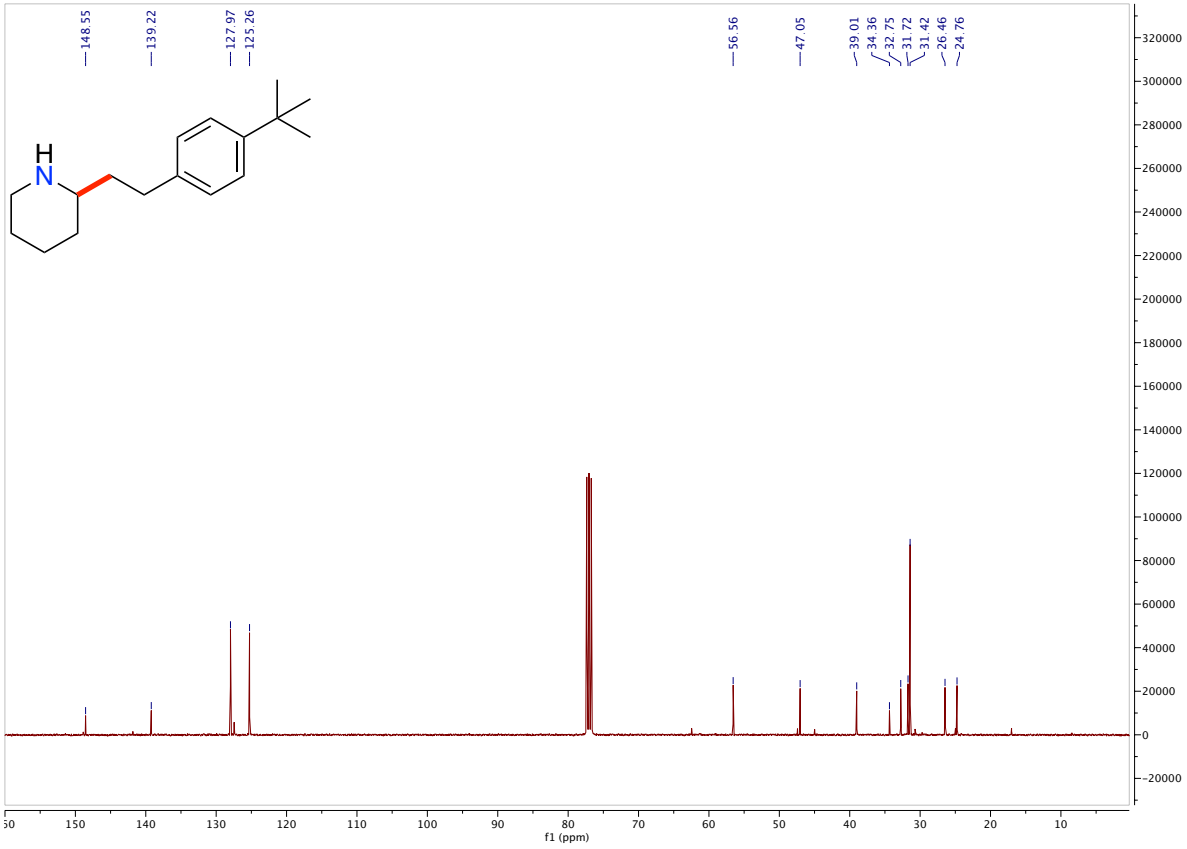

Figure. A.109. $^{13}C\{^{1}H\}$ NMR spectrum (101 MHz, $CDCl_3$, 298 K) 2-(4-(tert-butyl)phenethyl)piperidine.

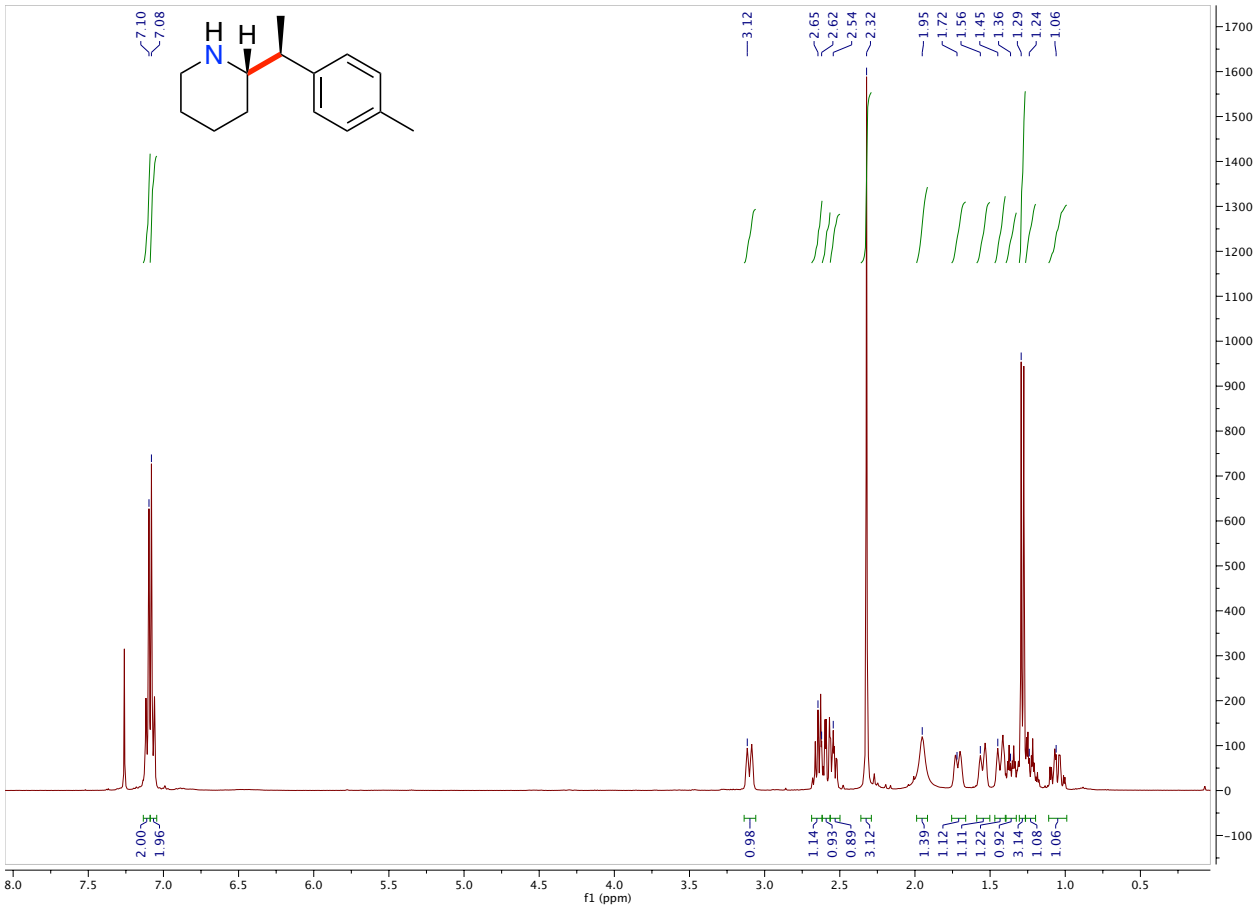

Figure. A.110. ^{1}H NMR spectrum (400 MHz, $CDCl_3$, 298 K) of 2-(1-(p-tolyl)ethyl)piperidine.

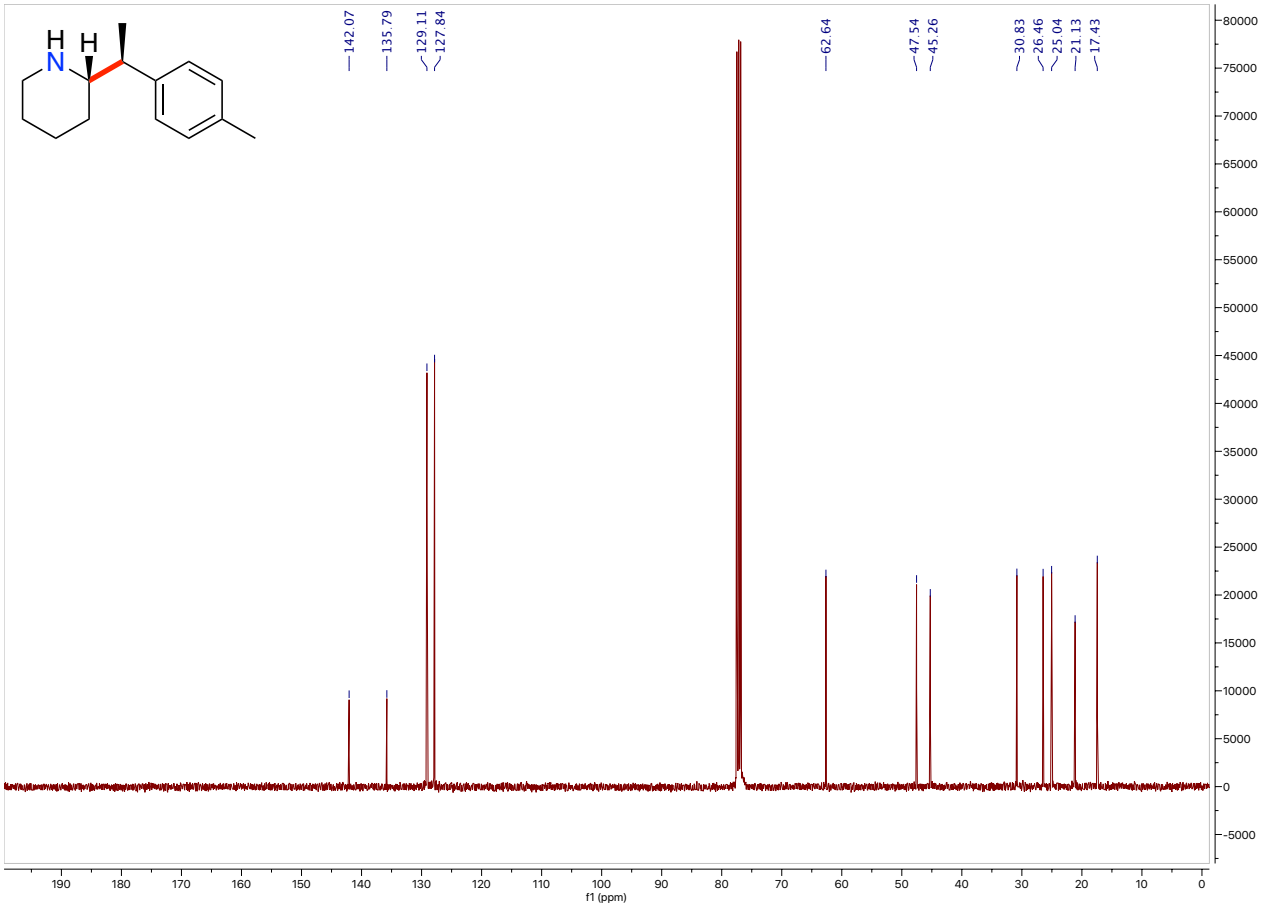

Figure. A.111. $^{13}C\{^{1}H\}$ NMR spectrum (101 MHz, $CDCl_3$, 298 K) of 2-(1-(p-tolyl)ethyl)piperidine.

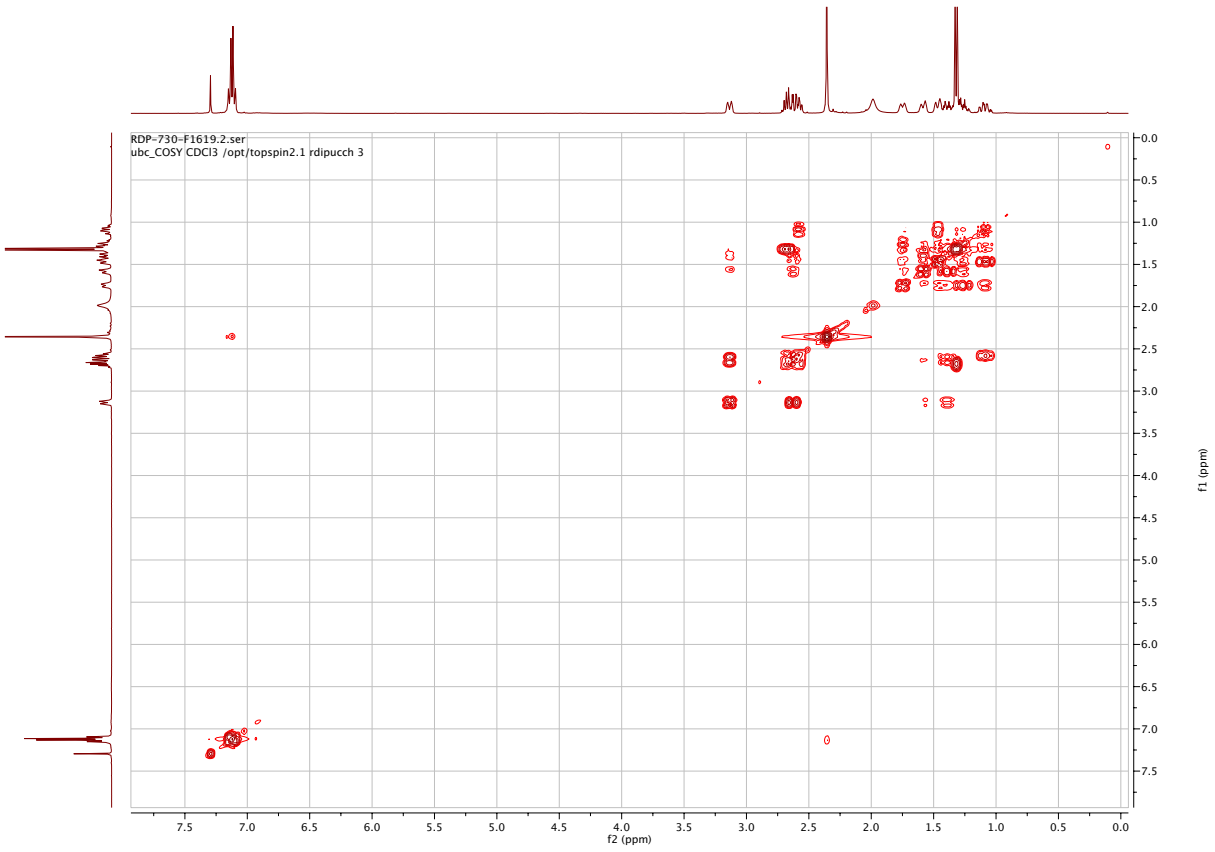

Figure. A.112. COSY spectrum (400 MHz, $CDCl_3$, 298 K) of 2-(1-(p-tolyl)ethyl)piperidine.

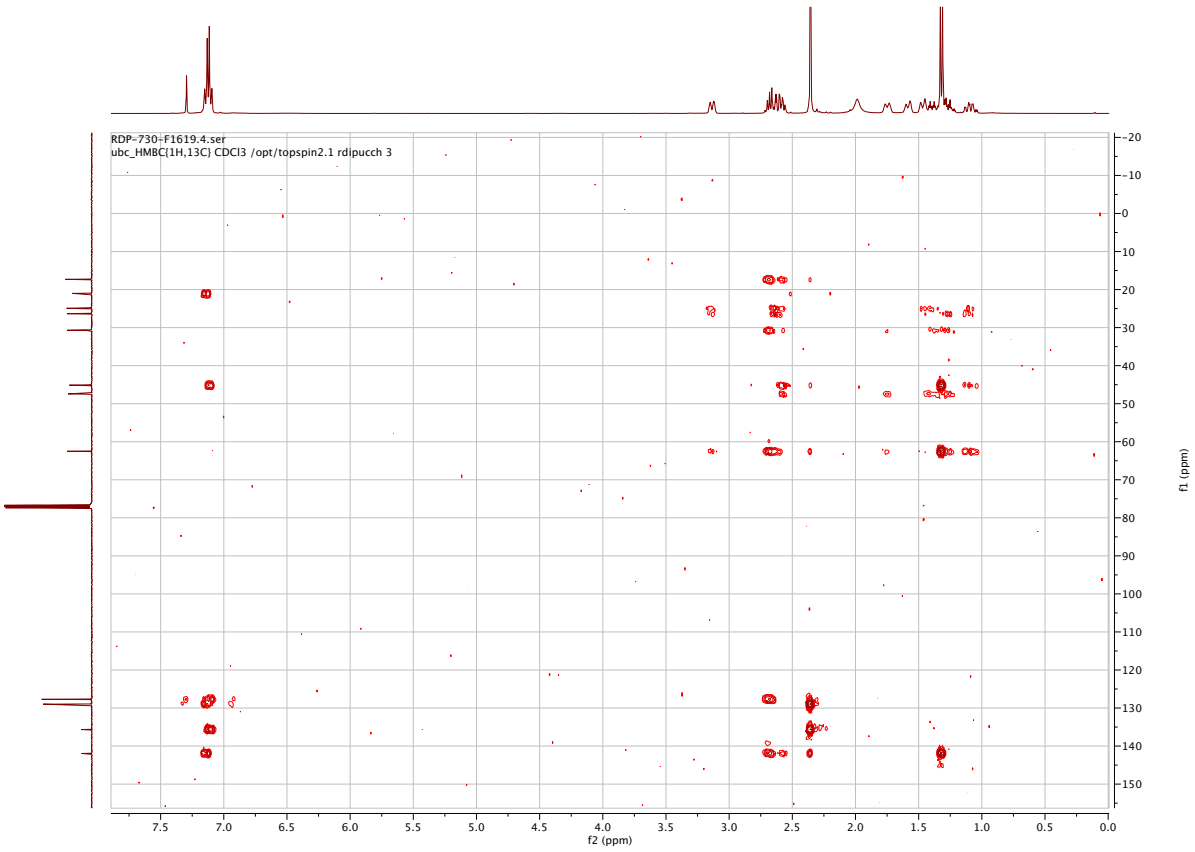

Figure. A.113. HMBC spectrum (101 MHz, $CDCl_3$, 298 K) 2-(1-(p-tolyl)ethyl)piperidine.

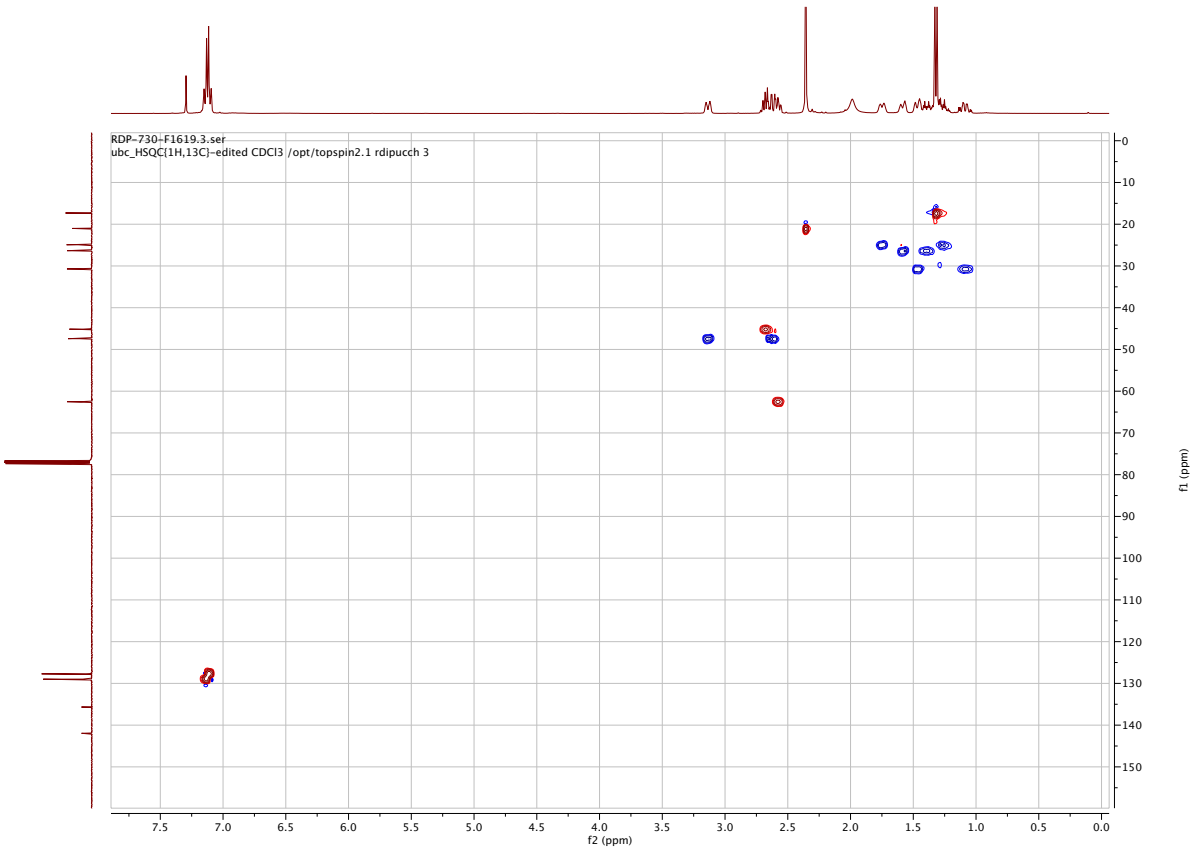

Figure. A.114. HSQC spectrum (101 MHz, $CDCl_3$, 298 K) 2-(1-(p-tolyl)ethyl)piperidine.

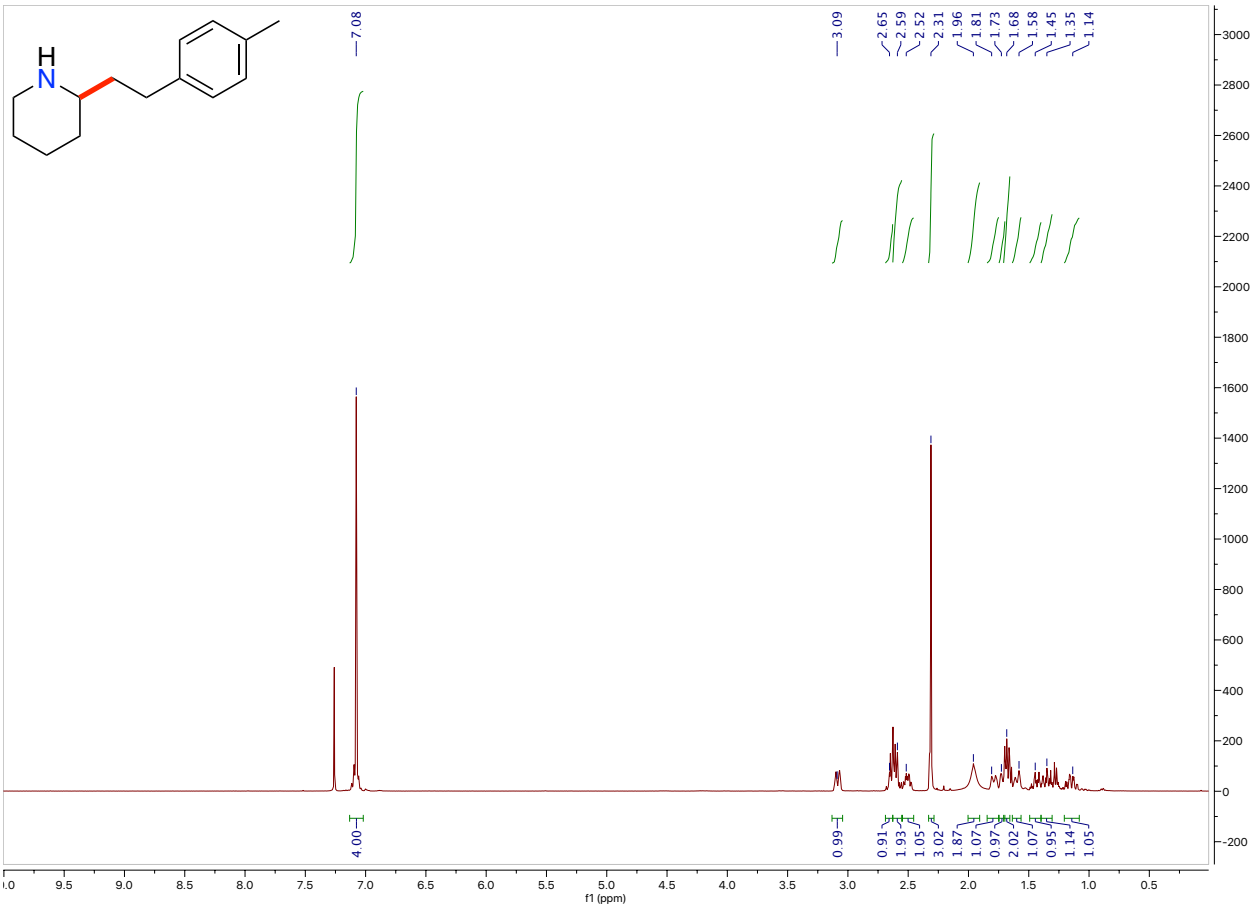

Figure. A.115. ^{1}H NMR spectrum (400 MHz, $CDCl_3$, 298 K) of 2-(4-methylphenethyl)piperidine.

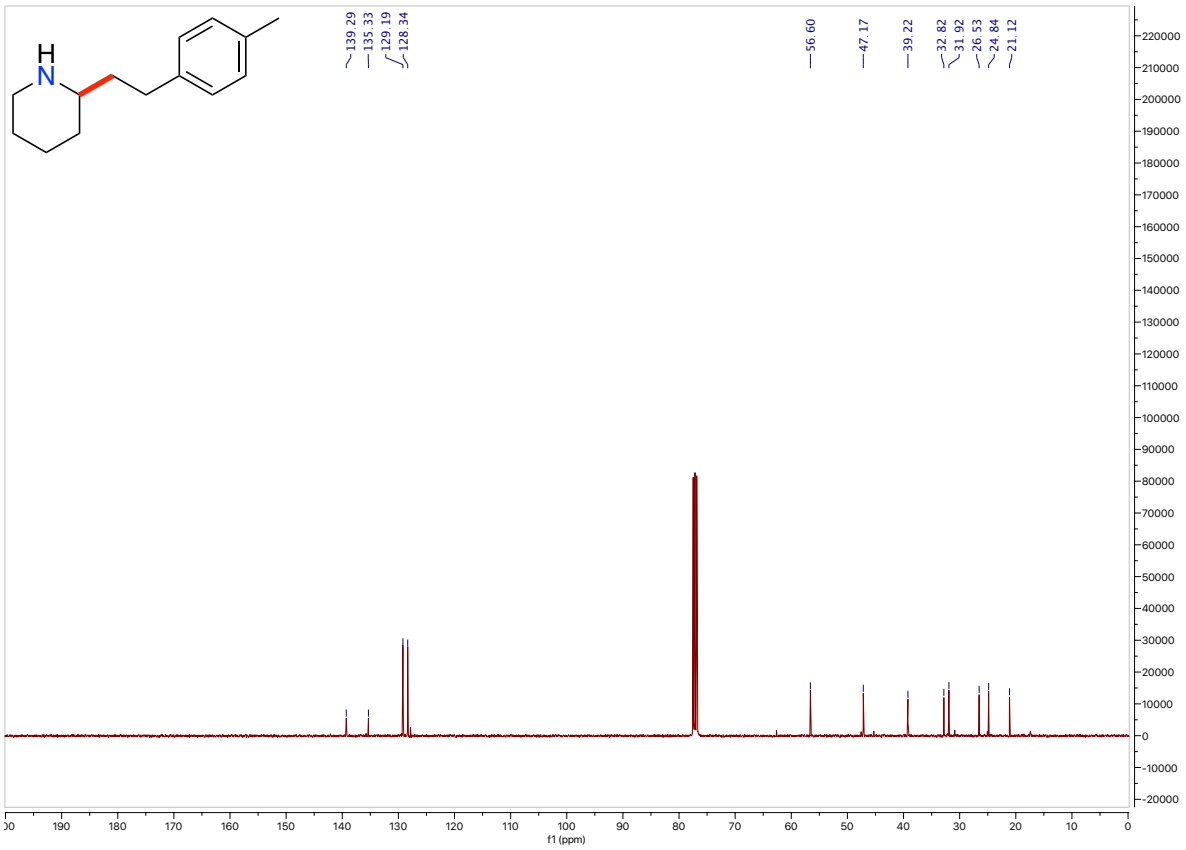

Figure. A.116. $^{13}C\{^{1}H\}$ NMR spectrum (101 MHz, $CDCl_3$, 298 K) of 2-(4-methylphenethyl)piperidine.

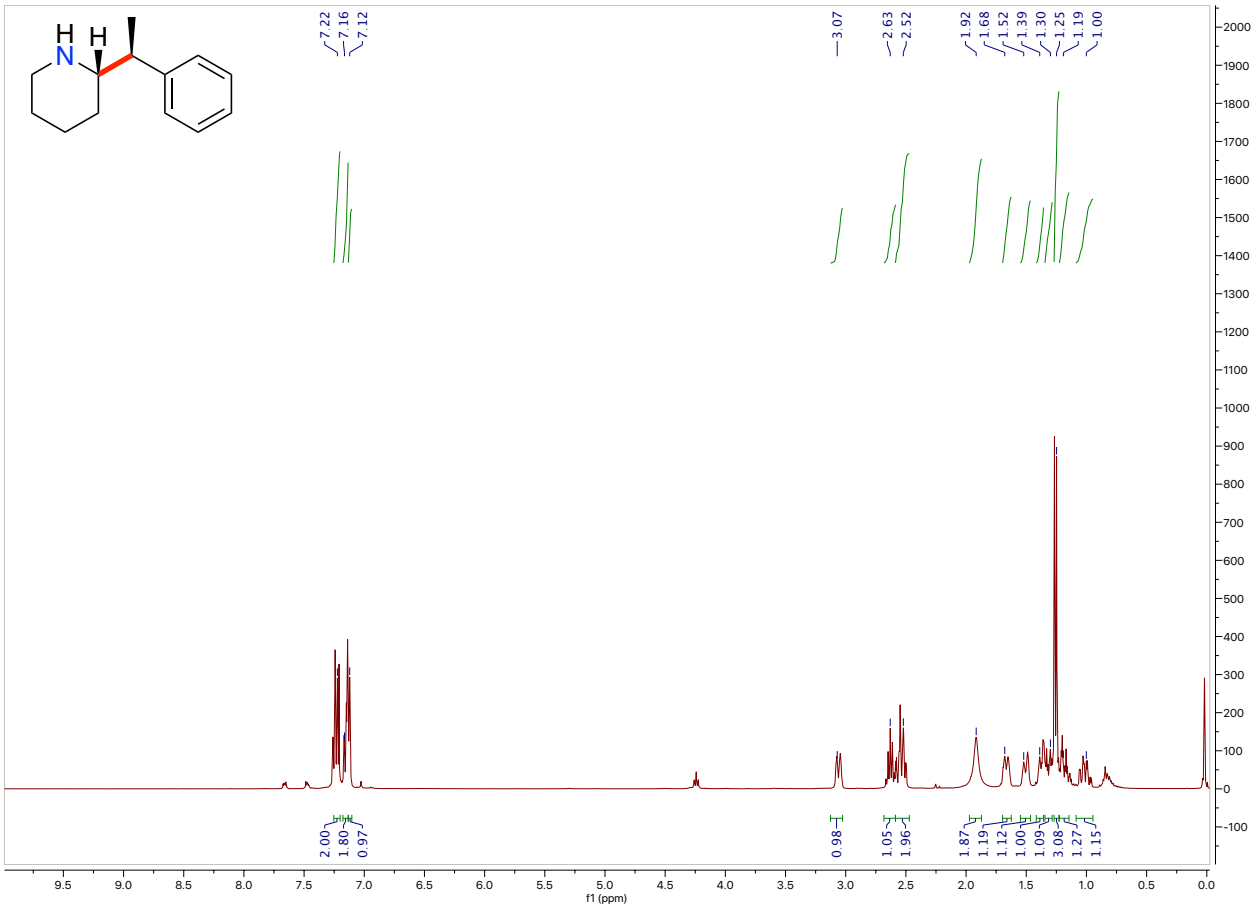

Figure. A.117. ^{1}H NMR spectrum (400 MHz, $CDCl_3$, 298 K) of 2-(1-phenylethyl)piperidine.

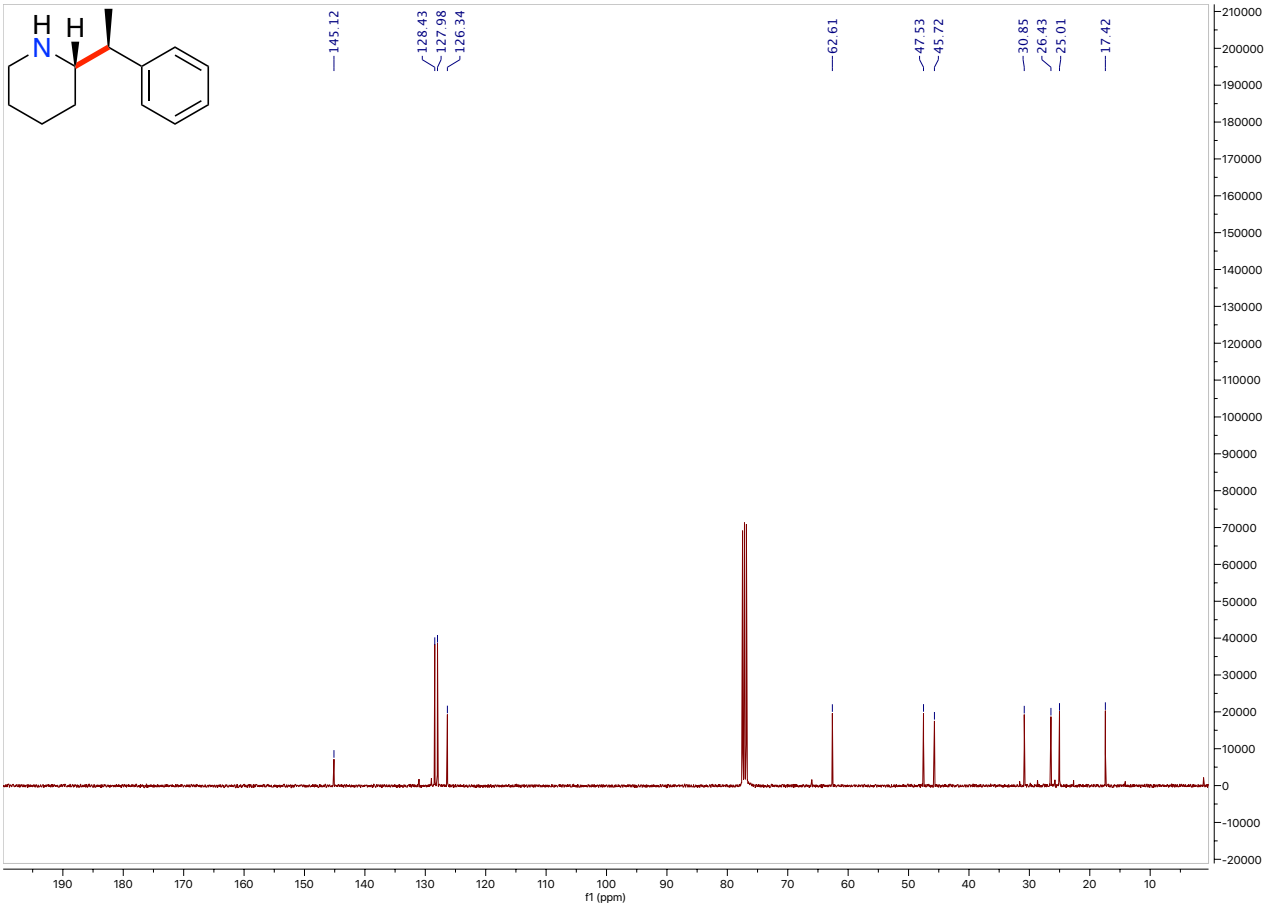

Figure. A.118. $^{13}C\{^{1}H\}$ NMR spectrum (101 MHz, $CDCl_3$, 298 K) of 2-(1-phenylethyl)piperidine.

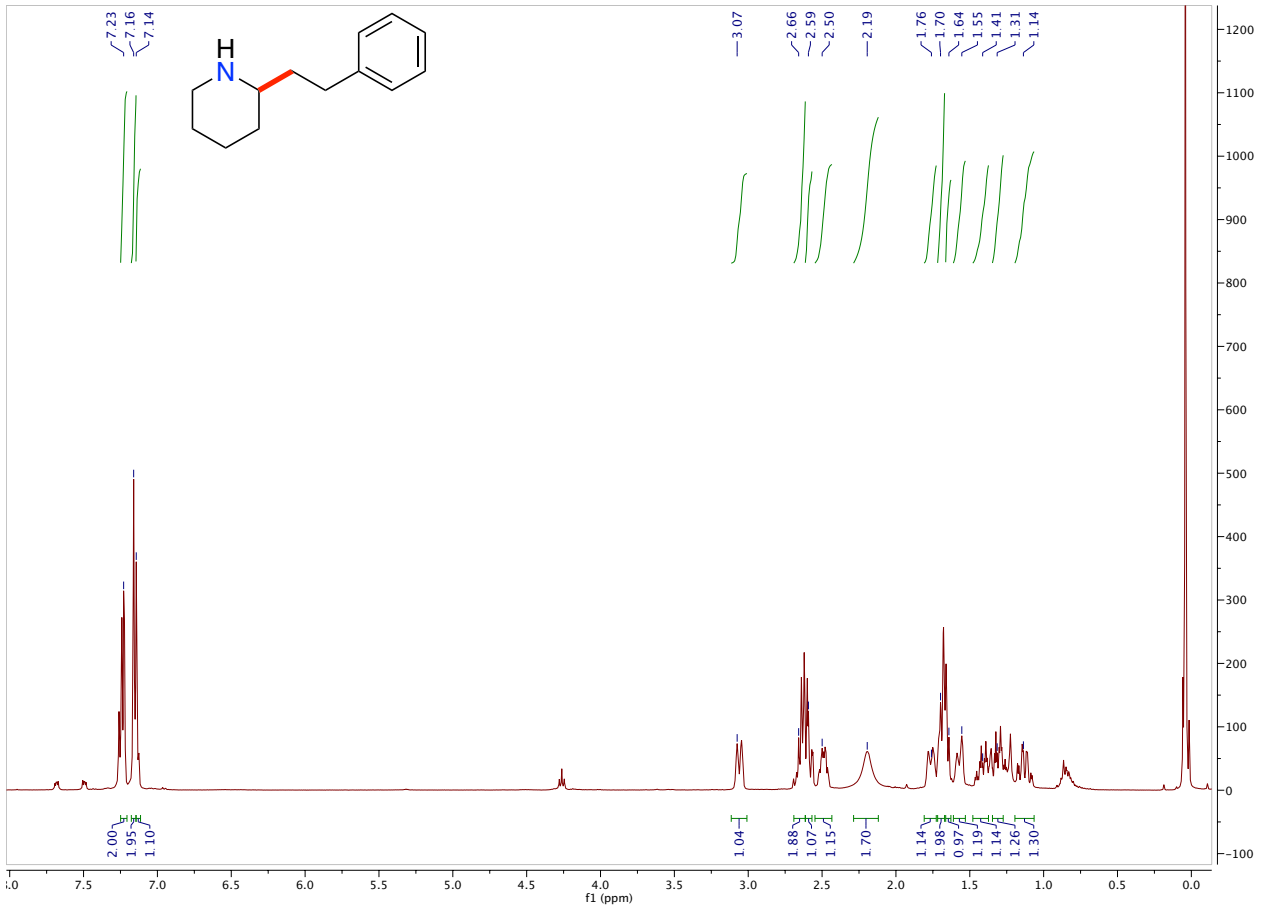

Figure. A.119. ^{1}H NMR spectrum (400 MHz, $CDCl_3$, 298 K) of 2-phenethylpiperidine.

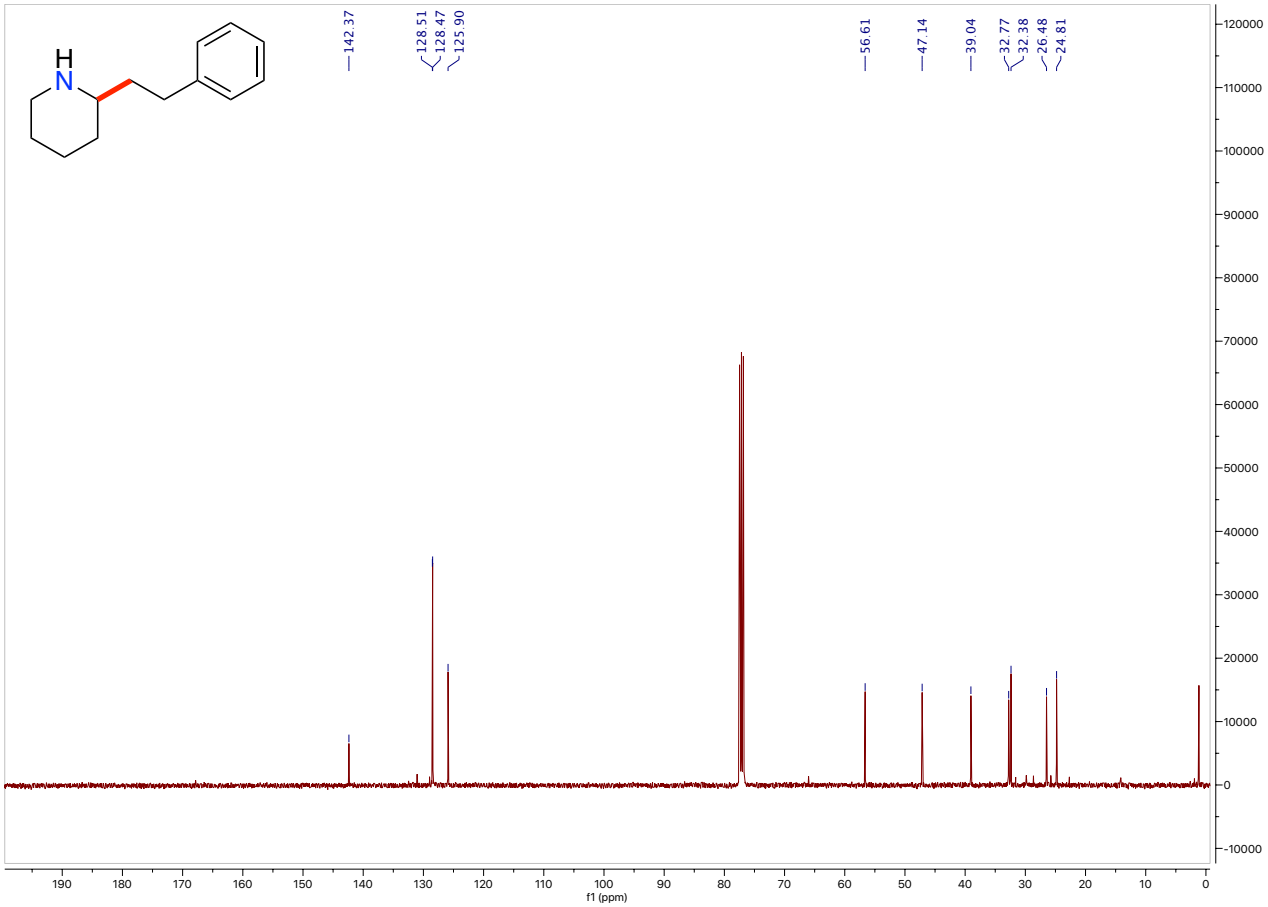

Figure. A.120. $^{13}C\{^{1}H\}$ NMR spectrum (101 MHz, $CDCl_3$, 298 K) of 2-phenethylpiperidine.

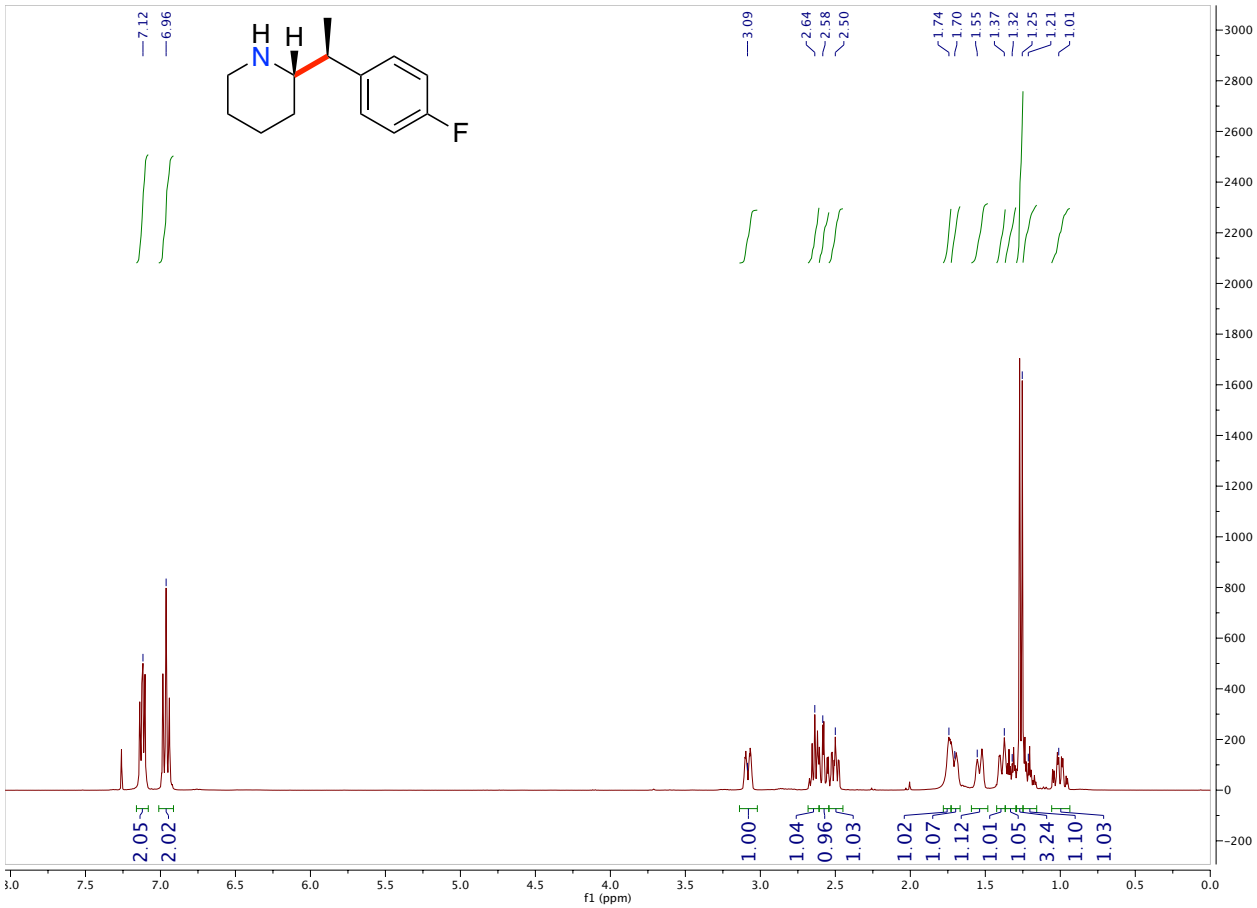

Figure. A.121. ^{1}H NMR spectrum (400 MHz, $CDCl_3$, 298 K) of 2-(1-(4-fluorophenyl)ethyl)piperidine.

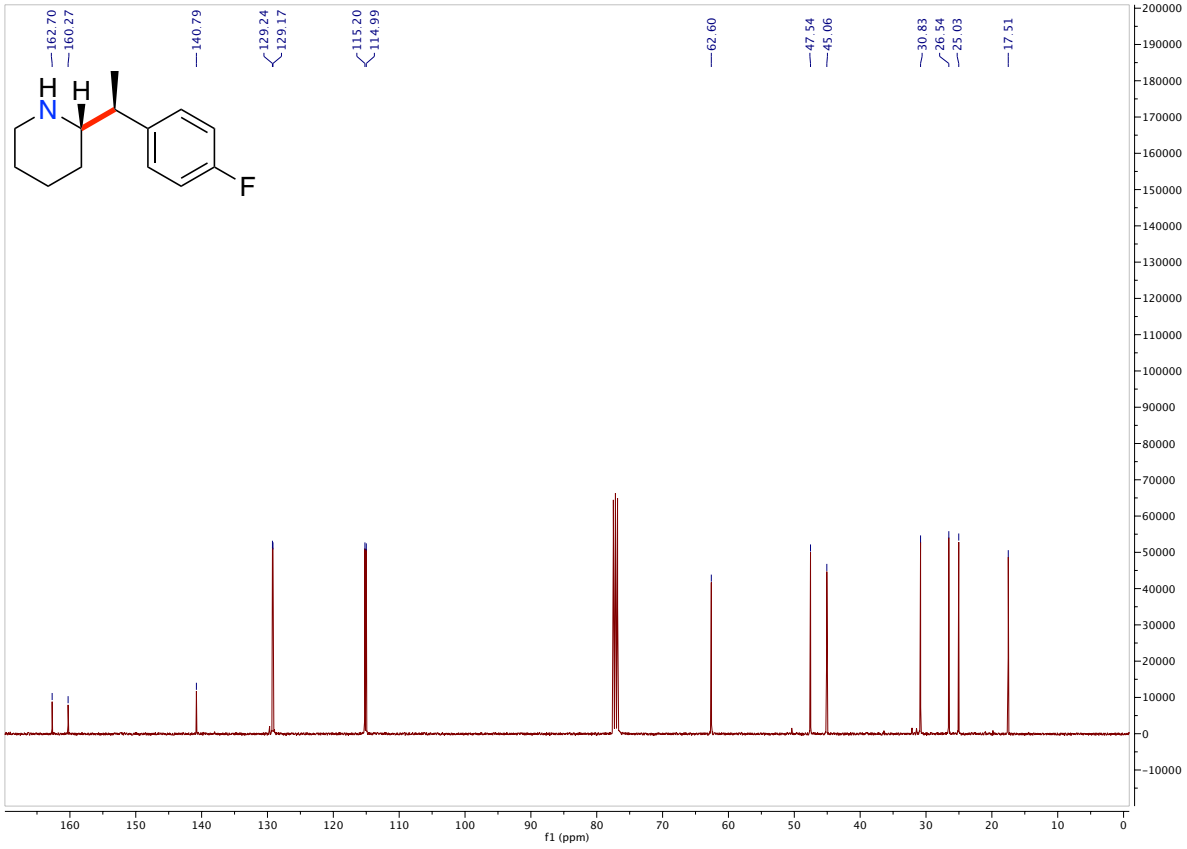

Figure. A.122. $^{13}C\{^{1}H\}$ NMR spectrum (101 MHz, $CDCl_3$, 298 K) 2-(1-(4-fluorophenyl)ethyl)piperidine.

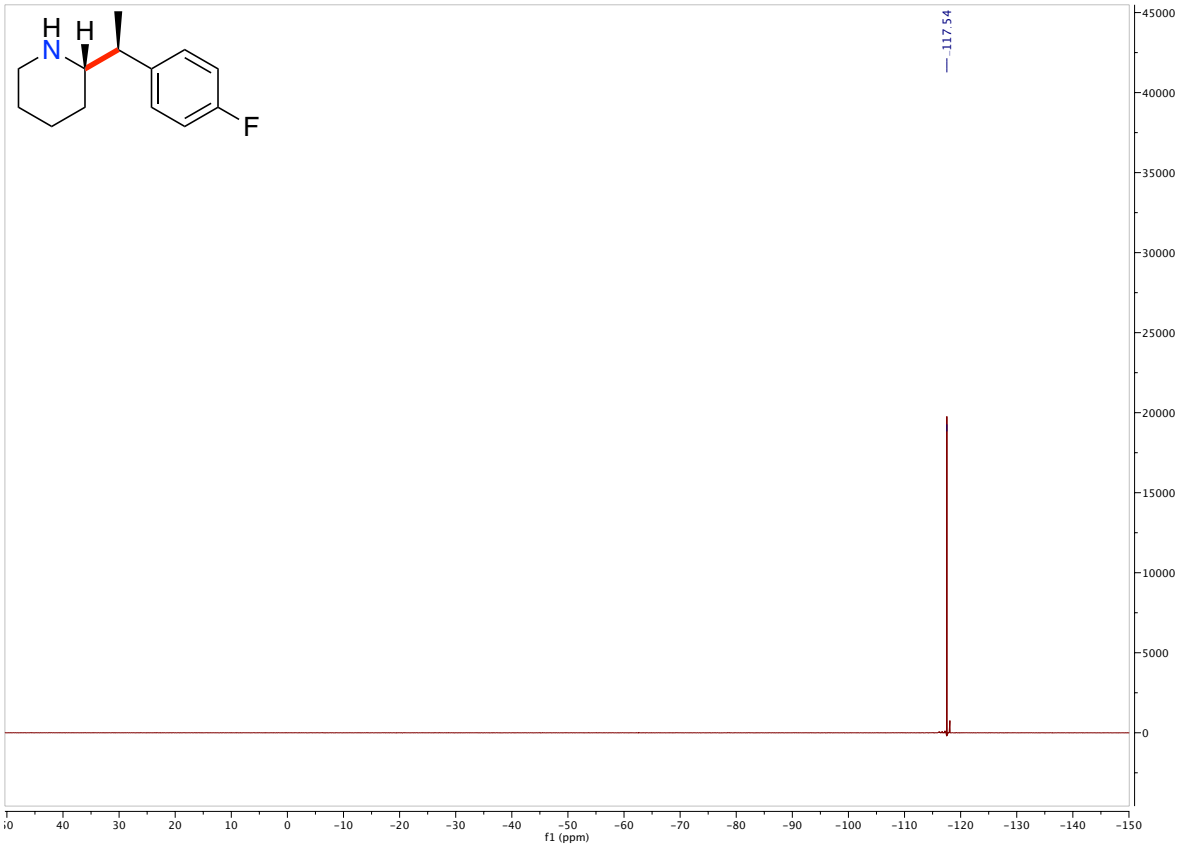

Figure. A.123. ^{19}F NMR spectrum (101 MHz, $CDCl_3$, 298 K) 2-(1-(4-fluorophenyl)ethyl)piperidine

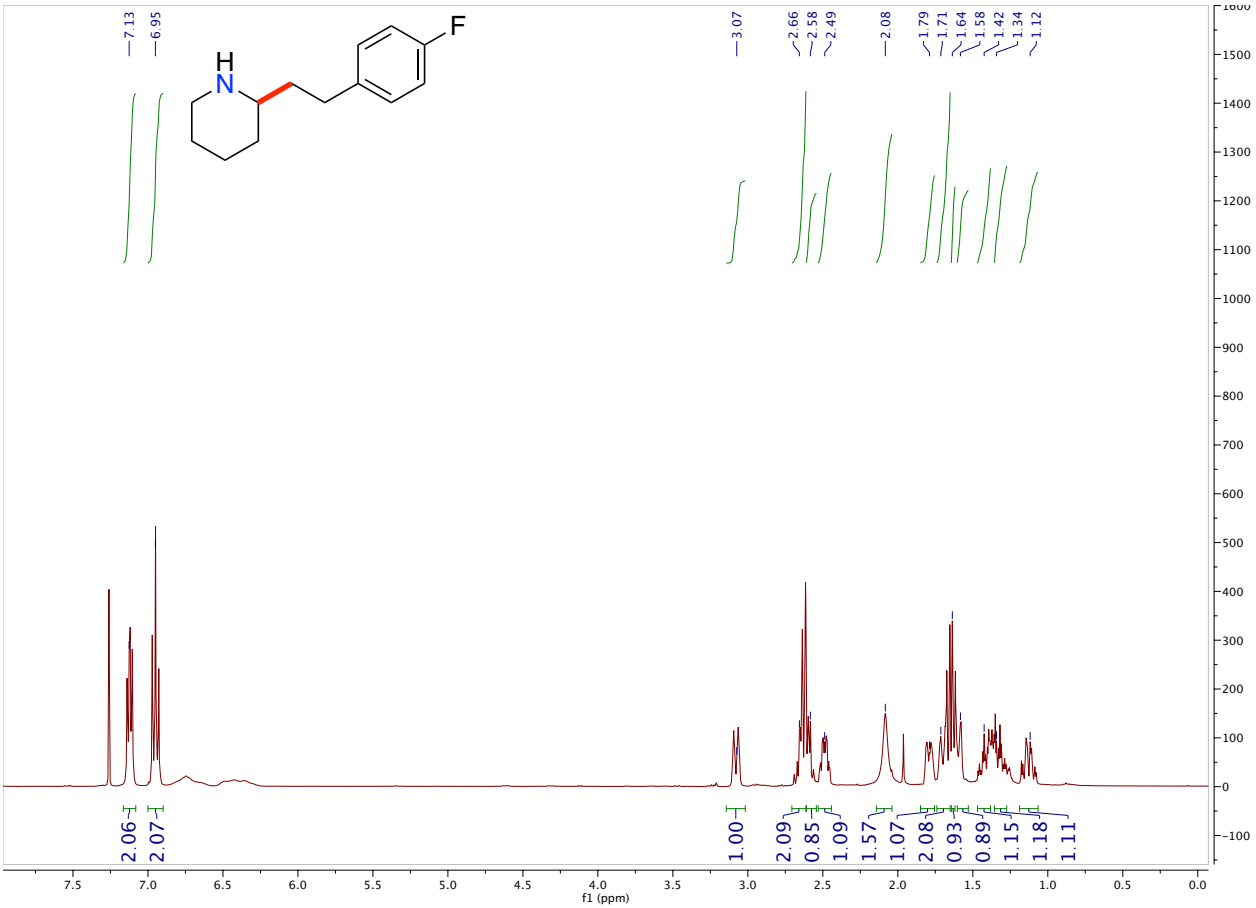

Figure. A.124. ^{1}H NMR spectrum (400 MHz, $CDCl_3$, 298 K) of 2-(4-fluorophenethyl)piperidine.

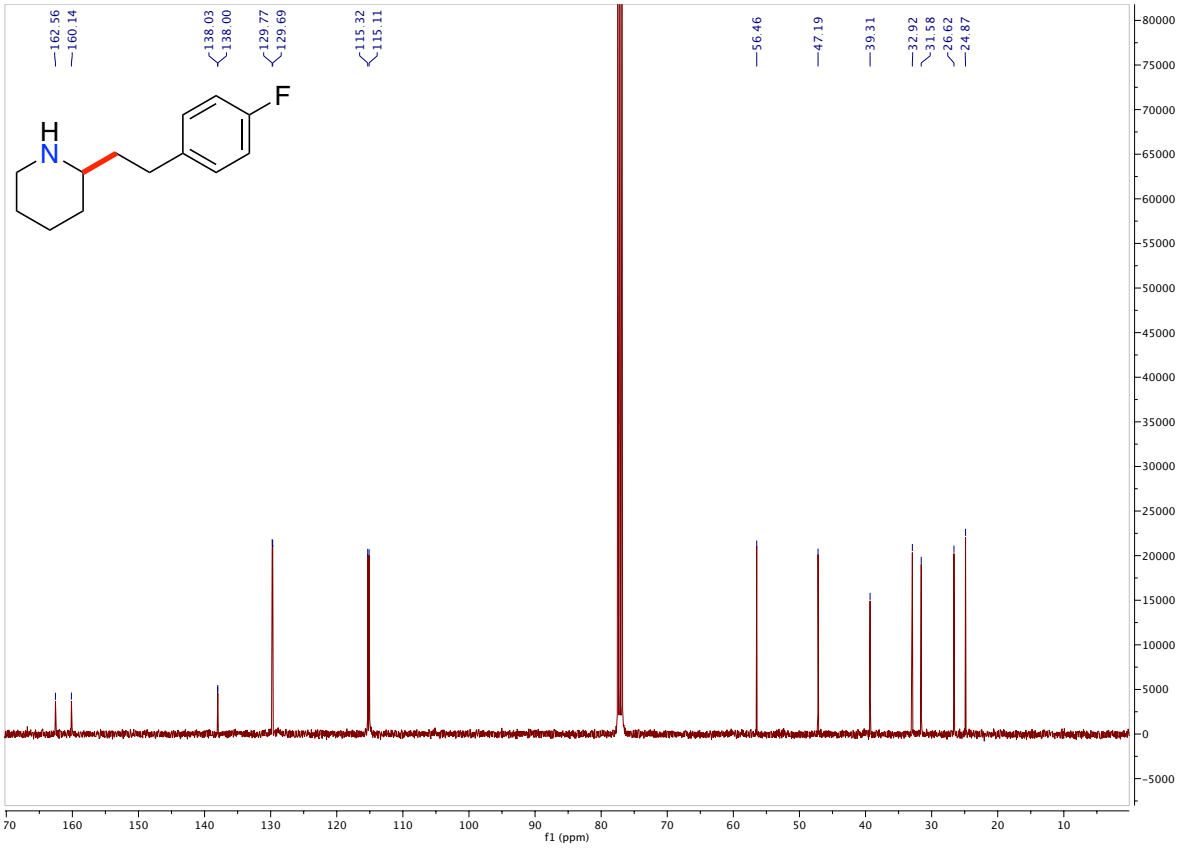

Figure. A.125. $^{13}C\{^{1}H\}$ NMR spectrum (101 MHz, $CDCl_3$, 298 K) 2-(4-fluorophenethyl)piperidine.

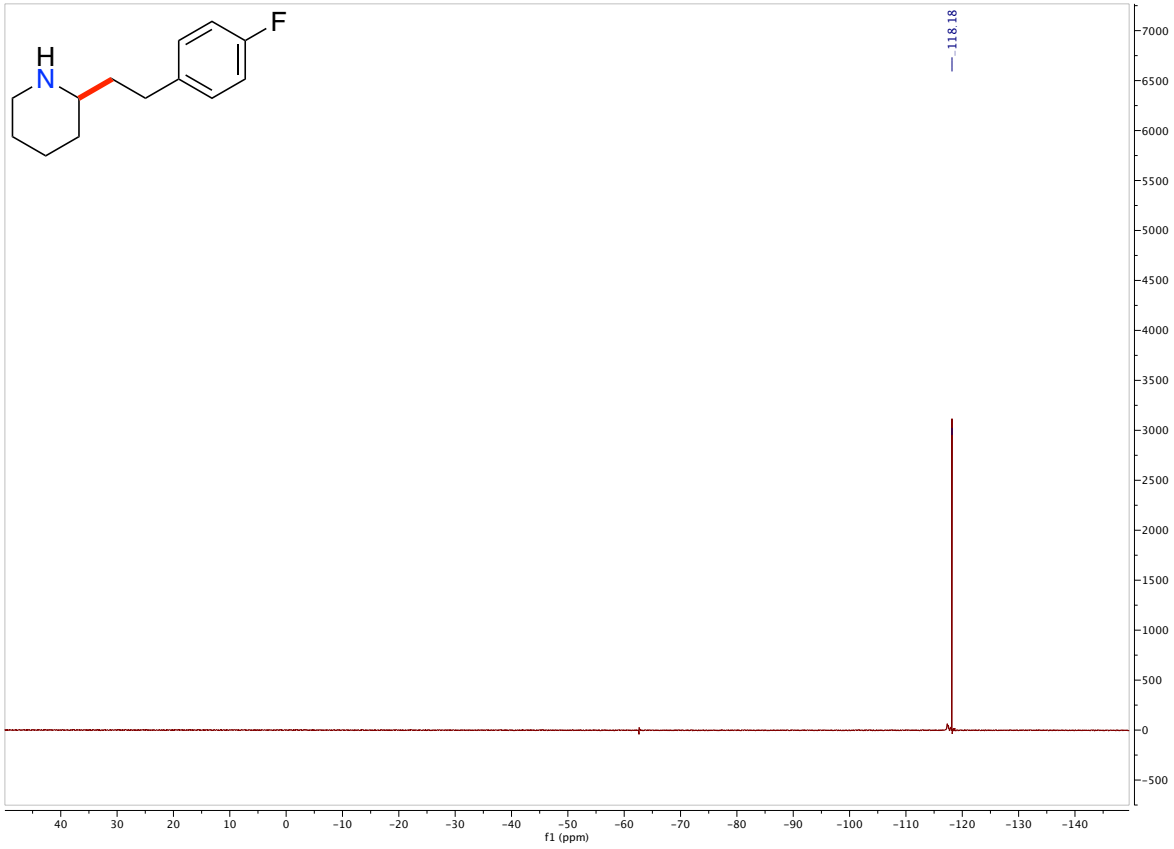

Figure. A.126. ^{19}F NMR spectrum (101 MHz, $CDCl_3$, 298 K) 2-(4-fluorophenethyl)piperidine.

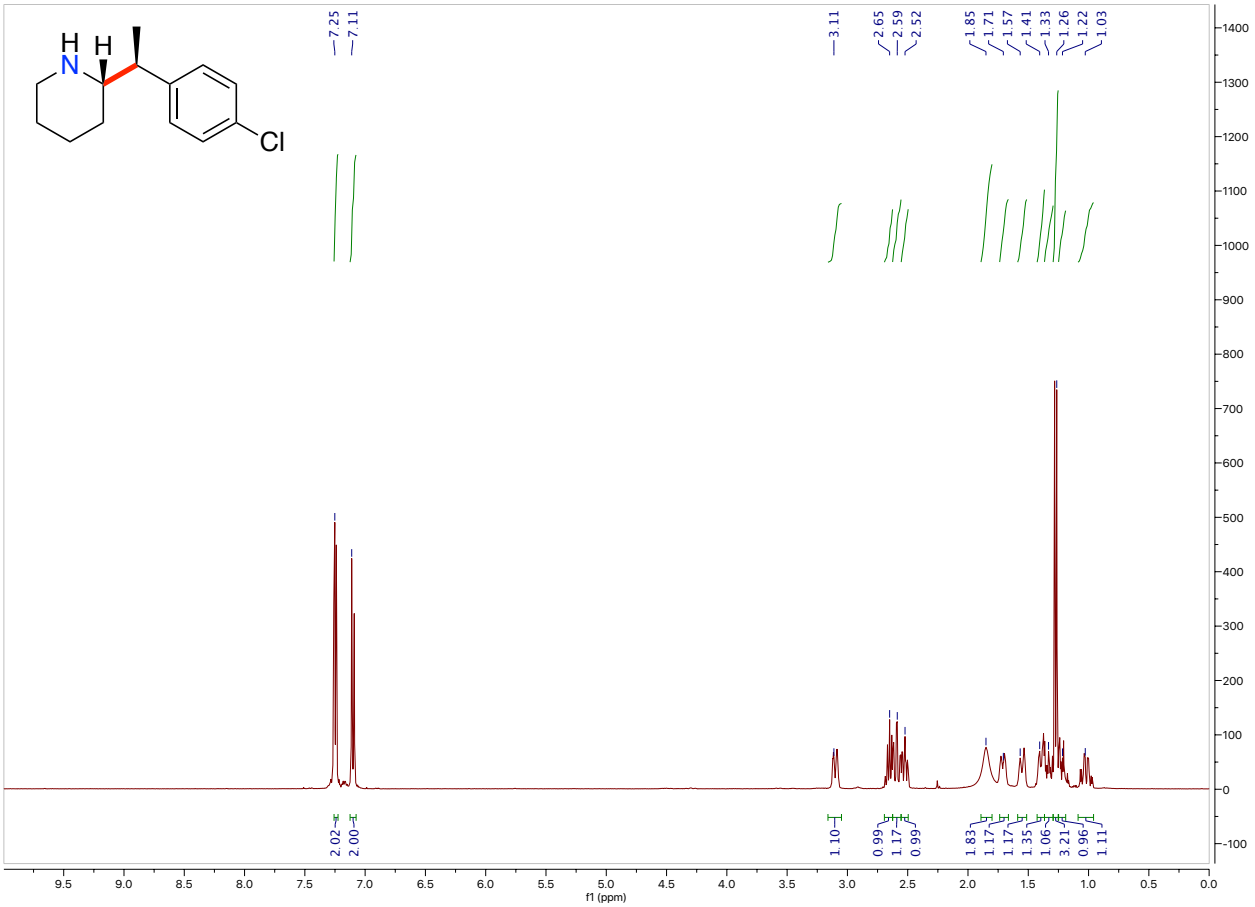

Figure. A.127. ^{1}H NMR spectrum (400 MHz, $CDCl_3$, 298 K) of 2-(1-(4-chlorophenyl)ethyl)piperidine.

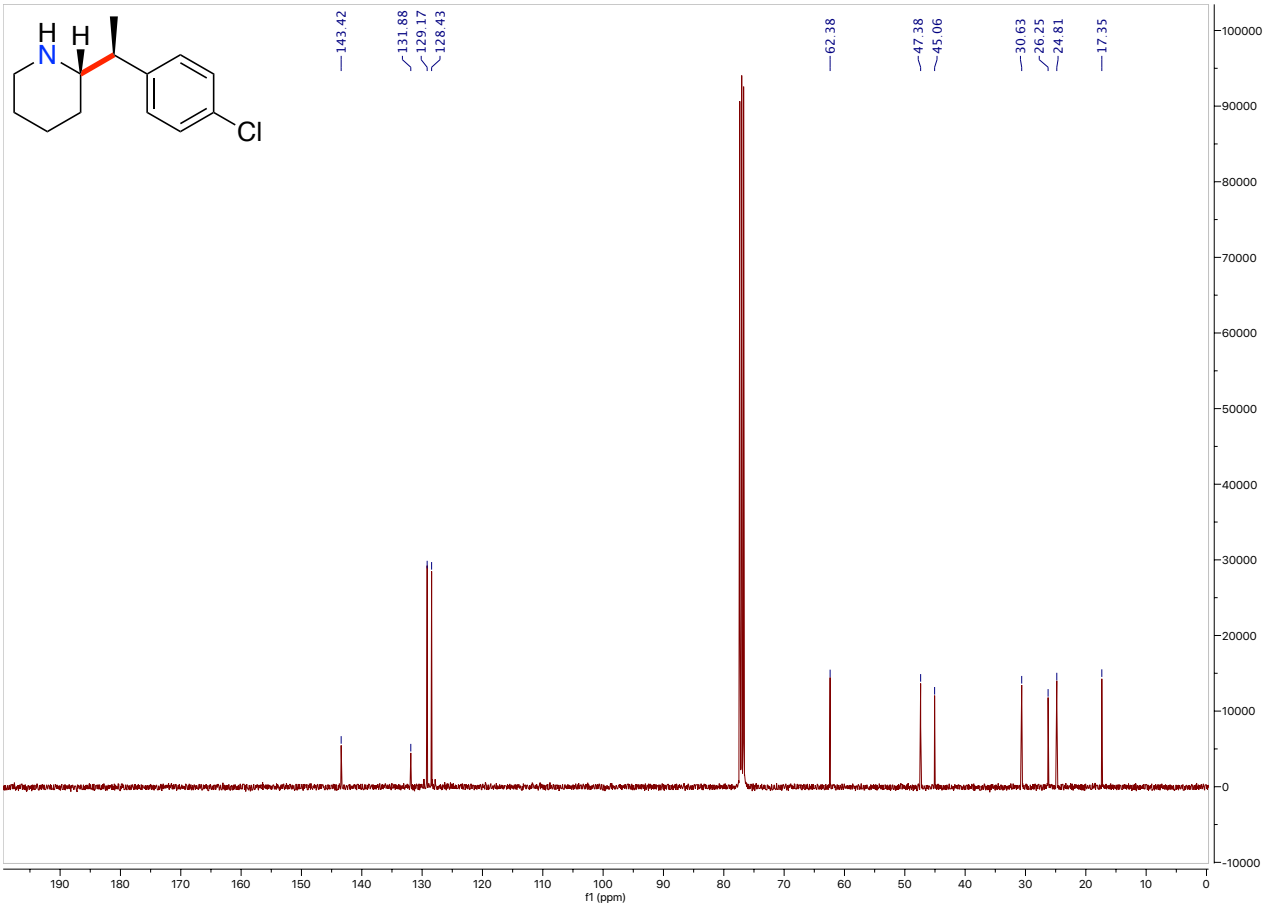

Figure. A.128. $^{13}C\{^{1}H\}$ NMR spectrum (101 MHz, $CDCl_3$, 298 K) of 2-(1-(4-chlorophenyl)ethyl)piperidine.

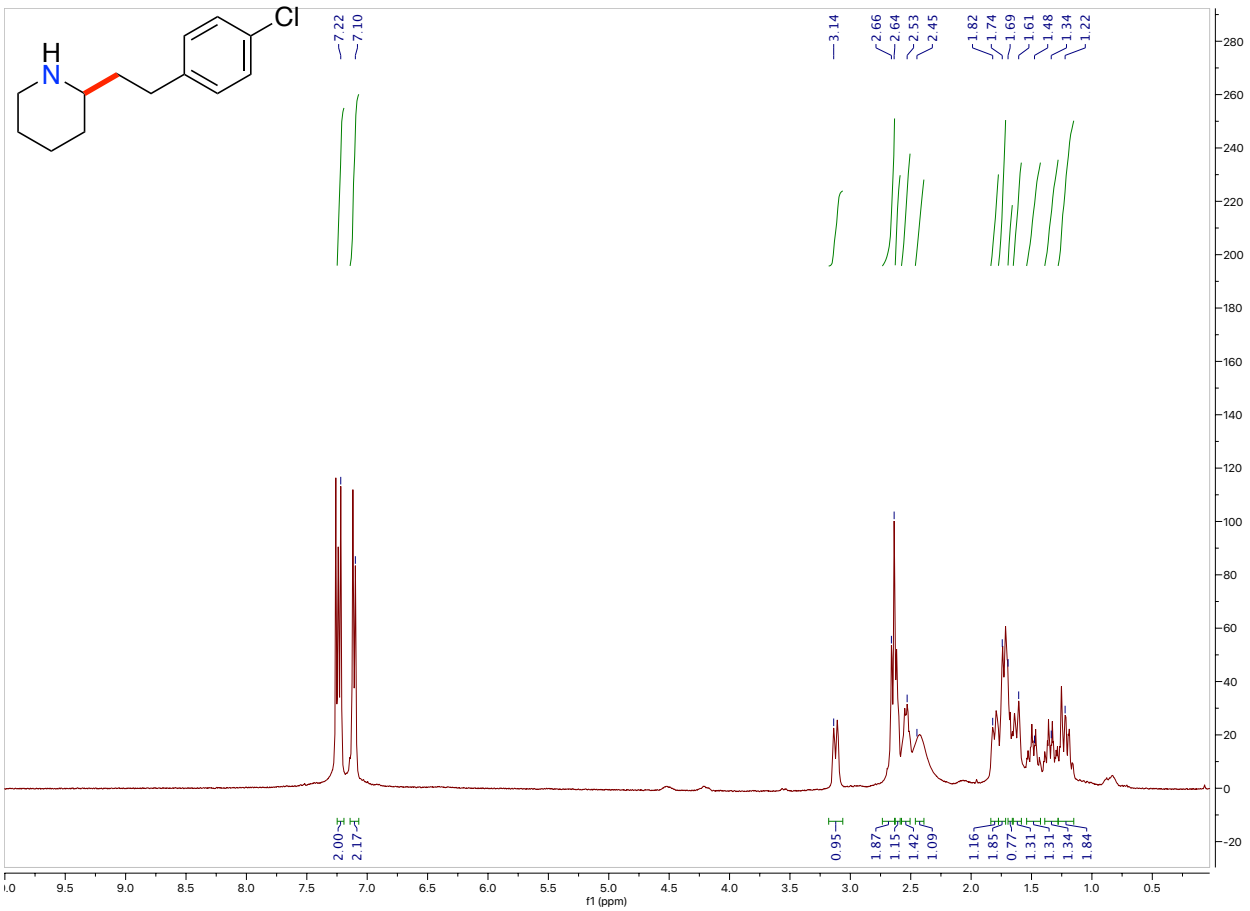

Figure. A.129. ^{1}H NMR spectrum (400 MHz, $CDCl_3$, 298 K) of 2-(4-chlorophenethyl)piperidine.

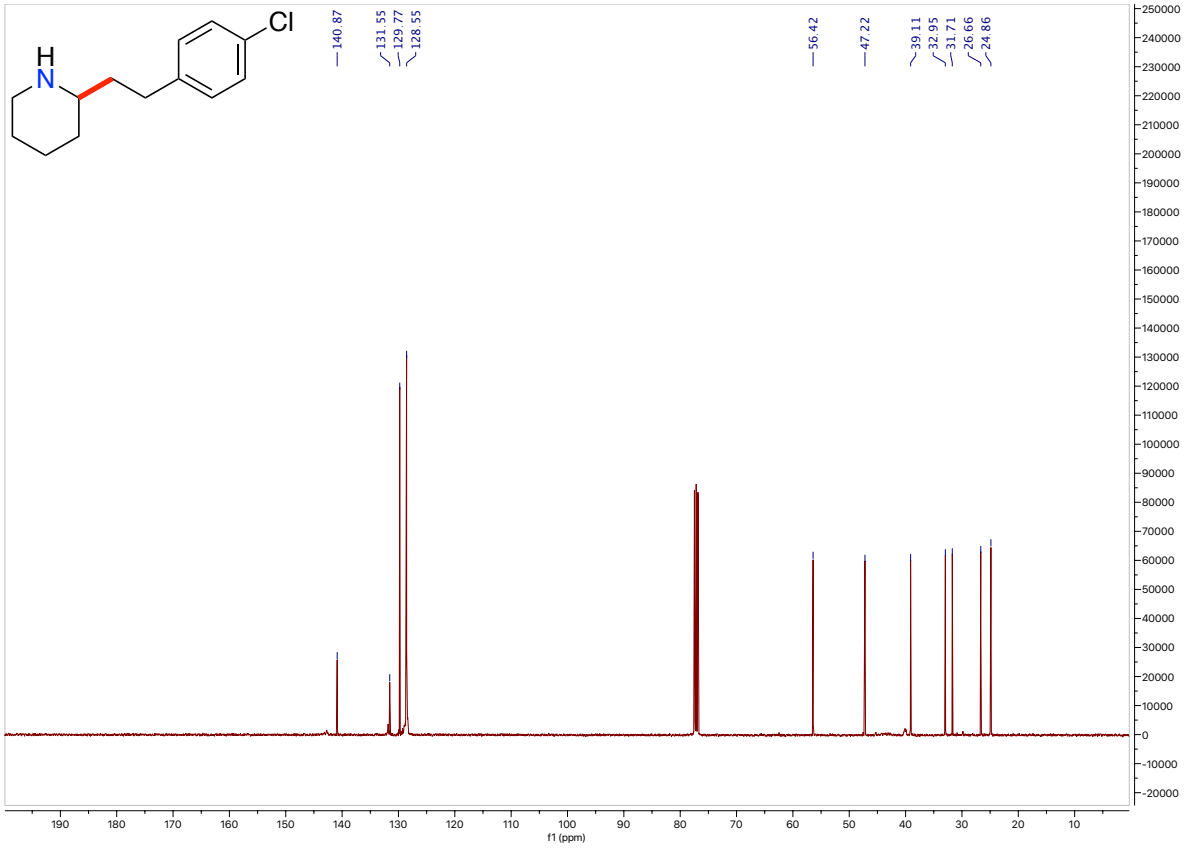

Figure. A.130. $^{13}C\{^{1}H\}$ NMR spectrum (101 MHz, $CDCl_3$, 298 K) of 2-(4-chlorophenethyl)piperidine.

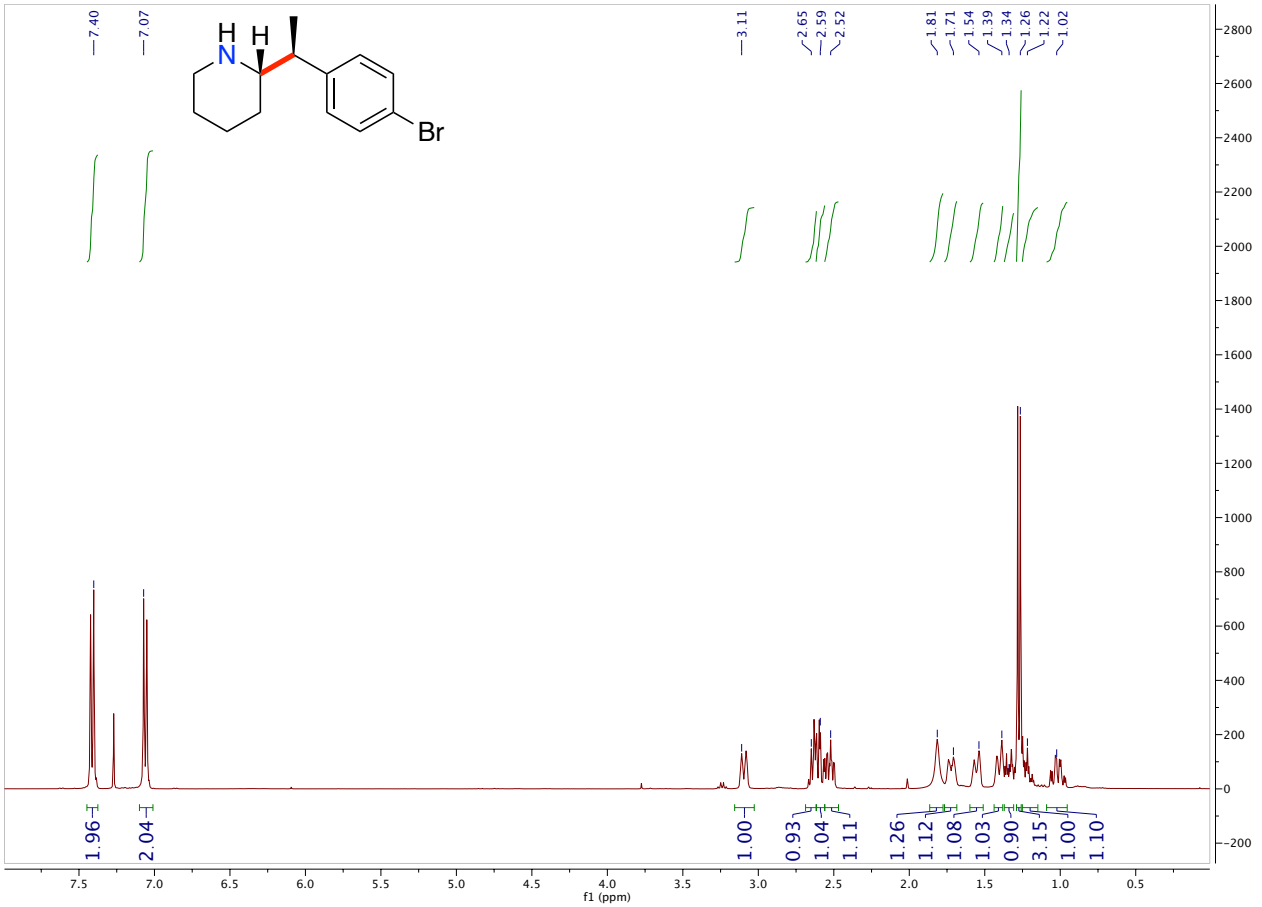

Figure. A.131. ^{1}H NMR spectrum (400 MHz, $CDCl_3$, 298 K) of 2-(1-(4-bromophenyl)ethyl)piperidine.

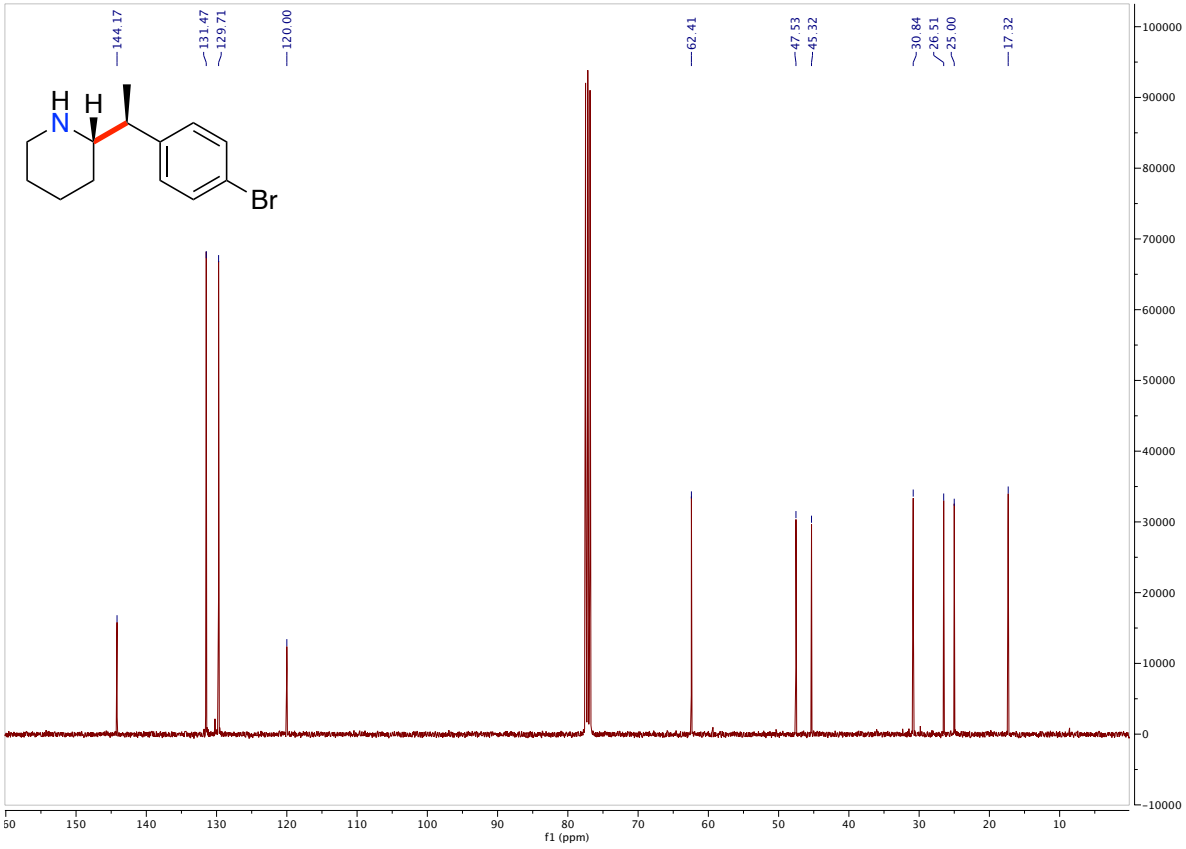

Figure. A.132. $^{13}C\{^{1}H\}$ NMR spectrum (101 MHz, $CDCl_3$, 298 K) 2-(1-(4-bromophenyl)ethyl)piperidine.

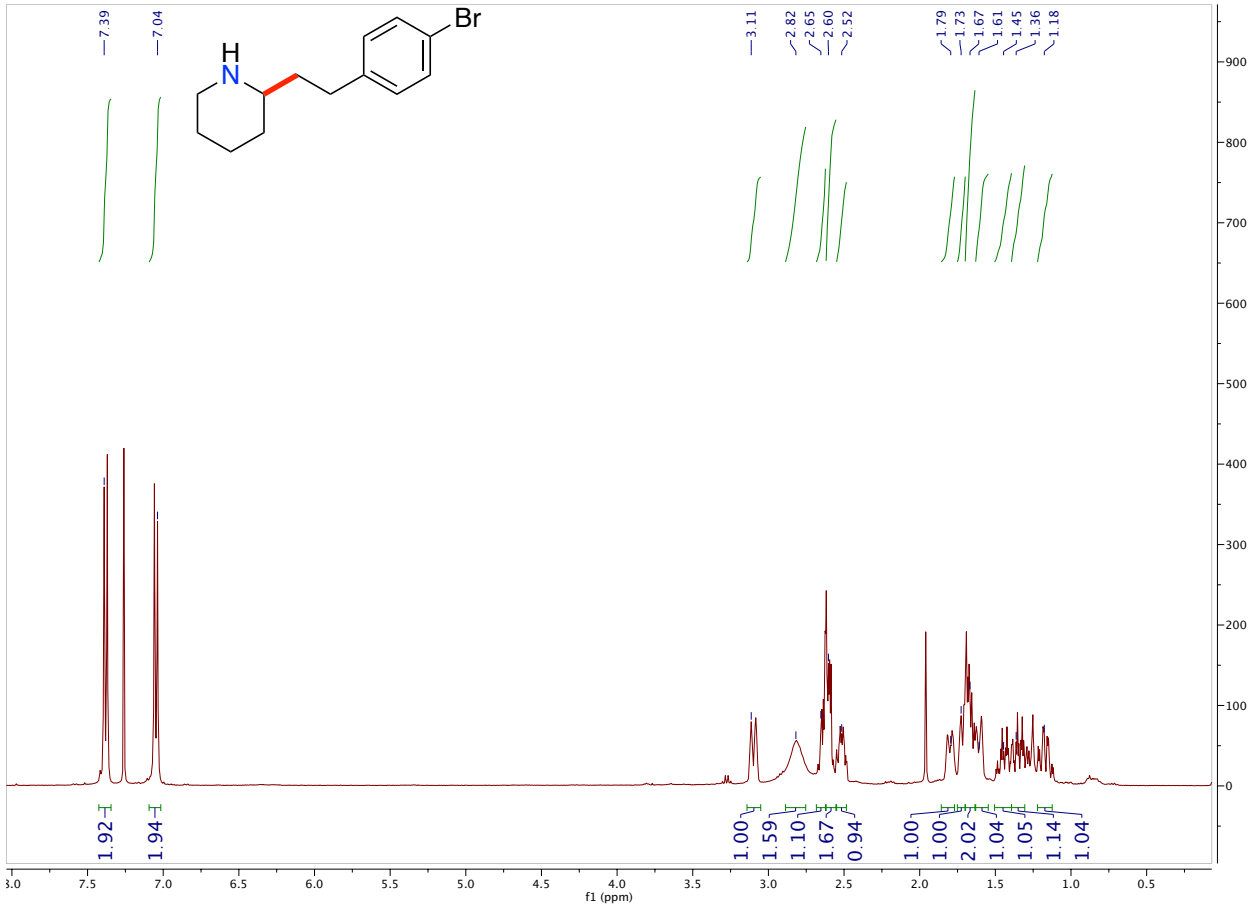

Figure. A.133. ^{1}H NMR spectrum (400 MHz, $CDCl_3$, 298 K) of 2-(4-bromophenethyl)piperidine.

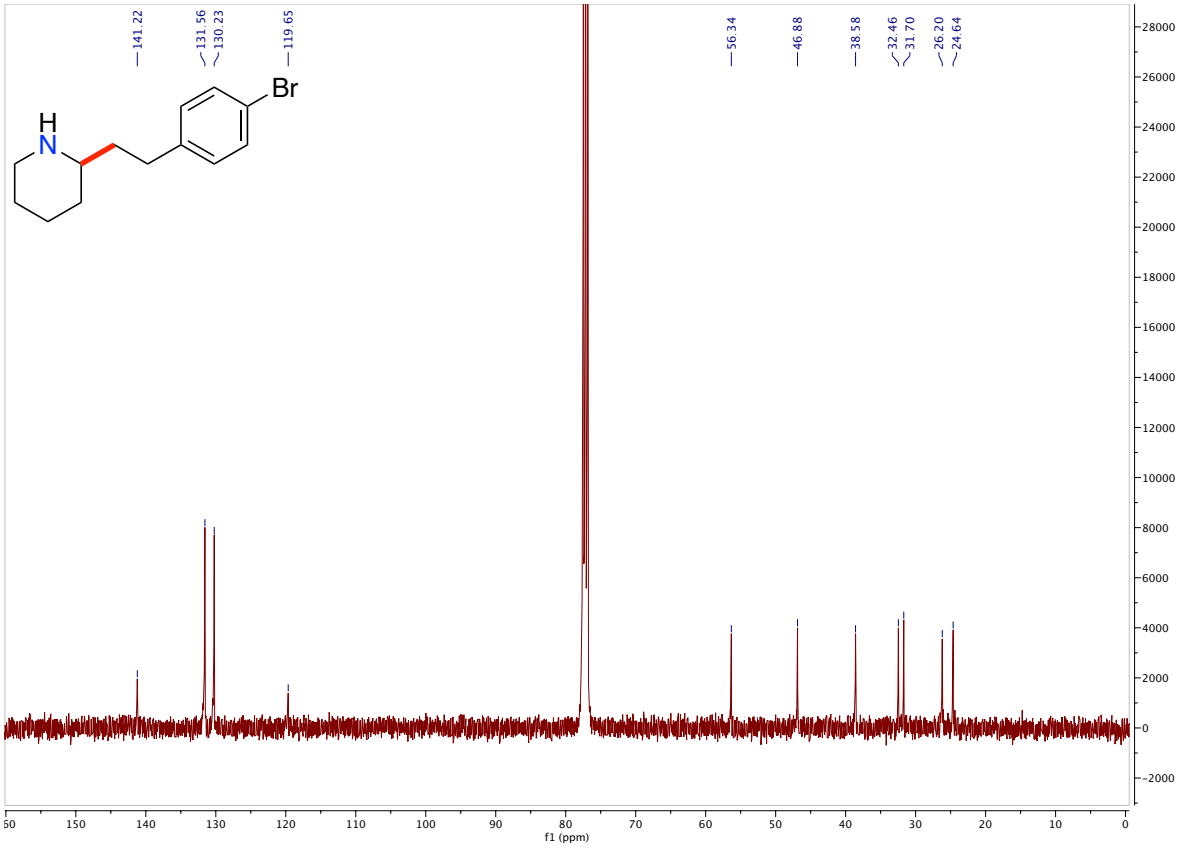

Figure. A.134. $^{13}C\{^{1}H\}$ NMR spectrum (101 MHz, $CDCl_3$, 298 K) 2-(4-bromophenethyl)piperidine.

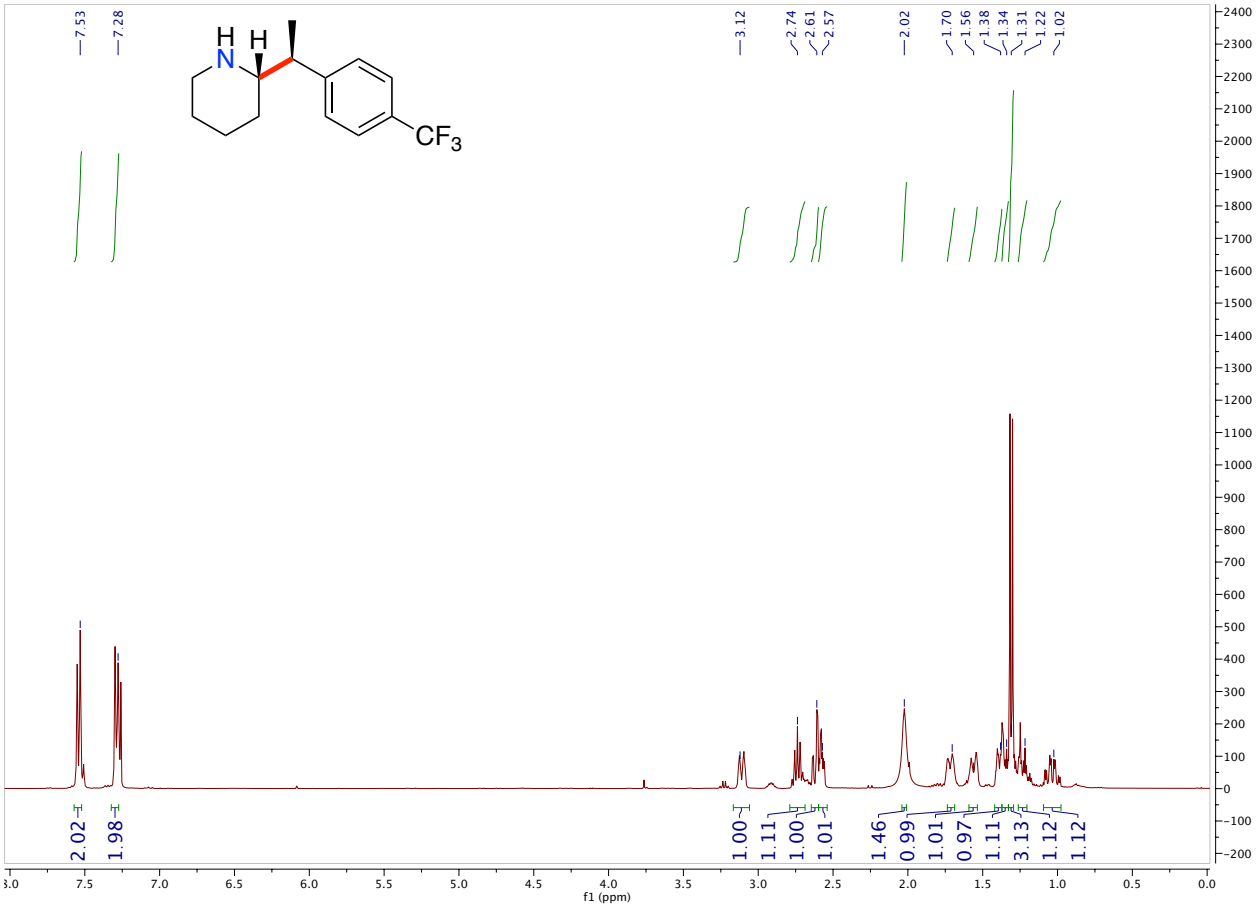

Figure. A.135. ^{1}H NMR spectrum (400 MHz, $CDCl_3$, 298 K) of 2-(1-(4-(trifluoromethyl)phenyl)ethyl)piperidine.

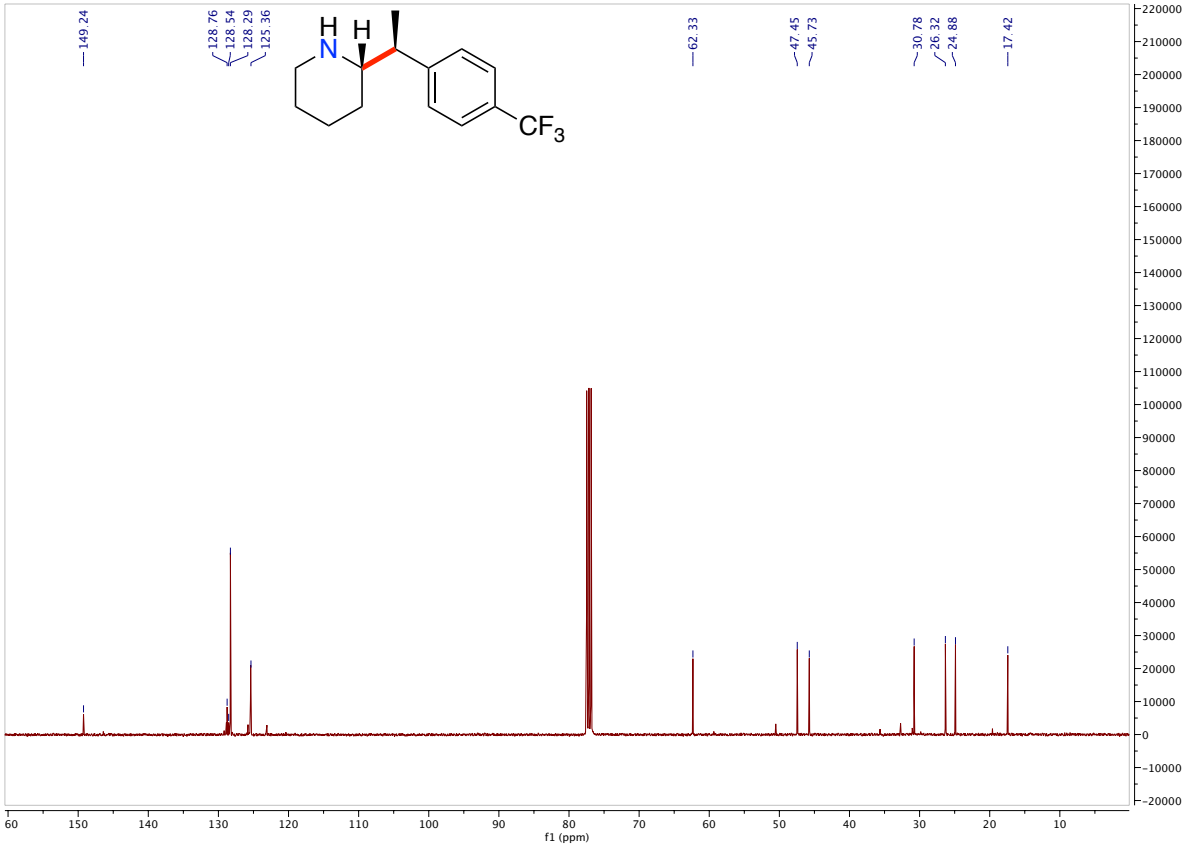

Figure. A.136. $^{13}C\{^{1}H\}$ NMR spectrum (101 MHz, $CDCl_3$, 298 K) 2-(1-(4-(trifluoromethyl)phenyl)ethyl)piperidine.

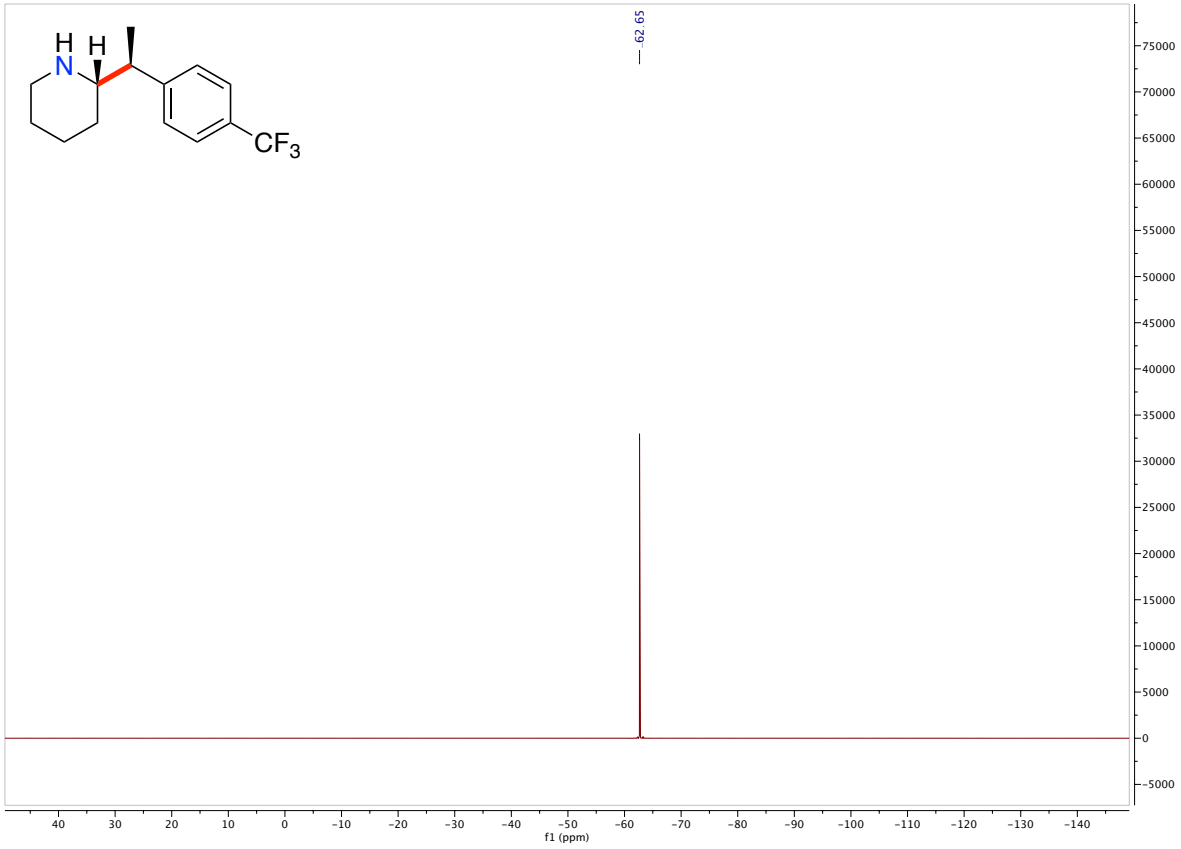

Figure. A.137. ^{19}F NMR spectrum (101 MHz, $CDCl_3$, 298 K) 2-(1-(4-(trifluoromethyl)phenyl)ethyl)piperidine.

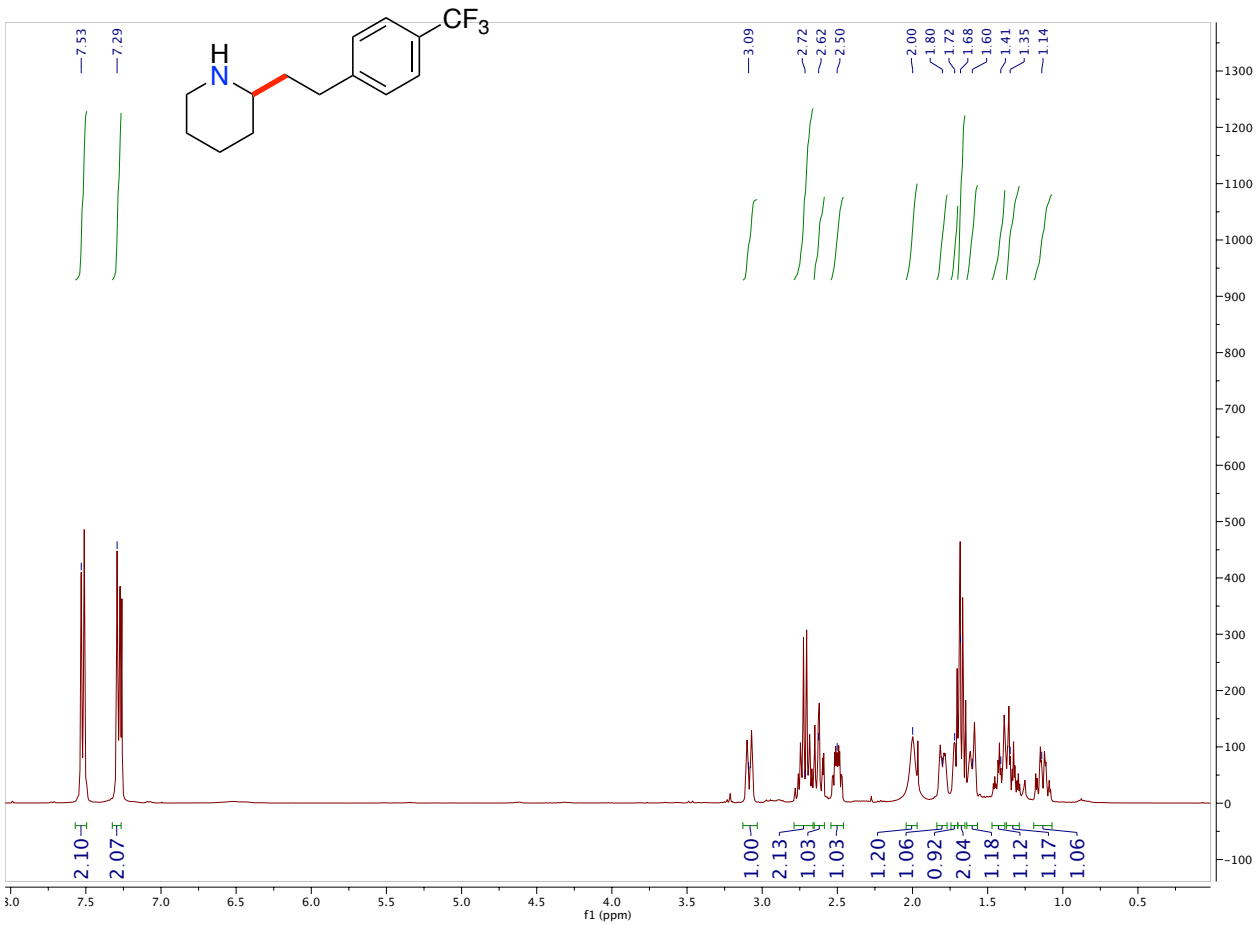

Figure. A.138. ^{1}H NMR spectrum (400 MHz, $CDCl_3$, 298 K) of 2-(4-(trifluoromethyl)phenethyl)piperidine.

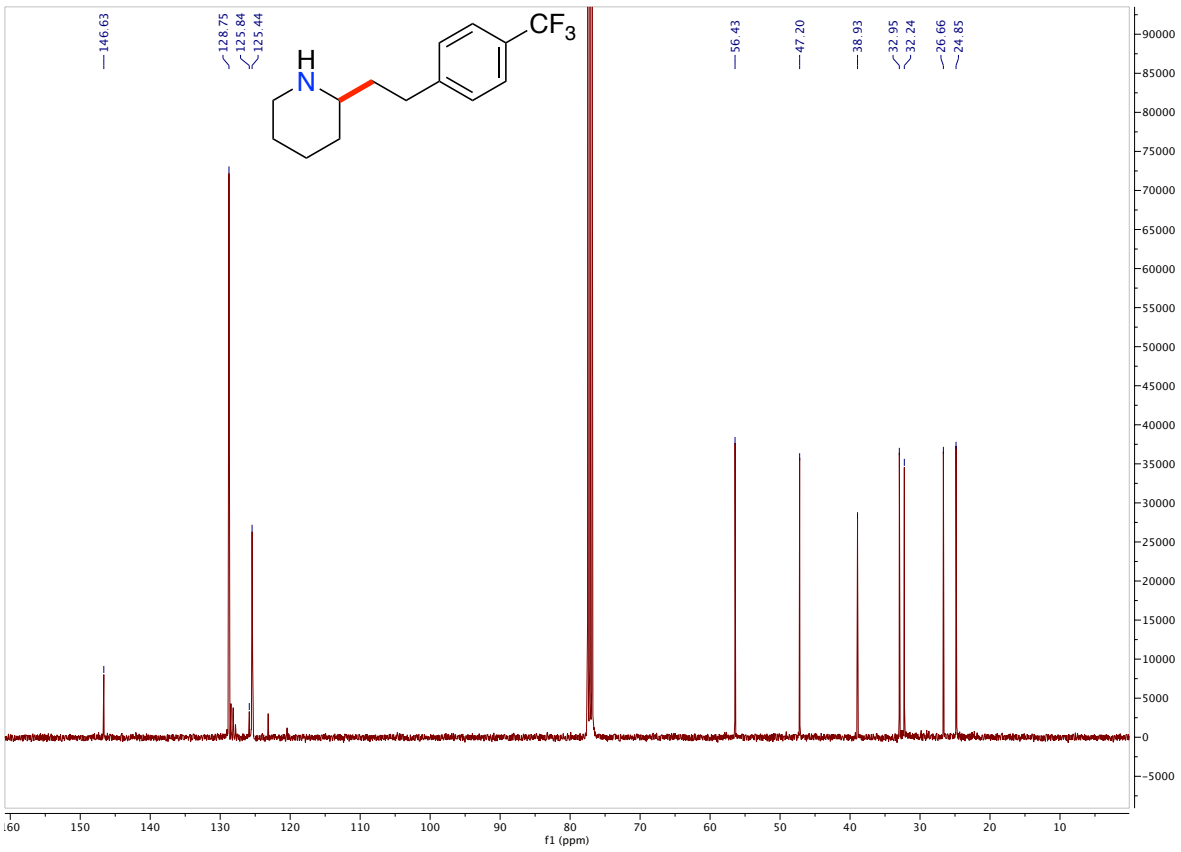

Figure. A.139. $^{13}C\{^{1}H\}$ NMR spectrum (101 MHz, $CDCl_3$, 298 K) 2-(4-(trifluoromethyl)phenethyl)piperidine.

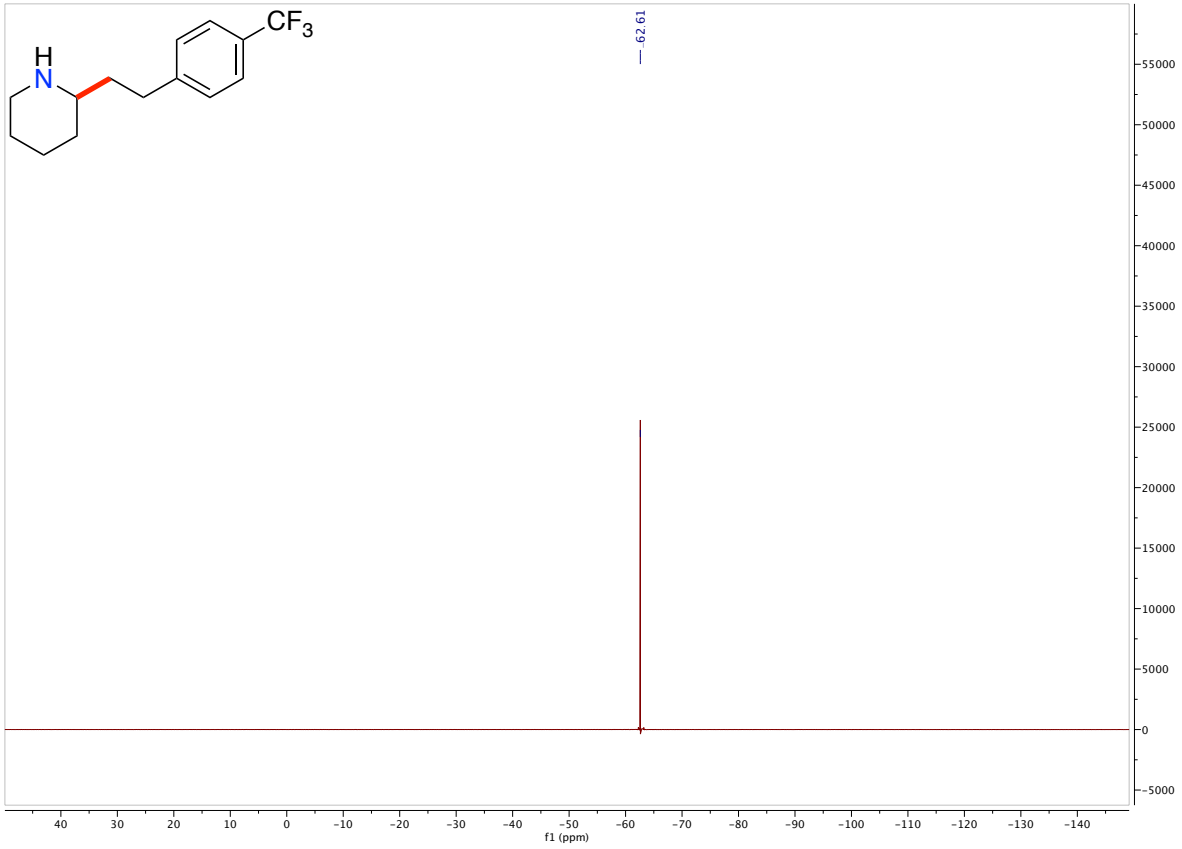

Figure. A.140. ^{19}F NMR spectrum (101 MHz, $CDCl_3$, 298 K) 2-(4-(trifluoromethyl)phenethyl)piperidine.

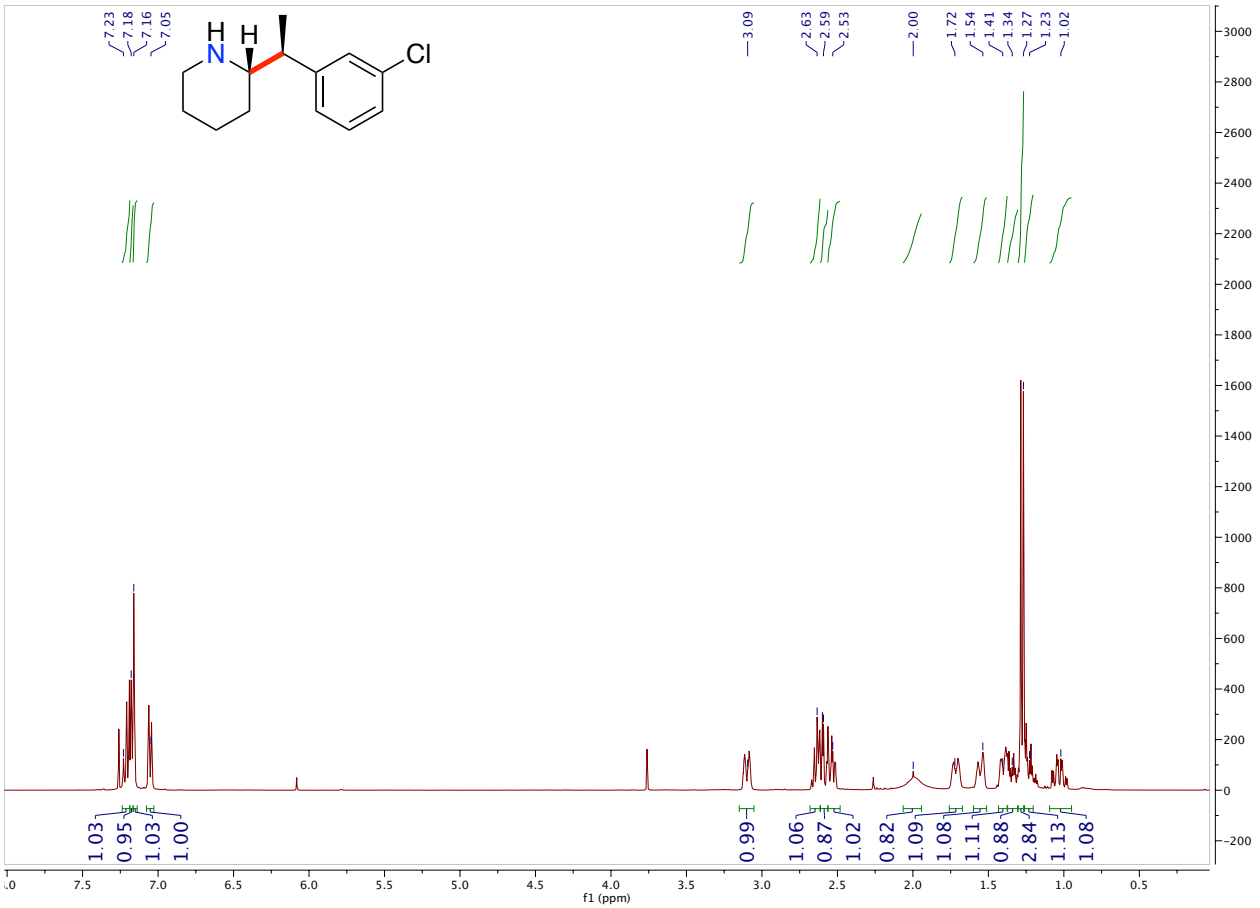

Figure. A.141. ^{1}H NMR spectrum (400 MHz, $CDCl_3$, 298 K) of 2-(1-(3-chlorophenyl)ethyl)piperidine.

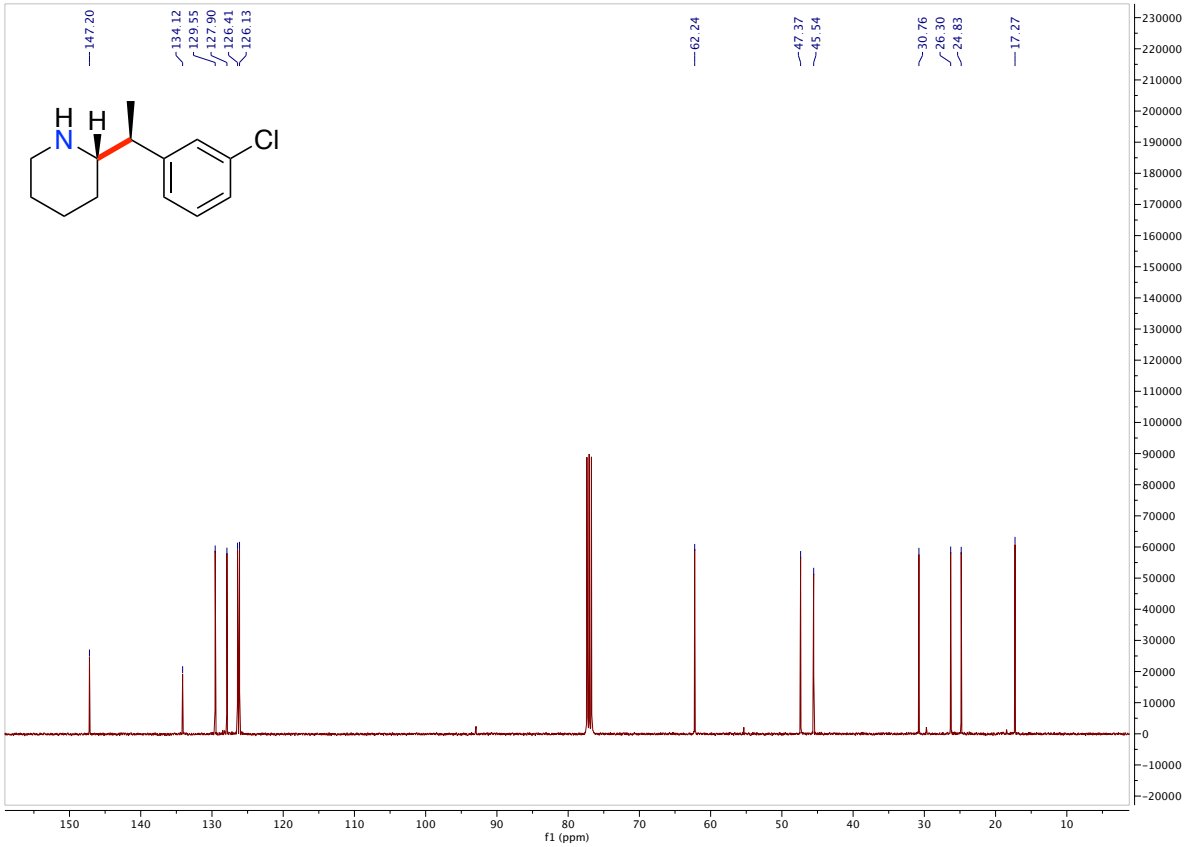

Figure. A.142. $^{13}C\{^{1}H\}$ NMR spectrum (101 MHz, $CDCl_3$, 298 K) 2-(1-(3-chlorophenyl)ethyl)piperidine.

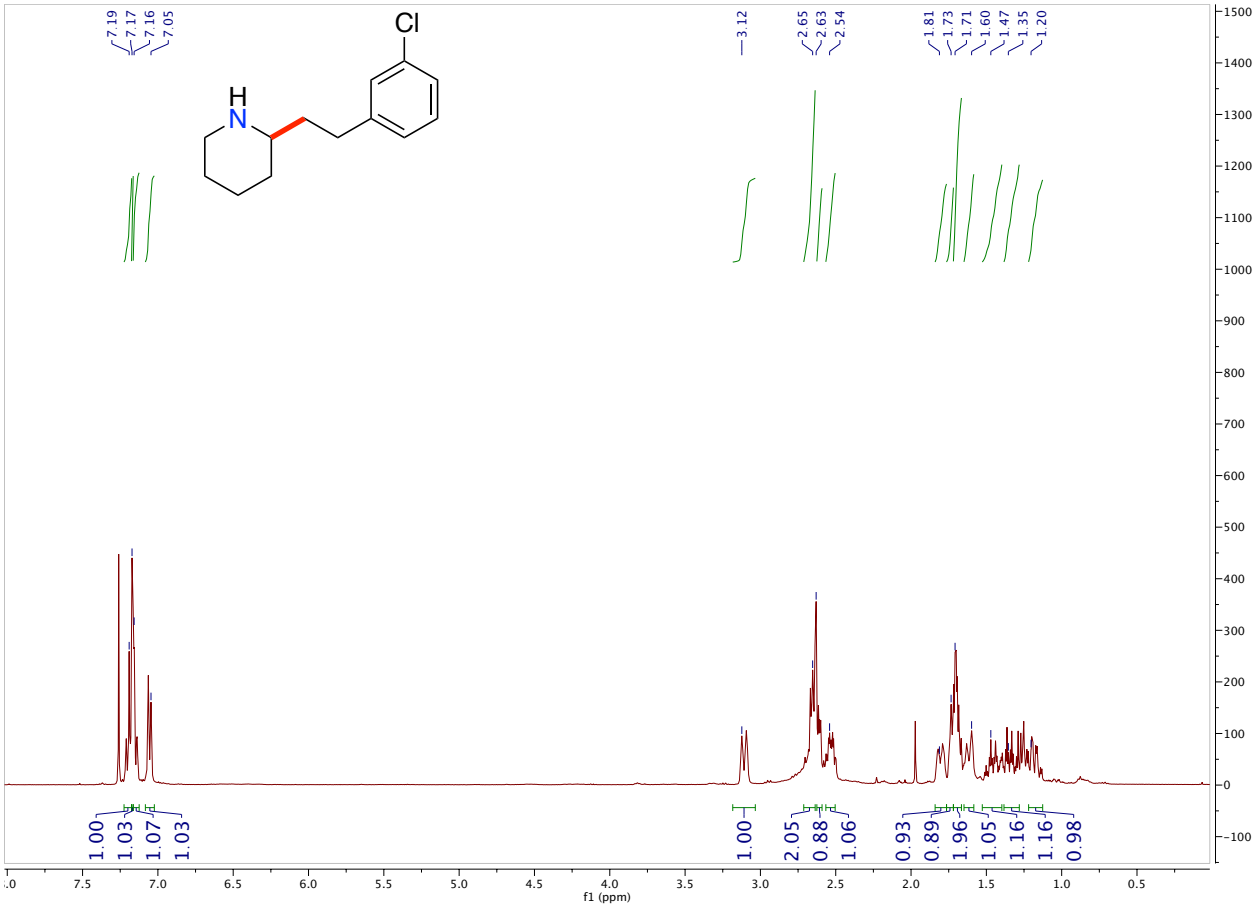

Figure. A.143. ^{1}H NMR spectrum (400 MHz, $CDCl_3$, 298 K) of 2-(3-chlorophenethyl)piperidine.

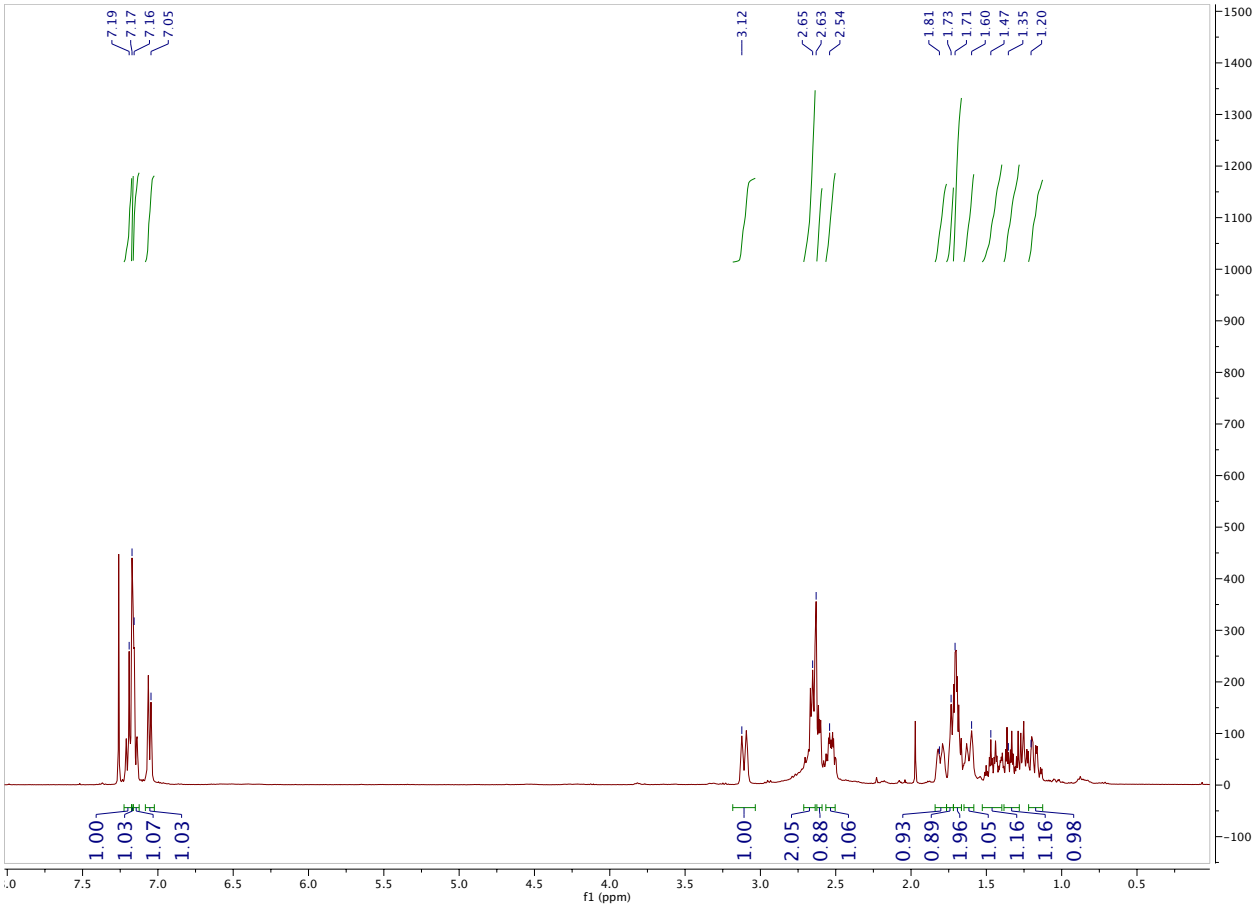

Figure. A.144. ^{1}H NMR spectrum (400 MHz, $CDCl_3$, 298 K) of 2-(3-chlorophenethyl)piperidine.

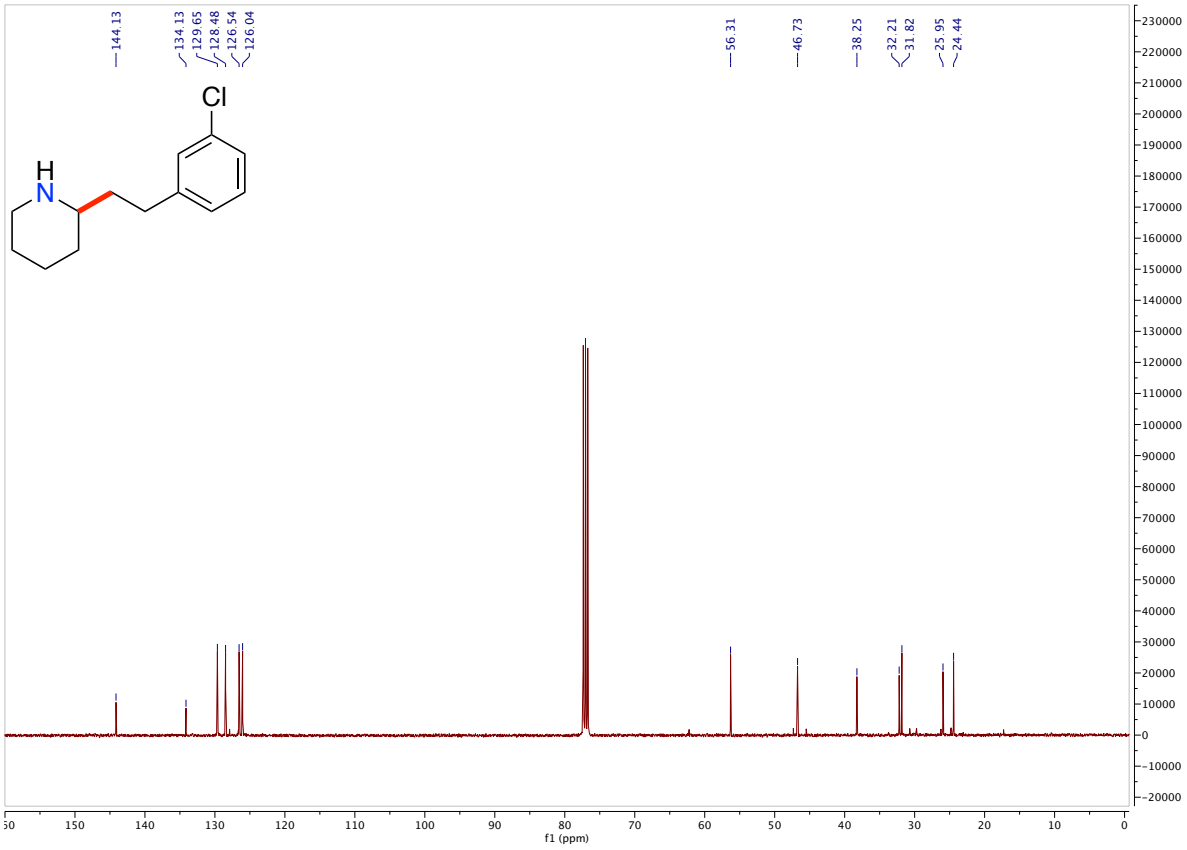

Figure. A.145. $^{13}C\{^{1}H\}$ NMR spectrum (101 MHz, $CDCl_3$, 298 K) 2-(3-chlorophenethyl)piperidine.

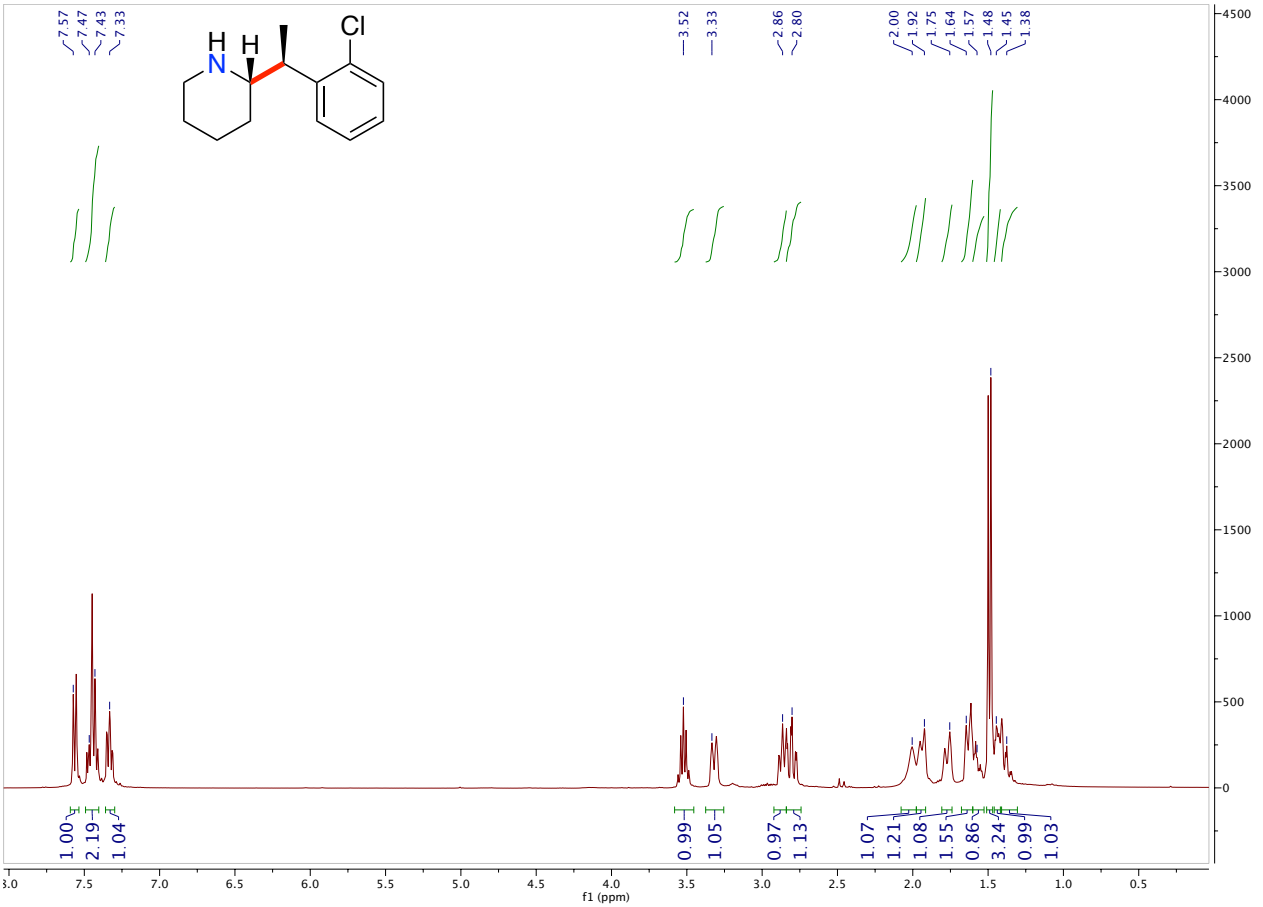

Figure. A.146. ^{1}H NMR spectrum (400 MHz, $CDCl_3$, 298 K) of 2-(1-(2-chlorophenyl)ethyl)piperidine.

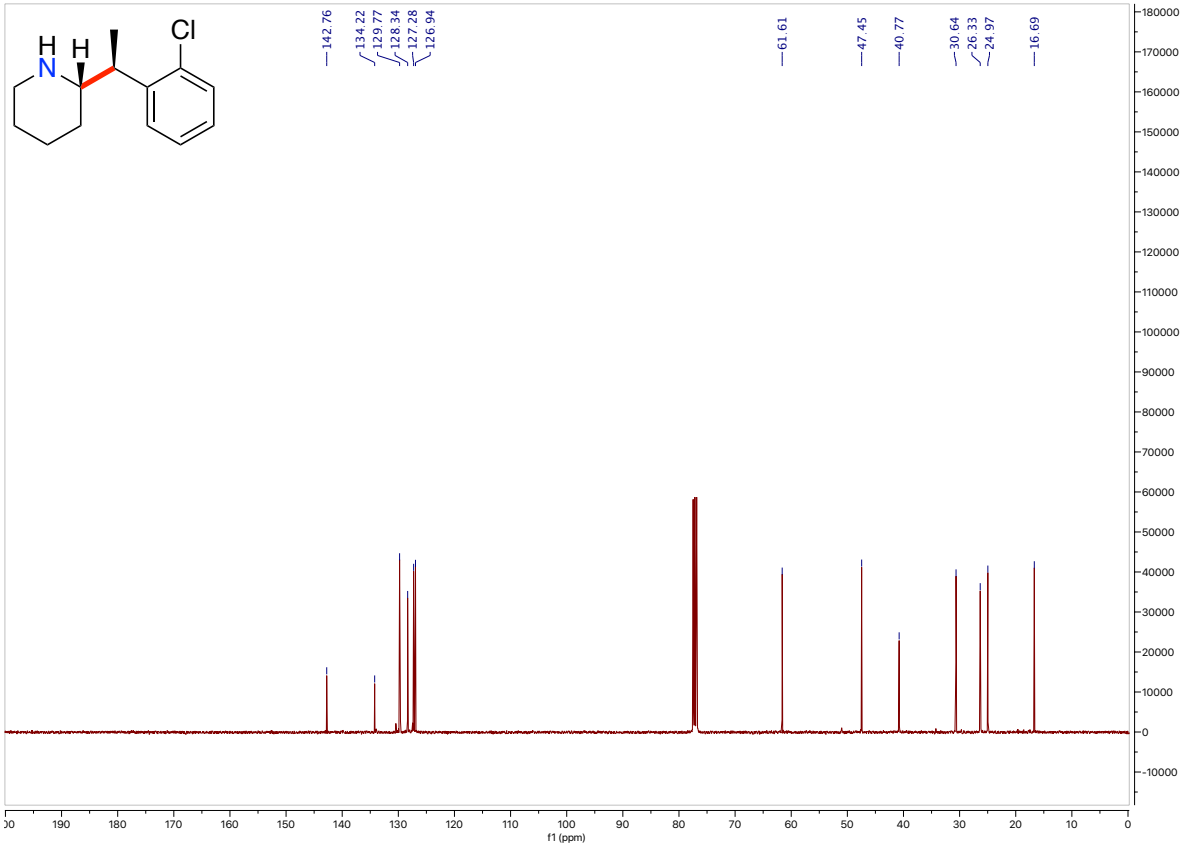

Figure. A.147. $^{13}C\{^{1}H\}$ NMR spectrum (101 MHz, $CDCl_3$, 298 K) of 2-(1-(2-chlorophenyl)ethyl)piperidine

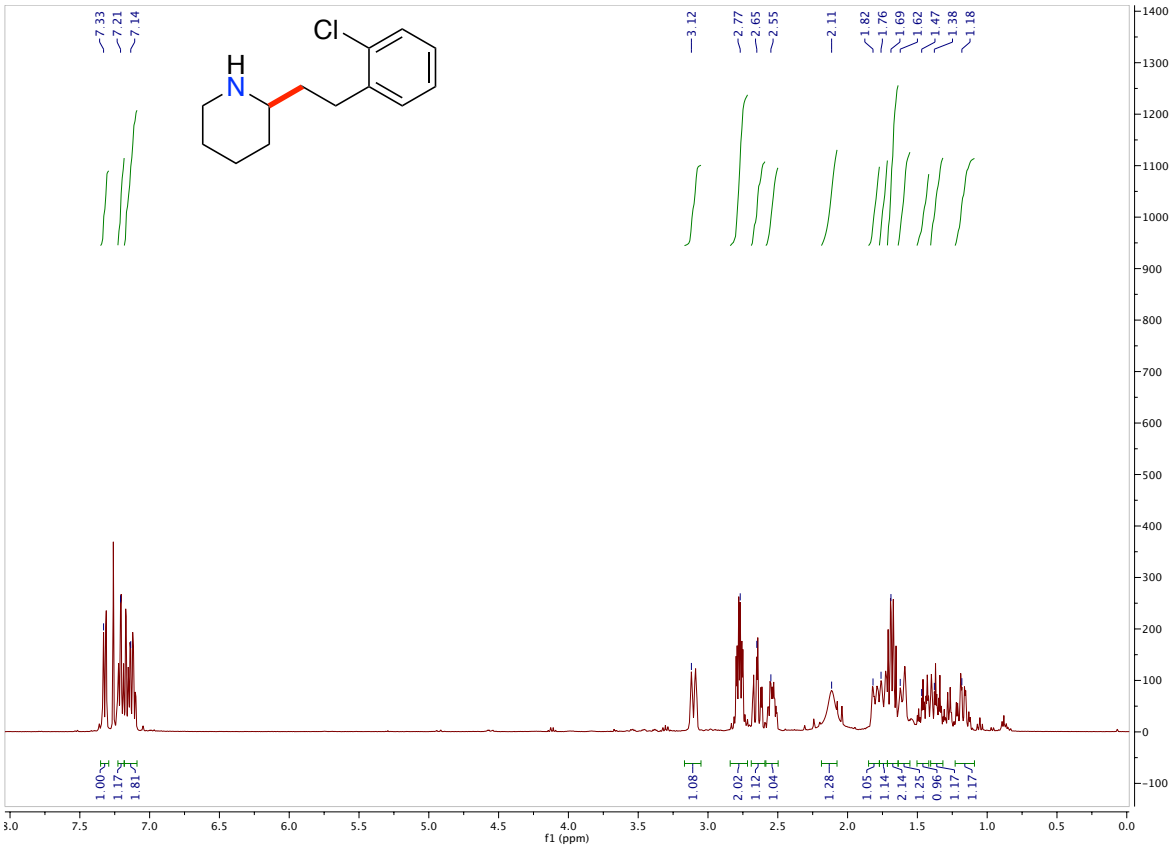

Figure. A.148. ^{1}H NMR spectrum (400 MHz, $CDCl_3$, 298 K) of 2-(1-(2-chlorophenyl)ethyl)piperidine.

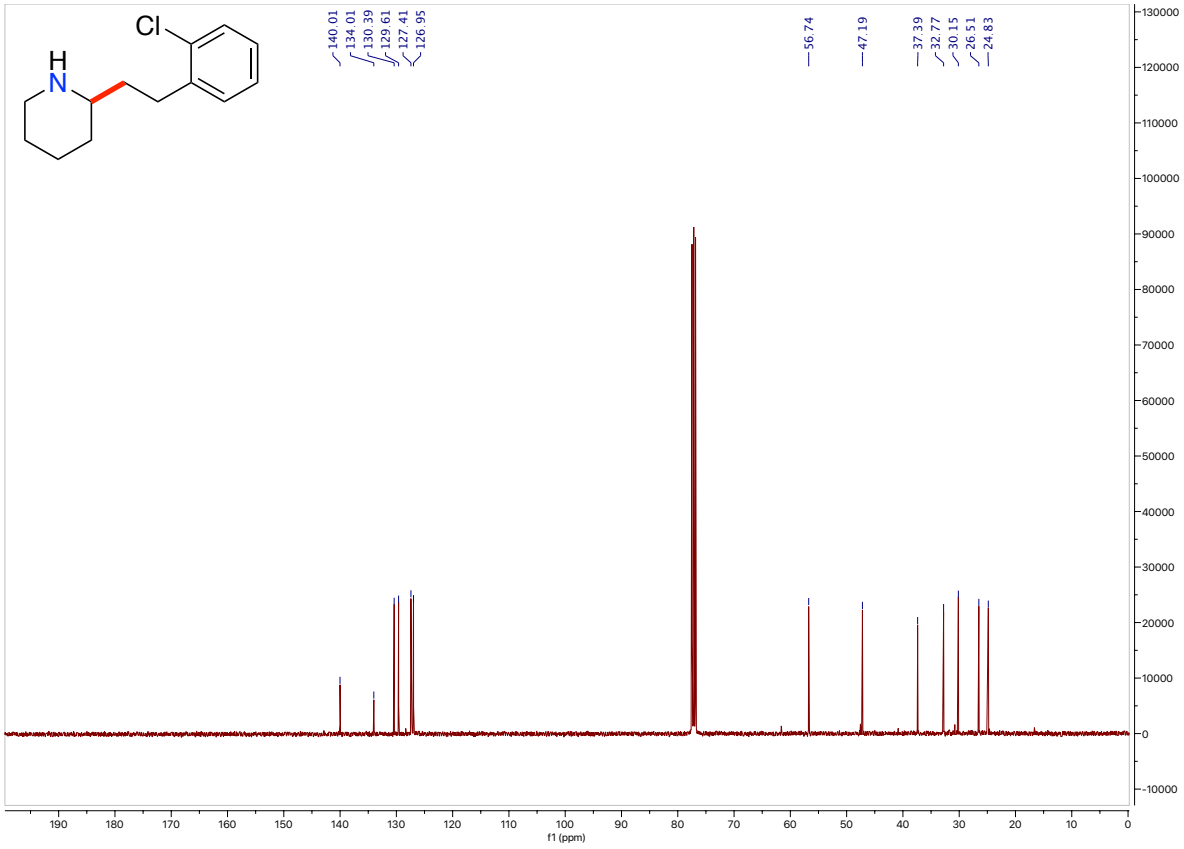

Figure. A.149. $^{13}C\{^{1}H\}$ NMR spectrum (101 MHz, $CDCl_3$, 298 K) of 2-(1-(2-chlorophenyl)ethyl)piperidine.

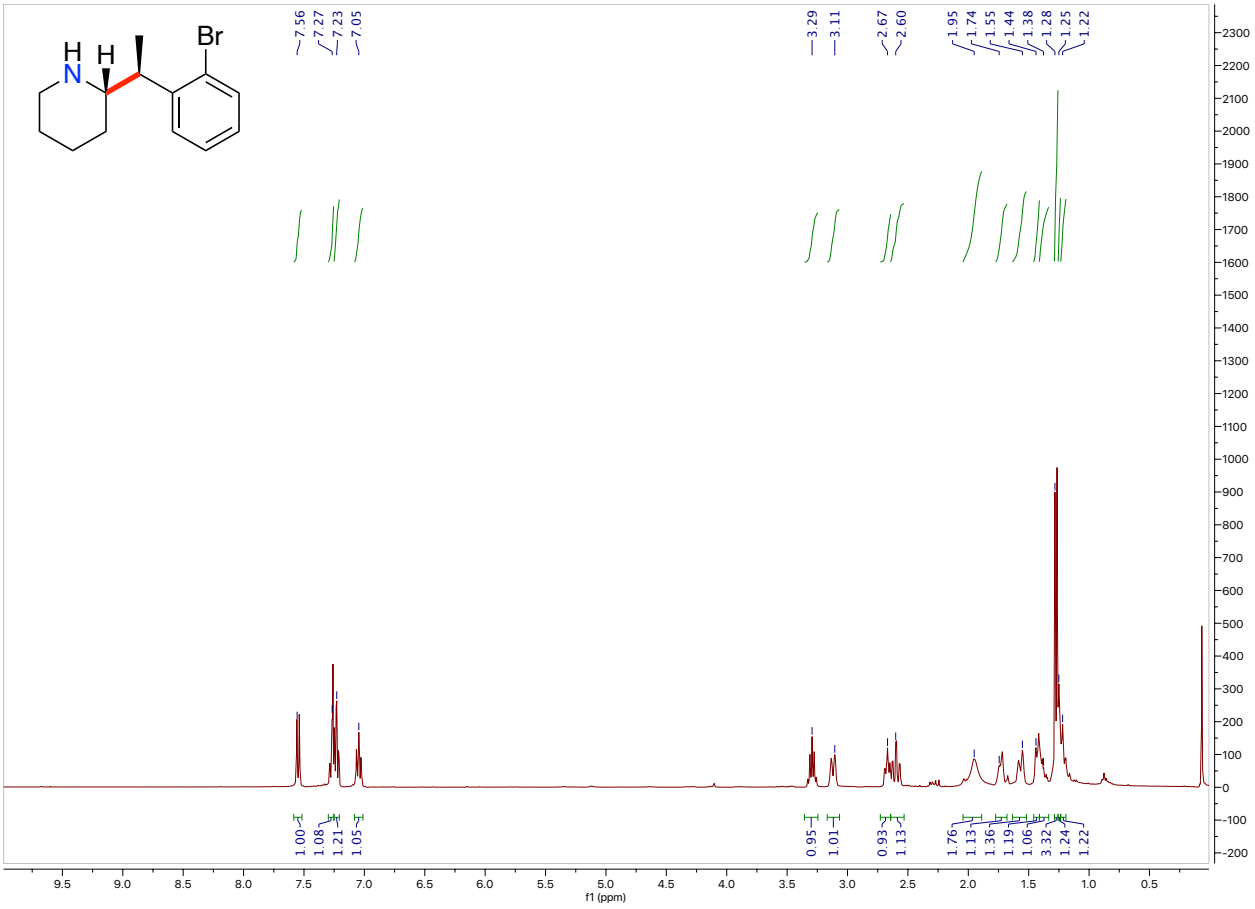

Figure. A.150. ^{1}H NMR spectrum (400 MHz, $CDCl_3$, 298 K) of 2-(1-(2-bromophenyl)ethyl)piperidine.

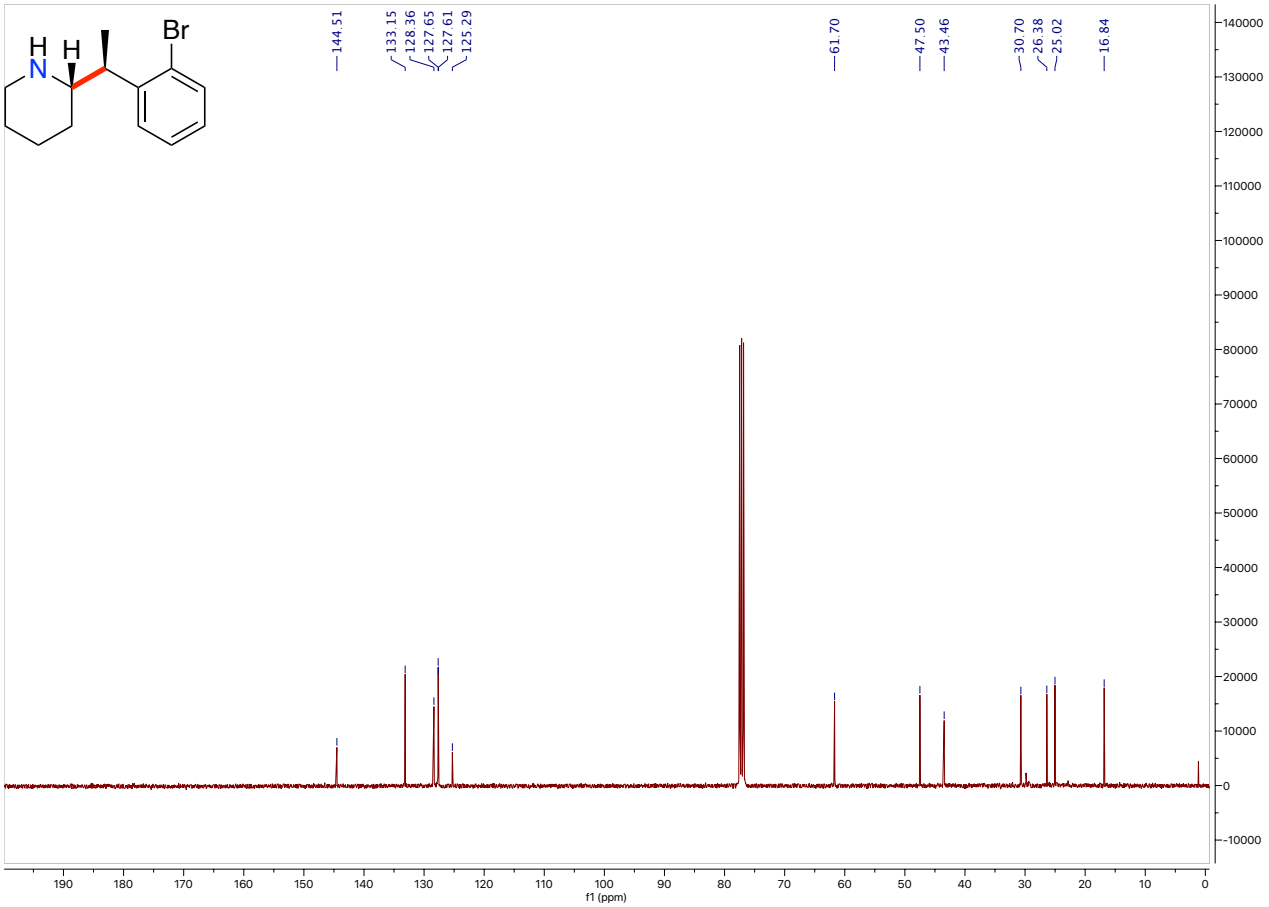

Figure. A.151. $^{13}C\{^{1}H\}$ NMR spectrum (101 MHz, $CDCl_3$, 298 K) of 2-(1-(2-bromophenyl)ethyl)piperidine.

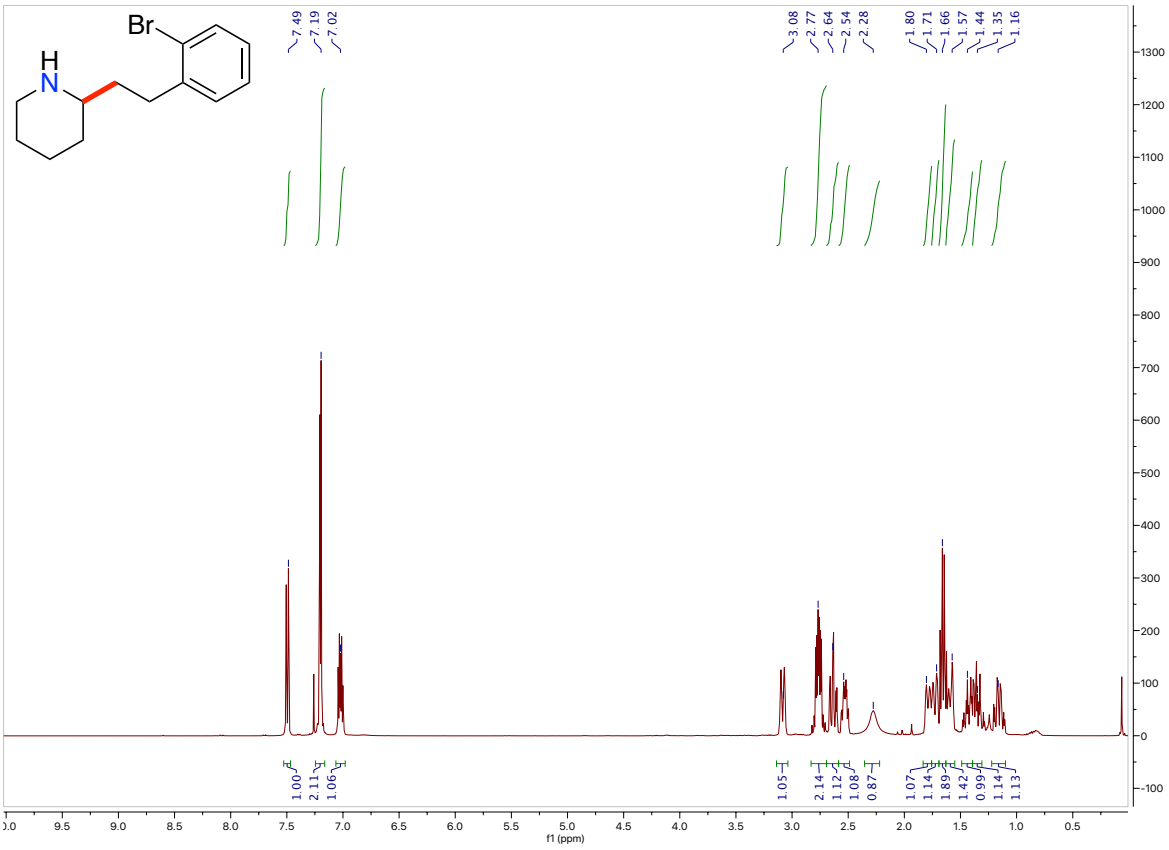

Figure. A.152. ^{1}H NMR spectrum (400 MHz, $CDCl_3$, 298 K) of 2-(2-bromophenethyl)piperidine.

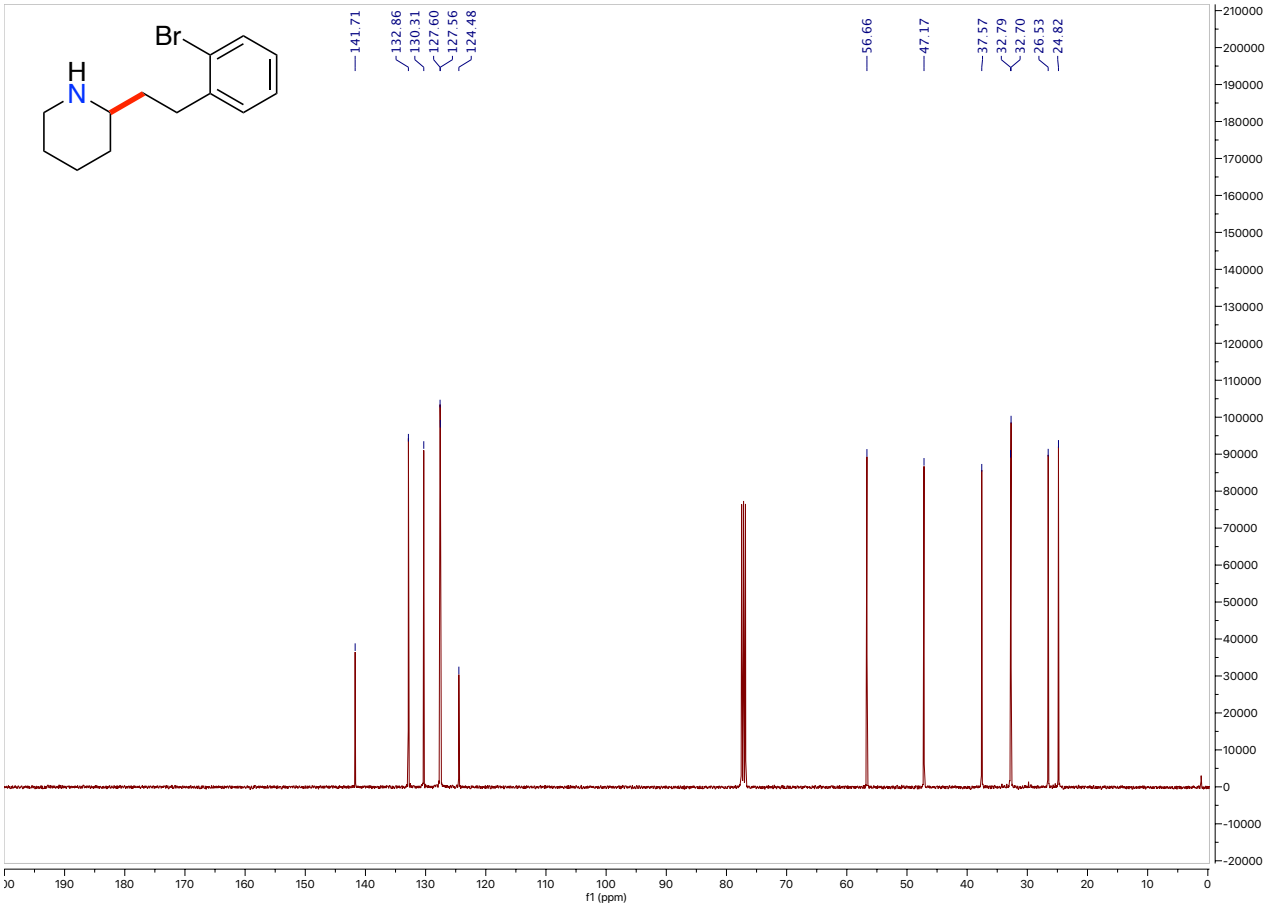

Figure. A.153. $^{13}C\{^{1}H\}$ NMR spectrum (101 MHz, $CDCl_3$, 298 K) of 2-(2-bromophenethyl)piperidine.

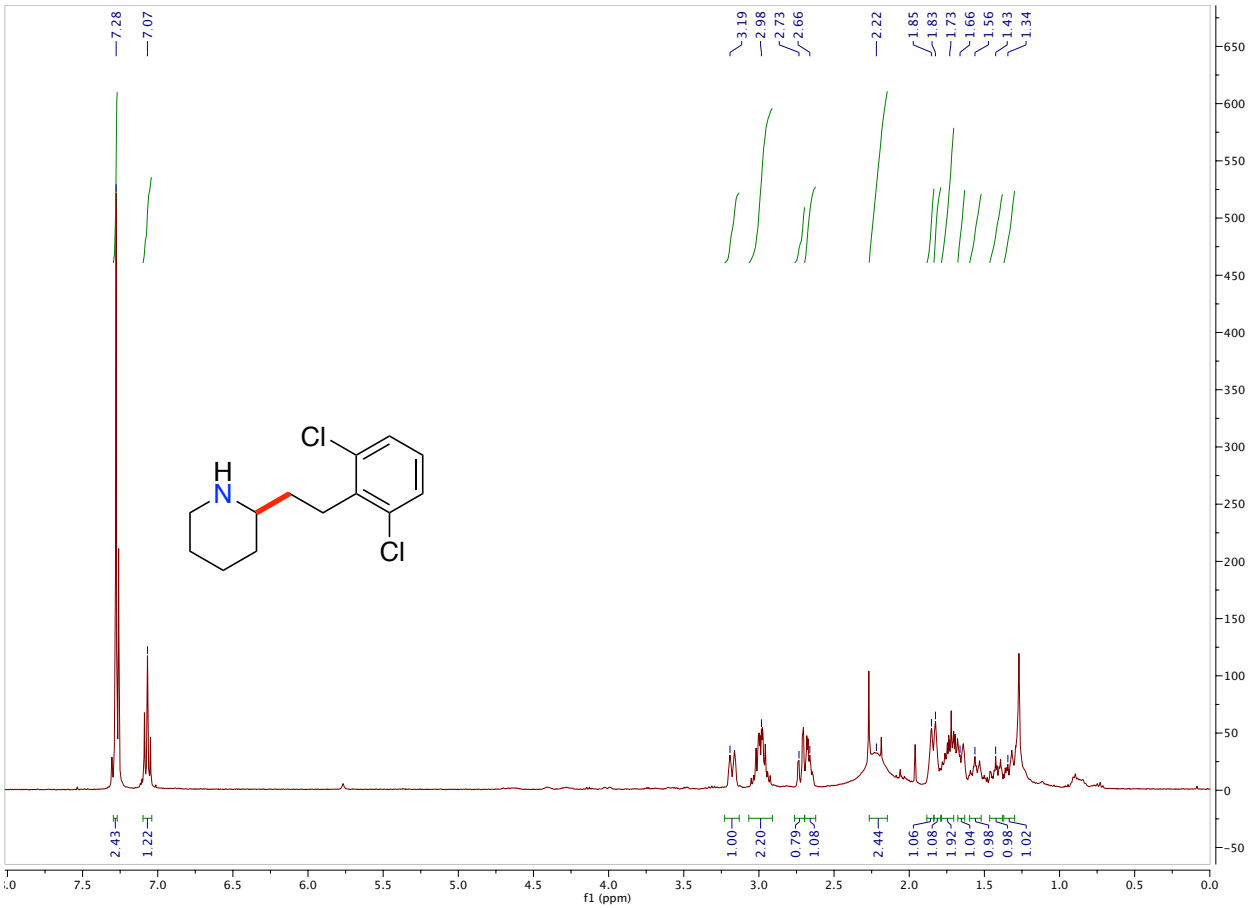

Figure. A.154. ^{1}H NMR spectrum (400 MHz, $CDCl_3$, 298 K) of 2-(2,6-dichlorophenethyl)piperidine.

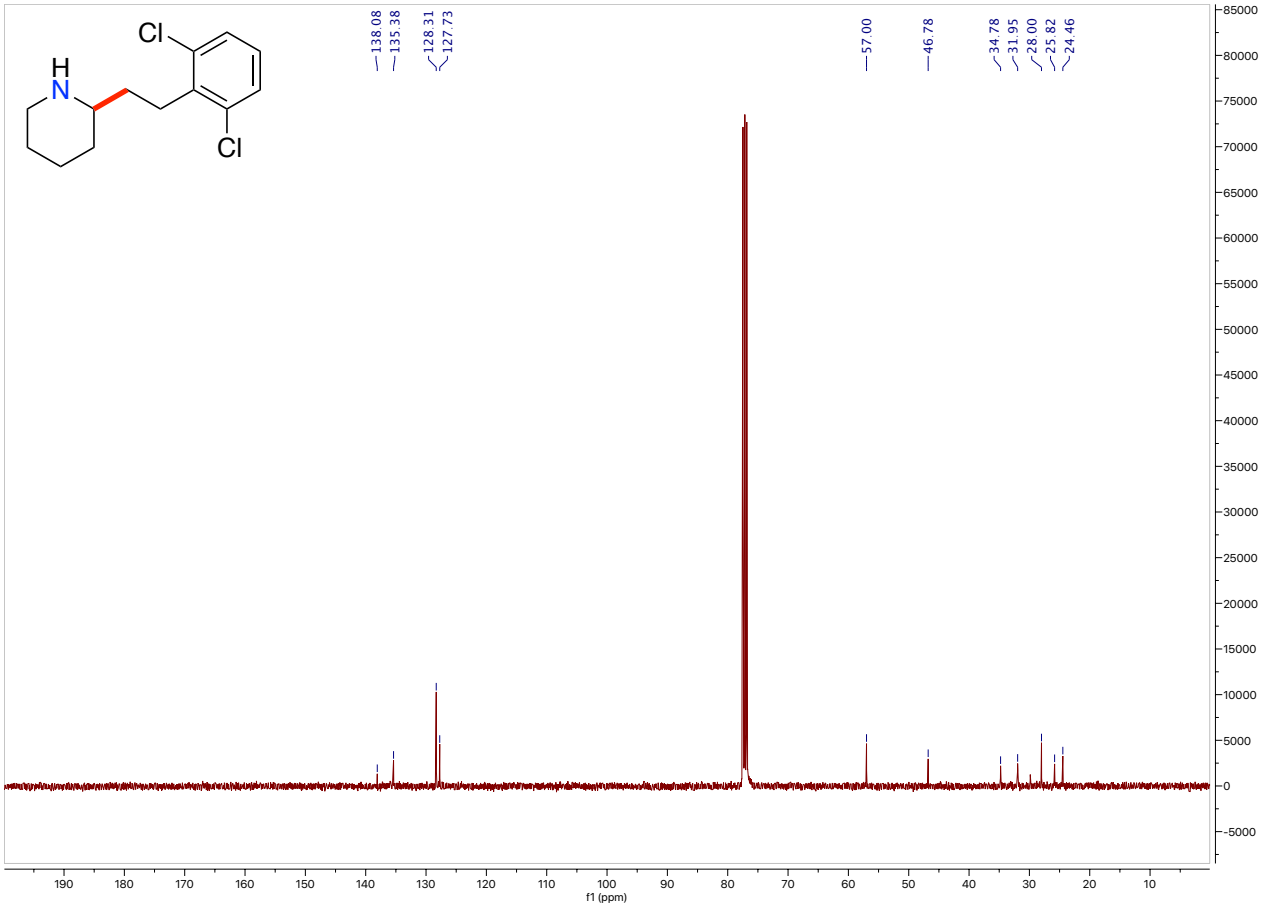

Figure. A.155. $^{13}C\{^{1}H\}$ NMR spectrum (101 MHz, $CDCl_3$, 298 K) of 2-(2,6-dichlorophenethyl)piperidine.

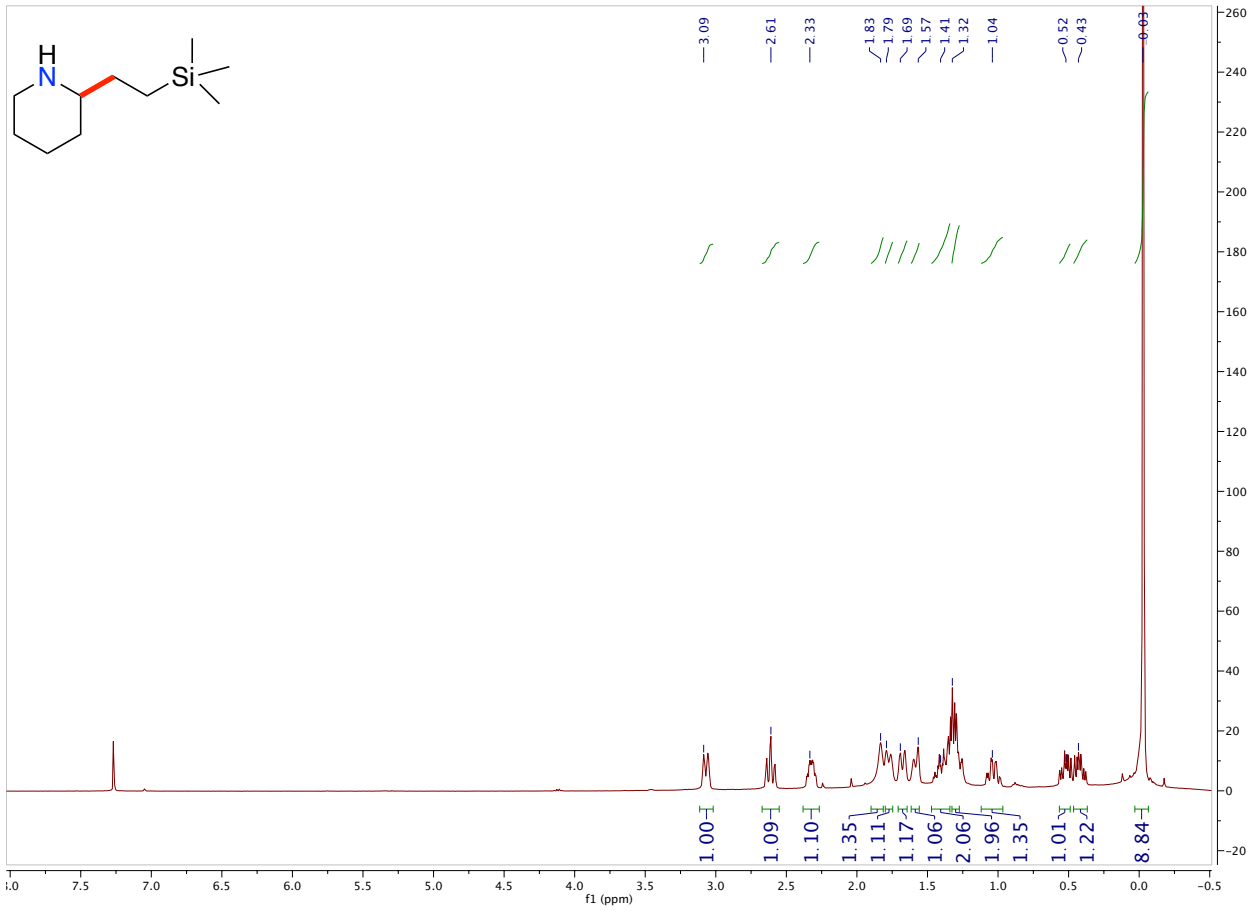

Figure. A.156. ^{1}H NMR spectrum (400 MHz, $CDCl_3$, 298 K) 2-(2-(trimethylsilyl)ethyl)piperidine.

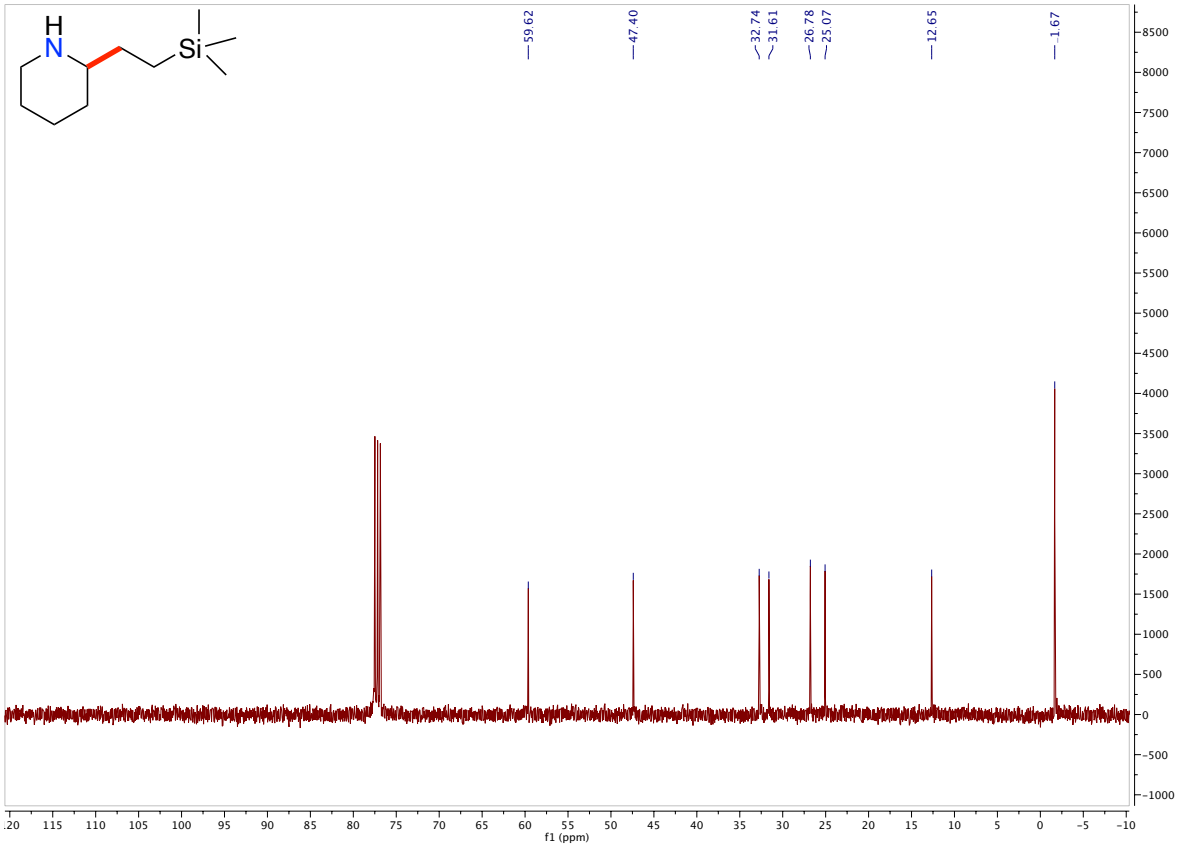

Figure. A.157. $^{13}C\{^{1}H\}$ NMR spectrum (101 MHz, $CDCl_3$, 298 K) of 2-(2-(trimethylsilyl)ethyl)piperidine.

A.13 Chapter 4 Amine Scope with 2-Chlorostyrene

Appendix B

This appendix is for GC-MS data.

B.1 Chapter 3 Pinene Scope GC-MS Data

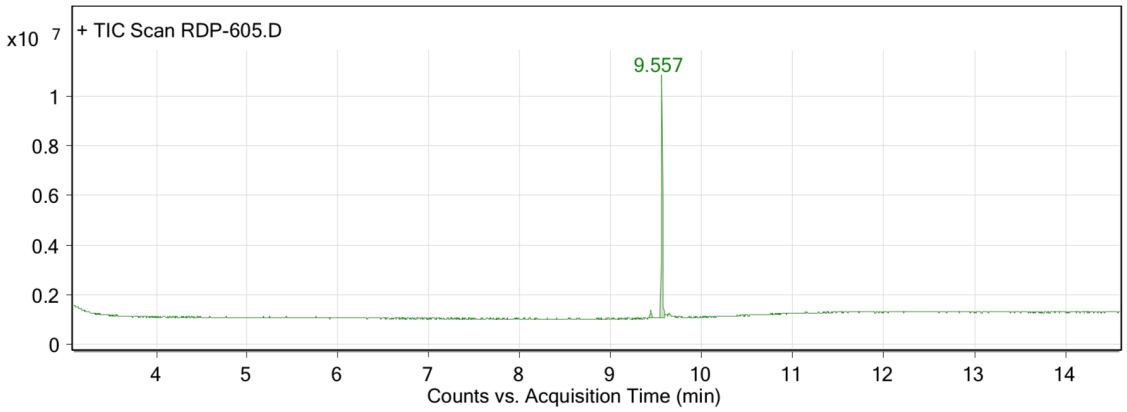

Integration Peak List

Peak	Start	RT	End	Height	Area	Area %
1	9.414	9.433	9.454	349924.76	317965.66	3.7
2	9.532	9.557	9.594	9824143.46	8582658.27	100

Figure. B.1. GC-MS chromatogram of *N*-((2,6,6-trimethylbicyclo[3.1.1]heptan-2-yl)methyl)aniline to confirm the d.r. value presented.

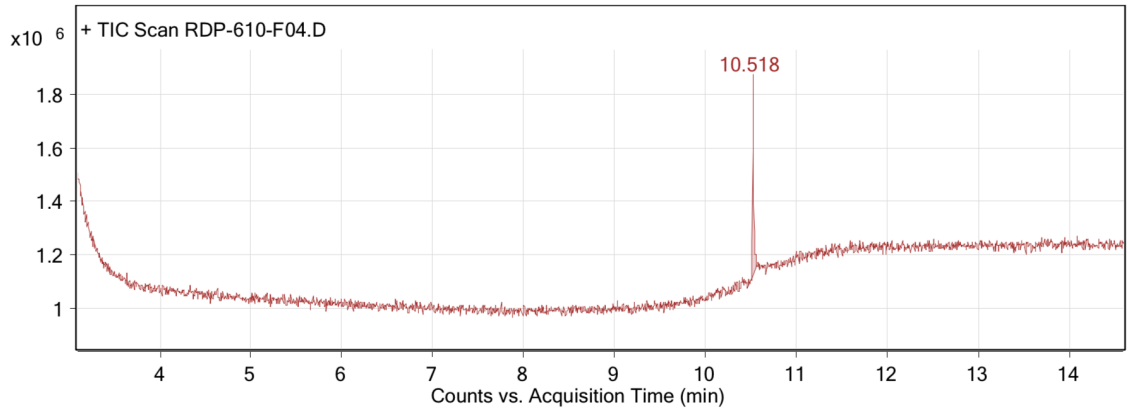

Integration Peak List

Peak	Start	RT	End	Height	Area	Area %
1	10.502	10.518	10.554	753673.62	754868.57	100

Figure. B.2. GC-MS chromatogram of 4-methoxy-*N*-((2,6,6-trimethylbicyclo[3.1.1]heptan-2-yl)methyl)aniline to confirm the d.r. value presented.

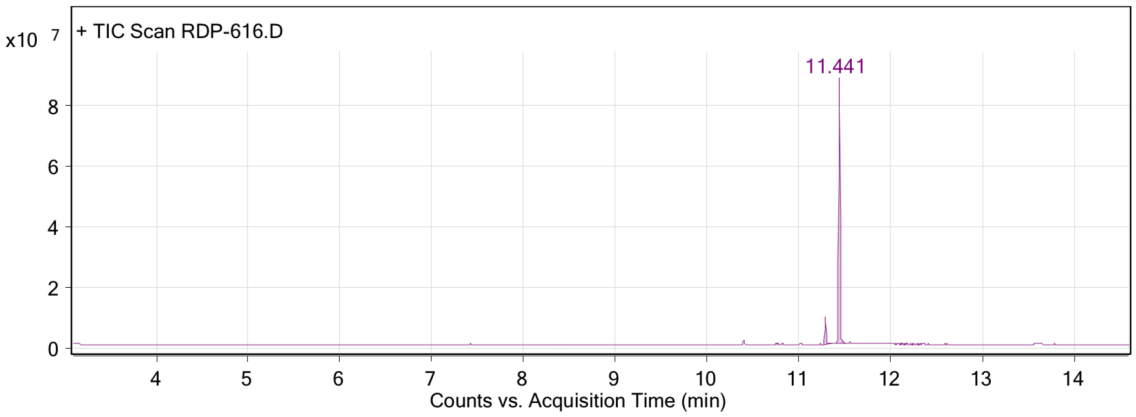

Integration Peak List

Peak	Start	RT	End	Height	Area	Area %
1	11.265	11.285	11.353	8874897.31	8744974.79	7.24
2	11.408	11.441	11.508	87422670.89	120739144.87	100

Figure. B.3. GC-MS chromatogram of 4-(methylthio)-*N*-((2,6,6-trimethylbicyclo[3.1.1]heptan-2-yl)methyl)aniline to confirm the d.r. value presented.

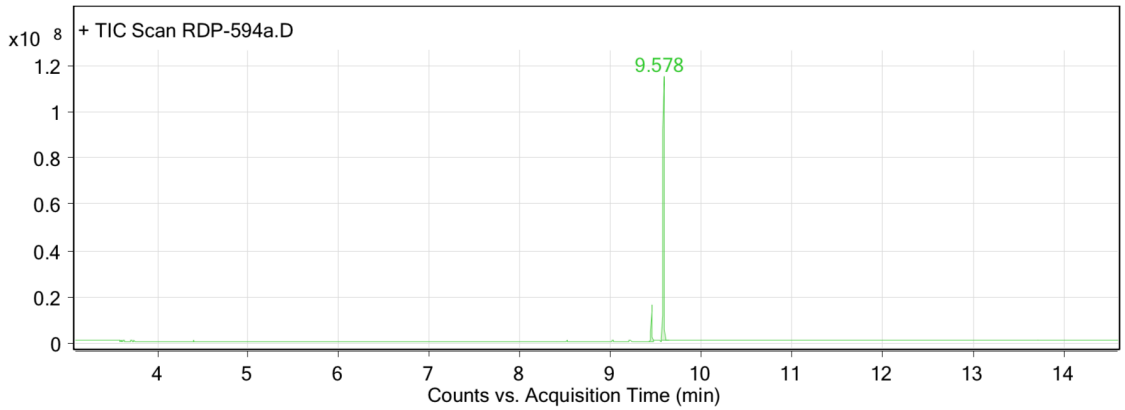

Integration Peak List

Peak	Start	RT	End	Height	Area	Area %
1	9.418	9.449	9.475	15782033.28	13356868.63	9.89
2	9.553	9.578	9.635	113929405.31	135121345.04	100

Figure. B.4. GC-MS chromatogram of 4-fluoro-*N*-(((1R,2S,5S)-2,6,6-trimethylbicyclo[3.1.1]heptan-2-yl)methyl)aniline to confirm the d.r. value presented.

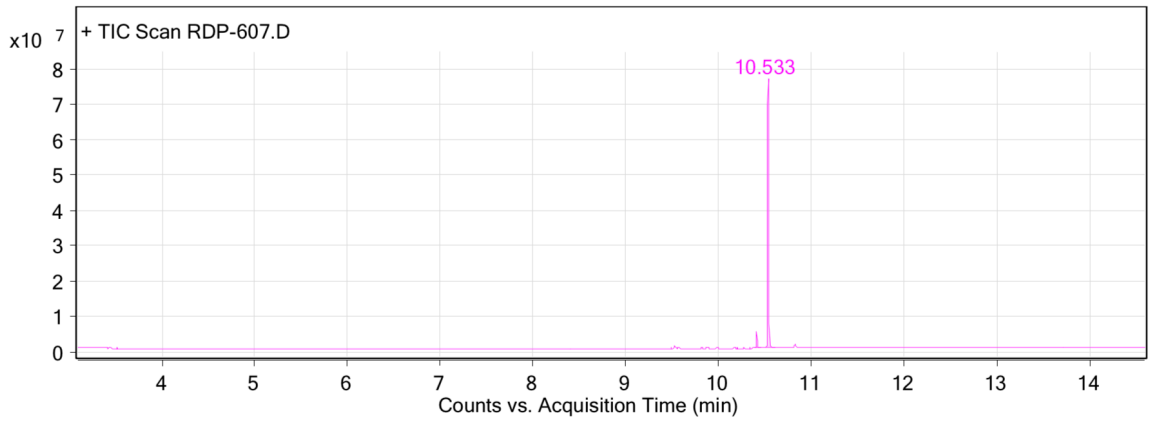

Integration Peak List

Peak	Start	RT	End	Height	Area	Area %
1	10.388	10.408	10.444	4518422.62	4031944.37	5.43
2	10.505	10.533	10.6	75993335.81	74304441.33	100

Figure. B.5. GC-MS chromatogram of 4-chloro-*N*-((2,6,6-trimethylbicyclo[3.1.1]heptan-2-yl)methyl)aniline to confirm the d.r. value presented.

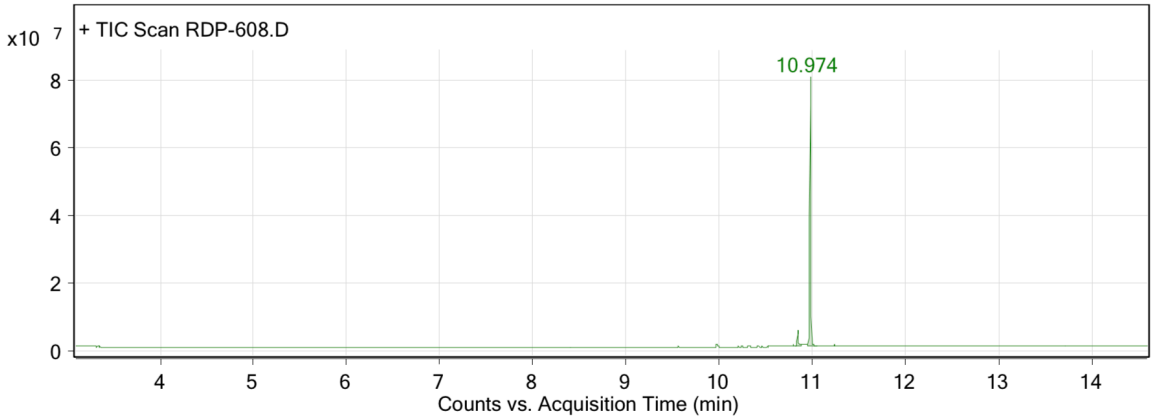

Integration Peak List

Peak	Start	RT	End	Height	Area	Area %
1	10.808	10.839	10.875	4738333.18	4845671.51	5.93
2	10.938	10.974	11.041	79615436.54	81762406.71	100

Figure. B.6. GC-MS chromatogram of 4-bromo-*N*-((2,6,6-trimethylbicyclo[3.1.1]heptan-2-yl)methyl)aniline to confirm the d.r. value presented.

B.2 Chapter 4 Amine Scope with 1-Octene GC-MS Data

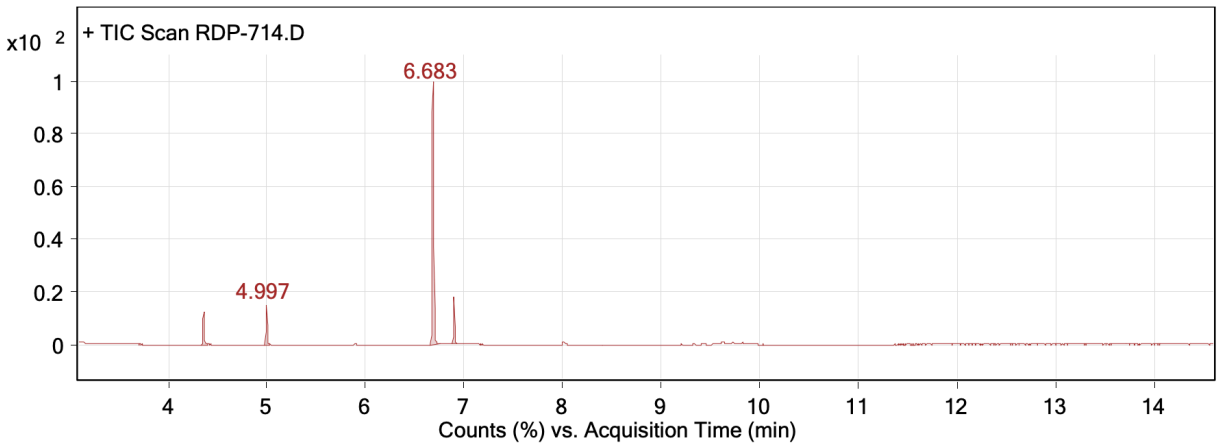

Figure. B.7. GC-MS chromatogram for the crude reaction mixture between piperidine and 1-

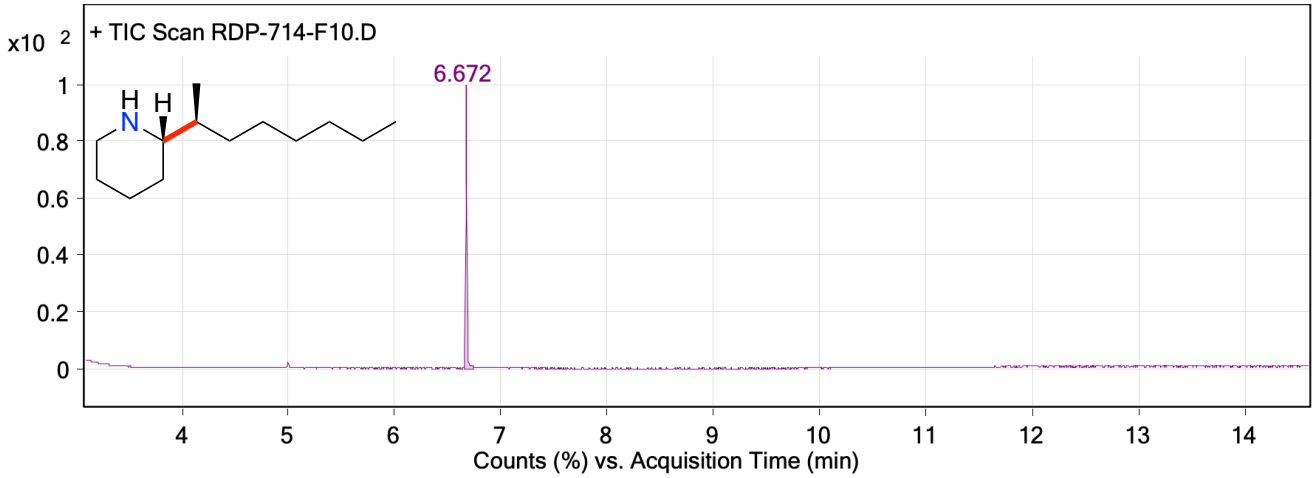

octene.

Figure. B.8. GC-MS chromatogram of 2-(octan-2-yl)piperidine.

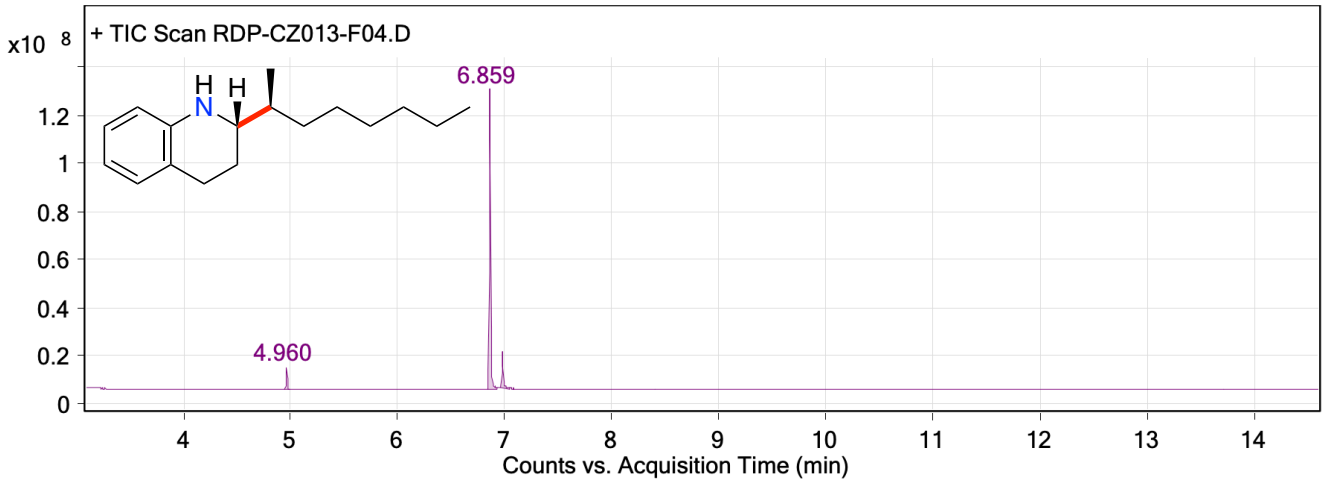

Figure. B.9. GC-MS chromatogram of 2-(octan-2-yl)-1,2,3,4-tetrahydroquinoline.

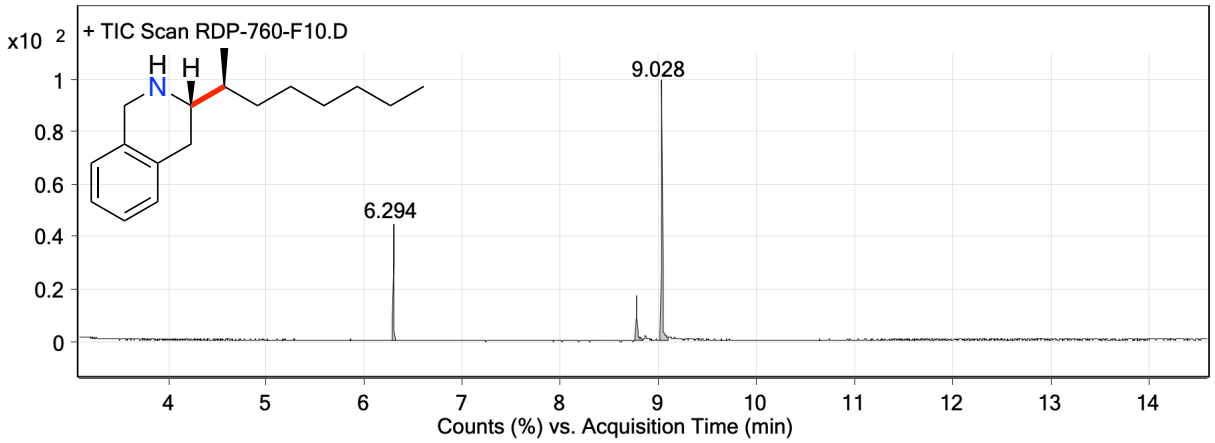

Figure. B.10. GC-MS chromatogram of 3-(octan-2-yl)-1,2,3,4-tetrahydroisoquinoline. Note that the peak at 6.294 represents residual internal standard.

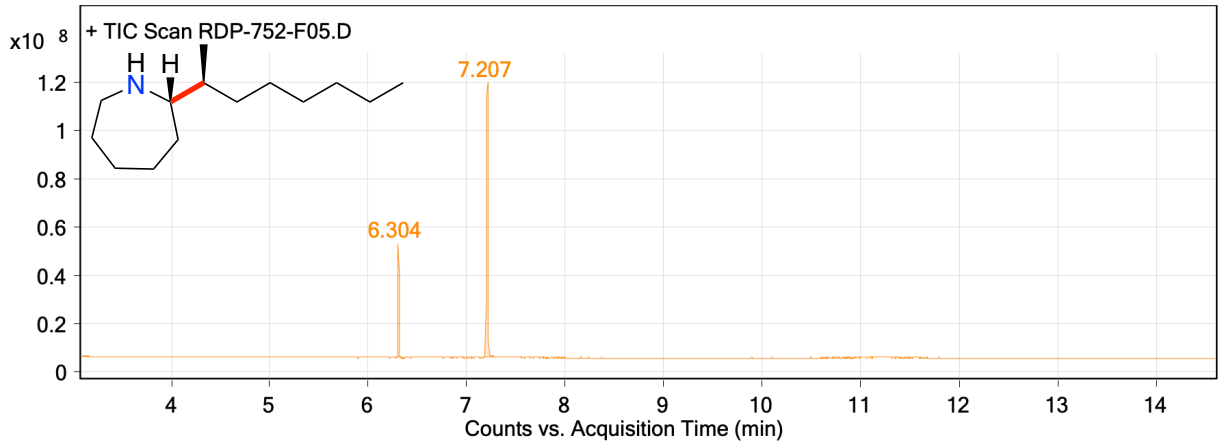

Figure. B.11. GC-MS chromatogram of 2-(octan-2-yl)azepane. Note that the peak at 6.304 min represents residual internal standard.

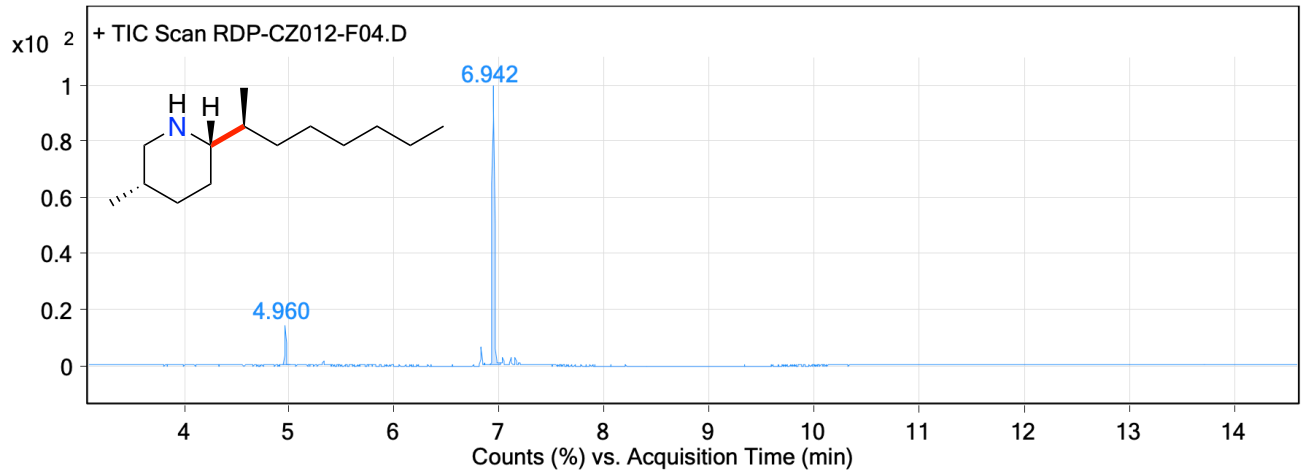

Figure. B.12. GC-MS chromatogram of 4-methyl-2-(octan-2-yl)piperidine.

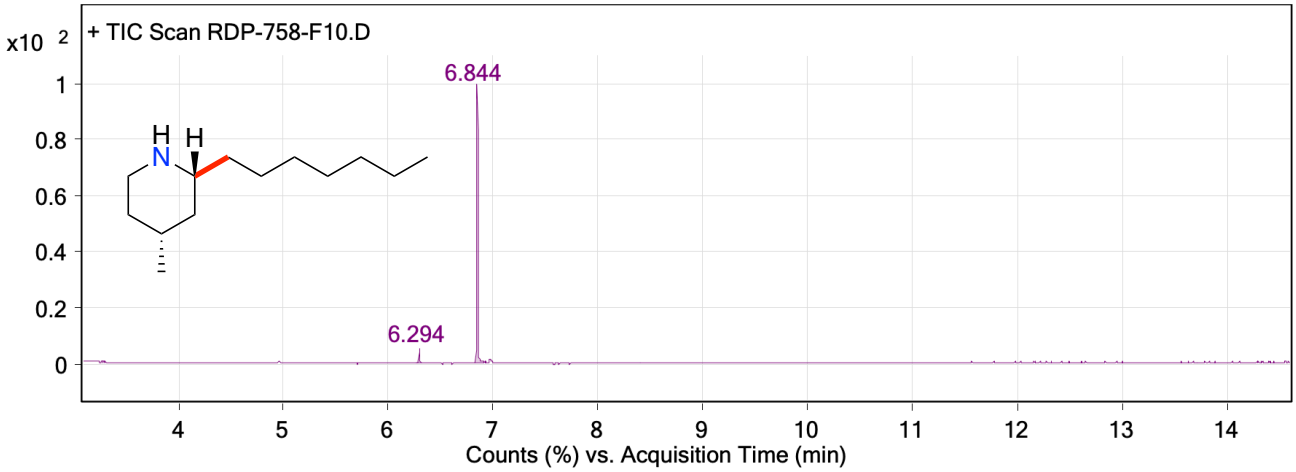

Figure. B.13. GC-MS chromatogram of 4-methyl-2-(octan-2-yl)piperidine.

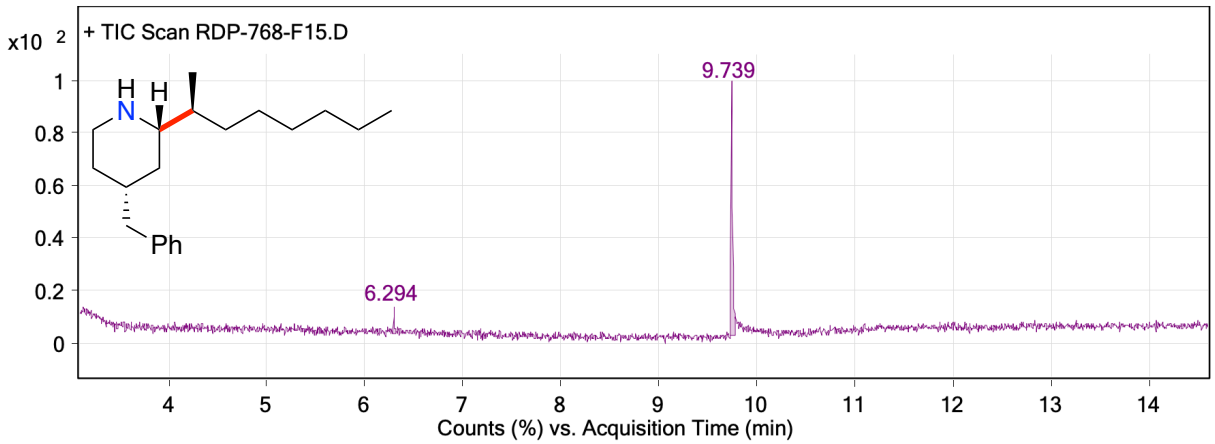

Figure. B.14. GC-MS chromatogram of 4-benzyl-2-(octan-2-yl)piperidine.

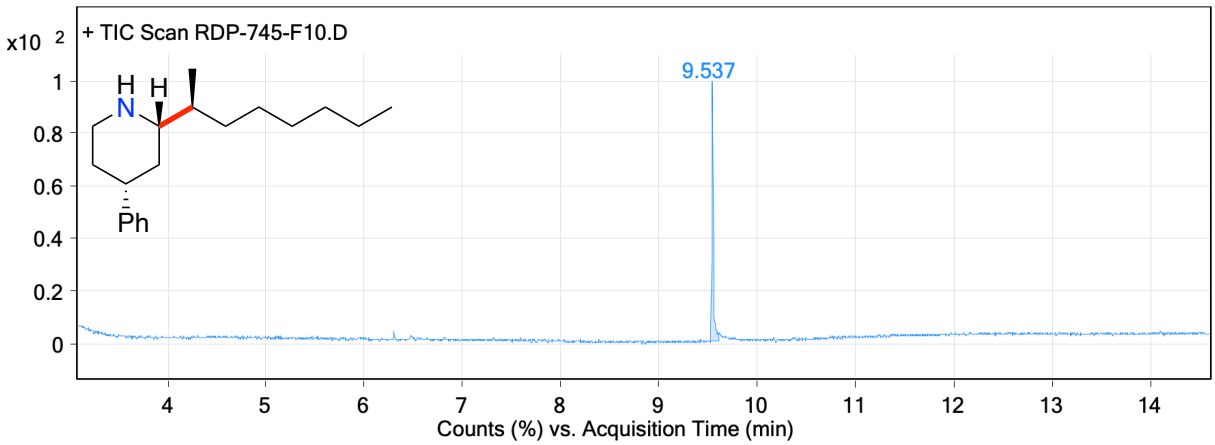

Figure. B.15. GC-MS chromatogram of 2-(octan-2-yl)-4-phenylpiperidine.

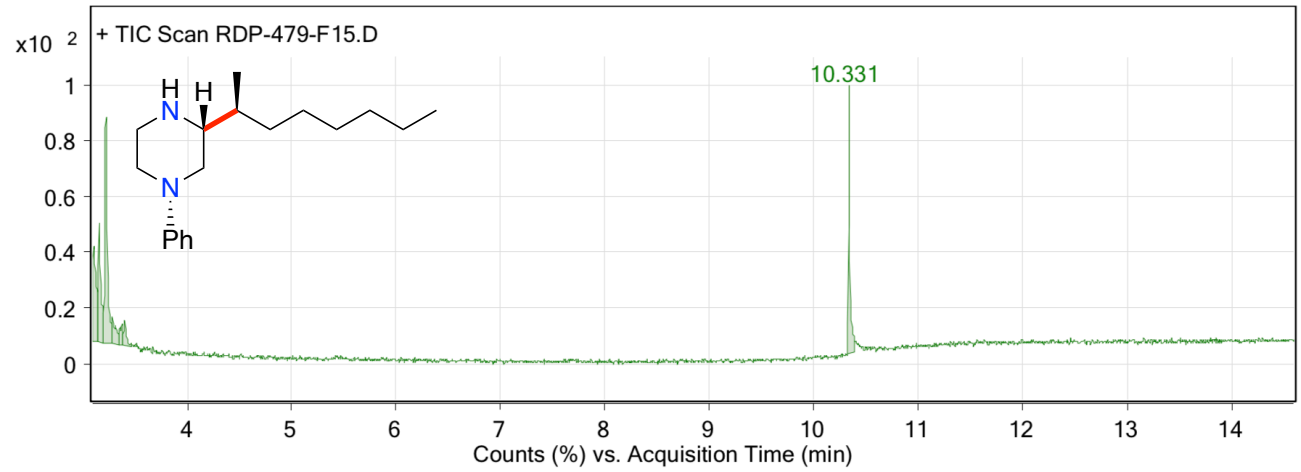

Figure. B.16. GC-MS chromatogram of 3-(octan-2-yl)-1-phenylpiperazine.

B.3 Chapter 4 Alkene Scope GC-MS Data

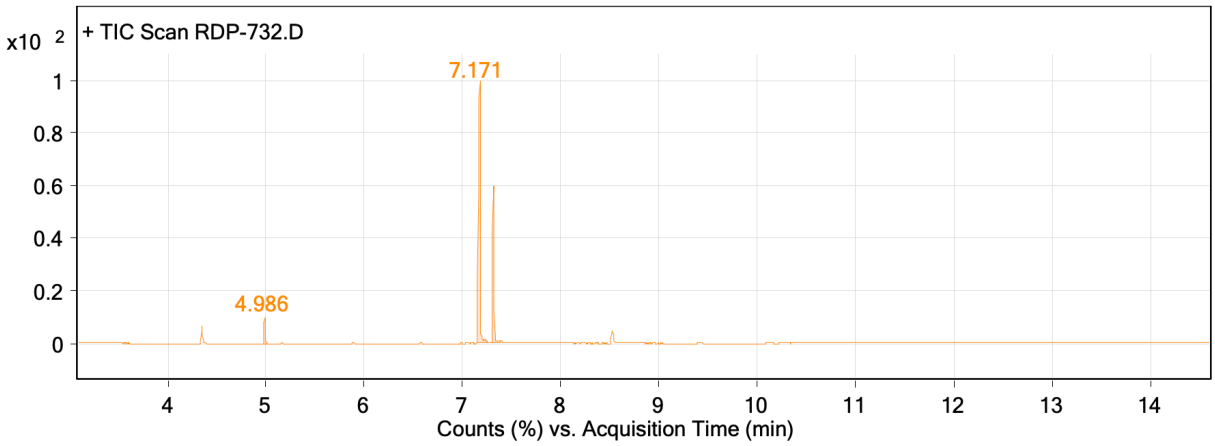

Figure. B.17. GC-MS chromatogram for crude reaction mixture between piperidine and vinylcyclohexene.

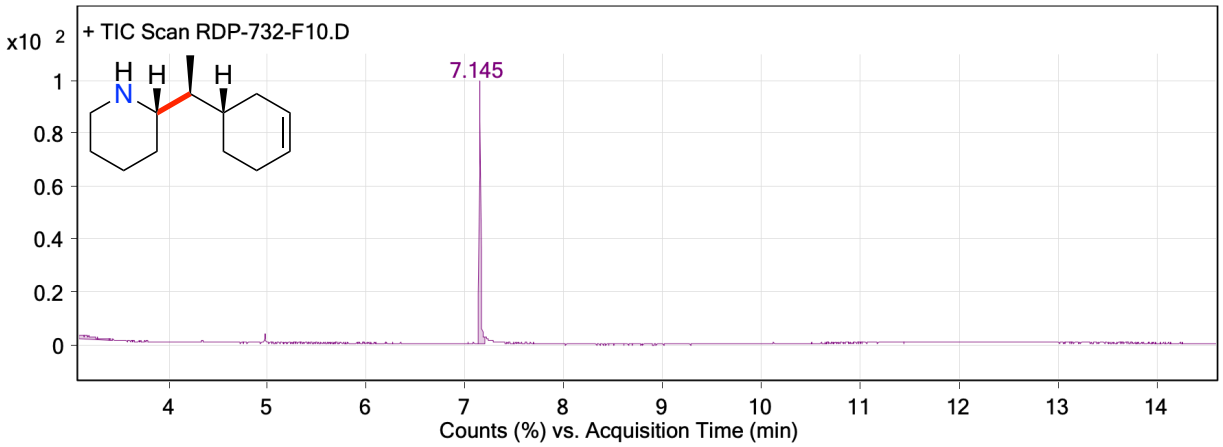

Figure. B.18. GC-MS chromatogram for the major diastereomer of 2-(1-(cyclohex-3-en-1-yl)ethyl)piperidine.

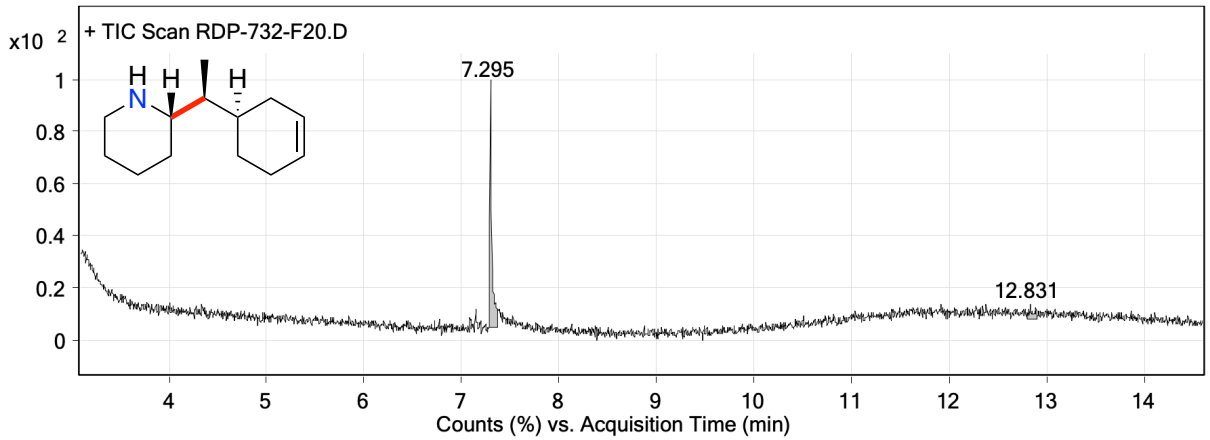

Figure. B.19. GC-MS chromatogram for the minor diastereomer of 2-(1-(cyclohex-3-en-1-yl)ethyl)piperidine.

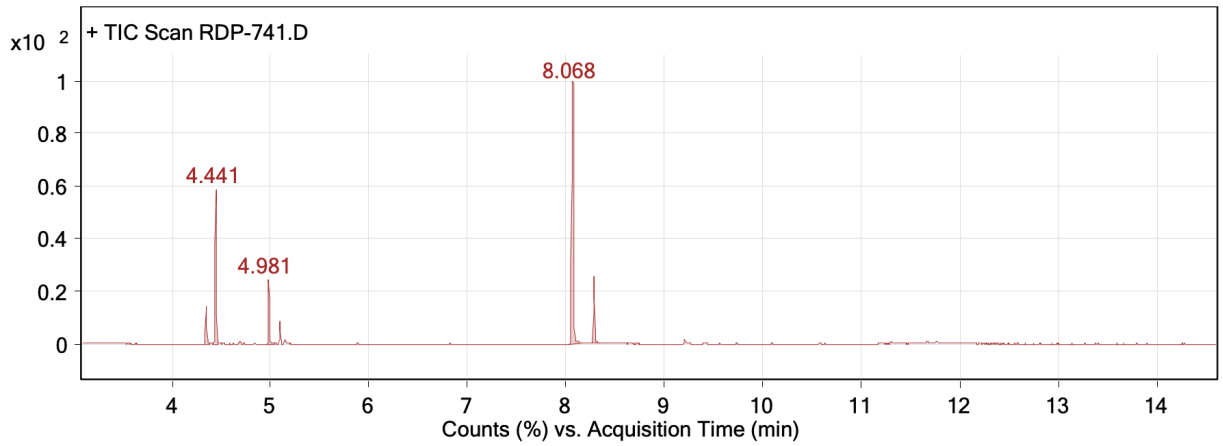

Figure. B.20. GC-MS chromatogram for the crude reaction mixture between piperidine and tert-butyldimethyl(pent-4-en-1-yloxy)silane.

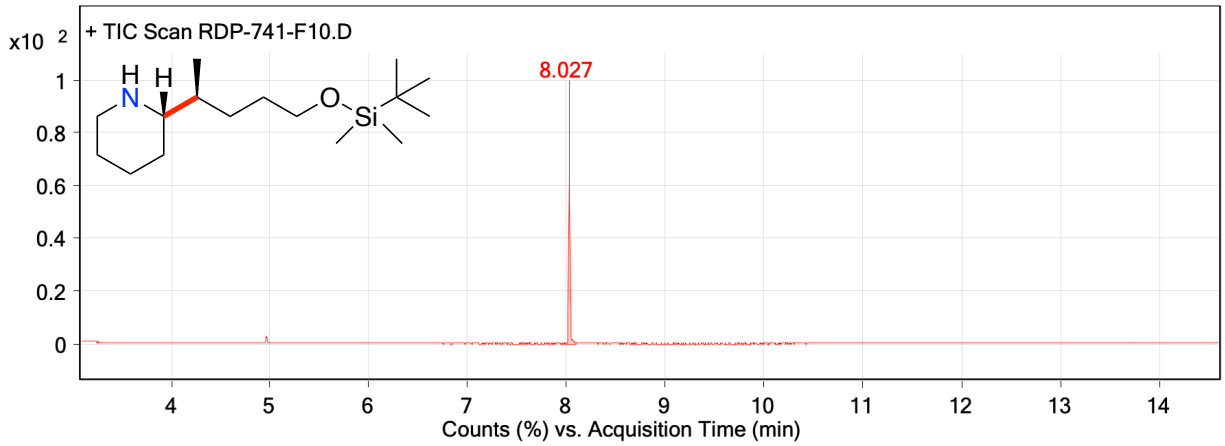

Figure. B.21. GC-MS chromatogram of 2-(5-((tert-butyldimethylsilyl)oxy)pentan-2-yl)piperidine.

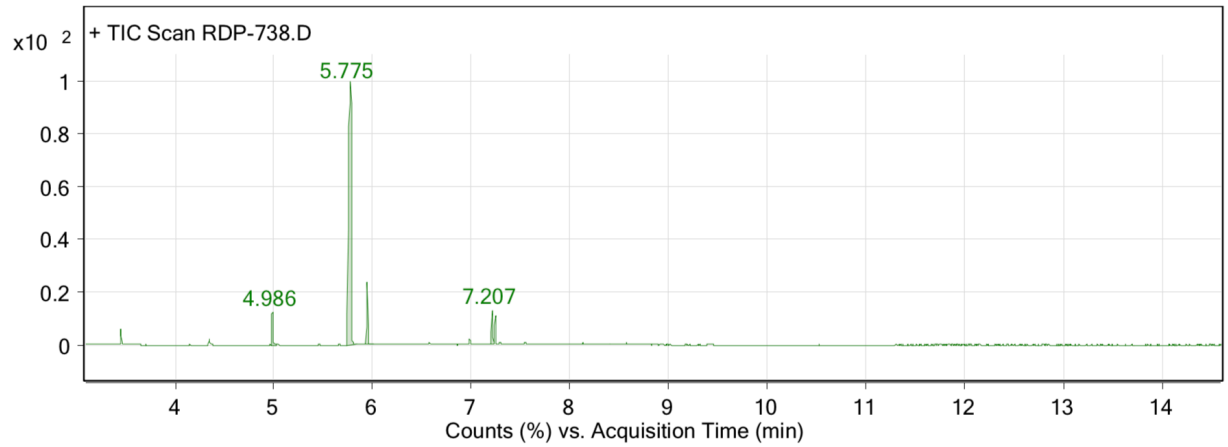

Figure. B.22. GC-MS chromatogram for the crude reaction between piperidine and allyltrimethylsilane.

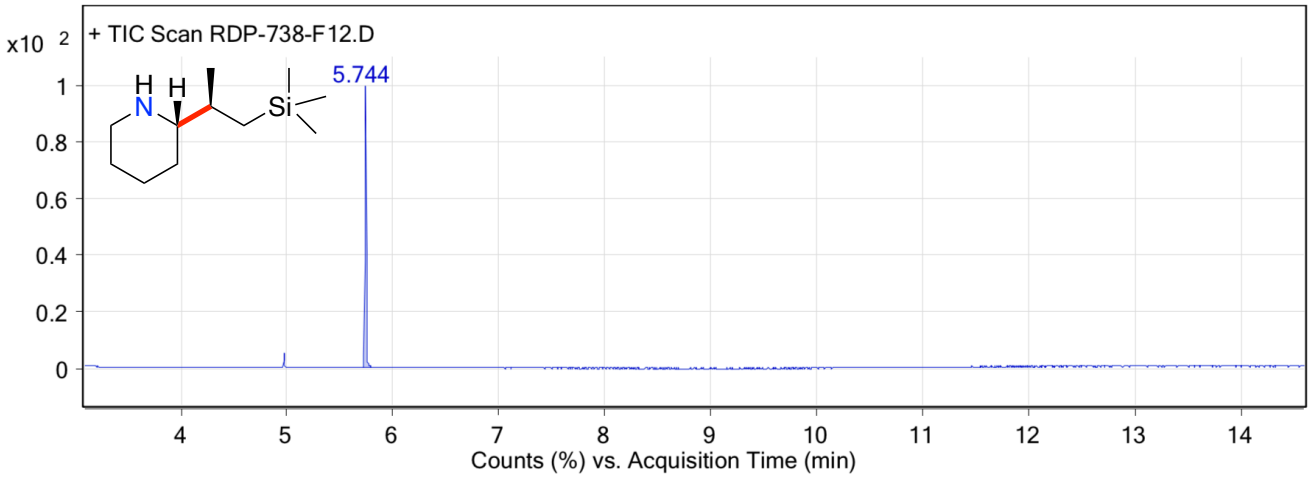

Figure. B.23. GC-MS chromatogram spectrum (101 MHz, $CDCl_3$, 298 K) of 2-(1-(trimethylsilyl)propan-2-yl)piperidine.

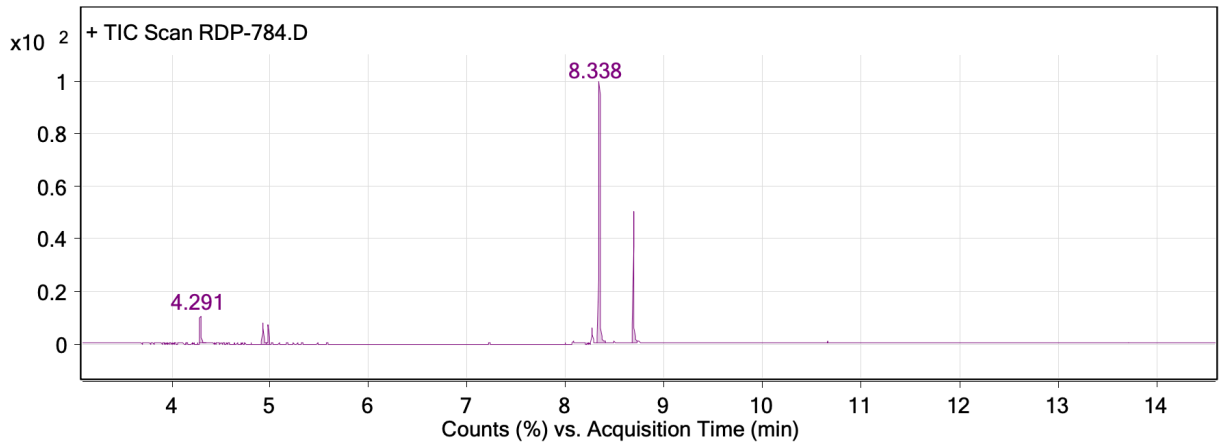

Figure. B.24. GC-MS chromatogram for the crude reaction mixture between piperidine and para-t-butylstyrene.

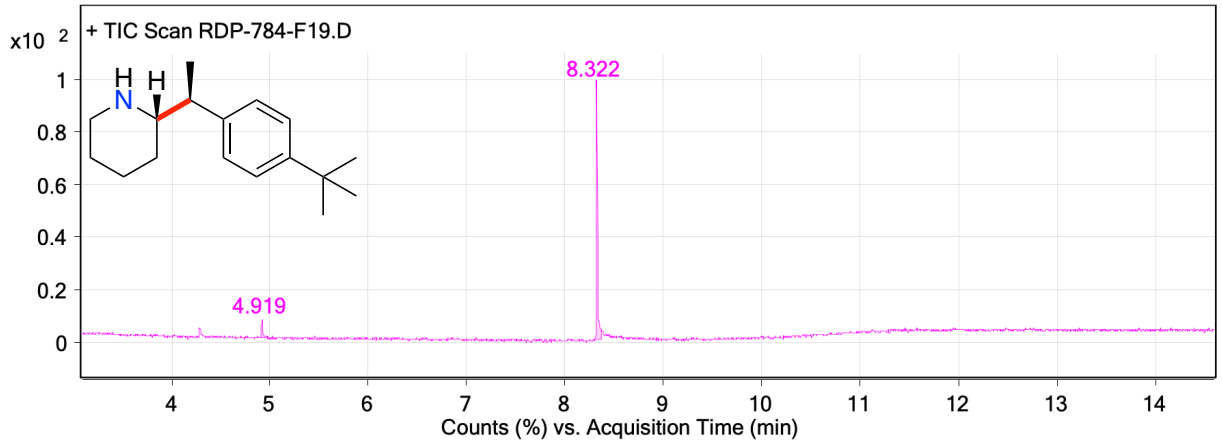

Figure. B.25. GC-MS chromatogram for 2-(1-(4-(tert-butyl)phenyl)ethyl)piperidine.

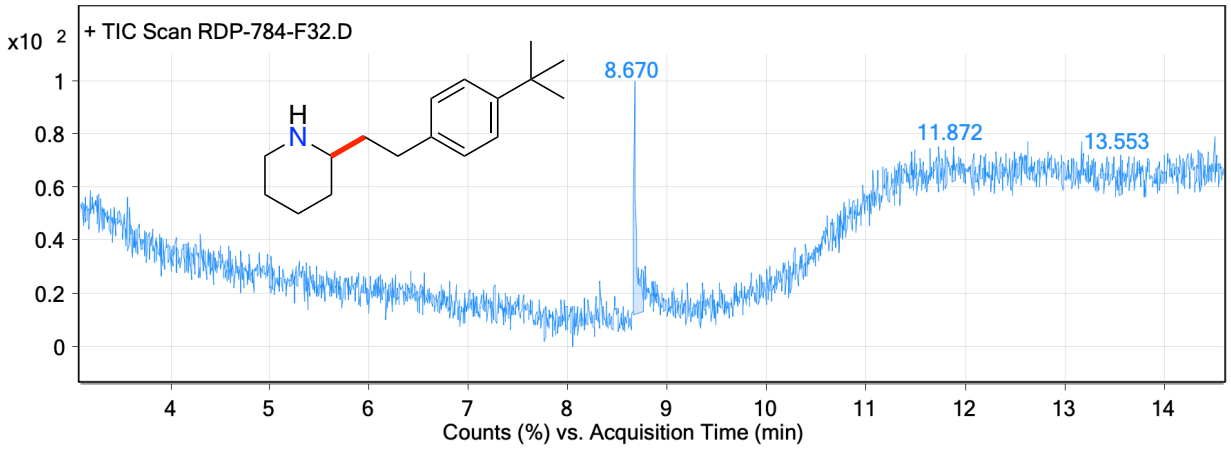

Figure. B.26. GC-MS chromatogram for 2-(4-(tert-butyl)phenethyl)piperidine.

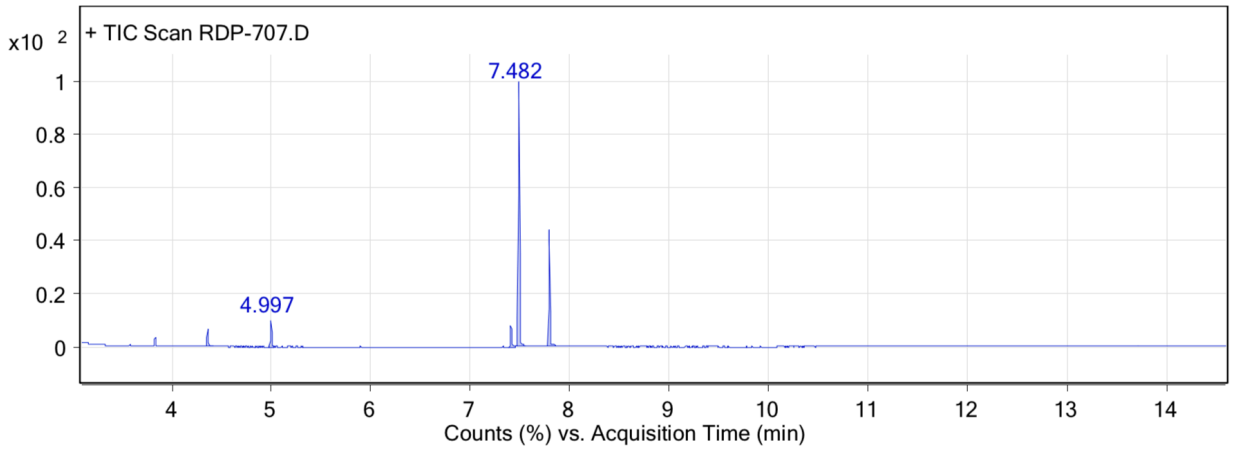

Figure. B.27. GC-MS chromatogram for the crude reaction mixture between piperidine and 4-methylstyrene.

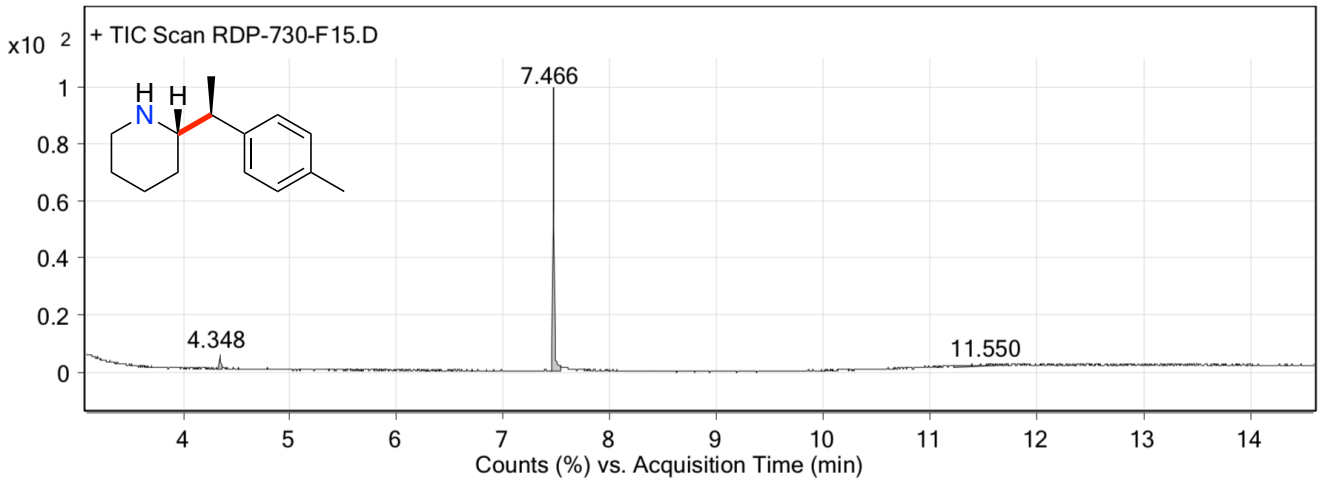

Figure. B.28. GC-MS chromatogram of 2-(1-(p-tolyl)ethyl)piperidine.

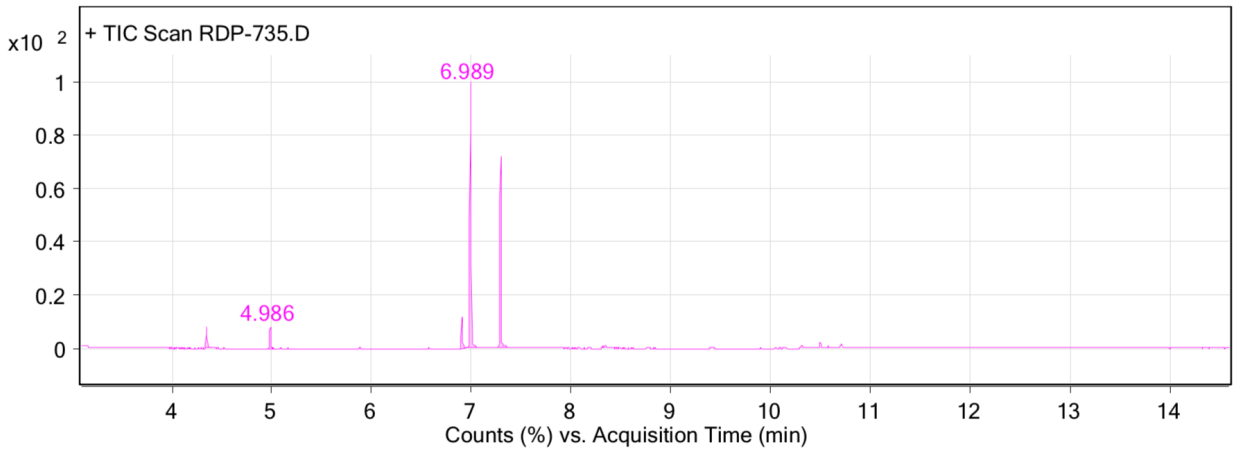

Figure. B.29. GC-MS chromatogram for the crude reaction mixture between piperidine and styrene

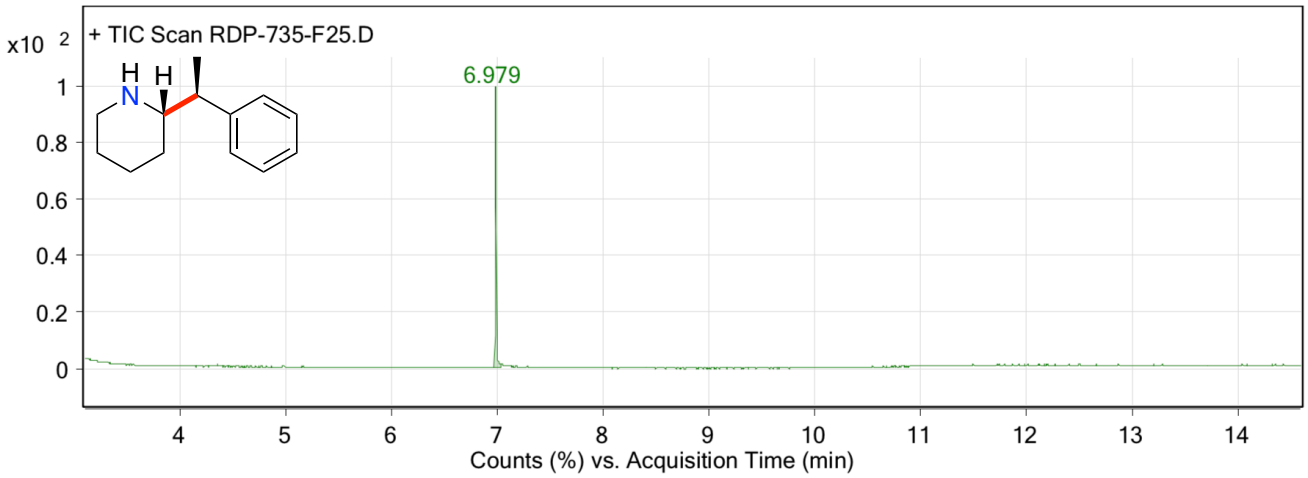

Figure. B.30. GC-MS chromatogram of 2-(1-phenylethyl)piperidine.

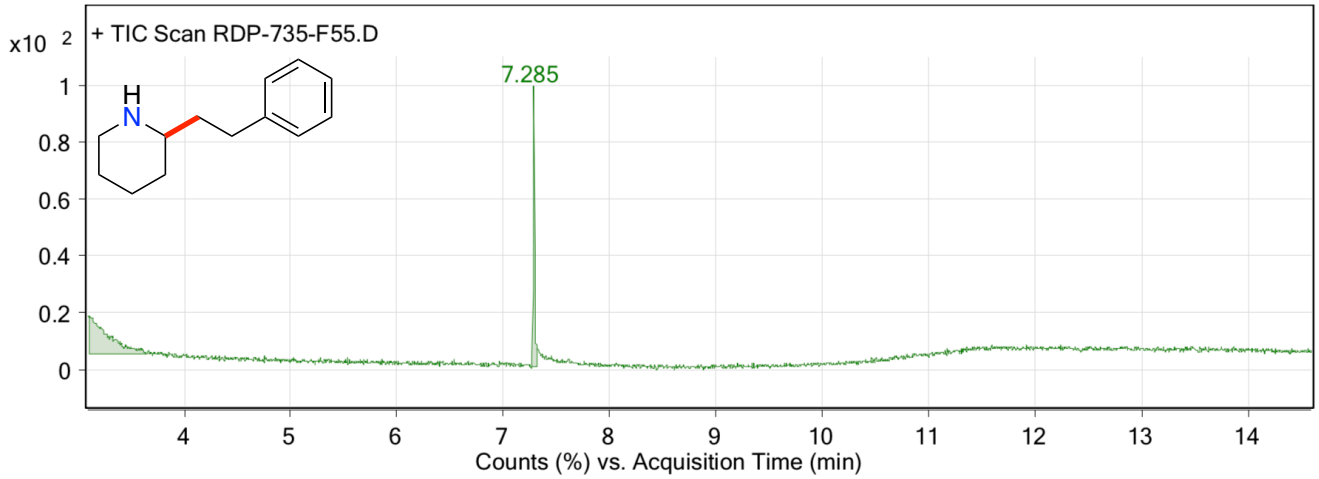

Figure. B.31. GC-MS chromatogram of 2-phenethylpiperidine.

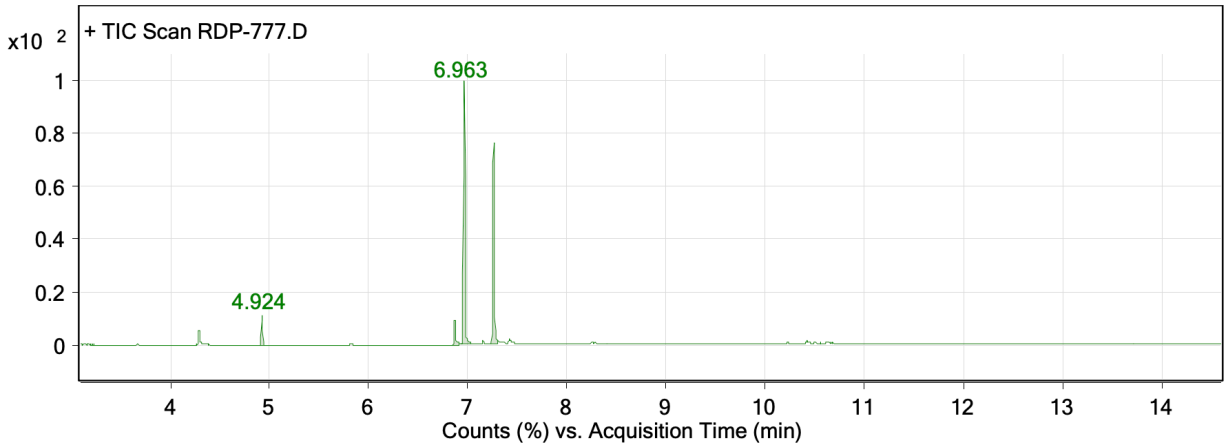

Figure. B.32. GC-MS chromatogram for crude reaction mixture between piperidine and para-fluorostyrene

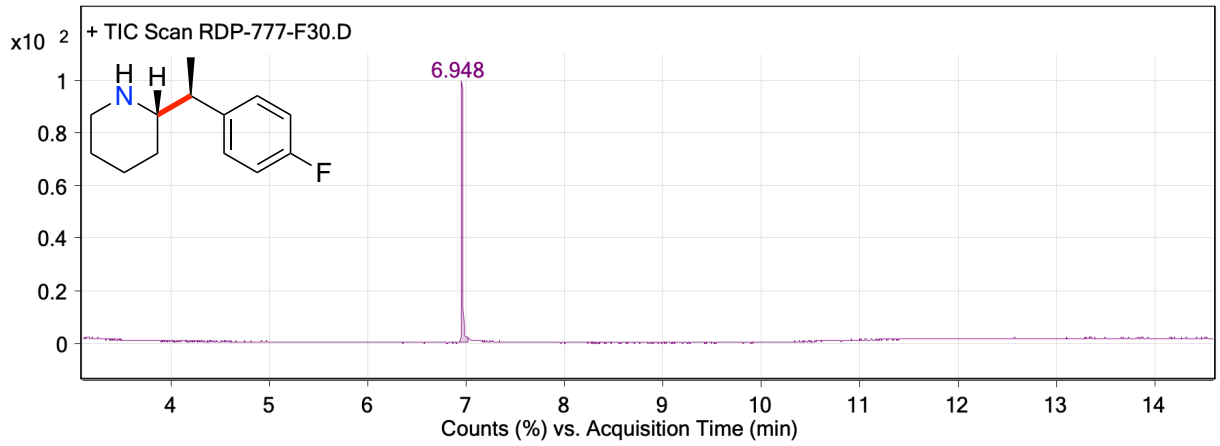

Figure. B.33. GC-MS chromatogram for 2-(1-(4-fluorophenyl)ethyl)piperidine.

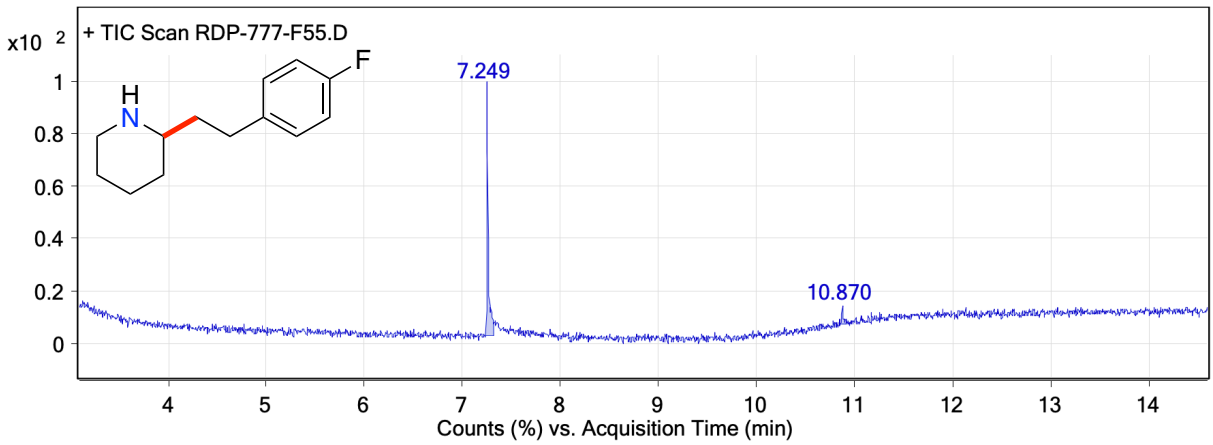

Figure. B.34. GC-MS chromatogram for 2-(4-fluorophenethyl)piperidine.

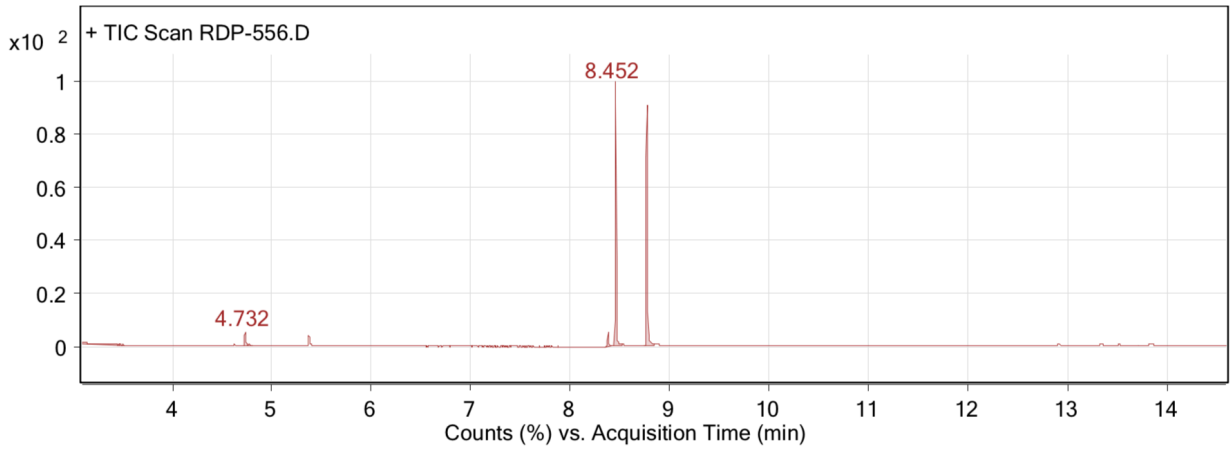

Figure. B.35. GC-MS chromatogram for the crude reaction mixture between piperidine and 4-chlorostyrene.

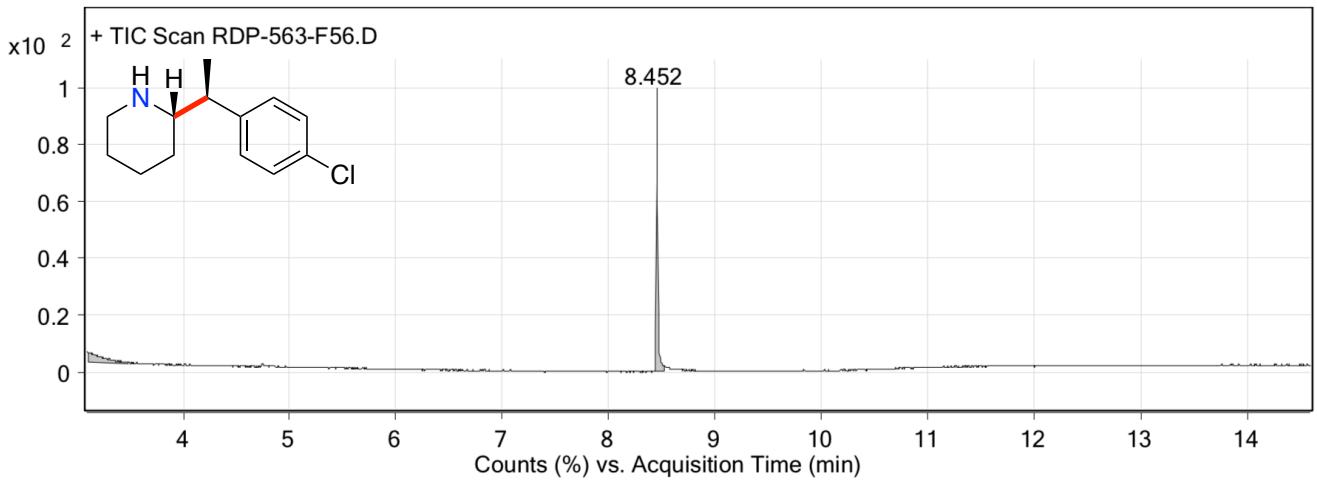

Figure. B.36. GC-MS chromatogram of 2-(1-(4-chlorophenyl)ethyl)piperidine.

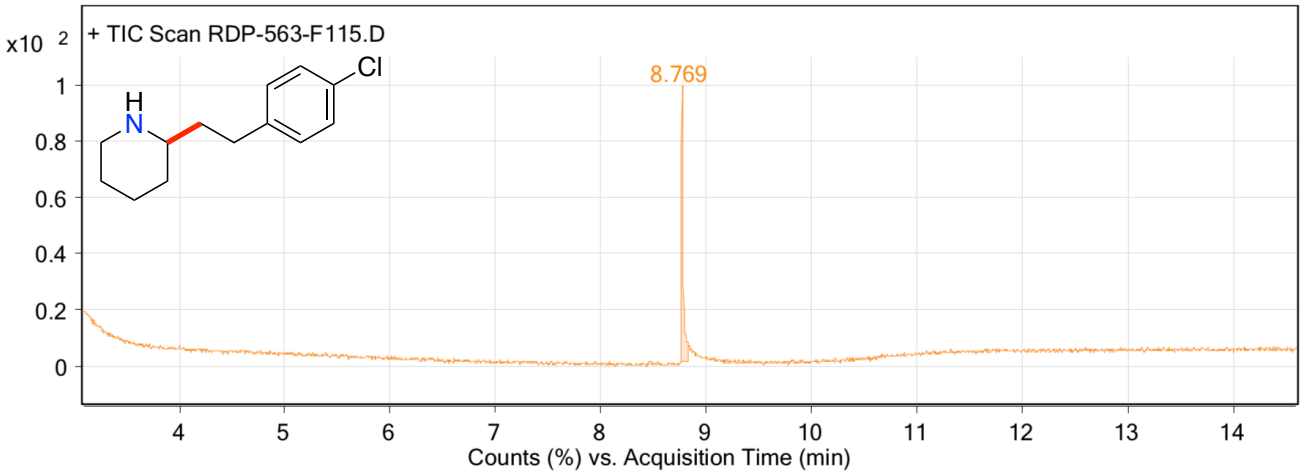

Figure. B.37. GC-MS chromatogram of 2-(4-chlorophenethyl)piperidine.

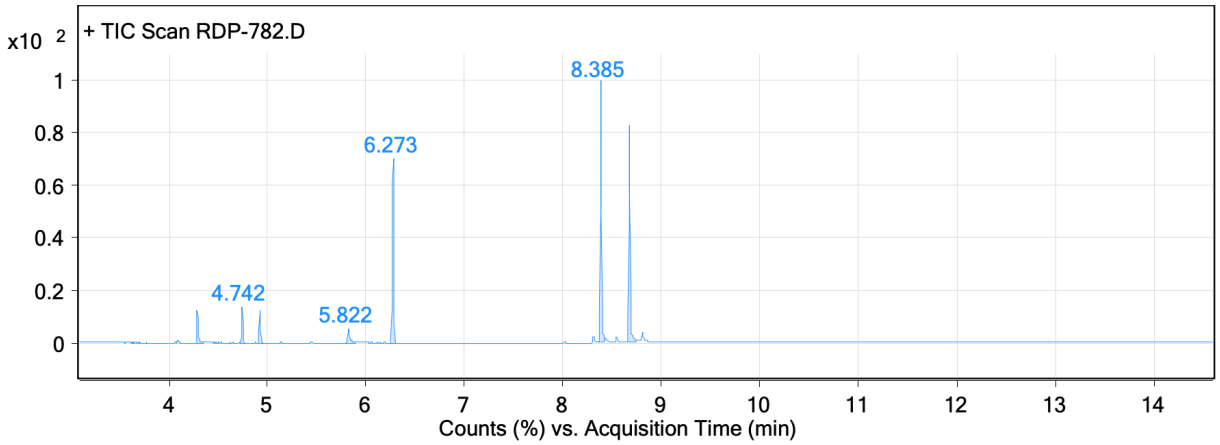

Figure. B.38. GC-MS chromatogram for the crude reaction mixture between piperidine and para-bromostyrene.

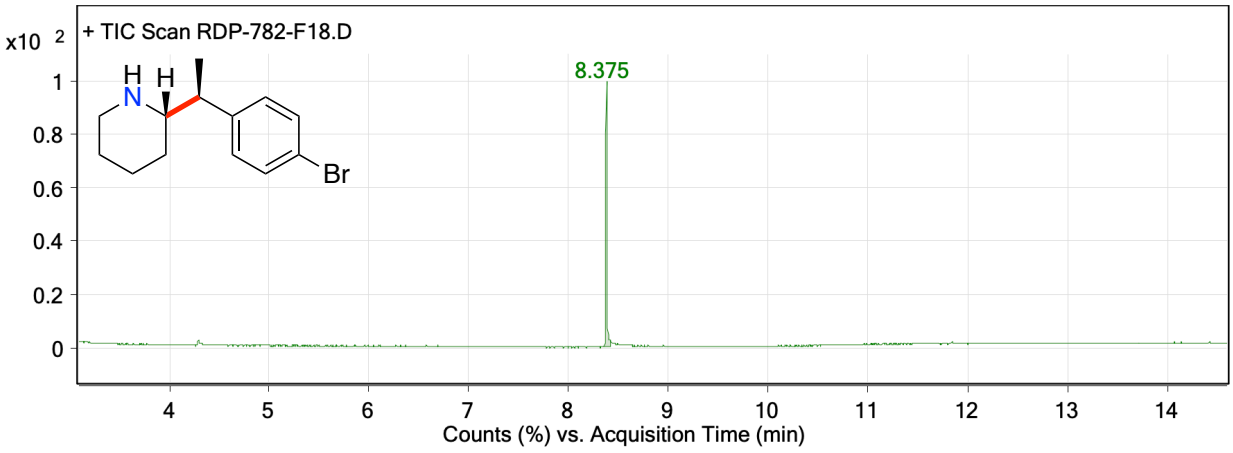

Figure. B.39. GC-MS chromatogram for 2-(1-(4-bromophenyl)ethyl)piperidine.

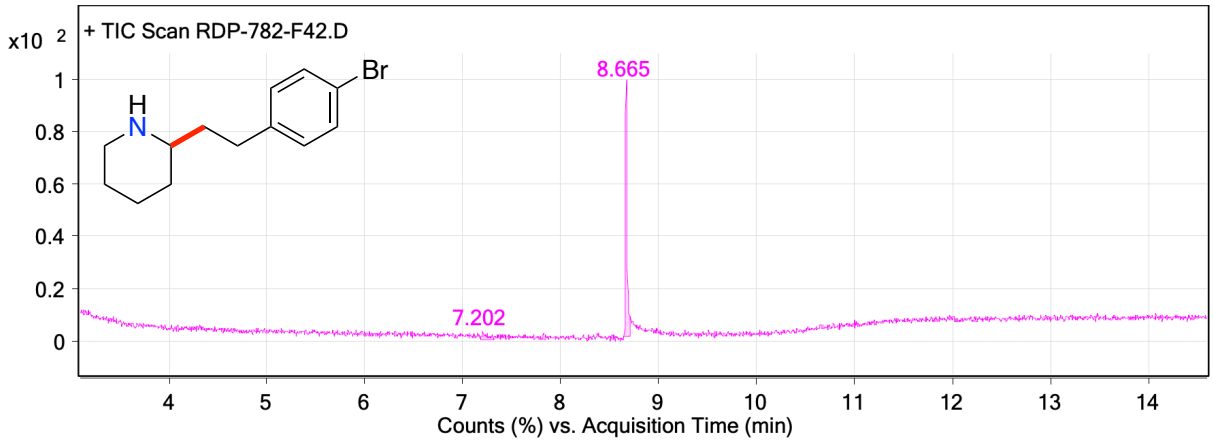

Figure. B.40. GC-MS chromatogram for 2-(4-bromophenethyl)piperidine.

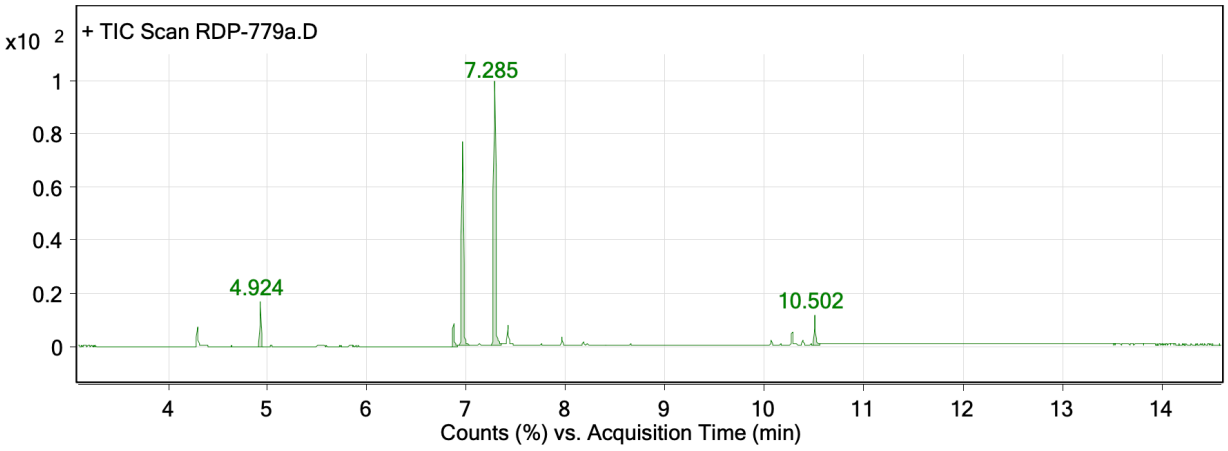

Figure. B.41. GC-MS chromatogram for the crude reaction mixture between piperidine and para-trifluoromethylstyrene.

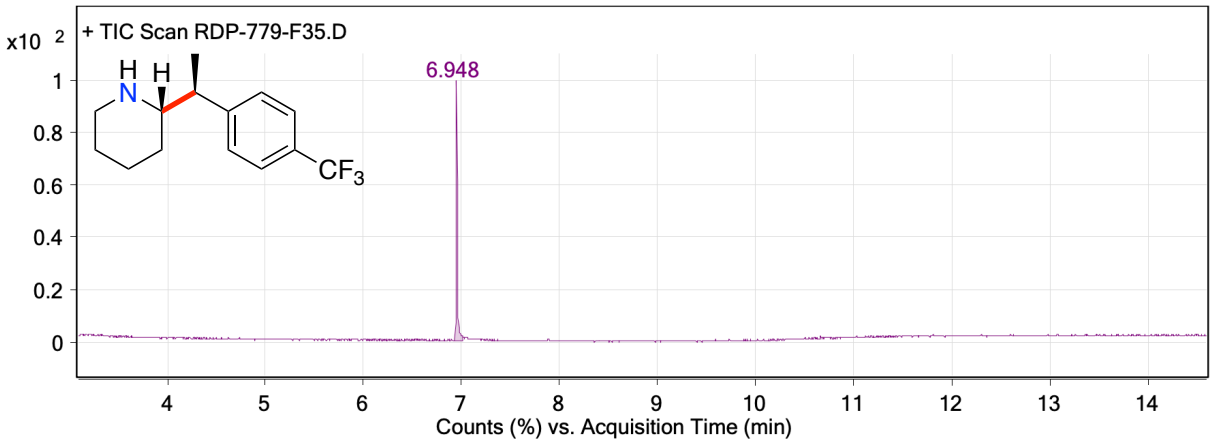

Figure. B.42. GC-MS chromatogram for 2-(1-(4-(trifluoromethyl)phenyl)ethyl)piperidine.

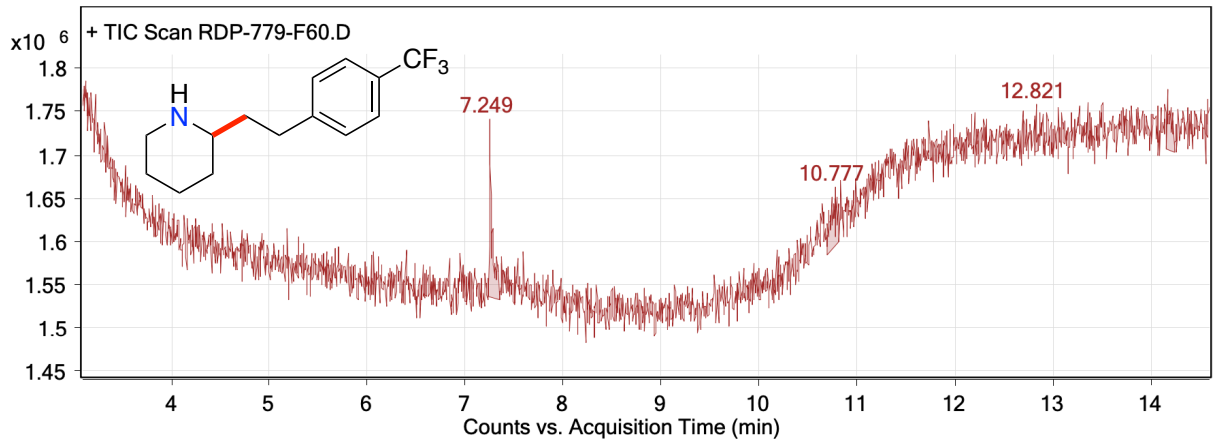

Figure. B.43. GC-MS chromatogram for 2-(4-(trifluoromethyl)phenethyl)piperidine.

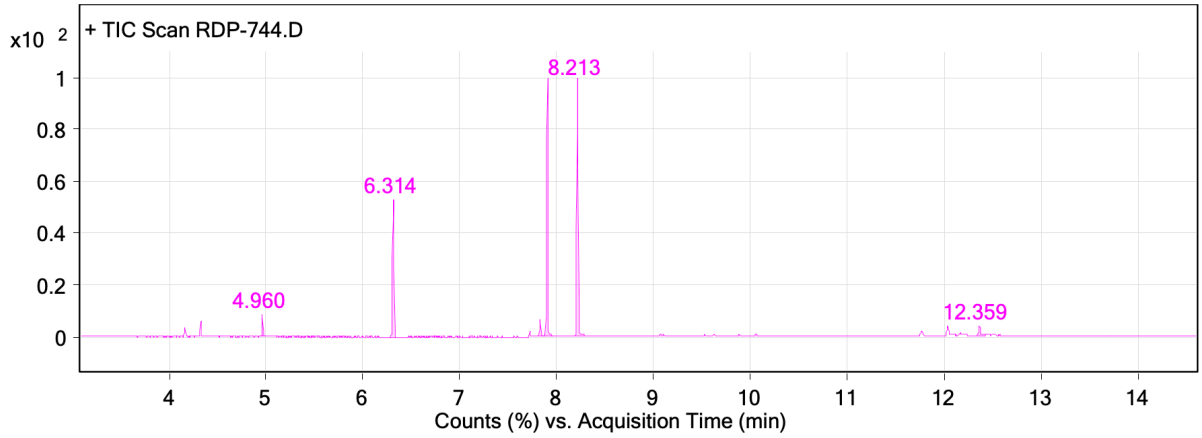

Figure. B.44. GC-MS chromatogram for the crude reaction mixture between piperidine and meta-chlorostyrene.

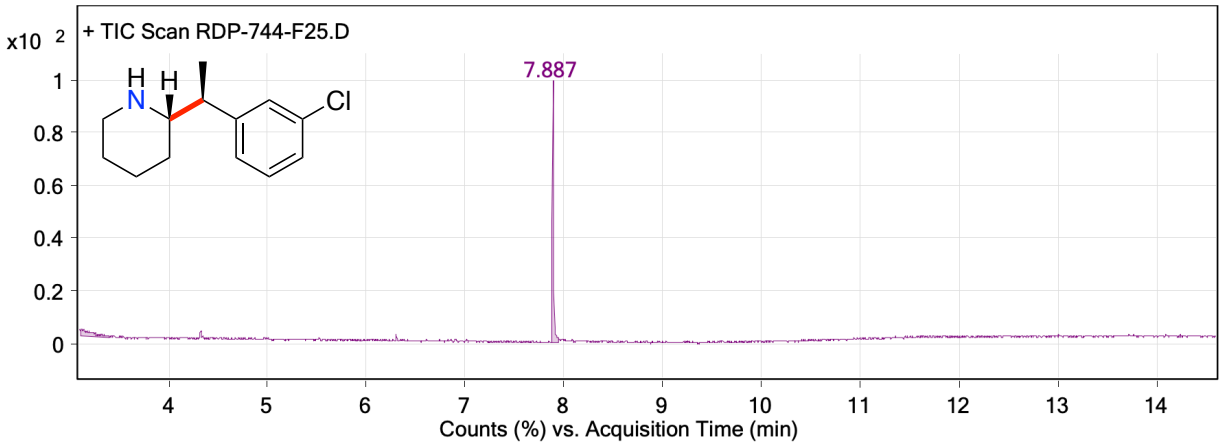

Figure. B.45. GC-MS chromatogram for 2-(1-(3-chlorophenyl)ethyl)piperidine.

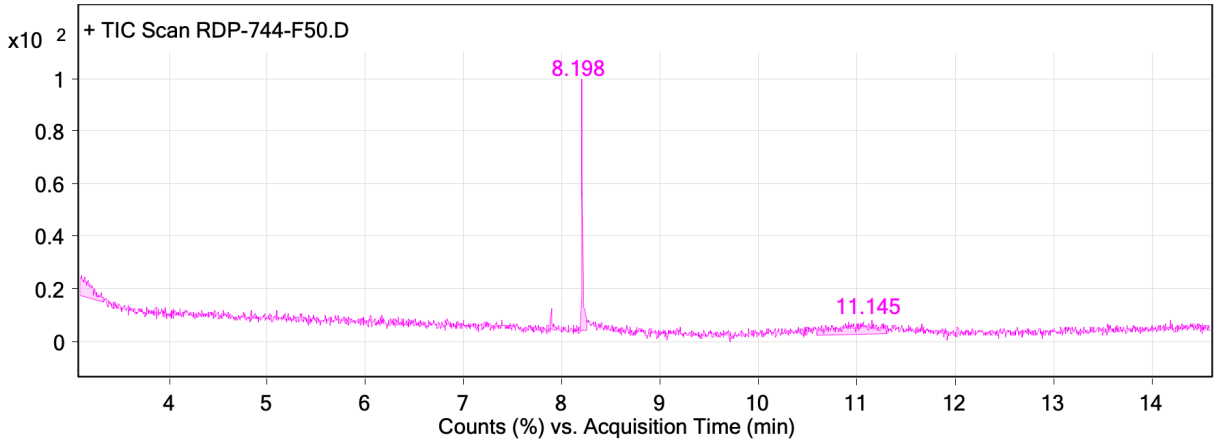

Figure. B.46. GC-MS chromatogram for 2-(3-chlorophenethyl)piperidine.

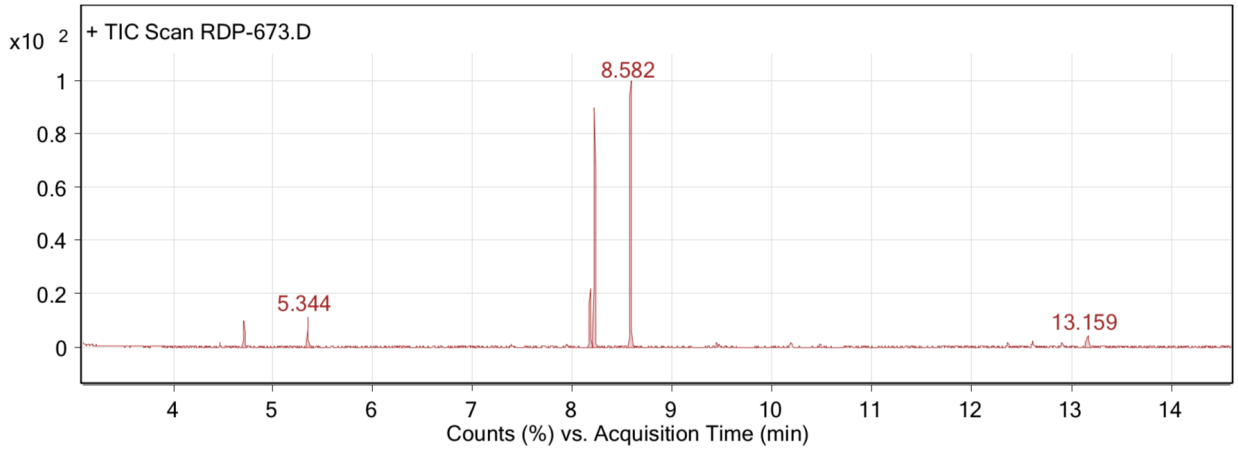

Figure. B.47. GC-MS chromatogram for the crude reaction between 2-chlorostyrene and piperidine.

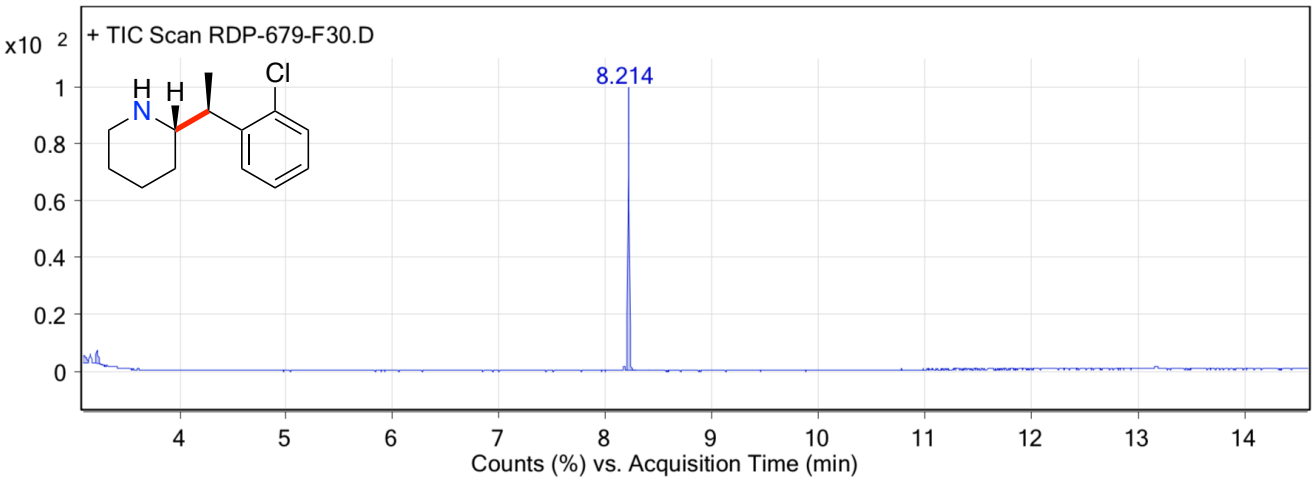

Figure. B.48. GC-MS chromatogram of 2-(1-(2-chlorophenyl)ethyl)piperidine.

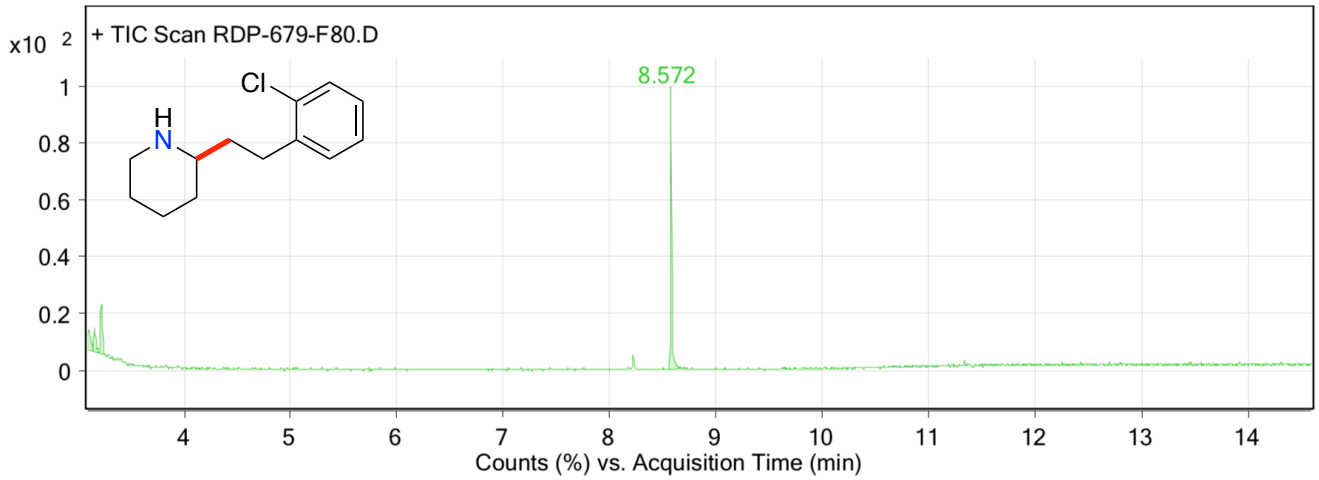

Figure. B.49. GC-MS chromatogram of 2-(1-(2-chlorophenyl)ethyl)piperidine.

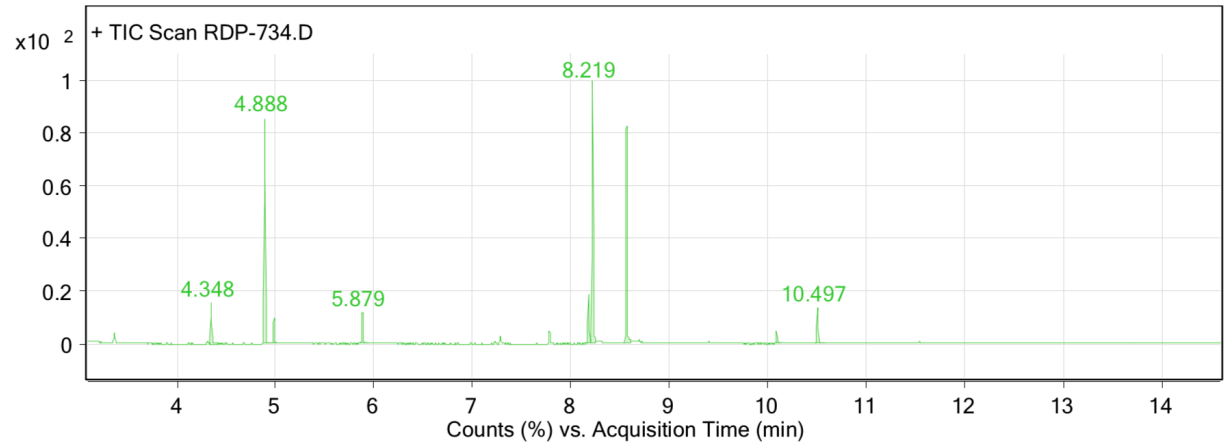

Figure. B.50. GC-MS chromatogram for the crude reaction mixture between piperidine and 2-chlorostyrene.

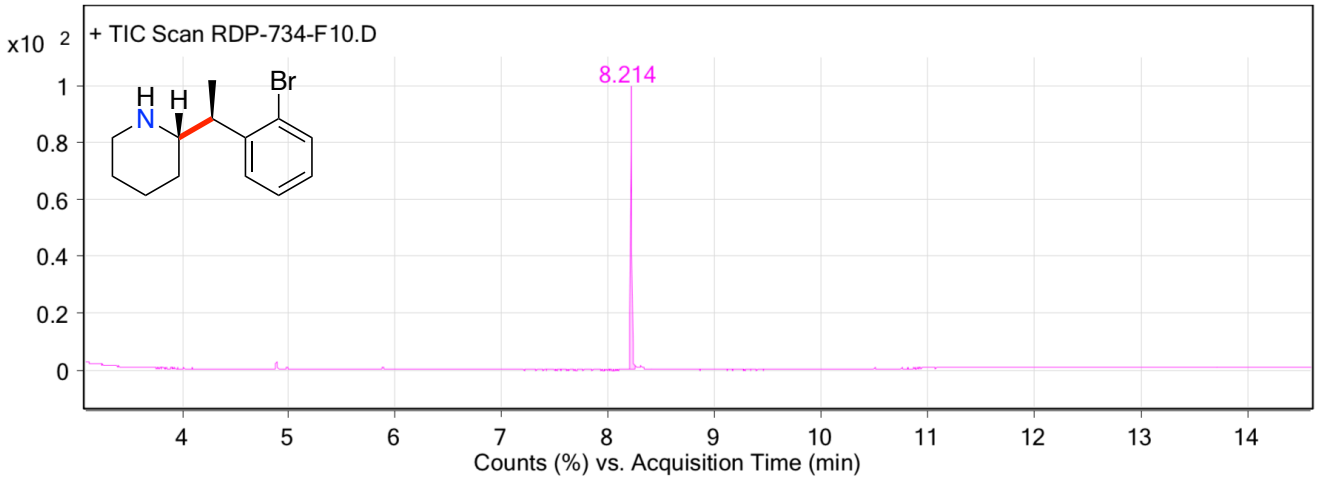

Figure. B.51. GC-MS chromatogram of 2-(1-(2-bromophenyl)ethyl)piperidine.

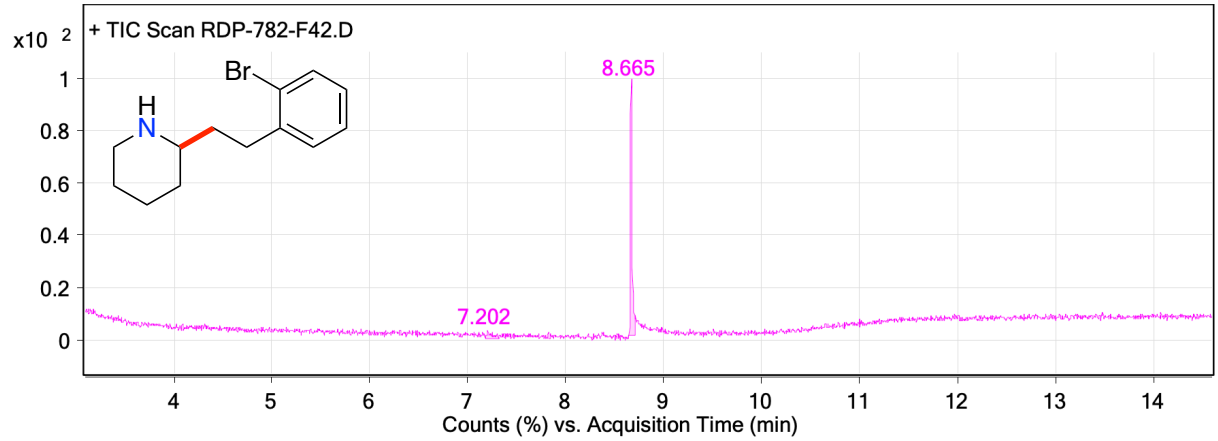

Figure. B.52. GC-MS chromatogram (101 MHz, $CDCl_3$, 298 K) of 2-(2-bromophenethyl)piperidine.

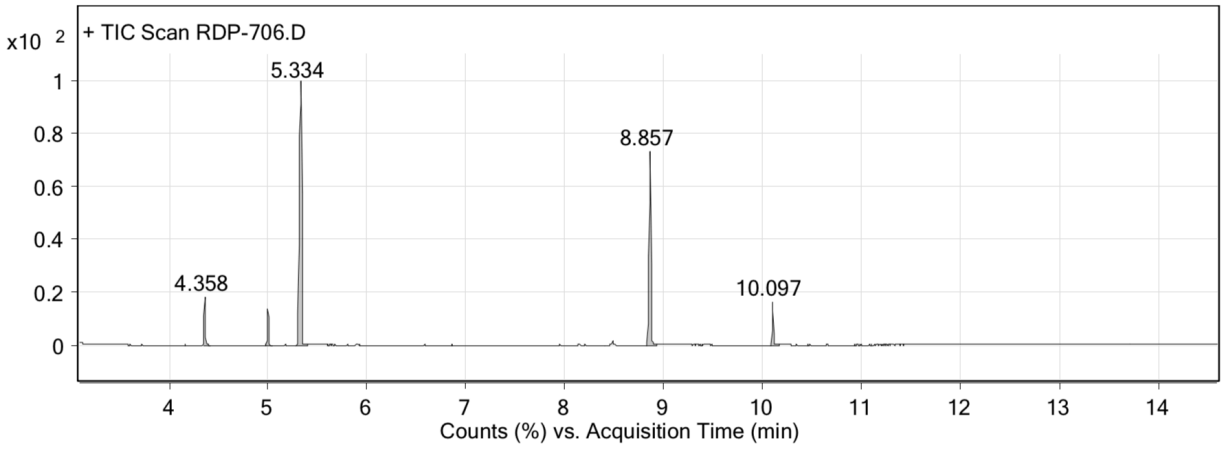

Figure. B.53. GC-MS chromatogram for the crude reaction mixture between piperidine and 2-chlorosrtyrene.

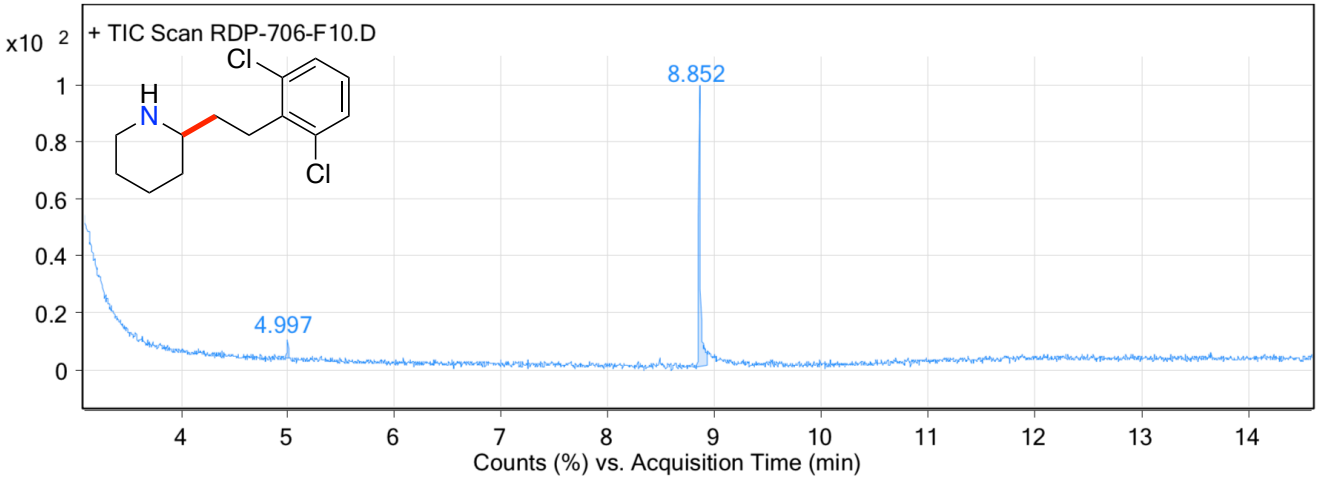

Figure. B.54. GC-MS chromatogram of 2-(2,6-dichlorophenethyl)piperidine.

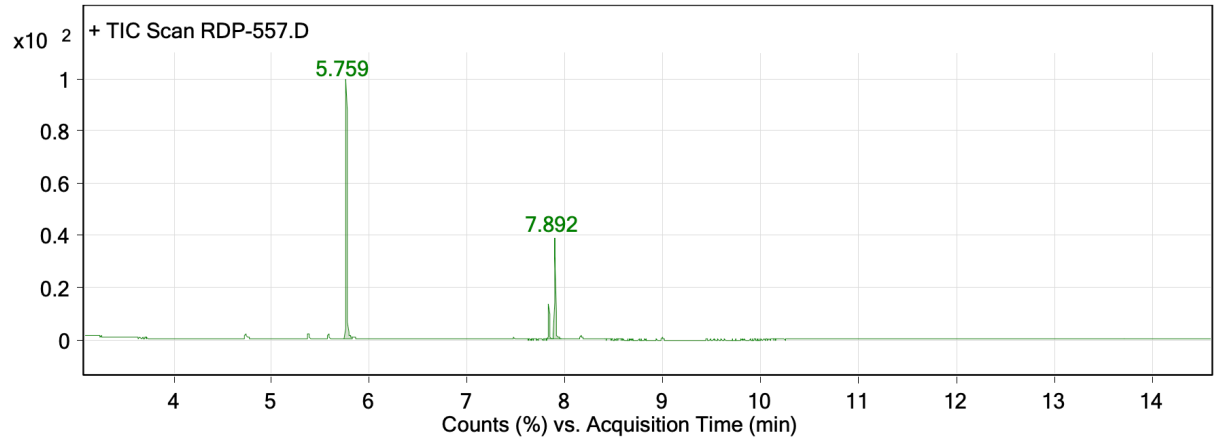

Figure. B.55. GC-MS chromatogram for the crude reaction mixture between piperidine and trimethylvinylsilane.

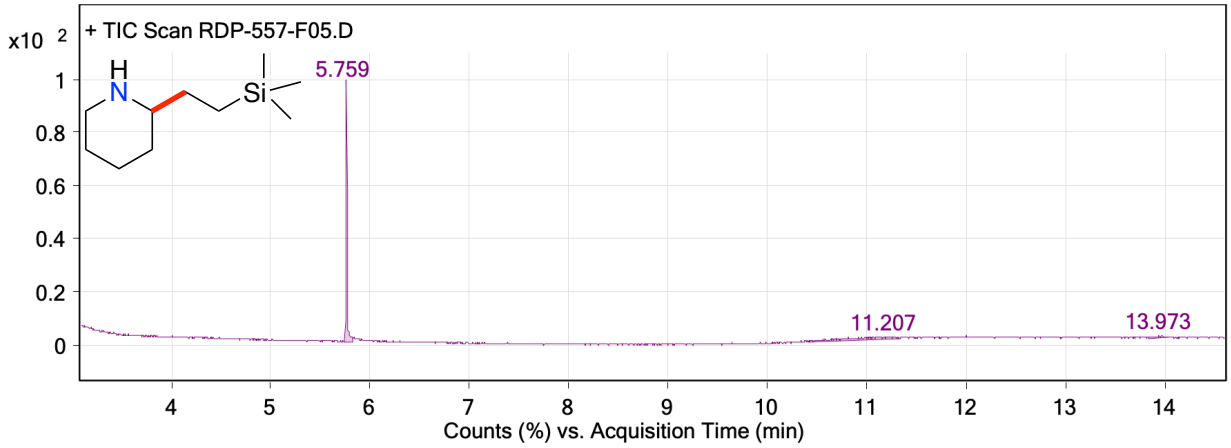

Figure. B.56. GC-MS chromatogram of 2-(2-(trimethylsilyl)ethyl)piperidine.

Appendix C

This appendix is for chiral HPLC data.

C.1 Chapter 3 HPLC Data

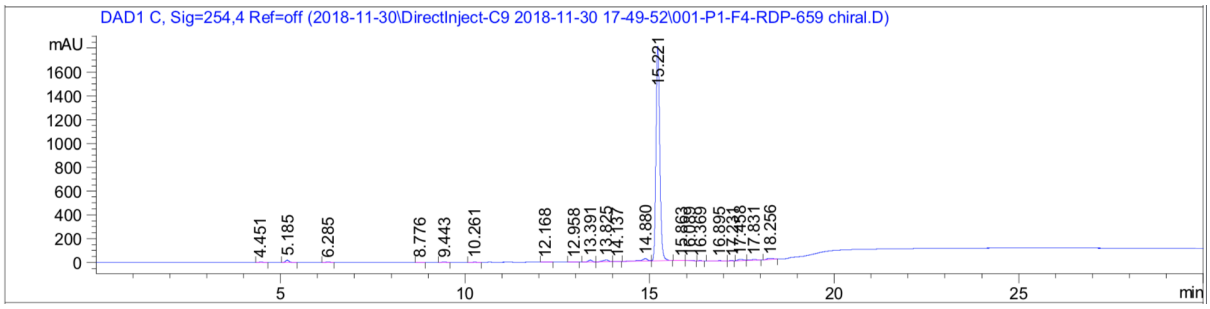

Figure. C.1. HPLC report of *N*-(2-methyl-2-(4-methylcyclohex-3-en-1-yl)propyl)aniline when (R)-(+)-limonene is used, indicating the presence of a single enantiomer when the product was made in the absence of any ligand salt.

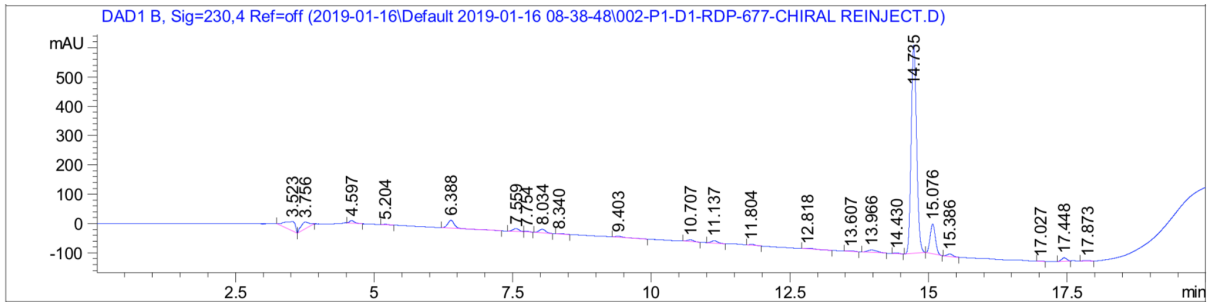

Figure. C.2. HPLC report of *N*-(2-methyl-2-(4-methylcyclohex-3-en-1-yl)propyl)aniline when (S)-(-)-limonene is used, indicating the presence of a majority single enantiomer when the product was made in the absence of any ligand salt. Note that the HPLC method used here is the same as that in Figure. C.1

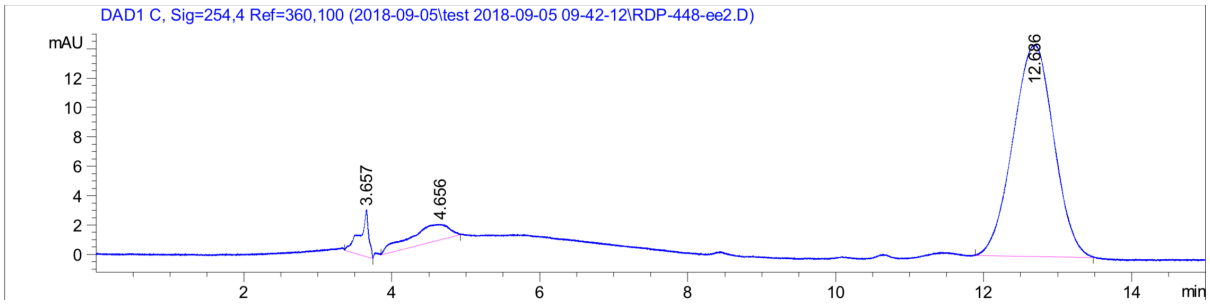

Figure. C.3. HPLC report of *N*-(2-methyl-2-(4-methylcyclohex-3-en-1-yl)propyl)aniline indicating the presence of a single enantiomer when a chiral ligand salt was employed.

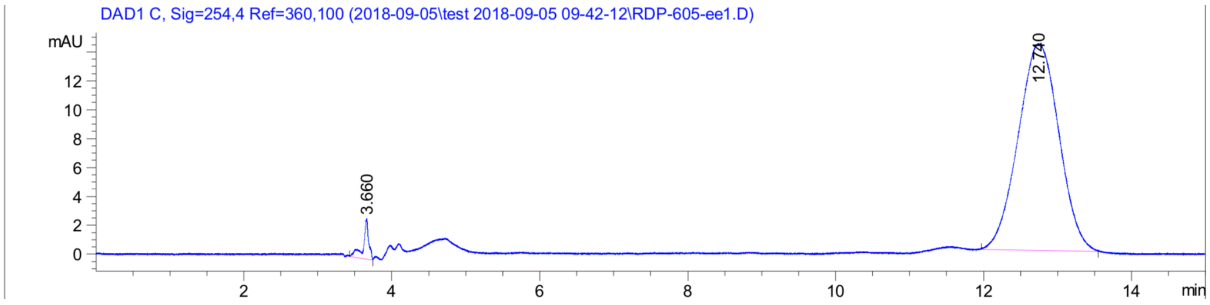

Figure. C.4. HPLC report of *N*-(2-methyl-2-(4-methylcyclohex-3-en-1-yl)propyl)aniline indicating the presence of a single enantiomer when a racemic ligand salt was employed.

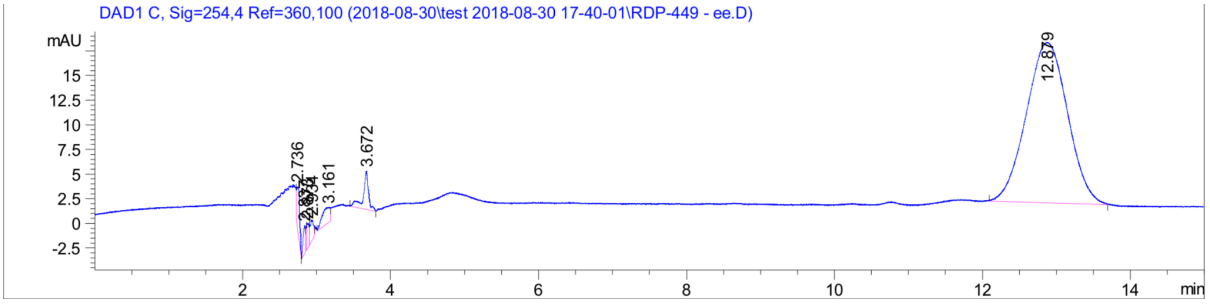

Figure. C.5. HPLC report of *N*-((2,6,6-trimethylbicyclo[3.1.1]heptan-2-yl)methyl)aniline indicating the presence of a single enantiomer when a chiral ligand salt was employed.

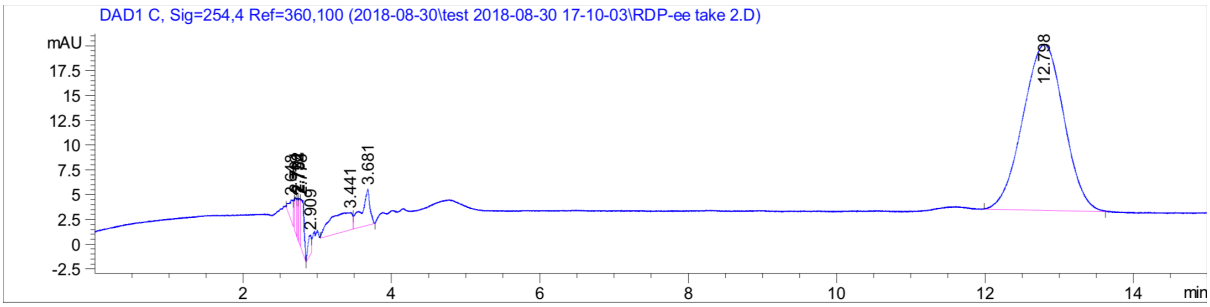

Figure. C.6. HPLC report of *N*-((2,6,6-trimethylbicyclo[3.1.1]heptan-2-yl)methyl)aniline indicating the presence of a single enantiomer when a racemic ligand salt was employed.

Appendix D

This appendix is for crystallographic data.

D.1 Chapter 2 Crystallographic Data

Table. D.1. List of crystallographic parameters for Mono(*N*-(2,6-dimethylphenyl)-*N*-piperidyl)carbamoylamidate)-tris(methylenetrimethylsilane)chlorotantalum (**2.40**)

Identification code	rhombo
Empirical formula	$C_{26}H_{52}ClN_2OSi_3Ta$
Formula weight	709.36
Temperature/K	296.15
Crystal system	trigonal
Space group	R3c
a/Å	26.1472(19)
b/Å	26.1472(19)
c/Å	28.646(3)
α/°	90
β/°	90
γ/°	120
Volume/Å^3	16961(3)
Z	18
ϱ_{calc}g/cm^3	1.250
μ/mm^{-1}	3.100
F(000)	6516.0
Crystal size/mm^3	0.14 × 0.12 × 0.08
Radiation	MoKα (λ = 0.71073)
2Θ range for data collection/°	3.116 to 60.222
Index ranges	-36 ≤ h ≤ 36, -34 ≤ k ≤ 36, -40 ≤ l ≤ 35
Reflections collected	67713
Independent reflections	10598 [R_{int} = 0.1022, R_{sigma} = 0.0768]
Data/restraints/parameters	10598/1/319
Goodness-of-fit on F^2	1.009
Final R indexes [I>=2σ (I)]	R_1 = 0.0401, wR_2 = 0.0729
Final R indexes [all data]	R_1 = 0.0642, wR_2 = 0.0802
Largest diff. peak/hole / e Å^{-3}	1.80/-0.92
Flack parameter	-0.014(11)

Table. D.2. List of crystallographic parameters for Mono(N-(2,6-dimethylphenyl)-N-methyl-N-(isopropyl)carbamoylamidate)-tris(methylenetrimethylsilane)chlorotantalum (**2.41**)

Identification code	platon_pl
Empirical formula	$C_{25}H_{52}ClN_2OSi_3Ta$
Formula weight	697.361
Temperature/K	296.15
Crystal system	orthorhombic
Space group	Pbca
a/Å	19.6155(6)
b/Å	16.9788(6)
c/Å	20.3172(6)
α/°	90
β/°	90
γ/°	90
Volume/Å^3	6766.6(4)
Z	8
ϱ_{calc}g/cm^3	1.369
μ/mm^{-1}	3.452
F(000)	2849.1
Crystal size/mm^3	0.21 × 0.16 × 0.14
Radiation	Mo Kα (λ = 0.71073)
2Θ range for data collection/°	3.76 to 59.22
Index ranges	-18 ≤ h ≤ 27, -23 ≤ k ≤ 23, -27 ≤ l ≤ 28
Reflections collected	252890
Independent reflections	9498 [R_{int} = 0.0573, R_{sigma} = 0.0181]
Data/restraints/parameters	9498/0/336
Goodness-of-fit on F^2	1.283
Final R indexes [I>=2σ (I)]	R_1 = 0.0331, wR_2 = 0.0569
Final R indexes [all data]	R_1 = 0.0534, wR_2 = 0.0808
Largest diff. peak/hole / e Å^{-3}	1.37/-0.93

Table. D.3. List of crystallographic parameters for Mono(N-(2,6-dimethylphenyl)-N-methyl-N-(benzhydryl)carbamoylamidate)-tris(methylenetrimethylsilane)chlorotantalum (**2.42**)

Identification code	ls810
Empirical formula	$C_{35}H_{56}ClN_2OSi_3Ta$
Formula weight	821.504
Temperature/K	90(2)
Crystal system	monoclinic
Space group	$P2_1/c$
a/Å	20.9753(18)
b/Å	17.1656(13)
c/Å	22.6226(17)
α/°	90
β/°	101.283(3)
γ/°	90
Volume/Å^3	7987.9(11)
Z	8
ϱ_{calc}g/cm^3	1.366
μ/mm^{-1}	2.936
F(000)	3361.3
Crystal size/mm^3	0.17 × 0.15 × 0.11
Radiation	Mo Kα (λ = 0.71073)
2Θ range for data collection/°	3 to 50.74
Index ranges	-25 ≤ h ≤ 24, 0 ≤ k ≤ 20, 0 ≤ l ≤ 27
Reflections collected	14575
Independent reflections	14573 [R_{int} = 0.0000, R_{sigma} = 0.1098]
Data/restraints/parameters	14573/0/798
Goodness-of-fit on F^2	1.024
Final R indexes [I>=2σ (I)]	R_1 = 0.0580, wR_2 = 0.1021
Final R indexes [all data]	R_1 = 0.1123, wR_2 = 0.1125
Largest diff. peak/hole / e Å^{-3}	2.12/-1.78

Table. D.4: List of crystallographic parameters for Mono(*N*-(2,6-trimethylphenyl)-*N*-methyl-*N*-(benzhydryl)carbamoylamidate)-tris(methylenetrimethylsilane)chlorotantalum (**2.43**)

Identification code	ls812 - AAU13Na
Empirical formula	$C_{34}H_{62}ClN_2OSi_3Ta$
Formula weight	815.52
Temperature/K	296.15
Crystal system	monoclinic
Space group	$P2_1/n$
a/Å	12.1904(8)
b/Å	18.7023(12)
c/Å	17.4187(12)
α/°	90
β/°	93.706(2)
γ/°	90
Volume/Å^3	3963.0(5)
Z	4
ρ_{calc}g/cm^3	1.367
μ/mm^{-1}	2.958
F(000)	1680.0
Crystal size/mm^3	0.18 × 0.15 × 0.068
Radiation	MoKα (λ = 0.71073)
2Θ range for data collection/°	3.198 to 61.112
Index ranges	$-17 \leq h \leq 16$, $-26 \leq k \leq 26$, $-24 \leq l \leq 24$
Reflections collected	55268
Independent reflections	12143 [R_{int} = 0.0612, R_{sigma} = 0.0511]
Data/restraints/parameters	12143/0/394
Goodness-of-fit on F^2	1.006
Final R indexes [I>=2σ (I)]	R_1 = 0.0280, wR_2 = 0.0535
Final R indexes [all data]	R_1 = 0.0438, wR_2 = 0.0582
Largest diff. peak/hole / e Å^{-3}	1.00/-1.41

Table. D.5. List of crystallographic parameters for Mono(*N*-(2,4,6-trimethylphenyl)-N-methyl-N-(benzhydryl)carbamoylamidate)-tris(methylenetrimethylsilane)chlorotantalum (**2.44**)

Identification code	ls814 - AAU17Na
Empirical formula	$C_{31}H_{56}ClN_2OSi_3Ta$
Formula weight	773.44
Temperature/K	296.15
Crystal system	orthorhombic
Space group	$P2_12_12_1$
a/Å	12.6400(7)
b/Å	15.6219(10)
c/Å	18.8874(12)
α/°	90
β/°	90
γ/°	90
Volume/Å^3	3729.5(4)
Z	4
ϱ_{calc}g/cm^3	1.377
μ/mm^{-1}	3.139
F(000)	1584.0
Crystal size/mm^3	0.26 × 0.15 × 0.12
Radiation	MoKα (λ = 0.71073)
2Θ range for data collection/°	3.384 to 61.058
Index ranges	-17 ≤ h ≤ 13, -21 ≤ k ≤ 22, -21 ≤ l ≤ 27
Reflections collected	50017
Independent reflections	11373 [R_{int} = 0.0637, R_{sigma} = 0.0585]
Data/restraints/parameters	11373/0/367
Goodness-of-fit on F^2	1.006
Final R indexes [I>=2σ (I)]	R_1 = 0.0296, wR_2 = 0.0593
Final R indexes [all data]	R_1 = 0.0356, wR_2 = 0.0615
Largest diff. peak/hole / e Å^{-3}	0.99/-1.05
Flack parameter	0.012(7)

Table. D.6. List of crystallographic parameters for Mono(N-(4-bromo-2,6-dimethylphenyl)-N-methyl-N-(benzhydryl)carbamoylamidate)-tris(methylenetrimethylsilane)chlorotantalum (**2.45**)

Identification code	ls816
Empirical formula	$C_{30}H_{53}BrClN_2OSi_3Ta$
Formula weight	838.32
Temperature/K	296.15
Crystal system	orthorhombic
Space group	$P2_12_12_1$
a/Å	12.6187(12)
b/Å	15.6891(14)
c/Å	18.9340(18)
α/°	90
β/°	90
γ/°	90
Volume/Å^3	3748.5(6)
Z	4
ϱ_{calc}g/cm^3	1.485
μ/mm^{-1}	4.189
F(000)	1688.0
Crystal size/mm^3	0.13 × 0.11 × 0.09
Radiation	MoKα (λ = 0.71073)
2Θ range for data collection/°	3.372 to 66.28
Index ranges	-19 ≤ h ≤ 10, -21 ≤ k ≤ 24, -29 ≤ l ≤ 28
Reflections collected	55371
Independent reflections	14259 [R_{int} = 0.0537, R_{sigma} = 0.0501]
Data/restraints/parameters	14259/0/366
Goodness-of-fit on F^2	0.994
Final R indexes [I>=2σ (I)]	R_1 = 0.0257, wR_2 = 0.0548
Final R indexes [all data]	R_1 = 0.0321, wR_2 = 0.0566
Largest diff. peak/hole / e Å^{-3}	1.06/-1.15
Flack parameter	0.103(5)

Table. D.7. List of crystallographic parameters for Mono(N-(4-chloro-2,6-dimethylphenyl)-N-methyl-N-(benzhydryl)carbamoylamidate)-tris(methylenetrimethylsilane)chlorotantalum (**2.46**)

Identification code	ls831_d
Empirical formula	$C_{30}H_{53}Cl_2N_2OSi_3Ta$
Formula weight	793.877
Temperature/K	296.15
Crystal system	orthorhombic
Space group	$P2_12_12_1$
a/Å	12.6181(4)
b/Å	15.5556(5)
c/Å	18.8201(7)
α/°	90
β/°	90
γ/°	90
Volume/Å^3	3694.0(2)
Z	4
ϱ_{calc}g/cm^3	1.427
μ/mm^{-1}	3.241
F(000)	1617.2
Crystal size/mm^3	0.34 × 0.33 × 0.22
Radiation	Mo Kα (λ = 0.71073)
2Θ range for data collection/°	3.4 to 61.26
Index ranges	-17 ≤ h ≤ 17, -21 ≤ k ≤ 22, -23 ≤ l ≤ 26
Reflections collected	58976
Independent reflections	11297 [R_{int} = 0.0381, R_{sigma} = 0.0435]
Data/restraints/parameters	11297/0/389
Goodness-of-fit on F^2	1.018
Final R indexes [I>=2σ (I)]	R_1 = 0.0272, wR_2 = 0.0504
Final R indexes [all data]	R_1 = 0.0323, wR_2 = 0.0524
Largest diff. peak/hole / e Å^{-3}	0.74/-0.58
Flack parameter	-0.012(5)

Table. D.8. List of crystallographic parameters for Bis(*N*-(2,6-dimethylphenyl)-*N*-piperidyl)carbamoylamidate)-tris(methylenetrimethylsilane)chlorotantalum (**2.47**)

Identification code	test
Empirical formula	$C_{40}H_{71}N_4O_2Si_3Ta$
Formula weight	905.22
Temperature/K	296.15
Crystal system	triclinic
Space group	P-1
a/Å	11.2624(6)
b/Å	13.2246(7)
c/Å	16.0849(9)
α/°	91.9850(10)
β/°	110.0120(10)
γ/°	100.4860(10)
Volume/Å^3	2201.2(2)
Z	2
ϱ_{calc}g/cm^3	1.366
μ/mm^{-1}	2.615
F(000)	940.0
Crystal size/mm^3	0.13 × 0.11 × 0.09
Radiation	MoKα (λ = 0.71073)
2Θ range for data collection/°	2.71 to 62.016
Index ranges	-16 ≤ h ≤ 16, -19 ≤ k ≤ 18, -21 ≤ l ≤ 23
Reflections collected	23822
Independent reflections	13801 [R_{int} = 0.0417, R_{sigma} = 0.0813]
Data/restraints/parameters	13801/0/464
Goodness-of-fit on F^2	1.029
Final R indexes [I>=2σ (I)]	R_1 = 0.0456, wR_2 = 0.0914
Final R indexes [all data]	R_1 = 0.0653, wR_2 = 0.0990
Largest diff. peak/hole / e Å^{-3}	6.18/-1.35

Table. D.9. List of crystallographic parameters for the mono *N,O*-chelated complex between **2.48** and $Ta(CH_2SiMe_3)_2Cl_2$ (**2.50**)

Formula	$C_{16}H_{37}ClN_5OTa$
M_w (g/mol); $d_{calcd.}$ (g/cm^3)	531.90; 1.557
T (K); F(000)	90; 532
Crystal System	Monoclinic
Space Group	$P2_1$
Unit Cell: a (Å)	9.9984(6)
b (Å)	8.1066(5)
c (Å)	14.0375(9)
α (°)	90
β (°)	94.491(3)
γ (°)	90
V (Å^3); Z	1134.29(12); 2
μ (mm^{-1}); Abs. Corr.	4.975; multiscan
θ range (°); completeness	2.42-30.09; 1
collected reflections; R_σ	24148; 0.0268
unique reflections; R_{int}	6631; 0.0310
R1(F) ($I > 2\sigma(I)$)	0.0322
wR(F^2) (all data)	0.0825
GoF(F^2); Flack-x	1.126; –0.013(12)
Residual electron density	0.994; –1.268

D.2 Chapter 3 Crystallographic Data

Table. D.10. List of crystallographic parameters for Mono(N-(4-chloro-2,6-dimethylphenyl)-N-methyl-N-(benzhydryl)carbamoylamidate)-tris(methylenetrimethylsilane)chlorotantalum

	ls781
Formula	$C_{17}H_{25}FNCl$
CCDC	1867183
Mol. wt.	297.83
Crystal system	orthorhombic
Space group	*P 21 21 2*
a(Å)	18.5454(13)
b(Å)	24.3387(16)
c(Å)	7.3121(5)
α(°)	90
β(°)	90
γ(°)	90
V(Å^3)	3300.5(4)
Z	8
Density (g/cm^3)	1.361
Abs. coeff., (mm^{-1})	0.233
F(000)	1280
Crystal size, mm	0.32×0.04×0.02
θ range, deg	1.38 to 24.71
Limiting indices	−21 < h < 18 −28 < k < 20 −8 < l < 8
R(int)	0.0465
Reflections collected	22975
Reflec. Unique [$I>2\sigma(I)$]	5632
Data/restraints/param.	4935 / 0 / 256
Goodness-of-fit	1.020
R_1 [$I>2\sigma(I)$] (all data)	0.0379 (0.0792)
wR_2 [$I>2\sigma(I)$] (all data)	0.0495 (0.0834)
Largest diff. e·A^{-3}	0.28 and –0.19

D.3 Chapter 4 Crystallographic Data

Table. D.11. List of crystallographic parameters for Mono(*N*-(4-chloro-2,6-dimethylphenyl)-*N*-methyl-*N*-(benzhydryl)carbamoylamidate)-tris(methylenetrimethylsilane)chlorotantalum

Identification code	ls806 - AAU10Na
Empirical formula	$C_{30}H_{54}ClN_2OSi_3Ta$
Formula weight	759.42
Temperature/K	273.15
Crystal system	monoclinic
Space group	$P2_1/n$
a/Å	12.6561(8)
b/Å	16.2013(10)
c/Å	17.5797(11)
α/°	90
β/°	90.103(2)
γ/°	90
Volume/Å^3	3604.6(4)
Z	4
ϱ_{calc}g/cm^3	1.399
μ/mm^{-1}	3.247
F(000)	1552.0
Crystal size/mm^3	0.15 × 0.12 × 0.09
Radiation	MoKα (λ = 0.71073)
2Θ range for data collection/°	3.418 to 59.178
Index ranges	-17 ≤ h ≤ 9, -22 ≤ k ≤ 20, -24 ≤ l ≤ 24
Reflections collected	28395
Independent reflections	10122 [R_{int} = 0.0546, R_{sigma} = 0.0685]
Data/restraints/parameters	10122/0/361
Goodness-of-fit on F^2	0.981
Final R indexes [I>=2σ (I)]	R_1 = 0.0345, wR_2 = 0.0612
Final R indexes [all data]	R_1 = 0.0556, wR_2 = 0.0673
Largest diff. peak/hole / e Å^{-3}	0.89/-0.78